Universidad Autónoma de Madrid

Facultad de Ciencias

Programa de Doctorado en Biociencias Moleculares

Utilidad de la biopsia líquida en pacientes con cáncer de pulmón no microcítico con translocación en *ALK*

Tesis Doctoral

Estela Sánchez Herrero

Madrid, 2022

Universidad Autónoma de Madrid

Departamento de Biología Molecular

Programa de Doctorado en Biociencias Moleculares

Utilidad de la biopsia líquida en pacientes con cáncer de pulmón no microcítico con translocación en *ALK*

Memoria de Tesis Doctoral presentada por:

Estela Sánchez Herrero

Graduada en Biología Sanitaria, para optar al grado de Doctora por la Universidad Autónoma de Madrid

Directores: **Dra. Atocha Romero Alfonso y Prof. Mariano Provencio**

Tutor de Empresa: **Dr. Víctor González Rumayor**

Tutor Académico: **Dr. Francisco Zafra Gómez**

Instituto de Investigación Sanitaria Puerta de Hierro – Segovia de Arana

Atrys Health SA

Atocha Romero Alfonso, Doctora en Bioquímica y Biología Molecular por la Universidad Complutense de Madrid y Directora Técnica del Laboratorio de Biopsia Líquida del Servicio de Oncología Médica del Hospital Universitario Puerta de Hierro; **Mariano Provencio Pulla**, Doctor en Medicina por la Universidad de Alcalá de Henares y Jefe de Servicio de Oncología Médica del Hospital Universitario Puerta de Hierro, Director Científico del Instituto de Investigación Sanitaria Puerta de Hierro – IDIPHIM y Catedrático de la Universidad Autónoma de Madrid; y **Víctor González Rumayor**, Doctor en Genética por la Universidad Complutense de Madrid y Director del Departamento de I+D de la empresa Atrys Health SA

CERTIFICAN:

Que Estela Sánchez Herrero ha realizado bajo nuestra dirección el presente trabajo de investigación "**Utilidad de la biopsia líquida en pacientes con cáncer de pulmón no microcítico con translocación en *ALK***" que, a nuestro juicio, reúne los requisitos de originalidad y rigor necesarios para ser presentado y juzgado por el tribunal correspondiente para optar al grado de Doctora en Biociencias Moleculares por la Universidad Autónoma de Madrid.

Para que conste a todos los efectos, firmamos el presente certificado en:

Madrid, 14 de Noviembre del 2022

Dra. Atocha Romero Alfonso	**Dr. Mariano Provencio Pulla**	**Dr. Víctor González Rumayor**
Directora de Tesis	**Co-Director de Tesis**	**Tutor de Empresa**

En primer lugar quiero agradecer a Atocha, mi directora de Tesis, la oportunidad que me dio hace 4 años, abriéndome las puertas de su equipo y del mundo maravilloso de la ciencia. Has logrado formar un laboratorio con los medios ideales para que descubramos y desarrollemos nuestro potencial. Gracias por cuidarnos, por luchar por nosotros y por contagiarnos esas ganas inagotables de avanzar y crecer. También quiero dar las gracias a mi co-director de Tesis, Mariano, por su confianza, por darme su visión clínica, junto con el resto de profesionales del grupo de Oncología Médica del Hospital Universitario Puerta de Hierro, y enseñarme que todo sale mejor cuando se trabaja en equipo.

También me gustaría agradecer a mi tutor de empresa Víctor por haberme ayudado a realizar esta Tesis, junto con la Comunidad de Madrid (con sus ayudas para la realización de Doctorados Industriales - IND2019/BMD-17258), y por darme la oportunidad de formar parte de Atrys Health y conocer a personas encantadoras que me han acogido de la mejor forma posible.

Pero este camino no hubiese sido posible sin el apoyo de las personas con las que he tenido la suerte de compartirlo, y a las cuales tengo mucho que agradecer.

Gracias M. Fanlo por contagiarnos tu pasión por la Biología y por seguir ahí en cada paso que damos. Y hablo en plural porque sé que es un sentimiento compartido con mis amigas de toda la vida Cris (aunque para mí siempre será mi Pekis) y Esther. Gracias a las dos por aparecer y por quedaros, por vuestro apoyo incondicional y por hacerme reír incluso en mis peores días. Espero que nunca os bajéis de mi cohete. También quiero dar las gracias a Andrea, que aunque esté a 17.000 km, siempre la siento cerca, transmitiéndome toda su buena energía. Más cerquita está mi otra Cris (o mi Franches), siempre disponible cuando me hace falta su sonrisa infatigable. Gracias también a mis súper mamis Anita y Carol por acompañarme en este camino que comenzamos las tres con el Funky y al que se han sumado mis dos peques Leo y Danielín.

Gracias a mis compañeros de carrera, *La Secta*. En especial, gracias a Bárbara por tu alegría, por las tardes de estudio, que terminaban siendo tardes de bares, por las clases de Candy Crush y Logo Quiz, pero sobre todo por ser mi amiga durante todos estos años.

Gracias a todos mis compañeros del Laboratorio de Biopsia Líquida, también conocidos como los *Atochos*, los que están y los que se han marchado. Gracias a Clara, Miguel y Nieves por enseñarme y por hacer mi comienzo más fácil. Sandra, gracias por ser mi compañera "mariprisillas", mi cómplice de fechorías y de lágrimas de risa y por ampliar mi vocabulario; pero sobre todo gracias por enseñarme a trabajar en equipo y por ayudarme en toda esta etapa, tanto que gran parte de esta Tesis también es tuya. Gracias a Alex por las fiestas y sus vueltas en cabify, por hacerme reír con tu estornudo-baile, por los innumerables cafés con charla y en definitiva por estar siempre ahí. Ha sido todo un placer empezar y terminar esta etapa con dos compañeros tan increíbles como vosotros. Rober, gracias por los escasos pero buenos momentos en los congresos (P.D. queda pendiente la revancha, aunque tampoco estuvo mal estar en el mismo equipo), por enseñarme a ahorrar muchos minutos en el coche, pero sobre todo por ayudarme a resolver mis numerosas dudas en el despachín, acompañándome y animándome siempre en este camino con sus días buenos y no tan buenos. Lucía, gracias por traernos tu alegría, tu locura, tus canturreos y tu entusiasmo por la ciencia al labo, pero sobre todo gracias por haberme ayudado este último año, tanto laboral como personalmente. Gracias

también a Patri, Cris, Raquel y Dunixe, así como a otros grupos y servicios del Instituto de Investigación Sanitaria Puerta de Hierro - Segovia de Arana.

Quiero agradecer también a todos mis amigos de Galve de Sorbe por estar siempre ahí, ayudándome a desconectar, ya sea de fiesta o de expedición por el campo, y particularmente a mis galvitas por crecer junto a mí y poder contar siempre con vuestro apoyo. En especial tengo que dar gracias infinitas a Vero, mi prima, amiga, confidente, compañera de fiestas y de vida. Gracias por estar pendiente y atenta de absolutamente todo (sobre todo de mis llaves y mi móvil), por ayudarme en todo momento y también gracias por haberme hecho reír tantísimo todos estos años, sobre todo con tus caídas. Tampoco puedo dejarme a mis *Cascanueces*, que tanto me han ayudado a desconectar sudando la gota gorda y que han hecho de mi comienzo en Guadalajara un camino mucho más fácil y divertido.

Por supuesto gracias a Pablo, mi chico, por luchar por mí desde tan pequeños, por quererme y respetarme como lo haces y por aguantarme todos estos años a pesar de los momentos de agobio y estrés. Gracias por las sonrisas y el apoyo que me das cada día, dándome ese impulso que en muchas ocasiones he necesitado. Gracias también por haberme traído a la alegría de nuestra casa, nuestro Bakun.

Por último, quiero dar las gracias a mi familia, que siempre me ha apoyado en mis decisiones y siempre ha estado ahí a mi lado. Gracias a mis padres por creer en mí más que nadie en el mundo. Gracias mamá por esforzarte siempre en entender mi trabajo, por escuchar los ensayos de mis charlas, por nuestra complicidad y por enseñarme tu forma de vivir la vida, siempre derrochando alegría y positivismo, enseñándome que las cosas no son tan importantes como parecen. Gracias papá por protegerme y cuidarme, por hacerme sentir que siempre seré tu niña y que, por mucho que pasen los años, nosotros seguiremos riéndonos con nuestras peleas; pero sobre todo, gracias por enseñarme que nunca hay que rendirse y que siempre hay que luchar por lo que es justo. Tate, gracias por ser el mejor hermano que se puede tener, por tu paciencia infinita y tu buen carácter. A mis abuelos, gracias por enseñarme vuestros valores, por consentirme con la merienda y por saber mejor que nadie cómo calmarme, os echo mucho de menos. A mis abuelas, gracias por vuestra fortaleza para seguir adelante y por vuestro amor y apoyo inquebrantable. No querría dejar de agradecer a todos mis tíos y primos, siempre tan pendientes de mis avances, siendo un apoyo fundamental en toda esta etapa.

RESUMEN

El cáncer de pulmón es la principal causa de mortalidad relacionada con el cáncer, diagnosticándose en estadios avanzados en el 80% de los casos. El manejo del cáncer de pulmón de células no pequeñas (CPCNP) avanzado ha mejorado notablemente gracias a la identificación de alteraciones moleculares y al desarrollo de fármacos dirigidos frente a las mismas. Las mutaciones más relevantes en el CPCNP ocurren en los genes *EGFR, ALK* y *ROS1*, dianas de terapias dirigidas basadas en inhibidores de tirosina kinasa (TKIs). En concreto, el 3-7% de los pacientes con CPCNP presentan translocaciones en *ALK*, originando un subtipo molecular observado especialmente en pacientes jóvenes, no fumadores y con histología de adenocarcinoma. El correcto diagnóstico de estos pacientes es crucial dada la mejora significativa en supervivencia y calidad de vida gracias al amplio abanico de TKIs dirigidos frente *ALK* (*ALK*-TKIs). Sin embargo, alrededor del 70% de los pacientes progresan tras 1 o 2 años de tratamiento debido a mutaciones de resistencia. Estas mutaciones, no obstante, no confieren resistencia a todos los TKIs disponibles. En este sentido, el estudio del perfil mutacional del tumor a la progresión, mediante técnicas de alta sensibilidad, puede suponer una estrategia eficiente para establecer una secuencia adecuada y personalizada de *ALK*-TKIs. Sin embargo, la biopsia tumoral en los pacientes con CPCNP no siempre es factible. La biopsia líquida, entendida como sangre y otros fluidos corporales, permite la detección tanto de las fusiones en *ALK* como de mecanismos de resistencia a *ALK*-TKIs de forma mínimamente invasiva. Sin embargo, la detección de fusiones en biopsia líquida sigue siendo un desafío dada su complejidad genómica. La Tesis doctoral se presenta como un compendio de publicaciones que tienen como objetivo perfeccionar los métodos diagnósticos y de seguimiento de los pacientes con CPCNP, especialmente aquellos con fusión en *ALK*. El primer trabajo demostró que la secuenciación masiva (NGS) del ADN circulante libre (cfDNA) basada en identificadores moleculares únicos (UMIs), con sensibilidad similar a técnicas como la PCR digital (dPCR), permite conocer el perfil mutacional del tumor con una alta concordancia con la dPCR. En el segundo trabajo, se demostró que el cfDNA procedente de fluidos corporales representa una fuente de información importante para identificar biomarcadores, en cáncer de pulmón, con mayor sensibilidad que el plasma. En el tercer artículo se analizaron mediante NGS 26 muestras de plasma y dos de líquido cefalorraquídeo (LCR), procedentes de 24 pacientes con CPCNP *ALK*-positivos, obtenidas en el momento de la progresión a un *ALK*-TKI. Mediante el desarrollo de un algoritmo bioinformático se identificaron mutaciones en el *locus* de *ALK* en el 35% de los pacientes, así como potenciales mutaciones de resistencia en otros genes. Estos resultados, junto con los del caso clínico descrito en el cuarto artículo, demostraron la validez de la NGS de muestras de biopsia líquida para la detección de mutaciones de resistencia en el *locus* de *ALK* y la utilidad de este abordaje para la toma de decisiones terapéuticas en los pacientes *ALK*-positivos. Por último, nuestra estrategia para el quinto trabajo fue el estudio de transcritos de fusión de *ALK* (ARN mensajero, mRNA) contenidos en vesículas extracelulares (EVs), donde se encuentran protegidos de las RNAasas del torrente sanguíneo. Así, la fusión de *EML4-ALK*, tanto en su forma proteica como en mRNA, se identificó en EVs aisladas de líneas celulares y, posteriormente, en 8 de las 16 muestras clínicas de plasma derivadas de pacientes con CPCNP *ALK*-positivos analizadas, especialmente en aquellas con mayor expresión de la tetraspanina CD81. El aislamiento de EVs supone una estrategia alternativa al tejido, no invasiva, automatizable y aplicable a la práctica clínica para la detección de fusiones como la translocación de *ALK*.

ASBTRACT

Lung cancer is the leading cause of cancer-related mortality worldwide, being diagnosed in advanced stages in 80% of cases. The management of advanced non-small cell lung cancer (NSCLC) has improved notably due to the identification of molecular alterations and the development of targeted drugs directed against them. The most relevant mutations in NSCLC occur in the *EGFR*, *ALK,* and *ROS1* genes, targets of tyrosine kinase inhibitors (TKIs). Specifically, 3-7% of NSCLC harbor translocations in the *ALK* gene, defining a molecular subtype observed especially in young patients, non-smokers, and with adenocarcinoma histology. The correct diagnosis of these patients is crucial given the significant improvement in survival and quality of life thanks to the development of a wide range of TKIs against *ALK* fusions (*ALK*-TKIs). However, approximately 70% of patients progress after 1 to 2 years of treatment due to the development of resistance mutations. These mutations, however, do not confer resistance to all available TKIs. In this sense, the study of the mutational profile of the tumor upon disease progression, using highly sensitive techniques, can be an efficient strategy to establish an adequate and personalized sequence of *ALK*-TKIs. Nevertheless, tumor biopsy in NSCLC patients is not always feasible. For this reason, liquid biopsy, understood as blood and other body fluids, allows the detection of both *ALK* fusions and resistance mechanisms to *ALK*-TKIs in a minimally invasive way. However, the detection of fusions in liquid biopsy samples remains challenging due to its genomic complexity.

The doctoral Thesis is presented as a compendium of publications aimed at improving diagnostic and follow-up methods for patients with NSCLC, especially those with ALK fusion. The first work showed that next-generation sequencing (NGS) of the cell-free DNA (cfDNA) using unique molecular identifiers (UMIs) during library preparation, with similar sensitivity to techniques such as digital PCR (dPCR), provides insight into the mutational profile of the tumor with a high concordance with dPCR. The second study demonstrated that cfDNA from body fluids represents an informative source for biomarker testing, in lung cancer patients, with greater sensitivity than plasma samples. In the third article, we analyzed by NGS 26 plasma samples and two cerebrospinal fluid (CSF) samples, from 24 *ALK*-positive NSCLC patients, collected upon disease progression while being treated with an *ALK*-TKI. Through the development of a bioinformatic algorithm, mutations in the *ALK locus* were identified in 35% of the patients. In addition, potential resistance mutations in other genes were identified. These results, together with those of the case report described in the fourth article, demonstrated the validity of NGS profiling of liquid biopsy samples for the detection of resistance mutations at the *ALK locus*, and the usefulness of this approach for therapeutic decision-making in *ALK*-positive patients. Finally, in the fifth article we showed that *ALK* fusions are present in EVs, both in their protein form and in messenger RNA (mRNA). Thus, the *EML4-ALK* fusion was identified in EVs isolated from cell lines and, subsequently, in 8 of the 16 clinical plasma samples derived from *ALK*-positive NSCLC patients analyzed, especially in those with increased expression of CD81 tetraspanin. The isolation of EVs represents an alternative approach to tissue, non-invasive, automatable, and applicable to clinical practice for the detection of fusions such as rearrangements in *ALK.*

ÍNDICE

ABREVIATURAS 3

INTRODUCCIÓN 5

1. Cáncer de pulmón 7

2. Cáncer de pulmón CPCNP 7

2.1. Clasificación histológica del CPCNP 7

2.2. Clasificación TNM del CPCNP 8

2.3. Clasificación molecular del CPCNP 10

2.3.1. CPCNP con mutación en *EGFR* 12

2.3.2. CPCNP con translocación en *ROS1* 13

3. CPCNP con translocación en *ALK* 13

3.1. Inhibidores Tirosina Kinasa frente *ALK*: *ALK*-TKIs 15

3.2. Mecanismos de resistencia frente *ALK*-TKIs 18

3.3. Estudio de los pacientes *ALK*-positivos CPCNP en la práctica clínica 19

4. Estudio de los pacientes con CPCNP *ALK*-positivos mediante biopsia líquida 21

4.1. ADN circulante tumoral (ctDNA, circulating tumor DNA) 21

4.2. ARN circulante tumoral (ctRNA, circulating tumor RNA) 23

4.3. Vesículas extracelulares (EVs, extracellular vesicles) 24

OBJETIVOS 27

RESULTADOS 37

ARTÍCULO 1: NEXT-GENERATION SEQUENCING FOR TUMOR MUTATION QUANTIFICATION USING LIQUID BIOPSIES 33

ARTÍCULO 2: ctDNA FROM BODY FLUIDS IS AN ADEQUATE SOURCE FOR *EGFR* BIOMARKER TESTING IN ADVANCED LUNG ADENOCARCINOMA 49

ARTÍCULO 3: NGS-BASED LIQUID BIOPSY PROFILING IDENTIFIES MECHANISMS OF RESISTANCE TO *ALK* INHIBITORS: A STEP TOWARD PERSONALIZED NSCLC TREATMENT. 62

ARTÍCULO 4: NEXT-GENERATION SEQUENCING TO DYNAMICALLY DETECT MECHANISMS OF RESISTANCE TO *ALK* INHIBITORS IN *ALK*-POSITIVE NSCLC PATIENTS: A CASE REPORT 92

ARTÍCULO 5: *ALK* FUSION TRANSCRIPTS CAN BE DETECTED IN EXTRACELLULAR VESICLES (EVs) FROM NON-SMALL CELL LUNG CANCER CELL LINES AND PATIENT PLASMA. TOWARDS EV-BASED NON-INVASIVE TESTING. 100

DISCUSIÓN 123

CONCLUSIONES 139

BIBLIOGRAFÍA 143

ANEXOS 161

ALK: Anaplastic Lymphoma Kinase

AMP: *Association for Molecular Pathology*

CAP: *College of American Pathologists*

cfDNA: ADN circulante libre

cfRNA: ARN circulante libre

CI: Intervalo de confianza

circRNAs: ARNs circulares

CNV: Alteración en el número de copias

CPCNP: Cáncer de pulmón de células no pequeñas

CPCP: Cáncer de pulmón de células pequeñas

CTC: Célula tumoral circulante

ctDNA: ADN circulante tumoral

ctRNA: ARN circulante tumoral

dPCR: PCR digital

EGFR: *Epithelial Growth Factor Receptor*

EMA: *European Medicines Agency*

EML4: EMAP Like 4 or Echinoderm Microtubule Associated Protein-Like 4

EVs: Vesículas extracelulares

FDA: *U.S. Food and Drug Administration*

FISH: Hibridación in situ fluorescente

HCPI: Hematopoyesis clonal de potencial indeterminado

HR: *Hazard Ratio*

IASLC: *International Association for the Study of Lung Cancer*

IHQ: Inmunohistoquímica

Indels: Inserciones y deleciones

ISET: *Isolation by size of epithelial tumor cells*

LCR: Líquido cefalorraquídeo

LOD: Límite de detección

lncRNA: *Long non-coding RNA*

MAF: Frecuencia alélica mutada

miRNA: Micro-ARN

MNP: *Multiple nucleotide polymorphism*

mRNA: ARN mensajero

mSLP: Mediana de supervivencia libre de progresión

NGS: *Next Generation Sequencing*

NPA: *Negative percentage agreement*

NTA: Análisis de rastreo de nanopartículas

OMS: Organización Mundial de la Salud

ORR: Tasa global de respuesta

PB: Pares de bases

PBMCs: *Peripheral blood mononuclear cells*

ρc: Coeficiente de correlación de Pearson

PPA: *Positive percentage agreement*

ROS1: *ROS Proto-oncogene 1, receptor tyrosine kinase*

RT-PCR: *reverse transcription polymerase chain reaction*

SEC: cromatografía de exclusión por tamaño

SG: Supervivencia global

SLP: Supervivencia libre de progresión

SNC: Sistema nervioso central

SNV: *Single-Nucleotide Variant*

TEM: Microscopía electrónica de trasmisión

TEPs: Plaquetas educadas en tumores

TKI: Inhibidor de tirosina kinasa

TNM: *Tumor, Node, Metastasis*

UC: Ultracentrifugación

UMI: Identificador molecular único

wt: *wild type*

INTRODUCCIÓN

1. Cáncer de pulmón

El cáncer de pulmón es la principal causa de mortalidad relacionada con el cáncer en todo el mundo, junto con el cáncer de mama (1), siendo el tabaco su mayor factor de riesgo. Según la Organización Mundial de la Salud (OMS), sólo en 2020 se diagnosticaron más de 2 millones de casos nuevos de cáncer de pulmón, siendo responsable de 1,79 millones de muertes (2).

El cáncer de pulmón se suele diagnosticar en estadios avanzados, cuando no es factible un tratamiento curativo (3), alcanzando una supervivencia a los 5 años de tan solo el 13,5% (4). Únicamente el 20% de los pacientes son diagnosticados en estadios tempranos, pudiendo ser beneficiarios de resección quirúrgica. Aun así, hasta el 50% de éstos sufren recidivas (5,6).

Las formas más comunes de cáncer de pulmón se clasifican según las características de las células de las que derivan (7), distinguiendo dos grandes grupos:

• Cáncer de pulmón de células pequeñas (CPCP): se trata de una neoplasia maligna muy agresiva que representa aproximadamente el 15% de los casos de cáncer de pulmón y se caracteriza por una mayor propensión al desarrollo temprano de metástasis generalizadas (8). El origen de las células tumorales del CPCP no se ha identificado formalmente, aunque comúnmente se cree que surgen de células neuroendocrinas en el bronquio (9). Finalmente, esta neoplasia se ha descrito principalmente en pacientes de la tercera edad con antecedentes de exposición prolongada al tabaco.

• Cáncer de pulmón de células no pequeñas (CPCNP): es el tipo más común de cáncer de pulmón, representa aproximadamente el 85% de todos los casos y es la forma más común en mujeres, adultos jóvenes y no fumadores (10). Además, este subtipo histológico de cáncer de pulmón no es tan letal como el CPCP, ya que generalmente crece y se disemina más lentamente. En este sentido, dependiendo de la estadificación, dichos pacientes suelen ser elegibles para una variedad más amplia de tratamientos, que van desde cirugía hasta radioterapia, quimioterapia, inmunoterapia y terapia dirigida.

2. Cáncer de pulmón CPCNP

2.1. Clasificación histológica del CPCNP

Dentro del CPCNP se pueden distinguir tres subtipos histológicos en base a sus características moleculares, fenotípicas y pronósticas:

- Adenocarcinoma: es el tipo más común de cáncer de pulmón y representa aproximadamente el 40% de los casos de CPCNP (10). Es el subtipo con el crecimiento más lento, por lo que puede diagnosticarse en estadios más tempranos. Por lo general, comienza en las células glandulares y tiende a desarrollarse en las vías respiratorias más pequeñas, como los alvéolos, y en los bordes externos de los pulmones, afectando con frecuencia a la pleura y a la pared torácica (11). Su aparición suele ser en edades más tempranas y constituye el subtipo más común en no fumadores y mujeres (12). Finalmente, en los últimos años, esta variante histológica ha cobrado especial interés debido al desarrollo de terapias dirigidas frente a determinadas alteraciones moleculares (13).
- Carcinoma de células escamosas: comprende entre el 25-30% de todos los casos de CPCNP (10). Surge de versiones tempranas de células escamosas en las células epiteliales de los

bronquios, causando síntomas de forma más temprana. Por otro lado, aunque este tipo de cáncer generalmente es de crecimiento lento, tiene el potencial de extenderse a múltiples localizaciones debido a su ubicación inicial (14). Además, este subtipo es el más fuertemente correlacionado con el tabaquismo (15,16).

- Carcinoma de células grandes o indiferenciado: representa del 5 al 10% de los cánceres de pulmón (10). Sin embargo, a medida que se utilizan métodos más exactos para diagnosticar el cáncer de pulmón, muchos tumores previamente etiquetados como carcinoma de células grandes indiferenciado pueden ahora clasificarse más apropiadamente como adenocarcinoma poco diferenciado o carcinoma de células escamosas (17). Por ello, la incidencia de este tipo de tumor sigue disminuyendo y muchas veces se diagnostica por defecto mediante la exclusión de otras posibilidades y donde no hay evidencia de maduración escamosa o glandular. Por lo general, comienza en las células epiteliales de los bordes externos de los pulmones y tiende a crecer y diseminarse rápidamente (18), lo que puede dificultar su tratamiento. Además, y como en los otros tipos, se concluye que el tabaquismo es la causa predominante de cáncer de pulmón de células grandes (19).
- Existen además otros tipos de CPCNP, como el sarcomatoide, los cuales son mucho menos frecuentes.

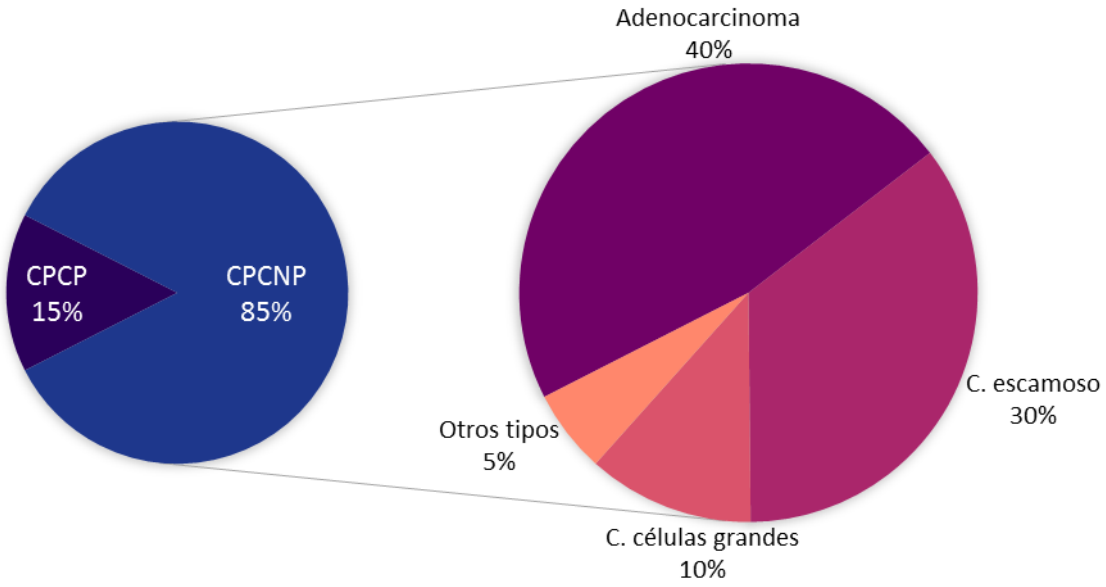

Figura 1. Clasificación histológica del cáncer de pulmón.

La distinción de estos subtipos histológicos ha sido crucial para el desarrollo de estrategias de tratamiento personalizadas (20).

2.2. Clasificación TNM del CPCNP

La estadificación del cáncer es un paso fundamental en el proceso de diagnóstico para determinar el tratamiento a seguir y establecer el pronóstico de los pacientes. La estructura fundamental de la clasificación se basa en el sistema TNM (*del inglés Tumor, Node, Metastasis*), que describe la extensión anatómica de la enfermedad y que usa códigos alfanuméricos para describir el estadio clínico del CPCNP en base a los resultados de un examen físico, biopsia y pruebas de imagen. El parámetro "*T*" se establece respecto al tamaño o extensión del tumor

primario; el parámetro "*N*" define la afectación a nivel de los ganglios linfáticos; y el parámetro "*M*" define la presencia o ausencia de metástasis.

T: Tumor	**Características del Tumor Primario**
Tx	El tumor primario no se puede evaluar o el tumor se prueba por la presencia de células malignas en el esputo o lavados bronquiales pero no visualizados por imágenes o broncoscopia
T0	Sin evidencia de tumor primario
Tis	Carcinoma *in situ*
T1	Tumor ≤ 3 cm, rodeado de pleura pulmonar o visceral, sin evidencia de invasión más proximal que el bronquio lobar (es decir, no en el bronquio principal)
T1mi	Adenocarcinoma mínimamente invasivo: solitario, ≤ 3 cm y ≤ 5 mm de invasión en un único foco
T1a	Tumor ≤ 1 cm
T1b	Tumor > 1 cm pero ≤ 2 cm
T1c	Tumor > 2 cm pero ≤ 3 cm
T2	Tumor > 3 cm pero ≤ 5 cm, o tumor con cualquiera de las siguientes características: • Afecta al bronquio principal sin comprometer la carina traqueal • Invade la pleura visceral • Asociado con atelectasia o neumonitis obstructiva que se extiende a la región hiliar, implicando parte del pulmón o todo el pulmón
T2a	Tumor > 3 cm pero ≤ 4 cm
T2b	Tumor > 4 cm pero ≤ 5 cm
T3	Tumor > 5 cm pero ≤ 7 cm o asociado con nódulos tumorales separados en el mismo lóbulo que el tumor primario o invade directamente cualquiera de las siguientes estructuras: pared torácica (incluyendo la pleura parietal y los tumores del surco superior), nervio frénico y pericardio parietal
T4	Tumor > 7 cm o asociado con nódulos tumorales separados en un lóbulo ipsolateral que el del tumor primario o invade cualquiera de las siguientes estructuras: diafragma, mediastino, corazón, grandes vasos, tráquea, nervio laríngeo recurrente, esófago, cuerpo vertebral y carina
N: Nódulos	**Ganglios Linfáticos Regionales**
Nx	No se pueden evaluar los ganglios linfáticos regionales
N0	Sin metástasis en los ganglios linfáticos regionales
N1	Metástasis en ganglios linfáticos peribronquial y/o hiliar ipsolaterales y ganglios intrapulmonares, incluida la afectación por extensión directa
N2	Metástasis en mediastino ipsilateral y/o ganglio(s) linfático subcarinal
N3	Metástasis en mediastino contralateral, hiliar contralateral, ganglio(s) linfático escaleno ipsilateral o contralateral o supraclavicular
M: Metástasis	**Metástasis Distantes**
M0	Sin metastasis distantes
M1	Con presencia de metástasis distantes
M1a	Nódulos tumorales separados en un lóbulo contralateral; tumor con nódulos pleurales o pericárdicos o derrame pleural o pericárdico maligno
M1b	Única metástasis extratorácica en un solo órgano
M1c	Varias metástasis extratorácicas en uno o varios órganos

Tabla 1. Clasificación del cáncer de pulmón en base a la 8ª edición del Sistema TNM.

Desde su introducción en la década de 1970, el sistema TNM ha sido objeto de importantes revisiones. Actualmente, la 8ª edición se encuentra en vigor internacionalmente desde el 2018 (21).

Clasificación de los estadios en base al sistema TNM:

Estadio		TNM
Carcinoma oculto		Tx N0 M0
Estadio 0		Tis N0 M0
Estadio I	**IA**	T1 N0 M0
	IB	T2a N0 M0
Estadio II	**IIA**	T2b N0 M0
	IIB	T1 N1 M0
		T2 N1 M0
		T3 N0 M0
Estadio III	**IIIA**	T1 N2 M0
		T2 N2 M0
		T3 N1 M0
		T4 N0 M0
		T4 N1 M0
	IIIB	T1 N3 M0
		T2 N3 M0
		T3 N2 M0
		T4 N2 M0
	IIIC	T3 N3 M0
		T4 N3 M0
Estadio IV	**IVA**	Cualquier T Cualquier N M1a/b
	IVB	Cualquier T Cualquier N M1c

Tabla 2. Estadificación del cáncer de pulmón según la 8ª edición del Sistema TNM.

Uno de los factores pronósticos más importantes es el estadio en el momento del diagnóstico. Sin embargo, la mayoría de los pacientes permanecen asintomáticos hasta que desarrollan una etapa avanzada, lo que dificulta el diagnóstico temprano (22).

2.3. Clasificación molecular del CPCNP

En la última década, el manejo del CPCNP avanzado ha mejorado notablemente gracias a la identificación y caracterización de alteraciones moleculares que impulsan el inicio y la progresión del cáncer y que son dianas terapéuticas de fármacos dirigidos. En definitiva, estas alteraciones se traducen a nivel funcional en la activación de oncogenes y en la inactivación de genes supresores de tumores (23,24), lo que activa de forma constitutiva determinadas vías de señalización jugando un papel crucial en la transducción de señales, proliferación celular, diferenciación, invasión a otros tejidos y otros mecanismos regulatorios.

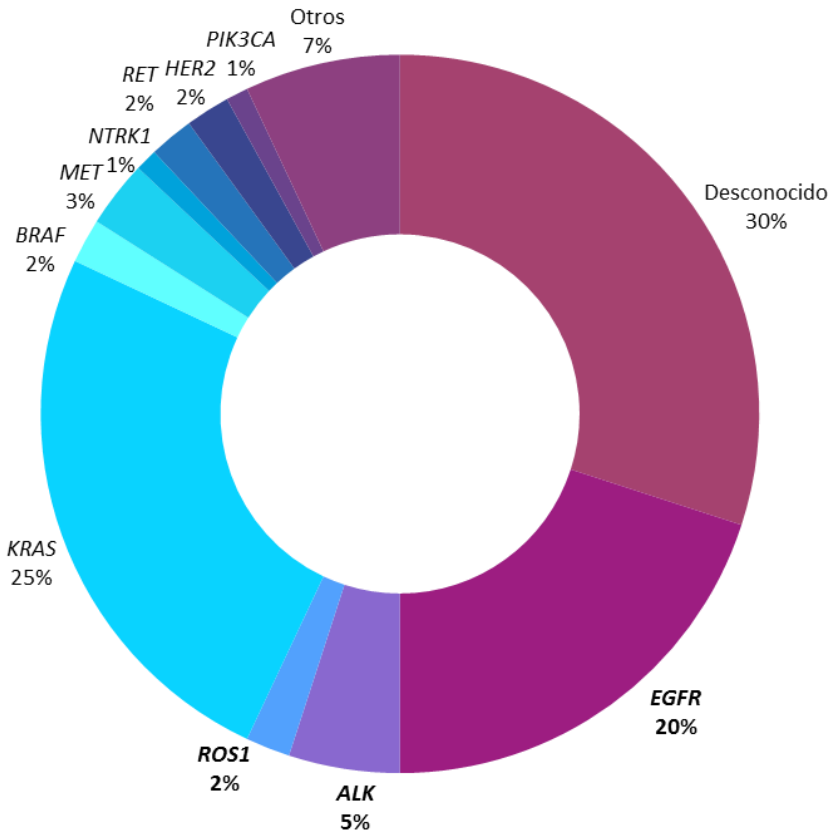

Figura 2. Clasificación molecular del cáncer de pulmón. Entre las alteraciones más prevalentes destacan las mutaciones en el gen *EGFR* y los reordenamientos de los genes *ALK* y *ROS1*.

Las mutaciones más prevalentes en el CPCNP ocurren en los genes de *EGFR, ALK, ROS1, KRAS, BRAF, RET, MET, NTRK1, ERBB2* (también llamado *HER2*) y *PIK3CA*, siendo hasta el 50% de todos los cánceres de pulmón portadores de una de estas alteraciones genéticas. Sin embargo, solo el 20% de las mutaciones son diana de terapias dirigidas aprobadas por la FDA (*del inglés U.S. Food and Drug Administration*) (25).

Dada la relevancia de estas alteraciones, especialmente en el adenocarcinoma, como biomarcadores y dianas terapéuticas de fármacos dirigidos, su estudio es recomendado según las guías clínicas ante un diagnóstico de adenocarcinoma, puesto que implica un mejor manejo terapéutico del paciente (26). Los primeros genes cuyo estudio molecular fue recomendado en los pacientes con CPCNP por las guías clínicas del *College of American Pathologists* (CAP), *International Association for the Study of Lung Cancer* (IASLC), y *Association for Molecular Pathology* (AMP) fueron *EGFR* y *ALK* en el 2013; seguido de *ROS1* en 2018. Las alteraciones en estos tres genes son mutuamente excluyentes en la mayoría de los pacientes, si bien se han descrito algunas excepciones (27). Más recientemente se recomienda el estudio de *KRAS*, *BRAF* y la alteración de salto del exón 14 de *MET*; reordenamientos en *NTRK1/2/3* y *RET*; y análisis de los niveles de expresión de PD-L1 (26).

Gen diana	Alteración	Terapias dirigidas	
KRAS	***p.G12C***	Sotorasib	
EGFR	***Deleción del exón 19, mutación p.L858R, etc.***	Gefitinib Erlotinib Afatinib	Osimertinib Dacomitinib
	Inserción en el exón 20	Amivantamab	Mobocertinib
Reordenamiento de ALK		Crizotinib Ceritinib Alectinib	Brigatinib Lorlatinib
Reordenamiento de ROS1		Crizotinib Entrectinib	Ceritinib Lorlatinib
Reordenamiento de MET		Capmatinib Tepotinib	Crizotinib
BRAF	***p.V600E***	Dabrafenib/Trametinib	
Reordenamiento de RET		Pralsetinib Selpercatinib	Cabozantinib Vandetanib
Fusión génica de NTRK		Larotrectinib	Entrectinib

Tabla 3. Alteraciones con terapias dirigidas aprobadas por la FDA.

2.3.1. CPCNP con mutación en *EGFR*

El gen que codifica el receptor del factor de crecimiento epitelial o *EGFR* (*epithelial growth factor receptor*) se encuentra en el brazo corto del cromosoma 7 (7p11.2) y fue identificado como potencial diana terapéutica en el cáncer en 1988 (28), convirtiéndose en la diana oncogénica más relevante en el CPCNP, presente en aproximadamente el 20% de estos pacientes. Las alteraciones activadoras o *sensitizing* en el gen *EGFR* más comunes son la deleción del exón 19 y la mutación p.L858R. Otras alteraciones oncogénicas incluyen las inserciones del exón 20 (*EGFR*ex20ins) y la mutación p.G719X del exón 18. La presencia de estas alteraciones implica una activación constitutiva de las vías de señalización PIK3CA/AKT1/MTOR y RAS/RAF1/MAP2K1/MAPK1 (29).

Los pacientes con CPCNP con mutaciones en el gen *EGFR* presentan respuestas excepcionales al tratamiento con inhibidores de tirosina kinasa frente *EGFR* (*EGFR*-TKIs) de primera, segunda y tercera generación (gefitinib y erlotinib; afatinib y dacomitib; y osimertinib, respectivamente) en comparación con la quimioterapia (30). Sin embargo, no todas las mutaciones activadoras de *EGFR* responden de igual manera a estos inhibidores. Un ejemplo de ello son los pacientes cuyos tumores son portadores de *EGFR*ex20ins (4-10%) (31,32), los cuales no responden a los *EGFR*-TKIs de generación temprana (31). Por ello, estos pacientes siguen siendo tratados con quimioterapia como primera línea estándar (33). Actualmente, se está llevando a cabo un gran esfuerzo de investigación para el desarrollo de terapias frente a estas inserciones, complejas genómicamente, para lo cual se están realizando ensayos clínicos con nuevos *EGFR*-TKIs como poziotinib (34) o CLN-081 (35), así como combinaciones de *EGFR*-TKIs con anticuerpos anti-*EGFR* (36,37) o con fármacos antiangiogénicos como bevacizumab (33).

2.3.2. CPCNP con translocación en *ROS1*

El gen *ROS1* (*ROS proto-oncogene 1, receptor tyrosine kinase*), localizado en el brazo largo del cromosoma 6 (6q22.1), codifica para un receptor tirosina kinasa perteneciente a la familia de la insulina cuya alteración se produce en aproximadamente el 2% de los pacientes con CPCNP. El oncogén *ROS1* fue identificado por primera vez en 1987 en una línea celular de glioblastoma (38). No fue hasta el 2007 cuando se describió el reordenamiento de *ROS1* en CPCNP, que da lugar a una proteína de fusión con activación constitutiva del dominio tirosina kinasa y, por consiguiente, produce la activación constitutiva de las señales de crecimiento para las células cancerosas mediante la vía de señalización de MAPK y la fosforilación de RAS. Hasta la fecha, se han descrito múltiples compañeros de fusión, entre los que se incluyen *CD74*, *TMP6, SDC4, EZR* o *CCDC6* (39).

Actualmente existen dos *ROS1*-TKIs aprobados por la FDA para el tratamiento de estos pacientes en primera línea: crizotinib y entrectinib, que mostraron una supervivencia libre de progresión (SLP) de 19,3 y 19 meses, respectivamente (40,41). Como se verá más adelante, estos fármacos se utilizan también en los pacientes con reordenamientos en el gen *ALK* debido a la similitud estructural del dominio tirosina kinasa de ambos genes.

3. CPCNP con translocación en *ALK*

El gen *Anaplastic lymphoma kinase* o *ALK*, localizado en el brazo corto del cromosoma 2 (2p23.2-p23.1), fue identificado en 1994 en el linfoma anaplásico de células grandes como parte de una fusión a la proteína nucleofosmina. Además de aparecer en linfomas, varios tumores sólidos como el CPCNP presentan fusiones del gen *ALK* con diferentes parejas génicas (3-7%), originando un subtipo molecular específico que se observa especialmente en pacientes más jóvenes (mediana de edad de 52 años) (42) y no fumadores con histología de adenocarcinoma (43,44). Se ha estimado una incidencia mundial de 40.000 casos al año de CPCNP con reordenamientos en *ALK* (42).

El gen *ALK* también codifica un receptor tirosina kinasa de la familia de la insulina con un dominio transmembrana (45), cuya alteración resulta en la activación constitutiva del mismo, generando actividad oncogénica (46,47).Todas las proteínas de fusión que involucran al gen *ALK* incluyen el dominio tirosina kinasa de *ALK*, necesario para la dimerización y activación constitutiva del receptor, seguida de la activación de diversas cascadas de señalización que desencadenan un aumento de la proliferación y la supervivencia celular. En general, *ALK* activa múltiples vías de señalización, como las vías PI3K-AKT-mTOR, RAS-RAF-MEK-ERK, MAPK y JAK-STAT3, en distinto grado dependiendo de la fusión exacta (48).

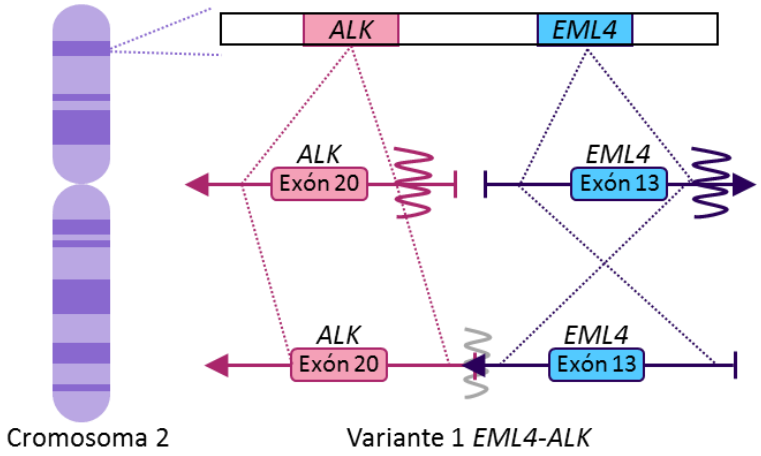

Figura 3. Fusión génica *EML4-ALK* variante 1 (E13:A20). La inversión paracéntrica del brazo corto del cromosoma 2 [Inv(2)(p21p23)] produce la unión de los exones 1–13 de *EML4* con los exones 20–29 de *ALK*.

Hasta ahora, se han identificado más de 19 compañeros de fusión de *ALK* en el CPCNP, siendo el más común *EML4* (*EMAP like 4 or echinoderm microtubule associated protein-like 4*), seguido de otros genes como *KIF5B, KLC1*, *TFG*, *TPR y HIP1* (49,50). Específicamente, el gen *EML4*, que codifica una proteína citoplasmática involucrada en la formación de microtúbulos, se fusiona con *ALK* mediante la inversión paracéntrica del brazo corto del cromosoma 2 [Inv(2)(p21p23)] y conlleva la unión de exones de *EML4* (cuyo número varía en función de la variante) con los exones 20–29 de *ALK*.

Las diferentes variantes originadas por la fusión *EML4-ALK* implican una estabilidad, actividad y sensibilidad a los inhibidores de *ALK* (*ALK-TKIs)* específica (51), terapia recomendada en este tipo de pacientes. En este sentido, los pacientes con la variante 1 de *EML4-ALK* (E13:A20) presentan una mediana de SLP (mSLP) significativamente mayor a aquellos pacientes con otra variante al ser tratados con crizotinib (11 *vs*. 4,2 meses, respectivamente) (52); mientras que los pacientes que tienen la variante 3 (E6:A20) tienen peor pronóstico con respecto a aquellos pacientes con otra variante (53). Por el contrario, entre los pacientes tratados con el *ALK*-TKI de tercera generación lorlatinib (después de progresar al tratamiento tanto con crizotinib como con al menos un inhibidor de *ALK* de segunda generación), la variante 3 se ha asociado con una SLP significativamente mayor que la variante 1 (mSLP 11 *vs*. 3,3 meses, respectivamente) (54). Por todo ello, no sólo es importante la identificación de la fusión en *ALK* si no también la de su compañero de fusión y la variante específica.

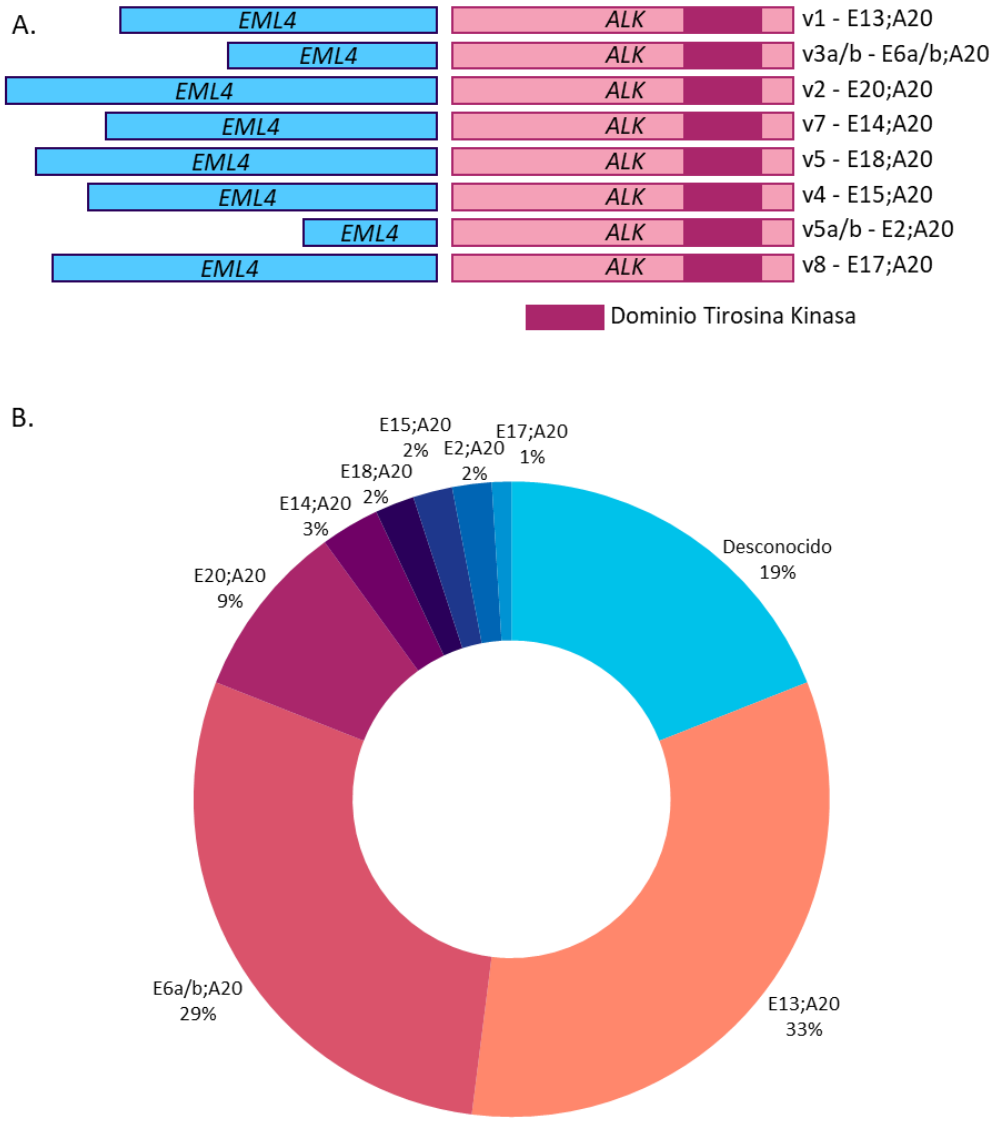

Figure 4. Variantes de fusión *EML4-ALK*. A. Puntos de corte y empalme de los exones de *EML4* y *ALK*. **B.** Prevalencia de las variantes de fusión *EML4-ALK*.

3.1. Inhibidores Tirosina Kinasa frente *ALK*: *ALK*-TKIs

Los pacientes con reordenamientos en el gen *ALK* son altamente sensibles a tratamientos con *ALK*-TKIs. Estas terapias dirigidas orales inhiben la activación constitutiva del receptor de *ALK* mutado, bloqueando las cascadas de señalización que desencadenan un aumento de la proliferación y supervivencia celular. Actualmente, existen 5 inhibidores de *ALK* aprobados por la FDA y englobados en 3 generaciones.

ALK-TKIs de primera generación

El primer inhibidor oral de *ALK* aprobado por la FDA fue el Crizotinib (Xalkori®), en 2011, siendo sus dianas terapéuticas *ALK*, *ROS1* y *MET*. En el estudio en fase III PROFILE 1014, se comparó la eficacia del crizotinib frente a la quimioterapia en primera línea en pacientes con CPCNP *ALK*-positivos, demostrándose una mayor SLP (10,9 *vs.* 7,0 meses) y una mayor tasa global de respuesta (ORR) (74% *vs.* 45%) en los pacientes tratados con crizotinib (55). El análisis final de supervivencia global (SG) fue de 59,8 meses con crizotinib frente a 19,2 meses con quimioterapia

(56). En base a estos datos, crizotinib fue aprobado tanto en primera línea como en líneas consecutivas en pacientes con CPCNP *ALK*-positivo.

Más tarde, el estudio PROFILE 1029, realizado con pacientes de Asia oriental, mostró resultados similares, obteniendo en los pacientes tratados con crizotinib en primera línea una mayor SLP (11,1 *vs.* 6,8 meses) y ORR (87,5 % *vs.* 48%) con respecto a la quimioterapia (57). A pesar de estos resultados, la mayoría de los pacientes terminan progresando durante el primer o segundo año de tratamiento, siendo el sistema nervioso central (SNC) la localización más frecuente (45-70%) (58).

***ALK-TKIs* de segunda generación**

Presentan la ventaja de ser activos frente a metástasis cerebrales, ya que atraviesan la barrera hematoencefálica. Actualmente hay tres inhibidores de *ALK* de segunda generación aprobados por la FDA:

a) Ceritinib (Zykadia®) es un inhibidor oral de segunda generación selectivo de *ALK* y *ROS1*, que fue aprobado por la FDA en 2014 como tratamiento en primera línea. Ceritinib demostró en el estudio en fase III ASCEND-4 una mayor SLP frente a la quimioterapia en primera línea en pacientes *ALK*-positivos CPCNP (16,6 *vs.* 8,1 meses). Además, ceritinib mostró un ratio de respuesta intracraneal del 72,7% frente al 27,3% con quimioterapia (59).
b) Alectinib (Alecensa®) es otro inhibidor oral de segunda generación frente *ALK* y *RET*, aprobado por la FDA en 2017 como tratamiento en primera línea. Alectinib demostró su superioridad con respecto a crizotinib en pacientes con CPCNP *ALK*-positivos (sin tratar previamente con quimioterapia) tanto a nivel de SLP (34,8 *vs.* 10,9 meses) como a nivel de seguridad. Estos datos se reportaron en dos estudios en fase III, J-ALEX y ALEX (60,61). Además, el uso de Alectinib mostró menor toxicidad y retraso en la progresión de la enfermedad a nivel del SNC (62), con un ratio de respuesta intracraneal del 81% frente al 50% con quimioterapia.
c) Brigatinib (Alunbrig®) es el último inhibidor oral de segunda generación, aprobado por la FDA en 2017 en pacientes con CPCNP *ALK*-positivos como tratamiento en segunda línea tras progresión a crizotinib. Este *ALK*-TKI, efectivo frente *ALK*, *ROS1* y *EGFR* con mutación p.T790M, demostró su superioridad con respecto a crizotinib en primera línea en el estudio en fase III ALTA-1L, con una SLP de 24 meses *vs.* 11 meses y una ORR de 74% *vs.* 62%, respectivamente (63). Este estudio incluyó 275 pacientes con CPCNP *ALK*-positivos, de los cuales 137 recibieron brigatinib y 138 crizotinib. Además, el ratio de respuesta intracraneal con brigatinib fue del 78% frente al 26% con crizotinib.

A pesar de la mayor efectividad de los inhibidores de segunda generación con respecto a crizotinib, alrededor de la mitad de los pacientes acaban desarrollando mutaciones de resistencia, mientras que en los pacientes que progresan al tratamiento con crizotinib, estas mutaciones ocurren sólo en un 20% de los casos (64). Así mismo, se han descrito mutaciones de resistencia específicas frente a *ALK*-TKIs de segunda generación, como la mutación p.G1202R del dominio *ALK* (65). Por lo tanto, son necesarias opciones de tratamiento adicionales, que generalmente implica el uso de inhibidores de *ALK* de tercera generación como lorlatinib.

***ALK-TKIs* de tercera generación**

Lorlatinib (Lorbrena®) es el único inhibidor de *ALK* de tercera generación aprobado por la FDA en 2018 y por la EMA (*European Medicines Agency*) en febrero del 2019. Este inhibidor ha demostrado eficacia frente a la mayoría de las mutaciones de resistencia de *ALK* conocidas actualmente, incluyendo la mutación p.G1202R; así como una mayor actividad intracraneal debido a su capacidad para penetrar la barrera hematoencefálica y lograr concentraciones terapéuticas en el SNC (64,65). Los datos de la parte de la fase I de un estudio en fase I/II en curso (NCT01970865), han demostrado que lorlatinib es más potente y selectivo que otros inhibidores de *ALK* conocidos, incluidos los inhibidores de segunda generación (66). En dicho estudio, la ORR con lorlatinib fue del 46% y la mSLP fue de 11,4 meses, aunque la mayoría de los pacientes habían recibido dos o más *ALK*-TKIs previamente. Además, este estudio demostró la capacidad de lorlatinib para disminuir el tamaño de las metástasis cerebrales (ORR intracraneal 63%).

Por otro lado, el estudio CROWN compara el tratamiento con lorlatinib frente a crizotinib en primera línea en pacientes con CPCNP *ALK*-positivos, demostrándose una mayor SLP a los 12 meses (78% *vs.* 39%) y una mayor ORR (76% *vs.* 58%) con lorlatinib (67). Sin embargo, a pesar de su eficacia, también se han descrito mecanismos de resistencia a lorlatinib (68).

Inhibidor *ALK*	**Ensayo Clínico**	**Fase del estudio**	**Resultados**	**Estado de aprobación**
Crizotinib	PROFILE 1014 Crizotinib *vs.* quimioterapia	Fase III	SLP: 10,9 *vs.* 7,0 meses (HR: 0,45)	Aprobado por FDA, primera línea
	PROFILE 1029 Crizotinib *vs.* quimioterapia	Fase III	SLP: 11,1 *vs.* 6,8 meses (HR: 0,40)	
Ceritinib	ASCEND-4 Ceritinib *vs.* crizotinib	Fase III	SLP: 16,6 *vs.* 8,1 meses (HR: 0,55)	Aprobado por FDA, primera línea
Alectinib	ALEX Alectinib *vs.* crizotinib	Fase III	SLP: 34,8 *vs.* 10,9 meses (HR: 0,5)	Aprobado por FDA, primera línea
	J-ALEX Alectinib *vs.* crizotinib	Fase III	SLP: NA *vs.* 10,2 meses (HR: 0,34)	
Brigatinib	ALTA-1L Brigatinib *vs.* crizotinib	Fase III	SLP a los 12 meses: 67% *vs.* 43% (HR: 0,49)	Aprobación por FDA, primera línea
Lorlatinib	NCT01970865 Brazo único	Fase II	SLP 11,4 meses ORR intracraneal: 63%	Aprobación acelerada por FDA, segunda y tercera línea
	CROWN Lorlatinib *vs.* crizotinib	Fase III	SLP a los 12 meses: 78% *vs.* 39% (HR: 0,21)	

Tabla 4. Inhibidores tirosina kinasa frente a *ALK* aprobados por la FDA y sus principales ensayos. HR, *Hazard Ratio*; NA, no alcanzado.

Aparte de los 5 *ALK*-TKIs aprobados por la FDA para la tratamiento de los pacientes con CPCNP portadores de reordenamientos en *ALK*, otras moléculas como ensartinib y entrectinib están esperando para su aprobación clínica en dichos pacientes (69,70). Además, se están desarrollando inhibidores de cuarta generación como TPX-0131 o NUV-655, con mayor potencia frente a mutaciones de resistencia como p.L1198F, p.G1202R o mutaciones compuestas en el *locus ALK* (71).

Con respecto a estrategias de combinación de tratamiento que incluyan un *ALK*-TKI, hoy en día no existe ninguna establecida pero se están evaluando algunas entre las que se incluyen inhibidores de *ALK* con quimioterapia (72), agentes anti-angiogénicos (NCT02521051) o inhibidores de *MAPK* (NCT03202940) o *mTOR* (NCT02321501). Por otro lado, la inmunoterapia parece no ser eficaz en estos pacientes, mostrando un aumento de la toxicidad cuando se combina con un *ALK*-TKI. Este es el caso del estudio fase I/II CheckMate 370, cerrado prematuramente debido a hepatotoxicidad severa por tratamiento en primera línea con crizotinib más nivolumab (tratamiento de inmunoterapia basado en la inhibición de la proteína PD-1) (71). Además, los pacientes con CPCNP *ALK*-positivos tratados con inhibidores de PD-1 en monoterapia no muestran buenas respuestas (73), lo cual podría deberse a que son pacientes no fumadores y con una baja carga tumoral en su mayoría (74), factores que se asocian a respuestas pobres frente al tratamiento de inmunoterapia. Sin embargo, se requieren más datos preclínicos para poder valorar los beneficios potenciales de la adición de inmunoterapia a la terapia con *ALK*-TKIs.

Con todo ello, los inhibidores de *ALK* son la mejor opción como tratamiento en primera línea en pacientes con CPCNP con reordenamientos en *ALK* actualmente, siendo alectinib y brigatinib los TKIs más recomendables en pacientes naïve (que no han sido sometidos a un tratamiento previo basado en TKI), debido a su mayor SLP en comparación con crizotinib; seguido de lorlatinib en caso de progresión, debido a su mayor actividad en el SNC. Como se ha citado anteriormente, estas terapias dirigidas han mejorado considerablemente los resultados clínicos de estos pacientes tanto en términos de calidad de vida, como de pronóstico, habiendo incrementado significativamente la SLP, la ORR y la SG con respecto a la quimioterapia (55,75). Por ello, la identificación de los pacientes cuyos tumores presentan reordenamiento en *ALK* es crucial.

Sin embargo, a pesar de la gran eficacia inicial de los inhibidores de *ALK*, en torno a un 70% de los pacientes acaba progresando tras el tratamiento debido al desarrollo de mutaciones de resistencia (76). En este sentido, la secuencia terapéutica de los diferentes *ALK*-TKIs disponibles necesita ser estudiada y optimizada en base al perfil molecular del tumor al momento de la progresión puesto que, en la práctica clínica actual, éstos se prescriben de forma empírica.

3.2. Mecanismos de resistencia frente *ALK*-TKIs

Existen multitud de mecanismos de resistencia frente a los *ALK*-TKIs, entre los que destacan los mecanismos dependientes de *ALK* como las mutaciones de resistencia en el dominio tirosina kinasa de *ALK* (77,78) y la amplificación del gen de fusión de *ALK* (79); y mecanismos independientes de *ALK*, como la activación de vías de señalización alternativas y la activación de la transición epitelio-mesenquimal mediante la pérdida de expresión de E-cadherina o el aumento de expresión de vimentina (80).

- **Dependientes de *ALK*:** el 20-36% de los pacientes resistentes a *ALK*-TKIs presentan mutaciones en el dominio tirosina kinasa de *ALK* (81), entre las que destacan p.G1269A, p.L1196M, p.F1174L, p.1151Tins, p.L1152R, p.S1206Y, p.I1171T, p.V1180L, p.G1202R, p.G1202del y p.D1203N. Además, se ha identificado la presencia simultánea de dos mutaciones en el *locus ALK* como mecanismo de resistencia al uso secuencial de *ALK*-TKIs, en especial a TKIs de segunda y tercera generación (brigatinib y lorlatinib) como p.E1210K+p.S1206C, p.E1210K+p.D1203N o p.L1198F+p.C1156Y (42). No todas las

mutaciones confieren resistencia a todos los TKIs. Por ejemplo, la mutación p.I1171S confiere resistencia a alectinib pero sensibilidad a ceritinib, mientras que la mutación p.F1174V crea resistencia a ceritinib pero no a alectinib (82,83). Así mismo, algunas mutaciones dobles incrementan la resistencia primaria a inhibidores de segunda/tercera generación, mientras que conducen a la re-sensibilización a crizotinib (84,85). Por otro lado, la amplificación de *ALK* confiere resistencia a crizotinib, aunque se da en menor frecuencia que las mutaciones puntuales en dicho gen (15%) (86). Además, esta alteración en el número de copias (CNV, *del inglés copy number variation*) no ha sido descrita en progresiones a *ALK*-TKIs de segunda y tercera generación.

- **Independientes de *ALK*:** se han descrito alteraciones en al menos un gen distinto de *ALK* en más de la mitad de los pacientes que progresan a un *ALK*-TKI de segunda generación (56%) (87), entre las que destacan mutaciones activadoras de los genes *PIK3CA*, *EGFR* (88), *HER2/3*, *IGF-1R*, *MAPK, BRAF, KRAS* o *SRC*; la amplificación de *KIT* (89), *MYC* o *MET* y la pérdida de función de *NF2* (68). Para combatir estas alteraciones, es necesaria la combinación de terapias que inhiban tanto al gen *ALK* como a las vías de señalización alternativas. Sin embargo, aún no se ha aprobado clínicamente ninguna terapia combinada, ni se ha desarrollado un inhibidor tirosina kinasa múltiple.

El difícil acceso del tumor de pulmón dificulta que se vuelva a realizar una biopsia de tejido (re-biopsia) en este tipo de pacientes, por lo que, en la práctica clínica, en la mayoría de los casos se desconocen los mecanismos de resistencia a los inhibidores de *ALK*, lo que implica una prescripción empírica de las sucesivas líneas de tratamiento.

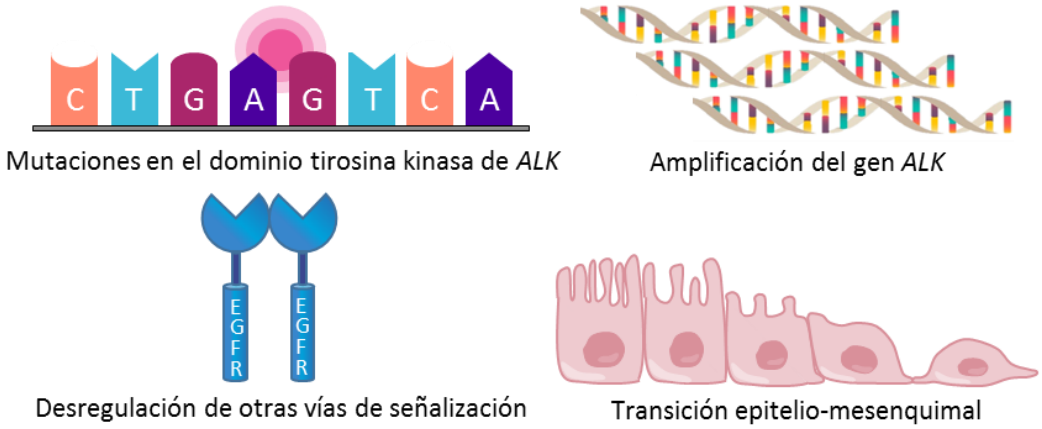

Figura 5. Mecanismos de resistencia frente *ALK*-TKIs. Los mecanismos dependientes de *ALK* engloban mutaciones en el dominio tirosina kinasa y la amplificación del gen *ALK*; mientras que los mecanismos independientes de *ALK* se producen por la desregulación de otras vías de señalización, como mutaciones en el gen *EGFR*, o la transición epitelio-mesenquimal.

3.3. Estudio de los pacientes *ALK*-positivos CPCNP en la práctica clínica

Como se ha dicho anteriormente, el estudio de biomarcadores en el cáncer de pulmón es crucial para asegurar un manejo adecuado de los pacientes. Por este motivo, los reordenamientos en el gen *ALK* deben ser evaluados en todos los pacientes diagnosticados con cáncer de pulmón estadio IV en la práctica clínica rutinaria (26).

El tejido tumoral es la muestra empleada en el estudio de los reordenamientos de *ALK*, siendo las técnicas de referencia la hibridación in situ fluorescente (FISH, *del inglés fluorescence in situ hybridization*), la inmunohistoquímica (IHQ) o la secuenciación masiva (NGS, *del inglés next generation sequencing*), siempre que la plataforma haya sido diseñada y validada adecuadamente para la detección de estas fusiones. Además, pueden utilizarse otras técnicas como la RT-PCR (*del inglés reverse transcription polymerase chain reaction*) (26). El método de FISH e IHQ tienen la desventaja de no ofrecer información acerca del compañero de fusión o las variantes en base a los puntos de corte, lo que podría influir potencialmente tanto en la elección del *ALK*-TKI como en el pronóstico de los pacientes (90). Además, algunos estudios han reportado hasta un 35% de falsos negativos usando la técnica FISH con respecto a la NGS del tumor (91). Por otro lado, la RT-PCR únicamente permite detectar parejas de fusión ya conocidas que involucran al gen *ALK*, mientras que la NGS es capaz de solventar este problema, permitiendo la detección simultánea de los reordenamientos conocidos de *ALK,* así como nuevas variables o compañeros de fusión. Sin embargo, hay muchos retos que superar antes de que se pueda establecer esta metodología en un laboratorio de diagnóstico patológico, como es la experiencia necesaria tanto para el análisis como para la interpretación de los resultados.

Por otro lado, la obtención del tejido tumoral presenta ciertas limitaciones. En primer lugar, el pulmón es un órgano de difícil acceso, por lo que obtener una muestra representativa y suficiente para realizar un estudio molecular adecuado puede ser complicado. Si la muestra no es adecuada, debe plantearse la re-biopsia, con el consecuente riesgo para el paciente, que debe volver a someterse a un procedimiento invasivo. Además, esto conlleva un retraso en el resultado que puede ser crucial para establecer el tratamiento más adecuado para el paciente. A esto se suma el aumento constante de biomarcadores conocidos para el cáncer de pulmón, cuyo estudio en ocasiones implica la obtención de biopsias con material suficiente, lo que no es factible siempre.

En segundo lugar, los tumores presentan una enorme heterogeneidad, de forma que cada zona del tumor puede presentar unas características genéticas propias. Esto puede provocar que la muestra analizada no sea representativa de la totalidad de las células tumorales, lo que puede producir resultados discordantes entre muestras de un mismo paciente.

En tercer lugar, los tumores no son estáticos, y sus características moleculares pueden ir cambiando con el desarrollo de la enfermedad. La selección de subclones resistentes debido al uso de fármacos dirigidos puede intervenir en la aparición de nuevas alteraciones genéticas, que producen diferencias moleculares entre el tumor primario y sus metástasis. Dichas alteraciones de resistencia pueden utilizarse a su vez como biomarcadores para nuevas estrategias terapéuticas, pero su caracterización resulta difícil mediante técnicas convencionales por el limitado acceso a las muestras.

4. Estudio de los pacientes con CPCNP *ALK*-positivos mediante biopsia líquida

El uso de la biopsia líquida, como método sensible y no invasivo que permite el análisis de los biomarcadores tumorales a través del estudio de fluidos corporales, prioritariamente la sangre, solventa las limitaciones anteriormente citadas de la biopsia sólida. Además, gracias a la posibilidad de obtener muestras secuenciales, permite la detección de recidivas y la monitorización de los tratamientos, detectando de forma precoz mecanismos de resistencia (92,93).

Las muestras de biopsia líquida provienen de diferentes fluidos corporales, principalmente sangre (suero o plasma), pero también esputo, orina, líquido cefalorraquídeo (LCR), líquido pleural, líquido ascítico, etc. Por otro lado, los biomarcadores pueden ser analizados a partir de distintos analitos presentes en los fluidos corporales como componentes celulares resultantes de la muerte de las células tumorales. Específicamente, en las muestras de biopsia líquida se puede analizar ADN circulante libre (cfDNA*, del inglés cell free DNA*), ARN circulante libre (cfRNA, *del inglés cell free RNA*), micro-ARNs (miRNAs), ARNs circulares (circRNAs), células tumorales circulantes (CTCs, *del inglés circulating tumor cells*), plaquetas educadas en tumores (TEPs, *del inglés tumor-educated platelets*) o vesículas extracelulares (EVs, *del inglés extracellular vesicles*), entre otros.

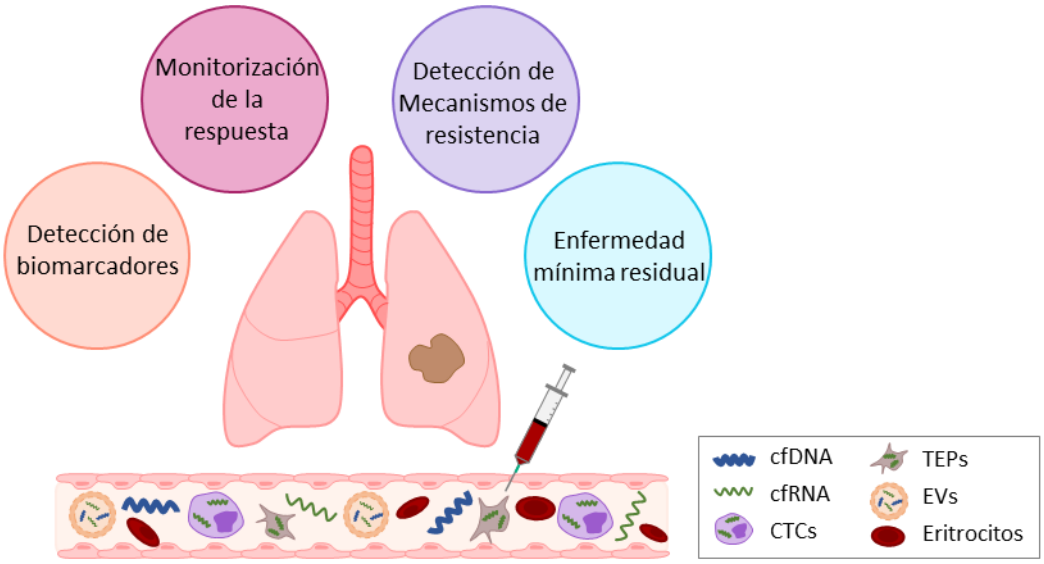

Figura 6. Elementos de interés en las muestras de biopsia líquida y su aplicación potencial. Todas las células del organismo vierten cfDNA y cfRNA debido a procesos de necrosis y apoptosis. En pacientes con CPCNP, parte de esos ácidos nucleicos circulantes proceden de células tumorales (ADN y ARN circulante tumoral: ctDNA y ctRNA), pudiendo ser capturados por otros elementos del torrente sanguíneo como las CTCs, plaquetas (TEPs) y EVs.

4.1. ADN circulante tumoral (ctDNA, circulating tumor DNA)

El cfDNA consiste principalmente en moléculas de ADN fragmentado [de aproximadamente 150-180 pares de bases (pb)], vertidas por las células al torrente sanguíneo tras procesos de necrosis y apoptosis fundamentalmente, con una vida media de 1,5 horas (94). Dentro de ese cfDNA, en los pacientes oncológicos se puede encontrar ADN proveniente de células tumorales, lo que se conoce como ADN circulante tumoral (ctDNA, *del inglés circulating tumor DNA*). Desde el punto de vista clínico, el ctDNA del plasma es la alternativa más extensamente estudiada y empleada

para el estudio del perfil molecular de tumores sólidos, incluido el CPCNP. En concreto, para los pacientes con cáncer de pulmón, el estudio del ctDNA se introdujo por primera vez en la práctica clínica para la detección de mutaciones en el gen *EGFR* (95). En dichos pacientes, el estudio del ctDNA se recomienda para la evaluación del estado mutacional de *EGFR* en pacientes naïve sin disponibilidad o con insuficiente tejido tumoral (detección de mutaciones *sensitizing* en el *locus EGFR*) o para la identificación de la mutación de resistencia p.T790M en el exón 20 de *EGFR* tras la resistencia adquirida a un *EGFR*-TKI de primera o segunda generación (96). Además, actualmente existen evidencias que apoyan el uso del ctDNA para el análisis de otras muchas mutaciones accionables, es decir, mutaciones para las cuales se dispone de un agente farmacológico; tanto en pacientes cuyo perfil molecular en biopsia tumoral ha resultado fallido, como de forma concurrente al mismo (97).

Por otro lado, el estudio de la evolución de mutaciones de resistencia mediante el análisis del ctDNA debe considerarse como un estándar de atención en pacientes con CPCNP con mutaciones accionables, proporcionando información muy valiosa para la guía de las siguientes líneas terapéuticas en los casos en los que no es factible la re-biopsia tumoral o es insuficiente para la realización del estudio molecular. Por todo ello, una alternativa prometedora para la identificación de los mecanismos de resistencia a terapias dirigidas como *ALK*-TKIs o *EGFR*-TKIs es el estudio del ctDNA.

En cuanto al estudio del ctDNA, dada su baja proporción en sangre con respecto al total del cfDNA (0,1-30%), se requieren tecnologías altamente sensibles como la PCR digital (dPCR) [frecuencia alélica mutada (MAF[1], *del inglés mutated allele frequency*) = 0,02%] o la NGS adaptada a muestras de biopsia líquida (MAF = 0,05%). Para conseguir estos niveles de sensibilidad mediante NGS, se emplean identificadores moleculares únicos (UMIs, *del inglés unique molecular identifiers*), pequeños fragmentos de ADN constituidos por bases nucleotídicas al azar, añadidos a las librerías de secuenciación antes de los pasos de enriquecimiento y amplificación, con el objetivo de detectar, cuantificar y secuenciar fragmentos de ADN únicos con alta sensibilidad, lo que permite la identificación y eliminación de artefactos que surgen en la preparación de la librería (98). Es decir, si una mutación no aparece en secuencias con más de un UMI diferente, probablemente se deba a un error de la amplificación o de la reacción de secuenciación. Por otro lado, la combinación de librerías optimizadas y algoritmos bioinformáticos se emplea para lograr un mejor rendimiento de los ensayos de NGS en la detección de variantes de muy baja frecuencia en el análisis de ctDNA, llegando a detectar MAFs de 0,1% (o incluso menores) sin sacrificar la especificidad (99). Además, gracias al avance de las tecnologías de secuenciación, recientes estudios han demostrado la alta concordancia entre la detección de mutaciones de resistencia a terapias dirigidas mediante el estudio del cfDNA y la biopsia tumoral (100,101). A esto se suma que, al contrario que la dPCR, la NGS permite la detección y cuantificación simultánea de múltiples alteraciones somáticas, conocidas y no conocidas.

[1] $MAF = \frac{Copias/\mu L\ FAM\ (mut)}{[Copias\ /\mu L\ VIC(wt) + Copias/\ \mu L\ FAM]}\ x\ 100$

El estudio del perfil mutacional a la progresión de un TKI mediante NGS es especialmente importante en los pacientes con CPCNP portadores de reordenamientos en el gen *ALK* puesto que, al contrario que los pacientes con mutaciones en el gen *EGFR* cuya mutación de resistencia a una primera línea de tratamiento con un *EGFR*-TKI es p.T790M en el 60% de los casos, los tumores *ALK*-positivos presentan múltiples mutaciones de resistencia a *ALK*-TKIs, que a su vez parecen tener diferentes sensibilidades a la gran variedad de *ALK*-TKIs disponibles actualmente. Por consiguiente, el análisis del cfDNA mediante NGS constituye un enfoque apropiado para el estudio de la dinámica mutacional del tumor a lo largo de la enfermedad, proporcionando información útil y clínicamente relevante, que permite un mejor manejo del paciente con CPCNP con reordenamiento en *ALK*.

4.2. ARN circulante tumoral (ctRNA, circulating tumor RNA)

A pesar del uso extendido del ctDNA para el estudio del perfil mutacional del tumor, las alteraciones genómicas complejas como las translocaciones constituyen un reto, ya que el punto de corte y empalme a nivel de ADN es desconocido muchas veces y dichas alteraciones implican un gran número de pares de bases. Por ello, la detección de reordenamientos mediante NGS requiere secuenciar un alto número de pares de bases a una alta profundidad, lo que implica una tecnología muy potente que no está al alcance de todos los laboratorios clínicos, en los cuales se suele optar por paneles de secuenciación dirigidos que cubren menos regiones genómicas.

Una buena alternativa para el estudio de las fusiones genómicas mediante paneles dirigidos de NGS es el análisis de los trascritos de fusión a nivel de ARN. Existen varios tipos de ARNs cuya utilidad como biomarcadores de diagnóstico o pronóstico está siendo evaluada en varios tipos de cáncer (102–104). Entre ellos destacan los ARNs mensajeros (mRNAs) derivados de fusiones génicas (transcritos de fusión). El análisis de los mRNAs a partir de muestras de tejido sólido han permitido la detección de transcritos de fusión como *BCR-ABL1* en pacientes con leucemia, *TMPRSS2-ERG* en pacientes con cáncer de próstata o *EML4-ALK* en pacientes con CPCNP (105–107). Sin embargo, el cfRNA es menos estable que el cfDNA, degradándose rápidamente por la acción de las ribonucleasas (RNasas) presentes en el torrente sanguíneo, por lo que el uso de la biopsia líquida para el estudio de tumores sólidos portadores de translocaciones sigue siendo un desafío. Una estrategia para el estudio de estas alteraciones complejas es el análisis del ARN contenido en distintos compartimentos presentes en el torrente sanguíneo, donde se encuentra protegido de la acción de las RNasas. Entre estos compartimentos destacan las CTCs, las TEPs o las EVs.

Tanto las CTCs, células cancerosas que se desprenden de la masa tumoral primaria o de metástasis; como las TEPs, plaquetas con capacidad de secuestrar ARN tumoral, son empleadas como biomarcadores en cáncer debido a su contenido genómico y a su papel en la estimulación de la supervivencia y la diseminación tumoral (108,109). Sin embargo, la cantidad de ambos compartimentos en el torrente circulatorio puede verse alterada debido a enfermedades inflamatorias, el uso de determinados tratamientos o condiciones pre-analíticas, afectando a la interpretación de los resultados (110). Además, el número de CTCs en sangre es muy escaso (1 CTC por cada 10^6–10^7 leucocitos) (111), y su aislamiento, al igual que el de las plaquetas, no está establecido en la rutina clínica de los pacientes con cáncer de pulmón. Aunque existe un instrumento aprobado por la FDA para el recuento de CTCs, CellSearch™ de Veridex, únicamente

ha sido autorizado para su uso clínico en pacientes con cáncer de mama, de próstata y colorrectal metastásico (112–114).

4.3. Vesículas extracelulares (EVs, extracellular vesicles)

Las EVs se postulan como un potente mecanismo de comunicación intercelular debido a su capacidad para actuar como un vehículo para el intercambio de material genético y proteico entre las células, tanto en condiciones fisiológicas como patológicas. Estas vesículas pueden desempeñar un papel funcional en la mediación de respuestas inmunitarias adaptativas a agentes infecciosos y tumores, reparación de tejidos y modulación del microambiente. Además, las EVs constituyen una fuente importante para la detección de biomarcadores, ya que son secretadas por todos los tipos celulares en cualquier condición (no solo en necrosis o apoptosis como es el caso del ctDNA), pueden aislarse a partir de casi todos los tipos de fluidos corporales y proporcionan estabilidad al material genético lábil que albergan, como el ARN, gracias a su membrana bicapa. Con respecto a las células sanas, las células cancerígenas liberan una cantidad mayor de EVs (con una estimación de 20000 vesículas por célula cada 48 horas) (115), con cambios significativos en su composición y que pueden transferirse a otras células para inducir nuevos procesos biológicos, como la angiogénesis, la adquisición de resistencia terapéutica, la formación de metástasis y un aumento de la proliferación (116,117).

Actualmente, se han descrito diferentes tipos de EVs, dentro de las cuales el término de exosomas se refiere a las nanovesículas o EVs pequeñas (30–200 nm) liberadas después de la fusión de cuerpos multivesiculares con la membrana plasmática al final de la ruta de reciclaje endocítico (118,119). Además, existen otros tipos de EVs entre las que se incluyen a los cuerpos apoptóticos y las microvesículas, que generalmente son más grandes que los exosomas (0.1-2 µm) y que no se originan en la vía endocítica, si no por brotes directos de la membrana plasmática (120). En general, las EVs se caracterizan por presentar proteínas de choque térmico (HSP60, HSP70, etc.), componentes del complejo ESCRT, proteínas involucradas en el transporte y fusión de membrana como Rab GTPasas y anexinas, integrinas y tetraspaninas (CD63, CD81 y CD9), que pueden estar en diferente cantidad en función de las subpoblaciones de EVs (121,122). Además, las EVs contienen lípidos, proteínas y una variedad de ácidos nucleicos, incluyendo ADN, ARN, mRNA, miRNA y ARNs largos no codificantes (lncRNA, *del inglés long non-coding RNA*) (120,123). Actualmente, para la caracterización de EVs se debe analizar al menos una proteína transmembrana propia de EVs, citadas anteriormente, y una proteína citosólica o derivada de estructuras/componentes no EVs como las flotilinas o las lipoproteínas, respectivamente, con el fin de demostrar tanto la naturaleza como el grado de pureza de las preparaciones de EVs (119).

Debido a que las EVs se pueden encontrar en distintos fluidos biológicos, como plasma, orina, saliva, LCR o exudados (124), éstas se han convertido en el foco de muchos estudios debido a su potencial aplicación clínica (87), en especial en el cáncer de pulmón, donde la re-biopsia no es siempre una opción factible. El reto actual reside en la obtención de un protocolo eficaz y estandarizado de aislamiento de EVs que permita utilizar pequeños volúmenes de muestra biológica para el diagnóstico y monitorización de la enfermedad mediante el estudio de la información genética contenida en ellas. Actualmente, los métodos de aislamiento de EVs se basan en las diferencias de tamaño entre las vesículas circulantes o la selección de marcadores

de superficie específicos. Las técnicas basadas en estos principios incluyen ultracentrifugación (UC), precipitación, filtración, cromatografía de exclusión por tamaño (SEC, *del inglés Size-exclusion chromatography*) y enfoques basados en microfluidos o inmunoafinidad (125). A pesar de los avances técnicos, la variedad de subtipos de EVs con diferente composición plantea desafíos continuos para evitar el sesgo dependiente de la metodología. Como complejidad añadida al desafío tecnológico, los reordenamientos genómicos de *ALK*, al contrario que las mutaciones en los genes *EGFR*, *BRAF* o *KRAS* (126), apenas se han estudiado mediante el análisis de los ácidos nucleicos contenidos en EVs.

OBJETIVOS

El objetivo principal de esta Tesis consiste en valorar la utilidad clínica de la biopsia líquida para el manejo del paciente con CPCNP con enfermedad avanzada (estadio IV) y translocación de *ALK.*

Los objetivos específicos de este trabajo son los siguientes:

1. Evaluar la concordancia de las nuevas estrategias de NGS basadas en UMIs y la PCR digital para el genotipado y cuantificación del ctDNA obtenido del plasma de pacientes con CPCNP.
2. Valorar la utilidad de los líquidos biológicos para el estudio del ctDNA como alternativa al plasma.
3. Desarrollar un algoritmo informático específicamente diseñado para la identificación de mutaciones somáticas en el domino tirosina kinasa de *ALK* a partir de los datos de NGS del ctDNA.
4. Estudiar las alteraciones moleculares del CPCNP con translocación de *ALK* a la progresión a un *ALK*-TKI mediante la NGS del ctDNA.
5. Evaluar el potencial de las EVs para la detección de las proteínas de fusión de *ALK* o sus correspondientes transcritos de fusión de ARN (mRNA) en muestras pre-tratamiento de pacientes con CPCNP *ALK*-positivos.

RESULTADOS

PUBLICACIONES CIENTÍFICAS

ARTÍCULO 1: NEXT-GENERATION SEQUENCING FOR TUMOR MUTATION QUANTIFICATION USING LIQUID BIOPSIES

Los pacientes con CPCNP portadores de alteraciones moleculares específicas, como las mutaciones en los genes de *EGFR* o *ALK*, se benefician de terapias dirigidas tanto en primera como en segunda línea de tratamiento. Sin embargo, raramente se lleva a cabo el estudio del perfil mutacional de estos tumores tras la progresión de la enfermedad, lo que impide la identificación de nuevas alteraciones que podrían ser dianas de otras terapias dirigidas. El análisis del ctDNA permite tanto la detección de biomarcadores como la monitorización de la respuesta tumoral al tratamiento de forma no invasiva. La dPCR, aunque es un método robusto, sólo permite el análisis, una a una, de un número limitado de alteraciones conocidas. Por el contrario, la NGS permite el análisis de un número significativamente grande de mutaciones de manera simultánea, conocidas o no.

En este manuscrito se describe el análisis de un total de 54 muestras de cfDNA procedentes de 52 pacientes con CPCNP (estadio III-IV) y 2 donantes sanos utilizando el panel de NGS Oncomine™ Lung cfDNA Assay kit y la dPCR.

Como resultado de este estudio, se demostró la correlación positiva y lineal entre las MAFs evaluadas por dPCR y NGS, calculadas mediante el coeficiente de correlación de concordancia de Lin y el coeficiente de correlación de Pearson (ρc = 0,986; 95% intervalo de confianza [CI] = 0,975–0,991; r = 0,987; p<0,0001, respectivamente). De manera similar, la concordancia entre NGS y dPCR para la detección de la mutación de resistencia a *EGFR*-TKIs p.T790M fue casi perfecta (K = 0,81; 95% CI = 0,62–0,99), con una excelente correlación en términos de MAFs (ρc = 0,991; 95% CI = 0,981–0,992 y Pearson r = 0,998; p<0,0001). Además, la mutación p.G1296A en el *locus ALK*, fue detectada en dos de los cuatro pacientes con CPCNP con translocación en *ALK*, con una muy buena correlación en cuanto a las MAFs obtenidas por NGS y por dPCR (0,87 *vs*. 0,42 y 2,99 *vs*. 2,81). Cabe destacar, que la secuenciación del cfDNA resultó satisfactoria incluso usando sólo 10 ng de cfDNA de entrada.

Como conclusión de este estudio, el cálculo de las MAFs por NGS está altamente correlacionada con el cálculo de las MAFs por dPCR, demostrando que la NGS basada en el uso de UMIs es una técnica robusta para la cuantificación del cfDNA procedente de muestras clínicas, permitiendo el control de la dinámica genómica del tumor a lo largo de la enfermedad, objetivo de la medicina de precisión.

Mi aportación a este estudio fue la cuantificación de muestras de cfDNA y la realización de experimentos de dPCR. Por último, y al igual que el resto de autores, llevé a cabo la revisión del manuscrito.

Mariano Provencio[a], Clara Pérez-Barrios[a], Miguel Barquin[a], Virginia Calvo, Fabio Franco, Estela Sánchez, Ricardo Sánchez, Daniel Marsden, Juan Cristóbal Sánchez, Paloma Martin Acosta, Raquel Laza-Briviesca, Alberto Cruz-Bermúdez and Atocha Romero*

Next-generation sequencing for tumor mutation quantification using liquid biopsies

https://doi.org/10.1515/cclm-2019-0745
Received July 21, 2019; accepted August 5, 2019

Abstract

Background: Non-small cell lung cancer (NSCLC) patients benefit from targeted therapies both in first- and second-line treatment. Nevertheless, molecular profiling of lung cancer tumors after first disease progression is seldom performed. The analysis of circulating tumor DNA (ctDNA) enables not only non-invasive biomarker testing but also monitoring tumor response to treatment. Digital PCR (dPCR), although a robust approach, only enables the analysis of a limited number of mutations. Next-generation sequencing (NGS), on the other hand, enables the analysis of significantly greater numbers of mutations.
Methods: A total of 54 circulating free DNA (cfDNA) samples from 52 NSCLC patients and two healthy donors were analyzed by NGS using the Oncomine™ Lung cfDNA Assay kit and dPCR.
Results: Lin's concordance correlation coefficient and Pearson's correlation coefficient between mutant allele frequencies (MAFs) assessed by NGS and dPCR revealed a positive and linear relationship between the two data sets ($\rho c = 0.986$; 95% confidence interval [CI] = 0.975–0.991; $r = 0.987$; $p < 0.0001$, respectively), indicating an excellent concordance between both measurements. Similarly, the agreement between NGS and dPCR for the detection of the resistance mutation p.T790M was almost perfect ($K = 0.81$; 95% CI = 0.62–0.99), with an excellent correlation in terms of MAFs ($\rho c = 0.991$; 95% CI = 0.981–0.992 and Pearson's $r = 0.998$; $p < 0.0001$). Importantly, cfDNA sequencing was successful using as low as 10 ng cfDNA input.
Conclusions: MAFs assessed by NGS were highly correlated with MAFs assessed by dPCR, demonstrating that NGS is a robust technique for ctDNA quantification using clinical samples, thereby allowing for dynamic genomic surveillance in the era of precision medicine.

Keywords: biomarker testing; cfDNA; ctDNA; digital PCR (dPCR); liquid biopsy; next-generation sequencing (NGS); non-small cell lung cancer (NSCLC).

[a]Mariano Provencio, Clara Pérez-Barrios and Miguel Barquin contributed equally to this work.
***Corresponding author: Atocha Romero,** PharmD, PhD, Medical Oncology Department, Puerta de Hierro Hospital, C/ Manuel de Falla 1, Majadahonda, Madrid 28222, Spain; and Molecular Oncology Laboratory, Biomedical Sciences Research Institute, Hospital Universitario Puerta de Hierro-Majadahonda, Madrid, Spain, E-mail: atocha10@hotmail.com. https://orcid.org/0000-0002-1634-7397
Mariano Provencio, Virginia Calvo, Fabio Franco, Daniel Marsden and Juan Cristóbal Sánchez: Medical Oncology Department, Hospital Universitario Puerta de Hierro-Majadahonda, Madrid, Spain
Clara Pérez-Barrios: Molecular Oncology Laboratory, Biomedical Sciences Research Institute, Hospital Universitario Puerta de Hierro-Majadahonda, Madrid, Spain; and Laboratory Medicine Department, Hospital Universitario Puerta de Hierro-Majadahonda, Madrid, Spain
Miguel Barquin, Estela Sánchez, Raquel Laza-Briviesca and Alberto Cruz-Bermúdez: Molecular Oncology Laboratory, Biomedical Sciences Research Institute, Hospital Universitario Puerta de Hierro-Majadahonda, Madrid, Spain
Ricardo Sánchez: Laboratorio de Hematología Traslacional, Servicio de Hematología, Instituto de Investigación Hospital 12 de Octubre (I+12), Hospital Universitario 12 de Octubre, Madrid, Spain
Paloma Martin Acosta: Pathology Department, Hospital Universitario Puerta de Hierro-Majadahonda, Madrid, Spain

Introduction

About 30% of non-small cell lung cancer (NSCLC) tumors harbor certain specific molecular alterations, such as activating mutations in the *EGFR* gene, which can be targeted by therapeutic agents. As personalized therapy has been shown to provide significant improvement in survival and quality of life in NSCLC patients, molecular profiling of lung cancer tumors is highly recommended in patients with advanced disease who might benefit from appropriately targeted treatments [1, 2]. Moreover, it has been suggested that molecular testing should be extended beyond recognized biomarkers for approved targeted therapies to include other molecular alterations which might guide investigational therapies with compelling evidence of efficacy [3]. Nevertheless, next-generation sequencing (NGS) analysis of lung cancer tumors remains a challenge. Specifically,

tumor molecular profiling after disease progression to first-line treatment is seldom performed in daily oncology as the availability of tumor tissue obtained from re-biopsies is limited. Detection of cancer mutations in blood by analyzing circulating tumor DNA (ctDNA) is a novel approach that avoids such limitation. Tumor cells shed ctDNA into the bloodstream, which can then be isolated from a noninvasive blood draw to be analyzed by ultrasensitive methods, such as digital PCR (dPCR). Moreover, ctDNA levels can be used to monitor tumor response to treatment within narrower time frames compared to imaged-based procedures [4–8]. However, dPCR has its own limitations, as this approach is designed to detect up to a few number of already-known mutations at a given time. Conversely, NGS enables simultaneous screening of multiple markers, in multiple samples, for a variety of genomic aberrations. However, until recent technological advances, NGS was not sensitive enough to detect and accurately quantify mutations that occur at a very low allele frequency (below 5%). Specifically, the use of unique molecular identifiers (UMIs), random nucleotide sequences that barcode DNA fragments prior to PCR amplification, during library preparation, can significantly reduce errors and quantitative bias introduced by DNA polymerases [9, 10].

In this study, we evaluated the feasibility of applying the new and more sensitive PCR-based NGS methodology for non-invasive biomarker testing and ctDNA quantification in routine clinical samples. To this aim, 52 samples from advanced NSCLC patients were sequenced using a panel specifically designed for circulating free DNA (cfDNA) analysis that screens 169 hotspots. Subsequently, results were validated by dPCR. We compared allele frequencies assessed by both technologies by applying statistical methods that are commonly used in the field of laboratory medicine [11]. Finally, we assessed the agreement as well as the correlation between NGS and dPCR for p.T790M identification and quantification.

Materials and methods

Study population

A total of 54 samples were obtained from 52 NSCLC patients and two healthy donors, after signing the appropriate informed consent. The study protocol was approved by the Hospital Puerta de Hierro Ethics Committee (internal codes 144/14 and 68/16). Eligible patients were both male and female, aged >18 years, with a pathologically confirmed diagnosis of stage III-IV NSCLC. In all cases, whole blood samples were collected in an 8.5 mL PPT™ tube (Becton Dickinson) containing a gel barrier to separate the plasma after centrifugation.

Laboratory procedures

All samples were processed as previously described [4, 5]. Briefly, samples were centrifuged at room temperature within 2 h from the time of blood extraction by two consecutive centrifugations: 1500 *g* for 10 min and 5000 *g* for 20 min. Hemolyzed samples were discarded for further analysis. cfDNA isolation was performed using the Maxwell® RSC (MR) ccfDNA Plasma Kit (Promega Corporation, Madison, WI, USA) according to the manufacturer's instructions and following the "1 mL cell free DNA custom" program. Fifty microliters of the supplied buffer was used for elution. After isolation, cfDNA was stored immediately at –20 °C until library preparation.

Before library preparation, samples were thawed in the refrigerator at 4 °C. Once thawed, cfDNAs were quantified using the QuantiFluor® dsDNA System Kit in a Quantus Fluorometer (Promega Corporation, Madison, WI, USA). Subsequently, library preparation was performed using the Oncomine™ Lung cfDNA Assay kit (Thermo Fisher, Palo Alto, CA, USA) according to the manufacturer's instructions. This multi-biomarker assay is optimized to detect 169 hotspots in 11 key genes (Supplementary Table 1). The panel is designed to detect tumor drivers (including actionable mutations) as well as resistant mutations to targeted therapies. All the purifications were carried out using AMPure XP magnetic beads (Beckman Coulter, Inc., Brea, CA, USA). Library quantification was performed using the Ion Library TaqMan® Quantitation Kit (Thermo Fisher, Palo Alto, CA, USA) in a StepOnePlus™ qPCR machine (Thermo Fisher, Palo Alto, CA, USA). The individual libraries were diluted to a final concentration of 100 pM. The final barcoded libraries were pooled and adjusted to a final concentration of 50 pM. Template preparation and chip loading were carried out on an Ion Chef™ System (Thermo Fisher, Palo Alto, CA, USA). Eight samples were loaded onto an Ion 530 Chip. Finally, loaded Ion 530™ chips were sequenced on an Ion S5™ Sequencer (Thermo Fisher, Palo Alto, CA, USA).

Analysis of raw sequencing data was performed using Torrent Suite Software (v5.6). For sequencing coverage analysis, the CoverageAnalysis (v. 5.6.0.1) plugin was used (Thermo Fisher, Palo Alto, CA, USA). Raw reads were aligned to the human reference genome hg19.

Variant calling, annotation and filtering were performed on the Ion Reporter (v5.6) platform using the Oncomine Lung Liquid Biopsy workflow (v1.3), which is specifically designed to annotate low frequency (up to 0.1% limit of detection [LOD]) variants (SNPs, InDels) from targeted DNA libraries from the Oncomine Lung cfDNA Assay. Briefly, sequencing reads were mapped to defined target regions (Oncomine Lung cfDNA Regions v1.2 and Oncomine Lung cfDNA Hotspots v1.2) and subjected to variant calling using the Oncomine Variant Annotator v2.3 plugin. For visualization of sequencing reads, the Integrative Genomics Viewer (IGV V.2.3.40, Broad Institute, Cambridge, MA, USA) was used.

Mutations with a minor allele frequency equal to or higher than 0.1%, detected in at least two molecular counts, were considered positive. Mutation confirmation was performed by dPCR. To this aim, cfDNA samples were analyzed using commercially available predesigned TaqMan® Liquid Biopsy dPCR assays and custom TaqMan® assays on a QuantStudio® 3D Digital PCR System (Applied Biosystems, South San Francisco, CA, USA) to confirm the previously detected mutations. For the dPCR reaction, 8.55 µL of template cfDNA was mixed with 0.45 µL of the aforementioned 40X TaqMan® assays and 9 µL of 20× QuantStudio 3D Master Mix, in an 18-µL reaction volume. As previously reported [6], 14.5 µL were loaded onto QuantStudio 3D Digital PCR 20K chips. The cycling conditions were

as follows: initial denaturation at 96 °C for 10 min, followed by 40 cycles at 56 °C for 2 min and 98 °C for 30 s and an elongation step of 72 °C for 10 min, and finally samples were maintained at 22 °C for at least 30 min. Chip fluorescence was read twice. Results were analyzed using QuantStudio® 3D Analysis Suite™ Cloud Software. The automatic call assignments for each data cluster were manually adjusted when needed. The result of the assay is reported as the ratio of mutant DNA molecules relative to the sum of mutant and wild-type (wt) DNA molecules. A negative control DNA was included in every run. Samples were considered positive when the mutant allele frequency (MAF) was greater than or equal to 0.1%. The LOD was assessed for all individual assays as previously described [4, 7]. In all cases, the LOD was below 0.1%.

Statistical analyses

Continuous variables are presented as means ± standard deviations (SD) or median and interquartile range and discrete variables are presented as proportions.

The nonparametric comparison of cfDNA concentration according to UICC tumor stage (stage III vs. IV) was evaluated using the Mann-Whitney U-test. The correlation between MAFs measured by dPCR and NGS was evaluated with simple linear regression analysis, using the concordance correlation coefficient (ρ) and Pearson's coefficient (r). In addition, Passing and Bablok [11] regression analysis was performed to assess the agreement and possible systematic bias between NGS and dPCR. Linear model validity was performed using the Cusum test for linearity. Similarly, MAF measurements by the two methodologies employed were graphically displayed in a Bland-Altman plot. Finally, the agreement between NGS and dPCR for the assessment of p.T790M status (detected vs. not detected) and the agreement between liquid and solid biopsy *EGFR* genotyping were evaluated using the kappa coefficient values and the corresponding 95% confidence intervals (95% CI). $p < 0.05$ was considered for statistical significance. The statistical analysis was performed using software R 3.0.1.

Results

Study cohort

All patients included in this study had biopsy-confirmed NSCLC (n = 52), most of them were classified as having adenocarcinoma (n = 40) and as having stage IV disease (n = 36). Study population characteristics are summarized in Supplementary Table 2. Additionally, two samples from healthy donors were sequenced as negative controls.

Overall, the median concentration of cfDNA isolated from clinical samples was 1.13 ng/μL. According to our data, cfDNA concentration was associated with the stage of disease, as cfDNA concentration was significantly higher in samples from stage IV NSCLC patients compared with those from stage III patients (1.5 ng/μL vs. 0.4 ng/μL; $p < 0.01$) (Supplementary Figure 1). The average number of mutations per sample, according to NGS analysis, was also higher in stage IV patients compared with non-metastatic patients, although this observation was not statistically significant (data not shown). Importantly, the number of mutations per sample was not dependent on cfDNA concentration.

NGS performance

For NGS analysis, the median cfDNA input amount per sample was 14.7 ng. Notably, using samples from daily routine, we failed to isolate cfDNA at 1.55 ng/μL in 34 cases (65.4% of cohort), and therefore the final input was below 20 ng (input amount recommended by the manufacturer). However, a somatic mutation could be detected in 24 (70.6%) of these cases.

On average, the chip density was 93.7%, resulting in 13.1 million average reads per run. The average mapped reads per sample was 1.4 million, resulting in a median overall sequencing depth of 28,090. The median read coverage and median molecular coverage per sample were 27,327 and 2519, respectively. In such a scenario, we were able to detect at least one somatic mutation in 36 of the 52 patients included (69.2%). No mutations were detected in the healthy donor samples.

A total of 61 mutations were accounted in the diseased population with an average of 1.2 mutations per patient and a median MAF of 0.64%. Most mutations identified were single-nucleotide polymorphisms (n = 49). We also detected deletions (n = 11) and one insertion (Supplementary Table 3).

Among samples without any mutations detected (n = 16), six corresponded to patients having stage III disease and the other 10 corresponded to patients having stage IV. No significant differences in sample concentration were observed between samples with positive and negative sequencing results ($p = 0.949$).

Using this panel, we detected mutations in eight of the 11 (72.7%) testable genes, with *EGFR* and *TP53* being the most frequently mutated genes. In this way, 38.5% of patients (n = 20) had a mutation in *EGFR* while 32.7% of patients (n = 17) had mutations in *TP53* (Figure 1). Interestingly, the resistance mutation to *ALK* inhibitors, p.G1269A in the kinase domain of *ALK*, was found in two *ALK*-positive NSCLC patients who had progressed on crizotinib (Figure 2). Additionally, the resistance mutation, p.T790M, was detected by NGS in 12 patients in which the plasma sample was obtained at first disease progression. Noteworthy, only two of these patients had re-biopsy

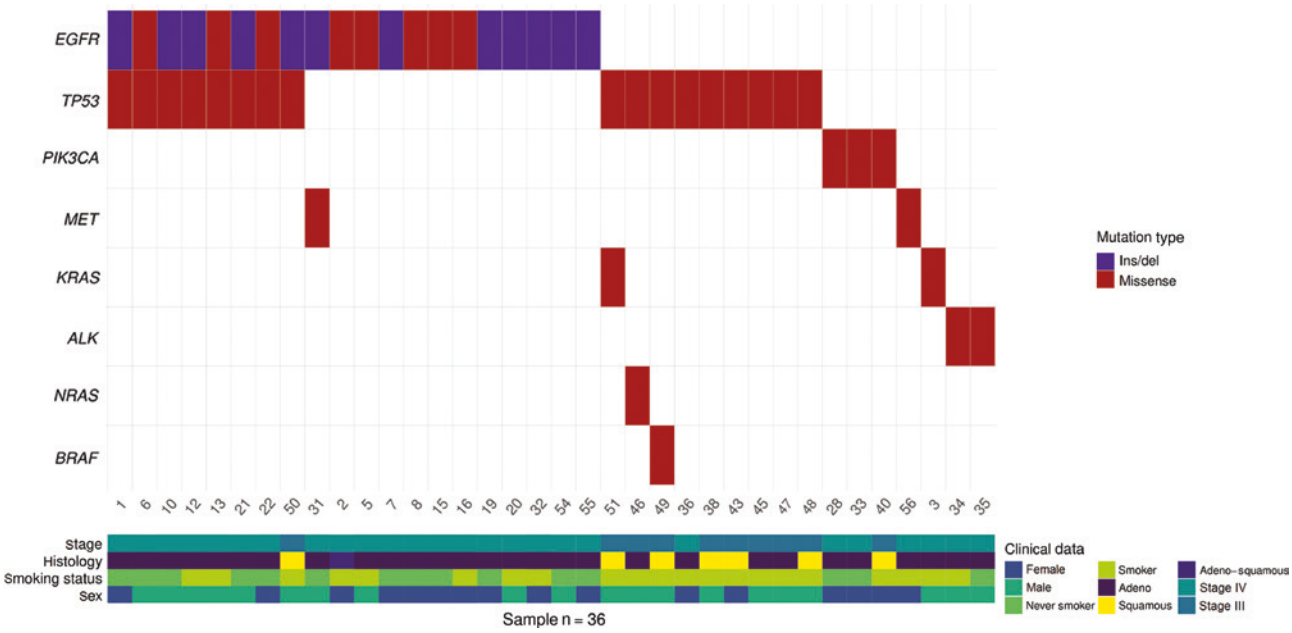

Figure 1: Co-mutation plot according to cfDNA analysis of NSCLC patients by NGS.
Each column represents data from a single patient. Indels are represented in blue whereas missense mutations are represented in red. Heat map at the bottom illustrates patient characteristics.

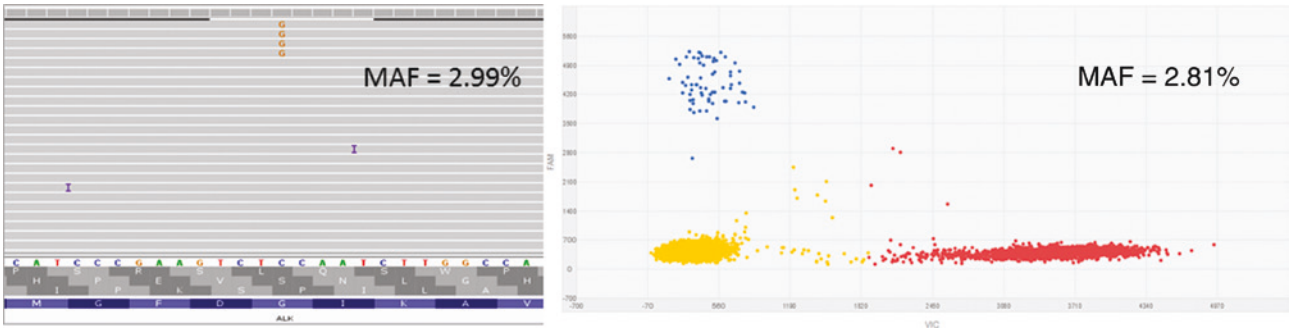

Figure 2: The p.G1269A mutation dPCR scatter plot and visualization of sequencing reads at the corresponding region by the Integrative Genomics Viewer.
On the dPCR scatter plot, the p.G1269A mutation in the kinase domain of *ALK* is labeled with FAM (blue data points), whereas the wild type is labeled with VIC (red data points).

available for p.T790M testing, and in both cases p.T790M was also detected in the tissue sample.

Agreement between solid and liquid biopsies

EGFR molecular data from tumor biopsy was available for 54 specimens. According to pathology reports, 31 patients had an *EGFR*-positive NSCLC tumor and a total of 33 mutations were reported (two patients had tumors harboring two *EGFR* sensitizing mutations). In addition, the *EGFR* mutation p.M766_A767insASV detected in a plasma sample from a patient with an *EGFR*-negative tumor according to clinical data was further confirmed by NGS in the tissue sample. Finally, there were 22 cases with negative results for *EGFR* testing. dPCR and NGS yielded concordant results with respect to the formalin-fixed paraffin-embedded (FFPE) *EGFR* genotyping (K = 0.65; 95% CI = 0.46–0.85, and K = 0.56; 95% CI = 0.35–0.77, respectively). Remarkably, all *EGFR* sensitizing mutations detected by NGS profiling of blood-derived samples (n = 20) were also identified in the matched FFPE sample (Figure 3). However, NGS failed to detect 13 *EGFR* sensitizing mutations that were reported by pathologist. In four of these cases, the original *EGFR* sensitizing mutation could be detected by dPCR.

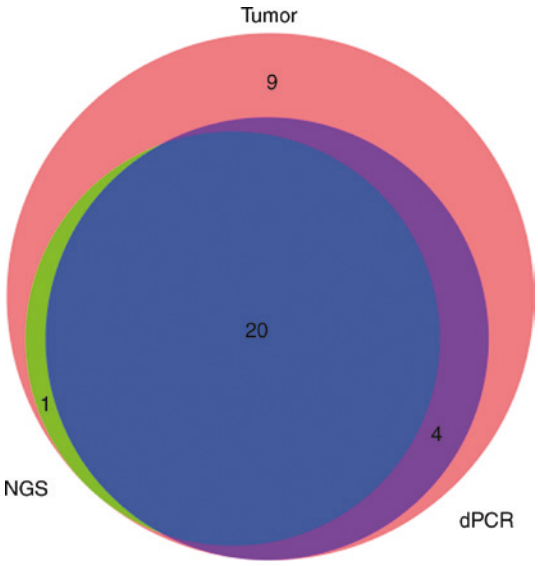

Figure 3: Venn diagram summarizing the number of mutations identified by NGS (green), dPCR (purple) and reported according to pathologist report (pink) and overlapping results (blue).

Concordance between NGS and dPCR

Among the total 61 mutations detected by the Oncomine™ Lung cfDNA Assay kit, we were able to perform 54 confirmations by dPCR (88.5%) using both custom TaqMan® assays and predesigned TaqMan® assays. For dPCR analysis, the median final input amount per sample was 9.8 ng (Supplementary Table 4).

Altogether, 34 out of 36 patients with an NGS-positive result were deemed evaluable for confirmation analysis between NGS and dPCR. This cohort had a total of 54 mutations detected by NGS. Of these, 49 were also detected by dPCR (89%). Five mutations were reported exclusively by NGS, which corresponded to samples in which mutations were detected at MAF close to the NGS and dPCR LOD (MAF ≤ 0.1%), except for the *EGFR* mutation p.M766_A767insASV, which was detected at an MAF of 12.5% by NGS. For its detection, we designed a custom TaqMan® dPCR assay. Nevertheless, dPCR technology is optimized for shorter insertions, which could explain this discrepancy; remarkably, this mutation was also identified by NGS in the corresponding FFPE sample.

Both Lin's concordance correlation coefficient and Pearson's correlation coefficient between MAFs obtained by NGS and dPCR revealed a positive and linear relationship between two sets of data (ρc = 0.986; 95% CI = 0.975–0.991 and r = 0.987; p < 0.0001, respectively).

Passing-Bablok regression analysis of the methods resulted in a regression equation y = 0.068 (95% CI = −0.017 to 0.152) + 0.893 (95% CI = 0.810–0.973) x, showing an excellent concordance between both methodologies (Figure 4A). The Cusum test for linearity indicated no significant deviation from linearity (p > 0.10). The Bland-Altman plot of the same data set (Figure 4B) showed little bias between the two methods (bias = −0.59; 95% limits of agreement −6.06 to 4.87) with only three measurements (close to LOD) being outside the CI. Similarly, when restricting the analysis to samples with a final input amount of cfDNA greater than or equal to 10 ng (n = 35), Lin's concordance correlation coefficient (ρc = 0.995; 95% CI = 0.990–0.997) and Pearson's correlation coefficient (r = 0.996; p < 0.0001) showed an almost perfect concordance between the MAFs obtained by each technology. Likewise, under these conditions, the Passing-Bablok regression equation was y = 0.079 (−0.023 to 0.173) + 0.883 (0.758–1.012) x. The Bland-Altman plot showed the same bias between the two methods that the previous situation showed (bias = −0.59) with more restrictive 95% limits of agreement (−3.98 to 2.80). Only two measurements were outside the CI. These results corroborated an almost perfect agreement between both methodologies when the cfDNA input was at least 10 ng.

Agreement between NGS and dPCR for p.T790M detection

As an exploratory analysis, we evaluated the agreement between NGS and dPCR for the detection of the resistant mutation p.T790M (n = 52). The proportion of observed agreement between NGS and dPCR was 92.3% with K = 0.81 (95% CI = 0.62–0.99), indicating an almost perfect agreement between the two methodologies. Remarkably, all cases in which the resistant mutation p.T790M was identified by NGS were confirmed by dPCR, with an excellent correlation in terms of MAF (ρc = 0.991; 95% CI = 0.981–0.992 and Pearson's r = 0.998; p < 0.0001) (Supplementary Figure 2).

Finally, in order to evaluate the accuracy of NGS for assessing the p.T790M status considering dPCR as the gold standard, the sensitivity, specificity and positive and negative predictive values were calculated, with 75% sensitivity and 100% specificity (Table 1).

Discussion

cfDNA sequencing can potentially overcome some limitations that solid biopsies have in terms of biomarker testing. Highly sensitive NGS techniques allow

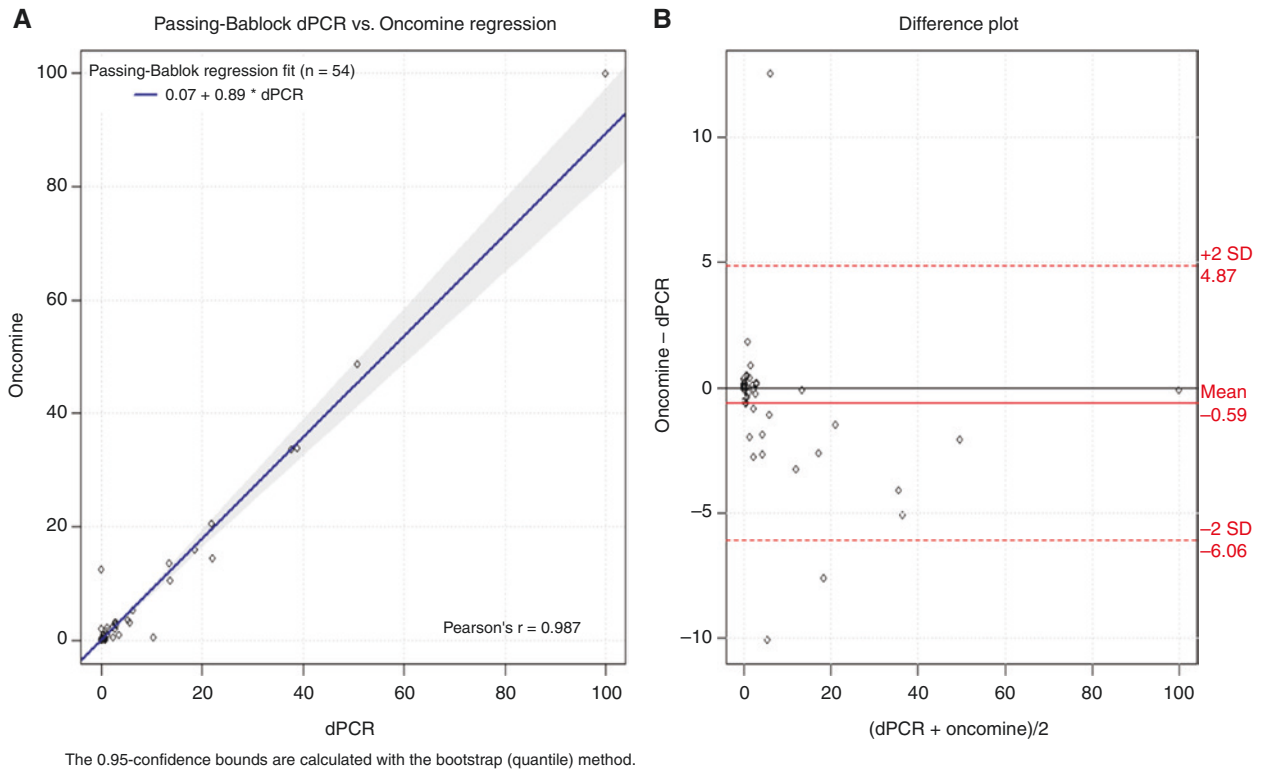

Figure 4: Comparison between dPCR and NGS for mutant allele frequency assessment.
(A) Passing-Bablok regression analysis showing good concordance between both methodologies. (B) Bland-Altman plot showing little bias between NGS and dPCR for mutant allele frequency quantification.

Table 1: Sensitivity, specificity, positive likelihood ratio and negative likelihood ratio of NGS for assessing the p.T790M status.

	Value	95% CI
Sensitivity	75%	48%–93%
Specificity	100%	90%–100%
Mutation prevalence	31%	19%–45%
Positive predictive value	100%	73%–100%
Negative predictive value	90%	76%–97%

for simultaneous analysis of clinically relevant alterations in plasma-derived cfDNA that occur at a very low allele frequency (lower than 0.5%), by non-invasive procedures.

In this study, we tested the feasibility of non-invasive biomarker testing and quantification of plasma genotype by NGS in routine clinical samples using the Oncomine™ Lung cfDNA Assay. A total of 61 mutations were reported across the study population (n = 52), with an average of 1.2 mutations per patient, consistent with previous findings [12]. In addition, the median MAF was 0.64%. Similar results have been reported in terms of MAF in NSCLC patients [13].

An important application of this approach is to detect resistance mutations in patients undergoing treatment with targeted therapies. This is especially relevant due to the difficulty of performing re-biopsies in real-world NSCLC patients. It has been recently reported that less than half of patients experiencing progression after *EGFR*-TKI therapy undergo re-biopsy [14]. Importantly, in our study, the agreement between NGS and dPCR to detect the resistance mutation p.T790M was high (K = 0.81; 95% CI = 0.62–0.99). Considering dPCR as the gold standard, in our hands, NGS provided excellent specificity (100%) for somatic mutation identification. Sensitivity, although acceptable (75%), could be limited by sample quality and probably by tumor stage. Altogether, our results suggest that cfDNA by itself could be considered an adequate approach when tissue biopsy is not available or is otherwise unsuccessful. Noteworthy, only two out of 12 patients in whom the resistance mutation p.T790M was detected by NGS had available tissue sample for molecular testing, thereby limiting the use of targeted therapies in second and subsequent lines of treatment. Finally, it is important to point out that a positive result is very likely to be true, which might obviate re-biopsies intended for biomarker testing.

On the other hand, we were able to identify the p.G1269A mutation in the kinase domain of *ALK* in two of the four patients harboring *ALK* rearrangements treated with crizotinib. This mutation has been reported as a crizotinib resistance mutation [15], although it does not seem to produce resistance to other second generation inhibitors such as ceritinib [16]. Unfortunately, second line treatment to *ALK* inhibitors is usually empirically prescribed, without first identifying the molecular alterations at disease progression. As a proof of concept, we show here that NGS profiling of blood-derived samples upon disease progression can be easily performed, being useful in guiding the subsequent targeted therapies in NSCLC patients. Noteworthy, NGS results can be obtained within a short time frame, ensuring an adequate turnaround time for the clinical setting.

It is well established that, unlike tumor biopsy, liquid biopsy can provide information regarding tumor burden in cancer patients and, therefore, somatic mutation allele frequencies can be used to monitor disease [4, 5, 7, 12, 17]. Importantly, our data indicate that there is an excellent concordance between NGS and dPCR when quantifying somatic mutations in cfDNA. Similarly, other researchers evaluating different NGS panels have reported a good correlation between other NGS panels and dPCR technologies for ctDNA quantification [12, 18, 19].

Of important note, input requirements for NGS are usually strict, which may be a limitation in its practical application. However, the concordance in MAF assessment was very high when the cfDNA input was below 20 ng, suggesting that the threshold of 0.1% could be achieved for samples with at least 10 ng cfDNA input consistent with previous findings [20].

A major limitation of cfDNA sequencing is false-positive plasma genotyping due to clonal hematopoiesis. Somatic mutations in cfDNA can be tumor-derived but also could represent mutations from peripheral blood cells (PBC) acquired during human aging [21]. Indeed, it has been reported that up to 3% of KRAS mutations in cfDNA can be attributable to clonal hematopoiesis, although the p.T790M mutation does not appear to be a common mutation in blood cells, suggesting that false-positive results in this circumstance would be rather exceptional [22]. However, larger studies sequencing paired plasma cfDNA and PBC DNA are of particular interest in order to estimate the impact of clonal hematopoiesis on biomarker testing using liquid biopsies.

In summary, in this paper, we have demonstrated the feasibility of NGS Oncomine™ Lung cfDNA Assay for non-invasive biomarker testing. Moreover, we have demonstrated that this approach is a robust methodology for ctDNA quantification in routine clinical samples from NSCLC patients, suggesting a pivotal role of cfDNA sequencing as a monitoring tool in NSCLC patients with the caveat that clonal hematopoiesis origin should be ruled out in some positive results.

Acknowledgments: We would like to thank the patients for their participation in the study.
Author contributions: AR conceived and coordinated the study. CBP, AR, MB and MM contributed to experimental design and data analysis. CBP, MB, ES, RS, RLB, ACB, PM and PM carried out the experiments. AR, MB and CPB performed the statistical analyses. MM, VC, JCS and FF selected the study population. AR and CPB contributed to manuscript preparation. All authors read and approved the final manuscript. All the authors have accepted responsibility for the entire content of this submitted manuscript and approved submission.
Research funding: This study was supported by the Carlos III Institute of Health, the Spanish Ministry of Science and Innovation and the European Regional Development Fund (grant numbers: PI16/01818 and PIE17/01977). MB was financed by i-PFIS predoctoral fellowship (grant number IFI18/00051) from the ISCIII-MINECO-AES-FEDER (Plan Estatal I+D+I 2013-2016). ES was financed by the Consejería de Educación, Juventud y Deporte of Comunidad de Madrid and by the Fondo Social Europeo (Programa Operativo de Empleo Juvenil, and Iniciativa de Empleo Juvenil, PEJ-2017-AI/SAL-6478).
Employment or leadership: None declared.
Honorarium: None declared.
Competing interests: The funding organization(s) played no role in the study design; in the collection, analysis, and interpretation of data; in the writing of the report; or in the decision to submit the report for publication.

References

1. Keedy VL, Temin S, Somerfield MR, Beasley MB, Johnson DH, McShane LM, et al. American Society of Clinical Oncology provisional clinical opinion: epidermal growth factor receptor (EGFR) mutation testing for patients with advanced non-small-cell lung cancer considering first-line EGFR tyrosine kinase inhibitor therapy. J Clin Oncol 2011;29:2121–7.
2. Novello S, Barlesi F, Califano R, Cufer T, Ekman S, Levra MG, et al. Metastatic non-small-cell lung cancer: ESMO Clinical Practice Guidelines for diagnosis, treatment and follow-up. Ann Oncol 2016;27(suppl_5):v1–27.
3. Kalemkerian GP, Narula N, Kennedy EB, Biermann WA, Donington J, Leighl NB, et al. Molecular Testing Guideline for the Selection of Patients with Lung Cancer for Treatment with Targeted Tyrosine Kinase Inhibitors: American Society of Clinical Oncology

Endorsement of the College of American Pathologists/International Association for the Study of Lung Cancer/Association for Molecular Pathology Clinical Practice Guideline Update. J Clin Oncol 2018;36:911–9.
4. Provencio M, Torrente M, Calvo V, Pérez-Callejo D, Gutiérrez L, Franco F, et al. Prognostic value of quantitative ctDNA levels in non small cell lung cancer patients. Oncotarget 2018;9:488–94.
5. Provencio M, Torrente M, Calvo V, Gutiérrez L, Pérez-Callejo D, Pérez-Barrios C, et al. Dynamic circulating tumor DNA quantificaton for the individualization of non-small-cell lung cancer patients treatment. Oncotarget 2017;8:60291–8.
6. Perez-Barrios C, Nieto-Alcolado I, Torrente M, Jimenez-Sanchez C, Calvo V, Gutierrez-Sanz L, et al. Comparison of methods for circulating cell-free DNA isolation using blood from cancer patients: impact on biomarker testing. Transl Lung Cancer Res 2016;5:665–72.
7. García-Saenz JA, Ayllón P, Laig M, Acosta-Eyzaguirre D, García-Esquinas M, Montes M, et al. Tumor burden monitoring using cell-free tumor DNA could be limited by tumor heterogeneity in advanced breast cancer and should be evaluated together with radiographic imaging. BMC Cancer 2017;17:210.
8. Oxnard GR, Thress KS, Alden RS, Lawrance R, Paweletz CP, Cantarini M, et al. Association between plasma genotyping and outcomes of treatment with osimertinib (AZD9291) in advanced non-small-cell lung cancer. J Clin Oncol 2016;34:3375–82.
9. Kivioja T, Vähärautio A, Karlsson K, Bonke M, Enge M, Linnarsson S, et al. Counting absolute numbers of molecules using unique molecular identifiers. Nat Methods 2012;9:72–4.
10. Schmitt MW, Kennedy SR, Salk JJ, Fox EJ, Hiatt JB, Loeb LA. Detection of ultra-rare mutations by next-generation sequencing. Proc Natl Acad Sci USA 2012;109:14508–13.
11. Passing H, Bablok, W. A new biometrical procedure for testing the equality of measurements from two different analytical methods. Application of linear regression procedures for method comparison studies in clinical chemistry, Part I. J Clin Chem Clin Biochem 1983;21:709–20.
12. Iwama E, Sakai K, Azuma K, Harada T, Harada D, Nosaki K, et al. Monitoring of somatic mutations in circulating cell-free DNA by digital PCR and next-generation sequencing during afatinib treatment in patients with lung adenocarcinoma positive for EGFR activating mutations. Ann Oncol 2017;28:136–41.
13. Chaudhuri AA, Chabon JJ, Lovejoy AF, Newman AM, Stehr H, Azad TD, et al. Early detection of molecular residual disease in localized lung cancer by circulating tumor DNA profiling. Cancer Discov 2017;7:1394–403.
14. Kim T-O, Oh I-J, Kho BG, Park HY, Chang JS, Park C-K, et al. Feasibility of re-biopsy and EGFR mutation analysis in patients with non-small cell lung cancer. Thorac Cancer 2018;9:856–64.
15. Katayama R, Lovly CM, Shaw AT. Therapeutic targeting of anaplastic lymphoma kinase in lung cancer: a paradigm for precision cancer medicine. Clin Cancer Res 2015;21:2227–35.
16. Friboulet L, Li N, Katayama R, Lee CC, Gainor JF, Crystal AS, et al. The ALK inhibitor ceritinib overcomes crizotinib resistance in non-small cell lung cancer. Cancer Discov 2014;4:662–73.
17. Garcia-Murillas I, Schiavon G, Weigelt B, Ng C, Hrebien S, Cutts RJ, et al. Mutation tracking in circulating tumor DNA predicts relapse in early breast cancer. Sci Transl Med 2015;7:302ra133.
18. Plagnol V, Woodhouse S, Howarth K, Lensing S, Smith M, Epstein M, et al. Analytical validation of a next generation sequencing liquid biopsy assay for high sensitivity broad molecular profiling. PLoS One 2018;13:e0193802.
19. Beije N, Helmijr JC, Weerts MJ, Beaufort CM, Wiggin M, Marziali A, et al. Somatic mutation detection using various targeted detection assays in paired samples of circulating tumor DNA, primary tumor and metastases from patients undergoing resection of colorectal liver metastases. Mol Oncol 2016;10:1575–84.
20. Garcia J, Dusserre E, Cheynet V, Bringuier PP, Brengle-Pesce K, Wozny A-S, et al. Evaluation of pre-analytical conditions and comparison of the performance of several digital PCR assays for the detection of majorEGFRmutations in circulating DNA from non-small cell lung cancers: the CIRCAN_0 study. Oncotarget 2017;8:87980–96.
21. Steensma DP, Bejar R, Jaiswal S, Lindsley RC, Sekeres MA, Hasserjian RP, et al. Clonal hematopoiesis of indeterminate potential and its distinction from myelodysplastic syndromes. Blood 2015;126:9–16.
22. Hu Y, Ulrich B, Supplee J, Kuang Y, Lizotte PH, Feeney N, et al. False positive plasma genotyping due to clonal hematopoiesis. Clin Cancer Res 2018;24:4437–43.

Supplementary Material: The online version of this article offers supplementary material (https://doi.org/10.1515/cclm-2019-0745).

GENE	START	END	EXON
NRAS	115256504	115256546	Exon 3
NRAS	115258729	115258763	Exon 2
ALK	29432658	29432693	Exon 25
ALK	29436821	29436865	Exon 24
ALK	29443594	29443638	Exon 23
ALK	29443670	29443708	Exon 23
ALK	29445156	29445220	Exon 22
ALK	29445255	29445324	Exon 22
ALK	29445424	29445485	Exon 21
PIK3CA	178936066	178936108	Exon 10
PIK3CA	178952065	178952102	Exon 21
ROS1	117641093	117641133	Exon 36
EGFR	55241670	55241715	Exon18
EGFR	55242453	55242493	Exon 19
EGFR	55248979	55249031	Exon 20
EGFR	55249059	55249104	Exon 20
EGFR	55259443	55259533	Exon 21
MET	116411985	116412078	Exon 14
MET	116417443	116417483	Exon 16
MET	116423398	116423433	Exon 19
MET	116423467	116423510	Exon 19
BRAF	140453089	140453156	Exon 15
BRAF	140481380	140481425	Exon 11
KRAS	25380260	25380289	Exon 3
KRAS	25398271	25398310	Exon 2
MAP2K1	66727422	66727467	Exon 2
MAP2K1	66729130	66729174	Exon 3
MAP2K1	66774107	66774155	Exon 6
TP53	7574010	7574045	Exon 11
TP53	7577080	7577141	Exon 8
TP53	7577519	7577592	Exon 7
TP53	7578165	7578248	Exon 6
TP53	7578387	7578477	Exon 5
TP53	7579280	7579326	Exon 4
ERBB2	37880965	37881007	Exon 20

Supplemental Table 1. List of the 11 genes and genomic regions tested by the Oncomine Lung cfDNA assay

Feature	Grouping	N	%
Age (years)	Median	64.5 (41-85)	
Sex	Male	29	56%
	Female	23	44%
Smoking status	Current/ex	32	62%
	Never	20	38%
Histology	Adenocarcinoma	40	77%
	Squamous cell carcinoma	10	19%
	Others	2	4%
Stage	IIIA	5	10%
	IIIB	11	25%
	IV	36	65%
Molecular status	EGFR mutation	31	60%
	ALK rearrangement	4	8%
	Negative	17	33%

Supplemental Table 2. Clinico-pathological features of study population.

Sample	*Gene*	*mutation designation (protein)*	*mutation designation (cDNA)*	*COSMIC ID*	*dPCR performed*	*assay type*	*dPCR result*
1	*EGFR*	p.Glu746_Ala750del	c.2236_2250delGAATTAAGAGAAGCA	COSM6225	YES	PREDESIGNED	detectable
1	*EGFR*	p.Thr790Met	c.2369C>T	COSM6240	YES	PREDESIGNED	detectable
1	*TP53*	p.Arg273Cys	c.817C>T	COSM10659	NO	-	NA
2	*EGFR*	p.Leu858Arg	c.2573T>G	COSM6224	YES	PREDESIGNED	detectable
3	*KRAS*	p.Gly13Asp	c.38G>A	COSM532	YES	PREDESIGNED	detectable
5	*EGFR*	p.Thr790Met	c.2369C>T	COSM6240	YES	PREDESIGNED	detectable
5	*EGFR*	p.Leu858Arg	c.2573T>G	COSM6224	YES	PREDESIGNED	detectable
6	*EGFR*	p.Leu858Arg	c.2573T>G	COSM6224	YES	PREDESIGNED	detectable
6	*TP53*	p.Tyr205Cys	c.614A>G	COSM43947	NO	-	NA
7	*EGFR*	p.Glu746_Ala750del	c.2235_2249delGGAATTAAGAGAAGC	COSM6223	YES	PREDESIGNED	detectable
7	*EGFR*	p.Thr790Met	c.2369C>T	COSM6240	YES	PREDESIGNED	detectable
8	*EGFR*	p.Thr790Met	c.2369C>T	COSM6240	YES	PREDESIGNED	detectable
8	*EGFR*	p.Leu858Arg	c.2573T>G	COSM6224	YES	PREDESIGNED	detectable
10	*EGFR*	p.Glu746_Ala750del	c.2235_2249delGGAATTAAGAGAAGC	COSM6223	YES	PREDESIGNED	detectable
10	*EGFR*	p.Thr790Met	c.2369C>T	COSM6240	YES	PREDESIGNED	detectable
10	*TP53*	p.Gly245Ser	c.733G>A	COSM6932	YES	PREDESIGNED	detectable
12	*EGFR*	p.Glu746_Ala750del	c.2236_2250delGAATTAAGAGAAGCA	COSM6225	YES	PREDESIGNED	detectable
12	*EGFR*	p.Thr790Met	c.2369C>T	COSM6240	YES	PREDESIGNED	detectable
12	*TP53*	p.Arg273His	c.818G>A	COSM10660	YES	PREDESIGNED	not detectable or below LOD
13	*EGFR*	p.Gly719Cys	c.2155G>T	COSM6253	YES	PREDESIGNED	detectable
13	*EGFR*	p.Ser768Ile	c.2303G>T	COSM6241	YES	PREDESIGNED	detectable
13	*EGFR*	p.Thr790Met	c.2369C>T	COSM6240	YES	PREDESIGNED	detectable
13	*TP53*	p.Tyr220Cys	c.659A>G	COSM10758	NO	-	NA
15	*EGFR*	p.Thr790Met	c.2369C>T	COSM6240	YES	PREDESIGNED	detectable
15	*EGFR*	p.Leu858Arg	c.2573T>G	COSM6224	YES	PREDESIGNED	detectable
16	*EGFR*	p.Thr790Met	c.2369C>T	COSM6240	YES	PREDESIGNED	detectable
16	*EGFR*	p.Leu858Arg	c.2573T>G	COSM6224	YES	PREDESIGNED	detectable
19	*EGFR*	p.Glu746_Ala750del	c.2236_2250delGAATTAAGAGAAGCA	COSM6225	YES	PREDESIGNED	detectable
20	*EGFR*	p.Glu746_Ala750del	c.2236_2250delGAATTAAGAGAAGCA	COSM6225	YES	PREDESIGNED	detectable
21	*EGFR*	p.Leu747_Pro753delinsSer	c.2240_2257delTAAGAGAAGCAACATCTC	COSM12370	YES	PREDESIGNED	detectable
21	*TP53*	p.Arg282Trp	c.844C>T	COSM10704	YES	PREDESIGNED	detectable
22	*EGFR*	p.Thr790Met	c.2369C>T	COSM6240	YES	PREDESIGNED	detectable
22	*EGFR*	p.Leu858Arg	c.2573T>G	COSM6224	YES	PREDESIGNED	detectable
22	*TP53*	p.Cys277Phe	c.830G>T	COSM10749	NO	-	NA

Supplemental Table 3. Mutations detected by NGS and further confirmed by dPCR.

28	*PIK3CA*	p.His1047Arg	c.3140A>G	COSM775	YES	PREDESIGNED	not detectable or below LOD
31	*EGFR*	p.Leu747_Thr751del	c.2240_2254delTAAGAGAAGCAACAT	COSM12369	YES	PREDESIGNED	detectable
31	*EGFR*	p.Thr790Met	c.2369C>T	COSM6240	YES	PREDESIGNED	detectable
31	*MET*	p.Thr1010Ile	c.3029C>T	COSM707	YES	PREDESIGNED	detectable
32	*EGFR*	p.Leu747_Ala750delinsPro	c.2239_2248delTTAAGAGAAGinsC	COSM12382	YES	PREDESIGNED	detectable
32	*EGFR*	p.Thr790Met	c.2369C>T	COSM6240	YES	PREDESIGNED	detectable
33	*PIK3CA*	p.Glu545Lys	c.1633G>A	COSM763	YES	PREDESIGNED	detectable
34	*ALK*	p.Gly1269Ala	c.3806G>C	COSM1169707	YES	PREDESIGNED	detectable
35	*ALK*	p.Gly1269Ala	c.3806G>C	COSM1169707	YES	PREDESIGNED	detectable
36	*TP53*	p.Arg273Gly	c.817C>G	COSM43843	YES	CUSTOM MADE	detectable
38	*TP53*	p.Arg273Ser	c.817C>A	COSM43909	YES	CUSTOM MADE	detectable
40	*PIK3CA*	p.Glu545Lys	c.1633G>A	COSM763	YES	PREDESIGNED	detectable
43	*TP53*	p.Val157Phe	c.469G>T	COSM10670	YES	PREDESIGNED	detectable
45	*TP53*	p.Val157Phe	c.469G>T	COSM10670	YES	PREDESIGNED	not detectable or below LOD
46	*NRAS*	p.Gly13Asp	c.38G>A	COSM573	YES	PREDESIGNED	not detectable or below LOD
46	*TP53*	p.Arg282Gly	c.844C>G	COSM10992	YES	CUSTOM MADE	detectable
47	*TP53*	p.Met237Ile	c.711G>T	COSM11063	NO	-	NA
48	*TP53*	p.Arg175His	c.524G>A	COSM10648	NO	-	NA
49	*BRAF*	p.Val600Glu	c.1799T>A	COSM476	YES	PREDESIGNED	detectable
49	*TP53*	p.Tyr234Cys	c.701A>G	COSM10725	NO	-	NA
50	*EGFR*	p.Met766_Ala767insAlaSerVal	c.2308_2309insCCAGCGTGG	COSM12426	YES	CUSTOM MADE	not detectable or below LOD
50	*TP53*	p.Arg283Pro	c.848G>C	COSM10743	YES	CUSTOM MADE	detectable
51	*KRAS*	p.Gly13Val	c.38G>T	COSM534	YES	PREDESIGNED	detectable
51	*TP53*	p.Ala159Val	c.476C>T	COSM11148	YES	CUSTOM MADE	detectable
54	*EGFR*	p.Glu746_Ala750del	c.2235_2249delGGAATTAAGAGAAGC	COSM6223	YES	PREDESIGNED	detectable
55	*EGFR*	p.Leu747_Pro753delinsSer	c.2240_2257delTAAGAGAAGCAACATCTC	COSM12370	YES	PREDESIGNED	detectable
56	*MET*	p.Thr1010Asn	c.3029C>A	-	YES	PREDESIGNED	detectable

Sample	Gene	Mutation (protein level)	CDS mutation	CHROM	POS	Oncomine MAF(%)	dPCR MAF (%)
1	*EGFR*	p.Glu746_Ala750del	c.2236_2250delGAATTAAGAGAAGCA	chr7	55242466	0,31	0,16
1	*EGFR*	p.Thr790Met	c.2369C>T	chr7	55249071	0,13	0,21
1	*TP53*	p.Arg273Cys	c.817C>T	chr17	7577121	0,12	NA
2	*EGFR*	p.Leu858Arg	c.2573T>G	chr7	55259515	33,88	38,95
3	*KRAS*	p.Gly13Asp	c.38G>A	chr12	25398281	0,19	0,13
3	*EGFR*	p.D770_N771insG	c.2310_2311insGGT	chr7	55181319	0,00	0,22
5	*EGFR*	p.Thr790Met	c.2369C>T	chr7	55249071	0,10	0,14
5	*EGFR*	p.Leu858Arg	c.2573T>G	chr7	55259515	2,32	2,39
6	*EGFR*	p.Leu858Arg	c.2573T>G	chr7	55259515	0,27	0,36
6	*TP53*	p.Tyr205Cys	c.614A>G	chr17	7578235	0,22	NA
7	*EGFR*	p.Glu746_Ala750del	c.2235_2249delGGAATTAAGAGAAGC	chr7	55242465	2,20	2,25
7	*EGFR*	p.Thr790Met	c.2369C>T	chr7	55249071	0,99	0,50
8	*EGFR*	p.Thr790Met	c.2369C>T	chr7	55249071	0,40	2,40
8	*EGFR*	p.Leu858Arg	c.2573T>G	chr7	55259515	0,91	3,66
10	*EGFR*	p.Glu746_Ala750del	c.2235_2249delGGAATTAAGAGAAGC	chr7	55242464	14,50	22,09
10	*EGFR*	p.Thr790Met	c.2369C>T	chr7	55249071	1,01	1,22
10	*TP53*	p.Gly245Ser	c.733G>A	chr17	7577548	0,14	0,14
12	*EGFR*	p.Glu746_Ala750del	c.2236_2250delGAATTAAGAGAAGCA	chr7	55242464	10,37	13,65
12	*EGFR*	p.Thr790Met	c.2369C>T	chr7	55249071	2,98	2,85
12	*TP53*	p.Arg273His	c.818G>A	chr17	7577120	0,13	0,05
13	*EGFR*	p.Gly719Cys	c.2155G>T	chr7	55241707	2,22	2,12
13	*EGFR*	p.Ser768Ile	c.2303G>T	chr7	55249005	2,17	1,28
13	*EGFR*	p.Thr790Met	c.2369C>T	chr7	55249071	0,92	0,48
13	*TP53*	p.Tyr220Cys	c.659A>G	chr17	7578190	0,11	NA
15	*EGFR*	p.Thr790Met	c.2369C>T	chr7	55249071	0,13	0,13
15	*EGFR*	p.Leu858Arg	c.2573T>G	chr7	55259515	0,10	0,10
16	*EGFR*	p.Thr790Met	c.2369C>T	chr7	55249071	0,67	0,65
16	*EGFR*	p.Leu858Arg	c.2573T>G	chr7	55259515	1,62	1,22
18	*EGFR*	p.Leu747_Thr751del	c.2240_2254delTAAGAGAAGCAACAT	chr7	55242464	0,00	0,46
19	*EGFR*	p.Glu746_Ala750del	c.2236_2250delGAATTAAGAGAAGCA	chr7	55242464	0,22	0,66
20	*EGFR*	p.Glu746_Ala750del	c.2236_2250delGAATTAAGAGAAGCA	chr7	55242464	0,41	10,50
21	*EGFR*	p.Leu747_Pro753delinsSer	c.2240_2257delTAAGAGAAGCAACATCTC	chr7	55242464	15,98	18,60
21	*TP53*	p.Arg282Trp	c.844C>T	chr17	7577094	13,42	13,54
22	*EGFR*	p.Thr790Met	c.2369C>T	chr7	55249071	0,29	0,11

Supplemental Table 4. MAFs for each mutation assessed by NGS and dPCR.

22	*EGFR*	p.Leu858Arg	c.2573T>G	chr7	55259515	0,13	0,80
22	*TP53*	p.Cys277Phe	c.830G>T	chr17	7577108	0,22	NA
28	*PIK3CA*	p.His1047Arg	c.3140A>G	chr3	178952085	0,11	0,08
28	*EGFR*	p.Glu746_Ala750del	c.2236_2250delGAATTAAGAGAAGCA	chr7	55242464	0,00	0,47
31	*EGFR*	p.Leu747_Thr751del	c.2240_2254delTAAGAGAAGCAACAT	chr7	55242464	0,49	0,90
31	*EGFR*	p.Thr790Met	c.2369C>T	chr7	55249071	0,19	0,80
31	*MET*	p.Thr1010Ile	c.3029C>T	chr7	116411990	99,83	99,95
32	*EGFR*	p.Leu747_Ala750delinsPro	c.2239_2248delTTAAGAGAAGinsC	chr7	55242464	48,68	50,76
32	*EGFR*	p.Thr790Met	c.2369C>T	chr7	55249071	33,60	37,70
33	*PIK3CA*	p.Glu545Lys	c.1633G>A	chr3	178936091	0,54	0,90
34	*ALK*	p.Gly1269Ala	c.3806G>C	chr2	29432682	0,87	0,42
35	*ALK*	p.Gly1269Ala	c.3806G>C	chr2	29432682	2,99	2,81
36	*TP53*	p.Arg273Gly	c.817C>G	chr17	7577121	0,55	0,17
38	*TP53*	p.Arg273Ser	c.817C>A	chr17	7577121	3,08	2,96
40	*PIK3CA*	p.Glu545Lys	c.1633G>A	chr3	178936091	1,96	2,81
43	*TP53*	p.Val157Phe	c.469G>T	chr17	7578461	3,50	5,39
45	*TP53*	p.Val157Phe	c.469G>T	chr17	7578461	0,16	0,00
46	*NRAS*	p.Gly13Asp	c.38G>A	chr1	115258736	0,32	0,00
46	*TP53*	p.Arg282Gly	c.844C>G	chr17	7577094	2,75	2,99
47	*TP53*	p.Met237Ile	c.711G>T	chr17	7577570	0,11	NA
48	*TP53*	p.Arg175His	c.524G>A	chr17	7578406	0,64	NA
49	*BRAF*	p.Val600Glu	c.1799T>A	chr7	140453136	0,25	0,17
49	*TP53*	p.Tyr234Cys	c.701A>G	chr17	7577580	0,14	NA
50	*EGFR*	p.Met766_Ala767insAlaSerVal	c.2308_2309insCCAGCGTGG	chr7	55248998	12,54	0,00
50	*TP53*	p.Arg283Pro	c.848G>C	chr17	7577090	20,41	21,88
51	*KRAS*	p.Gly13Val	c.38G>T	chr12	25398281	0,31	0,28
51	*TP53*	p.Ala159Val	c.476C>T	chr17	7578454	1,94	0,14
54	*EGFR*	p.Glu746_Ala750del	c.2235_2249delGGAATTAAGAGAAGC	chr7	55242464	5,31	6,39
54	*EGFR*	p.S768I	c.2303G>T	chr7	55181312	0,00	0,30
55	*EGFR*	p.Leu747_Pro753delinsSer	c.2240_2257delTAAGAGAAGCAACATCTC	chr7	55242464	3,02	5,70
56	*MET*	p.Thr1010Asn	c.3029C>A	chr7	116411990	0,17	0,25

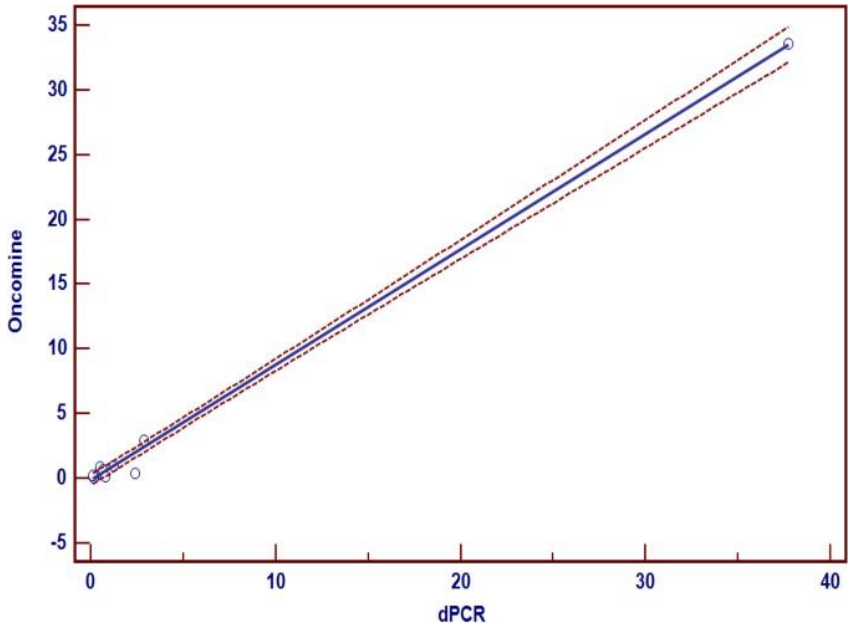

Supplemental Figure 1. Plot representing cfDNA concentration according to tumor stage.

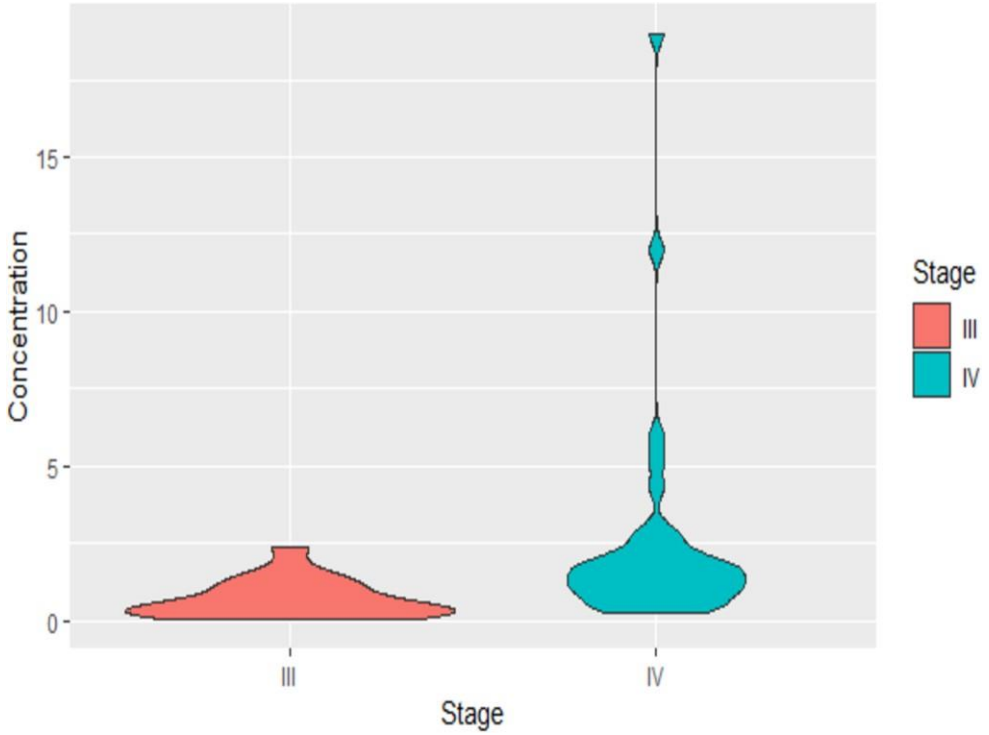

Supplemental Figure 2. Correlation between p.T790M mutation MAF values, assessed by NGS and dPCR.

ARTÍCULO 2: ctDNA FROM BODY FLUIDS IS AN ADEQUATE SOURCE FOR *EGFR* BIOMARKER TESTING IN ADVANCED LUNG ADENOCARCINOMA

La detección de biomarcadores a través del análisis de muestras de biopsia líquida sanguíneas sigue siendo un desafío dada la baja concentración del ctDNA en determinadas muestras de plasma. El objetivo de este estudio consiste en evaluar la utilidad del ctDNA procedente de derrames pleurales, LCRs y líquidos ascítico y pleural, obtenidos durante el manejo clínico, para el estudio del biomarcadores en pacientes con adenocarcinoma de pulmón.

Para llevar a cabo este estudio comparativo, se recolectaron 23 muestras pareadas de plasma y fluidos corporales procedentes de 17 pacientes con adenocarcinoma de pulmón *EGFR*-positivos. El ctDNA se genotipó mediante dPCR.

Los resultados de estos experimentos determinaron que los fluidos corporales presentaban una concentración superior de cfDNA que las muestras plasmáticas (1,90 *vs*. 0.36 ng/µL; p = 0,0130), así como un mayor número de muestras positivas para las mutaciones de *EGFR* (21 *vs*. 16 muestras), con un total de 28 *vs*. 22 variantes detectadas. Además, las MAFs de las mutaciones *sensitizing* de *EGFR* en los fluidos corporales fueron significativamente mayores que las determinadas en su correspondiente muestra pareada de plasma (mediana de MAFs = 15,8 *vs*. 0,8%; p = 0,0004). Esto mismo se observó para la mutación de resistencia p.T790M (mediana de MAFs = 8,69 *vs*. 0,16%; p = 0,0390). Cabe destacar, que dos pacientes progresados a un *EGFR*-TKI de primera generación con resultados dudosos para la mutación p.T790M en plasma (MAFs = 0,11%), presentaron un resultado claramente positivo en sus respectivas muestras de fluidos corporales (MAFs = 10,25 y 9,66%).

En conclusión, con este manuscrito se demostró que el cfDNA derivado de fluidos corporales es una fuente informativa para el estudio de biomarcadores, en concreto de *EGFR*, con una mayor sensibilidad que las muestras de plasma. Estos resultados sirvieron de base para la detección y monitorización de otros biomarcadores, como *ALK*, empleando tanto muestras plasmáticas como otros fluidos corporales que pudiesen ser más informativos.

Como aportación a este trabajo, ayudé a la recolección de muestras pareadas de plasma y fluidos corporales dentro de la colección de muestras de CPCNP del Laboratorio de Biopsia Líquida, así como a la búsqueda de datos clínicos de los pacientes de la cohorte final. Por otro lado, colaboré en la cuantificación del cfDNA y en los experimentos de dPCR para el análisis de las mutaciones *sensitizing* y la mutación de resistencia p.T790M en el gen *EGFR*. Finalmente, colaboré en la revisión del manuscrito.

Clara Pérez-Barrios*, Estela Sánchez-Herrero, Natalia Garcia-Simón, Miguel Barquín, Mariola Blanco Clemente, Mariano Provencio and Atocha Romero

ctDNA from body fluids is an adequate source for *EGFR* biomarker testing in advanced lung adenocarcinoma

https://doi.org/10.1515/cclm-2020-1465
Received October 2, 2020; accepted March 1, 2021;
published online March 11, 2021

Abstract

Objectives: Epidermal growth factor receptor (*EGFR*) biomarker testing using blood-based liquid biopsies remains challenging due to the low concentration of circulating tumor DNA (ctDNA) in certain plasma samples. The aim of this study is to evaluate the usefulness for *EGFR* biomarker testing of ctDNA from pleural effusions, cerebrospinal fluids, ascites and pericardial effusions obtained during the clinical management of lung adenocarcinoma patients.

Methods: For comparison purposes, 23 paired plasma and body fluid samples were collected from 17 patients with *EGFR*-positive lung adenocarcinoma. After circulating free DNA (cfDNA) isolation, samples were evaluated for the initial *EGFR*-sensitizing mutation and the p.T790M resistance mutation by array-based digital PCR (dPCR).

Results: Body fluids had more cfDNA than plasma samples (1.90 vs. 0.36 ng/μL; p=0.0130), and more samples tested positive for *EGFR* mutations (21 vs. 16 samples), with a total of 28 vs. 22 variants detected. Furthermore, mutant allele frequencies (MAFs) observed in body fluids were significantly higher than those assessed in the paired plasma samples for *EGFR*-sensitizing mutations (median MAFs = 15.8 vs. 0.8%; p=0.0004) as well as for the p.T790M resistance mutation (median MAFs = 8.69 vs. 0.16%; p=0.0390). Importantly, two patients who had progressed on first-generation *EGFR*-tyrosine kinase inhibitors with a dubious result for p.T790M plasma (MAFs = 0.11%) had an indisputably positive result in their respective body fluid samples (MAFs = 10.25 and 9.66%).

Conclusions: ctDNA derived from body fluids is an informative source for *EGFR* biomarker testing, with greater sensitivity than plasma samples.

Keywords: biomarker testing; body fluids; ctDNA; *EGFR*; liquid biopsy; lung adenocarcinoma.

Introduction

In the last decade, biomarker testing has become very important in the management of advanced lung adenocarcinoma because it allows for the selection of patients who can benefit from targeted therapies. For guiding treatment decisions, clinical guidelines strongly recommend testing for markers of a variety of genes, such as *EGFR, ALK, ROS1*, and *BRAF*, as well evaluating PDL-1 expression [1].

EGFR mutational status is typically evaluated in a tissue biopsy taken at the time of diagnosis, which enables response to *EGFR*-tyrosine kinase inhibitors (TKIs) to be predicted [2]. Additionally, some acquired mutations might appear under TKI treatment, of which p.T790M is the most frequent resistance mutation. However, the availability of tumor tissue obtained from biopsies in lung adenocarcinoma patients is sometimes low, which could limit the analysis of biomarkers. In addition, the analysis of liquid biopsies is significantly faster and enables the determination of the molecular profiles of the tumor throughout the course of the disease and the detection of clinically relevant alterations caused by the treatments. In this context, circulating tumor DNA (ctDNA), which is the fraction of

***Corresponding author: Clara Pérez Barrios**, PharmD, PhD, Laboratory Medicine Department, Hospital Universitario Puerta de Hierro-Majadahonda, C/Manuel de Falla 1, Majadahonda, Madrid 28222, Spain, E-mail: clara_pb@hotmail.com
Estela Sánchez-Herrero and Miguel Barquín, Molecular Oncology Laboratory, Biomedical Sciences Research Institute, Hospital Universitario Puerta de Hierro-Majadahonda, Madrid, Spain. https://orcid.org/0000-0002-2805-0312 (E. Sánchez-Herrero)
Natalia Garcia-Simón, Laboratory Medicine Department, Hospital Universitario Puerta de Hierro-Majadahonda, Madrid, Spain
Mariola Blanco Clemente and Mariano Provencio, Medical Oncology Department, Hospital Universitario Puerta de Hierro-Majadahonda, Madrid, Spain
Atocha Romero, Molecular Oncology Laboratory, Biomedical Sciences Research Institute, Hospital Universitario Puerta de Hierro-Majadahonda, Madrid, Spain; and Medical Oncology Department, Hospital Universitario Puerta de Hierro-Majadahonda, Madrid, Spain. https://orcid.org/0000-0002-1634-7397

circulating free DNA (cfDNA) that comes from cancerous cells and tumors, has been shown to be an adequate source for the identification and quantification of molecular alterations of the *EGFR* gene that can be used to monitor the course of the disease and detect relapse during targeted therapies [3, 4]. In addition, the analysis of ctDNA from plasma has the advantage that sample collection is straightforward, having been integrated into the clinical routine of many laboratories. Nonetheless, the amount of ctDNA in plasma is affected by many factors, such as tumor size or location [5, 6], which can limit the sensitivity of this approach in biomarker testing.

Body fluids, such as pleural effusion (PE), cerebrospinal fluid (CSF), ascites (ASC) and pericardial effusion (PC), are occasionally obtained from lung adenocarcinoma relapses in the course of clinical management. Although its collection is more invasive than that of blood, supernatant from other body fluids contains more ctDNA than its plasma counterparts [7, 8], making them more sensitive for tumor typing. Furthermore, the proximity of certain body fluids to the tumor site can be useful for obtaining molecular information from localized metastases, such as those in the brain, in which the amount of DNA released into the blood is usually very low [9].

In the present study, we evaluated the usefulness of ctDNA obtained from body fluids for *EGFR* molecular testing. To this end, 23 paired samples of plasma and body fluid were collected from 17 patients with *EGFR*-positive lung adenocarcinoma. After cfDNA isolation, the original sensitizing *EGFR* mutation and the p.T790M resistance mutation were assessed in both specimens using digital PCR (dPCR) for comparison purposes. Finally, we specifically analyzed the p.T790M mutation in body fluids obtained at progression to first- or second-generation TKIs to assess its impact on clinical decision-making.

Materials and methods

Study population

This is a non-interventional prospective study in which specimens were collected during routine clinical practice, according to the oncologist's criteria. Specifically, 23 body fluid samples from 17 non-small cell lung cancer (NSCLC) patients were collected between November 2015 and March 2020, after patients had provided their signed informed consent. All patients had been diagnosed with advanced lung adenocarcinoma disease (stage IV) and had biopsy-proven *EGFR*-sensitizing mutations using the Cobas® EGFR Mutation Test CE-IVD (Roche Molecular Systems, Pleasanton, CA, USA). Additionally, 23 blood samples were collected from the same cohort of patients, with a maximum of three weeks between body fluid and matched plasma sample collection. Information regarding clinicopathological features and tumor mutation status were obtained from clinical records. The study protocol was approved by the Hospital Puerta de Hierro Ethics Committee (internal code 144/14).

Laboratory procedures

Body fluids were collected in additive-free containers and blood samples were kept in 8.5 mL PPT™ tubes (Becton Dickinson). Immediately upon arrival at the laboratory, both samples were centrifuged at 1,500*g* for 10 min and the supernatant was separated using Falcon™ 15 mL conical tubes and stored at −80 °C. On the day the cfDNA was extracted, samples were thawed in the refrigerator at 4 °C and additional centrifugation was performed at 5,000 *g* for 20 min to ensure removal of cells and debris. The Maxwell® RSC (MR) ccfDNA Plasma Kit (Promega Corporation, Madison, WI, USA) was then used for cfDNA isolation, following the manufacturer's instructions and using the "1 mL cell free DNA custom" program. For the final elution, 50 µL of the supplied buffer were used. The cfDNA obtained was stored at −20 °C until further evaluation.

EGFR mutation quantification

Samples were thawed at 4 °C and cfDNA was quantified using the QuantiFluor® dsDNA System Kit in a Quantus Fluorometer (Promega Corporation, Madison, WI, USA). Subsequently, cfDNA was analyzed by array-based PCR QuantStudio® 3D Digital PCR System (Applied Biosystems, South San Francisco, CA, USA) using commercially available predesigned TaqMan® Liquid Biopsy dPCR assays for *EGFR* mutation detection and quantification. Specifically, five assays were used to detect some of the most frequent exon 19 deletions: *EGFR* p.E746_A750del (ELREA deletion, NM_005228.3:c.2235_2249del15 and NM_005228.3:c.2236_2250del15), *EGFR* p.L747_T751del (LREAT deletion, NM_005228.3:c.2239_2253del15), *EGFR* p.L747_S752del (LREATS deletion, NM_005228.3:c.2239_2256del18), and *EGFR* p.L747_A750delinsP (LREA>P indel, NM_005228.3:c.2239_2248delinsC), while the *EGFR* p.L858R and p.T790M (NM_005228.5:c.2573T>G and NM_005228.5:c.2369C>T, respectively) were analyzed through their specific assays.

For each reaction, 8.55 µL of template cfDNA was mixed with 0.45 µL of the 40× specific TaqMan® assay and 9 µL of QuantStudio® 3D Digital PCR Master Mix v2. After that, 14.5 µL of this mixture were loaded onto QuantStudio 3D Digital PCR 20K chips for the purpose of amplification. PCR cycling was carried out under the previously described conditions, and data were analyzed with QuantStudio® 3D Analysis Suite™ Cloud Software [10]. For each assay, results were reported as the mutant allele frequency (MAF), which is calculated as the ratio of mutant DNA molecules to the sum of mutant and wildtype (wt) DNA molecules. The limit of detection for each assay was calculated following the recommendations of The International Council for Harmonisation of Technical Requirements for Pharmaceuticals for Human Use (ICH) Guidelines [11], which have been published elsewhere [4]. The sensitivity and specificity of the assays, considering tissue genotyping to be the gold standard, have also been reported [12]. According to established custom, samples were considered to be positive when the MAF was greater than or equal to 0.1% and when there were at least 300 copies/mL of wt DNA. A negative control DNA (wt) and a blank sample (containing no DNA) were included in every run.

Statistical analysis

The nonparametric comparison of cfDNA concentration and MAFs in paired samples was evaluated using the Wilcoxon signed-rank test. MAFs were compared nonparametrically with respect to mutation type (del19 vs. p.L858R) and cytology result (positive vs. negative/insufficient) using Mann–Whitney U tests. Finally, Kruskal–Wallis tests were used for comparisons with respect to the time of sample collection (diagnosis, follow-up, or progression). Null hypotheses were rejected if the probability of a type I error was less than 0.05. Statistical analyses were carried out using packages in R 3.6.2.

Results

Study cohort

The study population consisted of 17 advanced lung adenocarcinoma patients with biopsy-proven *EGFR*-sensitizing mutations. Specifically, eight of them carried an exon 19 deletion and the other nine bore the p.L858R substitution. A majority of patients were female (n=10), and former or never smokers (n=15). Patient age ranged from 49 to 81 years. Comprehensive clinicopathological characteristics of the study population are summarized in Supplementary Table 1.

From this cohort of patients, a total of 23 body fluid samples were collected according to the oncologist's criteria: 15 PE, five CSF, two PC, and one ASC. Based on the time of collection, four samples were obtained at the time of diagnosis, six during follow-up and 13 at progression (Supplementary Figure 1). Cytological results were positive in 11 of the 16 available pathology reports. Additionally, 23 paired blood samples were collected for comparison.

Cell-free DNA concentration

Once cfDNA had been isolated, we quantified it and compared the results of the paired samples. Overall, cfDNA concentration was significantly higher in body fluids than in plasma samples (p=0.0130), with medians of 1.90 ng/μL [interquartile range (IQR) = 0.37–5.13 ng/μL] and 0.36 ng/μL [IQR = 0.14–0.76 ng/μL], respectively (Figure 1A). However, quantitation revealed a wide range of cfDNA concentrations in body fluid samples, from 0.04 to

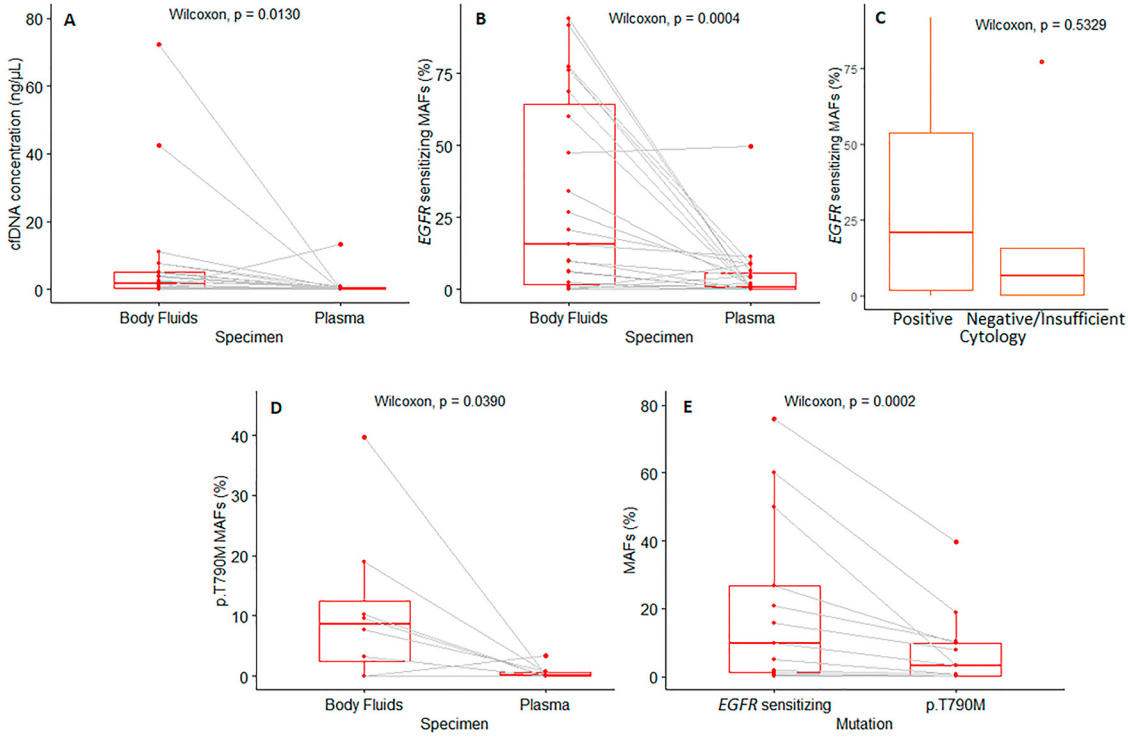

Figure 1: Box-plots representing the distribution of variables analyzed.
(A) cfDNA in paired body fluid vs. plasma samples. (B) *EGFR*-sensitizing mutation MAFs in paired body fluid vs. plasma samples (C) *EGFR*-sensitizing mutations in body fluid samples with a positive cytology result vs. samples with a negative result or reported as insufficient for cytological study. (D) p.T790M mutation MAFs in paired body fluid vs. plasma samples. (E) *EGFR*-sensitizing MAFs vs. p.T790M MAFs in samples presenting both mutations concomitantly.

72.20 ng/μL. Comparing the location of body fluids, the lowest median cfDNA concentration (0.18 ng/μL) was found in CSF (Supplementary Figure 2). No significant differences in cfDNA concentration with respect to their time of collection were found.

EGFR mutation detection

Overall, 28 and 22 *EGFR* variants were identified from body fluid and plasma samples, respectively. Of these mutations, 21 were detected in both samples, while seven were detected only in body fluids and one was only found in plasma samples (Table 1). Given that the *EGFR*-sensitizing mutations had been biopsy-proven in all patients, but the p.T790M resistance mutation was only acquired by some patients, we decided to analyze the molecular results separately.

EGFR-sensitizing mutations

Of the 23 body fluids analyzed, we were able to detect 21 *EGFR*-sensitizing mutations, representing a detection rate of 91.30%. The only two negative results (one exon 19 deletion and one p.L858R substitution) were obtained from cerebrospinal fluids collected at the time of disease progression. Interestingly, four of the five samples reported as negative or insufficient for cytological study were positive by cfDNA. On the other hand, 16 of 23 plasma samples were positive for their known *EGFR*-sensitizing mutation, representing a detection rate of 69.57%. All the mutations identified in plasma were also positive in the paired body-fluid samples. These results are summarized in Table 1.

Next, we compared the allele frequencies of the *EGFR*-sensitizing mutations between plasma and other body fluids. Overall, the median MAF observed in body fluids was 15.80% [IQR = 1.82–64.49%], while it was only 0.80% [IQR = 0.00–5.60%] in plasma samples. This difference was statistically significant according to the Wilcoxon test (p=0.0004; Figure 1B). We then analyzed whether the MAF differences depended on the type of *EGFR*-sensitizing mutation tested (exon 19 deletion and p.L858R substitution), or on the time of sample collection, but found no significant differences.

Finally, we compared the MAFs obtained in body fluids by cytology. We detected median MAFs of 20.74% [IQR = 1.82–53.85%] in samples with a positive result, and of 6.54% [IQR = 0.21–15.80%] in those reported to be negative or insufficient for cytological study. However, this difference was not statistically significant according to the Mann–Whitney independent samples test (Figure 1C).

p.T790M

The *EGFR* p.T790M resistance mutation was detected in seven fluids (including two for which the paired plasma sample was negative), and six plasma samples (including one for which the paired CSF sample was negative).

As shown in Figure 1D, the median MAF of the p.T790M mutation detected in body fluids was significantly higher than that observed in plasma samples (8.69% [IQR = 2.41–12.42%] vs. 0.16% [0.10–0.74%]; p=0.0390). Furthermore, in samples in which p.T790M was detected concomitantly with the *EGFR*-sensitizing mutation (n=13), we found that MAFs of the *EGFR*-sensitizing mutation were significantly higher than those of the concomitant p.T790M (p=0.0002) (Figure 1E).

Finally, we specifically analyzed the p.T790M results in 16 paired samples from the eight patients who relapsed while on first- or second-generation TKIs. Overall, we detected four p.T790M resistance mutations in body fluids and five in plasma samples. The only discordant result corresponded to a CSF. Remarkably, although all the p.T790M mutations detected in fluids were also positive in plasma (n=4), the mutation concentration was considerably higher in body fluids than in plasma samples, with respective median MAFs of 14.60% [IQR = 10.10–24.13%] and 0.16% [IQR = 0.11–0.33%]. This finding was especially interesting in two cases (Figures 2 and 3), in which the MAF at which the mutation was detected in plasma samples was close to the limit of detection (MAF = 0.1%), making it difficult to classify the result as positive or negative. In both examples, paired body fluid samples showed a clearly positive p.T790M result, with MAFs of 10.25 and 9.66%. The patients were treated with osimertinib and their responses lasted 18 and 11 months, respectively.

Discussion

EGFR biomarker testing from blood-based liquid biopsies has become an essential tool for the clinical management of advanced lung adenocarcinoma patients, providing updated molecular information throughout the course of the disease. However, these studies remain challenging owing to the limited amount of ctDNA present in plasma samples. In the current study, we have thoroughly assessed the clinical usefulness of body fluids for biomarker testing in one of the largest cohorts with paired

Table 1: Qualitative and quantitative results of *EGFR*-sensitizing and p.T790M mutations.

Paired sample reference	*EGFR* status by biopsy	Type of BF	Sensitizing mutation detected in BF/plasma by dPCR		Sensitizing (+/–) BD	Sensitizing (+/–) plasma	Sensitizing mutation discrepancy	Sensitizing MAF (%) BF	Sensitizing MAF (%) plasma	p.T790M (+/–) BF	p.T790M (+/–) plasma	p.T790M discrepancy	p.T790M MAF (%) BF	p.T790M MAF (%) plasma
			Nucleotide change	Amino acid change										
1	p.L858R	PE	c.2573T>G	p.L858R	+	+	No	20.74	0.52	+	+	No	10.25	0.11
2	del19	CSF	None	None	–	–	No	0.00	0.00	–	–	No	0.00	0.06
3	del19	PE	c.2236_2250del15	p.E746_A750del	+	+	No	9.66	0.43	+	–	yes	3.18	0.00
4	del19	PE	c.2236_2250del15	p.E746_A750del	+	–	yes	0.44	0.00	–	–	No	0.00	0.00
5	p.L858R	PE	c.2573T>G	p.L858R	+	–	yes	1.08	0.00	–	–	No	0.09	0.00
6	p.L858R	PE	c.2573T>G	p.L858R	+	+	No	15.80	4.84	+	+	No	7.71	0.85
7	del19	PE	c.2235_2249del15	p.E746_A750del	+	+	No	76.04	1.26	+	+	No	39.67	0.20
8	p.L858R	PE	c.2573T>G	p.L858R	+	–	Yes	0.94	0.00	–	–	No	0.00	0.00
9	p.L858R	PC	c.2573T>G	p.L858R	+	+	No	26.88	0.80	+	+	No	9.66	0.11
10	p.L858R	PE	c.2573T>G	p.L858R	+	+	No	47.47	0.29	–	–	No	0.00	0.00
11	p.L858R	PE	c.2573T>G	p.L858R	+	+	No	10.13	0.42	–	–	No	0.00	0.00
12	del19	PC	c.2239_2256del18	p.L747_S752del	+	+	No	77.45	8.84	–	–	No	0.00	0.00
13	del19	PE	c.2239_2256del18	p.L747_S752del	+	+	No	91.89	8.84	–	–	No	0.00	0.00
14	del19	PE	c.2235_2249del15	p.E746_A750del	+	+	No	6.18	4.59	–	–	No	0.00	0.00
15	p.L858R	ASC	c.2573T>G	p.L858R	+	+	No	60.23	2.00	+	+	No	18.95	0.70
16	p.L858R	CSF	None	None	–	–	No	0.00	0.00	–	–	No	0.00	0.00
17	p.L858R	PE	c.2573T>G	p.L858R	+	+	No	2.56	11.48	–	–	No	0.00	0.00
18	del19	PE	c.2235_2249del15	p.E746_A750del	+	+	No	0.21	6.36	+	–	Yes	0.10	0.07
19	p.L858R	PE	c.2573T>G	p.L858R	+	–	Yes	33.96	0.00	–	–	No	0.00	0.00
20	p.L858R	PE	c.2573T>G	p.L858R	+	+	No	6.54	4.15	–	–	No	0.01	0.00
21	del19	CSF	c.2235_2249del15	p.E746_A750del	+	+	No	77.17	49.87	–	+	Yes	0.00	3.32
22	del19	CSF	c.2239_2248delinsC	p.L747_A750delinsP	+	–	Yes	68.75	0.00	–	–	No	0.00	0.01
23	p.L858R	CSF	c.2573T>G	p.L858R	+	+	No	94.22	8.99	–	–	No	0.00	0.00

BD, body fluid; MAF, mutant allele frequency.

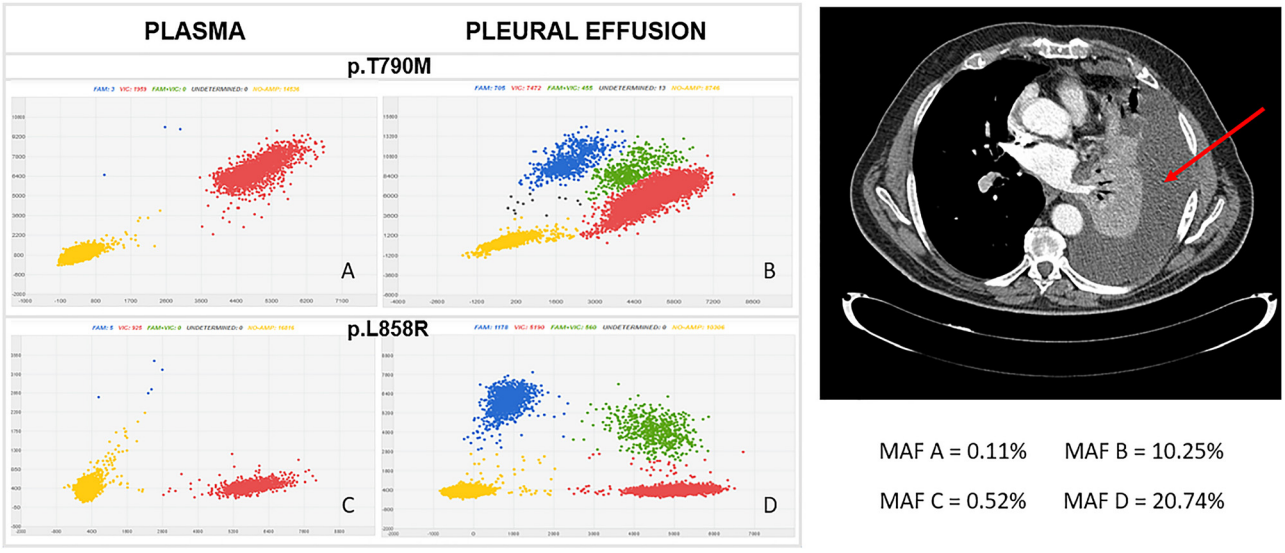

Figure 2: dPCR scatter-plots of p.T790M and p.L858R mutations in paired plasma (A, C) and pleural effusion (B, D) samples, which are evident in the 18-FDG PET-CT scan.
For each assay, the specific mutation is labeled with FAM (blue dots), and the wild type is labeled with VIC (red dots). Green dots represent simultaneous detection of fluorescence in VIC and FAM (more than one copy); yellow dots indicate wells in which there was no amplification. Figure corresponds to pair 1 in Table 1.

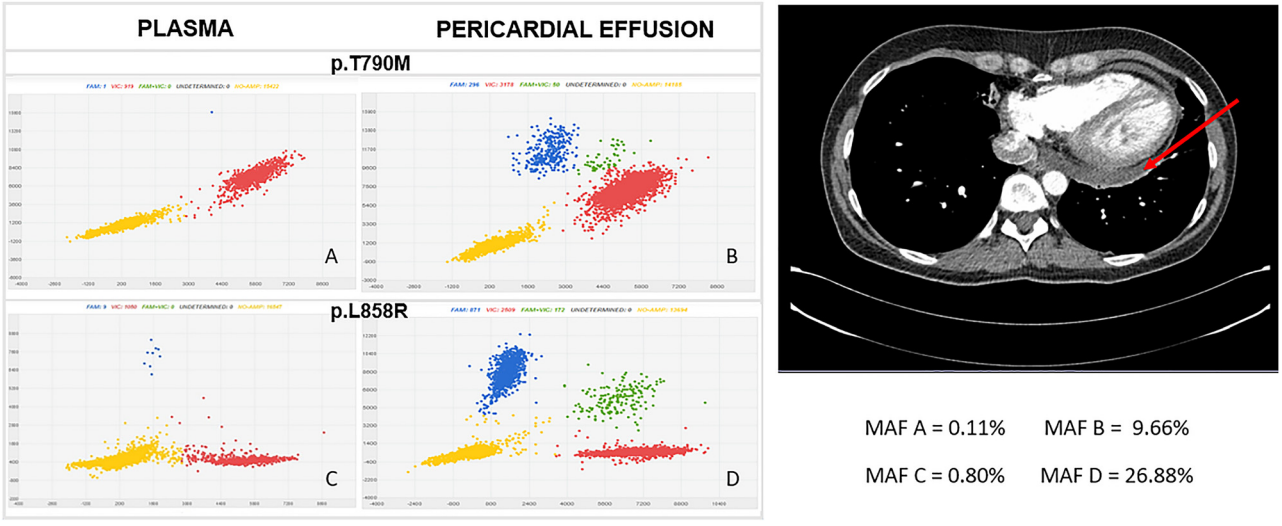

Figure 3: dPCR scatter-plots of p.T790M and p.L858R mutations in paired plasma (A, C) and pericardial effusion (B, D) samples, which is evident in the 18-FDG PET-CT scan.
For each assay, the specific mutation is labeled with FAM (blue dots), and the wild type is labeled with VIC (red dots). Green dots represent simultaneous detection of fluorescence in VIC and FAM (more than one copy); yellow dots indicate wells in which there was no amplification. The plasma sample gives a dubious result for p.T790M (A), with a MAF close to the limit of detection. However, the positive result for p.T790M in the pericardial effusion is beyond reasonable doubt, reinforcing the utility of biomarker testing in body fluids. Figure corresponds to pair 9 in Table 1.

plasma-body fluid reported. The results obtained prove that malignant fluids collected as part of routine clinical practice from advanced lung adenocarcinoma patients, such as PE, CSF, PC and ASC, are suitable alternative samples for molecular profiling, detecting a higher rate of mutations than observed in plasma samples.

First, we found that body fluids were enriched with cfDNA relative to blood. This feature could be especially pertinent for achieving maximum sensitivity when carrying out high-sensitivity next-generation sequencing (NGS), since library preparation frequently requires a minimum quantity of ctDNA input, which can be difficult to

obtain from plasma [13]. Moreover, this enrichment seems to have an important impact on biomarker testing, conferring greater sensitivity on body fluids than plasma. In this context, we have been able to detect 21 of the total 23 biopsy-proven *EGFR*-sensitizing mutations using cfDNA from body fluids. This detection rate (91.30%) is similar to that previously reported [14] and is higher than the sensitivity of 60–70% noted in plasma samples [15, 16]. Interestingly, the two negative body fluids were CSF, which had the lowest cfDNA concentration. However, several authors have demonstrated the utility of cfDNA from CSF for detecting genomic alterations in primary and metastatic brain tumors [17–20], obtaining superior results to those of plasma [9]. The remaining three CSF samples assessed were positive for *EGFR*-sensitizing mutations, with MAFs that ranged from 68.75 to 94.22%. On the other hand, negative results may also be due to an incorrect dPCR assay. In our study, biomarker testing in tissue samples was performed using the Cobas® system, which does not specify which of the *EGFR* exon 19 deletions is present in a given sample. Since we have used only five specific dPCR assays to detect the most frequent exon 19 deletions, lack of testing for other less common exon 19 deletions could explain the negative result observed in CSF from paired sample reference 2 (Table 1). Unfortunately, there was no tissue available to test the dPCR assays on the solid tumor. Regarding the other negative CSF (paired sample reference 16; Table 1), it belongs to a patient whose tumor harbors the *EGFR* p.L858R mutation, and therefore the possibility of an incorrect dPCR assay was discarded. Nevertheless, significantly more *EGFR*-sensitizing mutations were detected in the supernatant of body fluids than in plasma and cytological samples, in which only 16 and six sensitizing mutations, respectively, were reported, in agreement with earlier studies [14, 21].

The sensitivity of body fluids was also demonstrated quantitatively, as described in recent studies [8, 22]. Within this frame of reference, it has been reported [23] that the majority of discordant results between liquid biopsy approaches were found in plasma samples with MAFs <1%. According to our data, approximately half of the mutations detected in plasma samples (10/22) were below this MAF. Interestingly, this proportion dropped to 4/28 for body fluid samples, which offers a means of solving the specificity problems related to low ctDNA MAFs. Furthermore, we found no significant differences between the MAFs of samples with positive cytology results and those reported as negative or insufficient, in agreement with previous studies [24]. This implies that mutation detection in supernatant may be a useful adjunct for cytological samples with negative or indeterminate diagnoses.

Regarding the results with p.T790M, the frequency and abundance of the mutations detected were again significantly higher in body fluids than in plasma samples. As shown in Figures 2 and 3, this feature is especially useful for discriminating between a positive and a negative result in cases where the patient is relapsing to first- or second-generation TKIs, and in which p.T790M is present at a very low concentration in plasma. Finally, we obtained a positive p.T790M result in plasma (MAF = 3.32%) that was negative in CSF, which can be explained by the heterogeneous spatial distribution of the p.T790M mutation, as other studies have suggested [25].

The study has some limitations, the most important of which arises from the dPCR approach itself, whereby each mutation must be tested individually, making the study especially laborious when large numbers of them have to be tested. For this reason, and because more than 30 subtypes [26] of mutations are known, an exhaustive study of exon 19 deletions was not possible. Nevertheless, the detection rate for *EGFR*-sensitizing mutations in the supernatant of body fluids was notably high, exceeding 90%. On the other hand, although this study involved one of the largest cohorts with paired plasma-body fluid samples reported [8, 27], the fact that obtaining body fluids is more invasive than obtaining plasma limited the number of samples we were able to include (n=23).

However, these limitations did not prevent us from demonstrating that body fluids are extremely useful for biomarker testing, leading us to recommend they should form part of molecular analyses whenever possible. Furthermore, the use of alternative high-throughput approaches, such as NGS, may permit extended molecular profiling when tissue samples are exhausted or when a tumor sample is insufficient, of low quality or below the limit of detection for NGS. In this context, the analysis of ctDNA from body fluids by NGS at the time of *EGFR*-TKI progression can be useful for identifying acquired resistance mutations and planning subsequent treatments. It is worth noting that a wide range of resistance mechanisms are known to occur upon osimertinib failure, such as acquired *KRAS* mutations and other targetable gene fusions [28]. Likewise, several resistance mutations at the *ALK* locus are known, although not all of them confer resistance to all *ALK*-TKIs, highlighting the importance of genotyping following disease progression in patients receiving targeted therapies [29].

In summary, ctDNA obtained from body fluids is an adequate source for *EGFR* biomarker testing in advanced lung adenocarcinoma patients and is more sensitive than plasma samples.

Acknowledgments: We would like to thank the patients for their participation in the study.

Research funding: MB is supported by an i-PFIS predoctoral fellowship (Grant Number IFI18/00051) from ISCIII. ES is funded by the Consejería de Ciencia, Universidades e Innovación de la Comunidad de Madrid (Doctorados Industriales de la Comunidad de Madrid IND2019/BMD-17258), Spain.

Author contributions: All authors have accepted responsibility for the entire content of this manuscript and have approved its submission.

Competing interests: Authors state no conflict of interest.

Informed consent: Informed consent was obtained from all individuals included in this study.

Ethical approval: Our research involving human subjects complied with all the relevant national regulations and institutional policies, and was carried out in accordance with the tenets of the Helsinki Declaration (as revised in 2013), and was approved by the Hospital Puerta de Hierro Ethics Committee (internal code 144/14).

References

1. Lung cancer metastatic. Available from: NCCN.org/patients NCCN guidelines for patients NON-small cell lung cancer.
2. Gazdar AF. Activating and resistance mutations of EGFR in non-small-cell lung cancer: role in clinical response to EGFR tyrosine kinase inhibitors. Oncogene 2009;28:S24–31.
3. Provencio M, Torrente M, Calvo V, Gutiérrez L, Pérez-Callejo D, Pérez-Barrios C, et al. Dynamic circulating tumor DNA quantification for the individualization of non-small-cell lung cancer patients treatment. Oncotarget 2017;8:60291–8.
4. Provencio M, Torrente M, Calvo V, Pérez-Callejo D, Gutiérrez L, Franco F, et al. Prognostic value of quantitative ctDNA levels in non small cell lung cancer patients. Oncotarget 2018;9:488–94.
5. Dawson S-J, Tsui DWY, Murtaza M, Biggs H, Rueda OM, Chin S-F, et al. Analysis of circulating tumor DNA to monitor metastatic breast cancer. N Engl J Med 2013;368:1199–209.
6. Bettegowda C, Sausen M, Leary RJ, Kinde I, Wang Y, Agrawal N, et al. Detection of circulating tumor DNA in early- and late-stage human malignancies. Sci Transl Med 2014;6:224ra24.
7. Wang Y, Springer S, Zhang M, McMahon KW, Kinde I, Dobbyn L, et al. Detection of tumor-derived DNA in cerebrospinal fluid of patients with primary tumors of the brain and spinal cord. Proc Natl Acad Sci U S A 2015;112:9704–9.
8. Villatoro S, Mayo-de-las-Casas C, Jordana-Ariza N, Viteri-Ramírez S, Garzón-Ibañez M, Moya-Horno I, et al. Prospective detection of mutations in cerebrospinal fluid, pleural effusion, and ascites of advanced cancer patients to guide treatment decisions. Mol Oncol 2019;13:2633–45.
9. De Mattos-Arruda L, Mayor R, Ng CKY, Weigelt B, Martínez-Ricarte F, Torrejon D, et al. Cerebrospinal fluid-derived circulating tumour DNA better represents the genomic alterations of brain tumours than plasma. Nat Commun 2015;6:8839.
10. Pérez-Barrios C, Nieto-Alcolado I, Torrente M, Jiménez-Sánchez C, Calvo V, Gutierrez-Sanz L, et al. Comparison of methods for circulating cell-free DNA isolation using blood from cancer patients: impact on biomarker testing. Transl Lung Cancer Res 2016;5:665–72.
11. ICH Topic Q 2 (R1) Validation of Analytical Procedures: Text and Methodology Step 5 NOTE FOR GUIDANCE ON VALIDATION OF ANALYTICAL PROCEDURES: TEXT AND METHODOLOGY (CPMP/ICH/381/95) APPROVAL BY CPMP November 1994 DATE FOR COMING INTO OPERATION; 1995.
12. Romero A, Jantus-Lewintre E, García-Peláez B, Royuela A, Insa A, Cruz P, et al. Comprehensive cross-platform comparison of methods for non-invasive EGFR mutation testing: results of the RING observational trial. Mol Oncol 2021;15:43–56.
13. Provencio M, Pérez-Barrios C, Barquin M, Calvo V, Franco F, Sánchez E, et al. Next-generation sequencing for tumor mutation quantification using liquid biopsies. Clin Chem Lab Med 2020;58:306–13.
14. Liu D, Lu Y, Hu Z, Wu N, Nie X, Xia Y, et al. Malignant pleural effusion supernatants are substitutes for metastatic pleural tumor tissues in egfr mutation test in patients with advanced lung adenocarcinoma. PLoS One 2014;9. https://doi.org/10.1371/journal.pone.0089946.
15. Li Z, Zhang Y, Bao W, Jiang C. Insufficiency of peripheral blood as a substitute tissue for detecting EGFR mutations in lung cancer: a meta-analysis. Target Oncol 2014;9:381–8.
16. Douillard JY, Ostoros G, Cobo M, Ciuleanu T, Cole R, McWalter G, et al. Gefitinib treatment in EGFR mutated caucasian NSCLC: circulating-free tumor DNA as a surrogate for determination of EGFR status. J Thorac Oncol 2014;9:1345–53.
17. Jiang BY, Li YS, Guo WB, Zhang XC, Chen ZH, Su J, et al. Detection of driver and resistance mutations in leptomeningeal metastases of NSCLC by next-generation sequencing of cerebrospinal fluid circulating tumor cells. Clin Cancer Res 2017;23:5480–8.
18. Martínez-Ricarte F, Mayor R, Martínez-Sáez E, Rubio-Pérez C, Pineda E, Cordero E, et al. Molecular diagnosis of diffuse gliomas through sequencing of cell-free circulating tumor DNA from cerebrospinal fluid. Clin Cancer Res 2018;24:2812–9.
19. Pan W, Gu W, Nagpal S, Gephart MH, Quake SR. Brain tumor mutations detected in cerebral spinal fluid. Clin Chem 2015;61:514–22.
20. Boire A, Brandsma D, Brastianos PK, Le Rhun E, Ahluwalia M, Junck L, et al. Liquid biopsy in central nervous system metastases: a RANO review and proposals for clinical applications. Oxford: Oxford University Press; 2019, vol 21: 571–83 pp.
21. Lin J, Gu Y, Du R, Deng M, Lu Y, Ding Y. Detection of EGFR mutation in supernatant, cell pellets of pleural effusion and tumor tissues from non-small cell lung cancer patients by high resolution melting analysis and sequencing. Int J Clin Exp Pathol 2014;7:8813–22.
22. Guo Z, Xie Z, Shi H, Du W, Peng L, Han W, et al. Malignant pleural effusion supernatant is an alternative liquid biopsy specimen for comprehensive mutational profiling. Thorac Cancer 2019;10:823–31.
23. O'Leary B, Hrebien S, Beaney M, Fribbens C, Garcia-Murillas I, Jiang J, et al. Comparison of BEAMing and droplet digital PCR for circulating tumor DNA analysis. Clin Chem 2019;65:1405–13.

24. Song Z, Wang W, Li M, Liu J, Zhang Y. Cytological-negative pleural effusion can be an alternative liquid biopsy media for detection of EGFR mutation in NSCLC patients. Lung Cancer 2019;136:23–9.
25. Hata A, Katakami N, Yoshioka H, Kaji R, Masago K, Fujita S, et al. Spatiotemporal T790M heterogeneity in individual patients with EGFR-mutant non-small-cell lung cancer after acquired resistance to EGFR-TKI. J Thorac Oncol 2015;10:1553–9.
26. Su J, Zhong W, Zhang X, Huang Y, Yan H, Yang J, et al. Molecular characteristics and clinical outcomes of EGFR exon 19 indel subtypes to EGFR TKIs in NSCLC patients. Oncotarget 2017;8: 111246–57.
27. Zhang P, Wu X, Tang M, Nie X, Li L. Detection of *EGFR* gene mutation status from pleural effusions and other body fluid specimens in patients with lung adenocarcinoma. Thorac Cancer 2019;10:2218–24.
28. Oxnard GR, Hu Y, Mileham KF, Husain H, Costa DB, Tracy P, et al. Assessment of resistance mechanisms and clinical implications in patients with EGFR T790M-positive lung cancer and acquired resistance to osimertinib. JAMA Oncol 2018;4:1527–34.
29. Gainor JF, Dardaei L, Yoda S, Friboulet L, Leshchiner I, Katayama R, et al. Molecular mechanisms of resistance to first- and second-generation ALK inhibitors in ALK -rearranged lung cancer. Cancer Discov 2016;6:1118–33.

Supplementary Material: The online version of this article offers supplementary material (https://doi.org/10.1515/cclm-2020-1465).

Characteristics	**n=17**
Median age	66 [49-81]
Males Females	7 10
p.L858R del19	9 8
Current Smokers Former smokers Never smokers Smoking status unknown	1 6 9 1
With adenocarcinoma	17

Supplemental table 1: Clinicopatohological characteristics of the study cohort.

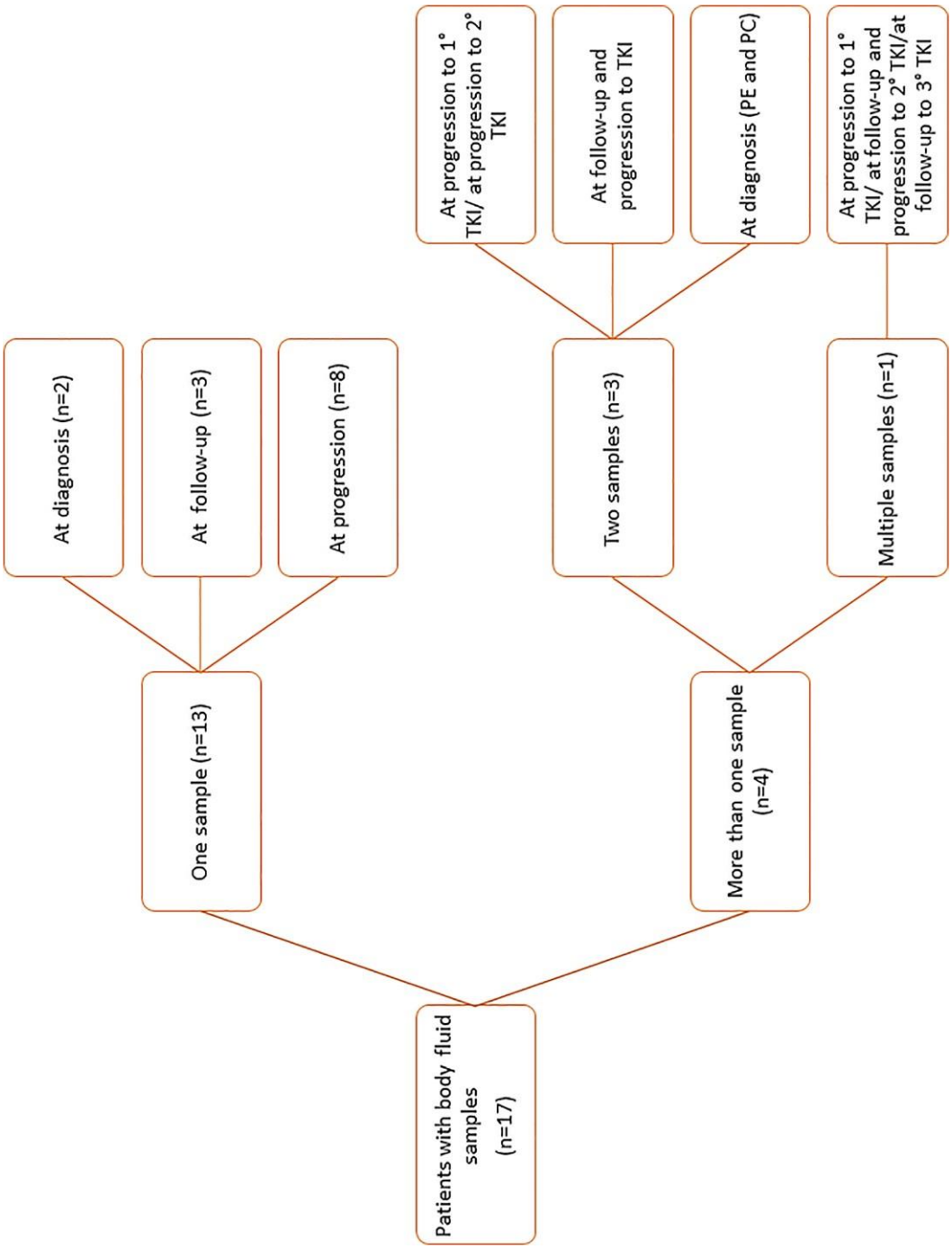

Supplemental figure 1. Diagram representing patient's distribution of the study cohort.

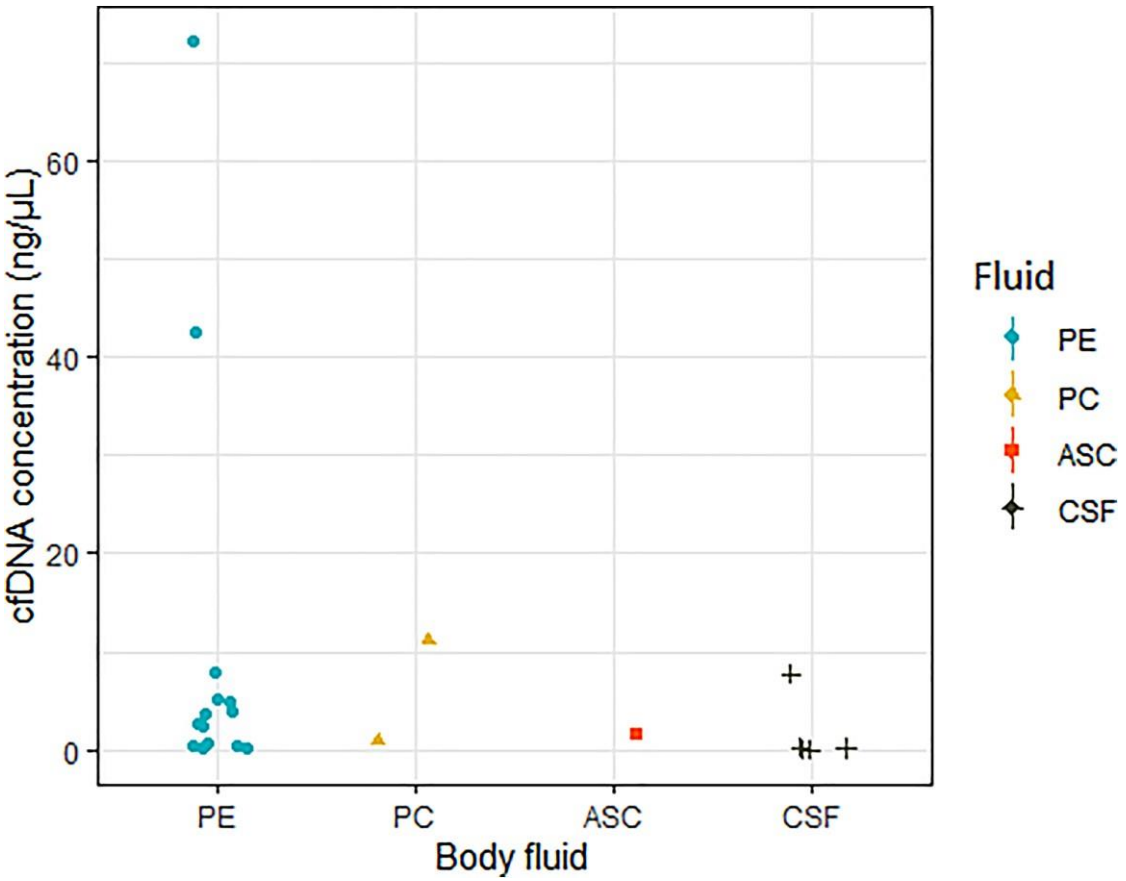

Supplemental figure 2: Dots diagram representing the distribution of cfDNA concentration data by type of body fluid.

ARTÍCULO 3: NGS-BASED LIQUID BIOPSY PROFILING IDENTIFIES MECHANISMS OF RESISTANCE TO *ALK* INHIBITORS: A STEP TOWARD PERSONALIZED NSCLC TREATMENT.

Aproximadamente el 3-7% de los pacientes con CPCNP presentan translocaciones en el gen *ALK*, siendo candidatos a terapias dirigidas con TKIs. Gracias a éstos, la supervivencia y calidad de vida de estos pacientes ha mejorado significativamente. Sin embargo, la mayoría de los pacientes acaban recayendo dentro de los primeros 3 años del tratamiento con un *ALK*-TKI debido al desarrollo de mecanismos de resistencia, entre los que se incluyen mutaciones en el dominio kinasa de *ALK,* así como mutaciones en genes implicados en otras vías de señalización.

En este trabajo se evaluó la utilidad clínica de la biopsia líquida para el estudio del perfil mutacional del tumor a la progresión de la enfermedad mediante NGS. Específicamente, se analizaron 26 muestras de plasma y dos de LCR procedentes de 24 pacientes con CPCNP *ALK*-positivos en estadios avanzados (IV) en el momento de la progresión a un inhibidor de *ALK*. Los datos obtenidos por NGS fueron analizados por un algoritmo bioinformático (V*ALK*), desarrollado y ajustado en base a las variantes confirmadas por dPCR. Este algoritmo fue validado con una segunda cohorte independiente.

El algoritmo desarrollado identificó al menos una mutación de resistencia en el *locus ALK* en el 38,5% de las muestras analizadas; siendo las mutaciones p.G1269A y p.G1202R las más prevalentes en los pacientes progresados a *ALK*-TKI de primera y segunda generación, respectivamente. En general, 61 mutaciones somáticas fueron detectadas en 14 genes: *TP53, ALK, PIK3CA, SMAD4, MAP2K1 (MEK1), FGFR2, FGFR3, BRAF, EGFR, IDH2, MYC, MET, CCND3* y *CCND1*. Específicamente, la deleción del exón 19 de *EGFR*, la mutación p.G466V de *BRAF* y la mutación p.F129L de *MAP2K1* fueron identificados en cuatro pacientes sin beneficio clínico con el tratamiento con *ALK*-TKIs. Por otro lado, se identificaron mutaciones puntuales en los genes *PIK3CA* e *IDH2*, que potencialmente podrían implicar resistencia a *ALK*-TKIs. Finalmente, se detectó la amplificación de *MYC* y la pérdida de expresión de *CCND1* y *FGFR3* en un paciente cuyo tumor progresó a crizotinib en primera línea.

Con este trabajo, se concluye que en torno al 35% de los pacientes de CPCNP *ALK*-positivos pueden beneficiarse de una secuenciación de *ALK*-TKIs basada en el perfil molecular a la progresión de la enfermedad, lo que podría suponer un enfoque eficiente para la toma de decisiones terapéuticas. Además, la NGS puede identificar mecanismos de resistencia en *loci* distintos.

En este trabajo me encargué de gran parte de la redacción del manuscrito y la posterior revisión del mismo tras las correcciones oportunas de mis directores de Tesis. A nivel experimental, mi aportación fue la extracción de los ácidos nucleicos de la cohorte final, así como la preparación de librerías de NGS y el posterior estudio de las variantes por dPCR para el correcto ajuste del algoritmo bioinformático desarrollado (V*ALK*). En este paso, también realicé el diseño de ensayos TaqMan custom. Finalmente, me encargué de la recopilación de los datos clínicos de los pacientes, con ayuda de los clínicos de los centros participantes, así como del análisis estadístico para el estudio de asociaciones significativas entre los datos moleculares y los datos clínicos o de supervivencia.

Molecular Oncology

FEBS PRESS science publishing by scientists

NGS-based liquid biopsy profiling identifies mechanisms of resistance to ALK inhibitors: a step toward personalized NSCLC treatment

Estela Sánchez-Herrero[1,2], Roberto Serna-Blasco[1], Vadym Ivanchuk[1], Rosario García-Campelo[3], Manuel Dómine Gómez[4], José M. Sánchez[5], Bartomeu Massutí[6], Noemi Reguart[7], Carlos Camps[8,9,10,11], Sandra Sanz-Moreno[1], Silvia Calabuig-Fariñas[8,9,12], Eloísa Jantus-Lewintre[8,9,13], Magdalena Arnal[14], Dietmar Fernández-Orth[15], Virginia Calvo[16], Víctor González-Rumayor[2], Mariano Provencio[1,16] and Atocha Romero[1,16]

1 Liquid Biopsy Laboratory, Biomedical Sciences Research Institute Puerta de Hierro-Majadahonda, Spain
2 Atrys Health, Barcelona, Spain
3 Medical Oncology Department, Complejo Hospitalario Universitario A Coruña, Spain
4 Medical Oncology Department, Hospital Universitario Fundación Jiménez Díaz, Oncohealth Institute, Universidad Autónoma de Madrid, Spain
5 Medical Oncology Department, Hospital La Princesa, Madrid, Spain
6 Medical Oncology Department, Hospital Universitario de Alicante, ISABIAL, Alicante, Spain
7 Medical Oncology Department, Hospital Clinic of Barcelona, Spain
8 Molecular Oncology Laboratory, Fundación Hospital General Universitario de Valencia, Spain
9 CIBERONC, Valencia, Spain
10 Department of Medical Oncology, Hospital General Universitario de Valencia, Spain
11 Department of Medicine, Universitat de València, Spain
12 Department of Pathology, Universitat de València, Spain
13 Department of Biotechnology, Universitat de València, Spain
14 MARGenomics, IMIM (Hospital del Mar Medical Research Institute), Barcelona, Spain
15 European Genome-phenome Archive, Centre for Genomic Regulation (CRG), Barcelona, Spain
16 Medical Oncology Department, Hospital Universitario Puerta de Hierro-Majadahonda, Spain

Keywords
ALK-TKI; *EML4-ALK*; liquid biopsy; NGS; NSCLC

Correspondence
A. Romero, Medical Oncology Department, Hospital Puerta de Hierro, Calle Joaquín Rodrigo, 1, 28222 Majadahonda, Madrid, Spain
Tel: +341917769
E-mail: atocha10@hotmail.com

(Received 13 January 2021, revised 21 May 2021, accepted 28 May 2021, available online 18 June 2021)

doi:10.1002/1878-0261.13033

Despite impressive and durable responses, nonsmall cell lung cancer (NSCLC) patients treated with anaplastic lymphoma kinase (*ALK*) inhibitors (*ALK*-Is) ultimately progress due to development of resistance. Here, we have evaluated the clinical utility of circulating tumor DNA (ctDNA) profiling by next-generation sequencing (NGS) upon disease progression. We collected 26 plasma and two cerebrospinal fluid samples from 24 advanced *ALK*-positive NSCLC patients at disease progression to an *ALK*-I. These samples were analyzed by NGS and digital PCR. A tool to retrieve variants at the *ALK* locus was developed (V*ALK* tool). We identified at least one resistance mutation in the *ALK* locus in ten (38.5%) plasma samples; the G1269A and G1202R mutations were the most prevalent among patients progressing to first- and second-generation *ALK*-Is, respectively. Overall, 61 somatic mutations were detected in 14 genes: *TP53*, *ALK*, *PIK3CA*, *SMAD4*, *MAP2K1 (MEK1)*, *FGFR2*, *FGFR3*,

Abbreviations
AF, allele frequency; *ALK*, anaplastic lymphoma kinase; *ALK*-Is, Anaplastic lymphoma kinase inhibitors; cfDNA, cell-free DNA; CNS, central nervous system; CNVs, copy-number variations; CSF, cerebrospinal fluid; CTC, circulating tumor cell; dPCR, digital PCR; ECOG, cooperative oncology group; LOD, limit of detection; MAF, mutant allele frequency; MNP, multiple-nucleotide polymorphism; NGS, next-generation sequencing; NPA, negative percentage agreement; NSCLC, nonsmall cell lung cancer; ORA, overall rates of agreement; OS, overall survival; PFS, progression-free survival; PPA, positive percentage agreement; SNVs, single nucleotide variants; UMIs, unique molecular identifiers; wt, wild-type.

BRAF, *EGFR*, *IDH2*, *MYC*, *MET*, *CCND3,* and *CCND1*. Specifically, a deletion in exon 19 in *EGFR*, a non-V600 *BRAF* mutation (G466V), and the F129L mutation in *MAP2K1* were identified in four patients who showed no objective survival benefit from *ALK*-Is. Potential *ALK*-I-resistance mutations were also found in *PIK3CA* and *IDH2*. Finally, a c-*MYC* gain, along with a loss of *CCND1* and *FGFR3*, was detected in a patient progressing on a first-line treatment with crizotinib. We conclude that NGS analysis of liquid biopsies upon disease progression identified different putative *ALK*-I-resistance mutations in most cases and could be a valuable approach for therapy decision making.

1. Introduction

Anaplastic lymphoma kinase (*ALK*) inhibitors (*ALK*-Is) have dramatically improved outcomes of nonsmall cell lung cancer (NSCLC) patients whose tumors harbor an *ALK* translocation [1,2]. A broad therapeutic arsenal is currently available to treat *ALK*-positive NSCLC tumors, and sequential treatment with different *ALK*-Is is the best therapeutic option for NSCLC patients with an *ALK* translocation [3,4]. However, it remains unclear how *ALK*-Is should be sequenced. It has been proposed that treatment sequencing can be established according to clinical characteristics of the patients or toxicity profile. In this way, second-generation *ALK*-Is have shown impressive central nervous system (CNS) efficacy in *ALK*-positive NSCLC patients [5,6]. On the other hand, crizotinib is associated with adverse events dominated by gastrointestinal and visual effects, increased transaminases and edema, whereas the most common adverse events of alectinib are anemia, myalgia, and increased blood bilirubin [7]. The tumor molecular profile can also determine the treatment response. In this way, among patients treated with the *ALK*-I lorlatinib, the *ALK* fusion variant 3 was associated with significantly longer progression-free survival (PFS) than variant 1 [8]. Finally, several resistance mutations have been identified upon progression to an *ALK*-I [9,10]. While some of them confer resistance to specific *ALK*-Is, others do not [11–13]. Paradoxically, therapy is seldom decided based on the tumor molecular profile upon disease progression, and *ALK*-Is are usually prescribed empirically. Conversely, biomarker testing after treatment failure is routinely performed in *EGFR*-positive NSCLC patients, as recommended by clinical guidelines [14].

Repeat tumor biopsy upon disease progression is not always feasible. Nevertheless, there is considerable evidence showing that genotyping cell-free DNA (cfDNA) is a valid and significantly faster approach than genotyping solid biopsies. Next-generation sequencing (NGS) enables the interrogation of a large number of mutations and can be used with liquid biopsies [15].

In this study, we have analyzed 26 plasma and two cerebrospinal fluid (CSF) samples, from 24 patients, collected upon disease progression while being treated with an *ALK*-I, in order to determine the clinical utility of liquid biopsies for *ALK*-Is sequencing. In addition, we provide a pipeline specifically designed to detect somatic mutations in the *ALK* domain. Finally, we evaluate the clinical significance of somatic alterations in genes other than *ALK*.

2. Methods

2.1. Study population

Between June 2015 and July 2019, 24 stage IV, *ALK*-positive NSCLC patients progressing on an *ALK*-I (the *ALK* cohort), were prospectively recruited from six hospitals across Spain. The study protocol was approved by the Hospital Puerta de Hierro Ethics Committee (internal code 79-18) and was conducted in accordance with the precepts of the Code of Ethics of The World Medical Association (Declaration of Helsinki). All patients provided their appropriate written informed consent to participate in the study prior to enrollment. Briefly, patients who were 18+ years of age and with a pathologically confirmed diagnosis of stage IV NSCLC with an *EML4-ALK* translocation were eligible for inclusion. The identification of *EML4-ALK* rearrangement was carried out by different methodologies, according to each participant center (Table S1). Specifically the *ALK* testing was performed by immunohistochemistry (IHC) using the Ventana *ALK* (D5F3) CDx assay on a Ventana BenchMark XT automated slide-processing system (Ventana Medical

Systems, Tucson, AZ, USA) or the mAb *ALK* (5A4) (Novocastra™; Leica Biosystems, Newcastle Upon Tyne, UK); Fluorescence *In Situ* Hybridization (FISH) using Vysis LSI *ALK* Dual Color Break Apart FISH probe kit (Vysis, Downers Grove, IL, USA) or *ALK* (2P23) Break Apart FISH probe kit (cYTOtEST, Rockville, MD, USA). The nCounter analysis system (NanoString Technologies, Seattle, WA, USA) was also used to detect *EML4-ALK* translocation. All plasma samples were collected upon disease progression, which was assessed according to RECIST criteria v.1.1. In total, 26 plasma and two CSF specimens were collected and analyzed.

2.2. Laboratory procedures

Peripheral whole-blood samples were collected in a 10-mL Streck cfDNA BCT® (Streck, Omaha, NE, USA) tube for cfDNA. CSF samples were collected in a 10-mL sterile tube with no additives or anticoagulants. CSF samples were taken from patients progressing at the brain level. Samples were centrifuged at room temperature in two consecutive centrifugations of 1500 ***g*** for 10 min and 5000 ***g*** for 20 min in order to separate plasma or CSF from the cellular fraction. cfDNA was isolated using QIAamp Circulating Nucleic Acid Kit (QIAgen, Valencia, CA, USA) according to the manufacturer's instructions. Libraries were prepared from at least 15ng of input cfDNA using the Oncomine™ Pan-Cancer Cell-Free Assay kit (Thermo Fisher, Palo Alto, CA, USA) according to the manufacturer's instructions. According to manufacturer, this amplicon-based targeted sequencing assay allows the detection of multiple variants in ctDNA isolated from liquid biopsy samples with a limit of detection (LOD) down to 0.1% mutant allele frequency (MAF). Specifically, the panel interrogates variants in 52 genes (Table S2). AMPureXP magnetic beads (Beckman Coulter, Inc., Brea, CA, USA) were used to purify all libraries. Subsequently, the individual libraries were quantified using the Ion Library TaqMan® Quantitation Kit (Thermo Fisher, Palo Alto, CA, USA) in a StepOnePlus™ qPCR machine (Thermo Fisher) and adjusted to a final concentration of 50 pM. Eight samples were pooled. Templating and Ion 550™ Chip loading were carried out with an Ion Chef™ System (Thermo Fisher). Finally, an Ion GeneStudio™ S5 Sequencer (Thermo Fisher) was used to sequence loaded Ion 550™ chips. TORRENT SUITE Software (v5.12) was used to analyze the raw sequencing data. The COVERAGE ANALYSIS (v. 5.12.0.0) plugin was used for sequencing coverage analysis (Thermo Fisher). Raw reads were aligned to the human reference genome hg19. Variant calling, annotation, and filtering were performed on the Ion Reporter (v5.10, Thermo Fisher) platform using the Oncomine TagSeq Pan-Cancer Liquid Biopsy workflow (v2.1, Thermo Fisher). All candidate mutations were manually reviewed using the Integrative Genomics Viewer v.2.3.40, (Broad Institute, Cambridge, MA, USA). The clinical significance of somatic variants was determined according to the Standards and Guidelines for the Interpretation and Reporting of Sequence Variants in Cancer [16].

The mutations identified by NGS were confirmed by digital PCR (dPCR) using a QuantStudio® 3D dPCR System (Applied Biosystems, South San Francisco, CA, USA). In accordance with the manufacturer's specifications, dPCR reactions were performed in an 18-μL volume comprising 9 μL of 20X QuantStudio 3D Master Mix, 0.45 μL of 40× commercially available predesigned or custom TaqMan® assays and 8.55 μL of cfDNA (minimum amount 2 ng). Subsequently, 14.5 μL of the PCR reaction was loaded onto a QuantStudio 3D dPCR 20K chip using QuantStudio™ 3D dPCR Chip Loader. Each dPCR run included a negative control DNA, as a wild-type (wt) control, a blank (with no cfDNA) and a positive control. PCR reactions were performed in a thermal cycler (Applied Biosystems) at 96 °C for 10 min, then 40 cycles at 56 °C for 2 min and 98 °C for 30 s, and a final elongation step at 72 °C for 10 min. Finally, samples were maintained at 22 °C for at least 30 min. Chips fluoresce was read twice two independent QuantStudio™ 3D dPCR Instruments. Results were visualized and analyzed using QuantStudio® 3D Analysis Suite™ Cloud Software (Thermo Fisher). The automatic call assignments for each data cluster were manually adjusted when needed. The MAF was calculated as the ratio of mutant DNA molecules to the sum of mutant and wt DNA molecules.

The LOD and limit of quantitation (LOQ) of the dPCR assays for *ALK* variants were evaluated for four custom TaqMan® assays by mixing DNA from two different plasmids an one patient sample harboring the specific *ALK* mutations in a background of wt DNA (from healthy donors) at different mutant allele concentrations (i.e., 1%, 0.5%, 0.1%, 0.05%). LOD and LOQ were estimated for an input of cfDNA of 7 ng. Specifically, LOD and LOQ for *ALK* G1202R assay were estimated using a patient sample. The mutation was previously confirmed by NGS. LOD and LOQ for *ALK* S1206Y were estimated using *ALK*_1 plasmid. Finally, LOD and LOQ for *ALK* L1196M and G1269A assays were estimated using *ALK*_3 plasmid. Plasmids were designed by Classic GeneArt Gene Synthesis Portal (Thermo Fisher). Schematic plasmid

maps are available upon request. LOD and LOQ were calculated based on the standard deviation of the response and the slope according to ICH Q2 (R1) guidelines (Validation of analytical procedures: text and methodology). The standard deviation of the response was calculated based on standard error of the y-intercept. Results of the detection sensitivity of TaqMan assays are displayed in Data S1. Overall, mutant allele frequencies correlated with the expected mutant allele frequencies in all cases (Pearson's correlation coefficient, 0.9999, 0.9991, 0.9994, and 0.9994 for G1202R, S1206Y, L1196M, and G1269A, respectively). LOD were 0.05%, 0.23%, 0.19%, and 0.18% for G1202R, S1206Y, L1196M, and G1269A, respectively. Additionally, 10 wt cfDNA from healthy donors were used to evaluate the false-positive signals. *ALK* mutations were not detected in any of the wt samples.

Samples were considered to be positive when the MAF was greater than or equal to 0.1% and when there were at least 300 copies·mL^{-1} of wt DNA. A negative control DNA (wt) and a blank sample (containing no DNA) were included in every run.

In order to discard that mutations detected by NGS were not clonal hematopoiesis-derived mutations (specifically those in *TP53*), DNA from peripheral blood mononuclear cells (PBMCs) was analyzed in 10 samples by dPCR or Sanger sequencing (Table S3). To this aim, DNA was isolated from PBMCs using Maxwell® RSC Whole Blood DNA Kit (Promega Corporation, Madison, WI, USA) according to the manufacturer's instructions. Custom primer sequences to target specific *TP53* regions (exon 2, exon 4, exon 7, and exon 8 splice site) were designed using the Primer3plus software. PCR reactions were performed in a 15-μL volume comprising 7.5 μL of 20X QuantStudio 3D Master Mix, 5.5 μL of H_2O, 0.5 μL of forward primer, 0.5 μL of reverse primer, and 1 μL of isolated DNA. PCR amplifications were carry out in the VeritiPro Thermal Cycler (Applied Biosystems). The thermal program included an initial step of 94 °C for 10 min, follow by 40 cycles of denaturation at 94 °C for 30 s, annealing at 60 °C for 1 min and extension at 72 °C for 30 s, and finally, at 72 °C for 7 min. Amplified DNA samples were subjected to electrophoresis with 2% agarose gel, stained with GelRed ™ Nucleic Acid Gel Stain, 10 000X in Water (Biotium, Hayward, CA, USA), and examined under an UV transilluminator. Products revealing clear PCR bands were purified by adding 2 μL of ExoSAP-IT reagent (GE Healthcare®, Madison, WI, USA) for each 5 μL of preamplification volume and incubated for 15 min at 37 °C followed by 15 min at 80 °C. One microliter of PCR product was subjected to Sanger sequencing using PCR primers and the BigDye™ Terminator v1.1 Cycle Sequencing Kit (Applied Biosystems). The thermal program included an initial step of 94 °C for 10 min, follow by 25 cycles of denaturation at 94 °C for 10 s, annealing at 50 °C for 10 s and extension at 60 °C for 2 min. The PCR product was purified with the protocol of the BigDye® XTerminator™ Purification Kit (Applied Biosystems) and sequenced with the forward and reverse PCR primers on ABI PRISM 310 Genetic Analyzer (Applied Biosystems). Sequence data were analyzed on SEQUENCING ANALYSIS Software 7 v7.0 (Applied Biosystems).

To increase the detection rate for variants at the *ALK* locus, we have developed a bioinformatic pipeline, called the V*ALK* tool (available at GitHub: https://github.com/AtochaHUPH/VALK-tool-), which is capable of fully automating the filtering generating a.csv file containing the output variants and a list of their properties. Specific conditions for single nucleotide variants (SNVs), indels, multiple-nucleotide polymorphisms (MNP), fusions and copy-number variation (CNV) calls were defined. The nonfiltered-oncomine.tsv file with variants in 'Variant Call Format' was obtained for the 28 samples. All variants that have passed the Oncomine Variants (v.5.12, Thermo Fisher) filter were included in the final analysis. In addition, we performed a second filtering process in order to rescue other somatic variants ruled out by the Oncomine Variants (v.5.12) filter. Specifically, parameters such as the overall error of the NGS assay, the LOD, the coverage depth, the percentage of targeted bases sequenced at that coverage depth, the total number of target reads covering a variant region, the number of reads supporting a specific variant, and the clinical significance, among others, were taken into account for the selection of the different thresholds. Figure S1 shows the selection criteria based on certain variables as presented in the nonfiltered-oncomine.tsv file.

All computations were performed in R v.3.6.3 (R Foundation for Statistical Computing, Vienna, Austria) using additional packages. Specifically, the Tcl/Tk package that was used to provide the end-user an intuitive graphical interface to carry out the entire filtering process. In addition, the Scales (v1.1.1; https://scales.r-lib.org/) package, which contains functions that convert data values to perceptual properties, was used to transform the raw data obtained from the nonfiltered-oncomine.tsv files into interpretable values for the end-user. Positive and negative percentage agreement (PPA and NPA) and overall rates of agreement (ORA) of the V*ALK* tool for detecting the *ALK* mutations specified in Table S4 were calculated considering the

imperfect reference standard the dPCR result and using the two independent data sets, the *ALK* cohort and the Valencia cohort, which consists of 54 cfDNA samples from NSCLC patients.

2.3. Statistical analysis

Median follow-up was estimated by the reverse Kaplan–Meier method. Overall survival (OS) was defined as the time from the start of treatment with an *ALK* inhibitor to death or last follow-up. PFS was defined as the time between the start of an *ALK* inhibitor and disease progression (as ascertained by RECIST criteria), death, or the censored date of the last assessment, whichever occurred first. The log-rank test was used to assess statistical differences between Kaplan–Meier survival curves. Hazard ratios were estimated from the Cox model using a multivariable approach adjusted for sex, cooperative oncology group (ECOG) performance status, and lines of *ALK*-TKI. Association between clinicopathological variables and genomic features was assessed by Mann–Whitney and Fisher's exact test as needed. Values of $P < 0.05$ were considered statistically significant. Statistical analyses were performed using Stata 15.1 (Stata Corporation, College Station, TX, USA).

3. Results

3.1. Study cohort

We collected and analyzed 26 plasma and two CSF specimens from 24 metastatic patients diagnosed with an *ALK*-positive NSCLC who were progressing on an *ALK*-I. Baseline clinicopathological characteristics of the study population ($N = 24$) are presented in Table 1. The median age at diagnosis was 53 years (range, 36–72 years) and 58.3% were females. The majority of the patients were never smokers (62.5%) and the most frequent histology was adenocarcinoma (95.8%). ECOG Performance Status at study entry varied from 0 to 2. As shown in Fig. 1, two samples from two patients were collected upon disease progression while on two consecutive lines of treatment with an *ALK*-I; three samples were obtained from one patient upon failure to three consecutive lines of *ALK*-I; all 21 other members of the cohort each provided a single sample.

As presented in Fig. 1, 13 samples corresponded to *ALK*-I-naïve patients who progressed on a first-line crizotinib ($N = 11$) or alectinib ($N = 2$) treatment. For these patients, the median PFS and OS were 11.6 months (95% CI: 6.5–20.9 months) and 24.6 months (95% CI: 11.8–NR months), respectively. In addition, 12 samples corresponded to patients who had received previously crizotinib and were treated with a second-generation *ALK*-I. Finally, the cohort included two samples from patients progressing on lorlatinib after failure of a prior second-generation *ALK*-I and one patient progressing on alectinib who had previously received crizotinib plus two second-generation *ALK*-I. Detailed information about treatment lines is presented in Table S5. The median PFS and OS for patients progressing on a second or subsequent line with an *ALK*-I were 5.4 months (95% CI: 2–9.1) and 11.2 months (95% CI: 3–NR) months, respectively.

Table 1. Baseline characteristics of the study cohort.

Feature		*N*	%
Age of diagnosis (years)	Median (range)	53 (36–72)	
Sex	Male	10	41.7
	Female	14	58.3
Smoking status	Current smoker	3	12.5
	Ex-smoker	6	25
	Never-smoker	15	62.5
ECOG performance status	0	12	50
	1	11	45.8
	2	1	4.2
Histology	Adenocarcinoma	23	95.8
	Neuroendocrine carcinoma	1	4.2
Clinical stage at diagnosis	III	6	25
	IV	18	75

3.2. Next-generation sequencing analysis upon disease progression

Overall plasma samples yielded higher cfDNA concentrations than CSF. Despite the small sample size of the study cohort, the median concentration of cfDNA isolated from CSF was significantly lower (0.20 $ng{\cdot}\mu L^{-1}$) than median concentration of cfDNA obtained from plasma samples (1.94 $ng{\cdot}\mu L^{-1}$; $P = 0.039$; calculated by Mann–Whitney test).

The average mapped reads per sample was 9 775 623, resulting in a median overall sequencing depth of 25 322. The median read coverage per sample was 21 261 and the median molecular coverage per sample was 1670.8. Regarding the two CSF samples, taken from patients with CNS disease, the average mapped reads per sample was 8 268 194, resulting in a median overall sequencing depth of 9318.

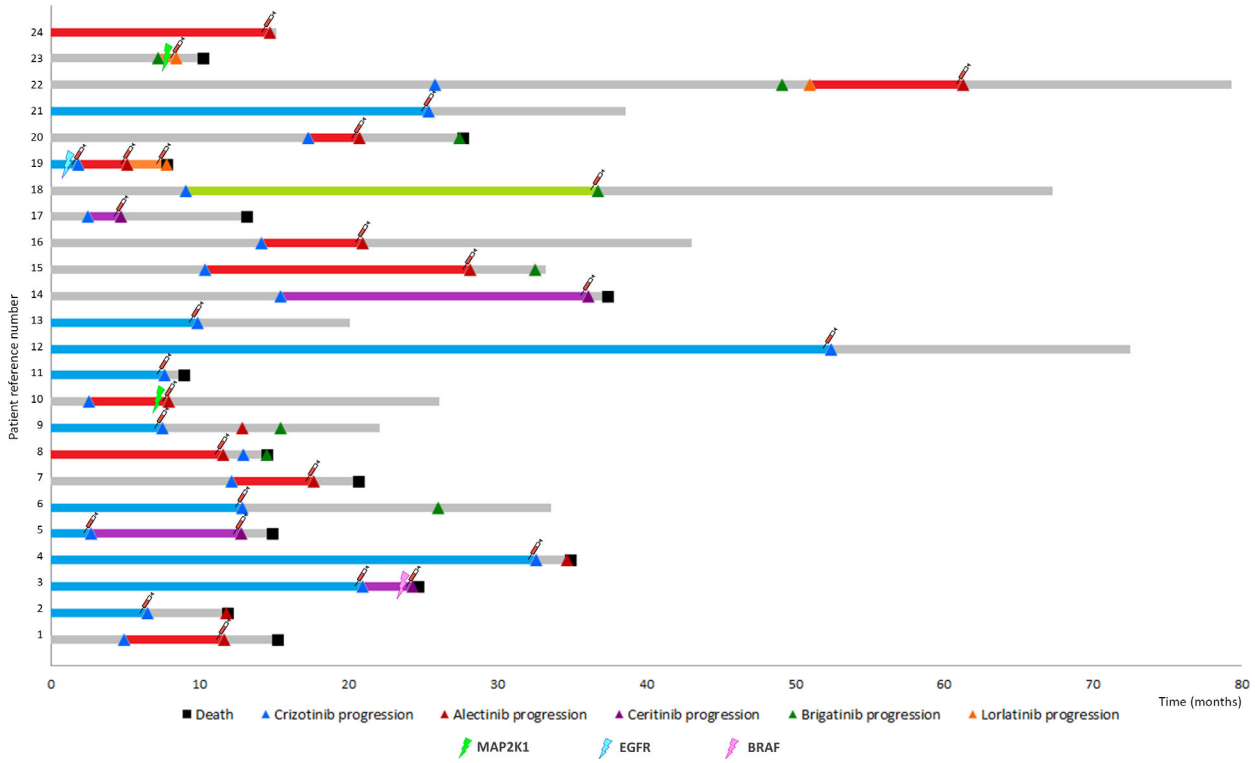

Fig. 1. Swimmer chart showing the individual treatment responses of the study cohort. Blue, red, purple, green, and orange bars correspond to response duration of patients who were treated with crizotinib, alectinib, ceritinib, brigatinib, and lorlatinib, respectively, and from whom a blood sample was taken at the time of disease progression (syringe icon). Gray bars denote treatments responses to therapy for which samples at disease progression could not be analyzed (out of study). Tumor progression is denoted by triangle, and patient's death is denoted by a squared. Mutations in *BRAF, EGFR,* and *MAP2K1* are indicated by a lightning.

In total, 61 somatic variants in ctDNA from 24 samples were detected. In three patients, no mutations were found. One of the patients with undetectable plasma ctDNA had progressed exclusively at the brain level. The average number of mutations per patient was 2.18 and the median MAF was 0.39%, with a minimum MAF of 0.02% and a maximum of 5.09%. As expected, SNPs were the most frequent mutation type ($N = 48$). In addition, we identified 10 indels and three CNVs (Fig. 2). Specifically, a c-*MYC* gain in conjunction with a *CCND1* and an *FGFR3* loss was detected in a patient progressing on a first line with crizotinib. This patient also harbored a mutation in *TP53* (Fig. 2).

As illustrated in Fig. 2, somatic mutations were detected in 14 genes: *TP53, ALK, PIK3CA, SMAD4, MAP2K1 (MEK) FGFR2, FGFR3, BRAF, EGFR, IDH2, MYC, MET, CCND3, and CCND1*. All the variants detected are listed in Table S6. Thirteen variants (12 of which were in the *ALK* locus and one was in the *EGFR* gene) were categorized as being of strong clinical significance. Mutations in *TP53* gene were further tested in PBMCs in order to discard a clonal hematopoietic origin (Table S3).

3.3. Identification of acquired resistance mutations in the *ALK* locus upon disease progression

To increase the sensitivity for detecting somatic mutations in the *ALK* locus, we developed an algorithm named V*ALK* tool. The tool has been specifically designed for the analysis of the NGS data obtained from liquid biopsies. Among other parameters, the algorithm takes into account the molecular depth and molecular counts as well as specific regions that are more likely for false-positive calls. In order to test the analytical performance of the tool, all SNPs in the *ALK* locus that were present in the nonfiltered-oncomine.tsv file were analyzed by dPCR. In total, 19 *ALK* variants from 22 samples were evaluated (Table S4). Considering the nonreference standard the dPCR result PPA, NPA, and overall percent agreement of *ALK* mutation detection for the V*ALK* tool

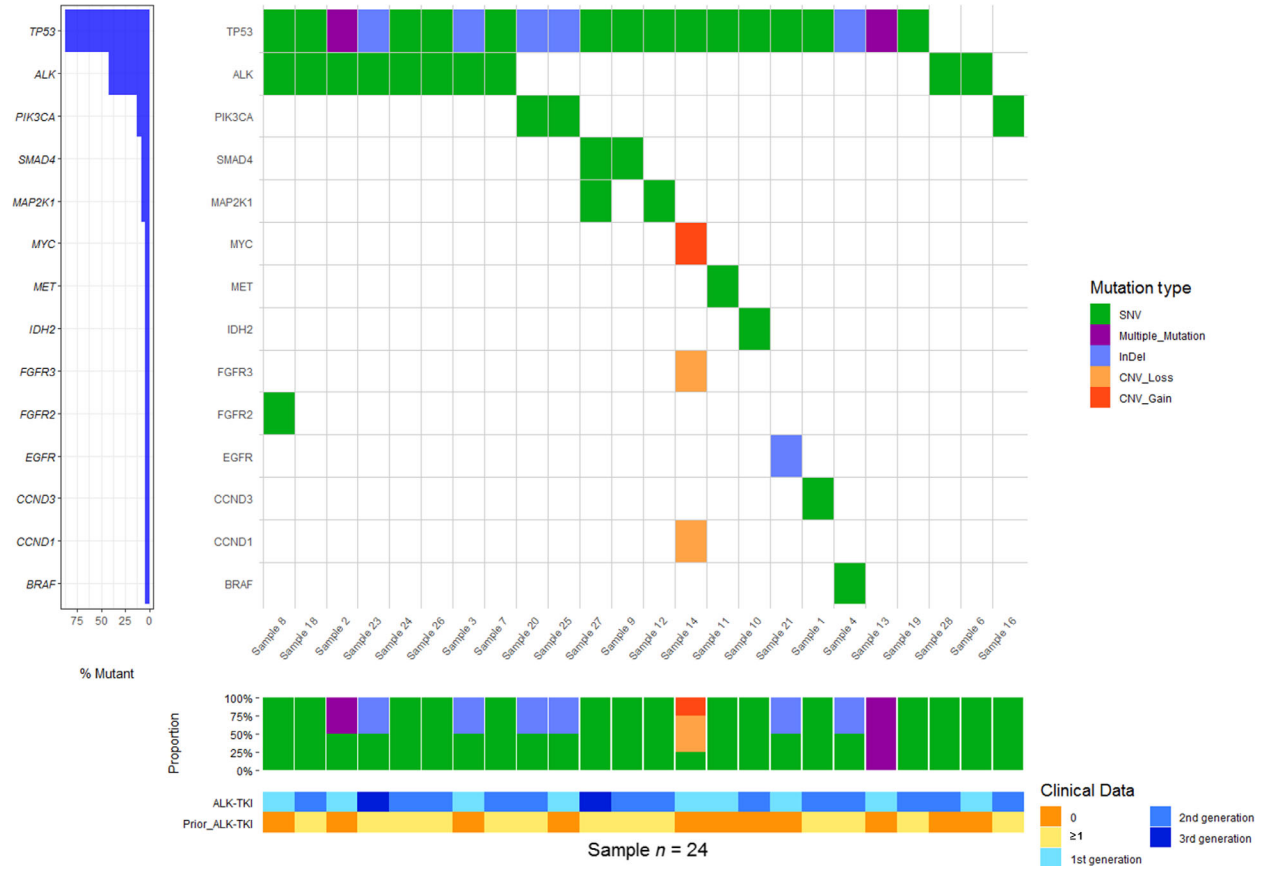

Fig. 2. Co-mutation plot according to ctDNA profiling by NGS. Each column represents data from a single patient. Each row represent data from a specific gene. Indels are represented in blue whereas missense mutations are represented in green. CNVs are colored in orange. Heat map at the bottom illustrates type of treatment received.

were 67% (95% CI: 35–90%), 93% (95% CI: 75–99%), and 85% (95% CI: 69–94%), respectively (Table S7). To validate the final algorithm (locked prior to analyses), a second independent batch of 54 samples provided by a different laboratory (Valencia cohort) was used. In this case, the PPA, NPA, and ORA were 100% (95% CI: 29–100%), 98% (95% CI: 90–100%), and 98% (95% CI: 90–100%), respectively. Cross-tables describing PPA, NPA, and ORA for the V*ALK* tool as well as for the Oncomine variants v5.10 using *ALK* and Valencia cohorts are presented in Table S7–S10.

Overall, in the *ALK* cohort we detected at least one *ALK* mutation in 10 (38.5%) plasma samples collected upon disease progression (Table 2, and Fig. S2). Notably, the Oncomine variants v5.10 filter only detected *ALK* mutations in three patients (Table 2).

The G1202R mutation was identified in four patients who had progressed on alectinib ($N = 3$) and ceritinib ($N = 1$; patient number 5). Specifically, in case of the patient progression on ceritinib (patient 5), this mutation was not detected at treatment initiation confirming its role as a resistance mutation (Table S11). In addition, the S1206Y mutation was detected along with the G1202R mutation in one of the aforementioned alectinib-progressing patients. This patient had been treated with crizotinib before initiating alectinib treatment. The low MAF of the S1206Y mutation suggests that it could be responsible for the previous crizotinib failure and it could have been decreased since alectinib therapy. In addition, the G1269A mutation was detected upon crizotinib failure in two cases and the L1196M mutation was identified after progression to crizotinib and lorlatinib. The latter was detected together with the R1275Q mutation in a patient diagnosed with an *ALK*-positive neuroendocrine carcinoma (patient 19). Of note, neither the L1196M mutation nor the R1275Q mutation was detected in the pre-treatment plasma sample from patient 19 (Table S11). Finally, the A1200V mutation

Table 2. Somatic mutations detected at the *ALK* locus upon treatment failure.

No. of patient	Nucleotide change	Amino acid change	Progression to	Line of treatment	Filter	MAF NGS (%)	MAF dPCR (%)	Total dPCR input (ng)
Patient 2	c.3599C>T	p.A1200V	Crizotinib	First line	nonfiltered-oncomine.tsv	0.02	0.04	42.07
Patient 3	c.3806G>C	p.G1269A	Crizotinib	First line	Oncomine 5.10/ *VALK* tool	3.36	2.82	4.64
Patient 5	c.3806G>C	p.G1269A	Crizotinib	First line	Oncomine 5.10/ *VALK* tool	0.88	0.42	7.20
Patient 5	c.3604G>A	p.G1202R	Ceritinib	Second line	Oncomine 5.10/ *VALK* tool	1.28	2.12	54.04
Patient 6	c.3586C>A	p.L1196M	Crizotinib	First line	nonfiltered-oncomine.tsv	0.02	0.06	27.10
Patient 16	c.3617C>A	p.S1206Y	Alectinib	Second line	*VALK* tool	0.06	0.01	26.50
Patient 16	c.3604G>A	p.G1202R	Alectinib	Second line	*VALK* tool	0.04	0.04	26.50
Patient 19	c.3586C>A	p.L1196M	Lorlatinib	Third line	nonfiltered-oncomine.tsv	0.05	0.05	29.24
Patient 19	c.3824G>A	p.R1275Q	Lorlatinib	Third line	nonfiltered-oncomine.tsv	0.03	0.04	21.80
Patient 20	c.3604G>A	p.G1202R	Alectinib	Second line	*VALK* tool	0.05	0.32	14.11
Patient 22	c.3604G>A	p.G1202R	Alectinib	Fourth line	*VALK* tool	0.03	0.01	48.05
Patient 24	c.3538G>C	p.V1180L	Alectinib	First line	nonfiltered-oncomine.tsv	0.37	0.35	16.67

($N = 1$) was detected in a sample collected after crizotinib failure, and the V1180L mutation ($N = 1$) was detected in a patient progressing on a first-line treatment with alectinib (Table 2).

3.4. Other molecular mechanisms underlying resistance to *ALK*-I

A deletion in exon 19 of the *EGFR* gene, a non-V600 *BRAF* mutation, and the F129L mutation in *MAP2K1* (MEK1) were identified in four patients who showed no objective survival benefit from *ALK*-Is. None of these patients had a secondary mutation in *ALK* locus.

Notably, the patient harboring the E746_A750del mutation in the *EGFR* gene had a PFS time of 1.8 months under first-line crizotinib treatment. The patient was subsequently treated with alectinib but tumor progression was assessed 3.1 months later prompting a switch of treatment to lorlatinib, but that also failed after 1.8 months, suggesting that the tumor had primary resistance to *ALK*-Is (Fig. 1, Table 3). Similarly, a non-V600 *BRAF* mutation, namely G466V, was identified in the CFS collected upon disease progression to ceritinib. While PFS with first-line crizotinib was 21 months, disease progression was assessed within 3 months of starting second-line ceritinib treatment (Fig. 1). Remarkably, the non-V600 *BRAF* mutation was absent in the plasma sample collected before ceritinib initiation (Table S11). Likewise, two patients harboring the F129L mutation in *MAP2K1* (*MEK1*) obtained little benefit from second-line *ALK*-I (Fig. 1, Table 3). This mutation was detected upon disease progression to alectinib (patient 10) and lorlatinib (patient 23). In case of patient 10, we could confirm that this mutation was not present in the pre-treatment plasma sample and tumor biopsy (Table S11). Noteworthy, the median PFS and OS for second-line treatment for these patients were less than one month (0.97) and 3 months, respectively, whereas median the PFS and OS for patients progressing on a second or subsequent lines with an *ALK*-I but without mutations in *MAP2K1* were 5.9 and 11.2 months (P log-rank < 0.05 in both cases; Fig. S3).

Potential *ALK*-I resistance mutations were also found in *IDH2, PIK3CA,* and *MYC* (Table 3). Specifically, the oncogenic mutations E545K and E545A in the *PIK3CA* gene were detected in the plasma sample of two patients progressing on ceritinib and brigatinib (Table 3). These mutations were not detected in the pre-treatment sample (Table S11). Likewise, the gain-of-function mutation in *IDH2*, R140Q, was detected upon disease progression to first-line alectinib treatment. Finally, as previously mentioned, a c-*MYC* amplification was detected jointly with a loss of *CCND1* and of *FGFR3*.

Table 3. Resistance mutations detected in loci other than *ALK* upon tumor progression.

Patient	Treatment	Treatment line	Sample	HUGO symbol	Amino acid change	Nucleotide change/CNV	Type	Variant class (Tier)	Transcript	rs	COSM
Patient 8	Alectinib	1st	Sample 10	*IDH2*	p.R140Q	c.419G>A	SNV	Potential clinical significance	NM_002168.3	–	COSM41590
Patient 14	Ceritinib	2nd	Sample 16	*PIK3CA*	p.E545K	c.1633G>A	SNV	Potential clinical significance	NM_006218	rs104886003	COSM763
Patient 18	Brigatinib	2nd	Sample 20	*PIK3CA*	p.E545A	c.1634A>C	SNV	Potential clinical significance	NM_006218	rs121913274	COSM12458
Patient 3	Ceritinib	2nd	Sample 4	*BRAF*	p.G466V	c.1397G>T	SNV	Potential clinical significance	NM_004333.4	rs121913351	COSM451
Patient 10	Alectinib	2nd	Sample 12	*MAP2K1*	p.F129L	c.385T>C	SNV	Potential clinical significance	NM_002755.3	rs1057519805	COSM1570285
Patient 12	Crizotinib	1st	Sample 14	*MYC*		Gain (3.08)	CNV	Potential clinical significance	NM_005359.5	–	
Patient 19	Crizotinib	1st	Sample 21	*EGFR*	p.E746_A750del	c.2235_2249delGGAATTAAGAGAAGC	InDel	Strong clinical significance	NM_005228.4	–	COSM6223
Patient 23	Lorlatinib	2nd	Sample 27	*MAP2K1*	p.F129L	c.385T>C	SNV	Potential clinical significance	NM_002755.3	rs1057519805	COSM1570285

4. Discussion

ALK-Is have dramatically improved outcomes in NSCLC patients [17]. However, despite the impressive responses they elicit, patients invariably relapse due to acquired resistance mutations. Solid biopsies remain the gold standard for biomarker testing. However, logistics for obtaining repeat tumor biopsies are complicated and seldom feasible leading to an empirical prescription of sequential *ALK*-Is. Nevertheless, blinding treatment sequential strategies might have a deleterious effect on patient's survival due to the incompletely overlapping *ALK* mutation coverage of different *ALK*-Is. In this exploratory analysis, we show that plasma NGS is feasible and we propose several different mechanisms which may underlie resistance to *ALK* Inhibitors (*ALK*-Is). Unfortunately, we did not have available data or plasma/tissue samples collected at baseline in 18 of the 24 patients included in the study, which may constitute an important limitation. Importantly, we also provide an algorithm capable of retrieving somatic mutations in the *ALK* locus that would otherwise be discarded by the commercial bioinformatic pipeline. As presented in Table 2, the commercial pipeline only detected three out of 12 mutations. MAFs of variants detected by the commercial pipeline were 2.8%, 2.1%, and 0.4%. According to the manufacturer's specifications, the LOD, in terms of MAF, for mutations is 0.1%. However, in our hands, mutations with a MAF below 0.5% are seldom detected by the commercial pipeline. By using the V*ALK* pipeline, some mutations that would otherwise have been missed can be rescued. Yet, confirmation using an alternative technique such as dPCR would be required to rule out false-positive calls.

Regarding acquired mutations in the *ALK* locus, our results are consistent with those of previous studies. Specifically, secondary mutations were detected in the plasma samples of 4 of the 11 (36%) patients treated with first-line crizotinib, with the G1269A mutation being detected in two cases. In this regard, mutation detection rate after crizotinib failure might vary from 60% [18] to 24% [19], G1269A being the most prevalent mutation. We also detected the L1196M and S1206Y mutations, which have been reported to occur in 7% and 2% of cases, respectively, of *ALK*-positive NSCLC patients treated with crizotinib [11]. Finally, we detected the A1200V mutation after crizotinib failure in one patient. This mutation is also known to appear upon crizotinib progression [18]. In addition, we found that the G1202R mutation was identified in three of the 10 patients (30%) progressing on alectinib. This mutation is known to arise after treatment with second-generation *ALK*-Is [11]. Recently, Noé *et al.* [20] reported a 53% *ALK* mutation detection rate in samples obtained post-progression on alectinib in which G1202R was the most frequent mutation. In our cohort, more than one mutation in *ALK* locus was detected in two samples collected during second- and third-generation *ALK*-I treatment. Likewise, it has been described that *ALK* resistance mutations become more frequent with each successive generation of *ALK*-I as sequential treatment may promote the appearance of resistance mutation at the *ALK* locus [21].

A reduced number of studies analyzing samples collected upon progression to an *ALK*-I by NGS have so far been conducted [11,18]. To our knowledge, there are only two studies describing NGS analysis of *EML4-ALK* NSCLC liquid biopsy samples using Oncomine™ Pan-Cancer Cell-Free Assay and both are case reports [22,23]. Overall all, our results are in agreement with other studies [11]. However, some genes such as *IGF-1R* and *SRC,* which have been described to be relevant for *ALK* resistance, were not included in the used panel. Genomic alterations responsible of treatment failure can be detected analyzing different components of bloodstream, most notably circulating tumor cells (CTCs) and cfDNA [19,24,25]. However, it has been proposed that cfDNA is the best strategy for sequencing analyses [26]. Nonetheless, assays for the detection of *EML4-ALK* fusion protein in CTCs have been developed [27]. Consistent with our results, mutations in *TP53, FGFR2, PIK3CA, and MET* have been identified in the tumor biopsy of patients progressing on ceritinib [11]. The E545K and E545A mutations in *PIK3CA* have not only been detected upon progression in advanced *ALK*-positive NSCLC patients, but also in *EGFR*-positive NSCLC patients [28,29]. The *IDH2* R140Q detected in our cohort is known to transform cells in vitro and induces myeloid and lymphoid neoplasms in mice [30,31]. This mutation is also frequent in angioimmunoblastic T-cell lymphoma [32]. In NSCLC, *IDH1/2* mutations are rarely detected in primary tumors but it has been suggested that they could be branching drivers leading to subclonal evolution, based on the MAFs at which these mutations are detected [33]. In this way, Zhao *et al.* [34] described a case of *an ALK*-positive tumor in which an *IDH1* variant was detected upon disease progression.

Also, we found the E746_A750del mutation in one patient who did not benefit from treatment with *ALK*-Is. Unfortunately, we could not orthogonally validate the presence of the *ALK* translocation nor the *EGFR* variant at baseline due to lack of tissue, which may constitute a limitation of the present study. However, it has been previously reported that mutations in *EGFR* in some NSCLC tumors coexist alongside *ALK*

rearrangements, although this is, at best, a rare event [35,36]. Concomitant *ALK* and *EGFR* alterations may lead to primary resistance to *ALK*-I [37]. Likewise, a non-V600 *BRAF* mutation was detected after 3 months of treatment with second-line ceritinib treatment, suggesting that resistance of the tumor to the *ALK*-I could be due to the acquisition of the *BRAF* mutation. It has been reported that ceritinib enhances the efficacy of trametinib, a MEK inhibitor, in *BRAF*/*NRAS*-wt melanoma cell lines [38], which makes it plausible that ceritinib would not have any effect in *BRAF*-mutated cells. Finally, two patients in whose plasma sample the F129L-activating mutation in *MAP2K1* (MEK1) was detected, exhibited marked resistance to second- and third-generation *ALK*-Is. Of note, we did not detect this mutation at baseline in one of these patients, supporting its role as a resistance mutation. In this way, this mutation has been identified as the molecular mechanism underlying *MEK*/*ERK* pathway activation in resistant clones of human HT-29 colon cancer cells [39]. Moreover, the activation of this downstream pathway is critical to the survival of *ALK*-positive NSCLC cells [40,41]. Indeed, the combination of *ALK* and *MEK* inhibition was highly effective at suppressing tumor growth in a preclinical model of *EML4-ALK* NSCLC [42]. Taken together, it is plausible that the F129L-activating mutation in *MAP2K1* is an acquired mutation that leads to tumor resistance to *ALK*-Is.

Mutations in the *FGFR2* and *FGFR3* genes were detected in two patients progressing on *ALK*-Is, suggesting sensitivity to fibroblast growth factor receptor inhibitors. It has been reported that alectinib, despite being a potent *ALK*-I, has limited inhibitory activity against other protein kinases such as *FGFR2* [43]. In this way, clinical trials evaluating the efficacy of combinations of *ALK*-Is with *FGFR* inhibitors would be of particular interest.

Three CNVs in c-*MYC*, *CCND1,* and *FGFR3* were detected upon disease progression in one patient, who was being treated with crizotinib. Remarkably, c-*MYC* amplification determines many oncogenic effects [44] and it has been identified as a potential mechanism of primary resistance to crizotinib in *ALK*-rearranged NSCLC patients [45]. It has been previously suggested by Alidousty *et al*. that co-occurrence of early *TP53* mutations in *ALK*$^+$ NSCLC can lead to chromosomal instability. Specifically, authors reported that, in a subset of 53 *ALK*$^+$ tumors, up to a quarter of *TP53*-mutated tumors showed amplifications of known cancer genes such as *MYC* or *CCND1* [46]. Consistent with this, we detected the P92A and V157F mutations in the *TP53* gene in the same plasma sample of this patient.

5. Conclusions

In conclusion, our data show that molecular mechanisms underlying treatment failure seem to involve different pathways. NGS analysis of liquid biopsies collected upon disease progression is feasible and a valuable approach toward personalized that will lead to better care for *ALK*-positive NSCLC patients.

Acknowledgements

The authors wish to thank the donors, and the BIOBANK HOSPITAL UNIVERSITARIO PUERTA DE HIERRO MAJADAHONDA (HUPHM)/INSTITUTO DE INVESTIGACIÓN SANITARIA PUERTA DE HIERRO-SEGOVIA DE ARANA (IDIPHISA) (PT17/0015/0020 in the Spanish National Biobanks Network) for the human specimens used in this study. This study has been funded by Instituto de Salud Carlos III through the project 'PI17/01977' (Co-funded by European Regional Development Fund/European Social Fund 'A way to make Europe'/'Investing in your future'). The work presented in this paper also received funding from the European Union's Horizon 2020 research and innovation program under grant agreement No 875160. ES was funded by the Consejería de Ciencia, Universidades e Innovación of the Comunidad de Madrid (Doctorados Industriales of the Comunidad de Madrid IND2019/BMD-17258). RS was funded by the Consejería de Educación, Juventud y Deporte of the Comunidad de Madrid and by the Fondo Social Europeo (Programa Operativo de Empleo Juvenil, and Iniciativa de Empleo Juvenil, PEJD-2018-PRE/BMD-8640).

Conflict of interest

MP reports personal fees from Roche, BMS, MSD Pfizer, Lilly, Novartis, and Takeda grants and personal fees from AstraZeneca, and Boehringer during the conduct of the study. VC reports personal fees from Roche BMS, MSD, Pfizer, Lilly, AstraZeneca, Boehringer, Novartis, Takeda, during the conduct of the study. MD reports personal fees from Astra-Zeneca, BMS, Boehringer Ingelheim, MSD, Pfizer and Roche. The rest of the authors have declared no conflict of interest.

Data accessibility

This paper is available as a preprint in Research Square server, https://doi.org/10.21203/rs.3.rs-86055/v1 (https://www.researchsquare.com/article/rs-86055/v1).

Author contributions

AR and MP conceived and /or designed the work. ES and RS have carried out statistical analyses. VI has developed V*ALK* tool. All authors have made substantial contributions to the acquisition and interpretation of data. AR and ES have drafted and revised the manuscript. All authors have approved the final version. Each author agreed to be accountable for all aspects of the work in ensuring that questions related to the accuracy or integrity of any part of the work are appropriately investigated and resolved.

Peer Review

The peer review history for this article is available at https://publons.com/publon/10.1002/1878-0261.13033.

References

1 Shaw AT, Yeap BY, Solomon BJ, Riely GJ, Gainor J, Engelman JA, Shapiro GI, Costa DB, Ou S-HI, Butaney M *et al.* (2011) Effect of crizotinib on overall survival in patients with advanced non-small-cell lung cancer harbouring ALK gene rearrangement: a retrospective analysis. *Lancet Oncol* **12**, 1004–1012.

2 Shaw AT, Kim DW, Nakagawa K, Seto T, Crinó L, Ahn MJ, De Pas T, Besse B, Solomon BJ, Blackhall F *et al.* (2013) Crizotinib versus chemotherapy in advanced ALK-positive lung cancer. *N Engl J Med* **368**, 2385–2394.

3 Gadgeel SM, Gandhi L, Riely GJ, Chiappori AA, West HL, Azada MC, Morcos PN, Lee R-M, Garcia L, Yu L *et al.* (2014) Safety and activity of alectinib against systemic disease and brain metastases in patients with crizotinib-resistant ALK-rearranged non-small-cell lung cancer (AF-002JG): results from the dose-finding portion of a phase 1/2 study. *Lancet Oncol* **15**, 1119–1128.

4 Duruisseaux M, Besse B, Cadranel J, Pérol M, Mennecier B, Bigay-Game L, Descourt R, Dansin E, Audigier-Valette C, Moreau L *et al.* (2017) Overall survival with crizotinib and next-generation ALK inhibitors in ALK-positive non-small-cell lung cancer (IFCT-1302 CLINALK): a French nationwide cohort retrospective study. *Oncotarget* **8**, 21903–21917.

5 Huber RM, Hansen KH, Paz-Ares Rodríguez L, West HL, Reckamp KL, Leighl NB, Tiseo M, Smit EF, Kim D-W, Gettinger SN *et al.* (2020) Brigatinib in crizotinib-refractory ALK+ NSCLC: 2-year follow-up on systemic and intracranial outcomes in the phase 2 ALTA trial. *J Thorac Oncol* **15**, 404–415.

6 Peters S, Camidge DR, Shaw AT, Gadgeel S, Ahn JS, Kim DW, Ou SI, Pérol M, Dziadziuszko R, Rosell R *et al.* (2017) Alectinib versus crizotinib in untreated ALK-positive non–small-cell lung cancer. *N Engl J Med* **377**, 829–838.

7 Camidge DR, Dziadziuszko R, Peters S, Mok T, Noe J, Nowicka M, Gadgeel SM, Cheema P, Pavlakis N, de Marinis F *et al.* (2019) Updated efficacy and safety data and impact of the EML4-ALK fusion variant on the efficacy of alectinib in untreated ALK-positive advanced non-small cell lung cancer in the global phase III ALEX study. *J Thorac Oncol* **14**, 1233–1243.

8 Lin JJ, Zhu VW, Yoda S, Yeap BY, Schrock AB, Dagogo-Jack I, Jessop NA, Jiang GY, Le LP, Gowen K *et al.* (2018) Impact of EML4-ALK variant on resistance mechanisms and clinical outcomes in ALK-positive lung cancer. *J Thorac Oncol* **14**, 1233–1243.

9 Doebele RC, Pilling AB, Aisner DL, Kutateladze TG, Le AT, Weickhardt AJ, Kondo KL, Linderman DJ, Heasley LE, Franklin WA *et al.* (2012) Mechanisms of resistance to crizotinib in patients with ALK gene rearranged non-small cell lung cancer. *Clin Cancer Res* **18**, 1472–1482.

10 Katayama R, Shaw AT, Khan TM, Mino-Kenudson M, Solomon BJ, Halmos B, Jessop NA, Wain JC, Yeo AT, Benes C *et al.* (2016) Cancer: mechanisms of acquired crizotinib resistance in ALK-rearranged lung cancers. *Sci Transl Med* **4**, 120ra17.

11 Gainor JF, Dardaei L, Yoda S, Friboulet L, Leshchiner I, Katayama R, Dagogo-Jack I, Gadgeel S, Schultz K, Singh M *et al.* (2016) Molecular mechanisms of resistance to first- and second-generation ALK inhibitors in ALK -rearranged lung cancer. *Cancer Discov* **6**, 1118–1133.

12 Okada K, Araki M, Sakashita T, Ma B, Kanada R, Yanagitani N, Horiike A, Koike S, Oh-hara T, Watanabe K *et al.* (2019) Prediction of ALK mutations mediating ALK-TKIs resistance and drug re-purposing to overcome the resistance. *EBioMedicine* **41**, 105–119.

13 Li J, Huang Y, Wu M, Wu C, Li X & Bao J (2018) Structure and energy based quantitative missense variant effect analysis provides insights into drug resistance mechanisms of anaplastic lymphoma kinase mutations. *Sci Rep* **8**, 10664.

14 Ettinger DS, Wood DE, Aisner DL, Akerley W, Bauman J, Chirieac LR, D'Amico TA, DeCamp MM, Dilling TJ, Dobelbower M *et al.* (2017) Non-small cell lung cancer, version 5.2017: clinical practice guidelines in oncology. *J Natl Compr Canc Netw* **15**, 504–535.

15 Provencio M, Pérez-Barrios C, Barquin M, Calvo V, Franco F, Sánchez E, Sánchez R, Marsden D, Cristóbal Sánchez J, Martin Acosta P *et al.* (2020) Next-generation sequencing for tumor mutation quantification using liquid biopsies. *Clin Chem Lab Med* **58**, 306–313.

16 Li MM, Datto M, Duncavage EJ, Kulkarni S, Lindeman NI, Roy S, Tsimberidou AM, Vnencak-Jones

CL, Wolff DJ, Younes A *et al.* (2017) Standards and guidelines for the interpretation and reporting of sequence variants in cancer. *J Mol Diagnostics* **19**, 4–23.
17 Gambacorti Passerini C, Farina F, Stasia A, Redaelli S, Ceccon M, Mologni L, Messa C, Guerra L, Giudici G, Sala E *et al.* (2014) Crizotinib in advanced, chemoresistant anaplastic lymphoma kinase-positive lymphoma patients. *J Natl Cancer Inst* **106**, djt378.
18 Yanagitani N, Uchibori K, Koike S, Tsukahara M, Kitazono S, Yoshizawa T, Horiike A, Ohyanagi F, Tambo Y, Nishikawa S *et al.* (2020) Drug resistance mechanisms in Japanese anaplastic lymphoma kinase-positive non–small cell lung cancer and the clinical responses based on the resistant mechanisms. *Cancer Sci* **111**, 932–939.
19 Horn L, Whisenant JG, Wakelee H, Reckamp KL, Qiao H, Leal TA, Du L, Hernandez J, Huang V, Blumenschein GR *et al.* (2019) Monitoring therapeutic response and resistance: analysis of circulating tumor DNA in patients with ALK+ lung cancer. *J Thorac Oncol* **14**, 1901–1911.
20 Noé J, Lovejoy A, Ou SHI, Yaung SJ, Bordogna W, Klass DM, Cummings CA & Shaw AT (2020) ALK mutation status before and after alectinib treatment in locally advanced or metastatic ALK-positive NSCLC: Pooled analysis of two prospective trials. *J Thorac Oncol* **15**, 601–608.
21 Dagogo-Jack I, Rooney M, Lin JJ, Nagy RJ, Yeap BY, Hubbeling H, Chin E, Ackil J, Farago AF, Hata AN *et al.* (2019) Treatment with next-generation ALK inhibitors fuels plasma ALK mutation diversity. *Clin Cancer Res* **25**, 6662–6670.
22 Sánchez-Herrero E, Clemente MB, Calvo V, Provencio M & Romero A (2020) Next-generation sequencing to dynamically detect mechanisms of resistance to ALK inhibitors in ALK-positive NSCLC patients: a case report. *Transl Lung Cancer Res* **9**, 366–372.
23 Berger LA, Janning M, Velthaus JL, Ben-Batalla I, Schatz S, Falk M, Iglauer P, Simon R, Cao R, Forcato C *et al.* (2018) Identification of a high-level MET amplification in CTCs and cfTNA of an ALK-positive NSCLC patient developing evasive resistance to crizotinib. *J Thorac Oncol* **13**, e243–e246.
24 Pailler E, Faugeroux V, Oulhen M, Mezquita L, Laporte M, Honore A, Lecluse Y, Queffelec P, NgoCamus M, Nicotra C *et al.* (2019) Acquired resistance mutations to ALK inhibitors identified by single circulating tumor cell sequencing in ALK-rearranged non–small-cell lung cancer. *Clin Cancer Res* **25**, 6671–6682.
25 Alix-Panabières C, Pantel K & Authors C (2021) Liquid biopsy: from discovery to clinical application. *Cancer Discov* **11**, 858–873.
26 Hofman P (2021) Detecting resistance to therapeutic ALK inhibitors in tumor tissue and liquid biopsy markers: an update to a clinical routine practice. *Cells* **10**, 168.
27 Rossi E, Aieta M, Tartarone A, Pezzuto A, Facchinetti A, Santini D, Ulivi P, Ludovini V, Possidente L, Fiduccia P *et al.* (2021) A fully automated assay to detect the expression of pan-cytokeratins and of EML4-ALK fusion protein in circulating tumour cells (CTCs) predicts outcome of non-small cell lung cancer (NSCLC) patients. *Transl Lung Cancer Res* **10**, 80–92.
28 Romero A, Serna-Blasco R, Alfaro C, Sánchez-Herrero E, Barquín M, Turpin MC, Chico S, Sanz-Moreno S, Rodrigez-Festa A, Laza-Briviesca R *et al.* (2020) ctDNA analysis reveals different molecular patterns upon disease progression in patients treated with osimertinib. *Transl Lung Cancer Res* **9**, 532–540.
29 Chaft JE, Arcila ME, Paik PK, Lau C, Riely GJ, Catherine Pietanza M, Zakowski MF, Rusch V, Sima CS, Ladanyi M *et al.* (2012) Coexistence of PIK3CA and other oncogene mutations in lung adenocarcinoma-rationale for comprehensive mutation profiling. *Mol Cancer Ther* **11**, 485–491.
30 Wang F, Travins J, DeLaBarre B, Penard-Lacronique V, Schalm S, Hansen E, Straley K, Kernytsky A, Liu W, Gliser C *et al.* (2013) Targeted inhibition of mutant IDH2 in leukemia cells induces cellular differentiation. *Science* **340**, 622–626.
31 Mylonas E, Janin M, Bawa O, Opolon P, David M, Quivoron C, Bernard OA, Ottolenghi C, DeBotton S & Penard-Lacronique V (2014) Isocitrate dehydrogenase (IDH)2 R140Q mutation induces myeloid and lymphoid neoplasms in mice. *Leukemia* **28**, 1343–1346.
32 Cairns RA, Iqbal J, Lemonnier F, Kucuk C, De Leval L, Jais JP, Parrens M, Martin A, Xerri L, Brousset P *et al.* (2012) IDH2 mutations are frequent in angioimmunoblastic T-cell lymphoma. *Blood* **119**, 1901–1903.
33 Rodriguez EF, De Marchi F, Lokhandwala PM, Belchis D, Xian R, Gocke CD, Eshleman JR, Illei P & Li MT (2020) IDH1 and IDH2 mutations in lung adenocarcinomas: evidences of subclonal evolution. *Cancer Med* **9**, 4386–4394.
34 Zhao P, Peng L, Wu W, Zheng Y, Jiang W, Zhang H, Tong Z, Liu L, Ma R, Wang L *et al.* (2019) Carcinoma of unknown primary with *EML4-ALK* fusion response to *ALK* inhibitors. *Oncologist* **24**, 449–454.
35 Yang JJ, Zhang XC, Su J, Xu CR, Zhou Q, Tian HX, Xie Z, Chen HJ, Huang YS, Jiang BY *et al.* (2014) Lung cancers with concomitant egfr mutations and ALK rearrangements: Diverse responses to EGFR-TKI and crizotinib in relation to diverse receptors phosphorylation. *Clin Cancer Res* **20**, 1383–1392.
36 Ulivi P, Chiadini E, Dazzi C, Dubini A, Costantini M, Medri L, Puccetti M, Capelli L, Calistri D, Verlicchi A *et al.* (2016) Nonsquamous, non-small-cell lung cancer patients who carry a double mutation of EGFR,

EML4-ALK or KRAS: frequency, clinical-pathological characteristics, and response to therapy. *Clin Lung Cancer* **17**, 384–390.

37 Tiseo M, Gelsomino F, Boggiani D, Bortesi B, Bartolotti M, Bozzetti C, Sammarelli G, Thai E & Ardizzoni A (2011) EGFR and EML4-ALK gene mutations in NSCLC: a case report of erlotinib-resistant patient with both concomitant mutations. *Lung Cancer* **71**, 241–243.

38 Verduzco D, Kuenzi BM, Kinose F, Sondak VK, Eroglu Z, Rix U & Smalley KSM (2018) Ceritinib enhances the efficacy of trametinib in BRAF/NRAS-wild-type melanoma cell lines. *Mol Cancer Ther* **17**, 73–83.

39 Wang H, Daouti S, Li WH, Wen Y, Rizzo C, Higgins B, Packman K, Rosen N, Boylan JF, Heimbrook D *et al.* (2011) Identification of the MEK1(F129L) activating mutation as a potential mechanism of acquired resistance to MEK inhibition in human cancers carrying the B-Raf V600E mutation. *Cancer Res* **71**, 5535–5545.

40 Hrustanovic G & Bivona TG (2015) RAS-MAPK in ALK targeted therapy resistance. *Cell Cycle* **14**, 3661–3662.

41 Hrustanovic G, Olivas V, Pazarentzos E, Tulpule A, Asthana S, Blakely CM, Okimoto RA, Lin L, Neel DS, Sabnis A *et al.* (2015) RAS-MAPK dependence underlies a rational polytherapy strategy in EML4-ALK-positive lung cancer. *Nat Med* **21**, 1038–1047.

42 Crystal AS, Shaw AT, Sequist LV, Friboulet L, Niederst MJ, Lockerman EL, Frias RL, Gainor JF, Amzallag A, Greninger P *et al.* (2014) Patient-derived models of acquired resistance can identify effective drug combinations for cancer. *Science* **346**, 1480–1486.

43 Sakamoto H, Tsukaguchi T, Hiroshima S, Kodama T, Kobayashi T, Fukami TA, Oikawa N, Tsukuda T, Ishii N & Aoki Y (2011) CH5424802, a selective ALK inhibitor capable of blocking the resistant gatekeeper mutant. *Cancer Cell* **19**, 679–690.

44 Lin CY, Lovén J, Rahl PB, Paranal RM, Burge CB, Bradner JE, Lee TI & Young RA (2012) Transcriptional amplification in tumor cells with elevated c-Myc. *Cell* **151**, 56–67.

45 Rihawi K, Alfieri R, Fiorentino M, Fontana F, Capizzi E, Cavazzoni A, Terracciano M, La Monica S, Ferrarini A, Buson G *et al.* (2019) MYC amplification as a potential mechanism of primary resistance to crizotinib in ALK-rearranged non-small cell lung cancer: a brief report. *Transl Oncol* **12**, 116–121.

46 Alidousty C, Baar T, Martelotto LG, Heydt C, Wagener S, Fassunke J, Duerbaum N, Scheel AH, Frank S, Holz B *et al.* (2018) Genetic instability and recurrent MYC amplification in ALK-translocated NSCLC: a central role of TP53 mutations. *J Pathol* **246**, 67–76.

Supporting information

Additional supporting information may be found online in the Supporting Information section at the end of the article.

Fig. S1. Flowchart of the bioinformatic pipeline optimized for the processing and assessment of variants at the *ALK* gene locus.

Fig. S2. Frequency of *ALK* missense mutations identified in the study population.

Fig. S3. PFS and OS curves according to F129L (*MAP2K1*) mutation status.

Table S1. Identification of *EML4-ALK* translocation.

Table S2. Genes included in the NGS panel used.

Table S3. DNA genotyping of PBMCs.

Table S4. List of mutations in *ALK* locus tested by dPCR.

Table S5. *ALK*-Is treatments of the study cohort.

Table S6. List of all somatic mutations detected in the study cohort.

Table S7. Cross-table describing PPA, NPA and ORA for *ALK* cohort using V*ALK* tool.

Table S8. Cross-tables describing PPA, NPA and ORA for Valencia cohort using V*ALK* tool.

Table S9. Cross-tables describing PPA, NPA and ORA for *ALK* cohort using the Oncomine Filter.

Table S10. Cross-tables describing PPA, NPA and ORA for Valencia cohort using the Oncomine Filter.

Table S11. List of the mutations detected at disease progression and status at baseline or in previous sample.

1. Supplemental Data

Limit of detection (LOD) and limit of quantitation (LOQ) for dPCR *ALK* variants custom TaqMan® assays

G1202R

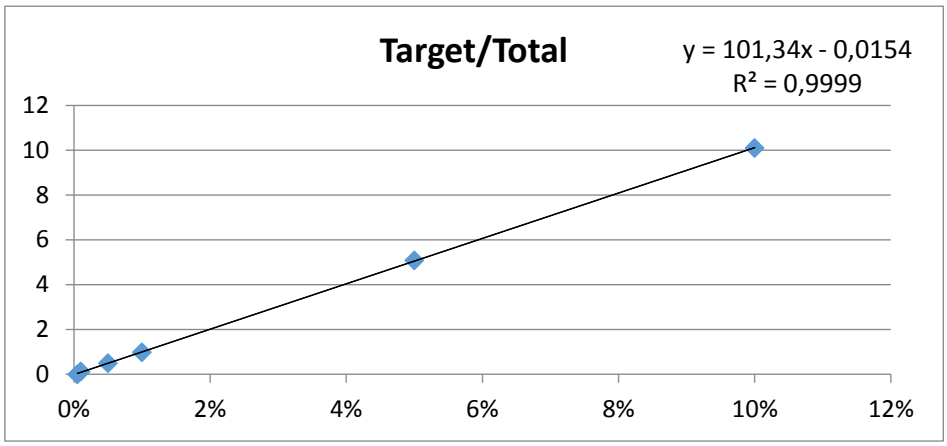

Summary Output

Regresion Statistics	
Multiple R	0.999974519
R Square	0.999949038
Adjusted R Square	0.999936297
Standard Error	0.032364871
Observations	6

ANOVA

	df	*SS*	*MS*	*F*	*Significance F*
Regression	1	82.21234139	82.21234139	78485.4679	9.73948E-10
Residual	4	0.00418994	0.001047485		
Total	5	82.21653133			

	Coefficients	*Standard Error*	*t Stat*	*P-value*	*Lower 95%*	*Upper 95%*
Intercept	-0.01540959	0.016593234	-0.92866704	0.40562786	-0.061479794	0.030660614
X Variable	101.3360813	0.361717466	280.1525797	9.7395E-10	100.3317926	102.34037

LOQ	0.16%
LOD	0.05%

Residual Output

Observation	*Predicted Y*	*Residuals*
1	10.11819854	-0.016198542
2	5.051394476	0.035605524
3	0.997951223	-0.017951223
4	0.491270817	0.000729183
5	0.085926491	0.033073509
6	0.035258451	-0.035258451

S1206Y

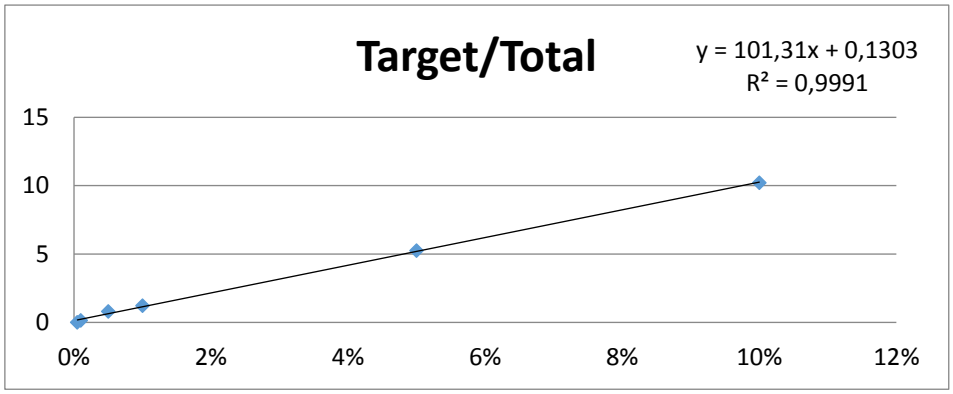

Summary Output

Regresion Statistics	
Multiple R	0.99954393
R Square	0.99908807
Adjusted R Square	0.99886008
Standard Error	0.13693202
Observations	6

ANOVA

	df	*SS*	*MS*	*F*	*Significance F*
Regression	1	82.1694818	82.1694818	4382.28387	3.1195E-07
Residual	4	0.07500151	0.01875038		
Total	5	82.2444833			

	Coefficients	*Standard Error*	*t Stat*	*P-value*	*Lower 95%*	*Upper 95%*
Intercept	0.13032351	0.07020405	1.85635311	0.13697766	-0.06459419	0.32524121
X Variable	101.309663	1.53038471	66.1988208	3.1195E-07	97.0606341	105.558692

LOQ	0.69%
LOD	0.23%

Residual Output

Observation	*Predicted Y*	*Residuals*
1	10.2612898	-0.04128983
2	5.19580667	0.05419333
3	1.14342014	0.07657986
4	0.63687183	0.16312817
5	0.23163318	-0.07163318
6	0.18097834	-0.18097834

L1196M

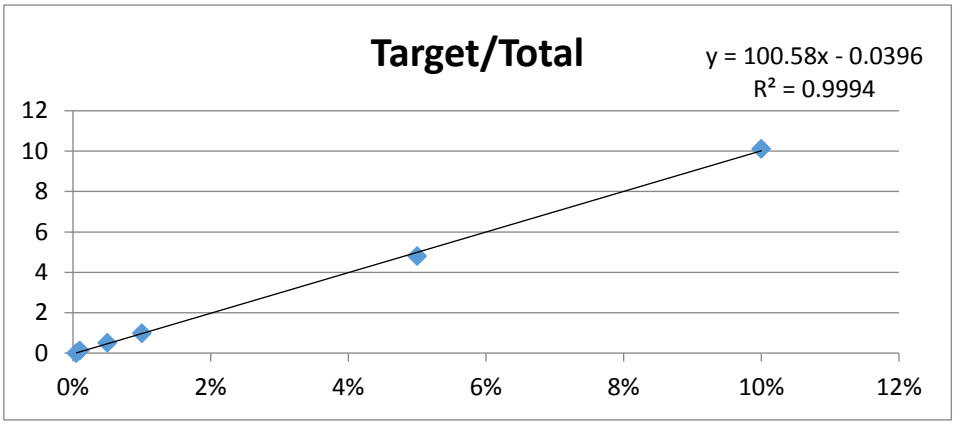

Summary Output

Regresion Statistics	
Multiple R	0.99969521
R Square	0.99939051
Adjusted R Square	0.99923813
Standard Error	0.11112779
Observations	6

ANOVA

	df	*SS*	*MS*	*F*	*Significance F*
Regression	1	80.9974858	80.9974858	6558.82716	1.3933E-07
Residual	4	0.04939754	0.01234939		
Total	5	81.0468833			

	Coefficients	*Standard Error*	*t Stat*	*P-value*	*Lower 95%*	*Upper 95%*
Intercept	-0.03955517	0.05697441	-0.69426204	0.52573106	-0.19774149	0.11863115
X Variable	100.584571	1.2419905	80.9865863	1.3933E-07	97.1362523	104.032889

LOQ	0.57%
LOD	0.19%

Residual Output

Observation	*Predicted Y*	*Residuals*
1	10.0189019	0.0910981
2	4.98967336	-0.18967336
3	0.96629054	0.01370946
4	0.46336768	0.03663232
5	0.0610294	0.0589706
6	0.01073711	-0.01073711

G1269A

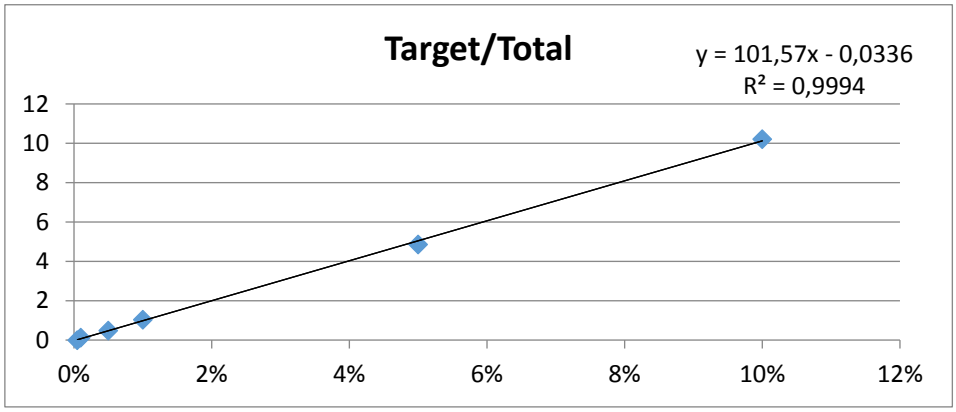

Summary Output

Regresion Statistics	
Multiple R	0.99971419
R Square	0.99942847
Adjusted R Square	0.99928558
Standard Error	0.10866516
Observations	6

ANOVA

	df	*SS*	*MS*	*F*	*Significance F*
Regression	1	82.5945175	82.5945175	6994.72402	1.2252E-07
Residual	4	0.04723247	0.01180812		
Total	5	82.64175			

	Coefficients	*Standard Error*	*t Stat*	*P-value*	*Lower 95%*	*Upper 95%*
Intercept	0.03360485	0.05571184	0.60319053	0.57891416	-0.18828571	0.12107601
X Variable	101.571346	1.21446755	83.6344667	1.2252E-07	98.1994436	104.943249

LOQ	0.55%
LOD	0.18%

Residual Output

Observation	*Predicted Y*	*Residuals*
1	10.1235298	0.08647025
2	5.04496245	-0.18496245
3	0.98210861	0.04789139
4	0.47425188	0.01574812
5	0.06796649	0.05203351
6	0.01718082	-0.01718082

2. Supplementary Figures.

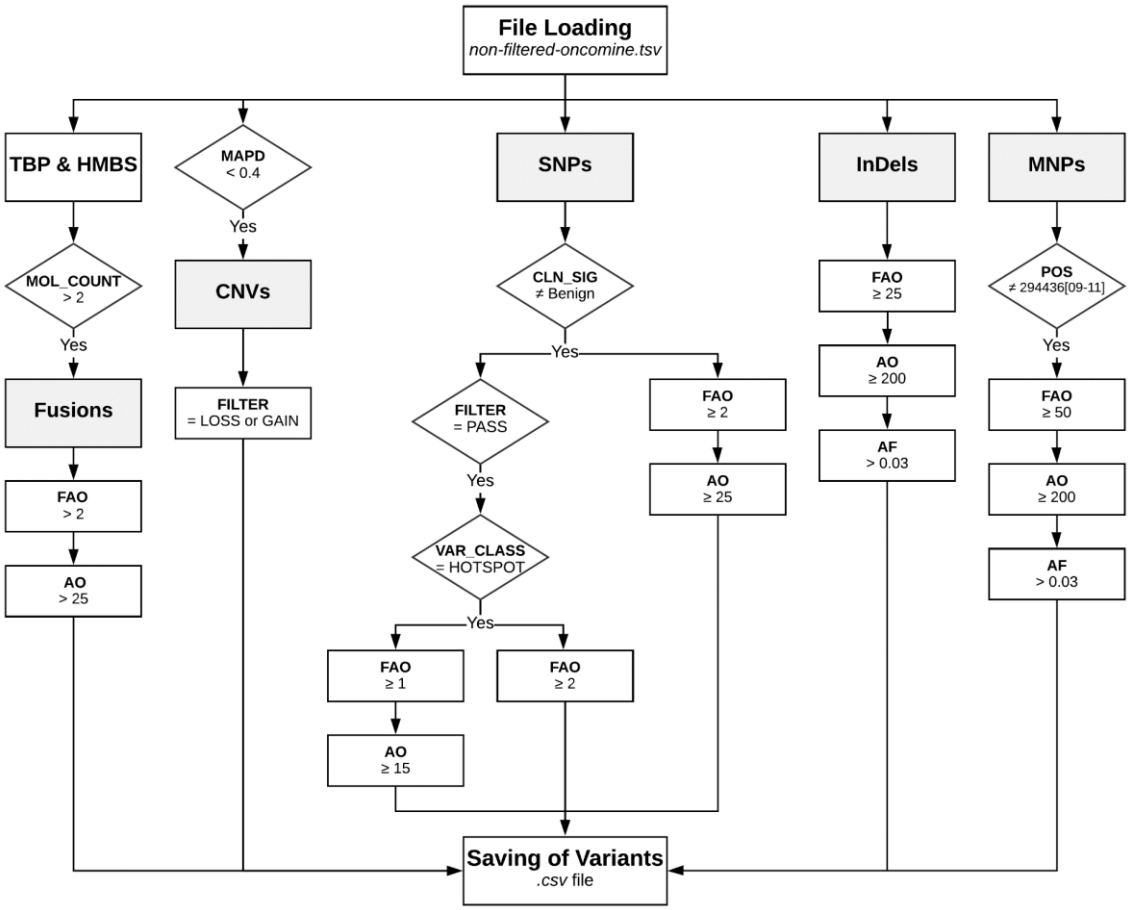

Figure S1. Flowchart of the bioinformatic pipeline optimized for the processing and assessment of variants at the *ALK* gene locus. FAO, molecular coverage; AO, read coverage; MAPD, median of the absolute values of all pairwise differences; FILTER: Ion Reporter™ internal filter (Oncomine™ Variants v5.12); CLN_SIG, clinical significance; VAR_CLASS: Oncomine™ Variant Class; POS: variant position; AF, allele frequency. **V*ALK* tool** selects fusion variants involving the *ALK* locus with molecular coverage >2 (INFO_MOL_COUNT) and fusion reads > 25 (INFO_READ_COUNT). The panel includes two control target genes, namely TBP and HMBS. Both controls must have a molecular count of >2 to pass QC (ROW_TYPE= "ProcControl"; FILTER= "PASS"). In addition, the tool selects *ALK* gene copy-number gains or losses (ROW_TYPE= "CNV"; FILTER= "GAIN" or FILTER= "LOSS") when CNV Ratio is >1.15 or >0.85, respectively. As recommended by the manufacturer, to make a CNV call the P-value must be $>10^{-5}$ and the MAPD (Median of the Absolute values of all Pairwise Differences) must be <0.4. MAPD is a quality metric that estimates coverage variability between adjacent amplicons in CNV analyses. The higher MAPD the lower coverage uniformity, resulting in a higher probability of erroneous CNV calls. Finally, according to our data false positives are less likely in SNPs and very likely in MNPs.

For this reason, the algorithm makes a positive call as long as any of the following five conditions is met:

1. SNPs in the HotSpot file that have passed the Oncomine Variants 5.10 filter and that were detected in at least one molecular count with ≥15 reads (Rowtype= “SNP”; INFO.A.FAO ≥1; INFO.A.AO ≥15; FILTER= “PASS”; FUNC1.oncomineVariantClass= "Hotspot");

2. SNPs that have passed the Oncomine Variants (5.10) filter and that were detected in at least two molecular counts (Rowtype= “SNP”; INFO.A.FAO ≥2; FILTER= “PASS”; FUNC1.oncomineVariantClass= "Hotspot”);

3. SNPs that have been detected in at least two molecular counts with ≥25 reads (Rowtype= “SNP”; INFO.A.FAO ≥2; INFO.A.AO ≥25);

4. Variants different from MNPs that have been detected in ≥25 molecular counts with ≥200 reads and AF ≥0.03 (Rowtype≠ “mnp”; INFO.A.FAO ≥25; INFO.A.AO ≥200; INFO.A.AF >0.03)

5. All variants that have been detected in ≥50 molecular counts with ≥200 reads and an AF ≥0.03, excluding the positions chr2: 29443609 to 29443611 in the ALK locus, which involves six consecutive guanines (G) (INFO.A.FAO ≥50; INFO.A.AO ≥200: INFO.A.AF >0.03; POS≠ “29443609”, “29443610”, “29443611”).

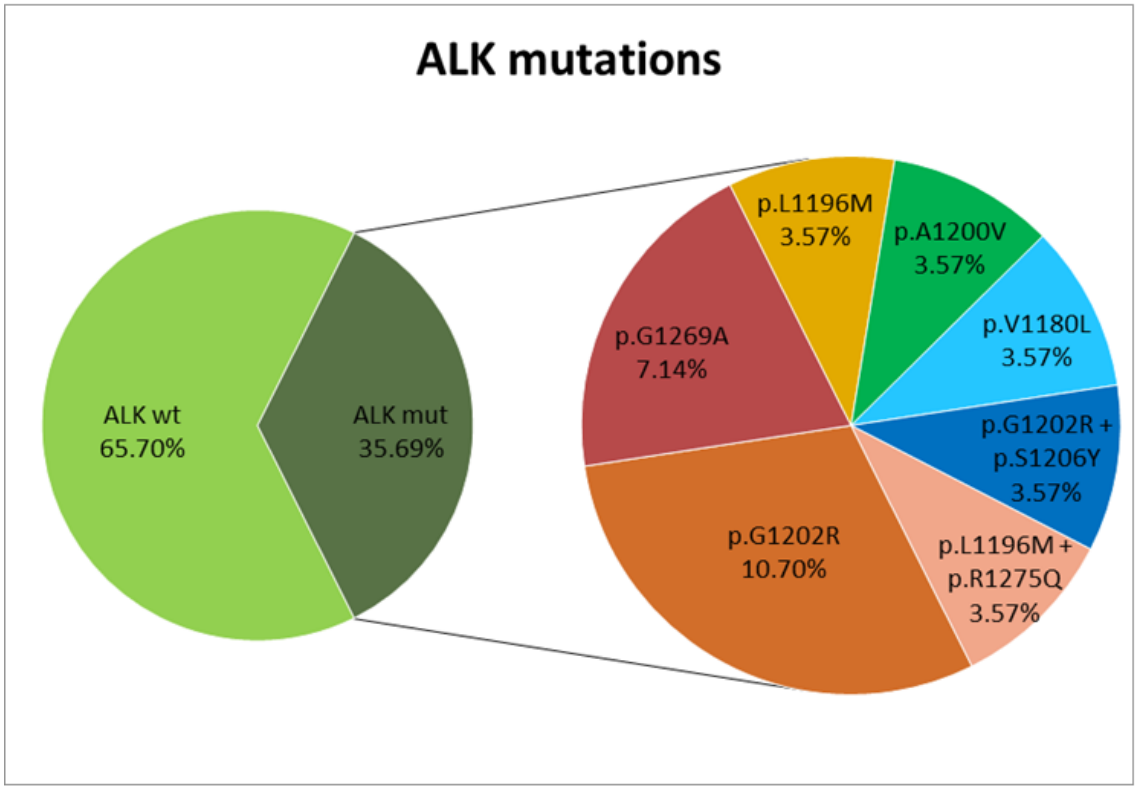

Figure S2. Frequency of *ALK* missense mutations identified in the study population

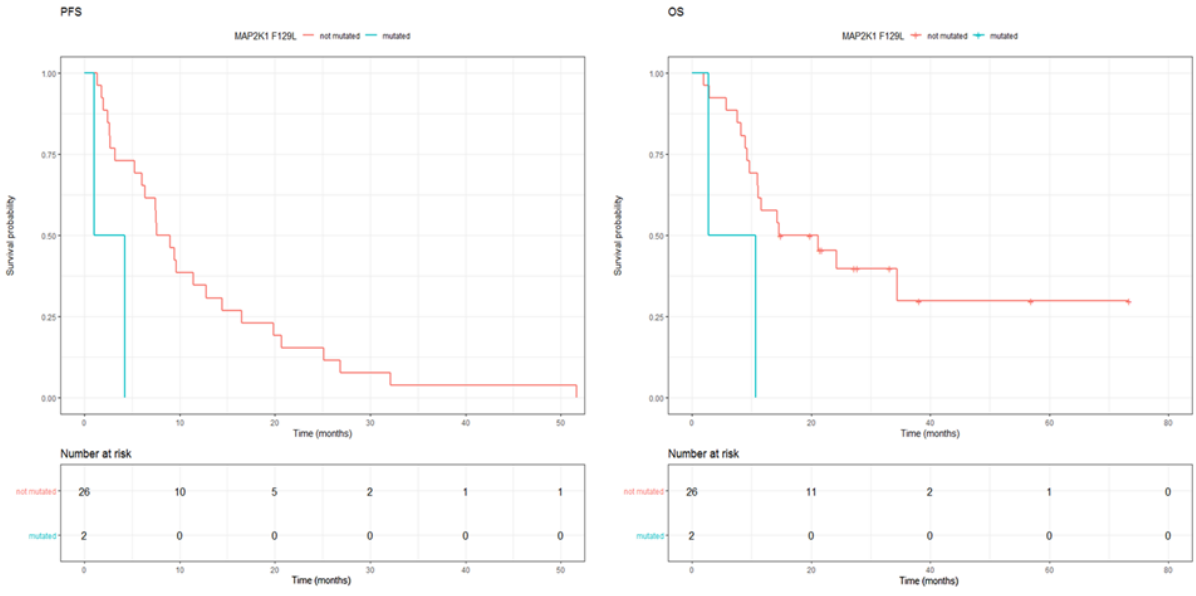

Figure S3. Progression free survival (PFS) and overall survival (OS) curves according to F129L (*MAP2K1*) mutation status. According to available clinical data there were not any clinicopathological feature that could explain the poor prognosis of F129L-positive cases (ECOG performance status was 1 in both cases, histology was adenocarcinoma in both positive cases and none of the F129L patients had brain metastases)

3. Supplementary Tables.

CENTER	IHC – *ALK* D5F3	IHC – *ALK* 5A4	FISH - Vysis LSI *ALK*	FISH - *ALK* (2P23)	nCounter
HUPH			X		
CHUAC	X				
FJD	X		X (confirmatory)		
HGUV		X		X (confirmatory)	
HClinic	X				X (confirmatory)
HUA	X		X (confirmatory)		

Table S1. Identification of *EML4-ALK* translocation. Methodology used by the Pathology Department of the six participant hospitals for *EML4-ALK* testing.

HUPH - Hospital Universitario Puerta de Hierro-Majadahonda

CHUAC - Complejo Hospitalario Universitario A Coruña

FJD - Hospital Universitario Fundación Jiménez Díaz

HGUV - Fundación Hospital General Universitario de Valencia

HClinic - Hospital Clinic of Barcelona

HUA - Hospital Universitario de Alicante

GENES IN TARGET PANEL	bp INTERROGATED	GENES IN TARGET PANEL	bp INTERROGATED
AKT1	*50*	*GNA11*	45
ALK	***434***	*GNAQ*	32
APC	*675*	*GNAS*	90
AR	*126*	*HRAS*	105
ARAF	*66*	*IDH1*	43
BRAF	***150***	*IDH2*	101
CCND1	*267*	***KIT***	609
CCND2	*410*	*KRAS*	188
CCND3	*537*	***MAP2K1***	198
CDK4	*388*	***MAP2K2***	127
CDK6	*351*	***MET***	682
CTNNB1	*67*	*MTOR*	522
CHEK2	*81*	*MYC*	246
DDR2	***141***	***NRAS***	186
EGFR	***910***	*NTRK1*	124
ERBB2	*743*	*NTRK3*	60
ERBB3	*265*	*PDGFRA*	492
ERG	*only fusions*	***PIK3CA***	409
ESR1	*144*	*PTEN*	343
ETV1	*only fusions*	*RAF1*	35
FBXW7	*290*	*RET*	392
FGFR1	*510*	*ROS1*	243
FGFR2	***778***	*SF3B1*	35
FGFR3	*590*	*SMAD4*	229
FGFR4	*96*	*SMO*	423
FLT3	*39*	*TP53*	979

Table S2. Genes included in the NGS panel used. Gene symbols in bold letter have been described to be potentially relevant for ALK resistance according to Gainor et al. (1)

1. Gainor JF, Dardaei L, Yoda S, Friboulet L, Leshchiner I, Katayama R, et al. (2016) Molecular mechanisms of resistance to first- and second-generation ALK inhibitors in ALK -rearranged lung cancer. Cancer Discov 6, 1118-1133.

Patient	Sample	Gene	Amino Acid Change	Nucleotide Change / CytoBand	Digital PCR	Sanger
Patient 2	Sample 2	*TP53*	p.A88Rfs	c.261_262insC		Negative
Patient 2	Sample 2	*TP53*	p.M133T	c.398T>C		Negative
Patient 2	Sample 2	*TP53*	p.P92A	c.274C>G	Negative	
Patient 6	Sample 8	*TP53*	p.P92A	c.274C>G	Negative	
Patient 6	Sample 8	*TP53*	p.R282W	c.844C>T	Negative	
Patient 7	Sample 9	*TP53*	p.V157F	c.469G>T		Negative
Patient 7	Sample 9	*TP53*	p.P92A	c.274C>G	Negative	
Patient 8	Sample 10	*TP53*	p.P92A	c.274C>G	Negative	
Patient 9	Sample 11	*TP53*	p.G105C	c.313G>T		Negative
Patient 10	Sample 12	*TP53*	p.P92A	c.274C>G	Negative	
Patient 16	Sample 18	*TP53*	p.R158C	c.472C>T		Negative
Patient 16	Sample 18	*TP53*	p.P250L	c.749C>T		Negative
Patient 16	Sample 18	*TP53*	p.?	c.919+10C>T		Negative
Patient 16	Sample 18	*TP53*	p.P92A	c.274C>G	Negative	
Patient 20	Sample 24	*TP53*	p.C176Y	c.527G>A		Negative
Patient 20	Sample 24	*TP53*	p.S241A	c.721T>G		Negative
Patient 20	Sample 24	*TP53*	p.P92A	c.274C>G	Negative	
Patient 21	Sample 25	*TP53*	p.Q16Rfs	c.45delT		Negative
Patient 22	Sample 26	*TP53*	p.P92A	c.274C>G	Negative	

Table S3. DNA genotyping of PBMCs. Mutations in *TP53* gene detected in ctDNA were interrogated in the DNA from PBMCs. The table shows the methodology by which each mutation was tested. The results discard a clonal hematopoiesis origin of the mutations

Sanger sequencing LOD has been established at 20% according to manufacturer

cDNA	protein	transcript	chromosome	position
c.3599C>T	p.A1200V	NM_004304.4	chr2	29443611
c.3806G>C	p.G1269A	NM_004304.4	chr2	29432682
c.3605_3606delGAinsAG	p.G1202E	NM_004304.4	chr2	29443611
c.3821C>T	p.A1274V	NM_004304.4	chr2	29432664
c.3824G>A	p.R1275Q	NM_004304.4	chr2	29432664
c.3604G>A	p.G1202R	NM_004304.4	chr2	29443611
c.3455T>C	p.L1152P	NM_004304.4	chr2	29445270
c.3626G>A	p.R1209Q	NM_004304.4	chr2	29443591
c.3606A>G	p.G1202G	NM_004304.4	chr2	29443611
c.3586C>A	p.L1196M	NM_004304.4	chr2	29443631
c.3691C>T	p.R1231W	NM_004304.4	chr2	29436902
c.3521T>C	p.F1174S	NM_004304.4	chr2	29443696
c.3367G>T	p.G1123C	NM_004304.4	chr2	29445466
c.3600G>A	p.A1200A	NM_004304.4	chr2	29443611
c.3600G>T	p.A1200A	NM_004304.4	chr2	29443611
c.3617C>A	p.S1206Y	NM_004304.4	chr2	29443600
c.3601G>A	p.G1201R	NM_004304.4	chr2	29443611
c.3807A>G	p.G1269G	NM_004304.4	chr2	29432681
c.3538G>C	p.V1180L	NM_004304.4	chr2	29443679

Table S4. List of mutations in *ALK* locus tested by dPCR

***ALK*-TKI**	**Number of samples**	***ALK*-TKI naive (N)**	**Treatment after crizotinib (N)**
Crizotinib	11	11	-
Alectinib	10	2	7
Ceritinib	4	0	4
Lorlatinib	2	0	0
Brigatinib	1	0	1

Table S5. *ALK*-Is treatments of the study cohort. Number of samples collected upon progression and according to *ALK*-TKIs. Number of samples collected upon progression to a first line treatment with an *ALK*-Is (*ALK*-TKI naive). Number of samples that correspond to patients who were previously treated with a previous line of treatment with crizotinib.

Sample	Gene (HUGO Symbol)	Amino Acid Change	Nucleotide Change / CytoBand	MAF NGS	Type of mutation	Variant Class (Tier)	Transcript	rs	COSM
Sample 1	*CCND3*	p.T191T	c.573A>T	0.93	SNV	Unknown	NM_001760	-	-
Sample 1	*TP53*	p.P92A	c.274C>G	0.30	SNV	unknown	NM_000546.5	-	COSM45844
Sample 2	*ALK*	p.A1200V	c.3599C>T	0.02	SNV	Strong Clinical Significance	NM_004304.4	rs200585833	COSM317003
Sample 2	*TP53*	p.A88Rfs	c.261_262insC	0.52	InDel	unknown	NM_000546.5	-	-
Sample 2	*TP53*	p.M133T	c.398T>C	0.55	SNV	unknown	NM_000546.5	rs28934873	COSM43723
Sample 2	*TP53*	p.P92A	c.274C>G	0.30	SNV	unknown	NM_000546.5	-	COSM45844
Sample 3	*ALK*	p.G1269A	c.3806G>C	3.36	SNV	Strong Clinical Significance	NM_004304.4	rs1057519781	COSM1169707
Sample 3	*TP53*	p.L35fs	c.104_105insC	0.30	InDel	unknown	NM_000546.5	-	-
Sample 4	*BRAF*	p.G466V	c.1397G>T	0.49	SNV	Potential Clinical Significance	NM_004333.4	rs121913351	COSM451
Sample 4	*TP53*	p.G262Rfs	c.784insC	1.00	InDel	unknown	NM_000546.5	-	-
Sample 4	*TP53*	p.V197Gfs	c.590delT	0.44	InDel	unknown	NM_000546.5	-	COSM44655
Sample 6	*ALK*	p.G1269A	c.3806G>C	0.88	SNV	Strong Clinical Significance	NM_004304.4	rs1057519781	COSM1169707
Sample 7	*ALK*	p.G1202R	c.3604G>A	1.28	SNV	Strong Clinical Significance	NM_004304.4	rs1057519783	COSM144250
Sample 7	*TP53*	p.P92A	c.274C>G	0.90	SNV	unknown	NM_000546.5	-	COSM45844
Sample 8	*ALK*	p.L1196M	c.3586C>A	0.02	SNV	Strong Clinical Significance	NM_004304.4	rs1057519784	COSM99137
Sample 8	*FGFR2*	p.G305R	c.913G>A	0.05	SNV	Unknown	NM_000141.5	-	COSM29824
Sample 8	*TP53*	p.P92A	c.274C>G	0.18	SNV	unknown	NM_000546.5	-	COSM45844
Sample 8	*TP53*	p.R282W	c.844C>T	0.17	SNV	unknown	NM_000546.5	rs28934574	COSM10704
Sample 9	*SMAD4*	p.A118V	c.353C>T	0.03	SNV	Unknown	NM_005359.6	-	COSM14215
Sample 9	*TP53*	p.P92A	c.274C>G	0.84	SNV	unknown	NM_000546.5	-	COSM45844
Sample 9	*TP53*	p.V157F	c.469G>T	0.99	SNV	unknown	NM_000546.5	rs121912654	COSM10670
Sample 10	*IDH2*	p.R140Q	c.419G>A	0.06	SNV	Potential Clinical Significance	NM_002168.3	-	COSM41590
Sample 10	*TP53*	p.P92A	c.274C>G	0.84	SNV	unknown	NM_000546.5	-	COSM45844
Sample 11	*MET*	p.L7P	c.20T>C	0.43	SNV	Unknown	NM_001127500	-	-
Sample 11	*TP53*	p.G105C	c.313G>T	0.42	SNV	unknown	NM_000546.5	-	COSM44481
Sample 12	*MAP2K1*	p.F129L	c.385T>C	1.00	SNV	Potential Clinical Significance	NM_002755.3	rs1057519805	COSM1235480
Sample 12	*TP53*	p.P92A	c.274C>G	1.37	SNV	unknown	NM_000546.5	-	COSM45844
Sample 13	*TP53*	p.A88Rfs	c.261_262insC	0.66	InDel	unknown	NM_000546.5	-	-
Sample 13	*TP53*	p.P92A	c.274C>G	0.45	SNV	unknown	NM_000546.5	-	COSM45844
Sample 14	*CCND1*		Loss (0,41)		CNV	Unknown	NM_053056	-	-
Sample 14	*FGFR3*		Loss (0,38)		CNV	Unknown	NM_000142	-	-
Sample 14	*MYC*		Gain (3,08)		CNV	Potential Clinical Significance	NM_005359.5	-	-
Sample 14	*TP53*	p.M160I	c.480G>T	0.75	SNV	unknown	NM_000546.5	rs772354334	COSM45674

Sample 16	*PIK3CA*	p.E545K	c.1633G>A	0.76	SNV	Potential Clinical Significance	NM_006218	rs104886003	COSM763
Sample 18	*ALK*	p.G1202R	c.3604G>A	0.04	SNV	Strong Clinical Significance	NM_004304.4	rs1057519783	COSM144250
Sample 18	*ALK*	p.S1206Y	c.3617C>A	0.06	SNV	Strong Clinical Significance	NM_004304.4	rs1057519782	COSM144251
Sample 18	*TP53*	p.?	c.919+10C>T	0.09	SNV	unknown	NM_000546.5	-	COSM45540
Sample 18	*TP53*	p.P250L	c.749C>T	0.08	SNV	unknown	NM_000546.5	rs1064794311	COSM10771
Sample 18	*TP53*	p.P92A	c.274C>G	0.18	SNV	unknown	NM_000546.5	-	COSM45844
Sample 18	*TP53*	p.R158C	c.472C>T	0.51	SNV	unknown	NM_000546.5	rs587780068	COSM43848
Sample 19	*TP53*	p.R273G	c.817C>G	0.64	SNV	unknown	NM_000546.5	rs121913343	COSM43843
Sample 20	*PIK3CA*	p.E545A	c.1634A>C	0.79	SNV	Potential Clinical Significance	NM_006218	rs121913274	COSM12458
Sample 20	*TP53*	p.S149Pfs	c.445delT	0.85	InDel	unknown	NM_000546.5	rs1064793929	COSM44099
Sample 21	*EGFR*	p.E746_A750del	c.2235_2249delGGAATTAAGAGAAGC	1.63	InDel	Strong Clinical Significance	NM_005228.4	-	COSM6223
Sample 21	*TP53*	p.R282W	c.844C>T	5.09	SNV	unknown	NM_000546.5	rs28934574	COSM10704
Sample 23	*ALK*	p.L1196M	c.3586C>A	0.05	SNV	Strong Clinical Significance	NM_004304.4	rs1057519784	COSM99137
Sample 23	*ALK*	p.R1275Q	c.3824G>A	0.03	SNV	Strong Clinical Significance	NM_004304.4	rs113994087	COSM28056
Sample 23	*TP53*	p.E221fs	c.662delA	0.10	InDel	unknown	NM_000546.5	-	COSM85959
Sample 23	*TP53*	p.I251fs	c.751_752insC	0.21	InDel	unknown	NM_000546.5	-	-
Sample 24	*ALK*	p.G1202R	c.3604G>A	0.05	SNV	Strong Clinical Significance	NM_004304.4	rs1057519783	COSM144250
Sample 24	*TP53*	p.C176Y	c.527G>A	0.15	SNV	unknown	NM_000546.5	rs786202962	COSM10687
Sample 24	*TP53*	p.P92A	c.274C>G	0.18	SNV	unknown	NM_000546.5	-	COSM45844
Sample 24	*TP53*	p.S241A	c.721T>G	0.09	SNV	unknown	NM_000546.5	rs1057520002	COSM44224
Sample 25	*PIK3CA*	p.I338F	c.1012A>T	0.32	SNV	Unknown	NM_006218	-	-
Sample 25	*TP53*	p.Q16Rfs	c.45delT	1.57	InDel	unknown	NM_000546.5	rs1555526997	COSM46341
Sample 26	*ALK*	p.G1202R	c.3604G>A	0.03	SNV	Strong Clinical Significance	NM_004304.4	rs1057519783	COSM144250
Sample 26	*TP53*	p.P92A	c.274C>G	1.23	SNV	unknown	NM_000546.5	-	COSM45844
Sample 27	*MAP2K1*	p.F129L	c.385T>C	0.06	SNV	Potential Clinical Significance	NM_002755.3	rs1057519805	COSM1235480
Sample 27	*SMAD4*	p.R361C	c.1081C>T	0.03	SNV	Unknown	NM_005359.5	rs80338963	COSM14140
Sample 27	*TP53*	p.P92A	c.274C>G	0.26	SNV	unknown	NM_000546.5	-	COSM45844
Sample 28	*ALK*	p.V1180L	c.3538G>C	0.37	SNV	Strong Clinical Significance	NM_004304.4	-	COSM4381101

Table S6. List of all somatic mutations detected in the study cohort.

***ALK* cohort**

		dPCR	
		+	-
VALK TOOL	+	8	2
	-	4	27

PPA (%)	66.67
NPA (%)	93.10
ORA (%)	85.37

Table S7. Cross-table describing PPA, NPA and ORA for *ALK* cohort using V*ALK* tool

Valencia cohort

		dPCR	
		+	-
VALK TOOL	+	3	1
	-	0	51

PPA (%)	100.00
NPA (%)	98.08
ORA (%)	98.18

Table S8. Cross-tables describing PPA, NPA and ORA for Valencia cohort using V*ALK* tool

***ALK* cohort**

		dPCR	
		+	-
Oncomine Filter	+	3	1
	-	9	27

PPA (%)	25.00
NPA (%)	96.43
ORA (%)	75.00

Table S9. Cross-tables describing PPA, NPA and ORA for *ALK* cohort using the Oncomine Filter

Valencia cohort

		dPCR	
		+	-
Oncomine Filter	+	1	0
	-	2	51

PPA (%)	33.33
NPA (%)	100.00
ORA (%)	96.30

Table S10. Cross-tables describing PPA, NPA and ORA for Valencia cohort using the Oncomine Filter

Nº Patient	**Nº Sample**	**Mutation**	**Method used in progression sample**	**Previous sample**	**Method used in previous sample**	**Result**
Patient 3	Sample 4	*BRAF*; p.G466V/c.1397G>T	NGS	PLASMA	NGS	Absence
Patient 5	Sample 6	*ALK*; p.G1269A/c.3806G>C	NGS + dPCR	PLASMA	dPCR	Absence
Patient 5	Sample 7	*ALK*; p.G1202R/c.3604G>A	NGS + dPCR	PLASMA	NGS + dPCR	Absence
Patient 10	Sample 12	*MAP2K1*; p.F129L/c.385T>C	NGS	PLASMA + TUMOR	NGS	Absence
Patient 14	Sample 16	*PIK3CA*; p.E545K/c.1633G>A	NGS + dPCR	PLASMA	dPCR	Absence
Patient 18	Sample 20	*PIK3CA*; p.E545A/c.1634A>C	NGS	TUMOR	dPCR	Absence
Patient 19	Sample 23	*ALK*; p.L1196M/c.3586C>A	NGS	PLASMA	NGS	Absence
Patient 19	Sample 23	*ALK*; p.R1275Q /c.3824G>A	NGS	PLASMA	NGS	Absence

Table S11. List of the mutations detected at disease progression and status at baseline or in previous sample.

ARTÍCULO 4: NEXT-GENERATION SEQUENCING TO DYNAMICALLY DETECT MECHANISMS OF RESISTANCE TO *ALK* INHIBITORS IN *ALK*-POSITIVE NSCLC PATIENTS: A CASE REPORT.

Los pacientes con CPCNP *ALK*-positivos, al contrario que los pacientes con CPCNP con mutaciones en el gen *EGFR*, cuyo mecanismo de resistencia a la primera línea de tratamiento con un TKI se debe fundamentalmente a la alteración p.T790M, presentan múltiples mutaciones de resistencia a *ALK*-TKIs, que a su vez parece que no confieren resistencia a todos los *ALK*-TKIs disponibles actualmente.

En este trabajo se presenta un caso clínico de un hombre de 52 años diagnosticado con CPCNP *ALK*-positivo, tratado con crizotinib en primera línea y con ceritinib en segunda línea. En este paciente se llevó a cabo el análisis por NGS de las muestras de biopsia líquida a la progresión de la enfermedad a las dos líneas de tratamiento, identificándose dos mutaciones en el *locus ALK* asincrónicas: p.G1269A en la muestra a la progresión de la primera línea de tratamiento y p.G1202R en la muestra a la progresión de la segunda línea de tratamiento. Además, distintas lesiones metastásicas podrían imputarse a cada una de las dos mutaciones de resistencia detectadas, lo que destaca la importancia de la heterogeneidad en la enfermedad avanzada. Específicamente, las pruebas de imagen mostraron lesiones a nivel de las vértebras T4 y T10 a la progresión a crizotinib, las cuales remitieron significativamente con el tratamiento con ceritinib. Por otro lado, nuevas lesiones óseas, especialmente en fémur e isquion, fueron detectadas a la progresión a ceritinib.

Por otro lado, las dos mutaciones en *ALK* fueron evaluadas retrospectivamente en muestras de biopsia líquida recolectadas a lo largo de todo el tratamiento, observándose una buena correlación entre los niveles plasmáticos de éstas y la respuesta tumoral evaluada por escáner y gammagrafía, sugiriendo que el estudio no invasivo del perfil mutacional del tumor mediante NGS permite la monitorización dinámica y eficiente de los pacientes con CPCNP *ALK*-positivos.

En conclusión, este caso clínico ejemplifica que es posible la monitorización molecular de los pacientes, lo que puede ser de utilidad para guiar las decisiones terapéuticas en los pacientes con CPCNP *ALK*-positivos basándose en el perfil mutacional al momento de la progresión a la enfermedad.

Mi aportación a este caso clínico, fue el procesamiento de las muestras de biopsia líquida del paciente, así como el análisis por NGS de las dos muestras a la progresión y el seguimiento por dPCR de las dos mutaciones identificadas en el resto de muestras. Además, junto con la ayuda de los clínicos del Hospital Puerta de Hierro, contribuí a la descripción de la clínica del paciente, así como a la búsqueda de lesiones metastásicas en las distintas pruebas por imagen realizadas. Finalmente, contribuí a la redacción del artículo mediante el escrito de una primera versión y posterior revisión del mismo.

Case Report

Next-generation sequencing to dynamically detect mechanisms of resistance to *ALK* inhibitors in *ALK*-positive NSCLC patients: a case report

Estela Sánchez-Herrero[1], Mariola Blanco Clemente[2], Virginia Calvo[2], Mariano Provencio[1,2], Atocha Romero[1,2]

[1]Molecular Oncology Laboratory, Biomedical Sciences Research Institute, [2]Medical Oncology Department, Puerta de Hierro-Majadahonda University Hospital, Madrid, Spain

Correspondence to: Atocha Romero. Medical Oncology Department, Puerta de Hierro-Majadahonda University Hospital, C/Manuel de Falla 1, Majadahonda-Madrid 28222, Spain. Email: atocha10@hotmail.com.

Abstract: Tyrosine kinase inhibitors (TKIs) of the anaplastic lymphoma kinase gene (*ALK*) have significantly improved the quality of life and survival of non-small cell lung cancer (NSCLC) patients whose tumors harbor an *ALK* translocation. However, most of these patients relapse within 2 to 3 years as the tumor acquires resistance mutations. Unlike beaming and digital PCR (dPCR), which only allow a few mutations to be analyzed, next-generation sequencing (NGS) approaches enable the simultaneous screening of multiple genetic alterations even when the frequencies of the variants are very low. We present the case of a 52-year-old man who was diagnosed with an *ALK*-positive NSCLC and was treated with crizotinib and, subsequently, ceritinib. The analysis of serial liquid biopsies by NGS detected two asynchronous mutations arising in the *ALK* locus during disease progression, namely p.Gly1269Ala (c.3806G>C) and p.Gly1202Arg (c.3604G>A), that conferred resistance to crizotinib and ceritinib, respectively. The resistance mutations were detected independently at different times, and could be imputed to different metastatic lesions, thereby highlighting the importance of heterogeneity in advance disease. Plasma levels of *ALK* resistance mutations correlated well with tumor responses assessed by CT scans and bone scintigraphy, demonstrating that non-invasive tumor molecular profiling by NGS allows the efficient dynamic monitoring of *ALK*-positive NSCLC patients, and outperforms dPCR and beaming because more somatic mutations can be tracked over the course of the treatment. In conclusion, this case report illustrates the usefulness NGS to guide therapeutic decisions in *ALK*-positive NSCLC patients based tumor molecular profile upon disease progression.

Keywords: Anaplastic lymphoma kinase (*ALK*); case report; liquid biopsy; next-generation sequencing (NGS); non-small cell lung cancer (NSCLC)

Submitted Dec 26, 2019. Accepted for publication Jan 18, 2020.
doi: 10.21037/tlcr.2020.02.07
View this article at: http://dx.doi.org/10.21037/tlcr.2020.02.07

Introduction

Approximately 3–7% of non-small cell lung cancer (NSCLC) patients have a genomic rearrangement of the anaplastic lymphoma kinase (*ALK*) gene (1), the most prevalent fusion partner being the echinoderm microtubule-associated protein-like 4 (*EML4-ALK*) (2). The development of molecular targeted therapies such as tyrosine kinase inhibitors (TKIs) of the *ALK* locus has dramatically changed the quality of life and prognosis of *ALK*-positive NSCLC patients, with significantly better survival than that provided by chemotherapy [median OS approximately 50 and 12 months, respectively (3)]. However, despite the efficacy of *ALK* inhibitors, patients ultimately relapse

Table 1 Clinico-pathological characteristics of the patient

Sex: Male
Age at diagnosis: 52 years
Smoking status: Former (10 cigarettes/day)
Histology: Adenocarcinoma
Clinical stage: IV (cT2N3M1)
Number of ALK-TKI lines during the study: 2
First line of treatment: Crizotinib
Second line of treatment: Ceritinib
Exitus date: 28/12/2016

within 2 to 3 years while receiving therapy (4). In order to detect molecular resistance mechanisms, tumor re-biopsy is required, although this is seldom feasible in routine clinical practice. Conversely, the analysis of liquid biopsies, can potentially overcome the aforementioned limitation, being a promising approach for identifying resistance mechanisms arising during disease progression. Resistance mutations in the *ALK* locus have been reported to occur in around 20% of *EML4-ALK* NSCLC patients treated with *ALK*-TKIs (5). Unlike patients with NSCLC who harbor an *EGFR* mutation, where the mechanism of resistance to first-line TKI treatment is mainly due to the p.Thr790Met (c.2369C>T) mutation (6), multiple resistance mutations to *ALK* inhibitors have been described in the *ALK* locus (7,8). On the other hand, distinct mutations in the *ALK* locus confer different sensitivities on a variety of *ALK*-TKIs (9,10); for example, pre-clinical evidence suggests that the p.Ile1171Asn (c.3512T>A) mutation confers resistance to crizotinib and alectinib, but not to ceritinib (5). Furthermore, the therapeutic arsenal against *ALK*-positive tumors has increased in recent years, with several *ALK*-TKIs recently being approved by the FDA (4). In routine clinical practice, these treatments are prescribed empirically upon first disease progression, rather than being based on the tumor molecular profile.

Digital PCR (dPCR), although an adequate approach for detecting and quantifying somatic mutations using liquid biopsies, can only detect a few already-known mutations at a given time, which means the method is of limited use for monitoring *ALK*-positive NSCLC patients. On the other hand, monitoring tumor burden by tracking single somatic mutations could be limited by tumor heterogeneity, especially in advanced stages (11). This limitation can be overcome by using novel NGS approaches that allow for simultaneous low-frequency variant calling of multiple mutations (12). We present the following case report in accordance with the CARE Guideline (13).

Case presentation

A 52-year-old Spanish man, a former smoker (10 cigarettes/day), with no significant past medical and family history, who developed cough, dysphonia and significant weight loss, with no relevant findings on physical examination, was diagnosed in June 2014 as having a poorly differentiated lung adenocarcinoma stage IV (cT2N3M1c TNM 7ª ed. with bone metastasis) by a positron emission computed tomography (CT) scan and a pathological examination. Clinico-pathological characteristics of the patient are described in *Table 1*.

A mutational study of the tumor biopsy was not performed in the hospital where the patient was initially diagnosed due to lack of material available for molecular analysis. Plasma samples were obtained in the Medical Oncology Department of Hospital Puerta de Hierro-Majadahonda. The patient was a participant in a research study that aimed to evaluate the clinical utility of liquid biopsies in NSCLC patients. The study protocol was approved by the Hospital Puerta de Hierro Ethics Committee (internal code PIE14/00064). The patient signed the appropriate informed consent on 9 October 2015.

The patient was initially treated with four cycles of cisplatin (75 mg/m^2) plus pemetrexed (500 mg/m^2) chemotherapy in August 2014 and he continued maintenance therapy with pemetrexed (500 mg/m^2). Unfortunately, after 12 months of chemotherapy a CT scan revealed progressive disease (PD), manifesting as new vertebral lesions.

A second biopsy was performed using a Vysis LSI ALK Dual Color Break Apart FISH probe kit (Vysis, Downers Grove, IL), which revealed an *EML4-ALK* rearrangement. Based on this new result, the patient received 250 mg crizotinib daily from October to December 2015. In December 2015, despite good treatment tolerance, a CT scan showed a new blastic metastasis in the axial skeleton and a slight increase in the size of the lung lesion (*Figure 1*), and the patient was diagnosed as having a PD. A plasma sample was obtained at this time and sequenced on an Ion S5™ Sequencer (Thermo Fisher, Palo Alto, CA)

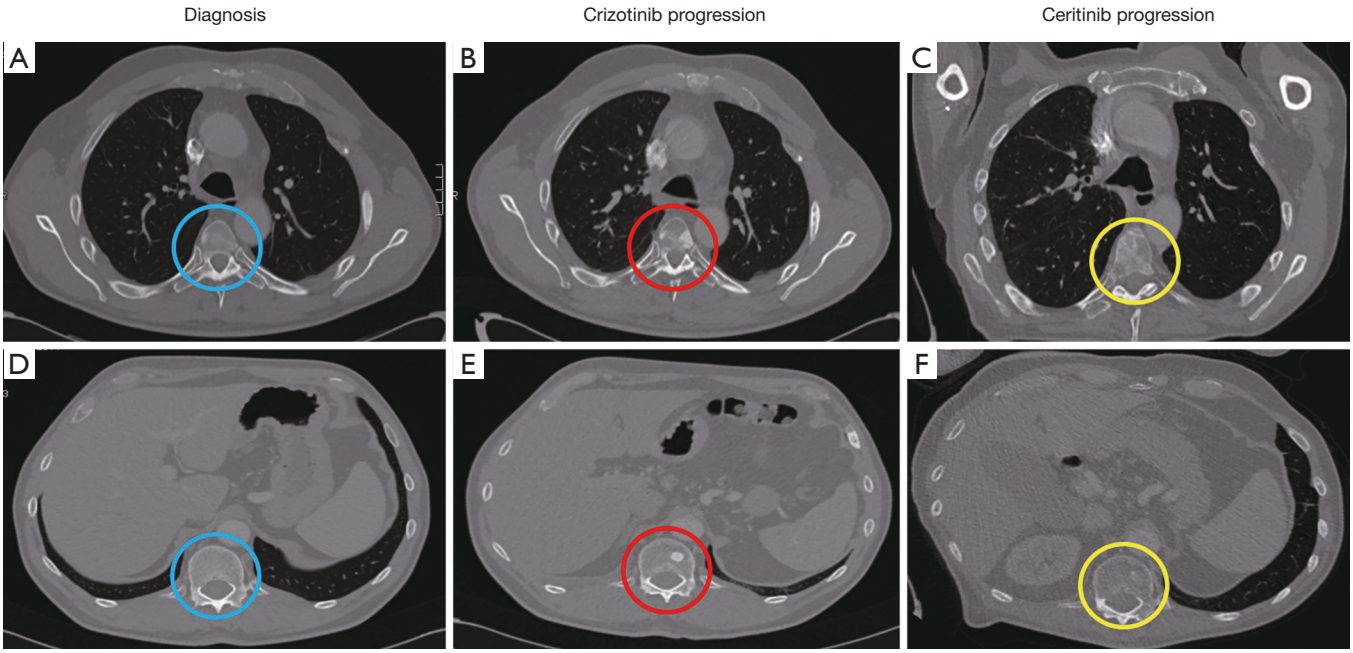

Figure 1 CT scans at times of diagnosis and progression during crizotinib and ceritinib treatment. (A) CT scan at time of diagnosis; (B) CT scan showing new T4 vertebral metastasis upon crizotinib progression; (C) The CT scan reveals a partial remission of T4 vertebral lesion with ceritinib treatment; (D) CT scan at time of diagnosis; (E) CT scan showing new T10 vertebral metastasis upon crizotinib progression; (F) The CT scan reveals a partial remission of T10 vertebral lesion with ceritinib treatment.

using the Oncomine™ Lung cfDNA Assay NGS panel (Thermo Fisher, Palo Alto, CA) to examine circulating tumor DNA (ctDNA). The NGS study revealed the presence of the p.Gly1269Ala (c.3806G>C) resistance mutation in the *ALK* gene (MAF =0.88%). This mutation was confirmed by dPCR (MAF =0.42%) using a custom TaqMan® assay in conjunction with a QuantStudio® 3D Digital PCR System (Applied Biosystems, South San Francisco, CA, USA). Next, using dPCR, we analyzed the p.Gly1269Ala (c.3806G>C) mutation in a plasma sample collected previously than the former. This technique did not detect the p.Gly1269Ala (c.3806G>C) mutation, correlating with tumor response to crizotinib at that time (November 2015) (*Figure 2*).

Upon progression to crizotinib treatment, the patient started treatment with ceritinib (600 mg per day). Throughout the course of this treatment there were no adverse events. Furthermore, ten plasma samples were collected and analyzed by dPCR. Partial response was assessed based on a CT scan performed in March 2016, correlating with undetectable plasma levels of p.Gly1269Ala (c.3806G>C) mutation, suggesting that ceritinib was able to eliminate the clone harboring the p.Gly1269Ala (c.3806G>C) mutation (*Figure 2*).

After 9 months of treatment (September 2016), the sequencing of a plasma sample using the Oncomine™ Pan-Cancer Cell-Free Assay NGS panel (Thermo Fisher, Palo Alto, CA) revealed the presence of the p.Gly1202Arg (c.3604G>A) resistance mutation in the *ALK* locus (MAF =1.28%) (*Figure 3A*), correlating with the symptomatology of the patient, who had reported a pain in his left hip. This mutation was confirmed by dPCR using another custom TaqMan® assay (MAF =2.12%) (*Figure 3B*).

Retrospective analysis of all 12 plasma samples collected by dPCR revealed that the p.Gly1202Arg (c.3604G>A) mutation was not present during the crizotinib treatment, but appeared between the fourth and sixth months (April-June 2016) after the start of the ceritinib treatment, albeit at very low allele frequencies (MAF =0.77% and 0.26%, respectively), coinciding with a hospital admission due to pneumonia. During the last 3 months of ceritinib therapy (October-December 2016), a dPCR study showed a significant increase of p.Gly1202Arg (c.3604G>A) mutation plasma levels (MAF = 2.11% in October 2016, and 6.70% in December 2016) (*Figure 2*), which was associated with the presence of the PD, as identified by scintigraphy performed

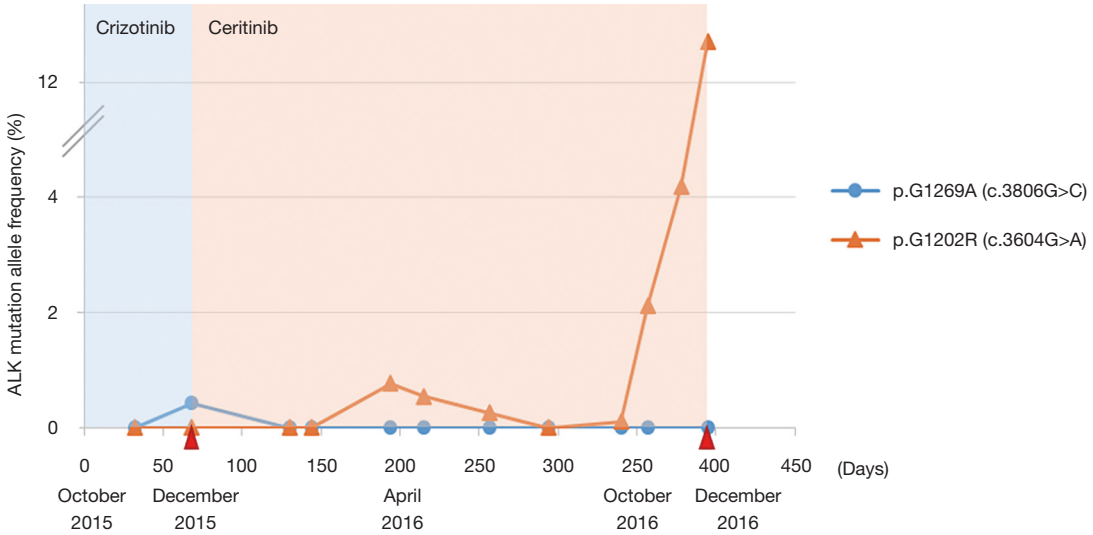

Figure 2 Monitoring molecular alterations using ctDNA in the two lines of *ALK*-TKI. The p.Gly1269Ala (c.3806G>C) mutation appeared upon crizotinib progression (December 2015) and was eliminated with ceritinib treatment. Conversely, the p.Gly1202Arg (c.3604G>A) mutation appeared during ceritinib treatment, increasing significantly upon ceritinib progression (October–December 2016). Red triangles indicate progressive disease.

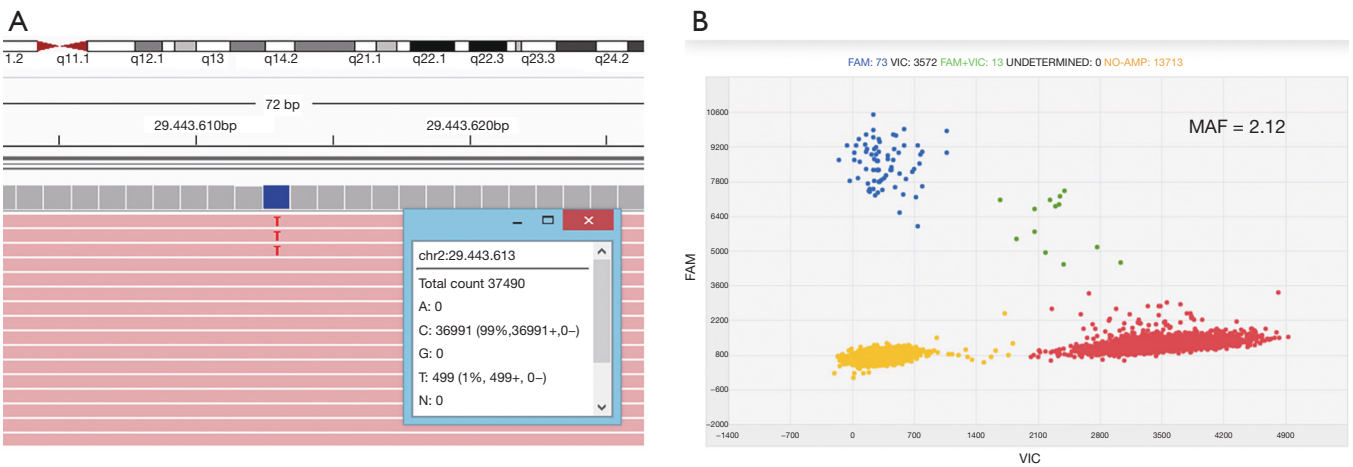

Figure 3 p.Gly1202Arg (c.3604G>A) mutation study. (A) p.Gly1202Arg (c.3604G>A) mutation detection by NGS: visualization of sequencing reads at the corresponding region by the Integrative Genomics Viewer; (B) On the dPCR scatter plot, the p.Gly1202Arg (c.3604G>A) mutation is labeled with FAM (blue data points), whereas the wild type is labeled with VIC (red data points). Green data points indicate the detection of both probes; yellow data points indicate no detection of probe.

in October 2016. Conversely, a CT scan on the same date showed a radiological response of some of the previous bone lesions detected at ceritinib initiation, and there was no evidence of new metastasis. In December 2016 the CT scan revealed PD with new bone blast lesions, especially in the femur and ischium (*Figure 4*). Finally, the patient died from the PD in December 2016, having attained an overall survival of 30 months.

Discussion

In this case report, we illustrate the usefulness of plasma

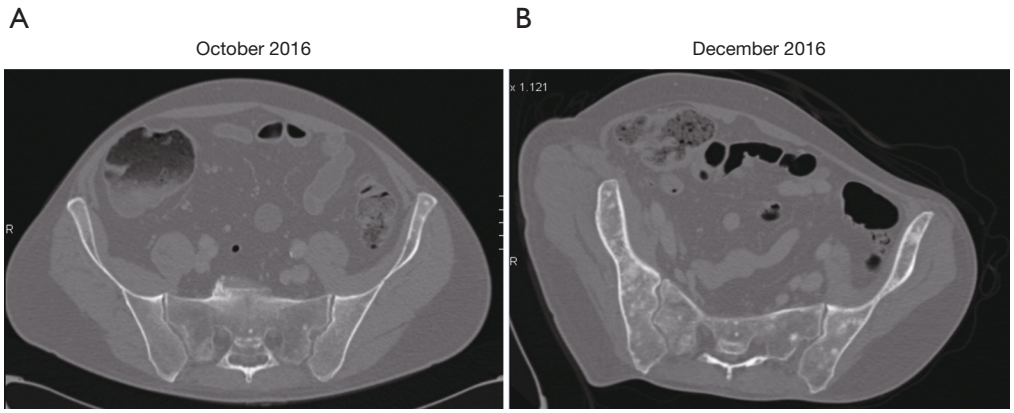

Figure 4 CT scans of new lesions observed upon ceritinib progression. (A) October 2016 CT scan with no evidence of PD; (B) December 2016 CT scan showed several new ischium lesions.

NGS profiling for detecting drug resistance mechanisms upon disease progression in NSCLC patients with an *EML4-ALK* rearrangement.

During the course of treatment, two *ALK* resistance mutations (p.Gly1269Ala (c.3806G>C) and p.Gly1202Arg (c.3604G>A)) were detected and quantified by NGS and dPCR. The p.Gly1269Ala (c.3806G>C) mutation has been described as a frequent event in crizotinib resistance in *ALK*-positive NSCLC patients, being detected in approximately 4% of cases (8). Next-generation *ALK*-TKIs such as ceritinib have demonstrated activity against the p.Gly1269Ala (c.3806G>C) mutation (14). In this way, plasma levels of this mutation dropped to undetectable levels soon after ceritinib treatment was initiated. Similarly, the p.Gly1202Arg (c.3604G>A) mutation occurs in 21% of patients following ceritinib treatment (5). Lorlatinib, the next-generation *ALK*-TKI, has demonstrated its efficacy against cells harboring the p.Gly1202Arg (c.3604G>A) mutation (15,16). Of note, the p.Gly1202Arg (c.3604G>A) resistance mutation was detected before disease progression, as ascertained by CT scan. In the same way, it has been reported that the p.Thr790Met (c.2369C>T) resistance mutation can be detected by ctDNA analysis approximately 50 days before PD is detected by CT scan in *EGFR*-positive NSCLC patients treated with a TKI (17,18), which suggests that ctDNA can complement imaging techniques to anticipate progression (19,20).

Technologies such as array-based dPCR or NGS allow the dynamic and quantitative analysis of somatic mutations in blood samples with high levels of sensitivity. However, dPCR can detect only a few, already-known genetic mutations in a single sample at a given time, while NGS enables the simultaneous screening of multiple mutations in multiple samples. Moreover, NGS allows to identify novel mutations. In this way the p.Gly1128Ala (c.3383G>C) mutation in *ALK* locus was recently identified in an *ALK*-positive NSCLC patient who progressed during treatment with crizotinib (21). As already mentioned, the use of dPCR is limited to monitoring a small number of mutations, and so is an unsuitable approach for screening resistance mutations in the *ALK* locus. However, as described in this case report, ctDNA profiling by NGS is feasible and can yield clinically useful information. Importantly, the laboratory turnaround time is short which make this a practical method for assisting oncologists in their clinical decision-making.

According to ctDNA analysis, in this case, ceritinib was able to eliminate the tumor cells that carried the resistance mutation p.Gly1269Ala (c.3806G>C), highlighting the high potency of the drug. Likewise, osimertinib, a third-generation *EGFR*-TKI, seems to be more potent than first- and second-generation TKIs such as erlotinib, gefitinib and afatinib, since it is more effective, in terms of survival, than standard *EGFR*-TKIs in first-line treatment (22). At the molecular level, unlike the first and second generations of *EGFR* inhibitors, in which the original *EGFR*-sensitizing mutation is always detected when disease progression occurs (23), osimertinib removes the tumor cells that carry both the original *EGFR* sensitizing mutation and the p.Thr790Met (c.2369C>T) resistance mutation in about half of the cases (24).

On the other hand, the two clones p.Gly1269Ala (c.3806G>C) and p.Gly1202Arg (c.3604G>A) were detected

at different times during the course of disease, and could be imputed to different cancer lesions upon disease progression. In this way, the bone metastasis detected in the T4 and T10 vertebral lesions could be imputed to the clone harboring the p.Gly1269Ala (c.3806G>C) mutation, since these lesions were diagnosed at the same time as the mutation was detected in the blood. Moreover, both lesions showed partial remission with ceritinib treatment, in association with a decrease in the plasma levels of the p.Gly1269Ala (c.3806G>C) mutation (*Figures 1*,*2*). The ischium metastasis could be imputed to the clone harboring the p.Gly1202Arg (c.3604G>A) mutation (*Figure 4*). The CT scan clearly showed its occurrence to be associated with a significant increase in the plasma levels of this mutation, as assessed by dPCR (*Figure 2*).

In conclusion, molecular profiling of liquid biopsies using NGS is feasible and can be useful for monitoring tumor heterogeneity and clonal evolution during *ALK*-TKI treatment of NSCLC patients harboring *EML4-ALK* translocation, helping clinicians prescribe the most appropriate subsequent treatment lines, and improve the quality of life and outcome of their patients.

Acknowledgments

We thank the patient in participating in our study.
Funding: This study was supported by the Carlos III Institute of Health, the Spanish Ministry of Science and Innovation and the European Regional Development Fund (grant number: PI17/01977 and PI16/01818). ES was funded by the Consejería de Educación, Juventud y Deporte of the Comunidad de Madrid and by the Fondo Social Europeo (Programa Operativo de Empleo Juvenil, and Iniciativa de Empleo Juvenil, PEJ-2017-AI/SAL-6478).

Footnote

Conflicts of Interest: All authors have completed the ICMJE uniform disclosure form (available at http://dx.doi.org/10.21037/tlcr.2020.02.07). The authors have no conflicts of interest to declare.

Ethical Statement: The authors are accountable for all aspects of the work in ensuring that questions related to the accuracy or integrity of any part of the work are appropriately investigated and resolved. The patient participated in a research study that aimed to evaluate the clinical utility of liquid biopsies in NSCLC patients. The study protocol was approved by the Hospital Puerta de Hierro Ethics Committee (internal code PIE14/00064). Written informed consent was obtained from the patient for publication of this case report as well as the accompanying images.

References

1. Sasaki T, Rodig SJ, Chirieac LR, et al. The biology and treatment of EML4-ALK non-small cell lung cancer. Eur J Cancer 2010;46:1773-80.
2. Yang L, Ling Y, Guo L, et al. Detection of ALK translocation in non-small cell lung carcinoma (NSCLC) and its clinicopathological significance using the Ventana immunohistochemical staining method: a single-center large-scale investigation of 1,504 Chinese Han patient. Chin J Cancer Res 2016;28:495-502.
3. Barrows SM, Wright K, Copley-Merriman C, et al. Systematic review of sequencing of ALK inhibitors in ALK-positive non-small-cell lung cancer. Lung Cancer (Auckl) 2019;10:11-20.
4. Singhi EK, Horn L, Sequist LV, et al. Advanced Non-Small Cell Lung Cancer: Sequencing Agents in the EGFR-Mutated/ALK-Rearranged Populations. Am Soc Clin Oncol Educ Book 2019;39:e187-97.
5. Gainor JF, Dardaei L, Yoda S, et al. Molecular Mechanisms of Resistance to First- and Second-Generation ALK Inhibitors in ALK-Rearranged Lung Cancer. Cancer Discov 2016;6:1118-33.
6. Provencio M, Pérez-Barrios C, Barquin M, et al. Next-generation sequencing for tumor mutation quantification using liquid biopsies. Clin Chem Lab Med 2020;58:306-13.
7. Doebele RC, Pilling AB, Aisner DL, et al. Mechanisms of resistance to crizotinib in patients with ALK gene rearranged non-small cell lung cancer. Clin Cancer Res 2012;18:1472-82.
8. Katayama R, Shaw AT, Khan TM, et al. Mechanisms of acquired crizotinib resistance in ALK-rearranged lung

Cancers. Sci Transl Med 2012;4:120ra17.
9. Okada K, Araki M, Sakashita T, et al. Prediction of ALK mutations mediating ALK-TKIs resistance and drug repurposing to overcome the resistance. EBioMedicine 2019;41:105-19.
10. Li J, Huang Y, Wu M, et al. Structure and energy based quantitative missense variant effect analysis provides insights into drug resistance mechanisms of anaplastic lymphoma kinase mutations. Sci Rep 2018;8:10664.
11. García-Saenz JA, Ayllón P, Laig M, et al. Tumor burden monitoring using cell-free tumor DNA could be limited by tumor heterogeneity in advanced breast cancer and should be evaluated together with radiographic imaging. BMC Cancer 2017;17:210.
12. Kivioja T, Vähärautio A, Karlsson K, et al. Counting absolute numbers of molecules using unique molecular identifiers. Nat Methods 2011;9:72-4.
13. Riley DS, Barber MS, Kienle GS, et al. CARE guidelines for case reports: explanation and elaboration document. J Clin Epidemiol 2017;89:218-35.
14. Sakamoto H, Tsukaguchi T, Hiroshima S, et al. CH5424802, a Selective ALK Inhibitor Capable of Blocking the Resistant Gatekeeper Mutant. Cancer Cell 2011;19:679-90.
15. Zou HY, Friboulet L, Kodack DP, et al. PF-06463922, an ALK/ROS1 Inhibitor, Overcomes Resistance to First and Second Generation ALK Inhibitors in Preclinical Models. Cancer Cell 2015;28:70-81.
16. Fontana D, Ceccon M, Gambacorti-Passerini C, et al. Activity of second-generation ALK inhibitors against crizotinib-resistant mutants in an NPM-ALK model compared to EML4-ALK. Cancer Med 2015;4: 953-65.
17. Provencio M, Torrente M, Calvo V, et al. Prognostic value of quantitative ctDNA levels in non small cell lung cancer patients. Oncotarget 2017;9:488-94.
18. Sorensen BS, Wu L, Wei W, et al. Monitoring of epidermal growth factor receptor tyrosine kinase inhibitor-sensitizing and resistance mutations in the plasma DNA of patients with advanced non-small cell lung cancer during treatment with erlotinib. Cancer 2014;120:3896-901.
19. Zheng D, Ye X, Zhang MZ, et al. Plasma EGFR T790M ctDNA status is associated with clinical outcome in advanced NSCLC patients with acquired EGFR-TKI resistance. Sci Rep 2016;6:20913.
20. De Carlo E, Schiappacassi M, Urbani M, et al. Therapeutic decision based on molecular detection of resistance mechanism in an ALK-rearranged lung cancer patient: a case report. Onco Targets Ther 2018;11:8945-50.
21. Ai X, Niu X, Chang L, et al. Next generation sequencing reveals a novel ALK G1128A mutation resistant to crizotinib in an ALK-Rearranged NSCLC patient. Lung Cancer 2018;123:83-6.
22. Soria JC, Ohe Y, Vansteenkiste J, et al. Osimertinib in untreated EGFR-Mutated advanced non-small-cell lung cancer. N Engl J Med 2018;378:113-25.
23. Gelatti ACZ, Drilon A, Santini FC. Optimizing the sequencing of tyrosine kinase inhibitors (TKIs) in epidermal growth factor receptor (EGFR) mutation-positive non-small cell lung cancer (NSCLC). Lung Cancer 2019;137:113-22.
24. Remon J, Caramella C, Jovelet C, et al. Osimertinib benefit in EGFR -mutant NSCLC patients with T790M -mutation detected by circulating tumour DNA. Ann Oncol 2017;28:784-90.

Cite this article as: Sánchez-Herrero E, Blanco Clemente B, Calvo V, Provencio M, Romero A. Next-generation sequencing to dynamically detect mechanisms of resistance to *ALK* inhibitors in *ALK*-positive NSCLC patients: a case report. Transl Lung Cancer Res 2020;9(2):366-372. doi: 10.21037/tlcr.2020.02.07

ARTÍCULO 5: *ALK* FUSION TRANSCRIPTS CAN BE DETECTED IN EXTRACELLULAR VESICLES (EVs) FROM NON-SMALL CELL LUNG CANCER CELL LINES AND PATIENT PLASMA. TOWARDS EV-BASED NON-INVASIVE TESTING.

El correcto diagnóstico de los pacientes con CPCNP *ALK*-positivos es crucial dada la mejora significativa de la supervivencia y la calidad de vida con la terapia basada en *ALK*-TKIs. Cuando no es posible la obtención de biopsia tumoral o la cantidad/calidad de la muestra no permite llevar a cabo el estudio de los reordenamientos en *ALK*, la biopsia líquida podría ser una buena alternativa. Sin embargo, el estudio de las fusiones en este tipo de muestras sigue siendo un reto debido a la complejidad de estas alteraciones genómicas. El ARN presente en el interior de las EVs se encuentra protegido de las RNAsas, constituyendo una fuente prometedora para la correcta detección de transcritos de fusión de manera no invasiva.

En este estudio, se aislaron las EVs del sobrenadante celular de dos líneas celulares derivadas de CPCNP: H3122 con la variante 1 de *EML4-ALK* (E13;A20) y H2228 con la variante 3 de *EML4-ALK* (E6a/b;A20), mediante UC. Además, las EVs fueron aisladas a partir de muestras de plasma pre-tratamiento de 16 pacientes con CPCNP *ALK*-positivos.

Las EVs derivadas de las líneas celulares fueron verificadas y caracterizadas mediante microscopía electrónica de trasmisión (TEM, *del inglés transmission electron microscopy*), análisis de rastreo de nanopartículas (NTA, *del inglés Nanoparticle Tracking Analysis*) y citometría de flujo. La expresión de tetraspaninas, marcadores específicos de EVs, así como la expresión de la proteína de fusión en *ALK* fue confirmada por Western Blot, dot blot y microscopía confocal. Asimismo, se detectó el transcrito de fusión de *ALK* a nivel de ARN (mRNA) por dPCR y NGS. Finalmente, con el estudio de las EVs aisladas a partir de las muestras de plasma pre-tratamiento de los 16 pacientes con CPCNP *ALK*-positivos, se identificaron por dPCR fusiones en *ALK* en un 50% de los casos (8/16), respaldando el hecho de que los transcritos de fusión en *ALK* se encuentran presentes en las EVs, especialmente en aquellas con mayor expresión de la tetraspanina CD81.

Por lo tanto, con este manuscrito se concluye, por primera vez, que los transcritos de fusión en *ALK* pueden ser detectados en fracciones enriquecidas de EVs. Estos resultados, sientan las bases para el desarrollo de métodos no invasivos basados en el análisis de las EVs para el estudio de las fusiones en las que se encuentra involucrado el gen *ALK*.

Para llevar a cabo este estudio, se estableció una colaboración con el grupo de la Dra. Mar Valés-Gómez del Centro Nacional de Biotecnología (CNB-CSIC), experta en EVs. Mi aportación al estudio, fue llevar a cabo el aislamiento y caracterización por Western Blot de las EVs derivadas de las líneas celulares, así como el mantenimiento del cultivo celular de las mismas. Además, cooperé con la obtención de las preparaciones de EVs para su posterior estudio por las demás técnicas empleadas en este estudio. Por otro lado, llevé a cabo los estudios a nivel de ARN para la detección de los transcritos de fusión por dPCR y NGS, tanto en las preparaciones de EVs derivadas de líneas celulares como en las derivadas de los pacientes con CPCNP *ALK*-positivo, de los cuales recolecté los datos clínicos. Por último, contribuí a la elaboración del manuscrito y la revisión del mismo.

ALK-Fusion Transcripts Can Be Detected in Extracellular Vesicles (EVs) from Nonsmall Cell Lung Cancer Cell Lines and Patient Plasma: Toward EV-Based Noninvasive Testing

Estela Sánchez-Herrero,[a,b,†] Carmen Campos-Silva,[c,†] Yaiza Cáceres-Martell,[c] Lucía Robado de Lope,[a] Sandra Sanz-Moreno,[a] Roberto Serna-Blasco,[a] Alejandro Rodríguez-Festa,[a] Dunixe Ares Trotta,[a] Paloma Martín-Acosta,[d] Cristina Patiño,[e] María José Coronado,[f] Alexandra Beneitez,[g] Ricardo Jara,[g] Nerea Lago-Baameiro,[h] Tamara Camino,[h] Alberto Cruz-Bermúdez,[a] María Pardo,[h] Víctor González-Rumayor,[b] Mar Valés-Gómez ,[c,*] Mariano Provencio,[a,i] and Atocha Romero [a,i,*]

BACKGROUND: *ALK* rearrangements are present in 5% of nonsmall cell lung cancer (NSCLC) tumors and identify patients who can benefit from *ALK* inhibitors. *ALK* fusions testing using liquid biopsies, although challenging, can expand the therapeutic options for *ALK*-positive NSCLC patients considerably. RNA inside extracellular vesicles (EVs) is protected from RNases and other environmental factors, constituting a promising source for noninvasive fusion transcript detection.

METHODS: EVs from H3122 and H2228 cell lines, harboring *EML4-ALK* variant 1 (E13; A20) and variant 3 (E6a/b; A20), respectively, were successfully isolated by sequential centrifugation of cell culture supernatants. EVs were also isolated from plasma samples of 16 *ALK*-positive NSCLC patients collected before treatment initiation.

RESULTS: Purified EVs from cell cultures were characterized by transmission electron microscopy (TEM), nanoparticle tracking analysis (NTA), and flow cytometry. Western blot and confocal microscopy confirmed the expression of EV-specific markers as well as the expression of *EML4-ALK*-fusion proteins in EV fractions from H3122 and H2228 cell lines. In addition, RNA from EV fractions derived from cell culture was analyzed by digital PCR (dPCR) and *ALK*-fusion transcripts were clearly detected. Similarly, plasma-derived EVs were characterized by NTA, flow cytometry, and the ExoView platform, the last showing that EV-specific markers captured EV populations containing *ALK*-fusion protein. Finally, *ALK* fusions were identified in 50% (8/16) of plasma EV-enriched fractions by dPCR, confirming the presence of fusion transcripts in EV fractions.

CONCLUSIONS: *ALK*-fusion transcripts can be detected in EV-enriched fractions. These results set the stage for the development of EV-based noninvasive *ALK* testing.

Introduction

Genomic rearrangements involving the oncogenic anaplastic lymphoma kinase (*ALK*) gene occur in 3 to 5% of nonsmall cell lung cancer (NSCLC) tumors (1, 2). So far, nearly 30 different *ALK*-fusion partners have been described, with *EML4* being the most common (3, 4). A wide therapeutic arsenal is currently available to tackle *ALK*-positive NSCLC tumors (5–7). Testing for *ALK* fusions is thus mandatory since the identification of *ALK* rearrangements significantly expands the therapeutic opportunities and life expectancy of these patients. However, the availability of tumor biopsies is sometimes limited for NSCLC patients, mostly due to the anatomical location of the tumor and the advanced age of these patients. Biomarker testing using liquid biopsies can

[a]Liquid Biopsy Laboratory, Medical Oncology Department, Instituto de Investigación Sanitaria Puerta de Hierro-Segovia de Arana, Majadahonda, Spain; [b]I+D Department, Atrys Health, Barcelona, Spain; [c]Department of Immunology and Oncology, Spanish National Centre for Biotechnology, CNB-CSIC, Madrid, Spain; [d]Pathology Department, Instituto de Investigación Sanitaria Puerta de Hierro-Segovia de Arana, Majadahonda, Spain; [e]Electron Microscopy Unit Centro Nacional de Biotecnología, CSIC, Madrid, Spain; [f]Confocal Microscopy Core Facility, Instituto de Investigación Sanitaria Puerta de Hierro-Segovia de Arana, Majadahonda, Spain; [g]Immunostep, S.L., Salamanca, Spain; [h]Grupo Obesidómica, Área de Endocrinología, Instituto de Investigación Sanitaria de Santiago (IDIS), Hospital Clínico Universitario de Santiago, Santiago de Compostela, Spain; [i]Medical Oncology Department, Hospital Universitario Puerta de Hierro-Majadahonda, Majadahonda, Spain.

*Address correspondence to: A.R. at Medical Oncology Department, Hospital Puerta de Hierro, Calle Joaquín Rodrigo, 1, 28222 Majadahonda, Madrid, Spain. Fax 911917872; e-mail atocha10@hotmail.com. M.V.-G. at Immunology and Oncology Department, Spanish National Centre for Biotechnology, CNB-CSIC, Calle Darwin, 3, 28049 Madrid, Spain. Fax 915854506; e-mail mvales@cnb.csic.es.

†These authors contributed equally to this work.

Received October 22, 2021; accepted January 12, 2022.
https://doi.org/10.1093/clinchem/hvac021

potentially overcome these limitations. Indeed, genomic profiling of liquid biopsies is integrated in NSCLC guidelines (8). Still, the identification of genomic rearrangements using liquid biopsies remains challenging. The identification of *ALK* translocation in circulating tumor DNA (ctDNA) is complicated as the rearrangement involves a large number of bases, breakpoints are usually unknown, and ctDNA is highly fragmented. Indeed, a sensitivity of 40% has been reported for next-generation sequencing assays in detecting oncogenic fusions in plasma cell-free DNA (9). Likewise, circulating free RNA (cfRNA) is rapidly degraded by RNases present in the bloodstream. However, RNAs carried in extracellular vesicles (EVs) are a priori protected from RNases. The use of EVs for noninvasive biomarker testing has several advantages. First, EVs are stable and they protect RNAs from degradation in the extracellular environment (10); second, nearly all types of cells can release EVs (11); and third, EV isolation methods from plasma samples can be automated so that the process can be scaled for high-throughput applications and therefore be adapted to the clinics.

In this preclinical study, we aimed to elucidate whether *ALK* fusions were detectable in EVs derived from NSCLC. To this aim, H3122 and H2228 NSCLC cell lines were used and EV enrichment protocols were followed to examine the presence of translocation messenger and protein products. The protocol was then optimized for the analysis of plasma samples from 16 *ALK*-positive NSCLC patients.

Materials and Methods

PLASMA SAMPLES

Plasma samples from 16 *ALK*-positive NSCLC patients were collected before treatment initiation at Hospital Puerta de Hierro-Majadahonda. The study protocol was approved by the Hospital Puerta de Hierro Ethics Committee (internal code 79-18). Appropriate written informed consent was obtained from all patients prior to enrollment in the study. Briefly, eligibility criteria included patients who were 18+ years of age and with a pathologically confirmed diagnosis of stage IV NSCLC with an *ALK* translocation.

EVS ISOLATION

Cell lines from NSCLC (H3122 and H2228) harboring an *ALK* translocation were grown. Conditions regarding tissue culture are available in the Methods in the online Data Supplement. As a control, the metastatic melanoma cell line (Ma-Mel-55) was used (12). Detailed information about EV isolation is available in the online Supplemental Methods. Briefly, cell culture supernatants (200 mL) were centrifuged twice for 10 min at 200*g*, followed by 2 centrifugations at 500*g* for 10 min and 1 centrifugation of 30 min at 10 000*g*. Finally, ultracentrifugation at 100 000*g* for 2 h at 4°C with no brake was carried out to collect EVs.

Plasma samples were collected in a 10-mL Streck Cell-Free DNA BCT® tube. Cell debris were removed by centrifugation at 2000*g* for 10 min at 4°C. Plasma samples were diluted in PBS (1:3) and centrifuged once at 110 000*g* for 2 h at 4°C with no brake to collect EVs.

EV QUANTITATION

The concentration and size of particles in the EV preparations were characterized by nanoparticle tracking analysis (NTA) in a NanoSight NS500 (Malvern Instruments Ltd) equipped with a 405 nm laser. Three different captures of 60 s were analyzed per sample. The settings used were camera level 12 (EVs from cell lines), 10 (EVs from NSCLC plasma samples), focus between −15 and +15, threshold 10, and temperature 25 °C.

TRANSMISSION ELECTRON MICROSCOPY (TEM) AND GOLD IMMUNOLABELING

Detailed information about TEM protocol is available in the online Supplemental Methods. Briefly, H3122 and H2228 EV preparations were diluted 1:10 in HBS and adsorbed on a formvar-carbon coated grid, and either stained with 2% uranyl acetate and analyzed directly in the TEM or labeled with antibodies as follows. After blocking, grids were incubated with the primary antibody, either anti-CD9 clone VJ120 (Immunostep, S.L.) or anti-CD81 clone 5A6 (Santa Cruz Biotechnology), blocked again and incubated with goat anti-mouse fab2'-gold 10 nm (BBI International). Finally, grids were stained with uranyl acetate 2%, dried, and analyzed using a Jeol JEM 1011 (JEOL Ltd) electron microscope operating at 100 kV with a CCD camera Gatan Erlangshen ES1000W (Gatan Ink).

CONFOCAL MICROSCOPY

Detailed information about confocal microscopy protocols is available in the Supplemental Methods. Briefly, a drop of EV pellet was put on a 35-mm imaging dish with a polymer coverslip bottom for high-end microscopy, dried, fixed with 4% *p*-formaldehyde and treated with NH_4Cl 50 mmol/L. After permeabilization with 0.2% Triton X-100, samples were blocked with 5% BSA, incubated with anti-CD63 antibody (Merck Millipore), and incubated with goat anti-mouse secondary antibody conjugated to ALEXA 546 or 488 (Invitrogen-Life Technologies). For a second immunodetection, samples were blocked again, incubated with anti-*ALK* antibody (Ventana D5F3; Cell Signaling Technology) or with anticalreticulin antibody (NB600-101; Novus Biologicals) and incubated with goat anti-

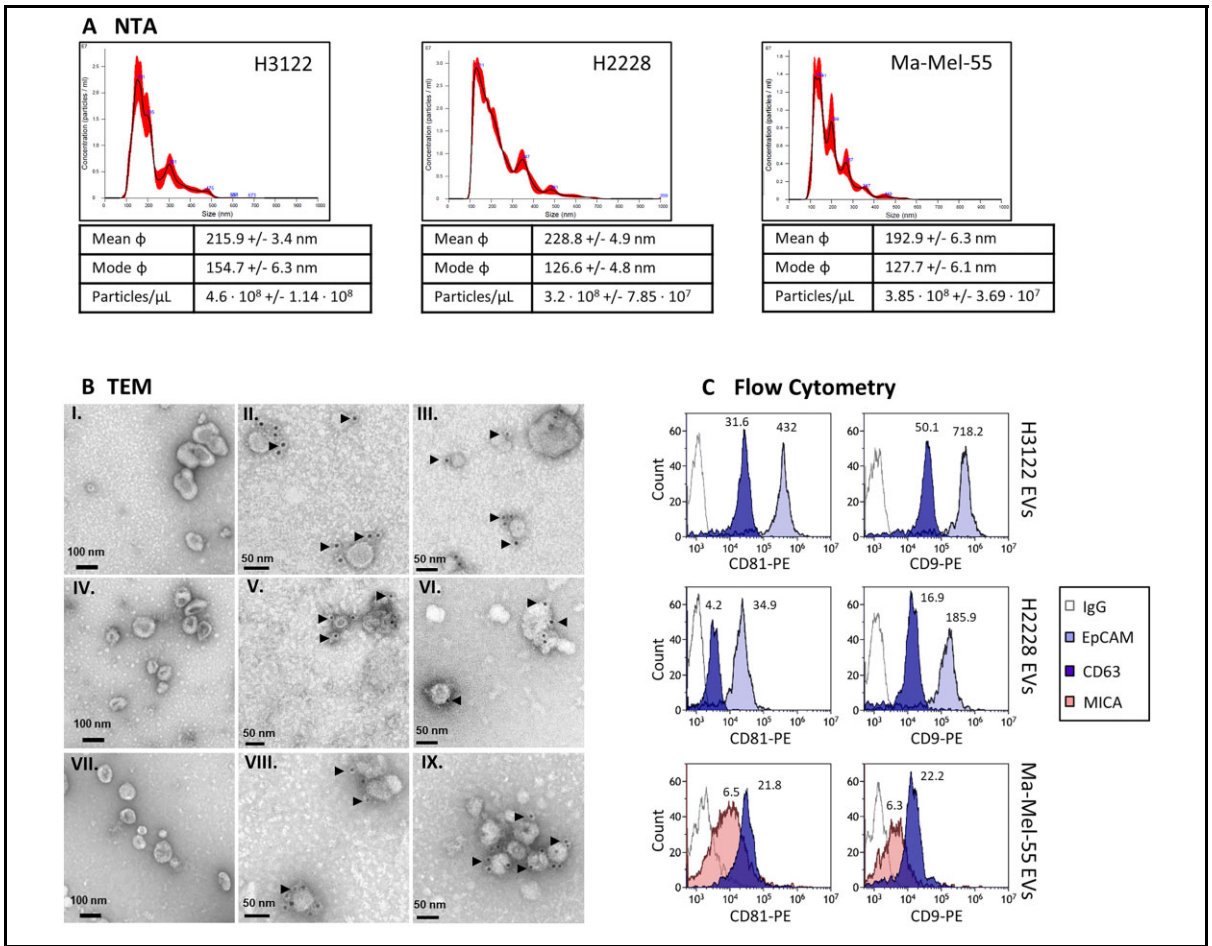

Fig. 1. Characterization of EV-enriched preparations from NSCLC cell lines. (A), Size and concentration analysis by Nanoparticle tracking analysis (NTA). Mean size and concentration listed in the table were obtained in a NanoSight equipment. Φ diameter; (B), Transmission electron microscopy (TEM) visualization. I. H3122 EV preparation unlabeled; II. labeled with CD9 antibody and III. labeled with CD81 antibody, respectively; IV. H2228 EV preparation unlabeled; V. labeled with CD9 antibody and VI. labeled with CD81 antibody; VII. Ma-Mel-55 EV preparation unlabeled; VIII. labeled with CD9 antibody and IX. labeled with CD81 antibody. Bar50 or 100 nm as indicated; (C), Bead-assisted flow cytometry. H3122, H2228, and Ma-Mel-55 EVs were incubated microbeads coated with anti-EpCAM, anti-MICA, anti-CD63, or IgG isotype control antibodies. Captured vesicles were detected by flow cytometry after incubation with either anti-CD81-PE (left panels) or anti-CD9-PE (right panels). Histograms from one representative experiment out of 3 are shown. Relative fluorescence intensity (RFI $= \frac{MFI\ sample}{MFI\ IgG}$) values are shown within each plot. MFI, median fluorescence intensity. PE, phycoerythrin.

rabbit secondary antibody conjugated to ALEXA 488 or 546 (Invitrogen-Life Technologies).

Fluorescence in situ hybridization (FISH) was performed using fixed EV-enriched samples and parent cells. EV-enriched samples and parent cells were permeabilized with 0.2% Triton X-100, dehydrated with 50%, 70%, and 100% ethanol, and incubated with a biotinylated *EML4-ALK* RNA probe. The specimens were incubated with hybridization buffer, washed, blocked with BSA 5%, and incubated with antistreptavidin antibody conjugated to ALEXA 546 (Invitrogen-Life Technologies). Nonpermeabilized and nondehydrated cells were incubated with a biotinylated *EML4-ALK* RNA probe, as a control condition. Nuclei were stained with TO-PRO-3 (Thermo Fisher Scientific). Images were collected with a TCS SP5 confocal microscope (Leica Microsystems) using a ×63 HCX PL APO (1.25–1.52 numerical aperture) oil-immersion objective and ×3 zoom. For immunofluorescence, the following excitation and emission parameters

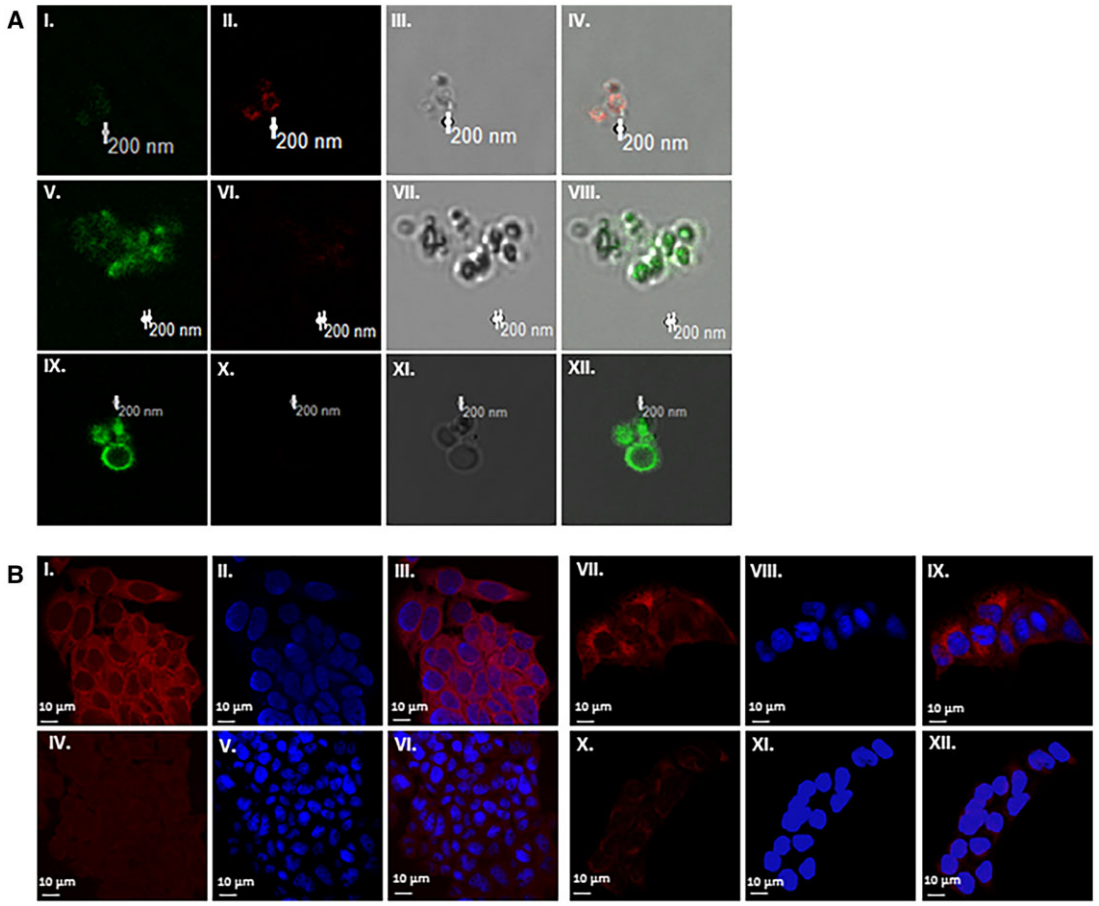

Fig. 2. Characterization of EV-enriched preparations from NSCLC cell lines by confocal microscopy visualization. (A), Double immunofluorescence in EV preparations. I. H3122 EVs stained with *EML4-ALK* antibody (green); II. H3122 EVs stained with CD63 antibody (red); III. H3122 EVs in bright field; IV. Merge; V. Ma-Mel-55 EVs stained with CD63 antibody (green); VI. Ma-Mel-55 EVs stained with *EML4-ALK* antibody (red); VII. Ma-Mel-55 EVs in bright field; VIII. Merge; IX. H3122 EVs stained with CD63 antibody (green); X. H3122 EVs stained with calreticulin antibody (red); XI. H3122 EVs in bright field; XII. Merge; (B), FISH RNA with biotinylated RNA assay for *EML4-ALK* variant 1 in H3122 cells, I. H3122 permeabilized cells labeled with *EML4-ALK* variant 1 biotinylated RNA assay (red); II. H3122 permeabilized cells labeled with TO-PRO-3 (blue); III. Merge; IV. H3122 nonpermeabilized cells labeled with *EML4-ALK* variant 1 biotinylated RNA assay (red); V. H3122 nonpermeabilized cells labeled with DAPI (blue); VI. Merge; VII. H2228 permeabilized cells labeled with *EML4-ALK* variant 3 biotinylated RNA assay (red); VIII. H2228 permeabilized cells labeled with DAPI (blue); IX. Merge; X. H2228 nonpermeabilized cells labeled with *EML4-ALK* variant 3 biotinylated RNA assay (red); XI. H2228 nonpermeabilized cells labeled with DAPI (blue); XII. Merge; (C), FISH RNA with biotinylated RNA assay for *EML4-ALK* variants in EV preparations, I. H2228 EVs with *EML4-ALK* variant 3 biotinylated RNA assay (red); II. H2228 EVs in bright field; III. H2228 Merge EV preparation; IV. Ma-Mel-55 EVs with *EML4-ALK* variant 3 biotinylated RNA assay (red); V. Ma-Mel-55 EVs in bright field; VI. Merge Ma-Mel-55 EV preparation; VII. H3122 EVs with *EML4-ALK* variant 1 biotinylated RNA assay (red); VIII. H3122 EVs in bright field; IX. H3122 Merge EV preparation; X. Ma-Mel-55 EVs with *EML4-ALK* variant 1 biotinylated RNA assay (red); XI. Ma-Mel-55 EVs in bright field; XII. Merge Ma-Mel-55 EV preparation. Bars represent 200 nm.

were used (546 nm, 557–572 nm) for CD63 and EML4-ALK signal, (488 nm, 500–540 nm) for EML4-ALK and calreticulin signal, and (633 nm, 645–750 nm) for TO-PRO-3 signal. Two different lasers were used independently for each fluorophore (ALEXA 488, ALEXA 546).

FLOW CYTOMETRY

Here 2 µL of purified EVs from H3122 (1×10^8 particles) and H2228 (1×10^9 particles) cell lines and 3 NSCLC plasma samples ($1.7–3.2 \times 10^8$ particles) were incubated overnight at room temperature with 3000 microbeads coated with anti-CD63 (Clone TEA3/18),

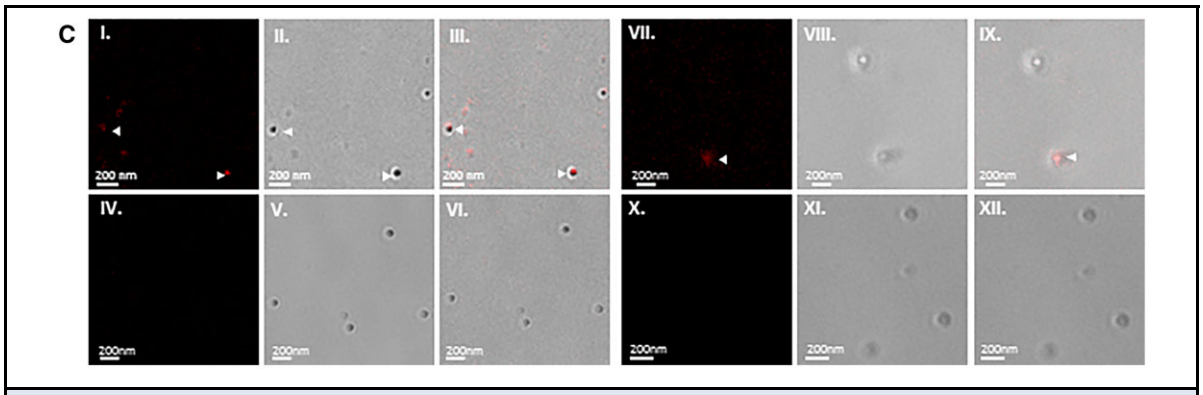

Fig. 2. (continued)

anti-EpCAM (Clone VU-1D9) or Isotype (IgG1; MOPC21) (Immunostep, S.L.) in a final volume of 25 µL of PBS containing 1% casein (Biorad, 1× PBS blocker). Subsequently, beads were stained with either anti-CD9 (VJ1/20) or anti-CD81 (M-38), PE-conjugated antibodies (Immunostep, S.L.) for 1 h at 4 °C. Data were acquired using CytoFLEX flow cytometer and analyzed using Kaluza software (both Beckman Coulter), as previously described (13).

DOT BLOT

Here, 3×10^8 particles from each EV preparation were treated with HBS 1% SDS or with HBS only, adsorbed onto a nitrocellulose membrane, dried, and blocked with PBS-T (PBS 0.1% Tween-20) containing 5% non-fat dry milk for 1 h, followed by a 1 h incubation with primary antibodies at 4°C; mouse anti-*EML4-ALK* variants [5A4 at 2.6 µg/mL (Leica Biosystems)] and anti-CD9 at 1 µg/mL (clone VJ120, Immunostep, S.L.). The membranes were then incubated for 1 h at RT with 0.4 µg/mL Alexa-700-conjugated goat anti-mouse secondary antibody (ThermoFisher). Proteins were visualized using the Odyssey Infrared system (LI-COR Biosciences).

CELL LYSATES AND WESTERN BLOT

Detailed information about cell lysates and western blot is available in the Supplemental Methods. Briefly, Cell lysates were prepared with 1% NP40 TNE buffer containing protease inhibitors. 50 µg of total lysate proteins and 50 µL of the EV-enriched preparation were run in 12% SDS–PAGE. Proteins were transferred to nitrocellulose membranes with Trans-Blot® Turbo™ Transfer Packs (BioRad). Membranes were blocked and incubated with primary antibodies for *EML4-ALK* variants [5A4 antibody (Leica Biosystems)], CD63, CD81 and CD9 tetraspanins [MEM259; MEM-38; and MEM62, respectively (a kind gift from Vaclav Horejsi, Czech Republic)], β-actin (AC-74, Sigma-Aldrich Co.) and calreticulin (NB600-101; Novus Biologicals). Membranes were then incubated with Alexa-700-conjugated goat anti-mouse secondary antibody or Alexa-790-streptavidin secondary antibody (ThermoFisher). Proteins were visualized using the Odyssey Infrared system (LI-COR Biosciences).

EXOVIEW ANALYSIS

Complete characterization of plasma-derived EVs ($N = 2$) was performed by ExoView R100 (NanoView Biosciences) using human tetraspanins kits (EV-DTETRA-C). Chips were prescanned using the provided protocol to identify any previously adhered particles during manufacturing. For incubation, chips were placed in 12-well plates, avoiding contact of the chip corners with the sides of the well. EVs were diluted at 1:100 in the provided incubation solution buffer; 50 µL of the diluted sample was incubated overnight without agitation. Following the manufacturer's protocol, several washes were performed the following day. Then, 1 µg/mL of fluorescently labeled antibodies provided by the kitanti-CD9 kit (CF 488A), anti-CD63 (CF 647A), and the protein of interest anti-*ALK*-(CF 594A) labeled by Alexa Fluor 594 Conjugation Kit Fast (ab269822, ABCAM) were incubated for 1 hour with gentle agitation. The chips were then washed and dried for analysis using ExoView Analyzer (Nanoview Biosciences).

RNA ISOLATION AND QUALITY ASSESSMENT

RNA from EV preparations (50 µL each) was isolated using exoRNeasy® Serum/Plasma Maxi Kit (QIAgen), following the manufacturer's instructions after EVs lysis with QIAzol reagent (QIAgen). Samples were eluted in 14 µL of RNase-free water. EV RNA samples were analyzed with the Agilent RNA 6000 Pico Kit using Agilent 2100 Bioanalyzer (Agilent Technologies).

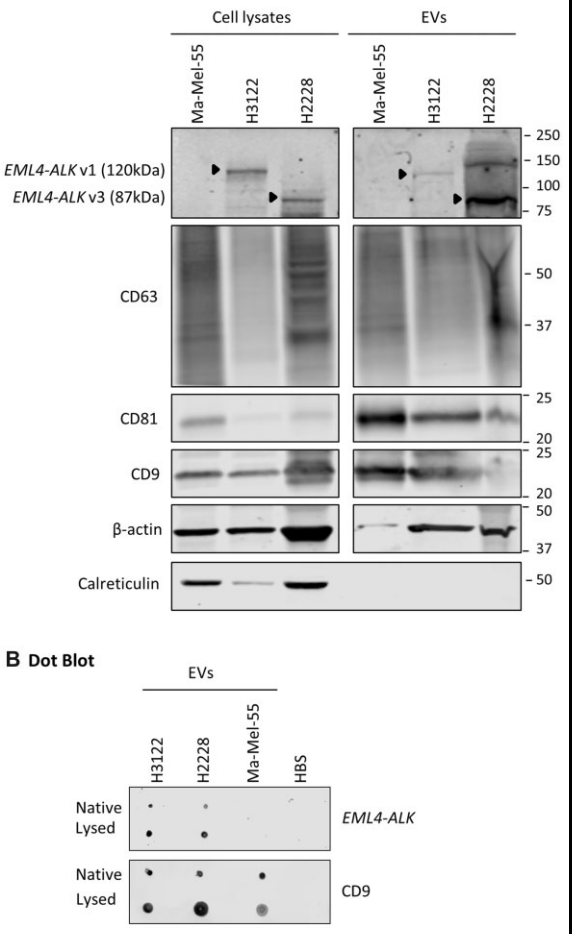

Fig. 3. ***EML4-ALK-fusion*** **protein detection in EV-enriched preparations. (A), Western blot. Total cell lysate proteins and EV-enriched preparations from H3122 and H2228 cell lines were run on SDS-PAGE and showed *EML4-ALK* variant 1 (120 kDa) and variant 3 (87 kDa), respectively, whereas Ma-Mel-55 cell line did not show the *EML4-ALK*-fusion protein. EV preparations showed CD63, CD81, and CD9 tetraspanins expression and did not show calreticulin (negative marker) expression; (B), Dot blot. 3 × 10^8 EVs from H3122 and H2228 cell lines were immobilized on nitrocellulose and *EML4-ALK*-fusion protein expression was analyzed both in native conditions and lysed with 1% SDS. Ma-Mel-55 EVs were used as a negative control. All EV preparations were positive for the CD9 tetraspanin.**

RNA from supernatants obtained by ultracentrifugation of cell medium and plasma were isolated using QIAamp® Circulating Nucleic Acid Kit (QIAgen), following the manufacturer's instructions.

Finally, 6.5 µL of total RNA was reverse-transcribed into complementary DNA (cDNA) using the PrimeScript RT Reagent Kit (TaKaRa) according to the manufacturer's recommendations.

DIGITAL PCR

ALK-fusion variants were analyzed by digital PCR (dPCR) using a QuantStudio® 3D Digital PCR System (Applied Biosystems) as previously described (14, 15). Assays for *ALK*-fusion variants are presented in Supplemental Table S1, as endogenous gene we used the *PUM1* (Hs00472881_m1) assay. A blank (with no cDNA), a negative control [a wild-type (WT) cDNA], and a positive control (H2228 and H3122 cell lysates) were included in each dPCR run. The mutant allele frequency (MAF) was calculated as the ratio of mutant (mut) DNA molecules to the total number of molecules (sum of mutant and WT molecules). Detailed information about the sensitivity of the dPCR *EML4-ALK* TaqMan® assays is available in the Supplemental Methods.

Results

EML4-ALK FUSION CAN BE DETECTED IN EV PREPARATIONS FROM NSCLC CELL LINES

To determine whether *EML4-ALK* translocations are present in NSCLC EV-enriched samples, we used culture supernatants from H3122 and H2228 cell lines. The metastatic melanoma cell line Ma-Mel-55, lacking these rearrangements, was used in parallel as a negative control. EV-enriched preparations were obtained by sequential centrifugation of the conditioned medium and were fully characterized following MISEV2018 guidelines (16). According to NTA the diameter of the particles ranged from 50 to 350 nm with means of 216 nm, 229 nm, and 193 nm and modes of 155 nm, 127 nm, and 128 nm, for H3122, H2228, and Ma-Mel-55 cell lines, respectively (Fig. 1, A), consistent with the size of small-medium EVs described in the literature. Similarly, TEM analysis of the EV-enriched preparations showed 50–300 nm spherical vesicles with the typical cup-shaped morphology, described to be caused by dehydration of vesicles during sample treatment processing for TEM (Fig. 1, B). Gold immunolabeling of CD9 and CD81 showed vesicles carrying these proteins in the EV preparations from the 3 cell lines. Moreover, to assess the presence of different EV-protein markers in the same particle, such as CD63, CD81, and CD9 tetraspanins, the preparation was analyzed by bead-assisted flow cytometry. EVs were captured on beads coated with either tetraspanin or tumor-associated protein markers, such as EpCAM or MICA, and detected with CD9 and CD81 antibodies. Both lung cancer and metastatic

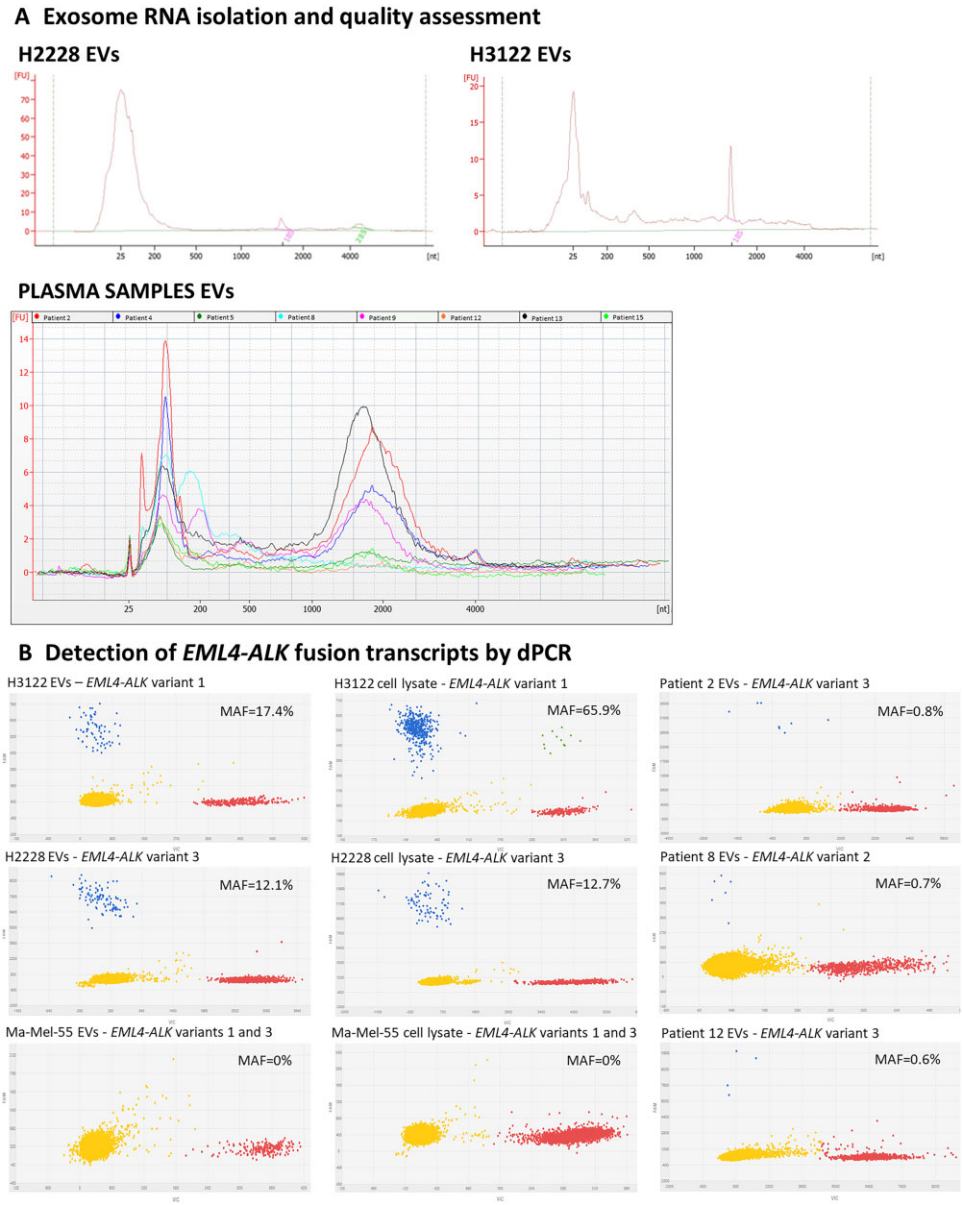

Fig. 4. EV-derived RNA quality assessment and *EML4-ALK*-fusion transcript detection. (A), RNA quality assessment by Agilent RNA 6000 Pico Kit. Bioanalyzer electropherograms showed the fluorescence intensity (FU) (*y* axis) and size distribution in nucleotides (nt) (*x* axis) of EV preparations RNA; (B), Detection of *EML4-ALK*-fusion transcripts by dPCR. *EML4-ALK* variants were labeled with FAM (blue data points), whereas the wild-type is labeled with VIC (red data points). Green and yellow data points indicated the detection of both probes and no detection of probes, respectively. The *y* axis corresponds to FAM measurement and *x* axis corresponds to VIC measurements.

melanoma-derived EVs were analyzed. Binding was measured as a Relative Fluorescence Index (RFI) above 1. NSCLC cells clearly contained EpCAM and CD63 in CD9- and CD81-positive vesicles while metastatic melanoma was positive for the immune-activating ligand MICA, indicating the presence of these protein combinations in the fraction of the EV preparations (Fig. 1, C).

Once the EV preparations were characterized using several standard techniques, the presence of *EML4-ALK*-fusion proteins was evaluated by confocal microscopy and western blot, together with transmembrane

EV-protein markers. Dual labeling of EVs with anti-*ALK* and anti-CD63 antibodies was observed, by confocal microscopy, in H3122 and H2228 EV preparations whereas Ma-Mel-55 EVs only showed CD63 expression (Fig. 2, A, Supplemental Fig. S1). In approximately 30% of EVs, we could detect both markers in the same vesicle. EV preparations were negative for the endoplasmic reticulum protein calreticulin expression (Fig. 2, A and Supplemental Fig. S1). RNA-FISH confirmed the presence of *ALK*-fusion transcripts in H3122 (variant 1) and H2228 (variant 3) derived EVs (Fig. 2, C). Likewise, we corroborated the presence of *ALK-EML4*-fusion protein in EVs by western blot analysis. As presented in Fig. 3, A *EML4-ALK* variant 1 (E13; A20) (120 kDa) and variant 3 (E6a/b; A20) (87 kDa) fusion proteins were clearly detected in H3122 and H2228 cell lysates and EV fractions, respectively, whereas no *ALK*-fusion variant was detected in either the EV fractions or in the lysates of the negative control Ma-Mel-55 cell line. CD63, CD9, and CD81 EV-protein markers, enriched in the EV fraction, were also detected in the same blot, as well as the cytosolic protein β-actin. Calreticulin, used as an EV-negative marker, was only detected in cell lysates. This result established that *EML4-ALK*-fusion protein variants are present and can be detected in EVs derived from tissue culture supernatants of NSCLC cell lines. In addition, we performed a dot blot analysis of the EVs either in their native state or after lysis with 1% SDS. As shown in Fig. 3, B, the tetraspanin CD9 was similarly detected on vesicles in their native state and in the lysed vesicles, indicating that this protein is recognized by the antibody at the vesicle surface. Regarding *EML4-ALK* protein, the positive signal was lower in the native state compared to the lysed vesicles, suggesting that the antibody was recognizing the protein predominantly inside the vesicle (Fig. 3, B). This result also supported the presence of the protein within EVs and not as a coprecipitating aggregate in the EV preparation. The low signal observed in native vesicles could be due to the disruption of a small proportion of the EV membranes on immobilization on the nitrocellulose. *EML4-ALK*-fusion proteins were not detected in Ma-Mel-55 cell lines.

EV-derived RNA from cell lines was analyzed by Agilent RNA 6000 Pico Kit using an Agilent 2100 Bioanalyzer. For both lung cancer cell lines, we mainly identified small RNAs (<200 nt) (H3122 EVs RNA area = 117.1 nt; H2228 EVs RNA area = 67.5 nt), although 18S and 28S rRNA peaks were weakly present (Fig. 4, A). Finally, as shown in Fig. 4, B, dPCR analysis detected *EML4-ALK* variant 1 and variant 3 transcripts in H3122 and H2228 cell lysates, respectively (MAF = 65.9% and MAF = 12.7%, respectively) and EV fractions (MAF = 17.4% and MAF = 12.1%, respectively), whereas the signal was negligible in the corresponding supernatant (Supplemental Fig. S4). Additionally, for the negative control Ma-Mel-55 cell line no *ALK*-fusion transcript variant was detected either in the EV fractions or in the lysates (Fig. 4, B).

EML4-ALK FUSION CAN BE DETECTED IN EV PREPARATIONS FROM NSCLC PATIENT PLASMA SAMPLES

To investigate whether *ALK* fusions were detectable in EVs isolated from clinical samples, plasma-derived EVs from NSCLC patients ($N = 3$) were characterized in terms of size distribution and number of particles by NTA (Fig. 5, A), showing a profile similar to that of the NSCLC cell-derived EVs (Fig. 1). Similarly, CD63, CD81, and CD9 tetraspanins coexpression was confirmed in plasma EVs by flow cytometry ($N = 3$) (Fig. 5, B). In addition, *ALK*-fusion protein was clearly detected in the plasma-derived-EVs from *ALK*-positive NSCLC patients ($N = 2$), using ExoView. Indeed, CD81, CD63, and CD9 captured EV populations contained *ALK*-fusion protein, most notably in CD81-captured EVs (Fig. 5, C and D and Supplemental Fig. S2).

To further characterize the presence of *ALK* rearrangements in plasma-derived EVs, we evaluated the detection of the 3 most common *EML4-ALK*-fusion variants (Supplemental Table S1) at the RNA level by analyzing their corresponding cDNA by dPCR (Fig. 4 and online Supplemental Fig. S3).

To this end, EVs were isolated from the pretreatment plasma sample from 16 *ALK*-positive NSCLC patients. Clinical characteristics of the study population are presented in Supplemental Table S2. Overall, the median concentration of EV-derived RNA from NSCLC patients was 0.618 ng/μL. Small RNAs (<500 nt) were detected in all EV preparations using Bioanalyzer 2100. In addition, 9 patients showed a 2000–4000 nt peak (Fig. 4).

As presented in Table 1, *EML4-ALK* variant 1 (E13; A20) was detected in 2 patients (12.5%), *EML4-ALK* variant 2 (E20; A20) was detected in 1 patient (6.3%) and *EML4-ALK* variant 3 (E6a/b; A20) was detected in 5 patients (31.3%), with a detection rate of 50%. No *ALK*-fusion transcript was detected in the supernatant obtained after plasma ultracentrifugation ($N = 2$) (Supplemental Fig. S4).

Discussion

Liquid biopsies are increasingly used in daily oncology practice as they provide a noninvasive way to identify biomarkers. Specifically, in NSCLC patients there is growing evidence supporting the use of liquid biopsies for Epidermal Growth Factor Receptor (*EGFR*) testing (17, 18). Nevertheless, robust methodologies for the identification of other alterations different from single nucleotide variations (SNVs), such as *EML4-ALK* fusions, are still

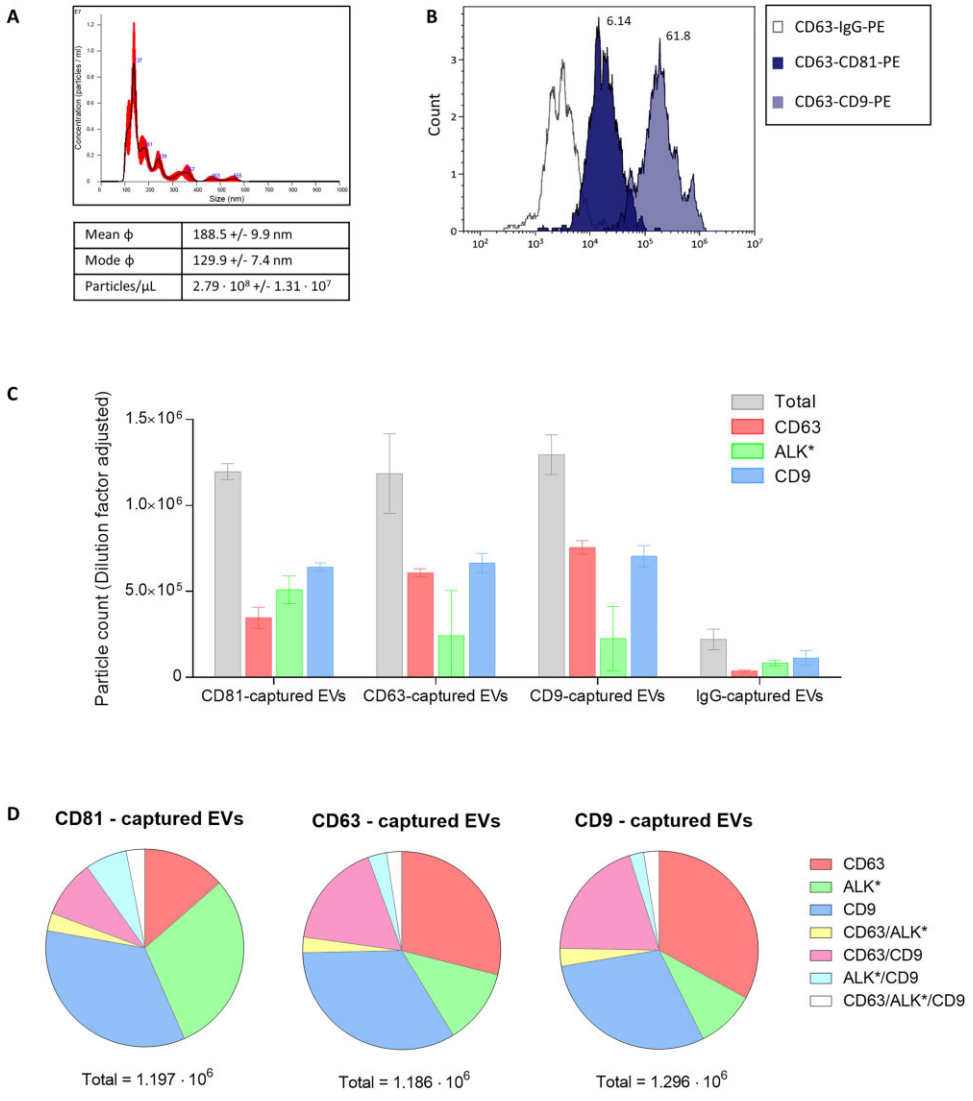

Fig. 5. Characterization of plasma-derived EVs from NSCLC patients. (A), Size and concentration analysis by Nanoparticle tracking analysis (NTA). Mean size and concentration listed in the table were obtained in a NanoSight equipment from a representative experiment out of 3. Φ diameter; (B), Bead-assisted flow cytometry. 2 µL of the EV preparations obtained by plasma ultracentrifugation were incubated with 3000 anti-CD63 coated microbeads in 25 µL of PBS 1% casein. Captured vesicles were detected by flow cytometry after incubation with anti-CD81-PE (left panel), anti-CD9-PE (right panel), or IgG-PE isotype control. Histograms of the fluorescence intensity detected from a representative experiment out of 3 are shown. Relative fluorescence intensity (RFI $= \frac{MFI\ sample}{MFI\ IgG}$) values are shown in each legend. MFI, median fluorescence intensity. PE, phycoerythrin; (C), Analysis of EVs by ExoView platform. Quantification of the number of particles captured by EV-specific tetraspanins. Anti-CD81, anti-CD63, and anti-CD9 antibodies were used for particle capture and fluorescently labeled anti-*ALK**(green), anti-CD63 (red), and anti-CD9 (blue) were subsequently used for particle detection. Anti-MIgG was used as a capture control. 3 capture spots were performed in each sample. Mean ± SD are represented. (D), Analysis of EVs by ExoView platform. Analysis of CD63, CD9, and *ALK** positive particle distribution in plasma-derived EVs. *ALK**, *ALK*-fusion protein.

lacking. Currently, the challenge is to increase the sensitivity of the blood tests for the detection of complex variants such as rearrangements in *ALK*, *ROS1*, *RET*, or *NTRK*. Notably, detecting these fusions using liquid biopsies, although challenging, could potentially expand therapeutic options in NSCLC patients.

Several studies have shown that *ALK* rearrangements can be detected within circulating tumor cells (CTCs)

Table 1. *ALK*-fusion variants detected by dPCR, in EVs derived from the plasma samples of 16 *ALK*-positive NSCLC patients.

Patient	*EML4-ALK* variant	*dPCR MAF*
Patient 1	–	–
Patient 2	Variant 3 (E6a/b; A20)	0.8%
Patient 3	–	–
Patient 4	Variant 3 (E6a/b; A20)	7.1%
Patient 5	Variant 3 (E6a/b; A20)	1.5%
Patient 6	–	–
Patient 7	–	–
Patient 8	Variant 2 (E20; A20)	0.7%
Patient 9	Variant 3 (E6a/b; A20)	16.7%
Patient 10	–	–
Patient 11	–	–
Patient 12	Variant 3 (E6a/b; A20)	0.6%
Patient 13	Variant 1 (E13; A20)	6.7%
Patient 14	–	–
Patient 15	Variant 1 (E13; A20)	0.3%
Patient 16	–	–

(19, 20), although there are important concerns about the feasibility of the implementation of these methodologies in the clinical setting. Likewise, there are a few reports showing that *ALK* fusions can be detected by NGS profiling of cfDNA (21, 22). In this way, McCoach et al. reported clinical benefit from *ALK* inhibitors in 3 patients who were *ALK*-positive by NGS profiling of cfDNA despite being negative *ALK* FISH (23). Nevertheless, the use of cfDNA may have some limitations as *ALK* translocations involve a large number of base pairs, and breakpoints are usually unknown. Complex variants such as large genomic rearrangements, including translocations, can be easily detected at the RNA level as fusion transcripts. However, unlike cfDNA, RNA degrades very quickly due to RNases present in the blood, constituting a major limitation. Thus, the analysis of encapsulated RNA, protected from RNases appears to be a promising approach. With this approach, encouraging results have been reported regarding the analysis of RNA isolated from tumor educated platelets (TEPs), which are thought to be able to sequester tumor-related RNA by a microvesicle dependent mechanism (24), with a 65% sensitivity and 100% specificity for the detection of *EML4-ALK* rearrangements (25).

Likewise, noninvasive biomarker testing using EVs appears to be a promising approach. Interest in EVs was re-energized when different laboratories described the presence of RNA in vesicles (26). To our knowledge, this is the first study thoroughly demonstrating that *ALK* fusions are present and can be detected in EV preparations from *ALK*-positive NSCLC cells and plasma samples from NSCLC patients. We were able to demonstrate the presence of an *ALK*-fusion transcript in EVs isolated from 8 plasma samples from patients who were previously diagnosed as having NSCLC harboring an *ALK*-fusion. Currently, there is intense research aimed to improve the technology for the characterization and phenotyping of EVs and validation of EVs for biomarker identification (27, 28). Size-exclusion chromatography (SEC) has been shown to perform well in separating EVs from clinical samples (29) and an automatic exosome isolation system based on SEC has been developed (qEV Automatic Fraction Collector). Likewise, high sensitivity methods for EV detection based on immune-capture have been described (13). Similarly, an automated, point-of-care device capable of isolating exosomes directly from whole blood has been developed by integrating acoustics and microfluidics (30), suggesting that robust high-throughput EV isolation methods will be available in the near future. In this regard, our results set the basis for noninvasive *ALK*-fusion transcript detection using EV preparations. Remarkably, unraveling the tetraspanin and *ALK*-fusion protein colocalization patterns will be vital for the development of EV-based diagnostic tests. As an exploratory analysis, our data, show that CD81-captured EVs are enriched in *ALK*-fusion protein. These findings should be confirmed in an appropriately sized cohort.

Different RNA populations have been identified in EVs (31–34). According to our data, the RNAs from EVs were mostly small RNAs (<200 nt), although 18S and 28S rRNA peaks were also detected in cell line samples. In some clinical samples, the electrophoretic pattern was compatible with the presence of long noncoding RNAs. Nevertheless, RNA obtained from EVs can be highly affected by the extraction method and studies on EV RNAs characterization remains lacking.

In summary, we have shown here that *ALK* fusions are present in EVs from NSCLC cells and patients. Although further improvements in EV isolation methods are needed, our results indicate that *ALK*-fusion testing through liquid biopsy is feasible. These results set the stage for high-throughput methodologies for fusion transcript detection on liquid biopsies.

ETHICS APPROVAL AND CONSENT TO PARTICIPATE

The study protocol was approved by the Hospital Puerta de Hierro Ethics Committee (internal code 79-18), and was conducted in accordance with the precepts of the Code of Ethics of The World Medical Association (Declaration of Helsinki). All patients provided their appropriate written informed consent to participate in the study prior to enrollment.

CONSENT FOR PUBLICATION

We have obtained consent to publish this paper from all of the study participants.

Supplemental Material

Supplemental material is available at *Clinical Chemistry* online.

Nonstandard Abbreviations: NSCLC, nonsmall cell lung cancer; EVs, extracellular vesicles; TEM, transmission electron microscopy; NTA, nanoparticle tracking analysis; dPCR, digital PCR; ALK, anaplastic lymphoma kinase; ctDNA, circulating tumor DNA; cfRNA, circulating free RNA; FISH, fluorescence in situ hybridization; cDNA, complementary DNA; WT, wild-type; MAF, mutant allele frequency; mut, mutant; RFI, relative fluorescence intensity; EGFR, epidermal growth factor receptor; SNVs, single nucleotide variations; CTCs, circulating tumor cells; TEPs, tumor educated platelets; SEC, size-exclusion chromatography; MFI, mean fluorescence intensity; PE, phycoerythrin; FU, fluorescence intensity

Human Genes: *ALK*, ALK receptor tyrosine kinase; *EGFR*, epidermal growth factor receptor; *EML4*, EMAP like 4; *NTRK*, neurotrophic receptor tyrosine kinase 1; *PUM1*, pumilio RNA binding family member 1; *RET*, ret proto-oncogene; *ROS1*, ROS proto-oncogene 1, receptor tyrosine kinase.

Acknowledgments: H. Peinado (CNIO) for the use of NanoSight; V. Horejsi (Inst. of Molecular Genetics Academy of Sciences of the Czech Republic, Prague) for tetraspanin antibodies. M. A. Molina for H3122 and H2228 cell lines; Annette Paschen (University Hospital Essen, Germany) for Ma-Mel-55 cell line.

Author Contributions: *All authors confirmed they have contributed to the intellectual content of this paper and have met the following 4 requirements(a) significant contributions to the conception and design, acquisition of data, or analysis and interpretation of data; (b) drafting or revising the article for intellectual content; (c) final approval of the published article; and (d) agreement to be accountable for all aspects of the article thus ensuring that questions related to the accuracy or integrity of any part of the article are appropriately investigated and resolved.*

Conception and design, V. González-Rumayor, M. Valés-Gómez, M. Provencio, and A. Romero. Development of methodology, E. Sánchez-Herrero, C. Campos-Silva, Y. Cáceres-Martell, S. Sanz-Moreno, A. Rodríguez-Festa, D. Ares Trotta, C. Patiño, M.J. Coronado, A. Beneitez, R. Jara, N. Lago-Baameiro, T. Camino, L. Robado de Lope, and A. Cruz-Bermúdez. Acquisition of data, E. Sánchez-Herrero, P. Martín-Acosta, M. Provencio, and A. Romero. Analysis and interpretation of data, E. Sánchez-Herrero, C. Campos-Silva, Y. Cáceres-Martell, R. Serna-Blasco, M. Valés-Gómez, and A. Romero. Writing, review, and/or revision of the manuscript, E. Sánchez-Herrero, C. Campos-Silva, Y. Cáceres-Martell, L. Robado de Lope, V. González-Rumayor, M. Valés-Gómez, M. Provencio, and A. Romero. Administrative, technical, or material support, P. Martín-Acosta, C. Patiño, M.J. Coronado, A. Beneitez, R. Jara, and M. Pardo. Study supervision, V. González-Rumayor, M. Valés-Gómez, M. Provencio, and A. Romero. Approved manuscript, All authors.

Authors' Disclosures or Potential Conflicts of Interest: *Upon manuscript submission, all authors completed the author disclosure form. Disclosures and/or potential conflicts of interest:*

Employment or Leadership: R. Jara is CEO of Immunostep, S.L.; A. Beneitez is employee of Immunostep, S.L.
Consultant or Advisory Role: A. Romero, Takeda and M. Provencio, BristolMyers Squibb, Takeda, Roche, AstraZeneca, Merck Sharpe & Dohme.
Stock Ownership: None declared.
Honoraria: None declared.
Research Funding: This study has been funded by Instituto de Salud Carlos III through the project "PI17/01977" (co-funded by European Regional Development Fund/European Social Fund "A way to make Europe"/"Investing in your future"). The work presented in this paper also received funding from the European Union's Horizon 2020 research and innovation program under grant agreement No 875160. E. Sánchez-Herrero was funded by the Consejería de Ciencia, Universidades e Innovación of the Comunidad de Madrid (Doctorados Industriales of the Comunidad de Madrid IND2019/BMD-17258). R. Serna-Blasco was funded by the Consejería de Educación, Juventud y Deporte of the Comunidad de Madrid and by the Fondo Social Europeo (Programa Operativo de Empleo Juvenil, and Iniciativa de Empleo Juvenil, PEJD-2018-PRE/BMD-8640). M. Valés-Gómez was funded by Spanish Ministry of Science and Innovation (MCIU/AEI/FEDER, EU) grant RTI2018-093569-B-I00 and Madrid Regional Government under grant "IMMUNOTHERCAN" (S2017/BMD-3733-2). This work was supported by GEIVEX, Network of Excellence in the Research and Innovation on Exosomes REDIEX, SAF2015-71231-REDT, Network of Excellence in Translational NeTwork for the CLinical application of Extracellular VesicleS (TeNTaCLES) (RED2018-102411-T). M. Provencio, grants from BristolMyers Squibb, Roche, and AstraZeneca.
Expert Testimony: None declared.
Patents: M. Valés-Gómez, Y. Cáceres-Martell, and C. Campos-Silva, EP1641.1562 Method for the detection and/or quantification of extracellular vesicles in fluid biological samples.
Other Remuneration: A. Romero reports personal fees from Takeda, outside the submitted work. M. Provencio reports personal fees, and travel expenses from BristolMyers Squibb, Roche, and AstraZeneca; and personal fees from Merck Sharpe & Dohme and Takeda, outside the submitted work. M. Valés-Gómez, Licence of ExostepTM to Immunostep S.L.

Role of Sponsor: The funding organizations played no role in the design of study, choice of enrolled patients, review and interpretation of data, preparation of manuscript, or final approval of manuscript.

REFERENCES

1. Gainor JF, Varghese AM, Ou SHI, Kabraji S, Awad MM, Katayama R, et al. ALK rearrangements are mutually exclusive with mutations in EGFR or KRASAn analysis of 1,683 patients with non-small cell lung cancer. Clin Cancer Res 2013;19:4273–81.
2. Koivunen JP, Mermel C, Zejnullahu K, Murphy C, Lifshits E, Holmes AJ, et al. EML4-ALK fusion gene and efficacy of an ALK kinase inhibitor in lung cancer. Clin Cancer Res 2008;14:4275–83.
3. Zhang X, Zhang S, Yang X, Yang J, Zhou Q, Yin L, et al. Fusion of EML4 and ALK is associated with development of lung adenocarcinomas lacking EGFR and KRAS mutations and is correlated with ALK expression. Mol Cancer 2010;9:188.
4. Childress MA, Himmelberg SM, Chen H, Deng W, Davies MA, Lovly CA. Fusion partners impact response to ALK inhibition differential effects on sensitivity, cellular phenotypes, and biochemical properties. Mol Cancer Res 2018;16:1724–36.
5. Shaw AT, Kim DW, Nakagawa K, Seto T, Crinó L, Ahn MJ, et al. Crizotinib versus chemotherapy in advanced ALK-positive lung cancer. N Engl J Med 2013;368:2385–94.
6. Gadgeel SM, Gandhi L, Riely GJ, Chiappori AA, West HL, Azada MC, et al. Safety and activity of alectinib against systemic disease and brain metastases in patients with crizotinib-resistant ALK-rearranged nonsmall-cell lung

cancer (AF-002JG). Results from the dose-finding portion of a phase 1/2 study. Lancet Oncol 2014;15:1119–28.
7. Duruisseaux M, Besse B, Cadranel J, Pérol M, Mennecier B, Bigay-Game L, et al. Overall survival with crizotinib and next-generation ALK inhibitors in ALK-positive non-small-cell lung cancer (IFCT-1302 CLINALK): a French nationwide cohort retrospective study. Oncotarget 2017;8:21903–17.
8. NCCN Guidelines. For Patients® nonsmall cell lung cancer metastatic. http://NCCN.org/patients (Accessed 22 Jul 2021).
9. Supplee JG, Milan MSD, Lim LP, Potts KT, Sholl LM, Oxnard GR, et al. Sensitivity of next-generation sequencing assays detecting oncogenic fusions in plasma cell-free DNA. Lung Cancer 2019;134:96–9.
10. Arroyo JD, Chevillet JR, Kroh EM, Ruf IK, Pritchard CC, Gibson DF, et al. Argonaute2 complexes carry a population of circulating microRNAs independent of vesicles in human plasma. Proc Natl Acad Sci USA 2011;108:5003–8.
11. Deatherage BL, Cookson BT. Membrane vesicle release in bacteria, eukaryotes, and archaea: a conserved yet underappreciated aspect of microbial life. Infect Immun 2012;80:1948–57.
12. López-Cobo S, Pieper N, Campos-Silva C, García-Cuesta EM, Reyburn HT, Paschen A, Valés-Gómez M. Impaired NK cell recognition of vemurafenib-treated melanoma cells is overcome by simultaneous application of histone deacetylase inhibitors. Oncoimmunology 2018;7:e1392426.
13. Campos-Silva C, Cáceres-Martell Y, López-Cobo S, Rodriguez MJ, Jara R, Yáñez-Mó M, Valés-Gómez M. An immunocapture-based assay for detecting multiple antigens in melanoma-derived extracellular vesicles. Methods Mol Biol 2021;2265:323–44.
14. Romero A, Serna-Blasco R, Alfaro C, Sánchez-Herrero E, Barquín M, Turpin MC, et al. ctDNA analysis reveals different molecular patterns upon disease progression in patients treated with osimertinib. Transl Lung Cancer Res 2020;9:532–40.
15. Sánchez-Herrero E, Serna-Blasco R, Ivanchuk V, García-Campelo R, Dómine Gómez M, Sánchez JM, et al. NGS-based liquid biopsy profiling identifies mechanisms of resistance to ALK inhibitors: a step toward personalized NSCLC treatment. Mol Oncol 2021;15:2363–76.
16. Théry C, Witwer KW, Aikawa E, Alcaraz MJ, Anderson JD, Andriantsitohaina R, et al. Minimal information for studies of extracellular vesicles 2018 (MISEV2018): a position statement of the International Society for Extracellular Vesicles and update of the MISEV2014 guidelines. J Extracell Vesicles 2018;7:1535750.
17. Romero A, Jantus-Lewintre E, García-Peláez B, Royuela A, Insa A, Cruz P, et al. Comprehensive cross-platform comparison of methods for non-invasive EGFR mutation testing: results of the RING observational trial. Mol Oncol 2021;15:43–56.
18. Ettinger DS, Wood DE, Aggarwal C, Aisner DL, Akerley W, Bauman JR, et al.; OCN. Non-small cell lung cancer, version 1.2020: featured updates to the NCCN guidelines. J Natl Compr Cancer Netw 2019;17:1464–72.
19. Aieta M, Facchinetti A, De Faveri S, Manicone M, Tartarone A, Possidente L, et al. Monitoring and characterization of circulating tumor cells (CTCs) in a patient with EML4-ALK–positive non–small cell lung cancer (NSCLC). Clin Lung Cancer 2016;17:e173–77.
20. Faugeroux V, Pailler E, Auger N, Taylor M, Farace F. Clinical utility of circulating tumor cells in ALK-positive non-small-cell lung cancer. Front Oncol 2014;4:281.
21. Odegaard JI, Vincent JJ, Mortimer S, Vowles JV, Ulrich BC, Banks KC, et al. Validation of a plasma-based comprehensive cancer genotyping assay utilizing orthogonal tissue- and plasma-based methodologies. Clin Cancer Res 2018;24:3539–49.
22. Paweletz CP, Sacher AG, Raymond CK, Alden RS, O'Connell A, Mach SL, et al. Bias-corrected targeted next-generation sequencing for rapid, multiplexed detection of actionable alterations in cell-free DNA from advanced lung cancer patients. Clin Cancer Res 2016;22:915–22.
23. McCoach CE, Blakely CM, Banks KC, Levy B, Chue BM, Raymond VM, et al. Clinical utility of cell-free DNA for the detection of ALK fusions and genomic mechanisms of ALK inhibitor resistance in non–small cell lung cancer. Clin Cancer Res 2018;24:2758–70.
24. Nilsson RJA, Balaj L, Hulleman E, Van Rijn S, Pegtel DM, Walraven M, et al. Blood platelets contain tumor-derived RNA biomarkers. Blood 2011;118:3680–3.
25. Nilsson RJA, Karachaliou N, Berenguer J, Gimenez-Capitan A, Schellen P, Teixido C, et al. Rearranged EML4-ALK fusion transcripts sequester in circulating blood platelets and enable blood-based crizotinib response monitoring in non-small-cell lung cancer. Oncotarget 2016;7:1066–75.
26. Valadi H, Ekström K, Bossios A, Sjöstrand M, Lee JJ, Lötvall JO. Exosome-mediated transfer of mRNAs and microRNAs is a novel mechanism of genetic exchange between cells. Nat Cell Biol 2007;9:654–9.
27. Liang Y, Lehrich BM, Zheng S, Lu M. Emerging methods in biomarker identification for extracellular vesicle-based liquid biopsy. J Extracell Vesicles 2021;10:e12090.
28. Bordanaba-Florit G, Royo F, Kruglik SG, Falcón-Pérez JM. Using single-vesicle technologies to unravel the heterogeneity of extracellular vesicles. Nat Protoc 2021;16:3163–85.
29. Böing AN, van der Pol E, Grootemaat AE, Coumans FAW, Sturk A, Nieuwland R. Single-step isolation of extracellular vesicles by size-exclusion chromatography. J Extracell Vesicles 2014;3:23430.
30. Fais S, O'Driscoll L, Borras FE, Buzas E, Camussi G, Cappello F, et al. Evidence-based clinical use of nanoscale extracellular vesicles in nanomedicine. ACS Nano 2016;10:3886–99.
31. Kim KM, Abdelmohsen K, Mustapic M, Kapogiannis D, Gorospe M. RNA in extracellular vesicles. Wiley Interdiscip Res RNA 2017;8:e1413.
32. Nolte-'t Hoen ENM, Buermans HPJ, Waasdorp M, Stoorvogel W, Wauben MHM, 't Hoen PAC. Deep sequencing of RNA from immune cell-derived vesicles uncovers the selective incorporation of small noncoding RNA biotypes with potential regulatory functions. Nucleic Acids Res 2012;40:9272–85.
33. Crescitelli R, Lässer C, Szabó TG, Kittel A, Eldh M, Dianzani I. Distinct RNA profiles in subpopulations of extracellular vesicles: apoptotic bodies, microvesicles and exosomes. J Extracell Vesicles 2013;2:20677.
34. Zhang S, Du L, Wang L, Jiang X, Zhan Y, Li J, et al. Evaluation of serum exosomal LncRNA-based biomarker panel for diagnosis and recurrence prediction of bladder cancer. J Cell Mol Med 2019;23:1396–405.

SUPPLEMENTAL METHODS

Cell lines

Cell lines from NSCLC (H3122 and H2228) were grown in RPMI 1640 (Sigma-Aldrich Co.) with 10% heat-inactivated fetal bovine serum (FBS) (Gibco) 1 mM L-Glutamine, 1 mM Sodium Pyruvate, 0.1 mM nonessential amino acids, 10 mM HEPES and Penicillin and Streptomycin at 100 µg/ml (Sigma-Aldrich Co.). As a control, the metastatic melanoma cell line (Ma-Mel-55) was used, which was grown in the same conditions. Cells were maintained at 37°C, in 5% CO_2/95% air, and passaged when cells reached 80-90% confluence. H3122 and H2228 cell lines were a gift from Miguel Angel Molina (Pangaea Oncology, Quiron Dexeus University Hospital, Barcelona, Spain) and they were authenticated by satellite analysis at the genomics service of the Institute of Biomedical Research (IIB-CSIC). Cells were assayed for mycoplasma contamination.

EVs isolation

For EV isolation cell lines were grown for 3-5 days in their appropriate medium supplemented with 1% vesicle-free serum (prepared by ultracentrifugation at 100,000 x *g* for 20 h using a Beckman Coulter Optima MAX-XP ultracentrifuge with an MLA-55 rotor (K-factor = 52) with no brake (Beckman Instruments). EVs were enriched by sequential centrifugation of cell culture supernatants (200mL). Briefly, supernatants were centrifuged twice for 10 min at 200 x *g*, followed by two centrifugations at 500 x *g* for 10 min, using a Thermo Scientific Sorvall Legend XFR Centrifuge (ThermoFisher) with an TX-750 rotor (K-factor = 9.783) with brake at maximum power, and one centrifugation of 30 min at 10,000 x *g* (using the ultracentrifuge above-mentioned). Finally, ultracentrifugation at 100,000 x *g* for 2 h at 4 °C with no brake was carried out to pellet EVs down and the supernatant was discarded by pouring it off. Pellets were air-dried at room temperature (RT) and re-suspended in 260 µL of HEPES-buffered saline buffer (HBS: 10 mM HEPES pH 7.2, 150 mM NaCl) pipetting up and down until the pellet was dissolved. Plasma samples were collected in a 10-mL Streck Cell-Free DNA BCT® (Streck) tube. Cell debris were removed by centrifugation at 2000 x *g* for 10 min at 4°C using a Thermo Scientific Sorvall Legend XFR Centrifuge with brake at maximum power. Plasma samples were diluted in PBS (1:3) and centrifuged once at 110,000 x *g* for 2 h at 4°C with no brake using a Beckman Coulter Optima MAX-XP ultracentrifuge. Pellets were air-dried and re-suspended in 50 µL of HEPES-buffered saline buffer by pipetting.

Transmission electron microscopy (TEM) and gold immunolabelling

1 µL of H3122 and H2228 EV preparation (4 x 10^8 particles) were diluted 1:10 in HBS, adsorbed for 2-3 min at RT on carbon-coated 400-mesh 240 formvar grid and either stained with 2% uranyl acetate for 1 min at RT and analyzed directly in the electron microscope or labeled with antibodies as follows. Grids were blocked for 15 min at RT with HBS containing 1.5% Bovine Serum Albumin (BSA), incubated for 25 min at RT with the primary antibody either anti-CD9 clone VJ120, (Immunostep, S.L.) or anti-CD81 clone 5A6 (Santa Cruz Biotechnology), both at 14 µg/ml, washed 4 times for 2 min at RT, blocked again for 10 min at RT with HBS 1.5% BSA, incubated 20 min at RT with goat anti-mouse fab2'-gold 10 nm (19 µg/ml, BBI International) diluted 1:40, in HBS 1.5% BSA, washed twice 5 min RT in HBS and 4 times 2 min RT in H_2O and finally stained with uranyl acetate 2% for 1 min, dried and analyzed using a Jeol JEM 1011 (JEOL Ltd.) electron microscope operating at 100 kV with a CCD camera Gatan Erlangshen ES1000W (Gatan Ink).

Confocal microscopy

A drop of EV pellet was put on a 35 mm imaging dish with a polymer coverslip bottom for high-end microscopy (ibidi), and dried. EVs were fixed with 4% p-formaldehyde for 10 min, washed with PBS, and treated with NH_4Cl 50 mM for 10 min. After permeabilization with 0.2% Triton X-100 for 10 min, samples were blocked with 5% BSA for 30 min and incubated with anti-CD63 antibody (1:100, 0.1 mg/mL, Merck Millipore) at 4°C overnight. The following day the specimens were washed with PBS and incubated with a goat anti Mouse secondary antibody conjugated to ALEXA 546 or 488 (1:500, 2 mg/mL, Invitrogen-Life Technologies), for 45 min at RT. For a second immunodetection, the samples were blocked again with BSA 5%, incubated with an undiluted rabbit anti-*ALK* antibody (Ventana D5F3; Cell Signaling Technology) or with a rabbit anti-calreticulin antibody at 250 µg/mL (NB600-101; Novus Biologicals) at 4°C overnight, washed with PBS, and incubated with a goat anti-rabbit secondary antibody conjugated to ALEXA 488 or 546 (1:500, 1 mg/mL, Invitrogen-Life Technologies) for 45 min at RT and washed with PBS.

Fluorescence in situ hybridization (FISH) was performed using fixed EV-enriched samples and parent cells which were washed with PBS. EV-enriched samples and parent cells were permeabilized with 0.2% Triton X-100 for 10 min, dehydrated with 50%, 70%, and 100% ethanol for 10 min and incubated with a biotinylated *EML4-ALK* RNA probe (40 nM) at 75°C for 5 min. The specimens were incubated with hybridization buffer (30% formamide, 0.01% SDS, 20mM Tris-HCl and 0.9 M ClNa) at 60°C overnight and washed with a washing buffer (1.8 M ClNa, 0.01% SDS and 20 mM Tris-HCl) at 65°C for 5 min and with PBS for 5 min. The samples were blocked with BSA 5% and incubated with anti-streptavidin antibody conjugated to ALEXA 546 (2 mg/mL, Invitrogen-Life Technologies) for 45 min at RT. Non-permeabilized and non-dehydrated cells were incubated with a biotinylated *EML4-ALK* RNA probe (40 nM) at 75°C for 5 min, as a control condition. Nuclei were stained with TO-PRO-3 (Thermo Fisher Scientific) diluted 1/500 in PBS for 20 min at RT. Finally, slides were washed 3 times in PBS and the coverslips were mounted in PBS/glycerol.

Images were collected with a TCS SP5 confocal microscope (Leica Microsystems) using a 63× HCX PL APO (1.25–1.52 numerical aperture) oil-immersion objective and 3x zoom. The two channels were acquired sequentially to avoid cross-talk between them. For immunofluorescence, the following excitation and emission parameters were used: (546 nm, 557-572 nm) for CD63 and *EML4-ALK* signal, (488 nm, 500-540 nm) for *EML4-ALK* and calreticulin signal and (633 nm, 645–750 nm) for TO-PRO-3 signal. Also, bright field was used. Two different lasers were used independently for each fluorophore (ALEXA 488, ALEXA 546). Laser intensity and detector sensitivity settings remained constant for all image acquisitions for experimental replicas.

Cell lysates and Western blot

Cell lysates were prepared with 1% NP40 TNE buffer (50 mM Tris, 150 mM NaCl, 5 mM EDTA, pH 7.5), containing protease inhibitors (1 µM Leupeptin and 1 µM Pepstatin A), incubated for 30 min on ice and centrifuged to pellet the nuclei. 50 µg of total lysate proteins and 50 µL of the EV-enriched preparation were run in SDS-PAGE either under reducing (loading buffer containing 1 mM DTT) or non-reducing conditions. Samples were boiled at 95 °C for 5 min and run on 12% PAGE. Proteins were transferred to nitrocellulose membranes with Trans-Blot® Turbo™ Transfer Packs (Bio-Rad). Membranes were blocked with PBS-T containing 5% non-fat dry milk for 1 h, followed by an overnight-incubation in primary antibodies at 4°C; *EML4-ALK* variants [5A4 antibody at 2.6 µg/mL (Leica Biosystems)] and CD63, CD81 and CD9 tetraspanins [MEM259 (1

μg/mL); MEM-38 (1 μg/mL); and MEM62 (1 μg/mL) respectively (kind gift from Vaclav Horejsi, Czech Republic)]. β-actin was detected with monoclonal anti-β-actin produced in mouse (Sigma-Aldrich Co.) at 0.13 μg/mL and calreticulin (EV-negative marker) was detected with a polyclonal anti-calreticulin produced in rabbit (NB600-101; Novus Biologicals) at 1 μg/mL, incubated for 1 h at RT. The membranes were then incubated with 0.4 μg/mL of the Alexa-700-conjugated goat anti-mouse secondary antibody or Alexa-790-streptavidin (0.4 μg/mL) secondary antibody (ThermoFisher) for 30 min at RT. Proteins were visualized using the Odyssey Infrared system (LI-COR Biosciences).

Platelets isolation

As it has been suggested that *ALK* fusion transcripts can be detected in tumor-educated platelets (TEPs), for cases 08 and 12 we obtained paired samples for plasma and platelets isolation.

Platelets were isolated from platelet-rich plasma obtained from plasma samples collected in EDTA tubes by centrifugation at 200 x *g* for 20 min at RT followed by centrifugation at 400 x *g* for 20 min at RT using a Thermo Scientific Sorvall Legend XFR Centrifuge with brake at maximum power. TEPs' pellet was stored at −80 °C until further use.

RNA from TEPs was isolated using QIAamp® Circulating Nucleic Acid Kit (QIAgen), adding to the pellet phosphate-buffered saline up to 1 mL and following the manufacturer's instructions. Finally, 6.5 μL of total RNA was reverse-transcribed into complementary DNA (cDNA) using the PrimeScript RT Reagent Kit (TaKaRa) according to the manufacturer's recommendations.

Statistical analysis

Discrete variables are displayed as proportions, and continuous variables as means, unless specified otherwise.

The mutant allele frequency (MAF) was calculated as the ratio of mutant (mut) DNA molecules to the total number of molecules (sum of mutant and wt molecules).

Limit of detection (LOD) and limit of quantitation (LOQ) for dPCR *EML4-ALK* variants TaqMan® assays.

To establish the limit of detection (LOD) and the limit of quantitation (LOQ) of the dPCR *EML4-ALK* variant 1 (Hs03654556_ft) and 3 (Hs03654558_ft) TaqMan® assays we adopted the recommendations of The International Council for Harmonisation of Technical Requirements for Pharmaceuticals for Human Use (ICH) Guidelines. ICH Q2 (R1) guidelines (Validation of analytical procedures: text and methodology).

To this aim RNA from H3122 and H2228 cell lysates harboring the specific *EML4-ALK* fusion transcript was reverse-transcribed into complementary DNA (cDNA). LOD and LOQ were estimated for an input of 10 ng of total RNA. Then, cDNA was mixed in a background of wt cDNA (from RNA from healthy donors) at different mutant allele concentrations (10%, 5%, 1%, 0.5%, 0.1%, 0.05%). The standard error of the y-intercept was used to calculate the standard deviation. Pearson's correlation coefficients were 0.9651 and 0.9996 for variant 1 and 3 assays, respectively, showing that the measured mutant allele frequency correlated with the expected mutant allele frequency in both cases. LOD was below 0.1% in both cases.

***EML4-ALK* variant 1**

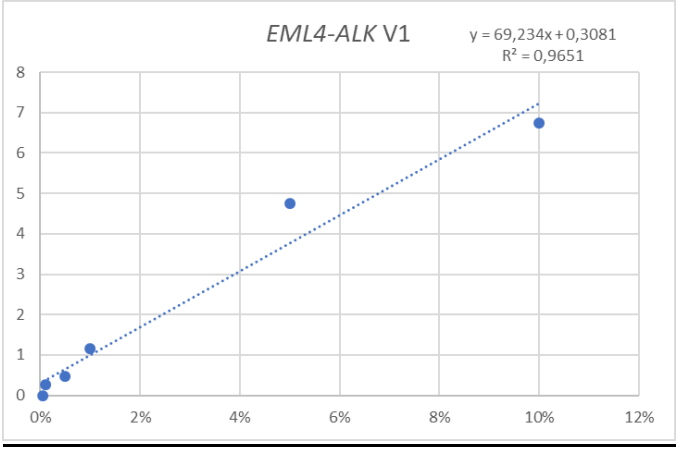

Summary Output

Regresion Statistics	
Multiple R	0,982404893
R Square	0,965119373
Adjusted R Square	0,956399217
Standard Error	0,588833506
Observations	6

ANOVA

	df	*SS*	*MS*	*F*	*Significance F*
Regression	1	38,37441574	38,3744157	110,676839	0,00046166
Residual	4	1,386899592	0,3467249		
Total	5	39,76131533			

	Coefficients	*Standard Error*	*t Stat*	*P-value*	*Lower 95%*	*Upper 95%*
Intercept	0,308102831	0,301890661	1,02057755	0,36515715	-0,53008002	1,14628568
X Variable	69,23353163	6,580942739	10,520306	0,00046166	50,9619054	87,5051579

LOD	0,044%
LOQ	0,014%

Residual Output

Observation	*Predicted Y*	*Residuals*
1	7,231455993	-0,492455993
2	3,769779412	0,978220588
3	1,000438147	0,153561853
4	0,654270489	-0,183270489
5	0,377336362	-0,113336362
6	0,342719597	-0,342719597

***EML4-ALK* variant 3**

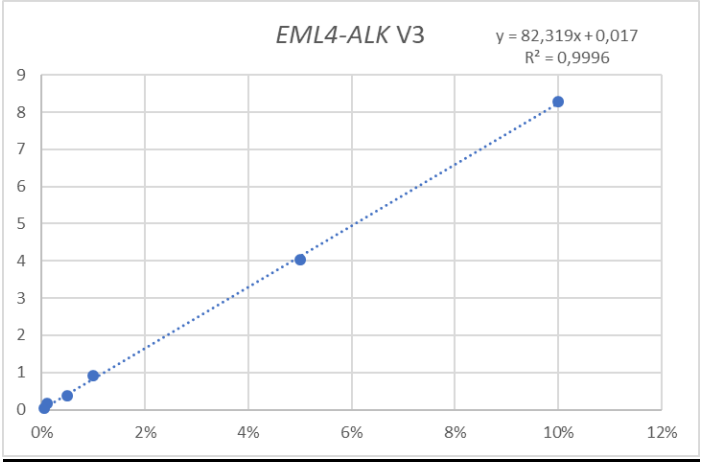

Summary Output

Regresion Statistics	
Multiple R	0,99978714
R Square	0,999574325
Adjusted R Square	0,999467907
Standard Error	0,075998798
Observations	6

ANOVA

	df	*SS*	*MS*	*F*	*Significance F*
Regression	1	54,25138006	54,2513801	9392,84896	6,7959E-08
Residual	4	0,023103269	0,00577582		
Total	5	54,27448333			

	Coefficients	*Standard Error*	*t Stat*	*P-value*	*Lower 95%*	*Upper 95%*
Intercept	0,016976314	0,038964032	0,43569193	0,68554113	-0,09120518	0,12515781
X Variable	82,31917186	0,849380573	96,9167114	6,7959E-08	79,9609133	84,6774304

LOD	0,0047%
LOQ	0,0016%

Residual Output

Observation	*Predicted Y*	*Residuals*
1	8,2488935	0,0431065
2	4,132934907	-0,093934907
3	0,840168033	0,065831967
4	0,428572174	-0,065572174
5	0,099295486	0,060704514
6	0,0581359	-0,0101359

SUPPLEMENTAL TABLES

Table S1. dPCR assays used.

Genes	*Variant*	*dPCR TaqMan assay*
EML4-ALK	*1 (E13;A20)*	*Hs03654556_ft*
EML4-ALK	*2 (E20;A20)*	*Hs03654557_ft*
EML4-ALK	*3 (E6a/b;A20)*	*Hs03654558_ft*

Table S2. Baseline characteristics of the study cohort.

Feature		***N***	***%***
Age of Diagnosis (years)	Median (Min-Max)	56.5 (37-86)	
Sex	Male Female	7 9	43.75% 56.25%
Smoking Status	Active smoker Former smoker Never smoker	2 4 10	12.50% 25% 62.50%
ECOG Performance Status	0 1 2	2 12 2	12.50% 75% 12.50%
Histology	Adenocarcinoma	16	100%
Clinical Stage at diagnosis	IIIA IVA IVB	1 8 7	6.25% 50% 43.75%

SUPPLEMENTAL FIGURES

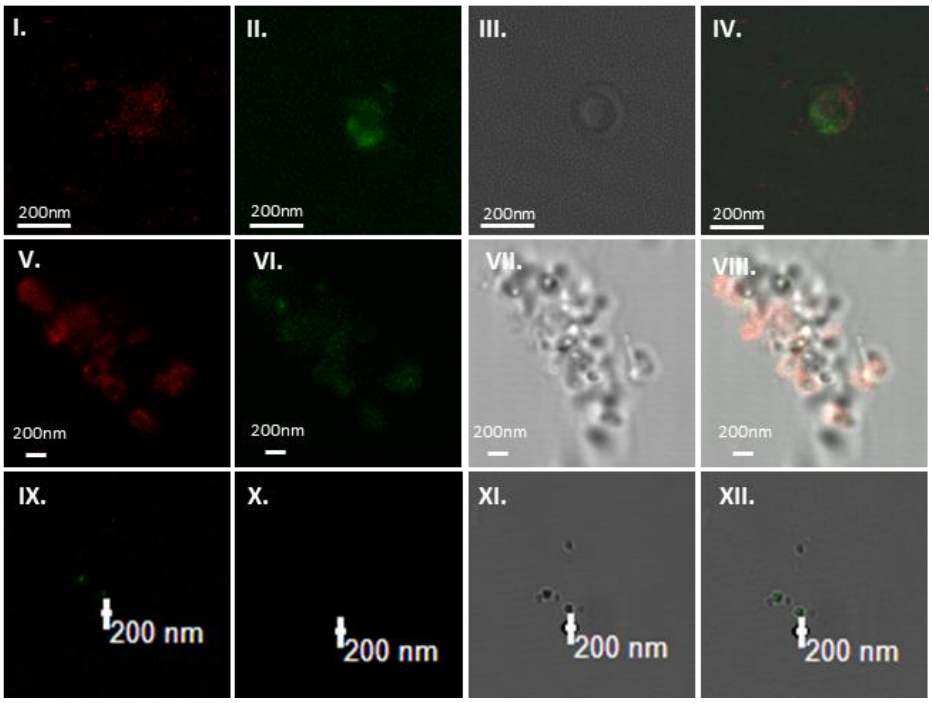

Figure S1. Dual labeling of H3122 and H2228 EVs preparations with CD63, *ALK,* and calreticulin antibodies: I. H3122 EVs with *ALK* (red); **II.** H3122 EVs with CD63 (green); **III.** H3122 Evs in bright field**; IV.** Merge; **V.** H2228 EVs with CD63 (red); **VI.** H2228 EVs with *ALK* (green); **VII.** H2228 Evs in bright field; **VIII.** Merge; **IX.** H2228 EVs stained with CD63 antibody (green); **X.** H2228 EVs stained with calreticulin antibody (red); **XI.** H2228 EVs in bright field; **XII.** Merge. Bars represent 200nm.

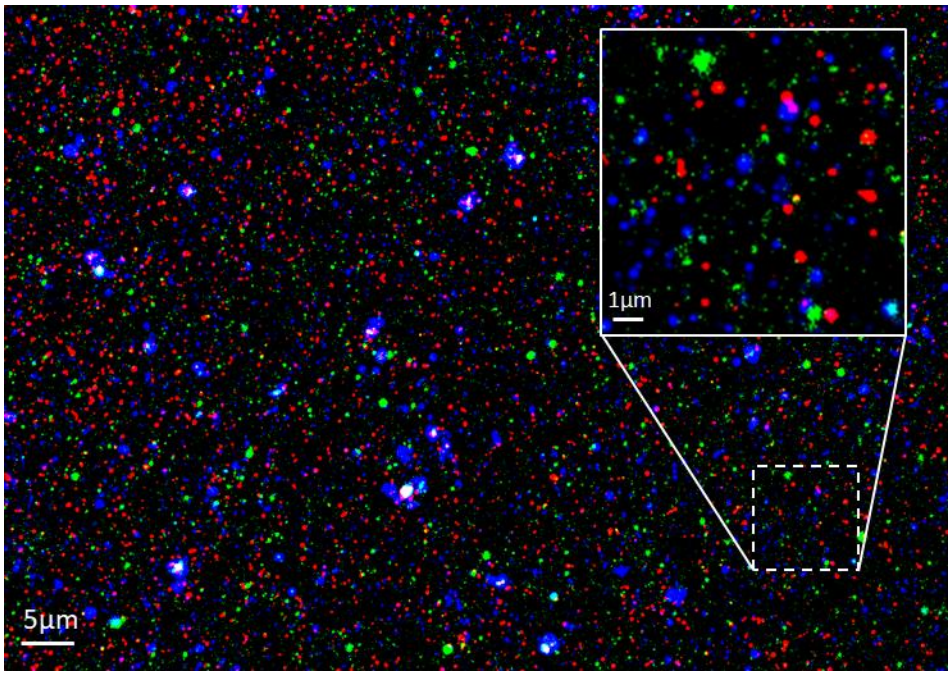

Figure S2. Characterization of EV-enriched preparations from NSCLC plasma samples by ExoView platform. CD9-captured EVs image in fluorescence mode: CD63 in red, CD9 in blue, *ALK** in green, CD63-*ALK** in yellow, CD63-CD9 in purple, *ALK**-CD9 in light blue, and CD63-CD9-*ALK** in white. *ALK**, *ALK* fusion protein.

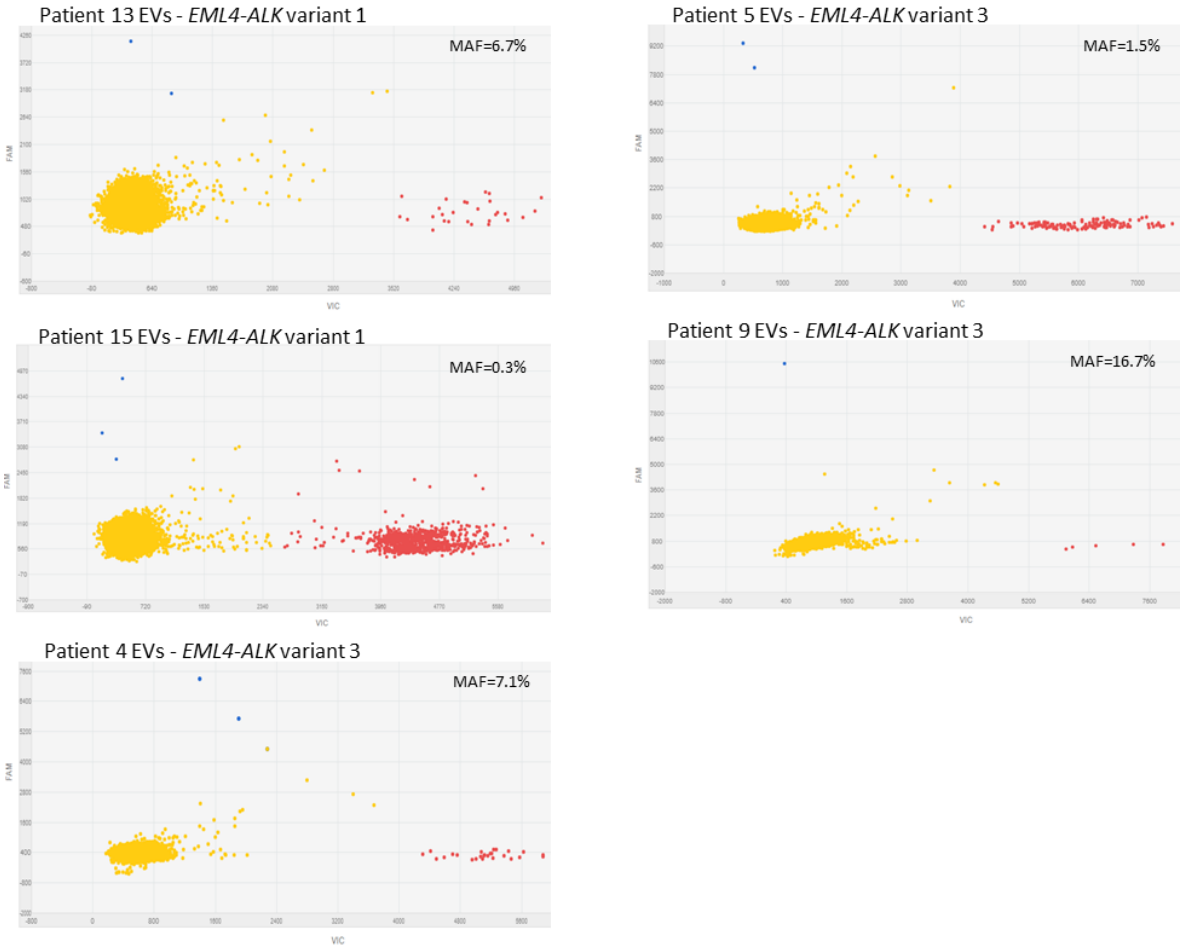

Figure S3. Detection of *EML4-ALK* fusion transcripts by dPCR. *EML4-ALK* variants were labeled with FAM (blue data points), whereas the wild type is labeled with VIC (red data points). Yellow data points indicate no detection of probes. Y-axis corresponds to FAM measurement and X-axis corresponds to VIC measurements**.**

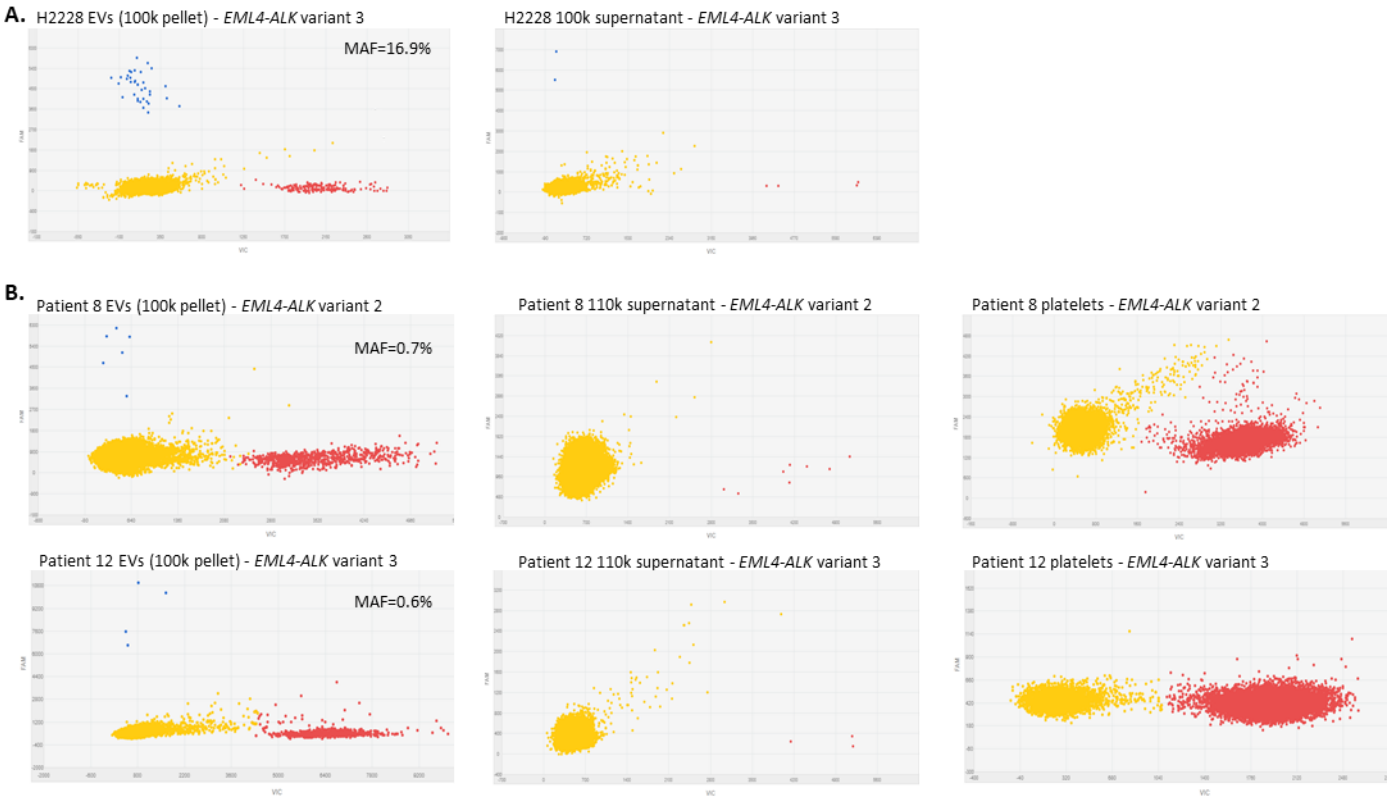

Figure S4. Comparison of ultracentrifugation pellet and supernatant as well as platelets for the detection of *EML4-ALK* fusion transcripts by dPCR. A. Analysis of the RNA contained in the pellet and the supernatant obtained by H2228 cell culture medium ultracentrifugation at 100,000 x *g* for 2 h at 4 °C with no brake. **B**. Analysis of the RNA found in platelets, EV preparations, and the supernatant obtained by plasma ultracentrifugation of patients 8 and 12 at 110,000 x *g* for 2 h at 4 °C with no brake. *EML4-ALK* variants are labeled with FAM (blue data points), whereas the wild type is labeled with VIC (red data points). Yellow data points no detection of probe (no amplification). Y-axis corresponds to FAM measurement and X-axis corresponds to VIC measurements**.**

DISCUSIÓN

Biopsia líquida en pacientes con CPCNP

La medicina de precisión ha tenido un impacto espectacular en el manejo clínico de los pacientes oncológicos, especialmente en aquellos con CPCNP, en gran parte debido al número creciente de oncogenes que son dianas moleculares de fármacos dirigidos; los cuales han supuesto una mejora significativa tanto en la supervivencia como en la calidad de vida de los pacientes. Las guías clínicas en cáncer de pulmón actualmente recomiendan el estudio de mutaciones en los genes de *EGFR*, *KRAS*, *BRAF;* la alteración de salto del exón 14 de *MET*; reordenamientos en *ALK*, *ROS1*, *NTRK1/2/3* y *RET*; y el análisis de los niveles de expresión de PD-L1 (26). Además, el incremento de nuevas terapias dirigidas en desarrollo clínico conlleva el estudio de biomarcadores emergentes como *ERBB2* (*HER2*).

A pesar de estos avances, algunos estudios han reportado un bajo número de pacientes con CPCNP con muestra de tejido tumoral adecuada y suficiente para el genotipado completo de estos biomarcadores (97,127). Actualmente, en España las guías clínicas recomiendan el estudio de *EGFR*, *ALK*, *ROS1* y *BRAF*. Por otro lado, la biopsia puede no representar la totalidad de las características genéticas del tumor, dada la enorme heterogeneidad tanto del tumor primario como de las distintas localizaciones metastásicas.

Por otro lado, existen estudios en los que se refleja que menos del 50% de los pacientes con CPCNP son re-biopsiados en el momento de la progresión a una línea de tratamiento con una muestra de suficiente calidad y/o cantidad (128). En concreto, en el estudio de Bosc C *et al*. tan sólo el 46% de los pacientes con mutación en *EGFR* o con fusión en *EML4-ALK* fueron re-biopsiados tras la progresión a una línea de *EGFR/ALK*-TKI, obteniéndose una muestra adecuada únicamente en el 42% de los mismos (129). La adaptabilidad dinámica de los tumores a las terapias dirigidas mediante la aparición de subclones, dentro de la lesión primaria o en distintas lesiones metastásicas (130), puede condicionar el comportamiento de la enfermedad y la sensibilidad a otras líneas de tratamiento. Además, la monitorización de la terapia es especialmente importante en los pacientes con CPCNP tratados con TKIs debido a la duración relativamente larga del tratamiento y a la aparición de resistencia adquirida, que por otro lado pude ser accionable con otro fármaco.

La biopsia líquida supone una herramienta no invasiva, eficaz y práctica para la identificación de alteraciones somáticas derivadas de tumores, permitiendo establecer una terapia dirigida en un mayor número de pacientes, así como la monitorización de la enfermedad a lo largo del tratamiento (131). Por otro lado, las muestras de biopsia líquida contienen una gran variedad de moléculas y compartimentos que contienen información genética procedente del tumor y cuya selección dependerá de la alteración que se quiera estudiar.

En esta Tesis se ha puesto especial interés en la evaluación de la utilidad clínica de la biopsia líquida para la monitorización de los pacientes con CPCNP a lo largo del tratamiento con terapias dirigidas basadas en TKIs, en especial aquellos tumores portadores de fusiones genómicas en las que el gen *ALK* se encuentra involucrado. Durante el desarrollo de esta Tesis se ha puesto a punto la detección de reordenamientos en *EML4-ALK,* a nivel de proteína y transcrito de fusión, a través del estudio de EVs. Esta alternativa mínimamente invasiva podría establecer las bases para el desarrollo de metodologías automatizadas que puedan implantarse en la práctica clínica,

incrementando la detección de pacientes con CPCNP portadores de fusiones génicas diagnosticados y, por consiguiente, tratados correctamente en base a su perfil molecular.

Utilidad del ctDNA para el estudio de biomarcadores en pacientes con CPCNP

El ctDNA presente en los fluidos corporales es un biomarcador no invasivo altamente específico y es el más estudiado y empleado en el análisis del perfil molecular de los tumores en la práctica clínica. Conjuntamente a la identificación de biomarcadores y mecanismos de resistencia, los niveles de ctDNA totales se emplean también como biomarcadores independientes de predicción de la respuesta a la terapia o de progresión de la enfermedad. En este sentido, los pacientes con bajos niveles de ctDNA en la muestra pre-tratamiento o los pacientes que logran alcanzar niveles indetectables de ctDNA en sangre a lo largo del tratamiento, presentan un mejor pronóstico y tiempos de respuesta más duraderos (132). Además, el ctDNA permite en algunos casos una detección más temprana de la progresión con respecto a las pruebas de imagen (92,133,134).

Actualmente, el genotipado del ctDNA está recomendado en pacientes con CPCNP en circunstancias clínicas en las que el paciente no esté en condiciones médicas para la obtención invasiva de muestras de tejido o si éstas son insuficientes para el análisis molecular en el contexto del diagnóstico inicial para la identificación de los principales biomarcadores, dianas de terapias dirigidas. Así mismo, el estudio del ctDNA también se recomienda en pacientes progresados a un *EGFR*-TKI de 1ª o 2ª generación para la evaluación de la mutación de resistencia p.T790M en caso de no disponer de una muestra de tejido o que ésta no sea suficiente (24). Este no es el caso de los pacientes progresados a un *ALK*-TKI, en los que el orden o secuencia terapéutica se establece en base a determinadas características clínicas de los pacientes (61,67) o a su perfil de toxicidad (59), a pesar de que los distintos inhibidores presentan diferentes sensibilidades a la multitud de mutaciones de resistencia en el dominio tirosina kinasa de *ALK* descritos (64). Por ello, el estudio del perfil molecular del tumor a la progresión a un *ALK*-TKI es una estrategia que puede ayudar en la prescripción de la siguiente línea de tratamiento. Además, la administración de más de una línea de *ALK*-TKI se ha asociado con una supervivencia significativamente superior en comparación con aquellos pacientes con CPCNP *ALK*-positivos tratados con una única línea (OS de 59 meses *vs*. 41 meses), lo que potencia la importancia de la identificación de mutaciones de resistencia en el *locus ALK* para mejorar la selección de las siguientes líneas de tratamiento (135).

- ***Condiciones pre-analíticas y analíticas***

No todo el cfDNA del torrente sanguíneo de los pacientes oncológicos es ctDNA, al igual que ocurre con el ctRNA. Se estima que entre el 0,1-89% del cfDNA está constituido por ctDNA, alcanzando un ratio superior en pacientes con enfermedad avanzada (aunque se ha descrito que alrededor del 20% de los pacientes con estadio IV no vierten ctDNA al torrente circulatorio (136)) y a medida que progresa el tumor (137). Por ello, el momento de la extracción de la muestra es clave a la hora de detectar las alteraciones derivadas del tumor en el ctDNA/ctRNA, ya que como se acaba de mencionar, el nivel de las mutaciones (medido en MAF) desciende cuando el paciente responde correctamente al tratamiento, mientras que alcanza niveles superiores en las muestras pre-tratamiento o a la progresión (138). Además, el estudio del ctDNA o ctRNA requiere consideraciones detalladas en cuanto a las condiciones pre-analíticas de las muestras

de biopsia líquida, entre las que destacan los tubos de plasma, el tiempo de procesamiento, la cantidad de plasma y el método de extracción de los ácidos nucleicos circulantes. En este sentido, el estudio BioCAST comprobó que el almacenamiento de muestras de sangre a temperatura ambiente hasta 24 horas antes del aislamiento del plasma, puede conllevar a la contaminación del ADN plasmático con el ADN germinal vertido por los glóbulos blancos necróticos, resultando en la dilución de los ácidos nucleicos circulantes tumorales en plasma, reduciendo el MAF de las mutaciones tumorales y, por consiguiente, afectando a la detección de las mismas (139). Todo ello implica que la proporción de ctDNA y ctRNA en sangre sea a menudo muy baja, requiriéndose de metodologías con una elevada sensibilidad para la identificación de mutaciones, en especial, para aquellas cuya fracción alélica sea inferior al 0,1%.

- ***Nuevas tecnologías de NGS para el estudio del ctDNA***

Las tecnologías actuales para el análisis del ctDNA incluyen la RT-PCR (capaz de detectar MAFs de hasta 0,1%), dPCR, BEAMing (combinación de PCR y citometría de flujo) y NGS (detectan MAFs de 0,01% o menos). Las metodologías basadas en PCR permiten el estudio de un número reducido de mutaciones conocidas; mientras que la NGS permite la secuenciación dirigida de un gran número de genes e incluso del exoma completo, sin necesidad de conocimiento previo de las mutaciones. Debido al aumento en el número de mutaciones que son diana de terapias dirigidas y de mutaciones de resistencia a las mismas, especialmente mutaciones de resistencia en el *locus ALK*, los paneles de NGS suponen un abordaje adecuado. Así mismo, la monitorización de una única mutación de resistencia puede ser errática debido a la heterogeneidad de los tumores, especialmente en estadios avanzados (130).

Uno de los enfoques actualmente empleados para lograr suficiente sensibilidad en la NGS y poder detectar mutaciones a baja frecuencia en el ctDNA, implica el uso de secuencias de UMIs, para reducir los errores técnicos. Usando un panel basado en UMIs, Leighl *et al*. demostraron la no-inferioridad de la biopsia líquida al analizar los biomarcadores recomendados por las guías en 307 pacientes con cáncer de pulmón metastásico, con un ratio de genotipado similar al tejido ($P < 0,0001$) y una reducción en el tiempo de obtención de los resultados (9 *vs.* 15 días; $P < 0,0001$) (97). Por otro lado, el desarrollo de algoritmos bioinformáticos también desempeña un papel clave a la hora de distinguir las verdaderas variantes tumorales en el ctDNA del ruido de fondo o de los errores técnicos producidos durante el proceso de NGS, debido a los errores de la ADN polimerasa en la PCR o el daño oxidativo del ADN (140,141).

En el *Artículo 1* de esta Tesis hemos comparado una metodología basada en PCR, la dPCR (138,142), con un panel de NGS basado en el uso de amplicones y de UMIs, Oncomine™ Lung cfDNA Assay kit, recién lanzado al mercado en el momento de dicho estudio. Para comprobar la viabilidad de esta nueva metodología de NGS basada en PCR para el genotipado y la cuantificación del ctDNA de forma no invasiva, se usaron muestras clínicas de rutina derivadas de 52 pacientes con CPCNP (*EGFR*-positivos = 31, *ALK*-positivos = 4, sin mutación conocida = 17). Considerando la dPCR como *gold standard*, la NGS del cfDNA demostró una excelente correlación en la cuantificación de la mutación de resistencia p.T790M de *EGFR*, con una especificidad del 100% y una sensibilidad del 75%. Los resultados obtenidos en este estudio son similares a otros estudios llevados a cabo en pacientes avanzados de CPCNP (143,144). En otro estudio, Paweletz *et al*. emplearon un panel de NGS basado en UMIs, distinto al nuestro, para

analizar el cfDNA de 48 pacientes con CPCNP avanzado, obteniendo una sensibilidad del 77% con respecto a tejido (145).

A pesar de los avances llevados a cabo en el análisis del ctDNA mediante NGS, a diferencia de los análisis basados en tejido, no se dispone de estándares establecidos en cuando al rendimiento analítico. De igual manera, se carece de un consenso sobre cómo medir los niveles del ctDNA y los umbrales de respuesta o progresión. Actualmente, se han utilizado distintos métodos de cuantificación del ctDNA mediante NGS entre los que se incluyen la máxima MAF, la media de las MAFs o el total de la concentración del ctDNA (146–148). Además, las alteraciones con bajas MAFs (<0,1%) y la concentración del ctDNA de partida pueden influir en la detección de alteraciones. En este sentido, además de la localización del tumor primario o de las lesiones metastásicas (142,149), determinadas mutaciones como las alteraciones en el gen *EGFR*, parecen influenciar en la concentración del ctDNA. De hecho, se ha descrito que los tumores *EGFR*-positivos vierten una mayor cantidad de ctDNA en comparación con los *ALK*-positivos, lo cual potencia el uso de dicho biomarcador en este importante subgrupo de pacientes (149). Esto podría deberse a la predilección de los tumores portadores de fusiones en *ALK* por las metástasis en el SNC (58,150), que vierten menos ctDNA debido a la barrera hematoencefálica (151).

Otros elementos que pueden afectar a los resultados de la NGS del ctDNA (152) son los umbrales del filtrado bioinformático, el ruido de fondo y el filtrado de las variables germinales y la hematopoyesis clonal de potencial indeterminado (HCPI).

- ***Hematopoyesis clonal de potencial indeterminado (HCPI)***

Como se acaba de mencionar, la secuenciación del cfDNA puede identificar alteraciones no tumorales derivadas de la HCPI (26), lo que supone una fuente de falsos positivos a tener en cuenta. Estas mutaciones somáticas de las células hematopoyéticas se acumulan con la edad pudiendo derivar en la expansión clonal de las mismas en ausencia de displasia pero que sí suponen un riesgo para neoplasias hematológicas y enfermedades cardiovasculares. La media de edad de diagnóstico, 70 años (153), así como otros factores asociados con la HCPI como son los tumores sólidos o el tabaco, hacen que la identificación de estas mutaciones sea aún más relevante en los pacientes con CPCNP (154). Numerosos estudios han descrito los genes en los que se producen la mayoría de las mutaciones derivadas de la HCPI, siendo *DNMT3A* y *TET2* los más frecuentes, seguidos de otros como *TP53, KRAS, IDH2* o *JAK2* (155,156). Por el contrario, no se han reportado mutaciones derivadas de la HCPI en los genes *EGFR* o *ALK*. Por ello, en el *Artículo 3* analizamos, mediante dPCR o secuenciación Sanger, las mutaciones en los genes *TP53* (19 de 33, 57,6%) e *IDH2* identificadas en las células mononucleares de sangre periférica (PBMCs, *del inglés peripheral blood mononuclear cells)* descartando que fuesen mutaciones derivadas de la HCPI.

- ***ctDNA derivado de otros fluidos corporales***

Debido a la proximidad, el análisis de derrames malignos a la progresión como los lavados peritoneales en el cáncer de ovario (157), fluidos pancreáticos en el cáncer de páncreas (158), fluidos peritoneales en el cáncer colorrectal (159), o el LCR en el CPCNP con metástasis cerebrales, podrían ser una buena alternativa; especialmente para aquellos con lesiones

cerebrales, tumores primarios o lesiones metastásicas, que no vierten ctDNA al torrente sanguíneo o vierten muy poco al tener íntegra la barrera hematoencefálica (160,161).

En este sentido, en el *Artículo 2* analizamos mediante dPCR muestras pareadas de plasma y otros fluidos corporales (todos ellos derrames malignos obtenidos a la progresión de la enfermedad) para evaluar la utilidad de estos últimos en el estudio del biomarcador *EGFR* en pacientes con adenocarcinoma de pulmón. En este estudio, detectamos la mutación activadora o *sensitizing* en el gen *EGFR* en el 91,30% de las muestras de ctDNA derivada de fluidos corporales, comparado con el 69,57% en las muestras de plasma. De forma similar, en estudios con cohortes más amplias como el de Guo *et al*., de 154 pacientes con cáncer de pulmón avanzado, se reportó un ratio de detección del 87% al analizar las 154 muestras de derrame pleural maligno (162). En cuanto a las MAFs, en los fluidos corporales fueron significativamente superiores a las obtenidas en las muestras plasmáticas (mediana de MAFs para mutaciones activadoras o *sensitizing* en el gen *EGFR* = 15,8 *vs*. 0,8%; p = 0,0004; mediana de MAFs para la mutación de resistencia p.T790M = 8,69 *vs*. 0,16%; p = 0,0390). Además, algunos estudios han reportado una mayor sensibilidad en estos fluidos para la detección de otro tipo de alteraciones más complejas y que requieren una mayor cantidad de ctDNA, como las CNVs (162,163).

<u>Identificación de mecanismos de resistencia a ALK-TKIs mediante la NGS del ctDNA</u>

Una vez demostrada la utilidad de las nuevas estrategias de NGS para la identificación de biomarcadores en pacientes con CPCNP a partir de muestras de biopsia líquida, tanto plasma como otros fluidos corporales, se evaluó su uso para el estudio del perfil mutacional de los pacientes con CPCNP con translocación en *ALK*. Específicamente, en el *Artículo 3* se analizaron mediante el panel Oncomine™ Pan-Cancer Cell-Free Assay 26 muestras de plasma y dos de LCR procedentes de 24 pacientes con CPCNP *ALK*-positivos en estadios avanzados (IV) al momento de la progresión a un inhibidor de *ALK*. El cambio al panel de NGS Oncomine™ Pan-Cancer Cell-Free Assay se realizó debido a que éste es de 52 genes y tiene el mismo límite de detección (LOD, *del inglés limit of detection*) para las mutaciones puntuales (SNVs, *del inglés Single-Nucleotide Variants*) (≥ 0,1%); mientras que el panel Oncomine™ Lung cfDNA Assay, usado en el *Artículo 1*, es de 11 genes. Por otro lado, aparte de SNVs, en los 52 genes se incluye el estudio de CNVs (cambio de 1,4 veces), la alteración de salto del exón 14 de *MET* (LOD ≥ 1%) y fusiones génicas (LOD ≥ 1%), entre las que se encuentran aquellas que involucran al gen *ALK*. Cabe destacar, que para la identificación de estas últimas se requiere el aislamiento del ctRNA de la fracción plasmática o de otros fluidos corporales, además del ctDNA.

- ***Algoritmo bioinformático para el gen ALK***

En relación a las mutaciones de resistencia dependientes de *ALK*, como resultado del *Artículo 3* se identificaron tres mutaciones somáticas en el *locus ALK* usando el algoritmo bioinformático comercial (Oncomine Variants v5.10), dos mutaciones p.G1269A (c.3806G>C) y una mutación p.G1202R (c.3604G>A) con MAFs de 3,36%, 0,88% y 1,28%, respectivamente. De acuerdo a las especificaciones del fabricante, el LOD para las mutaciones SNV en términos de MAF es de 0,1% (164); sin embargo, en nuestras manos rara vez se detectan mutaciones con MAF inferior al 0,5% usando este algoritmo comercial. En este sentido, el estudio de más de 1000 muestras de plasmas de pacientes con cáncer usando la tecnología de Guardant360 CDx™, mostró que la mitad de las SNVs detectadas tenían MAFs por debajo de ≈ 0,5% y un cuarto por debajo de ≈

0,2% (143). El empleo de algoritmos bioinformáticos adaptados puede permitir la distinción de las verdaderas variantes tumorales en el ctDNA con MAFs <0,5% del ruido de fondo o de los errores técnicos. Por consiguiente, y con el fin de incrementar la tasa de detección para las variantes en el *locus ALK*, desarrollamos un algoritmo bioinformático en lenguaje R llamado *VALK* (disponible en GitHub: https://github.com/AtochaHUPH/VALK-tool-).

El ajuste de nuestro algoritmo bioinformático *VALK* se llevó a cabo mediante el análisis por dPCR de las alteraciones obtenidas por NGS en la cohorte del *Articulo 3* (*Training set*), usando ensayos específicos para 19 mutaciones somáticas en el *locus ALK* y modificando los valores de filtrado de determinados parámetros del análisis de NGS: la cobertura de lectura, la cobertura molecular o la frecuencia alélica en función del tipo de alteración [SNVs, Indels (inserciones y deleciones sencillas), CNVs, fusiones o MNPs (*del inglés multiple nucleotide polymorphism*)]. Para validar el algoritmo final, se evaluó un segundo grupo o cohorte independiente de 54 muestras cedidas por un laboratorio independiente (*Validation set*). Una vez validado, el algoritmo *VALK* identificó 12 mutaciones en el *locus ALK*, es decir, que fuimos capaces de rescatar 9 alteraciones que son potenciales mecanismos de resistencia a *ALK*-TKIs con MAFs desde 0,02%. Cabe destacar, que a pesar de haber mejorado el LOD de nuestra secuenciación en cuanto al *locus ALK*, la sensibilidad de nuestro panel sigue siendo inferior a la de otros estudios como el de Newman *et al*., que combinan librerías optimizadas (CAPP-Seq) con algoritmos bioinformáticos (165).

Considerando la dPCR como método estándar de no referencia, el porcentaje de concordancia positivo y negativo (PPA y NPA, *del inglés positive or negative percentage agreement*)[2] (166), fue del 67% y 93% para el *locus ALK* usando nuestro algoritmo bioinformático *VALK*, respectivamente. Por el contrario, el PPA y NPA del algoritmo bioinformático comercial (Oncomine Variants v5.10) fue del 25% y 96% para el *locus ALK*, respectivamente. Es decir, que el PPA de nuestro algoritmo era superior al comercial, alcanzando valores más cercanos a los ensayos de NGS de ctDNA más sensibles (PPA relativo al tejido de entre 70-90%) (167–169). Las diferencias entre la sensibilidad del panel usado en el *Artículo 1* (Oncomine™ Lung cfDNA Assay), 75%, y el PPA del *Artículo 3* (Oncomine™ Pan-Cancer Cell-Free Assay) combinado con el algoritmo *VALK*, 67%, podrían deberse a las distintas especificaciones técnicas de ambos paneles, entre las que destacan el tamaño y la composición de los mismos, así como los análisis bioinformáticos, incluidos los tipos de mutaciones y los filtros de variantes utilizados (170,171).

[2] *Cuando una nueva prueba (herramienta VALK o filtro Oncomine) se compara con un estándar de no referencia (dPCR) en lugar de con un estándar de referencia, los cálculos habituales del tipo de sensibilidad y especificidad de la tabla 2x2 producirán estimaciones sesgadas de la sensibilidad y la especificidad porque el estándar no de referencia no siempre es correcto*. Por ello, para describir la frecuencia con la que una nueva prueba coincide con un estándar no de referencia, calculamos el PPA y el NPA:

		Non-reference Standard	
		+	−
New Test	+	a	b
	−	c	d
Total		a+c	b+d

PPA = 100% x a/(a+c); **NPA** = 100% x d/(b+d)

Con el algoritmo *VALK*, el 38,5% de las muestras a la progresión presentaron al menos una mutación en *ALK*, porcentaje similar a otros trabajos como el de Lin *et al*., en el que el 45,5% de los pacientes con CPCNP *EML4-ALK* positivos (N=77) presentaban una mutación de resistencia en el *locus ALK*, siendo mayor este porcentaje en aquellos pacientes con la variante 3 de *EML4-ALK* en comparación con los de la variante 1 (57% *vs.* 10%) (54). Lamentablemente, no disponíamos de la información de las variantes de los pacientes de la cohorte del *Artículo 3* para poder ver si se correlacionaba con estos datos.

De las mutaciones identificadas en nuestra cohorte (*Artículo 3*), las más frecuentes fueron p.G1202R (14,3%, n = 4 muestras: tres a la progresión a alectinib y una a ceritinib), p.G1269A (7,14%, n = 2 muestras a la progresión a crizotinib) y p.L1196M (7,14%, n = 2 muestras: una a la progresión a crizotinib y otra a lorlatinib). Estos resultados son similares a otros estudios (64,172,173). Así, por ejemplo, Gainor *et al*. identificaron la mutación p.G1202R en pacientes progresados a crizotinib, ceritinib, alectinib y brigatinib (2%, 21%, 29% y 43%, respectivamente); la mutación p.L1196M en pacientes progresados a crizotinib, ceritinib y alectinib (7%, 8%, 6%, respectivamente); y la mutación p.G1269A sólo en pacientes progresados a crizotinib (4%) (64). Con el fin de demostrar que las mutaciones de *ALK* detectadas se relacionan con la resistencia a distintos *ALK*-TKIs, cuatro de las 12 alteraciones se testaron en las muestras de plasma pre-tratamiento por NGS o dPCR, descartando en todos los casos la presencia de las mismas.

Las mutaciones concomitantes en el *locus ALK* parecen ser más frecuentes tras la exposición secuencial a *ALK*-TKIs (174). Así, en el estudio de Yu *et al*., la presencia de mutaciones activadores de *ALK* concomitantes se observó en el 29% de los pacientes tratados con múltiples líneas de *ALK*-TKIs, mientras que sólo se observó en el 6% de los pacientes tratados únicamente con crizotinib (175). Estos resultados se corresponden con los obtenidos en nuestro estudio (*Artículo 3*), en el que todas las muestras que presentaron más de una mutación en el *locus ALK* procedían de pacientes progresados a una segunda y tercera línea de *ALK*-TKI. Además, la identificación de mutaciones concomitantes en *ALK* fue del 7,14%, una frecuencia algo mayor con respecto a otros estudios de biopsia sólida (≈ 5,82%) (64), lo que refuerza el potencial de la biopsia líquida para reflejar la heterogeneidad y complejidad tumoral.

La NGS del ctDNA permite la identificación de la principal mutación impulsora de la resistencia a la terapia dirigida cuando se detecta más de una (173). Este es el caso del paciente 16 (*Artículo 3*), portador de la mutación p.G1202R (MAF dPCR = 0,04%) y p.S1206Y (MAF dPCR = 0,01%). La MAF superior de la mutación p.G1202R sugiere que ésta podría ser el principal mecanismo de resistencia al actual tratamiento con alectinib; mientras que la menor MAF de la mutación p.S1206Y podría deberse a que ésta es el mecanismo de resistencia a la línea de tratamiento anterior con crizotinib, y que disminuyó debido a la terapia con alectinib. Desafortunadamente, no disponíamos de muestra de biopsia líquida o tumoral previa para confirmarlo. Un caso similar fue descrito por Shaw *et al*., que identificaron una mutación compuesta, p.C1156Y+p.L1194F, en un paciente con CPCNP *ALK*-positivo que había progresado a una primera línea con crizotinib debido a la mutación p.C1156Y, seguido de ceritinib y lorlatinib secuencialmente (85). Los autores sugieren que, a pesar de la eficacia de lorlatinib frente a la mutación p.C1156Y, la adición de la segunda mutación interrumpe la unión del fármaco y conduce a la resistencia a lorlatinib.

Por último, el estudio del cfDNA permite recapitular el conjunto de mutaciones de cada localización (lesión primaria y distintas lesiones metastásicas), por lo que la identificación de

mutaciones de resistencias no se ve tan limitada por la heterogeneidad tumoral como con la biopsia sólida (176). En este sentido, los resultados del caso clínico (*Artículo 4*) sugieren que las lesiones metastásicas individuales podrían haberse desarrollado por distintos mecanismos de resistencia a terapias dirigidas. Específicamente, la presencia de la mutación p.G1269A se observó de forma conjunta con lesiones a nivel de la vértebra T4 y T10; mientras que la presencia de la mutación p.G1202R se observó junto con nuevas lesiones óseas, sobre todo en fémur e isquion. Lamentablemente, no disponíamos de biopsia de las distintas lesiones para corroborar nuestra hipótesis.

Estos resultados reflejan el potencial uso de la NGS de biopsia líquida a la progresión de la enfermedad para la detección de alteraciones moleculares clínicamente relevantes y, por consiguiente, para entender la heterogeneidad de la resistencia tumoral y guiar las subsecuentes líneas, de terapia dirigida, en pacientes con CPCNP *ALK*-positivos. Cabe destacar que los resultados de NGS se pueden obtener en un periodo de tiempo corto, lo que garantiza un tiempo de respuesta adecuado para el entorno clínico.

- ***Mecanismos de resistencia a ALK-TKIs en otros genes***

En el *Artículo 3*, la NGS de muestras de biopsia líquida permitió la detección de alteraciones en genes distintos a *ALK* en el 87,5% (n = 21) de los pacientes; siendo el tipo de mutación más frecuente SNVs, aunque también se detectaron 10 indels y tres CNVs. No se detectó ninguna fusión, probablemente debido al panel y tecnología empleados, como se discutirá más adelante. Cabe destacar, que uno de los tres pacientes en los que no se detectó ninguna alteración, progresó exclusivamente a nivel cerebral.

El gen más mutado en nuestra cohorte (*Artículo 3*) fue *TP53*, al igual que en muchos otros estudios (64,177). A pesar de que el porcentaje de pacientes mutados en dicho gen es algo superior a lo descrito en otros estudios (172,173,177), en el 57,6% de los casos se descartó, mediante dPCR o secuenciación Sanger, que estas alteraciones derivasen de la HCPI. Las alteraciones en *TP53* se han correlacionado con peores SLP y SG. Así, por ejemplo, en el estudio de Yu *et al*., la SLP en los pacientes con CPCNP *ALK*-positivos con mutaciones concomitantes en *TP53* fue de 8 meses en comparación con los pacientes *TP53 wt*, con una SLP de 13 meses (*Hazard Ratio* = 1,494, *P* value = 0,019) (175). Estas mutaciones dañan las funciones supresoras de la proteína p53, generando inestabilidad genómica y pudiendo favorecer la aparición de CNVs patogénicas (178). Este puede ser el caso del paciente 12 (*Artículo 3*), en el cual se identificó una amplificación de *MYC*, pérdida de expresión de *CCND1* y *FGFR3* junto con dos mutaciones puntuales en *TP53*. La presencia simultánea de mutaciones en *TP53* y alteraciones tipo CNV en los genes *MYC*, *CCND* y *FGFR* también ha sido descrita en uno de los participantes del ensayo piloto LIQUID IMPACT (CTRI/2019/02/017548), diagnosticados con cánceres de órganos sólidos refractarios avanzados (179).

Por otro lado, se identificaron otros potenciales mecanismos de resistencia a *ALK*-TKIs, incluyendo mutaciones en los genes *EGFR*, *BRAF, MAP2K1 (MEK1), PIK3CA*, *IDH2* (p.R140Q), *MET, FGFR2* y *CCND3*. Cabe destacar, que los pacientes (n = 5) con mutaciones en los tres primeros genes, no mostraron un beneficio clínico objetivo al tratamiento con inhibidores de *ALK*.

Las alteraciones en el gen *PIK3CA*, en concreto las mutaciones más comunes que involucran el codón 545 (180), también han sido descritas como mecanismos de resistencia a *ALK*- y *EGFR*-TKIs (138,181). Sin embargo, actualmente no disponemos de fármacos dirigidos frente a alteraciones en *PIK3CA*.

Por otro lado, las mutaciones en los oncogenes *RAS* y *B-RAF* ocurren frecuentemente en los tumores humanos (182,183), correlacionándose con progresión tumoral y peor pronóstico debido a la activación aberrante de la vía de señalización de MAPK, que incluye las kinasas RAS, Raf, MEK y ERK (184). Los inhibidores de *MEK* en combinación con otras terapias dirigidas que alberga la vía MAPK, como *ALK*-TKIs, puede ser una alternativa prometedora en pacientes con CPCNP con mutaciones en *KRAS*, *BRAF* o *MAP2K1 (MEK1)* (185). A pesar de que *KRAS* es el gen más comúnmente mutado en los pacientes con CPCNP (25%) (186) y que sus mutaciones se han descrito como mecanismo de resistencia en algunos estudios de pacientes *ALK*-positivos progresados a una línea de *ALK*-TKI (172,187), en nuestro estudio (*Artículo 3*), al igual que en muchos otros (64,87,173), no detectamos alteraciones en *KRAS.* Por el contrario, sí identificamos una mutación no-V600 en *BRAF* en un paciente, la p.G466V, y la mutación p.F129L en *MAP2K1* en dos pacientes, los cuales podrían beneficiarse de la combinación de *ALK*-TKIs e inhibidores de *MEK* (188–190).

Otras vías de señalización relacionadas con la vía de MAPK son las de los receptores tirosina kinasa FGFR y MET, cuyas alteraciones se han descrito también como mecanismos de resistencia a *EGFR*-TKIs (191,192). Para ambos genes se han desarrollado distintos TKIs, por lo que la combinación de *ALK*-TKIs con *FGFR*-TKIs (193) o *MET*-TKIs (194) podría ser una opción terapéutica en los pacientes con CPCNP *ALK*-positivos con mutaciones de resistencia en dichos genes.

Por último, aunque las mutaciones en *IDH* no son muy comunes en los pacientes con CPCNP *ALK*-positivos, si lo son en los pacientes diagnosticados con leucemia mieloide aguda (30%) (195), para los cuales la FDA ha aprobado dos inhibidores, ivosidenib y enasidenib, como inhibidores de *IDH1* e *IDH2* respectivamente (196). La combinación de estos inhibidores con *ALK*-TKIs podría suponer una nueva estrategia para pacientes con mutaciones concomitantes en *ALK* e *IDH*.

Aunque los estudios del ctDNA han demostrado una especificidad muy alta, su sensibilidad está comprometida, con una tasa de falsos negativos de incluso el 30% (197). Por ello, es importante tener en cuenta que, aunque la biopsia líquida proporciona una opción apropiada y prometedora para el perfil molecular en pacientes con CPCNP, su utilidad se limita principalmente a los casos en los que se detecta una mutación, mientras que un resultado negativo es menos informativo y requiere del estudio del perfil molecular basado en tejido. El desarrollo de algoritmos bioinformáticos mejora la detección de las mutaciones de resistencia, que al ser subclonales, aumentan de manera más tardía en la evolución del tumor y, por consiguiente, se presentan en MAFs más bajas (138). Con todo ello, las nuevas estrategias de NGS basadas en biopsia líquida constituyen un buen enfoque para el estudio del perfil mutacional a la progresión a un *ALK*-TKI en los pacientes con CPCNP *ALK*-positivos.

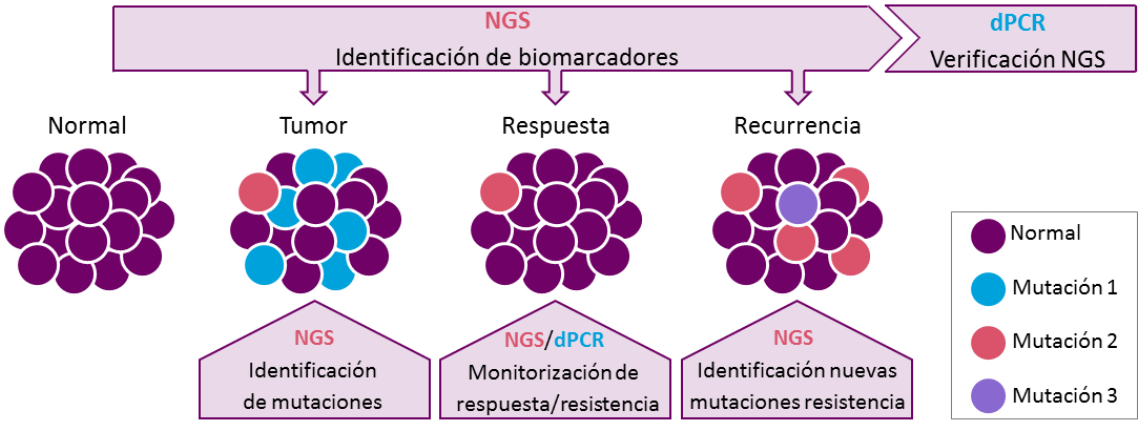

Figura 7. Evolución del tumor a lo largo del tratamiento: identificación y verificación de biomarcadores. La NGS permite la identificación de biomarcadores en el tumor, así como la correcta monitorización de la enfermedad, analizando tanto las mutaciones primarias como las mutaciones de resistencia adquiridas. La dPCR permite el estudio de pocas mutaciones (más adecuado para pacientes con CPCNP *EGFR*-positivos), mientras que los ensayos de NGS permiten el análisis de muchas mutaciones, conocidas y no conocidas (estrategia válida para pacientes con CPCNP *ALK*-positivo). Debido a las bajas MAFs de los subclones de resistencia, los resultados de la NGS deben verificarse por otras metodologías como la dPCR.

<u>Diagnóstico de pacientes con CPCNP con translocación en ALK mediante biopsia líquida</u>

La identificación de pacientes con CPCNP con reordenamientos genómicos mediante el análisis del ctDNA, al contrario que los pacientes con SNVs o pequeñas Indels, es más compleja debido al gran número de bases que implican dichas alteraciones, el pequeño tamaño de los fragmentos del ctDNA (≈ 150 pb) y los sesgos de amplificación en los ensayos de NGS basados en cfDNA. Asimismo, el punto de corte y empalme a nivel de ADN es a menudo desconocido. Todo ello, implica una secuenciación extensa y profunda del ctDNA para la detección del punto de ruptura cromosómico (172), que no siempre es viable dado su elevado coste. Una buena alternativa es el estudio de los transcritos de fusión a nivel de ARN. Sin embargo, el cfRNA es degradado rápidamente por las RNasas del torrente sanguíneo (198). Si bien los ácidos nucleicos circulantes libres son los biomarcadores tumorales más estudiados, las células tumorales también vierten al torrente circulatorio su información genómica embebida en otros compartimentos biológicos como las EVs y las CTCs.

- ***ctDNA y ctRNA***

El análisis de las fusiones de *ALK* usando ctDNA o ctRNA requieren consideraciones detalladas en cuanto a las condiciones pre-analíticas de las muestras de biopsia líquida, tal y como se ha explicado anteriormente. En cuanto a la analítica, se ha reportado un LOD de MAFs para las fusiones de ≥0,04% (172,199), mientras que el LOD del panel de NGS empleado en nuestros estudios (*Artículo 3* y *4*) para la identificación de fusiones es de hasta 1%. En esta línea, McCoach *et al*. describieron que las fusiones de *ALK* presentaban las MAFs más bajas comparado con las mutaciones activadoras o *sensitizing* y la mutación de resistencia p.T790M en *EGFR,* que presentaron las MAFs más elevadas (172). En el mismo sentido, en el estudio de NGS de ctDNA plasmático usando la plataforma IonTorrent, Couraud *et al*. obtuvieron una sensibilidad del 58% y una especificidad del 87% pero sin ser capaces de detectar reordenamientos o amplificaciones

(200). Estos resultados concuerdan con los obtenidos en los *Artículos 3* y *4*, donde se no detectó ninguna fusión de *ALK* usando la misma plataforma.

Existen otro tipo de metodologías para la generación de librerías, las basadas en hibridación con sondas de captura, cuya cobertura es más homogénea. Actualmente, hay dos ensayos basados en sondas de captura aprobados por la FDA, en 2020, que han demostrado sensibilidades de entorno al 50% en la detección de fusiones en pacientes con CPCNP a nivel del ctDNA: 56% Foundation-One Liquid CDx (201) y 44% Guardant360 CDx usando como *gold estandar* la muestra de tejido (202). Igualmente, otros estudios que han empleado estos paneles reportaron una incidencia de fusiones génicas menor a la esperada para pacientes con CPCNP o no las detectaron, aunque si se identificaron mutaciones de resistencia en el *locus ALK*, lo que podría deberse a la sensibilidad diferencial para la identificación de fusiones y mutaciones puntuales en el gen *ALK* (151,172,203). Otros paneles basados en hibridación con sondas de captura no aprobados por la FDA también han mostrado sensibilidades similares (204). Cabe destacar que la sensibilidad de la NGS basada en ADN no es satisfactoria si los puntos de ruptura de las fusiones involucran regiones intrónicas largas, ya que podrían no ser cubiertas por las sondas empleadas (205). Por ello, el diseño de las sondas es especialmente importante en la identificación de estas alteraciones debido a la variabilidad en la localización de los puntos de corte y a la fragmentación del ctDNA.

En cuanto al cfRNA, Hasegawa *et al*. observaron una mayor sensibilidad en la detección de fusiones génicas de *ALK* y *ROS1* en su cohorte de 20 pacientes con CPCNP mediante el empleo de un ensayo de cfRNA basado en RT-PCR y seguido de NGS en comparación con el ensayo de NGS de Guardant360 CDx basado en cfDNA (78% *vs*. 33%) (206). A pesar de que los ensayos de cfRNA basados en RT-PCR parecen identificar fusiones génicas con mayor sensibilidad (207), se encuentran limitados a unos pocos reordenamientos genómicos y requieren del conocimiento previo de las variantes, además de unas condiciones pre-analíticas concretas.

- ***Plaquetas y CTCs***

La metodología de RT-PCR también ha sido empleada para la identificación de fusiones en el ARN contenido en compartimentos biológicos presentes en el torrente sanguíneo como las plaquetas o las CTCs. En concreto, Nilsson *et al*. reportaron una mayor sensibilidad para la detección de reordenamientos de *EML4-ALK* analizando el ARN contenido en plaquetas en comparación con el cfRNA (65% vs. 21%), lo que atribuyen a la rápida degradación del cfRNA (208). Asimismo, Park *et al*. llevaron a cabo el análisis conjunto del cfRNA y el ARN de plaquetas mediante RT-PCR, obteniendo una sensibilidad del 78,8% y una especificidad del 89,3% con respecto al FISH de tejido (209). Aun así, obtuvieron altas tasas de resultados no válidos (46,8% en las muestras de cfRNA y 53,4% en las de plaquetas) (209). En cuanto a las CTCs, Ma *et al*. obtuvieron resultados altamente concordantes con respecto a la RT-PCR, IHQ y Western Blot de tejido, al analizar reordenamientos de *EML4-ALK* por RT-PCR en CTCs inmunocapturadas (210).

Otra de las técnicas empleadas para el estudio de fusiones en *ALK* en CTCs es la técnica de FISH, aunque ésta no permite la identificación del tipo concreto de fusión. Algunos estudios analizaron fusiones en *ALK* mediante un método de FISH en filtros (FA-FISH) en CTCs enriquecidas por ISET (*del inglés, isolation by size of epithelial tumor cells*) (211,212). En este último trabajo, Pailler *et al*. detectaron al menos cuatro CTCs positivas para la fusión de *ALK* por 1 mL de sangre en cada

paciente con CPCNP *ALK*-positivo analizado (N = 18), obteniendo un 100% de especificidad y sensibilidad (212). Sin embargo, los porcentajes de pacientes con al menos una CTC varían desde el 21% hasta el 41% dependiendo del estudio, partiendo de volúmenes muy superiores de sangre periférica (7,5 mL) (213–215), haciendo que estos resultados deban tomarse con precaución.

En cualquier caso, la presencia de plaquetas o CTCs *ALK*-positivas se ha asociado con tumores más agresivos y, por consiguiente, con un peor pronóstico (209,211,216); mientras que la no detección de la fusión parece ser indicativa de respuesta al tratamiento (208,209), pudiendo permitir la monitorización de la terapia. Sin embargo, el número de CTCs es muy escaso (111), dado que la mayoría sufren apoptosis inmediatamente después de su liberación en el torrente sanguíneo (217); y el número de plaquetas varía de forma significativa con determinados fármacos y enfermedades inflamatorias (110). Con todo ello, las EVs presentan la ventaja de ser compartimentos más estables (218), liberadas en gran cantidad por todas las células en cualquier estado, ya sea fisiológico o patológico (120,219,220).

- ***Vesículas extracelulares (EVs)***

A pesar del creciente interés en las EVs en el campo de la oncología, como se puede observar si se realiza una búsqueda en la colección de Web of Science™ (**Figura 8**), a nuestro entender, ningún grupo dedicado a la investigación ha descrito la identificación de fusiones génicas en *ALK* (en forma de proteína o transcrito de fusión) dentro de estos compartimentos.

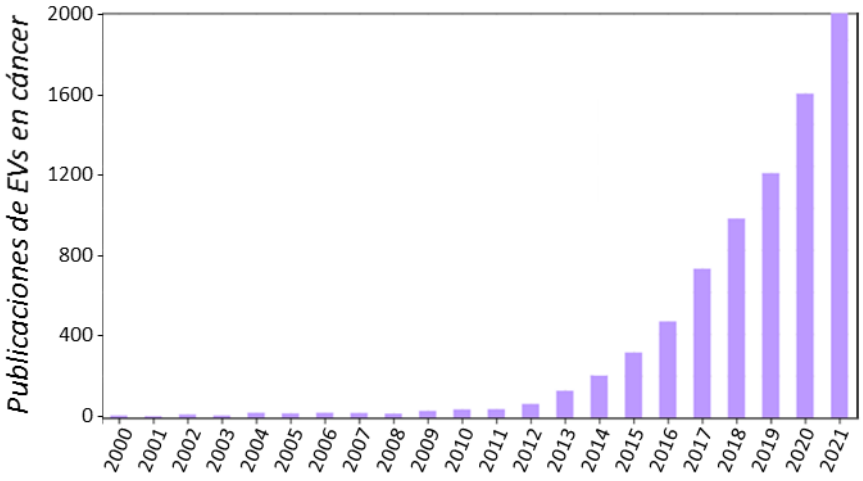

Figura 8. Publicaciones de los últimos años sobre la implicación y el empleo de EVs en cáncer.

Dentro del gran repertorio de métodos de enriquecimiento de EVs actualmente disponible (125), la filtración, la SEC y los enfoques basados en microfluidos o inmunoafinidad permiten la obtención de preparaciones con mayor pureza en un determinado tipo de EVs, discriminando por tamaño o por la expresión de marcadores; mientras que la UC y la precipitación con agentes como el *Poly-Ethylene Glycol* facilitan la obtención de un mayor rango de EVs (221–223). Dado el desconocimiento del tipo de EVs que podía contener la fusión de *ALK*, en el *Artículo 5* se eligió la tecnología de UC. Además, nuestro protocolo de UC fue modificado con el fin de no descartar las EVs más grandes (microvesículas) e incrementar así la sensibilidad en la detección de las fusiones en *ALK*. Posteriormente, confirmamos que dichos reordenamientos se encuentran, al

menos, en EVs que expresan las tetraspaninas CD9, CD81 y CD63, marcadores específicos de vesículas más pequeñas como los exosomas (224), y en especial en las vesículas CD81 positivas (Figura 5.D, *Artículo 5*). Sin embargo, no realizamos el estudio de otros marcadores de vesículas más grandes como son las selectinas, integrinas y otros marcadores menos estudiados que varían en función del tipo celular del que derivan (225,226); por lo que no podemos descartar que las fusiones de *ALK* puedan detectarse también en este tipo de EVs. De hecho, Vagner *et al*. sugirieron que, en pacientes con tumores de próstata, las alteraciones genómicas parecen estar principalmente en vesículas grandes como las microvesículas o los cuerpos apoptóticos (227).

Una vez seleccionado el método de aislamiento de EVs (UC) en base a los objetivos de nuestro estudio (*Articulo 5*), pusimos a punto nuestro protocolo con las líneas celulares más utilizadas en los estudios de fusiones de *EML4-ALK*, H3122 y H2228, derivadas de pacientes con CPCNP con la variante 1 [*EML4*(13)-*ALK*(20)] y 3 [*EML4*(6a/b)-*ALK*(20)] respectivamente (68,228). En el análisis de nuestra cohorte, fuimos capaces de identificar por dPCR una fusión de *ALK* en el 50% de los pacientes con CPCNP *ALK*-positivos analizados (N = 16). Cabe destacar, que tan solo analizamos las tres variantes de *EML4-ALK* más comunes, V1, V2 [*EML4*(20)-*ALK*(20)] y V3, debido a la escasez de muestra. Estas tres variantes fueron también las únicas analizadas en el estudio de Nilsson *et al*. mediante la RT-PCR del ARN de plaquetas, obteniendo una sensibilidad del 65% (208). En cuanto a la distribución de estas tres variantes de *EML4-ALK*, según los estudios realizados en tejido, la variante más común es la V1 (36-54%), seguida de la V3 (14-29,5%) y de la V2 (9-12%) (43,52,229,230). Sin embargo, en nuestra pequeña cohorte, la variante más común es la V3 (31,25%), seguida de la V1 (12,5%) y la V2 (6,25%). Estos resultados se observaron también en uno de los estudios, anteriormente citado, basado en CTCs: 15% V3, 10% V1 y 3,3% V2 (210). El resto de artículos basados en biopsia líquida que emplean técnicas que sí permiten la identificación de variantes (basadas en RT-PCR), no aportan dicha información, indicando exclusivamente los pacientes *ALK*-positivos (208,209,211,212). En línea a lo que ocurre con las CTCs de los tumores más agresivos, cuyo número aumenta notablemente en el torrente sanguíneo (211), los tumores con la V1 de *EML4-ALK*, cuya SLP es mayor en comparación con las otras variantes (11 *vs*. 4,2 meses) (90), podrían secretar un menor número de EVs. Esto implicaría una disminución en la comunicación basada en EVs y, por consiguiente, una posible reducción de la diseminación metastásica y progresión tumoral (231). Sin embargo, se necesitan nuevos estudios basados en la identificación de fusiones en EVs para esclarecer si las distintas variantes implican una menor o mayor concentración de vesículas en el torrente circulatorio.

Futuras direcciones - Implicaciones clínicas

La NGS del ctDNA permite el estudio del perfil mutacional a la progresión a un *ALK*-TKI en los pacientes con CPCNP *ALK*-positivos. Sin embargo, son necesarios nuevos estudios con cohortes más amplias, o estudios más profundos, para poder establecer la secuencia de *ALK*-TKIs más adecuada en base al perfil tumoral a la progresión y dilucidar nuevos mecanismos de resistencia potencialmente accionables por nuevas terapias dirigidas.

Por otro lado, las EVs parecen tener un gran potencial para la estudio de biomarcadores (232–234). Sin embargo, quedan muchas cuestiones por resolver entre las que destacan su papel en el cáncer y la mejor estrategia metodológica para el enriquecimiento de los subtipos de vesículas más informativas, y si estos varían en función de la alteración a estudiar. Estos estudios son de

vital importancia a la hora de desarrollar metodologías más sensibles para la identificación de fusiones en *ALK* u otros genes mediante muestras de biopsia líquida. Por ello, nuestro grupo está trabajando actualmente para identificar en qué tipo de EVs se encuentran enriquecidas las fusiones de *ALK*, puesto que una mejor caracterización de las EVs *ALK*-positivas podría optimizar el enriquecimiento de las mismas y posibilitar el desarrollo de métodos automatizados que puedan implantarse en la práctica clínica, mejorando el diagnóstico de los pacientes con CPCNP con reordenamientos. Para ello, se están empleando distintas estrategias metodológicas entre las que se incluye la inmunocaptura con distintos marcadores, el empleo de filtros con distintos tamaños de poro, la SEC, la plataforma *Exoview R100* y el microscopio de fluorescencia de super-resolución *Nanoimager*.

En definitiva, descifrar el potencial diagnóstico, pronóstico y de monitorización de la biopsia líquida en los pacientes con CPCNP con fusión en el gen *ALK* podría ayudar al establecimiento de secuencias terapéuticas de *ALK*-TKIs en base al perfil molecular del tumor a la progresión; así como al desarrollo de metodologías automatizadas de alto rendimiento para el enriquecimiento de EVs que permitan el diagnóstico de dichos pacientes, lo que supondría un mejor manejo clínico de los mismos.

CONCLUSIONES

Las conclusiones de este trabajo son las siguientes:

1. El análisis del cfDNA mediante NGS y dPCR presenta una elevada concordancia para el estudio de mutaciones somáticas en pacientes con CPCNP en estadios avanzados (III-IV).
2. La concentración del cfDNA obtenido de fluidos corporales en contacto con el tumor es superior al de muestras de plasma, mostrando un mayor número de variantes somáticas y MAFs significativamente superiores por dPCR en pacientes con CPCNP *EGFR*-mutados.
3. La NGS del cfDNA, de pacientes con CPCNP *ALK*-positivos a la progresión de la enfermedad, permite la identificación de potenciales mutaciones de resistencia a inhibidores de *ALK,* tanto en el *locus ALK* como en otros *loci.*
4. El algoritmo *VALK* permitió la detección de mutaciones en el dominio kinasa de *ALK* en el 35% de los pacientes con CPCNP *ALK*-positivos.
5. De acuerdo a nuestra experiencia, las mutaciones de resistencia más frecuentes en el *locus ALK* son la mutación p.G1269A, detectada en 2 de los 11 pacientes tratados con crizotinib en primera línea; y la mutación p.G1202R, detectada en 4 de los 15 pacientes tratados con *ALK*-TKIs de 2ª generación (alectinib, n = 3; ceritinib, n = 1).
6. Las fusiones en el gen *ALK* pueden ser detectadas a nivel de ARN y de proteína mediante el estudio de fracciones enriquecidas de EVs de líneas celulares derivadas de CPCNP *ALK*-positivo (H3122 y H2228).
7. El análisis por dPCR del ARN contenido en EVs aisladas a partir de muestras de biopsia líquida de pacientes con CPCNP *ALK*-positivo en estadios avanzados, permite la identificación de fusiones en *ALK* en 8 de 16 pacientes analizados.
8. El estudio de fusiones en el gen *ALK* mediante el análisis del ARN contenido en EVs supone un método no invasivo para el diagnóstico de los pacientes con CPCNP *ALK*-positivos cuando no haya disponibilidad de tejido tumoral.

BIBLIOGRAFÍA

1. Siegel RL, Miller KD, Jemal A. Cancer Statistics in USA, 2018. CA Cancer J Clin. 2018;68(1):7–30.
2. Cancer Today. 2022, Aug 31. https://gco.iarc.fr/today/
3. Hanna N, Neubauer M, Yiannoutsos C, McGarry R, Arseneau J, Ansari R, et al. Phase III Study of Cisplatin, Etoposide, and Concurrent Chest Radiation With or Without Consolidation Docetaxel in Patients With Inoperable Stage III Non–Small-Cell Lung Cancer: The Hoosier Oncology Group and U.S. Oncology. J Clin Oncol. 2008;26(35):5755–60.
4. Allemani C, Matsuda T, Di Carlo V, Harewood R, Matz M, Nikšić M, et al. Global surveillance of trends in cancer survival 2000–14 (CONCORD-3): analysis of individual records for 37 513 025 patients diagnosed with one of 18 cancers from 322 population-based registries in 71 countries. Lancet. 2018;391(10125):1023-1075.
5. Ohno Y, Koyama H, Dinkel J. Lung cancer. Med Radiol. 2018;0(9783319426167):293–341.
6. Uramoto H, Tanaka F. Recurrence after surgery in patients with NSCLC. Transl Lung Cancer Res. 2014;3(4):242-9.
7. Travis WD, Brambilla E, Nicholson AG, Yatabe Y, Austin JHM, Beasley MB, et al. The 2015 World Health Organization Classification of Lung Tumors: Impact of Genetic, Clinical and Radiologic Advances since the 2004 Classification. J Thorac Oncol. 2015;10(9):1243-1260.
8. Kalemkerian GP, Akerley W, Bogner P, Borghaei H, Chow LQ, Downey RJ, et al. Small cell lung cancer: Clinical practice guidelines in oncology. J Natl Compr Cancer Netw. 2013;11(1):78–98.
9. Calbó J, Meuwissen R, Van Montfort E, Van Tellingen O, Berns A. Genotype-phenotype relationships in a mouse model for human small-cell lung cancer. Cold Spring Harb Symp Quant Biol. 2005;70:225-32.
10. Zappa C, Mousa SA. Non-small cell lung cancer: Current treatment and future advances. Transl Lung Cancer Res. 2016;5(3):288–300.
11. Lung Cancer Basics | American Lung Association. 2020, Sep 7. https://www.lung.org/
12. Zhu Z, Liang Z, Tong J, Mao X, Yin Y, Manor LC, et al. Survival analysis in Caucasian pulmonary adenocarcinoma patients based on differential targets between Caucasian and Asian population. Saudi J Biol Sci. 2018;25(5):1003–6.
13. Berardi R, Mazzanti P, Caramanti M, Santoni M, De Lisa M, Morgese F, et al. Squamous cell carcinoma of the lung: clinical criteria for treatment strategy. J Cancer Metastasis Treat. 2015;1(2):90-3.
14. Quint LE, Tummala S, Brisson LJ, Francis IR, Krupnick AS, Kazerooni EA, et al. Distribution of distant metastases from newly diagnosed non-small cell lung cancer. Ann Thorac Surg. 1996;62(1):246–50.
15. Proctor RN. Tobacco and the global lung cancer epidemic. Nat Rev Cancer. 2001;1(1):82–6.
16. Walser T, Cui X, Yanagawa J, Lee JM, Heinrich E, Lee G, et al. Smoking and lung cancer: The role of inflammation. In: Proceedings of the American Thoracic Society. 2008
17. Rosenzweig KE, Chen CP, Yom SS, Krug LM. Tumors of the Lung, Pleura, and Mediastinum. Leibel and Phillips Textbook of Radiation Oncology. 2010:737–71.
18. Ihde DC, Minna JD. Non-small cell lung cancer part: I Biology, diagnosis, and staging. Curr Probl Cancer. 1991;15(2):65–104.

19. Muscat JE, Stellman SD, Zhang ZF, Neugut AI, Wynder EL. Cigarette smoking and large cell carcinoma of the lung. Cancer Epidemiol Biomarkers Prev. 1997;6(7):477–80.
20. Calvayrac O, Pradines A, Pons E, Mazières J, Guibert N. Molecular biomarkers for lung adenocarcinoma. Eur Respir J. 2017;49(4):1601734.
21. Lim W, Ridge CA, Nicholson AG, Mirsadraee S. The 8th lung cancer TNM classification and clinical staging system: Review of the changes and clinical implications. Quant Imaging Med Surg. 2018;8(7):709-718.
22. Tylski E, Goyal M. Low Dose CT for Lung Cancer Screening: The Background, the Guidelines, and a Tailored Approach to Patient Care. Mo Med. 2019;116(5):414-419.
23. Sidransky D. Emerging molecular markers of cancer. Nat Rev Cancer. 2002;2(3):210-9.
24. Santarius T, Shipley J, Brewer D, Stratton MR, Cooper CS. A census of amplified and overexpressed human cancer genes. Nat Rev Cancer. 2010;10(1):59-64.
25. Barlesi F, Mazieres J, Merlio JP, Debieuvre D, Mosser J, Lena H, et al. Routine molecular profiling of patients with advanced non-small-cell lung cancer: results of a 1-year nationwide programme of the French Cooperative Thoracic Intergroup (IFCT). Lancet. 2016;387(10026):1415-1426.
26. Ettinger DS, Wood DE, Aisner DL, Akerley W, Bauman JR, Bharat A, et al. Non-Small Cell Lung Cancer, Version 3.2022, NCCN Clinical Practice Guidelines in Oncology. J Natl Compr Canc Netw. 2022 May;20(5):497-530. 27. Yang JJ, Zhang XC, Su J, Xu CR, Zhou Q, Tian HX, et al. Lung cancers with concomitant EGFR mutations and ALK rearrangements: diverse responses to EGFR-TKI and crizotinib in relation to diverse receptors phosphorylation. Clin Cancer Res. 2014;20(5):1383–92.
28. Mendelsohn J. Growth factor receptors as targets for antitumor therapy with monoclonal antibodies. Prog Allergy. 1988;45:147–60.
29. Antonicelli A, Cafarotti S, Indini A, Galli A, Russo A, Cesario A, et al. EGFR-targeted therapy for non-small cell lung cancer: focus on EGFR oncogenic mutation. Int J Med Sci. 2013;10(3):320–30.
30. Lynch TJ, Bell DW, Sordella R, Gurubhagavatula S, Okimoto RA, Brannigan BW, et al. Activating mutations in the epidermal growth factor receptor underlying responsiveness of non-small-cell lung cancer to gefitinib. N Engl J Med. 2004;350(21):2129–39.
31. Riess JW, Gandara DR, Frampton GM, Madison R, Peled N, Bufill JA, et al. Diverse EGFR Exon 20 Insertions and Co-Occurring Molecular Alterations Identified by Comprehensive Genomic Profiling of Non-Small Cell Lung Cancer. J Thorac Oncol. 2018;13(10):1560.
32. Yasuda H, Park E, Yun CH, Sng NJ, Lucena-Araujo AR, Yeo WL, et al. Structural, biochemical and clinical characterization of epidermal growth factor receptor (EGFR) exon 20 insertion mutations in lung cancer. Sci Transl Med. 2013;5(216):216ra177.
33. Hou J, Li H, Ma S, He Z, Yang S, Hao L, et al. EGFR exon 20 insertion mutations in advanced non-small-cell lung cancer: current status and perspectives. Biomark Res. 2022;10(1):1–12.
34. Le X, Goldman JW, Clarke JM, Tchekmedyian N, Piotrowska Z, Chu D, et al. Poziotinib shows activity and durability of responses in subgroups of previously treated EGFR exon 20 NSCLC patients. J Clin Oncol. 2020;38(15_suppl):9514–9514.
35. Piotrowska Z, Nguyen D, Koczywas M, Tchekmedyian N, Clancy MS, Witter D, et al. 1345P Preliminary safety and activity of CLN-081 in NSCLC with EGFR exon 20 insertion mutations (Ins20). Ann Oncol. 2020;31:S862–3.

36. van Veggel B, de Langen AJ, Hashemi SMS, Monkhorst K, Heideman DAM, Thunnissen E, et al. Afatinib and Cetuximab in Four Patients With EGFR Exon 20 Insertion-Positive Advanced NSCLC. J Thorac Oncol. 2018;13(8):1222–6.
37. Riess JW, Groshen SG, Reckamp KL, Wakelee HA, Oxnard GR, Padda SK, et al. Osimertinib (Osi) plus necitumumab (Neci) in EGFR-mutant NSCLC: An ETCTN California cancer consortium phase I study. J Clin Oncol. 2019;37(15_suppl):9057–9057.
38. Birchmeier C, Sharma S, Wigler M. Expression and rearrangement of the ROS1 gene in human glioblastoma cells. Proc Natl Acad Sci U S A. 1987;84(24):9270–4.
39. Azelby CM, Sakamoto MR, Bowles DW. ROS1 Targeted Therapies: Current Status. Curr Oncol Rep. 2021;23(8):94.
40. Shaw AT, Riely GJ, Bang YJ, Kim DW, Camidge DR, Solomon BJ, et al. Crizotinib in ROS1-rearranged advanced non-small-cell lung cancer (NSCLC): updated results, including overall survival, from PROFILE 1001. Ann Oncol. 2019;30(7):1121-1126.
41. Drilon A, Siena S, Dziadziuszko R, Barlesi F, Krebs MG, Shaw AT, et al. Entrectinib in ROS1 fusion-positive non-small-cell lung cancer: integrated analysis of three phase 1-2 trials. Lancet Oncol. 2020;21(2):261-270.
42. Singh A, Chen H. Optimal Care for Patients with Anaplastic Lymphoma Kinase (ALK)-Positive Non-Small Cell Lung Cancer: A Review on the Role and Utility of ALK Inhibitors. Cancer Manag Res. 2020;12:6615-6628.
43. Sasaki T, Rodig SJ, Chirieac LR, Jänne PA. The biology and treatment of EML4-ALK non-small cell lung cancer. Eur J Cancer. 2010;46(10):1773–80.
44. Yang L, Ling Y, Guo L, Ma D, Xue X, Wang B, et al. Detection of ALK translocation in non-small cell lung carcinoma (NSCLC) and its clinicopathological significance using the Ventana immunohistochemical staining method: a single-center large-scale investigation of 1,504 Chinese Han patient. Chinese J Cancer Res. 2016;28(5):495–502.
45. Shaw AT, Yeap BY, Mino-Kenudson M, Digumarthy SR, Costa DB, Heist RS, et al. Clinical features and outcome of patients with non-small-cell lung cancer who harbor EML4-ALK. J Clin Oncol. 2009;27(26):4247–53.
46. Soda M, Choi YL, Enomoto M, Takada S, Yamashita Y, Ishikawa S, et al. Identification of the transforming EML4-ALK fusion gene in non-small-cell lung cancer. Nature. 2007;448(7153):561–6.
47. Chia PL, Dobrovic A, Dobrovic A, John T. Prevalence and natural history of ALK positive non-small-cell lung cancer and the clinical impact of targeted therapy with ALK inhibitors. Clin Epidemiol. 2014;6:423-32.
48. Lin JJ, Shaw AT. Differential Sensitivity to Crizotinib: Does EML4-ALK Fusion Variant Matter? J Clin Oncol. 2016;34(28):3363–5.
49. Zhang X, Zhang S, Yang X, Yang J, Zhou Q, Yin L, et al. Fusion of EML4 and ALK is associated with development of lung adenocarcinomas lacking EGFR and KRAS mutations and is correlated with ALK expression. Mol Cancer. 2010;9(1):1–12.
50. Childress MA, Himmelberg SM, Chen H, Deng W, Davies MA, Lovly CM. ALK Fusion Partners Impact Response to ALK Inhibition: Differential Effects on Sensitivity, Cellular Phenotypes, and Biochemical Properties. Mol Cancer Res. 2018;16(11):1724–36.
51. Heuckmann JM, Hölzel M, Sos ML, Heynck S, Balke-Want H, Koker M, et al. ALK mutations conferring differential resistance to structurally diverse ALK inhibitors. Clin Cancer Res. 2011;17(23):7394-401.

52. Yoshida T, Oya Y, Tanaka K, Shimizu J, Horio Y, Kuroda H, et al. Differential crizotinib response duration among ALK fusion variants in ALK-positive non-small-cell lung cancer. J Clin Oncol. 2016;34(28):3383-9.
53. Woo CG, Seo S, Kim SW, Jang SJ, Park KS, Song JY, et al. Differential protein stability and clinical responses of EML4-ALK fusion variants to various ALK inhibitors in advanced ALK-rearranged non-small cell lung cancer. Ann Oncol. 2017;28(4):791–7.
54. Lin JJ, Zhu VW, Yoda S, Yeap BY, Schrock AB, Dagogo-Jack I, et al. Impact of EML4-ALK variant on resistance mechanisms and clinical outcomes in ALK-positive lung cancer. J Clin Oncol. 2018;36(12):1199-1206.
55. Solomon BJ, Mok T, Kim D-W, Wu Y-L, Nakagawa K, Mekhail T, et al. First-Line Crizotinib versus Chemotherapy in ALK -Positive Lung Cancer. N Engl J Med. 2014;371(23):2167–77.
56. Solomon BJ, Kim DW, Wu YL, Nakagawa K, Mekhail T, Felip E, et al. Final overall survival analysis from a study comparing first-line crizotinib versus chemotherapy in alk-mutation-positive non–small-cell lung cancer. J Clin Oncol. 2018;36(22):2251–8.
57. Wu YL, Lu S, Lu Y, Zhou J, Shi Y kai, Sriuranpong V, et al. Results of PROFILE 1029, a Phase III Comparison of First-Line Crizotinib versus Chemotherapy in East Asian Patients with ALK-Positive Advanced Non–Small Cell Lung Cancer. J Thorac Oncol. 2018;13(10):1539–48.
58. Costa DB, Kobayashi S, Pandya SS, Yeo WL, Shen Z, Tan W, et al. CSF concentration of the anaplastic lymphoma kinase inhibitor crizotinib. J Clin Onco. 2011;29(15):e443-5.
59. Soria J-C, Tan DSW, Chiari R, Wu Y-L, Paz-Ares L, Wolf J, et al. First-line ceritinib versus platinum-based chemotherapy in advanced ALK -rearranged non-small-cell lung cancer (ASCEND-4): a randomised, open-label, phase 3 study. Lancet. 2017;389(10072):917–29.
60. Hida T, Nokihara H, Kondo M, Kim YH, Azuma K, Seto T, et al. Alectinib versus crizotinib in patients with ALK-positive non-small-cell lung cancer (J-ALEX): an open-label, randomised phase 3 trial. Lancet. 2017;390(10089):29–39.
61. Camidge DR, Dziadziuszko R, Peters S, Mok T, Noe J, Nowicka M, et al. Updated Efficacy and Safety Data and Impact of the EML4-ALK Fusion Variant on the Efficacy of Alectinib in Untreated ALK-Positive Advanced Non–Small Cell Lung Cancer in the Global Phase III ALEX Study. J Thorac Oncol. 2019;14(7):1233-1243.
62. Peters S, Camidge DR, Shaw AT, Gadgeel S, Ahn JS, Kim DW, et al. Alectinib versus crizotinib in untreated ALK-positive non–small-cell lung cancer. N Engl J Med. 2017;377(9):829-838.
63. Camidge DR, Kim HR, Ahn M-J, Yang JC-H, Han J-Y, Lee J-S, et al. Brigatinib versus Crizotinib in ALK -Positive Non–Small-Cell Lung Cancer. N Engl J Med. 2018;379(21):2027–39.
64. Gainor JF, Dardaei L, Yoda S, Friboulet L, Leshchiner I, Katayama R, et al. Molecular mechanisms of resistance to first- and second-generation ALK inhibitors in ALK -rearranged lung cancer. Cancer Discov. 2016;6(10):1118-1133.
65. Lin JJ, Riely GJ, Shaw AT. Targeting ALK: Precision medicine takes on drug resistance. Cancer Discov. 2017;7(2):137-155.
66. Solomon BJ, Bauer TM, Felip E, Besse B, James LP, Clancy JS, et al. Safety and efficacy of lorlatinib (PF-06463922) from the dose-escalation component of a study in patients with advanced ALK+ or ROS1+ non-small cell lung cancer (NSCLC). J Clin Oncol. 2016;34(15_suppl):9009.
67. Shaw AT, Bauer TM, de Marinis F, Felip E, Goto Y, Liu G, et al. First-Line Lorlatinib or Crizotinib in Advanced ALK -Positive Lung Cancer. N Engl J Med. 2020;383(21):2018–29.

68. Recondo G, Mezquita L, Facchinetti F, Planchard D, Gazzah A, Bigot L, et al. Diverse resistance mechanisms to the third-generation ALK inhibitor lorlatinib in ALK-rearranged lung cancer. Clin Cancer Res. 2020;26(1):242-255.
69. Horn L, Wang Z, Wu G, Poddubskaya E, Mok T, Reck M, et al. Ensartinib vs Crizotinib for Patients with Anaplastic Lymphoma Kinase-Positive Non-Small Cell Lung Cancer: A Randomized Clinical Trial. JAMA Oncol. 2021;7(11):1617-1625.
70. Liu D, Offin M, Harnicar S, Li BT, Drilon A. Entrectinib: An orally available, selective tyrosine kinase inhibitor for the treatment of NTRK, ROS1, and ALK fusion-positive solid tumors. Ther Clin Risk Manag. 2018;14:1247-1252.
71. Cui JJ, Rogers E, Zhai D, Deng W, Ung J, Nguyen V, et al. Abstract 5226: TPX-0131: A next generation macrocyclic ALK inhibitor that overcomes ALK resistant mutations refractory to current approved ALK inhibitors. Cancer Res. 2020;80(16 Supplement):5226–5226.
72. McCusker MG, Russo A, Scilla KA, Mehra R, Rolfo C. How i treat ALK-positive non-small cell lung cancer. ESMO Open. 2019;4(Suppl 2):e000524.
73. Gainor JF, Shaw AT, Sequist L V., Fu X, Azzoli CG, Piotrowska Z, et al. EGFR mutations and ALK rearrangements are associated with low response rates to PD-1 pathway blockade in non-small cell lung cancer: A retrospective analysis. Clin Cancer Res. 2016;22(18):4585–93.
74. Govindan R, Ding L, Griffith M, Subramanian J, Dees ND, Kanchi KL, et al. Genomic Landscape of Non-Small Cell Lung Cancer in Smokers and Never-Smokers. Cell. 2012;150(6):1121–34.
75. Shaw AT, Kim TM, Crinò L, Gridelli C, Kiura K, Liu G, et al. Ceritinib versus chemotherapy in patients with ALK-rearranged non-small-cell lung cancer previously given chemotherapy and crizotinib (ASCEND-5): a randomised, controlled, open-label, phase 3 trial. Lancet Oncol. 2017;18(7):874–86.
76. Zhou J, Zheng J, Zhang X, Zhao J, Zhu Y, Shen Q, et al. Crizotinib in patients with anaplastic lymphoma kinase-positive advanced non-small cell lung cancer versus chemotherapy as a first-line treatment. BMC Cancer. 2018;18(1):10.
77. Doebele RC, Pilling AB, Aisner DL, Kutateladze TG, Le AT, Weickhardt AJ, et al. Mechanisms of resistance to crizotinib in patients with ALK gene rearranged non-small cell lung cancer. Clin Cancer Res. 2012;18(5):1472-82.
78. Toyokawa G, Hirai F, Inamasu E, Yoshida T, Nosaki K, Takenaka T, et al. Secondary mutations at I1171 in the ALK gene confer resistance to both crizotinib and alectinib. J Thorac Oncol. 2014;9(12):e86-7.
79. Katayama R, Khan TM, Benes C, Lifshits E, Ebi H, Rivera VM, et al. Therapeutic strategies to overcome crizotinib resistance in non-small cell lung cancers harboring the fusion oncogene EML4-ALK. Proc Natl Acad Sci U S A. 2011;108(18):7535-40.
80. Kogita A, Togashi Y, Hayashi H, Sogabe S, Terashima M, De Velasco MA, et al. Hypoxia induces resistance to ALK inhibitors in the H3122 non-small cell lung cancer cell line with an ALK rearrangement via epithelial-mesenchymal transition. Int J Oncol. 2014;45(4):1430-6.
81. Fukuda K, Takeuchi S, Arai S, Katayama R, Nanjo S, Tanimoto A, et al. Epithelial-to-Mesenchymal Transition Is a Mechanism of ALK Inhibitor Resistance in Lung Cancer Independent of ALK Mutation Status. Cancer Res. 2019;79(7):1658–70.
82. Katayama R, Friboulet L, Koike S, Lockerman EL, Khan TM, Gainor JF, et al. Two novel ALK mutations mediate acquired resistance to the next generation ALK inhibitor alectinib. Clin Cancer Res. 2014;20(22):5686-96.

83. Ou SH, Milliken JC, Azada MC, Miller VA, Ali SM, Klempner SJ. ALK F1174V mutation confers sensitivity while ALK I1171 mutation confers resistance to alectinib. The importance of serial biopsy post progression. Lung Cancer. 2016;91:70–2.
84. Okada K, Araki M, Sakashita T, Ma B, Kanada R, Yanagitani N, et al. Prediction of ALK mutations mediating ALK-TKIs resistance and drug re-purposing to overcome the resistance. EBioMedicine. 2019;41:105–19.
85. Shaw AT, Friboulet L, Leshchiner I, Gainor JF, Bergqvist S, Brooun A, et al. Resensitization to Crizotinib by the Lorlatinib ALK Resistance Mutation L1198F. N Engl J Med. 2016;374(1):54.
86. Camidge DR, Pao W, Sequist L V. Acquired resistance to TKIs in solid tumours: learning from lung cancer. Nat Rev Clin Oncol. 2014;11(8):473–81.
87. Yoda S, Lin JJ, Lawrence MS, Burke BJ, Friboulet L, Langenbucher A, et al. Sequential ALK Inhibitors Can Select for Lorlatinib-Resistant Compound ALK Mutations in ALK-Positive Lung Cancer. Cancer Discov. 2018;8(6):714–29.
88. Sasaki T, Koivunen J, Ogino A, Yanagita M, Nikiforow S, Zheng W, et al. A novel ALK secondary mutation and EGFR signaling cause resistance to ALK kinase inhibitors. Cancer Res. 2011;71(18):6051-60.
89. Katayama R, Shaw AT, Khan TM, Mino-Kenudson M, Solomon BJ, Halmos B, et al. Mechanisms of acquired crizotinib resistance in ALK-rearranged lung Cancers. Sci Transl Me . 2012;4(120):120ra17.
90. Antoni D, Burckel H, Noel G. Combining Radiation Therapy with ALK Inhibitors in Anaplastic Lymphoma Kinase-Positive Non-Small Cell Lung Cancer (NSCLC): A Clinical and Preclinical Overview. Cancers. 2021;13(10):2394.
91. Ali SM, Hensing T, Schrock AB, Allen J, Sanford E, Gowen K, et al. Comprehensive Genomic Profiling Identifies a Subset of Crizotinib-Responsive ALK -Rearranged Non-Small Cell Lung Cancer Not Detected by Fluorescence In Situ Hybridization. Oncologist. 2016;21(6):762–70.
92. Provencio M, Torrente M, Calvo V, Gutiérrez L, Pérez-Callejo D, Pérez-Barrios C, et al. Dynamic circulating tumor DNA quantificaton for the individualization of non-small-cell lung cancer patients treatment. Oncotarget. 2017;8(36):60291–8.
93. Provencio M, Torrente M, Calvo V, Pérez-Callejo D, Gutiérrez L, Franco F, et al. Prognostic value of quantitative ctDNA levels in non small cell lung cancer patients. Oncotarget. 2018;9(1):488–94.
94. Kustanovich A, Schwartz R, Peretz T, Grinshpun A. Life and death of circulating cell-free DNA. Cancer Biol Ther. 2019;20(8):1057-1067.
95. Cescon DW, Bratman S V., Chan SM, Siu LL. Circulating tumor DNA and liquid biopsy in oncology. Nat Cancer. 2020;1(3):276–90.
96. Canale M, Pasini L, Bronte G, Delmonte A, Cravero P, Crinò L, et al. Role of liquid biopsy in oncogene-addicted non-small cell lung cancer. Transl Lung Cancer Res. 2019;8:S265–79.
97. Leighl NB, Page RD, Raymond VM, Daniel DB, Divers SG, Reckamp KL, et al. Clinical Utility of Comprehensive Cell-free DNA Analysis to Identify Genomic Biomarkers in Patients with Newly Diagnosed Metastatic Non-small Cell Lung Cancer. Clin Cancer Res. 2019;25(15):4691–700.
98. Kou R, Lam H, Duan H, Ye L, Jongkam N, Chen W, et al. Benefits and Challenges with Applying Unique Molecular Identifiers in Next Generation Sequencing to Detect Low Frequency Mutations. PLoS One. 2016;11(1):e0146638.

99. Sater V, Viailly PJ, Lecroq T, Ruminy P, Bérard C, Prieur-Gaston É, et al. UMI-Gen: A UMI-based read simulator for variant calling evaluation in paired-end sequencing NGS libraries. Comput Struct Biotechnol J. 2020;18:2270-80.
100. Provencio M, Pérez-Barrios C, Barquin M, Calvo V, Franco F, Sánchez E, et al. Next-generation sequencing for tumor mutation quantification using liquid biopsies. Clin Chem Lab Med. 2020;58(2):306-313
101. Mok TS, Wu Y-L, Ahn M-J, Garassino MC, Kim HR, Ramalingam SS, et al. Osimertinib or Platinum-Pemetrexed in EGFR T790M-Positive Lung Cancer. N Engl J Med. 2017;376(7):629–40.
102. Meng W, Li Y, Chai B, Liu X, Ma Z. miR-199a: A Tumor Suppressor with Noncoding RNA Network and Therapeutic Candidate in Lung Cancer. Int J Mol Sci. 2022;23(15):8518
103. Wang S, Cheng L, Wu H, Li G. Mechanisms and prospects of circular RNAs and their interacting signaling pathways in colorectal cancer. Front Oncol. 2022;12:949656.
104. Azizidoost S, Ghaedrahmati F, Sheykhi-Sabzehpoush M, Uddin S, Ghafourian M, Mousavi Salehi A, et al. The role of LncRNA MCM3AP-AS1 in human cancer. Clin Transl Oncol. 2022.
105. Berman E, Jhanwar S, Hedvat C, Arcila ME, Wahab OA, Levine R, et al. Resistance to imatinib in patients with chronic myelogenous leukemia and the splice variant BCR-ABL1(35INS). Leuk Res. 2016;49:108–12.
106. Soda M, Choi YL, Enomoto M, Takada S, Yamashita Y, Ishikawa S, et al. Identification of the transforming EML4-ALK fusion gene in non-small-cell lung cancer. Nature. 2007;448(7153):561–6.
107. Hagen RM, Adamo P, Karamat S, Oxley J, Aning JJ, Gillatt D, et al. Quantitative analysis of ERG expression and its splice isoforms in formalin-fixed, paraffin-embedded prostate cancer samples: association with seminal vesicle invasion and biochemical recurrence. Am J Clin Pathol. 2014;142(4):533–40.
108. Yap TA, Lorente D, Omlin A, Olmos D, De Bono JS. Circulating Tumor Cells: A MultifunctionalBiomarkerCirculating Tumor Cells. Clin Cancer Res. 2014;20(10):2553–68.
109. Nilsson RJA, Balaj L, Hulleman E, Van Rijn S, Pegtel DM, Walraven M, et al. Blood platelets contain tumor-derived RNA biomarkers. Blood. 2011;118(13):3680–3.
110. Joosse SA, Pantel K. Tumor-Educated Platelets as Liquid Biopsy in Cancer Patients. Cancer Cell. 2015;28(5):552–4.
111. Salloum E, Reiss M, Cooper D. Detection and viability of tumor cells in peripheral blood stem cell and bone marrow collections from breast cancer patients. Blood. 1994;83(7):2007–8.
112. Cristofanilli M, Budd GT, Ellis MJ, Stopeck A, Matera J, Miller MC, et al. Circulating Tumor Cells, Disease Progression, and Survival in Metastatic Breast Cancer. N Engl J Med. 2004;351(8):781–91.
113. De Bono JS, Scher HI, Montgomery RB, Parker C, Miller MC, Tissing H, et al. Circulating tumor cells predict survival benefit from treatment in metastatic castration-resistant prostate cancer. Clin Cancer Res. 2008;14(19):6302–9.
114. Cohen SJ, Punt CJA, Iannotti N, Saidman BH, Sabbath KD, Gabrail NY, et al. Relationship of circulating tumor cells to tumor response, progression-free survival, and overall survival in patients with metastatic colorectal cancer. J Clin Oncol. 2008;26(19):3213–21.
115. Balaj L, Lessard R, Dai L, Cho YJ, Pomeroy SL, Breakefield XO, et al. Tumour microvesicles contain retrotransposon elements and amplified oncogene sequences. Nat Commun. 2011;2(1):180.

116. Sundararajan V, Sarkar FH, Ramasamy TS. The versatile role of exosomes in cancer progression: diagnostic and therapeutic implications. Cell Oncol (Dordr). 2018 Aug;41(4):463.
117. Robado de Lope L, Sánchez-Herrero E, Serna-Blasco R, Provencio M, Romero A. Cancer as an infective disease: the role of EVs in tumorigenesis. Mol Oncol. 2022.
118. Février B, Raposo G. Exosomes: endosomal-derived vesicles shipping extracellular messages. Curr Opin Cell Biol. 2004;16(4):415–21.
119. Théry C, Witwer KW, Aikawa E, Alcaraz MJ, Anderson JD, Andriantsitohaina R, et al. Minimal information for studies of extracellular vesicles 2018 (MISEV2018): a position statement of the International Society for Extracellular Vesicles and update of the MISEV2014 guidelines. J Extracell Vesicles. 2018;7(1):1535750..
120. Yáñez-Mó M, Siljander PRM, Andreu Z, Zavec AB, Borràs FE, Buzas EI, et al. Biological properties of extracellular vesicles and their physiological functions. J Extracell Vesicles. 2015;4:27066.
121. Witwer KW, Buzás EI, Bemis LT, Bora A, Lässer C, Lötvall J, et al. Standardization of sample collection, isolation and analysis methods in extracellular vesicle research. J Extracell Vesicles. 2013;2(1).
122. Durcin M, Fleury A, Taillebois E, Hilairet G, Krupova Z, Henry C, et al. Characterisation of adipocyte-derived extracellular vesicle subtypes identifies distinct protein and lipid signatures for large and small extracellular vesicles. J Extracell Vesicles. 2017;6(1):1305677.
123. Simons M, Raposo G. Exosomes--vesicular carriers for intercellular communication. Curr Opin Cell Biol. 2009;21(4):575–81
124. Barreiro K, Dwivedi OP, Leparc G, Rolser M, Delic D, Forsblom C, et al. Comparison of urinary extracellular vesicle isolation methods for transcriptomic biomarker research in diabetic kidney disease. J Extracell vesicles. 2020;10(2):e12038.
125. Sidhom K, Obi PO, Saleem A. A review of exosomal isolation methods: Is size exclusion chromatography the best option? Int J Mol Sci. 2020;21(18):6466.
126. Möhrmann L, Huang HJ, Hong DS, Tsimberidou AM, Fu S, Piha-Paul SA, et al. Liquid Biopsies Using Plasma Exosomal Nucleic Acids and Plasma Cell-Free DNA Compared with Clinical Outcomes of Patients with Advanced Cancers. Clin Cancer Res. 2018;24(1):181–8.
127. Ruggiero JE, Rughani J, Neiman J, Swanson S, Revol C, Green RJ. Real-world concordance of clinical practice with ASCO and NCCN guidelines for EGFR/ALK testing in aNSCLC. J Clin Oncol. 2017;35(8_suppl):212.
128. Chouaid C, Dujon C, Do P, Monnet I, Madroszyk A, Le Caer H, et al. Feasibility and clinical impact of re-biopsy in advanced non small-cell lung cancer: A prospective multicenter study in a real-world setting (GFPC study 12-01). Lung Cancer. 2014;86(2):170–3.
129. Bosc C, Ferretti GR, Cadranel J, Audigier-Valette C, Besse B, Barlesi F, et al. Rebiopsy during disease progression in patients treated by TKI for oncogene-addicted NSCLC. Target Oncol. 2014;10(2):247–53.
130. Parikh AR, Leshchiner I, Elagina L, Goyal L, Levovitz C, Siravegna G, et al. Liquid versus tissue biopsy for detecting acquired resistance and tumor heterogeneity in gastrointestinal cancers. Nat Med. 2019;25(9):1415–21.
131. Romero A, Serna-Blasco R, Calvo V, Provencio M. Use of Liquid Biopsy in the Care of Patients with Non-Small Cell Lung Cancer. Curr Treat Options Oncol. 2021;22(10):86.
132. Provencio M, Serna-Blasco R, Nadal E, Insa A, García-Campelo MR, Casal Rubio J, et al. Overall Survival and Biomarker Analysis of Neoadjuvant Nivolumab Plus Chemotherapy in

Operable Stage IIIA Non-Small-Cell Lung Cancer (NADIM phase II trial). J Clin Oncol. 2022;40(25):2924-2933.

133. Provencio M, Serna-Blasco R, Franco F, Calvo V, Royuela A, Auglytė M, et al. Analysis of circulating tumour DNA to identify patients with epidermal growth factor receptor-positive non-small cell lung cancer who might benefit from sequential tyrosine kinase inhibitor treatment. Eur J Cancer. 2021;149:61–72.

134. Angeles AK, Christopoulos P, Yuan Z, Bauer S, Janke F, Ogrodnik SJ, et al. Early identification of disease progression in ALK-rearranged lung cancer using circulating tumor DNA analysis. NPJ Precis Oncol. 2021;5(1):1–12.

135. Elsayed M, Bozorgmehr F, Kazdal D, Volckmar AL, Sültmann H, Fischer JR, et al. Feasibility and Challenges for Sequential Treatments in ALK-Rearranged Non-Small-Cell Lung Cancer. Front Oncol. 2021;11:670483.

136. Malapelle U, Tiseo M, Vivancos A, Kapp J, Serrano MJ, Tiemann M, et al. Liquid Biopsy for Biomarker Testing in Non-Small Cell Lung Cancer: A European Perspective. J Mol Pathol. 2021;2(3):255-273.

137. Adashek JJ, Janku F, Kurzrock R, Troncone G, Siravegna G. Signed in Blood: Circulating Tumor DNA in Cancer Diagnosis, Treatment and Screening. Cancers (Basel). 2021;13(14):3600.

138. Romero A, Serna-Blasco R, Alfaro C, Sánchez-Herrero E, Barquín M, Turpin MC, et al. ctDNA analysis reveals different molecular patterns upon disease progression in patients treated with osimertinib. Transl Lung Cancer Res. 2020;9(3):532-540.

139. Schwarzenbach H, Hoon DSB, Pantel K. Cell-free nucleic acids as biomarkers in cancer patients. Nat Rev Cancer. 2011;11(6):426-37.

140. Costello M, Pugh TJ, Fennell TJ, Stewart C, Lichtenstein L, Meldrim JC, et al. Discovery and characterization of artifactual mutations in deep coverage targeted capture sequencing data due to oxidative DNA damage during sample preparation. Nucleic Acids Res. 2013;41(6):e67.

141. Kinde I, Wu J, Papadopoulos N, Kinzler KW, Vogelstein B. Detection and quantification of rare mutations with massively parallel sequencing. Proc Natl Acad Sci U S A. 2011;108(23):9530–5.

142. Romero A, Jantus-Lewintre E, García-Peláez B, Royuela A, Insa A, Cruz P, et al. Comprehensive cross-platform comparison of methods for non-invasive EGFR mutation testing: results of the RING observational trial. Mol Oncol. 2021;15(1):43–56.

143. Lanman RB, Mortimer SA, Zill OA, Sebisanovic D, Lopez R, Blau S, et al. Analytical and clinical validation of a digital sequencing panel for quantitative, highly accurate evaluation of cell-free circulating tumor DNA. PLoS One. 2015;10(10):e0140712.

144. Rolfo C, Mack PC, Scagliotti G V., Baas P, Barlesi F, Bivona TG, et al. Liquid Biopsy for Advanced Non-Small Cell Lung Cancer (NSCLC): A Statement Paper from the IASLC. J Thorac Oncol. 2018;13(9):1248–68.

145. Paweletz CP, Sacher AG, Raymond CK, Alden RS, O'Connell A, Mach SL, et al. Bias-Corrected Targeted Next-Generation Sequencing for Rapid, Multiplexed Detection of Actionable Alterations in Cell-Free DNA from Advanced Lung Cancer Patients. Clin Cancer Res. 2016;22(4):915–22.

146. Goldberg SB, Narayan A, Kole AJ, Decker RH, Teysir J, Carriero NJ, et al. Early Assessment of Lung Cancer Immunotherapy Response via Circulating Tumor DNA. Clin Cancer Res. 2018;24(8):1872–80.

147. Ococks E, Frankell AM, Masque Soler N, Grehan N, Northrop A, Coles H, et al. Longitudinal tracking of 97 esophageal adenocarcinomas using liquid biopsy sampling. Ann Oncol. 2021;32(4):522–32.
148. Nabet BY, Esfahani MS, Moding EJ, Hamilton EG, Chabon JJ, Rizvi H, et al. Noninvasive Early Identification of Therapeutic Benefit from Immune Checkpoint Inhibition. Cell. 2020;183(2):363-376.e13.
149. Lam VK, Zhang J, Wu CC, Tran HT, Li L, Diao L, et al. Genotype-Specific Differences in Circulating Tumor DNA Levels in Advanced NSCLC. J Thorac Oncol. 2021;16(4):601–9.
150. Crizotinib versus Chemotherapy in Advanced ALK -Positive Lung Cancer. N Engl J Med. 2015;373(16):1582.
151. Aggarwal C, Thompson JC, Black TA, Katz SI, Fan R, Yee SS, et al. Clinical Implications of Plasma-Based Genotyping With the Delivery of Personalized Therapy in Metastatic Non–Small Cell Lung Cancer. JAMA Oncol. 2019;5(2):173–80.
152. Stetson D, Ahmed A, Xu X, Nuttall BRB, Lubinski TJ, Johnson JH, et al. Orthogonal Comparison of Four Plasma NGS Tests With Tumor Suggests Technical Factors are a Major Source of Assay Discordance. JCO Precis Oncol. 2019;(3):1–9.
153. Thandra KC, Barsouk A, Saginala K, Aluru JS, Barsouk A. Epidemiology of lung cancer. Contemp Oncol. 2021;25(1):45.
154. Ptashkin RN, Mandelker DL, Coombs CC, Bolton K, Yelskaya Z, Hyman DM, et al. Prevalence of clonal hematopoiesis mutations in tumor-only clinical genomic profiling of solid tumors. JAMA Oncol. 2018.
155. Hu Y, Ulrich BC, Supplee J, Kuang Y, Lizotte PH, Feeney NB, et al. False-positive plasma genotyping due to clonal hematopoiesis. Clin Cancer Res. 2018;4(11):1589-1593.
156. Liu J, Chen X, Wang J, Zhou S, Wang CL, Ye MZ, et al. Biological background of the genomic variations of cf-DNA in healthy individuals. Ann Oncol. 2019;30(3):464-470.
157. Barquín M, Maximiano C, Pérez-Barrios C, Sanchez-Herrero E, Soriano M, Colmena M, et al. Peritoneal washing is an adequate source for somatic BRCA1/2 mutation testing in ovarian malignancies. Pathol Res Pract. 2019;215(2):392–4.
158. Ideno N, Mori Y, Nakamura M, Ohtsuka T. Early Detection of Pancreatic Cancer: Role of Biomarkers in Pancreatic Fluid Samples. Diagnostics (Basel, Switzerland). 2020;10(12):1056.
159. van't Erve I, Rovers KP, Constantinides A, Bolhuis K, Wassenaar ECE, Lurvink RJ, et al. Detection of tumor-derived cell-free DNA from colorectal cancer peritoneal metastases in plasma and peritoneal fluid. J Pathol Clin Res. 2021;7(3):203–8.
160. Jiang BY, Li YS, Guo WB, Zhang XC, Chen ZH, Su J, et al. Detection of driver and resistance mutations in leptomeningeal metastases of NSCLC by next-generation sequencing of cerebrospinal fluid circulating tumor cells. Clin Cancer Res. 2017;23(18):5480–8.
161. Pan W, Gu W, Nagpal S, Gephart MH, Quake SR. Brain Tumor Mutations Detected in Cerebral Spinal Fluid. Clin Chem. 2015;61(3):514-22.
162. Guo Z, Xie Z, Shi H, Du W, Peng L, Han W, et al. Malignant pleural effusion supernatant is an alternative liquid biopsy specimen for comprehensive mutational profiling. Thorac Cancer. 2019;10(4):823-31.
163. Tong L, Ding N, Tong X, Li J, Zhang Y, Wang X, et al. Tumor-derived DNA from pleural effusion supernatant as a promising alternative to tumor tissue in genomic profiling of advanced lung cancer. Theranostics. 2019;9(19):5532-41.

164. Cao R, Lea K, Jasti M, Schageman J, Hanif K, Li Y, et al. Characterization of Genetic Mutation Spectra and Identification of Gene Amplification and Fusion Variants in Cell-Free Nuclei Acid from Cultured Cancer Cell Media and Liquid Biopsy Specimens Using Oncomine™ Pan-Cancer Cell-Free Assay. https://www.thermofisher.com/es/es/home.html.
165. Newman AM, Bratman S V, To J, Wynne JF, Eclov NCW, Modlin LA, et al. An ultrasensitive method for quantitating circulating tumor DNA with broad patient coverage. Nat Med. 2014;20(5):548-54.
166. Meier K. Guidance for Industry and FDA Staff - Statistical Guidance on Reporting Results from Studies Evaluating Diagnostic Tests. 2007. http://www.fda.gov/dockets/ecomments.
167. Lanman RB, Mortimer SA, Zill OA, Sebisanovic D, Lopez R, Blau S, et al. Analytical and Clinical Validation of a Digital Sequencing Panel for Quantitative, Highly Accurate Evaluation of Cell-Free Circulating Tumor DNA. PLoS One. 2015;10(10):e0140712.
168. Schwaederlé MC, Patel SP, Husain H, Ikeda M, Lanman RB, Banks KC, et al. Utility of genomic assessment of blood-derived circulating tumor DNA (ctDNA) in patients with advanced lung adenocarcinoma. Clin Cancer Res. 2017;23(17):5101–11.
169. Kim ST, Lee WS, Lanman RB, Mortimer S, Zill OA, Kim K-M, et al. Prospective blinded study of somatic mutation detection in cell-free DNA utilizing a targeted 54-gene next generation sequencing panel in metastatic solid tumor patients. Oncotarget. 2015;6(37):40360–9.
170. Deveson IW, Gong B, Lai K, LoCoco JS, Richmond TA, Schageman J, et al. Evaluating the analytical validity of circulating tumor DNA sequencing assays for precision oncology. Nat Biotechnol. 2021;39(9):1115-28.
171. Merino DM, McShane LM, Fabrizio D, Funari V, Chen SJ, White JR, et al. Establishing guidelines to harmonize tumor mutational burden (TMB): in silico assessment of variation in TMB quantification across diagnostic platforms: phase I of the Friends of Cancer Research TMB Harmonization Project. J Immunother Cancer. 2020;8(1):147.
172. McCoach CE, Blakely CM, Banks KC, Levy B, Chue BM, Raymond VM, et al. Clinical utility of cell-free DNA for the detection of ALK fusions and genomic mechanisms of ALK inhibitor resistance in non–small cell lung cancer. Clin Cancer Res. 2018;24(12):2758–70.
173. Dagogo-Jack I, Brannon AR, Ferris LA, Campbell CD, Lin JJ, Schultz KR, et al. Tracking the Evolution of Resistance to ALK Tyrosine Kinase Inhibitors Through Longitudinal Analysis of Circulating Tumor DNA. JCO Precis Oncol. 2018;2(2):1–14.
174. Dagogo-Jack I, Rooney M, Lin JJ, Nagy RJ, Yeap BY, Hubbeling H, et al. Treatment with Next-Generation ALK Inhibitors Fuels Plasma ALK Mutation Diversity. 2019;25(22):6662-6670.
175. Yu Y, Ou Q, Wu X, Bao H, Ding Y, Shao YW, et al. Concomitant resistance mechanisms to multiple tyrosine kinase inhibitors in ALK-positive non-small cell lung cancer. Lung Cancer. 2019;127:19–24.
176. Russo M, Siravegna G, Blaszkowsky LS, Corti G, Crisafulli G, Ahronian LG, et al. Tumor heterogeneity and Lesion-Specific response to targeted therapy in colorectal cancer. Cancer Discov. 2016;6(2):147–53.
177. Christopoulos P, Dietz S, Kirchner M, Volckmar AL, Endris V, Neumann O, et al. Detection of TP53 mutations in tissue or liquid rebiopsies at progression identifies ALK + lung cancer patients with poor survival. Cancers (Basel). 2019;11(1)_124.
178. Brosh R, Rotter V. When mutants gain new powers: News from the mutant p53 field. Nature Reviews Cancer. 2009;9(10):701-13.

179. Nagarkar R, Crook T, Plowman N, Gaya A, Patil D, Akolkar D, et al. A Pilot Basket Study to Evaluate Multi-Analyte Liquid Biopsies for Personalized Treatments in Advanced Refractory Cancers. medRxiv. 2021.
180. Lin YT, Chiang CL, Hung JY, Lee MH, Su WC, Wu SY, et al. Resistance profiles of anaplastic lymphoma kinase tyrosine kinase inhibitors in advanced non–small-cell lung cancer: a multicenter study using targeted next-generation sequencing. Eur J Cancer. 2021;156:1-11.
181. Scheffler M, Bos M, Gardizi M, König K, Michels S, Fassunke J, et al. PIK3CA mutations in non-small cell lung cancer (NSCLC): Genetic heterogeneity, prognostic impact and incidence of prior malignancies. Oncotarget. 2015;6(2):1315-26.
182. Schubbert S, Shannon K, Bollag G. Hyperactive Ras in developmental disorders and cancer. Nat Rev Cancer. 2007;7(4):295-308
183. Davies H, Bignell GR, Cox C, Stephens P, Edkins S, Clegg S, et al. Mutations of the BRAF gene in human cancer. Nature. 2002;417(6892):949-54.
184. Sebolt-Leopold JS, Herrera R. Targeting the mitogen-activated protein kinase cascade to treat cancer. Nat Rev Cancer. 2004;4(12):937-47.
185. Han J, Liu Y, Yang S, Wu X, Li H, Wang Q. MEK inhibitors for the treatment of non-small cell lung cancer. J Hematol Oncol. 2021;14(1):1.
186. Ryan MB, Corcoran RB. Therapeutic strategies to target RAS-mutant cancers. Nat Rev Clin Oncol. 2018;15(11):709-720.
187. Kemper M, Evers G, Schulze AB, Sperveslage J, Schülke C, Lenz G, et al. Polyclonal on-And off-target resistance mutations in an EML4-ALK positive non-small cell lung cancer patient under ALK inhibition. Oncotarget. 2021;12(19):1946-1952.
188. Verduzco D, Kuenzi BM, Kinose F, Sondak VK, Eroglu Z, Rix U, et al. Ceritinib enhances the efficacy of trametinib in BRAF/NRAS-wild-type melanoma cell lines. Mol Cancer Ther. 2018;17(1):73–83.
189. Crystal AS, Shaw AT, Sequist L V., Friboulet L, Niederst MJ, Lockerman EL, et al. Patient-derived models of acquired resistance can identify effective drug combinations for cancer. Science. 2014;346(6216):1480–6.
190. Hrustanovic G, Olivas V, Pazarentzos E, Tulpule A, Asthana S, Blakely CM, et al. RAS-MAPK dependence underlies a rational polytherapy strategy in EML4-ALK-positive lung cancer. Nat Med. 2015;21(9):1038–47.
191. Collisson EA, Campbell JD, Brooks AN, Berger AH, Lee W, Chmielecki J, et al. Comprehensive molecular profiling of lung adenocarcinoma: The cancer genome atlas research network. Nature. 2014;511(7511):543-50.
192. Zhao Y, Wang H, He C. Drug resistance of targeted therapy for advanced non-small cell lung cancer harbored EGFR mutation: from mechanism analysis to clinical strategy. J Cancer Res Clin Oncol. 2021;147(12):3653-3664.
193. Moes-Sosnowska J, Chorostowska-Wynimko J. Fibroblast Growth Factor Receptor 1-4 Genetic Aberrations as Clinically Relevant Biomarkers in Squamous Cell Lung Cancer. Front Oncol. 2022;12:780650
194. Fujino T, Suda K, Mitsudomi T. Emerging MET tyrosine kinase inhibitors for the treatment of non-small cell lung cancer. Expert Opin Emerg Drugs. 2020;25(3):229-249.
195. Figueroa ME, Abdel-Wahab O, Lu C, Ward PS, Patel J, Shih A, et al. Leukemic IDH1 and IDH2 mutations result in a hypermethylation phenotype, disrupt TET2 function, and impair hematopoietic differentiation. Cancer Cell. 2010;18(6):553–67.

196. McMurry H, Fletcher L, Traer E. IDH Inhibitors in AML—Promise and Pitfalls. Curr Hematol Malig Rep. 2021;16(2):207–17.
197. Oxnard GR, Thress KS, Alden RS, Lawrance R, Paweletz CP, Cantarini M, et al. Association Between Plasma Genotyping and Outcomes of Treatment With Osimertinib (AZD9291) in Advanced Non–Small-Cell Lung Cancer. J Clin Oncol. 2016;34(28):3375.
198. Pös O, Biró O, Szemes T, Nagy B. Circulating cell-free nucleic acids: characteristics and applications. Eur J Hum Genet. 2018;26(7):937–45.
199. Vowles J, Odegaard J, Mortimer S, Fairclough S, Sikora M, Abdueva D, et al. Abstract 5705: Analytical validation of Guardant360 v2.10. Cancer Res. 2017;77 (13_Supplement):5705–5705.
200. Couraud S, Vaca-Paniagua F, Villar S, Oliver J, Schuster T, Blanché H, et al. Noninvasive diagnosis of actionable mutations by deep sequencing of circulating free DNA in lung cancer from never-smokers: a proof-of-concept study from BioCAST/IFCT-1002. Clin Cancer Res. 2014;20(17):4613–24.
201. Rafal Dziadziuszko A, Hung T, Wang K, Choeurng V, Drilon A, Doebele RC, et al. Pre- and post-treatment blood-based genomic landscape of patients with ROS1 or NTRK fusion-positive solid tumors treated with entrectinib. Mol Oncol. 2022;16(10):2000-2014.
202. Supplee JG, Milan MSD, Lim LP, Potts KT, Sholl LM, Oxnard GR, et al. Sensitivity of next-generation sequencing assays detecting oncogenic fusions in plasma cell-free DNA. Lung Cancer. 2019;134:96–9.
203. Odegaard JI, Vincent JJ, Mortimer S, Vowles J V., Ulrich BC, Banks KC, et al. Validation of a plasma-based comprehensive cancer genotyping assay utilizing orthogonal tissue- and plasma-based methodologies. Clin Cancer Res. 2018;24(15):3539–49.
204. Cui S, Zhang W, Xiong L, Pan F, Niu Y, Chu T, et al. Use of capture-based next-generation sequencing to detect ALK fusion in plasma cell-free DNA of patients with non-small-cell lung cancer. Oncotarget. 2017;8(2):2771–80.
205. Solomon JP, Benayed R, Hechtman JF, Ladanyi M. Identifying patients with NTRK fusion cancer. Ann Oncol Off J Eur Soc Med Oncol. 2019;30 Suppl 8(Suppl_8):viii16–22.
206. Hasegawa N, Kohsaka S, Kurokawa K, Shinno Y, Takeda Nakamura I, Ueno T, et al. Highly sensitive fusion detection using plasma cell-free RNA in non-small-cell lung cancers. Cancer Sci. 2021;112(10):4393.
207. Tong Y, Zhao Z, Liu B, Bao A, Zheng H, Gu J, et al. 5′/ 3′ imbalance strategy to detect ALK fusion genes in circulating tumor RNA from patients with non-small cell lung cancer. J Exp Clin Cancer Res. 2018;37(1):68.
208. Nilsson RJA, Karachaliou N, Berenguer J, Gimenez-Capitan A, Schellen P, Teixido C, et al. Rearranged EML4-ALK fusion transcripts sequester in circulating blood platelets and enable blood-based crizotinib response monitoring in non-small-cell lung cancer. Oncotarget. 2016;7(1):1066-75.
209. Park CK, Kim JE, Kim MS, Kho BG, Park HY, Kim TO, et al. Feasibility of liquid biopsy using plasma and platelets for detection of anaplastic lymphoma kinase rearrangements in non-small cell lung cancer. J Cancer Res Clin Oncol. 2019;145(8):2071-2082
210. Ma AP, Guo WX, Gao DH, Ke MY, Luo Q, Liu Q. Construction of CTC-ALK gene fusion detection system based on the multi-site magnetic separation in lung cancer and its clinical verification. Neoplasma. 2020;67(6):1233–43.

211. Ilie M, Long E, Butori C, Hofman V, Coelle C, Mauro V, et al. ALK-gene rearrangement: a comparative analysis on circulating tumour cells and tumour tissue from patients with lung adenocarcinoma. Ann Oncol. 2012;23(11):2907–13.
212. Pailler E, Adam J, Barthélémy A, Oulhen M, Auger N, Valent A, et al. Detection of circulating tumor cells harboring a unique ALK rearrangement in ALK-positive non–small-cell lung cancer. J Clin Oncol. 2013;31(18):2273-81.
213. Tanaka F, Yoneda K, Kondo N, Hashimoto M, Takuwa T, Matsumoto S, et al. Circulating tumor cell as a diagnostic marker in primary lung cancer. Clin Cancer Res. 2009;15(22):6980-6.
214. Allard WJ, Matera J, Miller MC, Repollet M, Connelly MC, Rao C, et al. Tumor cells circulate in the peripheral blood of all major carcinomas but not in healthy subjects or patients with nonmalignant diseases. Clin Cancer Res. 2004;10(20):6897-904.
215. Krebs MG, Sloane RS, Greystoke A. Evaluation and Prognostic Significance of Circulating Tumor Cells in Patients With Non-Small-Cell Lung Cancer. J Clin Oncol. 2011;29(12):1556-63.
216. Rossi E, Aieta M, Tartarone A, Pezzuto A, Facchinetti A, Santini D, et al. A fully automated assay to detect the expression of pan-cytokeratins and of EML4-ALK fusion protein in circulating tumour cells (CTCs) predicts outcome of non-small cell lung cancer (NSCLC) patients. Transl Lung Cancer Res. 2021;10(1):80–92
217. Kowalik A, Kowalewska M, Góźdź S. Current approaches for avoiding the limitations of circulating tumor cells detection methods—implications for diagnosis and treatment of patients with solid tumors. Transl Res. 2017;185:58-84.e15.
218. Jeyaram A, Jay SM. Preservation and Storage Stability of Extracellular Vesicles for Therapeutic Applications. AAPS J. 2017;20(1):1.
219. Ibrahim SA, Khan YS. Histology, Extracellular Vesicles. StatPearls. 2022.
220. Pettersen Hessvik N, Llorente A. Current knowledge on exosome biogenesis and release. Cell Mol Life Sci. 2018;75:193–208.
221. De Sousa KP, Rossi I, Abdullahi M, Ramirez MI, Stratton D, Inal JM. Isolation and characterization of extracellular vesicles and future directions in diagnosis and therapy. Wiley Interdiscip Rev Nanomedicine Nanobiotechnology. 2022;e1835.
222. Clos-Sansalvador M, Monguió-Tortajada M, Roura S, Franquesa M, Borràs FE. Commonly used methods for extracellular vesicles' enrichment: Implications in downstream analyses and use. Eur J Cell Biol. 2022;101(3):151227.
223. Stam J, Bartel S, Bischoff R, Wolters JC. Isolation of extracellular vesicles with combined enrichment methods. J Chromatogr B Anal Technol Biomed Life Sci. 2021;1169:122604.
224. Kowal J, Arras G, Colombo M, Jouve M, Morath JP, Primdal-Bengtson B, et al. Proteomic comparison defines novel markers to characterize heterogeneous populations of extracellular vesicle subtypes. Proc Natl Acad Sci U S A. 2016;113(8):E968-77.
225. Shah R, Patel T, Freedman JE. Circulating Extracellular Vesicles in Human Disease. N Engl J Med. 2018;379(22):2179-80.
226. Surman M, Stępień E, Przybyło M. Melanoma-derived extracellular vesicles: Focus on their proteome. Proteomes. 2019;7(2):21.
227. Vagner T, Spinelli C, Minciacchi VR, Balaj L, Zandian M, Conley A, et al. Large extracellular vesicles carry most of the tumour DNA circulating in prostate cancer patient plasma. J Extracell Vesicles. 2018;7(1):1505403.
228. Liu P, Zhao L, Pol J, Levesque S, Petrazzuolo A, Pfirschke C, et al. Crizotinib-induced immunogenic cell death in non-small cell lung cancer. Nat Commun. 2019;10(1):1486.

229. Lei YY, Yang JJ, Zhang XC, Zhong WZ, Zhou Q, Tu HY, et al. Anaplastic Lymphoma Kinase Variants and the Percentage of ALK-Positive Tumor Cells and the Efficacy of Crizotinib in Advanced NSCLC. Clin Lung Cancer. 2016;17(3):223-31.
230. Mitiushkina N V., Tiurin VI, Iyevleva AG, Kholmatov MM, Filippova EA, Moiseyenko F V., et al. Variability in lung cancer response to ALK inhibitors cannot be explained by the diversity of ALK fusion variants. Biochimie. 2018;154:19-24.
231. Becker A, Thakur BK, Weiss JM, Kim HS, Peinado H, Lyden D. Extracellular Vesicles in Cancer: Cell-to-Cell Mediators of Metastasis. Cancer Cell. 2016;30(6):836-848.
232. Koi Y, Tsutani Y, Nishiyama Y, Ueda D, Ibuki Y, Sasada S, et al. Predicting the presence of breast cancer using circulating small RNAs, including those in the extracellular vesicles. Cancer Sci. 2020;111(6):2104-15.
233. Matsuzaki K, Fujita K, Jingushi K, Kawashima A, Ujike T, Nagahara A, et al. MiR-21-5p in urinary extracellular vesicles is a novel biomarker of urothelial carcinoma. Oncotarget. 2017;8(15):24668-78.
234. Pu C, Huang H, Wang Z, Zou W, Lv Y, Zhou Z, et al. Extracellular Vesicle-Associated mir-21 and mir-144 Are Markedly Elevated in Serum of Patients With Hepatocellular Carcinoma. Front Physiol. 2018;9:930.

ANEXOS

Otras publicaciones relacionadas con la Tesis Doctoral

Artículo 1: Romero A, Serna-Blasco R, Alfaro C, **Sánchez-Herrero E**, Barquín M, Turpin MC, Chico S, Sanz-Moreno S, Rodrigez-Festa A, Laza-Briviesca R, Cruz-Bermudez A, Calvo V, Royuela A, Provencio M. ctDNA analysis reveals different molecular patterns upon disease progression in patients treated with osimertinib. Transl Lung Cancer Res. 2020; 9:532-540.

Artículo 2: Barquín M, Calvo V, García-García F, Nuñez B, **Sánchez-Herrero E**, Serna-Blasco R, Auglytė M, Carcereny E, Rodriguez-Abreu D, López Castro R, Guirado M, Camps C, Bosch-Barrera J, Massuti B, Ortega AL, Del Barco E, Gonzalez-Larriba JL, Aguiar D, García-Campelo R, Dómine M, Agraso S, Sala MA, Oramas J, Bernabé R, Blanco R, Parejo C, Cruz A, Menasalvas E, Royuela A, Romero A, Provencio M. Sex is a strong prognostic factor in stage IV non-small-cell lung cancer patients and should be considered in survival rate estimation. Cancer Epidemiol. 2020; 67:101737.

Artículo 3: Serna-Blasco R, **Sánchez-Herrero E**, Berrocal Renedo M, Calabuig-Fariñas S, Molina-Vila MÁ, Provencio M, Romero A. R-Score: A New Parameter to Assess the Quality of Variants' Calls Assessed by NGS Using Liquid Biopsies. Biology (Basel). 2021; 10:954.

Artículo 4: Serna-Blasco R, **Sánchez-Herrero E**, Sanz-Moreno S, Rodriguez-Festa A, García-Veros E, Casarrubios M, Sierra-Rodero B, Laza-Briviesca R, Cruz-Bermúdez A, Mielgo-Rubio X, Sánchez-Hernández A, Uribelarrea EA, Calvo V, Romero A, Provencio M. KRAS p.G12C mutation occurs in 1% of EGFR-mutated advanced non-small-cell lung cancer patients progressing on a first-line treatment with a tyrosine kinase inhibitor. ESMO Open. 2021; 6:100279.

Artículo 5: Campos-Silva C, Cáceres-Martell Y, **Sánchez-Herrero E**, Sandúa A, Beneitez-Martínez A, González Á, Provencio M, Romero A, Jara-Acevedo R, Yáñez-Mó M, Valés-Gómez M. A simple immunoassay for extracellular vesicle liquid biopsy in microliters of non-processed plasma. J Nanobiotechnology. 2022; 20:72.

Artículo 6: Provencio M, Serna-Blasco R, Nadal E, Insa A, García-Campelo MR, Casal Rubio J, Dómine M, Majem M, Rodríguez-Abreu D, Martínez-Martí A, De Castro Carpeño J, Cobo M, López Vivanco G, Del Barco E, Bernabé Caro R, Viñolas N, Barneto Aranda I, Viteri S, Pereira E, Royuela A, Calvo V, Martín-López J, García-García F, Casarrubios M, Franco F, **Sánchez-Herrero E**, Massuti B, Cruz-Bermúdez A, Romero A. Overall Survival and Biomarker Analysis of Neoadjuvant Nivolumab Plus Chemotherapy in Operable Stage IIIA Non-Small-Cell Lung Cancer (NADIM phase II trial). J Clin Oncol. 2022; JCO2102660.

Artículo 7: Serna-Blasco, R, Sánchez-Herrero, E, Robado de Lope, L, Sanz-Moreno, S, Rodríguez-Festa, A, Ares-Trotta, D, Cruz-Bermúdez, A, Franco, F, Sánchez-Hernández, A, Campayo, MJ, García-Girón, C, Dómine, M, Blasco, A, Sánchez, JM, Oramas, J, Bosch-Barrera, J, Sala, MÁ, Sereno, M, Romero, A, Provencio, M. Molecular Divergence upon EGFR-TKI Resistance Could Be Dependent on the Exon Location of the Original EGFR-Sensitizing Mutation. Cancers. 2022; 14:4446.

Otros documentos relacionados con la Tesis Doctoral

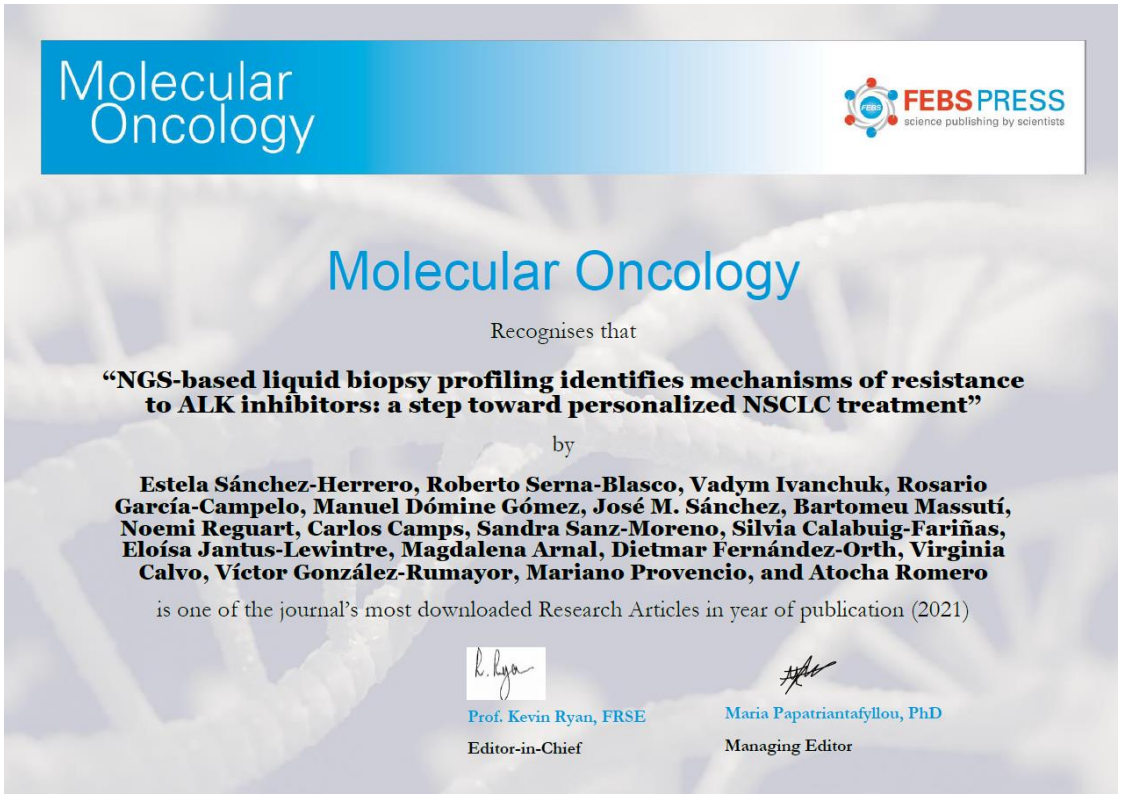

Molecular Oncology

FEBS PRESS
science publishing by scientists

Molecular Oncology

Recognises that

"NGS-based liquid biopsy profiling identifies mechanisms of resistance to ALK inhibitors: a step toward personalized NSCLC treatment"

by

Estela Sánchez-Herrero, Roberto Serna-Blasco, Vadym Ivanchuk, Rosario García-Campelo, Manuel Dómine Gómez, José M. Sánchez, Bartomeu Massutí, Noemi Reguart, Carlos Camps, Sandra Sanz-Moreno, Silvia Calabuig-Fariñas, Eloísa Jantus-Lewintre, Magdalena Arnal, Dietmar Fernández-Orth, Virginia Calvo, Víctor González-Rumayor, Mariano Provencio, and Atocha Romero

is one of the journal's most downloaded Research Articles in year of publication (2021)

Prof. Kevin Ryan, FRSE
Editor-in-Chief

Maria Papatriantafyllou, PhD
Managing Editor

Original Article

ctDNA analysis reveals different molecular patterns upon disease progression in patients treated with osimertinib

Atocha Romero[1,2], Roberto Serna-Blasco[2], Cristina Alfaro[1], Estela Sánchez-Herrero[2], Miguel Barquín[2], María Carmen Turpin[3], Sofía Chico[2], Sandra Sanz-Moreno[2], Alejandro Rodrigez-Festa[2], Raquel Laza-Briviesca[2], Alberto Cruz-Bermudez[2], Virginia Calvo[1], Ana Royuela[4], Mariano Provencio[1,2]

[1]Medical Oncology Department, Hospital Universitario Puerta de Hierro-Majadahonda, Madrid, Spain; [2]Molecular Oncology Laboratory, Biomedical Sciences Research Institute Puerta de Hierro-Majadahonda University Hospital, Madrid, Spain; [3]School of Medicine, Universidad Francisco de Vitoria, Madrid, Spain; [4]Biostatistics Unit, Idiphisa, Hospital Universitario Puerta de Hierro-Majadahonda, Madrid, Spain

Contributions: (I) Conception and design: A Romero, M Provencio; (II) Administrative support: A Cruz-Bermudez; (III) Provision of study materials or patients: C Alfaro, A Romero, V Calvo, C Alfaro, MC Turpín, R Laza-Briviesca, M Provencio; (IV) Collection and assembly of data: E Sánchez-Herrero, R Serna-Blasco, S Chico, M Barquín, S Sanz-Moreno, A Rodrigez-Festa; (V) Data analysis and interpretation: A Romero, R Serna-Blasco, E Sánchez-Herrero, M Barquín, S Sanz-Moreno, A Rodrigez-Festa, A Royuela; (VI) Manuscript writing: All authors; (VII) Final approval of manuscript: All authors.

Correspondence to: Atocha Romero; Mariano Provencio. Medical Oncology Department, Hospital Universitario Puerta de Hierro-Majadahonda, C/ Manuel de Falla 1, Madrid 28222, Spain. Email: atocha10@hotmail.com; mariano.provencio@salud.madrid.org.

Background: Several clinical trials have demonstrated the efficacy and safety of osimertinib in advanced non-small-cell lung cancer (NSCLC). However, there is significant unexplained variability in treatment outcome.

Methods: Observational prospective cohort of 22 pre-treated patients with stage IV NSCLC harboring the epidermal growth factor receptor (*EGFR*) p.T790M resistance mutation and who were treated with osimertinib. Three hundred and twenty-six serial plasma samples were collected and analyzed by digital PCR (dPCR) and next-generation sequencing (NGS).

Results: The median progression-free survival (PFS), since the start of osimertinib, was 8.9 [interquartile range (IQR): 4.6–18.0] months. The median treatment durations of sequential gefitinib + osimertinib, afatinib + osimertinib and erlotinib + osimertinib treatments were 30.1, 24.6 and 21.1 months, respectively. The p.T790M mutation was detected in 19 (86%) pre-treatment blood samples. Undetectable levels of the original *EGFR*-sensitizing mutation after 3 months of treatment were associated with superior PFS (HR: 0.2, 95% CI: 0.05–0.7). Likewise, re-emergence of the original *EGFR* mutation, alone or together with the p.T790M mutation was significantly associated with shorter PFS (HR: 8.8, 95% CI: 1.1–70.7 and HR: 5.9, 95% CI: 1.2–27.9, respectively). Blood-based monitoring revealed three molecular patterns upon progression to osimertinib: sensitizing+/T790M+/C797S+, sensitizing+/T790M+/C797S–, and sensitizing+/T790M–/C797S–. Median time to progression in patients showing the triplet pattern (sensitizing+/T790M+/C797S+) was 12.27 months compared with 4.87 months in patients in whom only the original *EGFR* sensitizing was detected, and 2.17 months in patients showing the duplet pattern (sensitizing+/T790M+). Finally, we found that mutations in exon 545 of the *PIK3CA* gene were the most frequent alteration detected upon disease progression in patients without acquired *EGFR*-resistance mutations.

Conclusions: Different molecular patterns identified by plasma genotyping may be of prognostic significance, suggesting that the use of liquid biopsy is a valuable approach for tumor monitoring.

Keywords: Circulating tumor DNA (ctDNA); epidermal growth factor receptor (*EGFR*); non-small-cell lung cancer (NSCLC); osimertinib

Submitted Sep 20, 2019. Accepted for publication Mar 13, 2020.
doi: 10.21037/tlcr.2020.04.01
View this article at: http://dx.doi.org/10.21037/tlcr.2020.04.01

Introduction

Epidermal growth factor receptor (*EGFR*) tyrosine kinase inhibitors (TKIs) have been the standard of care for patients with advanced *EGFR*-mutant non-small-cell lung cancer (NSCLC) (1,2). However, most patients progress within 1 to 2 years (3). The *EGFR* p.T790M mutation is the most common resistance mechanism to first- and second-generation *EGFR* TKIs (4). Osimertinib, a third-generation TKI, has demonstrated its clinical efficacy in NSCLC tumors harboring the p.T790M mutation at disease progression after treatment with first- or second-generation *EGFR* TKIs (5). Moreover, in the randomized phase III FLAURA trial, osimertinib exceeded the standard of care gefitinib or erlotinib in treatment-naive NSCLC patients harboring *EGFR* exon 19 deletions and the p.L858R point mutation, giving rise to a significant improvement in median progression-free survival (PFS) compared with standard TKIs (6).

Nevertheless, acquired *EGFR* mutations conferring osimertinib resistance invariably emerge, such as the p.C797S mutation, which accounts for approximately 20–40% of the cases (7,8). Other resistance mechanisms have also been described (9,10). A better understanding of the diversity of mechanisms by which tumors acquire resistance to third-generation *EGFR* inhibitors is of particular relevance to the better clinical management of patients, making the analysis of circulating tumor DNA (ctDNA) during disease progression an attractive means of deriving new insights into tumor biology at different stages of the disease. In this paper, we describe an observational prospective cohort of 22 unselected patients treated with osimertinib with a median follow-up of 62 months. In addition, ctDNA analysis was performed on 326 samples collected throughout the course of disease.

Methods

Study cohort

The present observational study was conducted on 22 prospectively enrolled patients. Patients were followed from their diagnosis of stage IV disease. The study was approved by the Hospital Puerta de Hierro Ethics Committee and was conducted in accordance with the precepts of the Code of Ethics of The World Medical Association (Declaration of Helsinki). Written informed consent was obtained from all patient. Briefly, eligible patients were males and females with a pathologically confirmed diagnosis of stage IIIB–IV NSCLC tumor harboring an *EGFR* mutation, who were treated with a TKI, and who were candidates for receiving osimertinib. A complete staging workup was performed prior to recruitment. Data on demographic characteristics, clinicopathological features, tumor mutational status, vital status, disease status, drug dose adjustments and discontinuation of medication were collected in the study's electronic database. Computed tomography (CT) measurements and magnetic resonance imaging (MRI) were obtained as clinically indicated. The clinical response was evaluated according to RECIST v1.1 criteria combined with a blinded medical judgment about the benefits of the treatment. Additionally, whole-body 18F-fluoro-2-deoxy-D-glucose positron emission tomography (18FDG-PET) CT scans were performed as clinically indicated.

Laboratory procedures

Three hundred and twenty-six whole blood samples were collected in an 8.5 mL PPT™ tube (Becton Dickinson Franklin Lakes, NJ, USA) containing a gel barrier to separate the plasma after centrifugation. Samples were processed as previously described (11-13). Briefly, after two consecutive centrifugations, cfDNA was isolated from plasma using the Maxwell® RSC (MR) ccfDNA Plasma Kit (Promega Corporation, Madison, WI, USA). The original *EGFR*-sensitizing mutation, and the p.T790M and p.C797S resistant mutations were analyzed by digital PCR (dPCR). Specifically, cfDNA was analyzed using commercially available predesigned TaqMan® Liquid Biopsy dPCR assays as well as custom TaqMan® assays in a QuantStudio® 3D Digital PCR System (Applied Biosystems, South San Francisco, CA, USA). dPCR reactions were carried out in a final volume of 18 µL and using 8.55 µL of cfDNA template. Subsequently, 14.5 µL were loaded into a QuantStudio 3D Digital PCR 20K chip. The cycling conditions were as follows: initial denaturation at 96 ℃ for 10 min, followed by 40 cycles at 56 ℃ for 2 min, and 98 ℃ for 30 s, a step of 72 ℃ for 10 min, and finally samples were maintained at 22 ℃ for at least 30 min. Chip fluorescence was measured twice. Results were analyzed with QuantStudio® 3D AnalysisSuite™ Cloud Software. The automatic call assignments for each data cluster were manually adjusted when needed. The result of the assay is reported as the ratio of mutant DNA molecules relative to the sum of mutant and wild-type (wt) DNA molecules. A negative and a positive control DNA were included in every run.

Libraries were prepared using the Oncomine™ Pan-

Table 1 Clinico-pathological features of the study population

Feature	Grouping	N	%
Age (years)	Median	65.2	–
Sex	Male	9	41
	Female	13	59
Smoking status	Current/ex	9	41
	Never	13	59
ECOG performance status	0	7	32
	1	12	55
	2	3	14
Histology	Adenocarcinoma	22	100
Stage at first diagnosis	III	4	18
	IV	18	82
EGFR mutation	Deletion exon 19	12	55
	L858R	10	45
1st Stage IV treatment	Afatinib	10	45
	Erlotinib	4	18
	Gefitinib	5	23
	Other	3	14

EGFR, epidermal growth factor receptor.

Cancer Cell-Free Assay (Thermo Fisher, Palo Alto, CA, USA) according to manufacturer's instructions. All the purifications were done using AMPure XP magnetic beads (Beckman Coulter, Inc., Brea, CA, USA). Library quantification was performed using the Ion Library TaqMan® Quantitation kit (Thermo Fisher, Palo Alto, CA, USA) in a StepOnePlus™ qPCR machine (Thermo Fisher, Palo Alto, CA, USA). The individual libraries were diluted to a final concentration of 100 pM. The final barcoded libraries were pooled and adjusted to a final concentration of 50 pM. Template preparation and chip loading were carried out on an Ion Chef™ System (Thermo Fisher, Palo Alto, CA, USA). Eight samples were loaded onto an Ion 550™ chip. Finally, Ion 550™ chips were sequenced in an Ion S5™ Sequencer (Thermo Fisher, Palo Alto, CA, USA).

Raw sequencing data were analyzed using Torrent Suite Software (v5.10.0). Sequencing coverage was analyzed using the Coverage Analysis (v.5.10.0.3) plug-in (Thermo Fisher, Palo Alto, CA, USA). Raw reads were aligned to the human reference genome hg19.

Variant calling, annotation and filtering were carried out on the Ion Reporter (v5.10) platform using the Oncomine TaqSeq Pan-Cancer Liquid Biopsy workflow (v5.10). The clinical significance of somatic variants was determined according to the Standards and Guidelines for the Interpretation and Reporting of Sequence Variants in Cancer (14). Mutations with an allele frequency (AF) greater than or equal to 0.1% were considered positive.

Statistical analysis

Discrete variables are presented as frequencies and proportions, and continuous variables as means and standard deviations (SDs), unless otherwise specified. The median follow-up was estimated by the reverse Kaplan-Meier method (15). Overall survival (OS) and PFS were evaluated using the Kaplan-Meier survival function and Cox proportional hazards models. For OS analysis, time from the start of treatment with osimertinib to death or last follow-up was measured. PFS was defined as the time between the start of osimertinib treatment and disease progression, as assessed by RECIST criteria, or all-cause death. Patients who were alive on the last date of assessment and who had not experienced any event were censored at that time. Time to treatment discontinuation (TTD) of targeted therapy was defined as the time between the date when first-line treatment with a TKI began to the date of osimertinib discontinuation or death. Similarly, time to osimertinib discontinuation was also analyzed. Hazard ratios (HRs) were calculated from univariate Cox models. Significance was concluded for P values less than 0.05. Statistical analyses were performed using Stata 15.1 and R 3.1.2 software.

Results

Clinical outcomes

The study cohort included 22 patients. Clinico-pathological characteristics of the study population are presented in *Table 1*. The median age at diagnosis was 65 (range, 41–75) years. We found an unusually high prevalence of tobacco consumption, whereby 41% (9/22) of the patients were smokers (3/22) or former-smokers (6/22), with a mean consumption of 35 (SD: 28.5) pack-years. According to the pathologist's report, 54.5% of the cases (12/22) harbored exon 19 deletions. In one case, a deletion in exon 19 co-occurred with the p.S768I mutation in exon 20. In addition, 45.5% (10/22) harbored the point mutation p.L858R in exon 21. These frequencies

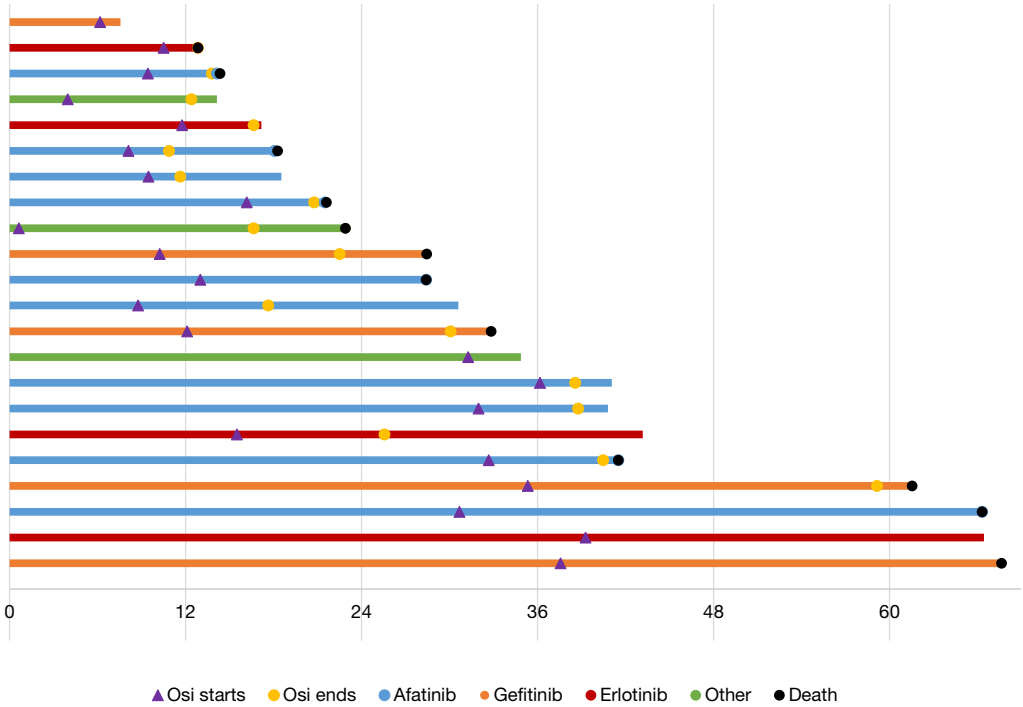

Figure 1 Swimmer chart showing the individual treatment responses since the start of first TKI therapy. Blue, red and orange bars correspond to patients who were treated with afatinib, erlotinib and gefitinib, respectively, in first-line treatment prior to osimertinib treatment. Initiation of osimertinib treatment is denoted by a purple triangle. TKI, tyrosine kinase inhibitor.

are as expected, based on previously published data. No significant differences were observed in OS and PFS with respect to the original *EGFR*-sensitizing mutation. At the start of osimertinib treatment, patients had a median of three metastatic sites, the most frequent locations being the lung (73%), the bone (64%), the pleura (59%), the central nervous system (23%) and the peritoneum (14%). The ECOG Performance Status varied from 0 to 2. Patients with an ECOG Performance Status of 0 exhibited improved OS (P=0.026).

The median follow-up was 62 months. During the study, 12 deaths were recorded and progressive disease (PD) to osimertinib was observed in 16 patients (73%). Interestingly, in one patient, a transformation from NSCLC to small-cell lung cancer (SCLC) was observed upon disease progression. Median PFS, since the start of osimertinib treatment, was 8.9 [interquartile range (IQR): 4.6–18.0] months, whereas median OS, since osimertinib initiation, was 20.7 (IQR: 8.8–27.7) months. Osimertinib was used as a second-line treatment in 11 (50%) patients, while 11 (50%) patients had received two or more lines of treatment prior to that with osimertinib. As expected, the latter group of patients had a significantly poorer outcome in terms of PFS and OS than the former (P<0.004 and 0.020, respectively). Clinical objective response rates (RECIST criteria) were observed in 14 (64%) patients. Oligoprogressive disease (oligo-PD) was noted in 9 (41%) patients, and in 7 of whom (78%) osimertinib was maintained for a median of 3.8 (IQR: 1.2–9.1) months beyond oligo-PD.

Median treatment durations of sequential gefitinib + osimertinib, afatinib + osimertinib and erlotinib + osimertinib were 30.1, 24.6 and 21.1 months, respectively, indicating that time on targeted therapy was longest in patients treated with the combination gefitinib + osimertinib combination. However, no significant differences were observed in OS and PFS according to first TKI treatment (afatinib, gefitinib, erlotinib). *Figure 1* shows the times on targeted therapy and the time under osimertinib treatment for each patient.

Considering toxicity, 12 patients reported adverse events, 82.6% of which were mild (G1). The most frequent toxicities were neutropenia (9%), diarrhea (9%), hypertransaminasemia (9%) and asthenia (9%). Only one G3 event was recorded (asymptomatic hyperamylasemia).

Longitudinal ctDNA monitoring

To analyze the evolution of these tumors throughout the course of treatment, *EGFR* somatic mutations within ctDNA were prospectively collected from 326 samples and analyzed by dPCR. A blood sample obtained before starting osimertinib treatment was available for all patients. At baseline, the p.T790M mutation was detected in 19 (86%) patients, with a median AF of 4.11% (minimum 0.1%; maximum 37.7%). In the other three cases, the p.T790M mutation was detected only in the re-biopsy (N=2) and in the cerebrospinal fluid (N=1). Noteworthy, two of these plasma-negative T790M patients each had metastases exclusively at the brain level. The original *EGFR*-sensitizing mutation was detected in all pre-treatment samples. Neither p.T790M AF nor the original *EGFR*-sensitizing mutation AF at the start of treatment predicted a survival benefit from osimertinib. Nevertheless, ctDNA levels across serial plasma samples were correlated with treatment responses. Specifically, undetectable levels of the original *EGFR*-sensitizing mutation after 3 months of osimertinib treatment were associated with improved PFS (HR: 0.19, 95% CI: 0.05–0.7). Similarly, patients in whom plasma levels of the original *EGFR*-sensitizing decreased after 3 months had a better prognosis in terms of PFS (HR: 0.14, 95% CI: 0.23–0.86). On the other hand, re-emergence of the original *EGFR* mutation, alone or together with the p.T790M mutation, was significantly associated with shorter PFS (HR: 8.8, 95% CI: 1.1–70.7 and HR: 5.9, 95% CI: 1.2–27.9, respectively), indicating that ctDNA quantification is informative in terms of prognosis also in this group of patients.

Molecular patterns upon disease progression

In order to assess the frequency of the p.C797S (c.2389T>A and c.2390G>C) mutation at the time of osimertinib progression in our population, dPCR was performed in all samples collected at osimertinib progression (N=16) (*Figure 2A*). At this time, the p.C797S mutation was found along with the p.T790M mutation as well as the original *EGFR*-sensitizing mutation in 3 (19%) patients (two cases with the p.L858R mutation and one with a deletion in exon 19). Specifically, two cases harbored the c.2390 G>C mutation and one featured the c.2389T>A mutation. Remarkably, dPCR analysis did not identify the p.C797S mutation in any of the previously collected samples, indicating that cells with this mutation were positively selected over the course of therapy. The p.C797S mutation was detected at a lower AF than p.T790M mutation levels, which, at the same time, were lower than the sensitizing mutation AF (*Figure 2B*). Interestingly enough, patients showing this "triplet pattern" (sensitizing+/T790M+/C797S+) tended to exhibit longer PFS and OS than patients who did not (P=0.1, *Figure S1*). In 2 patients (12.5%), plasma levels of the original *EGFR*-sensitizing mutation were again detected at the time of disease progression alongside the p.T790M mutation (*Figure 2C*). This "duplet pattern" (sensitizing+/T790M+) was detected in patients with a high tumor load. Finally, in the other 11 (69%) cases, there was a prominent increase in the original *EGFR*-sensitizing mutation, with null or residual levels of the p.T790M mutation detected (*Figure 2D*), suggesting that osimertinib was able to eliminate the p.T790M-mutated clone in this subset of patients (sensitizing+), even though the tumor was able to become resistant to treatment. The median time to progression in patients showing the triplet pattern (sensitizing+/T790M+/C797S+) was 12.27, 4.87 months in patients in whom only the original *EGFR*-sensitizing mutation was detected, and 2.17 months in patients with the duplet pattern (sensitizing+/T790M+). *Figure S2* shows how early the appearance of the resistance mechanism was detected during ctDNA monitoring.

Next-generation sequencing (NGS) analysis upon osimertinib progression

ctDNA collected at the time of disease progression was available from seven patients for NGS analysis. In this subset of patients, *PIK3CA* mutations were the alterations most frequently detected upon disease progression, being found in four patients. Specifically, we identified the p.E545K mutation in one patient (*Table 2*). The analysis of previous plasma samples by dPCR revealed that this mutation was not present at the start of the treatment (*Figure 3*). Likewise, the mutation p.E545A was detected at disease progression in three patients. Curiously, we detected the p.S464L mutation in the *EGFR* gene in a patient who was treated with cetuximab plus afatinib prior to osimertinib therapy. In addition, the p.A750P mutation in the *EGFR* gene was found in another patient who harbored the deletion in exon 19 p.L747_A750>P. Retrospective analysis of plasma samples revealed that the A750P mutation was also present at the start of osimertinib treatment although at a very low AF. Finally, an *EGFR* copy-number gain was detected by NGS in one case. However, this alteration

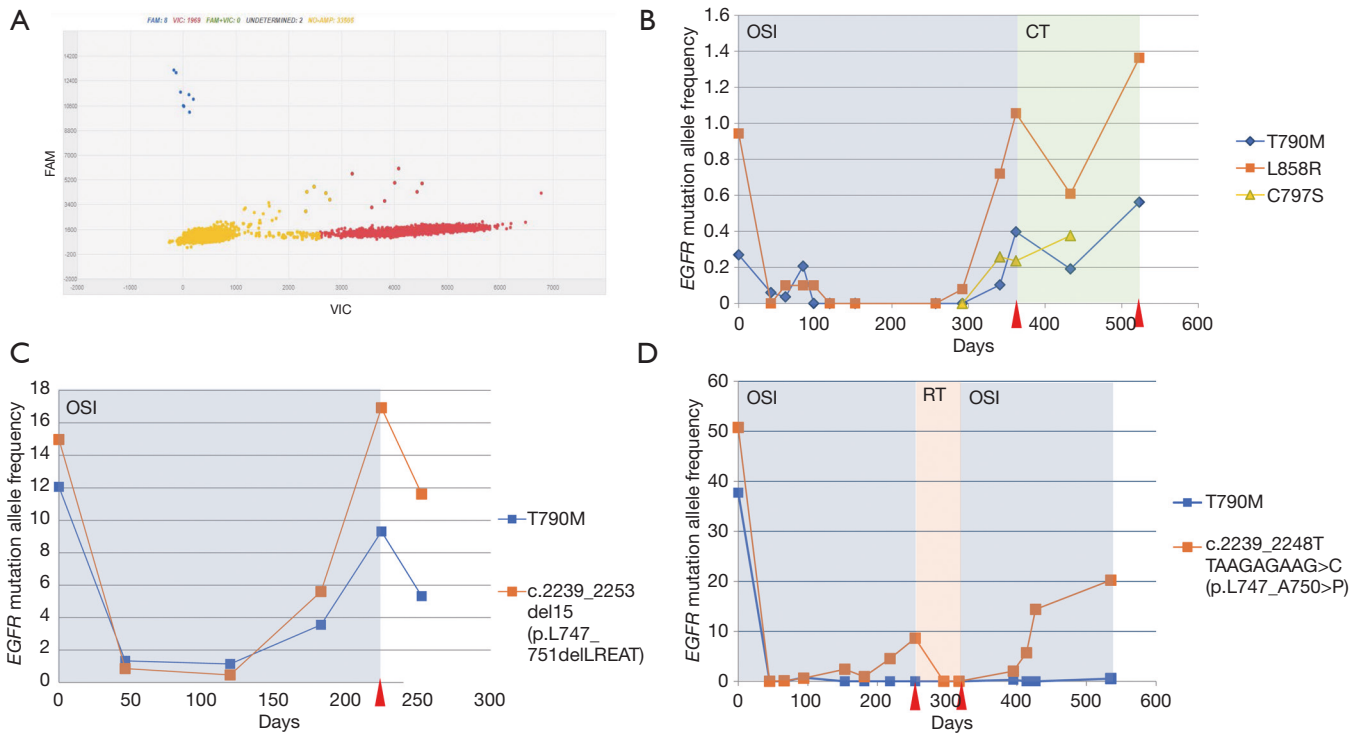

Figure 2 Different molecular patterns upon disease progression. (A) Two-dimensional fluorescence plot. The C797S (c.2390G>C) mutation is labelled with FAM (blue data points), whereas the wild-type is labelled with VIC (red data points); (B,C,D) longitudinal quantitative analyses of *EGFR* mutations in plasma samples. ctDNA levels (AF%) of patients with a triplet, duplet and single pattern (B, C and D respectively) are presented. Therapies are denoted by different-colored shading. PD, ascertained by CT scans at different times, is indicated with a red triangle. *EGFR*, epidermal growth factor receptor; ctDNA, circulating tumor DNA; AF, allele frequency; PD, progressive disease; CT, computed tomography; OSI, osimertinib.

Table 2 Molecular alterations detected in ctDNA upon progression to osimertinib treatment

Number of cases	Gene	Genomic alteration	Method
3	*EGFR*	p.C797S	dPCR
3	*PIK3CA*	p.E545A	NGS, dPCR
1	*PIK3CA*	p.E545K	NGS, dPCR
1	*EGFR*	p.A750P	NGS, dPCR
1	*EGFR*	p.S464L	NGS, dPCR
1	*EGFR*	Amplification	NGS

ctDNA, circulating tumor DNA; *EGFR*, epidermal growth factor receptor; NGS, next-generation sequencing; dPCR, digital PCR.

could not be confirmed by any other alternative technique.

On the other hand, we found that the median TTD was 8.7 (IQR: 2.8–10.1) months in patients whose tumors harbored co-mutations in TP53, compared with 18 (IQR: 7.8–28.2) months in patients whose tumors were negative for *TP53* mutations. However, the difference noted was not statistically significant, given the small sample size.

Discussion

There is growing evidence of the usefulness of liquid biopsy as an effective tool for biomarker testing and treatment

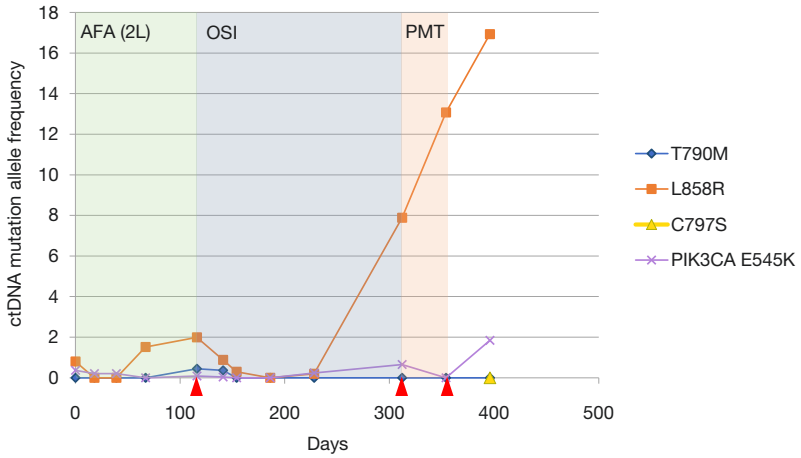

Figure 3 A 67-year-old male with metastatic lung adenocarcinoma treated with afatinib (AFA) as second-line treatment. Subsequently, the patient started treatment with osimertinib (OSI). Further disease progression was observed. The patient then began treatment with pemetrexed, which resulted in a slight decrease in ctDNA levels of the E545K mutation (*PIK3CA*). However, an increase in the mutant AF of the L858R mutation (*EGFR*) was observed during treatment, and PD was diagnosed soon after (denoted by a red triangle). ctDNA, circulating tumor DNA; *EGFR*, epidermal growth factor receptor; AF, allele frequency; PD, progressive disease.

monitoring. In the present study, the p.T790M mutation was detected in the plasma of 19 (86%) patients at baseline, supporting the clinical utility of liquid biopsies for decision-making about treatment. Nevertheless, the possibility of a false-negative result should be ruled out using tumor tissue obtained by biopsy (16). The reported sensitivities of the different assays for *EGFR* mutation detection using cfDNA from advanced NSCLC patients vary as much as from 30% to 100% (17). Although the cohort presented in this study is rather limited our results supports the usefulness of dPCR for plasma p.T790M testing. On the other hand, levels of the original *EGFR*-sensitizing mutation after 3 months of osimertinib treatment were of prognostic significance. Noteworthy, the effect size was substantive (HR: 0.19, 95% CI: 0.05–0.7). Several studies have reported that *EGFR* mutation tracking correlates with treatment outcome (11,12). However, it is important to mention that in the case of NSCLC patients resistant to first/second-generation *EGFR*-TKIs, treated with osimertinib, only the original *EGFR*-sensitizing mutation is informative for monitoring purposes. According to our data, a complete clearance of the p.T790M mutation was found in 69% of the patients with PD, and therefore, the p.T790M mutation is not useful in monitoring the response to osimertinib. In the same way, previous studies have reported similar results (18,19).

According to plasma genotyping, we were able to define three molecular patterns upon disease progression in patients treated with osimertinib, highlighting the importance heterogeneity in advanced disease. These patterns were also reported in a study cohort of 22 patients who became resistant to osimertinib and from whom cfDNA was collected during the phase I AURA study (7). Similarly, other studies have shown that the p.C797S mutation is always detected in conjunction with the p.T790M mutation as well as the original *EGFR*-sensitizing mutation (9,12,20). According to our data, these patterns may determine different prognoses. In our study, patients showing the "triplet pattern" (sensitizing+/T790M+/C797S+) tended to have better PFS and OS (P=0.1), suggesting that tumors that become resistant to osimertinib through p.T790M loss may have a poorer outcome. Likewise, Oxnard *et al.* reported that acquired resistance to osimertinib mediated by loss of the p.T790M mutation was associated with early treatment failure (21). However, despite its pertinence in this context, this observation requires confirmation in larger cohorts. NGS profiling of plasma samples has proved to be a valuable approach for identifying resistance mutations. In our hands, the activating mutations in codon 545 of the *PIK3CA* gene were frequently observed upon osimertinib progression. Likewise, other researchers have proposed that mutations in codon 545 of the *PIK3CA* gene constitute a common resistance mechanism of third-generation TKIs (22). Similarly, Yang *et al.* reported that mutations in *PIK3CA* potentially contribute to osimertinib resistance in patients without secondary *EGFR* mutations (23). In addition, we found the p.S464L mutation in the *EGFR*

gene in the tumor of a patient treated with cetuximab plus afatinib prior to osimertinib therapy. Remarkably, this mutation has been reported in colorectal tumors that are refractory to cetuximab (24).

On the other hand, our results show that the efficacy of osimertinib in real-world practice was similar to that observed in clinical trials, with a favorable adverse effect profile. Similar results have recently been reported in a large sized real-world study (25). Strikingly, time on targeted therapy was longer in patients treated with the gefitinib + osimertinib combination, than those who received one of the other two combinations, although no significant difference in PFS according to first-line TKI was found.

It is important to mention that the small sample size of the present study is an important limitation and therefore although our results are of particular interest they need to be tested in appropriately sized cohorts.

Conclusions

In summary, we report a comprehensive descriptive study of a real-world cohort of patients treated with osimertinib as second-line treatment. Analysis of ctDNA during the course of the disease revealed three molecular patterns that might confer different prognoses. Besides the p.C797S mutation, putative *PIK3CA* mutations might underlie osimertinib resistance in patients without secondary *EGFR* mutations.

Acknowledgments

The authors wish to thank all the patients that participated in this study.

Funding: This study was supported by Carlos III Institute of Health, Spanish Ministry of Science and Innovation, and European Regional Development Fund (grant number: PI16/01818 and PI17/00064). E Sánchez-Herrero is supported by Plan de Empleo Juvenil Comunidad de Madrid (PEJ-2017-AI/SAL-6478), R Serna-Blasco is supported by Plan de Empleo Juvenil Comunidad de Madrid (PEJD-2018-PRE/BMD-8640), S Sanz-Moreno is supported by Plan de Empleo Juvenil Comunidad (PEJ-2017-TL/SAL-7476) and Alejandro Rodriguez-Festa is supported by Plan de Empleo Juvenil Comunidad (PEJ-2017-TL/SAL-7481).

Footnote

Conflicts of Interest: All authors have completed the ICMJE uniform disclosure form (available at http://dx.doi.org/10.21037/ tlcr.2020.04.01). AR reports other from Boehringer, Takeda during the conduct of the study. VC reports other from Roche, BMS, MSD, Pfizer, Lilly, AstraZeneca, Boehringer, Novartis, Takeda during the conduct of the study. MP reports other from Roche, BMS, MSD, Pfizer, Lilly, grants and other from AstraZeneca, Boehringer, other from Novartis, Takeda during the conduct of the study. MP serves as an unpaid editorial board member of *Translational Lung Cancer Research* from Sep 2019 to Sep 2021. The other authors have no conflicts of interest to declare.

Ethical Statement: The authors are accountable for all aspects of the work in ensuring that questions related to the accuracy or integrity of any part of the work are appropriately investigated and resolved. The study was conducted in accordance with the Declaration of Helsinki (as revised in 2013). The study was approved by the Hospital Puerta de Hierro Ethics Committee (approval number: internal code Acta nº02.16.). Written informed consent was obtained from the patients.

References

1. Maemondo M, Inoue A, Kobayashi K, et al. Gefitinib or chemotherapy for non-small-cell lung cancer with mutated EGFR. N Engl J Med 2010;362:2380-8.
2. Rosell R, Carcereny E, Gervais R, et al. Erlotinib versus standard chemotherapy as first-line treatment for European patients with advanced EGFR mutation-positive non-small-cell lung cancer (EURTAC): a multicentre, open-label, randomised phase 3 trial. Lancet Oncol 2012;13:239-46.
3. Hirsch FR, Suda K, Wiens J, et al. New and emerging targeted treatments in advanced non-small-cell lung cancer. Lancet 2016;388:1012-24.
4. Shih JY, Gow CH, Yang PC. EGFR mutation conferring primary resistance to gefitinib in non-small-cell lung

cancer. N Engl J Med 2005;353:207-8.
5. Mok TS, Wu YL, Ahn MJ, et al. Osimertinib or platinum-pemetrexed in EGFR T790M-positive lung cancer. N Engl J Med 2017;376:629-40.
6. Soria JC, Ohe Y, Vansteenkiste J, et al. Osimertinib in untreated EGFR-mutated advanced non-small-cell lung cancer. N Engl J Med 2018;378:113-25.
7. Thress KS, Paweletz CP, Felip E, et al. Acquired EGFR C797S mutation mediates resistance to AZD9291 in non-small cell lung cancer harboring EGFR T790M. Nat Med 2015;21:560-2.
8. Planchard D, Loriot Y, André F, et al. EGFR-independent mechanisms of acquired resistance to AZD9291 in EGFR T790M-positive NSCLC patients. Ann Oncol 2015;26:2073-8.
9. Ou SI, Cui J, Schrock AB, et al. Emergence of novel and dominant acquired EGFR solvent-front mutations at Gly796 (G796S/R) together with C797S/R and L792F/H mutations in one EGFR (L858R/T790M) NSCLC patient who progressed on osimertinib. Lung Cancer 2017;108:228-31.
10. Bersanelli M, Minari R, Bordi P, et al. L718Q mutation as new mechanism of acquired resistance to AZD9291 in EGFR-mutated NSCLC. J Thorac Oncol 2016;11:e121-3.
11. Provencio M, Torrente M, Calvo V, et al. Dynamic circulating tumor DNA quantificaton for the individualization of non-small-cell lung cancer patients treatment. Oncotarget 2017;8:60291-8.
12. Provencio M, Torrente M, Calvo V, et al. Prognostic value of quantitative ctDNA levels in non small cell lung cancer patients. Oncotarget 2017;9:488-94.
13. Provencio M, Pérez-Barrios C, Barquin M, et al. Next-generation sequencing for tumor mutation quantification using liquid biopsies. Clin Chem Lab Med 2020;58:306-13.
14. Li MM, Datto M, Duncavage EJ, et al. Standards and guidelines for the interpretation and reporting of sequence variants in cancer: A Joint Consensus Recommendation of the Association for Molecular Pathology, American Society of Clinical Oncology, and College of American Pathologists. J Mol Diagn 2017;19:4-23.
15. Clark TG, Bradburn MJ, Love SB, et al. Survival analysis part I: basic concepts and first analyses. Br J Cancer 2003;89:232-8.
16. Merker JD, Oxnard GR, Compton C, et al. Circulating tumor DNA analysis in patients with cancer: American Society of Clinical Oncology and College of American Pathologists Joint Review. J Clin Oncol 2018;36:1631-41.
17. Mayo-de-Las-Casas C, Jordana-Ariza N, Garzón-Ibañez M, et al. Large scale, prospective screening of EGFR mutations in the blood of advanced NSCLC patients to guide treatment decisions. Ann Oncol 2017;28:2248-55.
18. Del Re M, Bordi P, Rofi E, et al. The amount of activating EGFR mutations in circulating cell-free DNA is a marker to monitor osimertinib response. Br J Cancer 2018;119:1252-8.
19. Del Re M, Rofi E, Cappelli C, et al. The increase in activating EGFR mutation in plasma is an early biomarker to monitor response to osimertinib: a case report. BMC Cancer 2019;19:410.
20. Yu HA, Tian SK, Drilon AE, et al. Acquired resistance of EGFR-mutant lung cancer to a T790M-specific EGFR inhibitor: emergence of a third mutation (C797S) in the EGFR tyrosine kinase domain. JAMA Oncol 2015;1:982-4.
21. Oxnard GR, Hu Y, Mileham KF, et al. Assessment of resistance mechanisms and clinical implications in patients with EGFR T790M-positive lung cancer and acquired resistance to osimertinib. JAMA Oncol 2018;4:1527-34.
22. Chabon JJ, Simmons AD, Lovejoy AF, et al. Circulating tumour DNA profiling reveals heterogeneity of EGFR inhibitor resistance mechanisms in lung cancer patients. Nat Commun 2016;7:11815.
23. Yang Z, Yang N, Ou Q, et al. Investigating novel resistance mechanisms to third-generation EGFR tyrosine kinase inhibitor osimertinib in non-small cell lung cancer patients. Clin Cancer Res 2018;24:3097-107.
24. Arena S, Bellosillo B, Siravegna G, et al. Emergence of multiple EGFR extracellular mutations during cetuximab treatment in colorectal cancer. Clin Cancer Res 2015;21:2157-66.
25. Marinis F, Wu YL, de Castro G Jr, et al. ASTRIS: a global real-world study of osimertinib in >3000 patients with EGFR T790M positive non-small-cell lung cancer. Future Oncol 2019;15:3003-14.

Cite this article as: Romero A, Serna-Blasco R, Alfaro C, Sánchez-Herrero E, Barquín M, Turpin MC, Chico S, Sanz-Moreno S, Rodrigez-Festa A, Laza-Briviesca R, Cruz-Bermudez A, Calvo V, Royuela A, Provencio M. ctDNA analysis reveals different molecular patterns upon disease progression in patients treated with osimertinib. Transl Lung Cancer Res 2020;9(3):532-540. doi: 10.21037/tlcr.2020.04.01

Cancer Epidemiology 67 (2020) 101737

Contents lists available at ScienceDirect

Cancer Epidemiology

journal homepage: www.elsevier.com/locate/canep

Sex is a strong prognostic factor in stage IV non-small-cell lung cancer patients and should be considered in survival rate estimation

Miguel Barquín[a], Virginia Calvo[a], Francisco García-García[b], Beatriz Nuñez[a], Estela Sánchez-Herrero[a], Roberto Serna-Blasco[a], Milda Auglytė[a], Enric Carcereny[c], Delvys Rodriguez-Abreu[d], Rafael López Castro[e], María Guirado[f], Carlos Camps[g], Joaquín Bosch-Barrera[h], Bartomeu Massuti[i], Ana Laura Ortega[j], Edel del Barco[k], José Luis Gonzalez-Larriba[l], David Aguiar[m], Rosario García-Campelo[n], Manuel Dómine[o], Sara Agraso[p], Mª Angeles Sala[q], Juana Oramas[r], Reyes Bernabé[s], Remei Blanco[t], Consuelo Parejo[u], Alberto Cruz[a], Ernestina Menasalvas[v], Ana Royuela[w], Atocha Romero[a,*], Mariano Provencio[a,*]

[a] Hospital Universitario Puerta de Hierro-Majadahonda, Madrid, Spain
[b] Bioinformatics & Biostatistics Unit, Príncipe Felipe Research Center, Valencia, Spain
[c] Institut Català d'Oncologia Badalona-Hospital Germans Trias i Pujol, B-ARGO GROUP Badalona Applied Research Group in Oncology, Badalona, Spain
[d] Hospital Insular de Gran Canaria, Las Palmas de Gran Canaria, Spain
[e] Hospital Clínico Universitario de Valladolid, Valladolid, Spain
[f] Hospital General Universitario de Elche, Elche, Spain
[g] Hospital General Universitario de Valencia, Valencia, Spain
[h] Catalan Institute of Oncology, Girona, Spain
[i] Hospital Universitario General de Alicante, Alicante, Spain
[j] Complejo Hospitalario de Jaen, Jaen, Spain
[k] Hospital Universitario de Salamanca, Salamanca, Spain
[l] Hospital Clínico San Carlos, Madrid, Spain
[m] Hospital Universitario de Gran Canaria Dr Negrin, Las Palmas, Spain
[n] Hospital Universitario de la Coruña, La Coruña, Spain
[o] Hospital Fundación Jiménez Díaz, Madrid, Spain
[p] Complejo Hospitalario Universitario de Vigo, Vigo, Spain
[q] Hospital de Basurto, Bilbao, Spain
[r] Hospital Universitario de Canarias, Tenerife, Spain
[s] Hospital Universitario Virgen del Rocio, Seville, Spain
[t] Hospital de Terrassa, Barcelona, Spain
[u] TIC Unit, Medical Oncology Department, Hospital Universitario Puerta de Hierro-Majadahonda, Madrid, Spain
[v] Center for Biomedical Technology, Universidad Politécnica de Madrid, Madrid 28000, Spain
[w] Biostatistics Unit, CIBERESP, Hospital Universitario Puerta de Hierro-Majadahonda, Madrid, Spain

ARTICLE INFO

Keywords:
Non-small cell lung cancer
EGFR
Gender
Female
Sex

ABSTRACT

Background: Biological differences between the sexes have a major impact on disease and treatment outcome. In this paper, we evaluate the prognostic value of sex in stage IV non-small-cell lung cancer (NSCLC) in the context of routine clinical data, and compare this information with other external datasets.

Methods: Clinical data from stage IV NSCLC patients from Hospital Puerta de Hierro (HPH) were retrieved from electronic health records using big data analytics (N = 397). In addition, data from the Spanish Lung Cancer Group (GECP) Tumor Registry (N = 1382) and from a published study available from the cBioPortal (MSK) (N = 601) were analyzed. Survival curves were estimated using the Kaplan–Meier method. A Cox proportional hazards regression model was used to assess the prognostic value of sex. A meta-analysis to compare the outcome for males and females in terms of overall survival (OS) and progression free survival (PFS) was performed.

Results: The median OS time was 12 months for males and 19 months for females (overall HR = 0.77; 95% CI: 0.68–0.87; P < 0.001). Similarly, females with stage IV NSCLC harboring an *EGFR*-sensitizing mutation lived

* Corresponding authors at: Medical Oncology Department, Puerta de Hierro Hospital, C/ Manuel de Falla 1, Majadahonda, Madrid 28222, Spain.
E-mail addresses: atocha10@hotmail.com (A. Romero), mariano.provencio@salud.madrid.org (M. Provencio).

https://doi.org/10.1016/j.canep.2020.101737
Received 3 October 2019; Received in revised form 30 March 2020; Accepted 20 April 2020

significantly longer than males (median OS: males, 19 months; females, 32 months) with a lower risk of death compared with males (overall HR = 0.75; 95% CI: 0.67–0.84). In addition, female patients benefited more from *EGFR* inhibitors in terms of PFS and OS (overall HR = 0.45; 95% CI: 0.32–0.64, and HR = 0.62; 95% CI: 0.48–0.80, respectively). Median PFS was 21 months in females and 12 months in males (P < 0.001).

Conclusions: Using routine clinical data we confirmed the previous finding that among stage IV NSCLC patients, females had a significantly better prognosis than males. The effect size of the sex was notable, highlighting the fact that survival rates are usually estimated and patients are generally managed without considering the sexes separately, which may lead to suboptimal results.

1. Introduction

There is increasing evidence that sex has a major impact in health and disease [1–3]. According to recent The National Institutes of Health policy, the inclusion of sex as a biological variable is mandatory in vertebrate and human studies [4]. Paradoxically, although it is obvious that males and females are biologically different, drug prescriptions, prognostic estimates and overall patient management are seldom adjusted for sex. In the context considered here, lung cancer is no exception, even though its clinical presentation and outcomes differ between the sexes [5–8]. Previous studies have demonstrated that among non-small-cell lung cancer (NSCLC) patients, females have a lower risk of progression and death than males [6,9–12]. NSCLC comprises a wide range of diseases and the impact of the sex of patients on their survival needs to be addressed in each specific cancer type. *EGFR*-positive NSCLC can be considered as a different clinical entity. This tumor is more frequent in non-smokers and is associated with adenocarcinoma histology. Moreover, patients with this disease are candidates for receiving tyrosine kinase inhibitor with a prognosis significantly better compared with *EGFR* negative NSCLC population.

Evidence from the analysis of routine clinical practice can be a valuable source for evaluating treatment benefit besides of randomized clinical trials in which only a small proportion of patients are enrolled, and those who are do not necessarily reflect the general oncological population, which is typically older, with more comorbidities and lower performance status. Big data analytics allow data to be retrieved, homogenized and analyzed, although studies addressing the impact of sex on survival using these approaches are particularly scarce. As there are significant differences in drug pharmacokinetics according to sex, it is worthwhile exploring the prognostic value of sex in homogenous subsets of patients that are likely to be treated in a similar manner. In this paper, we explore sex differences in stage IV NSCLC patients using data retrieved by big data analytics from electronic health records (EHR). In addition we use data of the Spanish Lung Cancer Group (GECP) Tumor Registry and data from a study published on the cBioPortal [13] and particularly we focus on the subset of patients with an *EGFR*-activating mutation

2. Material and methods

2.1. Data sources

The prognostic value of sex was evaluated in three independent datasets, which are described below.

First, data from EHR of 397 patients diagnosed with stage IV lung cancer, between 2012 and 2019, and treated at the Medical Oncology Department of the Puerta de Hierro University Hospital, were retrieved using big data analytics (HPH dataset). Before their inclusion in the study, each participant signed the appropriate informed consent form. The study protocol was approved by the Hospital Puerta de Hierro Ethics Committee (internal code PI55/17), and was conducted in accordance with the Declaration of Helsinki. Big data analytics were used to retrieve, curate and homogenize data. Briefly, the system ingests the text of clinical records and performs enriched Natural Language Processing (NLP) to structure the information from a syntactical point of view and to label all the medical concepts with annotators developed for the purpose (diagnosis, TNM, dates, *etc.*). Once the data have been structured, another process is applied to integrate and validate the information for every patient using the concepts annotated in the various documents that medical doctors generate for a particular patient. This results in the natural history of the patient being available, along with all the structured information, making it possible to interrogate the data.

Second, the scientific literature was reviewed to identify relevant studies for which clinical data were available for re-analysis. To this end GEO, PubMed and the cBioPortal platform were used. The searched terms were “NSCLC”, “lung adenocarcinoma” and “lung cancer survival” (Search performed on August 2018). Supplemental Fig. 1 shows the PRISMA flow diagram. The initial search returned 5131 unique citations. Titles and abstracts were reviewed by MB and FGG and those studies considered out of scope were excluded. Case reports, clinical trials and other studies not representing routine clinical data studies were also excluded. Full papers were obtained from 43 selected studies. Next, eligible papers were selected according to the following criteria: studies that included stage IV NSCLC patients and with the following information available: sex, age at diagnosis, histology, *EGFR* status and overall survival (OS). Only one study was found to fulfil these criteria. This involved the Memorial Sloan Kettering (MSK) dataset [13], which comprises clinical data collected from 601 patients tested by MSK-IMPACT. It is available in digital form from the cBioPortal for Cancer Genomics [13–15].

Finally, data from 1382 stage IV NSCLC patients diagnosed between 2016 and 2018 were identified through the Spanish Lung Cancer Group (GECP) tumor registry (GECP dataset), which was approved by the Hospital Puerta de Hierro Ethics Committee (Internal Code: PI148/15) and Agencia Española de Medicamentos y Productos Sanitarios. The GECP registry prospectively collects data from 52 hospitals across Spain. The registry actively conducts an annual follow-up of each patient. It contacts the medical oncologist and updates information on the most recent contact date, vital status, and recurrence status. The age, sex, *EGFR* status, treatment, smoking status and follow-up information were obtained from all patients.

Information regarding stage was collected according to the TNM staging system (version 8th [16]) and tumor histology was recorded according to the World Health Organization classification

2.2. Statistical analysis

Discrete variables are summarized as absolute frequencies and proportions, and continuous variables as means and standard deviations (SD), unless otherwise specified. The median follow-up time was estimated by the reverse Kaplan–Meier method [17]. Student’s *t*-test was used to compare mean age at diagnosis of the two sexes. In order to evaluate the comparability of the three cohorts, differences in sex and other clinicopathological variables across cohorts were assessed by the chi-square and Kruskal–Wallis tests, respectively.

OS was defined as the time from diagnosis of stage IV NSCLC to death from any cause, or the censored date of the last follow-up for patients who were alive when the data were extracted. For progression-free survival (PFS), the events considered were disease progression

assessed by RECIST criteria, death from any cause, or the censored date of the last assessment, whichever was earliest. PFS for the subset of *EGFR*-positive patients was considered as the time between the start of tyrosine kinase inhibitor (TKI) treatment and disease progression, as assessed by RECIST criteria, death from any cause, or the censored date of the last follow-up, whichever was earliest. Survival was evaluated by the Kaplan–Meier method and with Cox proportional hazards models assuming an exponential distribution of the survival data. The log-rank test was used to assess statistical differences between Kaplan–Meier survival curves. The proportional hazard assumption in cox model was checked based scaled Schoenfeld residuals using Stata software. Hazard ratios (HRs) were estimated from the Cox model using a multivariable approach adjusted for potential confounding factors. In the adjusted model, sex, age and *EGFR* status were included as covariates. The Eastern Cooperative Oncology Group (ECOG) performance status was also included in the analysis of the HPH and GECP datasets. HRs and two-sided 95% confidence intervals (CIs) for sex, for each dataset, were estimated using random effects analyses of forest plots. Heterogeneity was assessed with Cochrane's χ^2 test, values of $P < 0.10$ being taken as evidence of significant heterogeneity. The degree of heterogeneity was measured by the I-square index, significant values being taken to be those with a corresponding value of $P < 0.05$. Statistical analyses were performed using Stata 14.1 and in the R 3.1.2 environment.

3. Results

3.1. Clinicopathological features

We report here on data from 2380 NSCLC patients, of whom 1415 (59.45%) were male and 965 (40.55%) were female. The median age of diagnosis was 63 years (SD = 10.97 years). Females were diagnosed with NSCLC at a significantly younger age than males (61.4 *vs*. 63.5 years; P = 0.0054). In terms of histology, adenocarcinoma was the most frequently diagnosed type of tumor (78.99% of cases). The median follow-up was 46, 31 and 16 months for the HPH, GECP and MSK datasets, respectively. 22.94% (546) of the patients were diagnosed with an *EGFR*-positive tumor. Regarding the type of *EGFR*-sensitizing mutation, 43.95% (240) of tumors harbored a mutation in exon 19, while 29.12% (159) of them were located in exon 21. Mutations in exons 18 and 20 were detected in 11.53% (63) of the tumors. As expected, tumors harboring a deletion in exon 19 had better OS (HR: 0.46; 95% CI: 0.37–0.56). There were no significant differences in the distributions of mutations between the sexes.

Demographic and pathological characteristics of study participants, and distributions of characteristics by each dataset are presented inTable 1 .

3.2. Survival analysis

The median OS time was 12 months for males and 19 months for females (P < 0.001) (Supplemental Table 1). In univariate analyses, sex, age, mutation status, and ECOG performance status proved to be significant prognostic factors (P < 0.05 in all cases). The effect of sex was still significant after adjustment by Cox regression for age, ECOG performance status and *EGFR* status in the HPH and GECP datasets. The adjusted HRs for sex were 0.69 (95% CI: 0.54–0.88, P = 0.003), 0.84 (95% CI: 0.66–1.07, P = 0.158) and 0.73 (95% CI: 0.63–0.85, P < 0.001) for the HPH, MSK and GECP data sets, respectively, in favor

Table 1
Distribution of clinicopathological characteristics of the study population according to each data set.

		HPH		MSK		GECP		p-Value	TOTAL	
Total		397		601		1382			2380	
Median age at diagnosis		63	± 10.79	64	± 11.82	63	± 10.64	NS	63	± 10.97
		N	%	N	%	N	%		N	%
Sex	Women	140	35.26 (30.5–40.1)	354	58.9 (54.8–62.8)	471	34.09 (31.5–36.6)		965	40.55
	Men	257	64.74 (59.8–69.4)	247	41.1 (37.1–57.1)	911	65.91 (63.3–68.4)	< 0.05	1415	59.45
Stage	IV	397	100	601	100	1382	100		2380	100
EGFR status	Wild type	326	82.12 (77.9–85.7)	427	71.04(67.2–74.6)	1081	78.22 (75.9–80.3)		1834	77.05
	Mutated	71	17.88(14.2–22)	174	28.95 (25.3–32.7)	301	21.78 (19.6–24)	< 0.05	546	22.95
EGFR mutation	exon_18	5	7.04	2	1.15	11	3.65		18	3.29
	exon_19	35	49.30	45	25.86	160	53.16		240	43.95
	exon_20	5	7.04	40	22.99	0	0		45	8.26
	exon_21	25	35.21	49	28.16	85	28.24		159	29.12
	Unknown mutation	1	1.41	38	21.84	45	14.95	< 0.05	84	15.38
ECOG	0	135	34.01	NA	NA	353	25.54		NA	NA
	1	175	44.08	NA	NA	783	56.65		NA	NA
	2	68	17.13	NA	NA	189	13.67		NA	NA
	3	17	4.28	NA	NA	45	3.26		NA	NA
	4	2	0.50	NA	NA	6	0.44		NA	NA
	5	0	0	NA	NA	6	0.44		NA	NA
Histology	Adenocarcinoma	330	83.12	601	100	949	68.67		1880	78.99
	Adenosquamous	67	16.88	0	0	315	22.79		382	16.06
	Others	0	0	0	0	118	8.54	< 0.05	118	4.95
Smoking status	Never	75	18.9	207	34.45	277	20.04		559	23.48
	Smoker	322	81.10	394	65.55	1088	78.72		1804	75.79
	Unknown	0	0	0	0	17	1.24	< 0.05	17	0.73
Treatment	Gefitinib	20	5.04	NA	NA	93	6.75		NA	NA
	Erlotinib	27	6.8	NA	NA	54	3.9		NA	NA
	Afatinib	24	6.04	NA	NA	72	5.2		NA	NA
	Platinum-based chemotherapy	244	61.47	NA	NA	NA	NA		NA	NA
	Immunotherapy	12	3.02	NA	NA	NA	NA		NA	NA
	Others	70	17.63	NA	NA	NA	NA		NA	NA

Abbreviations: N: Number of patients. %: percentage of patients; MSK: Memorial Sloan Kettering; HPH: Hospital Puerta de Hierro; GECP Spanish Lung Cancer Group.

of female patients.

Females with stage IV NSCLC who harbored an *EGFR*-sensitizing mutation lived longer than their male counterparts, with a median OS of 32 and 19 months, respectively (Supplemental Table 1). Univariate analyses showed that patients with specific characteristics (female, ECOG performance status of 0–1) had a significantly better OS than those with the opposite characteristics ($P < 0.05$ in all cases). The Kaplan–Meier curves for each dataset, presented in Fig. 1, illustrate a tendency of longer OS for females compared with males for all the datasets. The sex-adjusted HRs were 0.67 (95% CI: 0.33–1.35, $P = 0.261$), 0.61 (95% CI: 0.36–1.03, $P = 0.06$) and 0.61 (95% CI: 0.44–0.84, $P = 0.003$) for the HPH, MSK and GECP datasets, respectively.

Differences in PFS were evaluated for the subset of patients who harbored an *EGFR*-sensitizing mutation and who were treated with a TKI using data from the HPH and GECP datasets (N = 220). There were no significant differences in survival with respect to treatment in the GECP and HPH cohorts. Median PFS was significantly longer in females than males (21 *vs.* 12 months; $P < 0.001$). Specifically, sex-adjusted HRs were 0.48 (95% CI: 0.32–0.74, $P < 0.001$) for the GECP cohort and 0.38 (95% CI: 0.20–0.71, $P = 0.003$) for the HPH patients.

3.3. Meta-analysis

No significant heterogeneity was observed between the three datasets. Forest plots of meta-analysis for the three datasets separately and combined are displayed in Fig. 2. An overall HR of 0.75 (95%CI: 0.67–0.84) for OS was obtained for stage IV patients, indicating that females with metastatic NSCLC had a 33% increase in OS time compared to male. When restricting the analysis to patients harboring an *EGFR* mutation, a significantly lower risk of lung cancer death in females was observed, with an overall HR of 0.62 (95%CI: 0.48–0.80), resulting in a 61% increase in OS time in female sex compared with males, assuming a constant risk over time. Finally, the PFS of females was 2.2 times that of males, with an overall HR of 0.45 (95% CI: 0.32–0.64), suggesting that, at worst, females sex have a 56% increase in PFS time compared to male.

4. Discussion

In this paper we show that females diagnosed with stage IV NSCLC tend to live longer than males. Noteworthy, female sex with stage IV NSCLC had a 33% increase in OS time compared to male. This difference rises to 61% in the subgroup of *EGFR*-positive NSCLC patients.

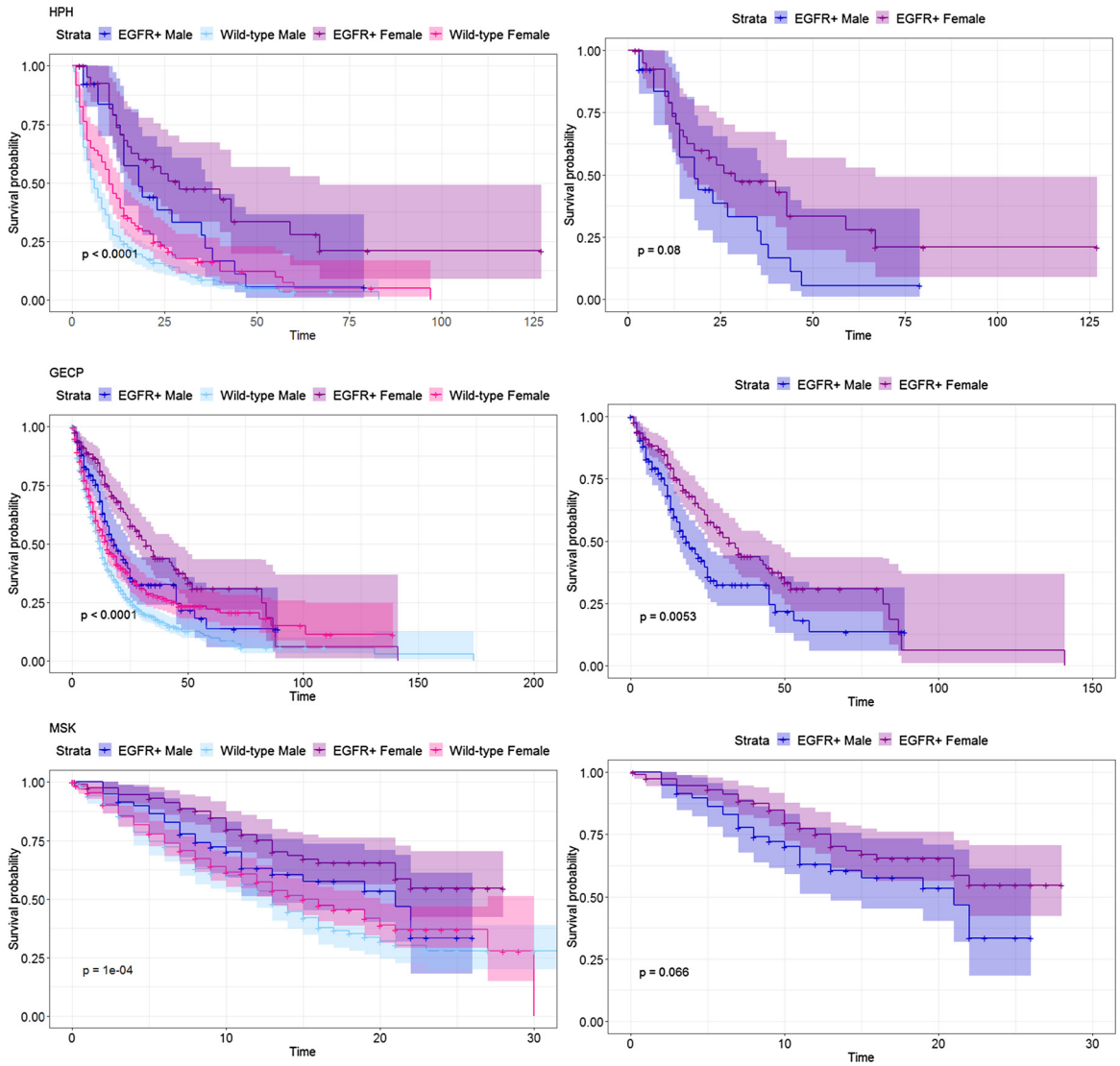

Fig. 1. Overall survival curves by sex and *EGFR* status for HPH, GECP and MSK datasets. Values of P are those associated with the log-rank test. Abbreviations: MSK, Memorial Sloan Kettering; HPH, Hospital Puerta de Hierro; GECP, Spanish Lung Cancer Group.

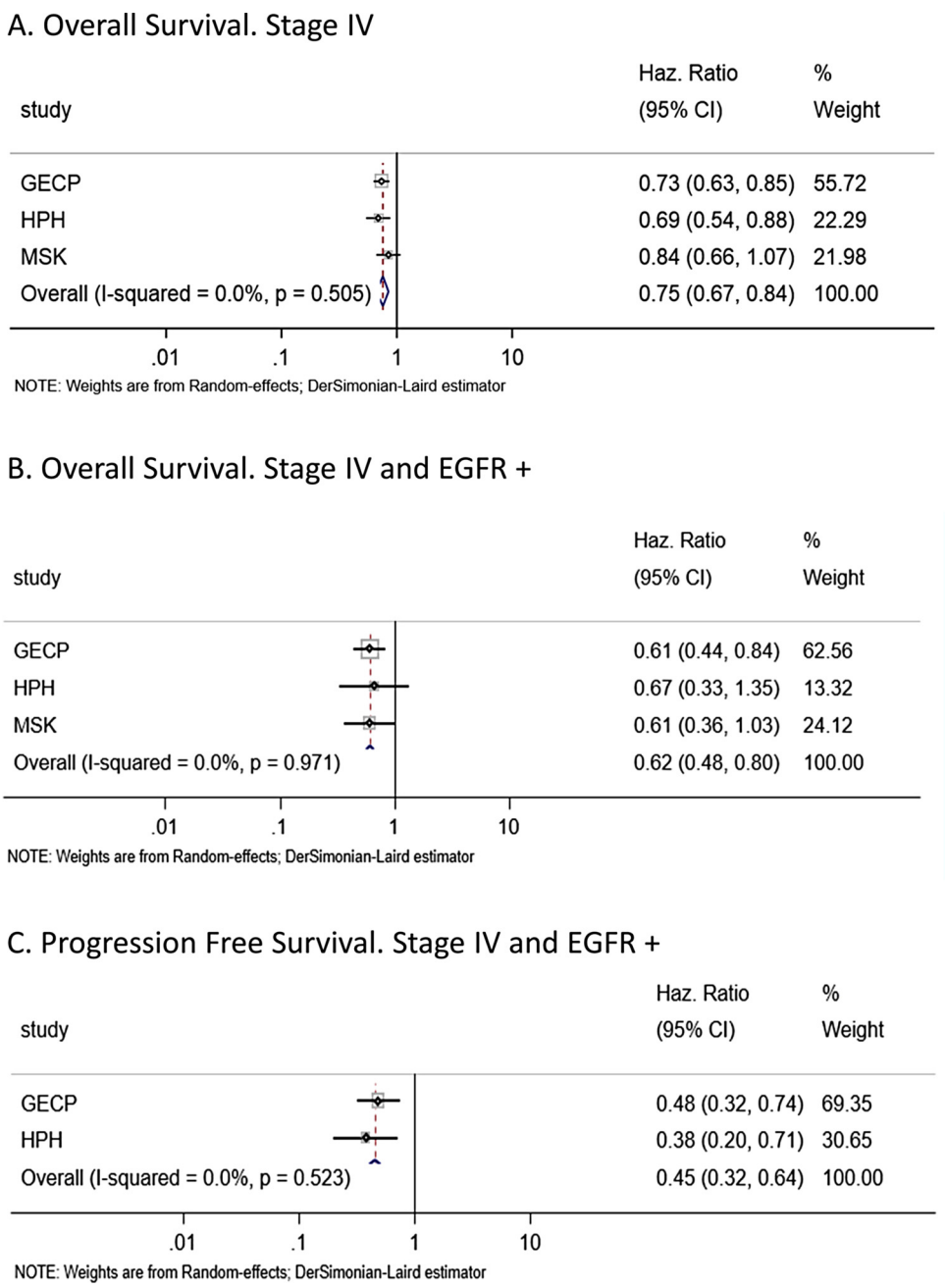

Fig. 2. Survival analysis by sex. (A) OS analysis of stage IV patients. Pooled analysis shows significant OS benefits to women. (B) OS analysis of stage IV patients with tumors harboring an *EGFR* mutation. Pooled analysis shows a significant OS benefit to women. (C) PFS analysis in stage IV patients with tumors harboring an *EGFR* mutation. Pooled analysis shows a significant PFS benefit to women. Abbreviations: Haz. Ratio, hazard ratio; CI, confidence interval; MSK, Memorial Sloan Kettering; HPH, Hospital Puerta de Hierro; GECP, Spanish Lung Cancer Group.

Likewise, PFS was significantly longer in females with an *EGFR*-positive NSCLC, whereby they had 50% the risk of progression of males. Previous studies have reported a significant improved survival in female NSCLC patients relative to males [5,6,9,12]. Data from clinical trials showed that treatment with *EGFR* tyrosine kinase inhibitors was more effective in females than males [18]. Similar results were noted in a meta-analysis conducted by Pinto et al. [19], in which female and male OS and PFS in phase III randomized clinical trials were compared. However, unlike previous reports, in this study, data were retrieved from EHR, using big data approaches. Our results, confirmed the previous findings of clinical trials, indicating that females diagnosed with metastatic NSCLC have significantly better survival than males with the same condition. Data from daily clinical routine has been shown to be useful for extending the information provided by traditional clinical trials as they recapitulate outcomes from patients who are not usually enrolled in such studies [20]. Moreover, routine clinical data were compared with independent data sets. Importantly, no significant heterogeneity was found between the three datasets. According to the meta-analysis the effect size of sex was notable (HR = 0.62 for OS and HR = 0.45 for PFS for *EGFR*-positive cases), highlighting the importance of sex as a prognostic factor, and suggesting the need to estimate survival rates separately for each sex, rather than combined, as is currently usually done. The effect size of sex prompts us to reconsider whether overall patient management should take sex differences into account (*e.g.*, should the scheduling of follow-up consultations differ for women and men?). There is growing evidence indicating that sex stratification has not been sufficiently studied in medicine, and that efforts need to be made to incorporate sex as a factor in healthcare

planning and patient management [21,22].

It is important to point out the similarities we have found between the data retrieved from EHR and those of a recent study by Westergaard et al. of the complete Danish population [23]. According to the latter study, age at first diagnosis was typically younger in males than females, with some exceptions, including cancer diagnosis, in which the opposite trend prevailed. Data retrieved from EHR were therefore concordant with other larger studies and with other independent databases (GECP and MSK), suggesting that the deep learning approaches employed in this study produced reliable data.

It is not clear whether the sex differences in OS and PFS arise from differences in biology, behavior and lifestyle, or from sociological factors, including gender socialization. On one hand, women are known to be more likely to adopt beneficial health behaviors and personal health practices that promote longevity [24]. For example, the proportion of smokers among men is known to be higher than among women [25], although the difference has been narrowing in recent times. On the other hand, there is increasing evidence that biological differences between the sexes have been underestimated and genetic, metabolic, and hormonal factors might be responsible for the survival advantage of females [26–29]. In this way, it has been reported that postmenopausal women with NSCLC have a longer OS than premenopausal women [10]. However, the proportion of NSCLC premenopausal women is low [30] which makes difficult to evaluate whether hormones are responsible for this effect on lung cancer survival and larger cohorts of this specific group of patients are needed to confirm this observation.

Likewise, the molecular mechanisms underlying the clear differences in survival outcomes between the sexes among targeted therapies such as TKI remain unknown, stressing the need to conduct research studies addressing this issue.

5. Conclusions

Precision medicine and biomarker-defined care has attracted the attention of medical oncologists. However, classical prognostic factors such as sex should not be left behind. According to our findings, sex is a strong prognostic factor of OS and PFS in stage IV NSCLC patients. The omission of sex as a factor in developing clinical management of patients is likely to be to the detriment of more efficient health care. In other words, personalized medicine cannot be performed without taking sex into consideration as a fundamental prognostic factor.

Credit author statement

AR: Conceptualization, Supervision, Writing – Review & Editing, Project administration; FG: Methodology, Formal analysis; AR: Formal analysis; MB: Formal analysis, Visualization, Investigation; EM: Software; CP: Software; EC: Resources; DR: Resources; RLC: Resources; MG: Resources; CC: Resources; JB: Resources; BM: Resources; ALO: Resources; EDB: Resources; JLGL: Resources; DA: Resources; RGC: Resources; MD: Resources; SA: Resources; MAS: Resources; JO: Resources; RB: Resources; RB : Resources; VC: Validation; BN: Validation; ESH: Validation; RSB: Validation; MA : Validation; AC: Validation; MP: Supervision, Funding acquisition.

Funding

This study was supported by European Research Council (H2020-SC1-PM-18-2016, Project ID: 727658 and H2020-SC1-DTH-01-2019 Project ID: 875160). M Barquin is supported by an i-PFIS predoctoral fellowship (grant number IFI18/00051) from ISCIII. E Sanchez-Herrero is supported by the Plan de Empleo Juvenil Comunidad de Madrid (PEJ-2017-AI/SAL-6478). R Serna-Blasco is supported by the Plan de Empleo Juvenil Comunidad de Madrid (PEJD-2018-PRE/BMD-8640).

Authorship contribution statement

AR conceived the study. FG contributed to the analysis design. FG, AR and MB contributed to statistical analysis. EM and CP retrieved the clinical data from electronic records. EC, DR, RLC, MG, CC, JB, BM, ALO, EDB, JLGL, DA, RGC, MD, SA, MAS, JO, RB, RB provided and validated the clinical data from GECP data set. VC, BN, ESH, RSB, MA and AC validated the clinical data from HPH data set. AR and MP supervised every aspect of the study. AR wrote the manuscript.

Declaration of Competing Interest

The authors declare no competing interests.

Appendix A. Supplementary data

Supplementary material related to this article can be found, in the online version, at doi:https://doi.org/10.1016/j.canep.2020.101737.

References

[1] A.J. McGregor, W. Frank Peacock, A. Marie Chang, B. Safdar, D. Diercks, Sex- and gender-specific research priorities for the emergency management of heart failure and acute arrhythmia: proceedings from the 2014 Academic Emergency Medicine Consensus Conference Cardiovascular Research Workgroup, Acad. Emerg. Med. 21 (2014) 1361–1369, https://doi.org/10.1111/acem.12526.

[2] A.J. McGregor, The effects of sex and gender on pharmacologic toxicity: implications for clinical therapy, Clin. Ther. 39 (2017) 8–9, https://doi.org/10.1016/j.clinthera.2016.12.007.

[3] C.J. Peer, J.D. Strope, S. Beedie, A.M. Ley, A. Holly, K. Calis, R. Farkas, J. Parepally, A. Men, E.O. Fadiran, P. Scott, M. Jenkins, W.H. Theodore, T.M. Sissung, Alcohol and aldehyde dehydrogenases contribute to sex-related differences in clearance of zolpidem in rats, Front. Pharmacol. 7 (2016) 260, https://doi.org/10.3389/fphar.2016.00260.

[4] NOT-OD-15-102: Consideration of Sex as a Biological Variable in NIH-funded Research, (2015) Retrieved from https://grants.nih.gov/grants/guide/notice-files/not-od-15-102.html.

[5] M.K. Ferguson, J. Wang, P.C. Hoffman, D.J. Haraf, J. Olak, G.A. Masters, E.E. Vokes, Sex-associated differences in survival of patients undergoing resection for lung cancer, Ann. Thorac. Surg. 69 (2000) 245–249 discussion 249-250.

[6] E. Radzikowska, P. Głaz, K. Roszkowski, Lung cancer in women: age, smoking, histology, performance status, stage, initial treatment and survival. Population-based study of 20 561 cases, Ann. Oncol. Off. J. Eur. Soc. Med. Oncol. 13 (2002) 1087–1093.

[7] H. Minami, M. Yoshimura, Y. Miyamoto, H. Matsuoka, N. Tsubota, Lung cancer in women: sex-associated differences in survival of patients undergoing resection for lung cancer, Chest 118 (2000) 1603–1609.

[8] K.A. Moore, C.M. Mery, M.T. Jaklitsch, A.P. Estocin, R. Bueno, S.J. Swanson, D.J. Sugarbaker, J.M. Lukanich, Menopausal effects on presentation, treatment, and survival of women with non-small cell lung cancer, Ann. Thorac. Surg. 76 (2003) 1789–1795.

[9] L.-H. Hsu, N.-M. Chu, C.-C. Liu, S.Y.C. Tsai, D.-L. You, J.-S. Ko, M.-C. Lu, A.-C. Feng, Sex-associated differences in non-small cell lung cancer in the new era: is gender an independent prognostic factor? Lung Cancer 66 (2009) 262–267, https://doi.org/10.1016/j.lungcan.2009.01.020.

[10] V. Rodríguez-Lara, L.A. Ramírez-Tirado, F. Barrón, Z.L. Zatarain-Barrón, D. Flores-Estrada, O. Arrieta, Characteristics of non-small cell lung cancer: differences by sex and hormonal status in a Mexican population, Salud Publica Mex. 61 (2019) 265–275, https://doi.org/10.21149/10094.

[11] M. de Perrot, M. Licker, C. Bouchardy, M. Usel, J. Robert, A. Spiliopoulos, Sex differences in presentation, management, and prognosis of patients with non-small cell lung carcinoma, J. Thorac. Cardiovasc. Surg. 119 (2000) 21–26.

[12] A.L. Visbal, B.A. Williams, F.C. Nichols, R.S. Marks, J.R. Jett, M.-C. Aubry, E.S. Edell, J.A. Wampfler, J.R. Molina, P. Yang, Gender differences in non–small-cell lung cancer survival: an analysis of 4,618 patients diagnosed between 1997 and 2002, Ann. Thorac. Surg. 78 (2004) 209–215, https://doi.org/10.1016/j.athoracsur.2003.11.021.

[13] E.J. Jordan, H.R. Kim, M.E. Arcila, D. Barron, D. Chakravarty, J. Gao, M.T. Chang, A. Ni, R. Kundra, P. Jonsson, G. Jayakumaran, S.P. Gao, H.C. Johnsen, A.J. Hanrahan, A. Zehir, N. Rekhtman, M.S. Ginsberg, B.T. Li, H.A. Yu, P.K. Paik, A. Drilon, M.D. Hellmann, D.N. Reales, R. Benayed, V.W. Rusch, M.G. Kris, J.E. Chaft, J. Baselga, B.S. Taylor, N. Schultz, C.M. Rudin, D.M. Hyman, M.F. Berger, D.B. Solit, M. Ladanyi, G.J. Riely, Prospective comprehensive molecular characterization of lung adenocarcinomas for efficient patient matching to approved and emerging therapies, Cancer Discov. 7 (2017) 596–609, https://doi.org/10.1158/2159-8290.CD-16-1337.

[14] E. Cerami, J. Gao, U. Dogrusoz, B.E. Gross, S.O. Sumer, B.A. Aksoy, A. Jacobsen, C.J. Byrne, M.L. Heuer, E. Larsson, Y. Antipin, B. Reva, A.P. Goldberg, C. Sander, N. Schultz, The cBio Cancer genomics portal: an open platform for exploring

multidimensional Cancer genomics data: figure 1, Cancer Discov. 2 (2012) 401–404, https://doi.org/10.1158/2159-8290.CD-12-0095.
[15] J. Gao, B.A. Aksoy, U. Dogrusoz, G. Dresdner, B. Gross, S.O. Sumer, Y. Sun, A. Jacobsen, R. Sinha, E. Larsson, E. Cerami, C. Sander, N. Schultz, Integrative analysis of complex Cancer genomics and clinical profiles using the cBioPortal, Sci. Signal. 6 (2013), https://doi.org/10.1126/scisignal.2004088 pl1–pl1.
[16] F.C. Detterbeck, D.J. Boffa, A.W. Kim, L.T. Tanoue, The eighth edition lung cancer stage classification, Chest 151 (2017) 193–203, https://doi.org/10.1016/j.chest.2016.10.010.
[17] T.G. Clark, M.J. Bradburn, S.B. Love, D.G. Altman, Survival analysis part I: basic concepts and first analyses, Br. J. Cancer 89 (2003) 232–238, https://doi.org/10.1038/sj.bjc.6601118.
[18] M. Maemondo, A. Inoue, K. Kobayashi, S. Sugawara, S. Oizumi, H. Isobe, A. Gemma, M. Harada, H. Yoshizawa, I. Kinoshita, Y. Fujita, S. Okinaga, H. Hirano, K. Yoshimori, T. Harada, T. Ogura, M. Ando, H. Miyazawa, T. Tanaka, Y. Saijo, K. Hagiwara, S. Morita, T. Nukiwa, North-east japan study group, gefitinib or chemotherapy for non–Small-Cell lung Cancer with mutated EGFR, N. Engl. J. Med. 362 (2010) 2380–2388, https://doi.org/10.1056/NEJMoa0909530.
[19] J.A. Pinto, C.S. Vallejos, L.E. Raez, L.A. Mas, R. Ruiz, J.S. Torres-Roman, Z. Morante, J.M. Araujo, H.L. Gómez, A. Aguilar, D. Bretel, C.J. Flores, C. Rolfo, Gender and outcomes in non-small cell lung cancer: an old prognostic variable comes back for targeted therapy and immunotherapy? ESMO Open 3 (2018) e000344, , https://doi.org/10.1136/esmoopen-2018-000344.
[20] R.A. Miksad, A.P. Abernethy, Harnessing the power of real-world evidence (RWE): a checklist to ensure regulatory-grade data quality, Clin. Pharmacol. Ther. 103 (2018) 202–205, https://doi.org/10.1002/cpt.946.
[21] E. Ortona, F. Delunardo, G. Baggio, W. Malorni, A sex and gender perspective in medicine: a new mandatory challenge for human health. Preface, Ann. Ist. Super. Sanita. 52 (2020) 146–148, https://doi.org/10.4415/ANN_16_02_02 (n.d.).
[22] R.I. Shader, More on women's health, gender medicine, and the complexities of personalized medicine, Clin. Ther. 38 (2016) 233–235, https://doi.org/10.1016/j.clinthera.2016.01.011.
[23] D. Westergaard, P. Moseley, F.K.H. Sørup, P. Baldi, S. Brunak, Population-wide analysis of differences in disease progression patterns in men and women, Nat. Commun. 10 (2019) 666, https://doi.org/10.1038/s41467-019-08475-9.
[24] W.H. Courtenay, Constructions of masculinity and their influence on men's well-being: a theory of gender and health, Soc. Sci. Med. 50 (2000) 1385–1401.
[25] S. Gallus, R. Pacifici, P. Colombo, V. Scarpino, P. Zuccaro, C. Bosetti, E. Fernandez, G. Apolone, C. La Vecchia, Prevalence of smoking and attitude towards smoking regulation in Italy, 2004, Eur. J. Cancer Prev. 15 (2006) 77–81.
[26] J.D. Patel, Lung Cancer in women, J. Clin. Oncol. 23 (2005) 3212–3218, https://doi.org/10.1200/JCO.2005.11.486.
[27] D. Ryberg, A. Hewer, D.H. Phillips, A. Haugen, Different susceptibility to smoking-induced DNA damage among male and female lung cancer patients, Cancer Res. 54 (1994) 5801–5803.
[28] S. Mollerup, D. Ryberg, A. Hewer, D.H. Phillips, A. Haugen, Sex differences in lung CYP1A1 expression and DNA adduct levels among lung cancer patients, Cancer Res. 59 (1999) 3317–3320.
[29] S. Mollerup, G. Berge, R. Bæra, V. Skaug, A. Hewer, D.H. Phillips, L. Stangeland, A. Haugen, Sex differences in risk of lung cancer: expression of genes in the PAH bioactivation pathway in relation to smoking and bulky DNA adducts, Int. J. Cancer 119 (2006) 741–744, https://doi.org/10.1002/ijc.21891.
[30] P. Garrido, N. Viñolas, D. Isla, M. Provencio, M. Majem, A. Artal, E. Carcereny, R. Garcia Campelo, P. Lianes, R. De La Peñas, E. Felip, Lung cancer in Spanish women: the WORLD07 project, Eur. J. Cancer Care 28 (2019) e12941, , https://doi.org/10.1111/ecc.12941.

biology

MDPI

Article

R-Score: A New Parameter to Assess the Quality of Variants' Calls Assessed by NGS Using Liquid Biopsies

Roberto Serna-Blasco [1], Estela Sánchez-Herrero [1,2], María Berrocal Renedo [1], Silvia Calabuig-Fariñas [3,4,5], Miguel Ángel Molina-Vila [6], Mariano Provencio [7] and Atocha Romero [1,7,*]

1 Liquid Biopsy Laboratory, University Hospital Puerta de Hierro, Majadahonda, 28222 Madrid, Spain; rserna@idiphim.org (R.S.-B.); esanchez@idiphim.org (E.S.-H.); mariaberrocal18@gmail.com (M.B.R.)
2 Atrys Health, I+D Department, 08025 Barcelona, Spain
3 CIBERONC, Liquid Biopsy WM, 28029 Madrid, Spain; calabuix_sil@gva.es
4 Mixed Unit TRIAL, Príncipe Felipe Research Center & General University Hospital of Valencia Research Foundation, 46012 Valencia, Spain
5 Department of Pathology, Universitat de València, 46010 Valencia, Spain
6 Laboratory of Oncology/Pangaea Oncology, Quirón-Dexeus University Hospital, 08028 Barcelona, Spain; mamolina@panoncology.com
7 Medical Oncology, University Hospital Puerta de Hierro, Majadahonda, 28222 Madrid, Spain; mariano.provencio@salud.madrid.org
* Correspondence: aromero@idiphim.org; Tel.: +34-1917769

check for updates

Citation: Serna-Blasco, R.; Sánchez-Herrero, E.; Berrocal Renedo, M.; Calabuig-Fariñas, S.; Molina-Vila, M.Á.; Provencio, M.; Romero, A. R-Score: A New Parameter to Assess the Quality of Variants' Calls Assessed by NGS Using Liquid Biopsies. *Biology* **2021**, *10*, 954. https://doi.org/10.3390/biology10100954

Academic Editors: Shibiao Wan, Yiping Fan, Chunjie Jiang, Shengli Li and Dirk Rades

Received: 3 August 2021
Accepted: 4 September 2021
Published: 24 September 2021

Publisher's Note: MDPI stays neutral with regard to jurisdictional claims in published maps and institutional affiliations.

Simple Summary: Circulating tumor DNA profiling by next-generation sequencing (NGS) is becoming essential for guiding targeted therapies. However, it remains challenging. Here, we show that variant allele fraction and the median of absolute values of all pairwise differences impact the agreement between digital PCR and NGS calls. Therefore, we propose a new parameter, named R-score, which integrates both variables, and we evaluate its usefulness for optimizing NGS variant calling.

Abstract: Next-generation sequencing (NGS) has enabled a deeper knowledge of the molecular landscape in non-small cell lung cancer (NSCLC), identifying a growing number of targetable molecular alterations in key genes. However, NGS profiling of liquid biopsies risk for false positive and false negative calls and parameters assessing the quality of NGS calls remains lacking. In this study, we have evaluated the positive percent agreement (PPA) between NGS and digital PCR calls when assessing *EGFR* mutation status using 85 plasma samples from 82 *EGFR*-positive NSCLC patients. According to our data, variant allele fraction (VAF) was significantly lower in discordant calls and the median of the absolute values of all pairwise differences (MAPD) was significantly higher in discordant calls ($p < 0.001$ in both cases). Based on these results, we propose a new parameter that integrates both variables, named R-score. Next, we sought to evaluate the PPA for *EGFR* mutation calls between two independent NGS platforms using a subset of 40 samples from the same cohort. Remarkably, there was a significant linear correlation between the PPA and the R-score ($r = 0.97$; $p < 0.001$). Specifically, the PPA of samples with an R-score ≤ -1.25 was 95.83%, whereas PPA falls to 81.63% in samples with R-score ≤ 0.25. In conclusion, R-score significantly correlates with PPA and can assist laboratory medicine specialists and data scientists to select reliable variants detected by NGS.

Keywords: NGS; ctDNA; VAF; liquid biopsy; filtering; variant calling

1. Introduction

The analysis of circulating tumor DNA (ctDNA) has become an attractive approach for non-invasive biomarker testing as well as for real-time monitoring of cancer patients; its usefulness is especially remarkable in lung cancer patients [1–4]. These tumors are

mostly diagnosed at advanced stages, in elderly patients with a median age at diagnosis of approximately 65 years [5], and they are difficult to access owing to their anatomical location, which makes it sometimes difficult to obtain sufficient material for molecular analysis [6]. Moreover, in the last decades, there has been a major paradigm shift in the management of metastatic non-small cell lung cancer (NSCLC), with the advent of targeted therapies for patients harbouring druggable alterations such as *EGFR* or *BRAF* mutations, as well as *ALK*, *ROS*, and *RET* rearrangements, and so on [7]. Furthermore, novel *KRAS* inhibitors constitute a promising therapeutic approach for advanced NSCLC patients [8,9]. Specifically, 30% of NSCLC tumours harbour activating mutations in the *EGFR* gene, which identify patient candidates to receive tyrosine kinase inhibitors (TKIs) [10]. For this subset of patients, liquid biopsy has been proven to be extremely useful, saving time in the process of diagnosis. In this way, guidelines recommend testing for the T790M *EGFR* mutation in the blood after progression to an *EGFR* TKI as a first choice, and re-biopsies are suggested in the case of a negative result in order to identify patients that can benefit from osimertinib (a third-generation TKI) [11]. Moreover, ctDNA plasma levels have been shown to be of prognostic significance for these patients, and monitoring *EGFR* mutation levels in the plasmas has been proven useful for response to treatment monitoring [5,12,13].

Next-generation sequencing (NGS) enables simultaneous detection of multiple alterations in a single test. Incorporation of unique molecular identifiers (UMIs), random nucleotide sequences assigned to each DNA fragment prior to PCR amplification during library preparation, enables the detection, quantification, and sequencing of unique DNA fragments with high-resolution, allowing the identification and removal of amplification artifacts arising from library preparation and the reduction of the limit of detection (LOD) [14,15]. Nonetheless, ctDNA is present at very low levels in the plasma and its profiling is still challenging with working conditions sometimes close to the edge of this technology. Therefore, there is a need to develop new parameters assessing the quality of the reads in order to avoid false positive and false negative calls.

Here, we assess the impact of two parameters, namely, variant allele fraction (VAF) and median of the absolute values of all pairwise differences (MAPD), separately and together on variant calls when using the Oncomine Pan-Cancer Cell-Free Assay™ (ThermoFisher Scientific®, Palo Alto, CA, USA) by evaluating the agreement between digital PCR (dPCR) and NGS for the assessment of *EGFR* mutation status. Based on our data, we propose a new parameter named R-score and, finally, we evaluate the agreement in NGS calls between two independent NGS methods according to R-score.

2. Materials and Methods

2.1. Patients and Samples

A total of 85 samples from advanced *EGFR*-positive NSCLC patients were recruited upon disease progression to a first-line with a TKI, between February 2016 and March 2019. The study was approved by the Hospital Puerta de Hierro Ethics Committee. All patients provided the appropriate written informed consent to participate in the study prior to enrolment. Briefly, eligible patients were both male and female, age >18 years, with a pathologically confirmed diagnosis of stage IV NSCLC harbouring an *EGFR* mutation. Blood samples were collected in 8.5 mL PPT™ tubes (Becton Dickinson, Franklin Lakes, NJ, USA).

2.2. Laboratory Procedures

Two independent laboratories were involved in this study: laboratory 1 (L1) and laboratory 2 (L2). Samples for which we did not have available at least 8 mL of plasma (N = 45) were processed only by L1 exclusively, and they were used to test the agreement between dPCR and NGS exclusively. For 40 plasma samples, we had available at least 8 mL of plasma, and samples were divided into two aliquots, which were then distributed to L1 and L2. L1 carried out dPCR assays and NGS analysis using the Oncomine Pan-Cancer Cell-Free Assay and an Ion S5 sequencer (ThermoFisher Scientific®, Palo Alto, CA, USA),

whereas L2 carried out NGS with QIAact Lung DNA UMI Panel using the GeneRead Platform (QIAgen, Valencia, CA, USA).

Isolation of plasma was achieved by two consecutive centrifugations at room temperature, the first one at 1500× *g* for 10 min and the second at 5000× *g* for 20 min. cfDNA was extracted with the QIAamp Circulating Nucleic Acid Kit (QIAgen, Valencia, CA, USA) according to the manufacturer's protocol (QIAamp Circulating Nucelic Acid Handbook 10/2013). DNA concentration was measured by Qubit 2.0 Fluorometer with Qubit 1X dsDNA HS Assay Kit (ThermoFisher Scientific®, Palo Alto, CA, USA) and fragment length and sample quality were evaluated using the Agilent High Sensitivity DNA Kit using Agilent 2100 Bioanalyzer (Agilent Technologies, Santa Clara, CA, USA). Supplementary Figure S1 shows the observed size of the cfDNA fragments, which was approximately 180 bp. cfDNA was stored at −80 °C until further analysis.

In order to detect somatic mutation in the *EGFR* gene, dPCRs were performed using predesigned TaqMan® dPCR assays in a QuantStudio® 3D Digital PCR (Applied Biosystems®, South San Francisco, CA, USA). dPCR reaction was carried out in a final volume of 18 µL; this reaction included 8.55 µL of template cfDNA, 9 µL of 20X QuantStudio® Master Mix, and 0.45 µL 40X TaqMan assay. Subsequently, 14.5 µL of final reaction volume was loaded to QuantStudio® 3D digital PCR 20K chip. The thermal cycler conditions were as follows: initial denaturalization at 96 °C for 10 min, 40 cycles at 56 °C for 2 min, 98 °C for 30 s, 72 °C for 10 min, and finally samples were maintained at 22 °C for at least 30 min. Chips were read using QuantStudio® 3D Digital PCR instrument. The results were analysed with QuantStudio® 3D AnalysisSuite™ Cloud. Default call assignments for each data cluster were manually adjusted when needed. A positive and a negative control were included in every run. The LOD and limit of quantitation of the dPCR TaqMan® assays were estimated based on the standard deviation of the response and the slope according to the recommendations of The International Council for Harmonisation of Technical Requirements for Pharmaceuticals for Human Use; ICH Q2 (R1) guidelines (validation of analytical procedures: text and methodology), and they have been published elsewhere [13]. The sensitivity and specificity of the assays, considering tissue genotyping to be the gold standard, have also been reported [16].

The presence of *EGFR* mutations was evaluated in parallel by two independent NGS platforms, Ion S5™ XL and GeneReader™, and using two different gene panels, Oncomine™ Pan-Cancer Cell-Free Assay (ThermoFisher Scientific®, Palo Alto, CA, USA) and the QIAact Lung DNA UMI Panel (QIAgen, Valencia, CA, USA), respectively. The comparison was performed using 40 samples.

For NGS analysis using the Oncomine Pan-Cancer Cell-Free Assay (NGS-Oncomine), library preparation was performed with a minimum input of 10 ng of cfDNA according to manufacturer's instructions. The final pool was loaded in an Ion 550™ Chip using Ion Chef™ Instrument (ThermoFisher Scientific®, Palo Alto, CA, USA). Finally, loaded chips were sequenced on an Ion GeneStudio™ S5 Sequencer (ThermoFisher Scientific®, Palo Alto, CA, USA). Torrent Suite Software (v5.12) was used to perform raw sequencing data analysis. The CoverageAnalysis (v. 5.12.0.0) plugin was used for sequencing coverage analysis (ThermoFisher Scientific®, Palo Alto, CA, USA). As recommended by the manufacturer, a median read coverage >25,000 and median molecular coverage >2500 were required to detect a variant with a VAF of 0.1%. Raw reads were aligned to the human reference genome hg19. Variant calling, annotation, and filtering were performed on the Ion Reporter (v5.10) platform using the OncomineTagSeq Pan-Cancer Liquid Biopsy workflow (v2.1). Briefly, sequencing reads were mapped to defined target regions (Oncomine Pan-Cancer DNA Regions v1.0 (5.10)) and subjected to variant calling using Oncomine Pan-Cancer Annotations v1r.0.

For NGS analysis using the QIAact Lung DNA UMI Panel (NGS-GeneReader), libraries were performed with an input of 16.75 µL and ~10–70 ng of purified cfDNA, according to manufacturer's instructions. Then, libraries were quantified using a QIAxcel Advanced System and Qubit dsDNA HS Assay kit in order to pool in batches of six samples.

GeneRead Clonal Amp Q Kit was used to clonal amplification of pooled libraries. After bead enrichment, pooled libraries were sequenced using the GeneRead UMI Advanced Sequencing Q kit in a GeneReader instrument. Finally, FASTQ files alignment was performed using hg19 as reference genome, and variant calling and report generation of sequencing results were performed by QIAGEN Clinical Insight Analyze software.

2.3. Parameters

VAF was defined as the number of mutant molecules at a specific nucleotide location relative to the sum of total DNA molecules (mutant + wild type). VAF was provided for each detected mutation after dPCR and NGS analysis. In dPCR analysis, VAF was calculated, following the next equation, by QuantStudio® 3D AnalysisSuite™ Cloud:

$$\text{VAF} = (\text{FAMcopies}/\mu\text{L})/(\text{FAMcopies}/\mu\text{L} + \text{VICcopies}/\mu\text{L}) \times 100 \quad (1)$$

where FAM copies = number of reads of mutated sequences and VIC copies = number of reads of wild-type sequences.

In the case of NGS-Oncomine, VAF was calculated, using the CoverageAnalysis (v. 5.12.0.0) plugin. Likewise, using NGS-GeneReader, VAF was calculated with QIAGEN Clinical Insight Analyze software in the same way as NGS-Oncomine.

NGS-Oncomine platform also provides a quality sequencing parameter, MAPD, as a pair is defined as adjacent amplicons in terms of genomic distances. Assuming that adjacent amplicons in the genome most likely have the same underlying copy number in a sample, the difference between the log2c(read count ratio) values against the reference baseline for all adjacent amplicons contains information for the noise level of the data. The MAPD is an estimation of coverage variability between adjacent amplicons. The default threshold is 0.5 [17]. As a result, sample results with an MAPD above this value should be reviewed with caution

$$\text{MAPD} = \text{median}(|x_{i+1} - x_i|) \quad (2)$$

where x_i = log2 ratio for marker i.

2.4. Statistical Analysis

The primary objective was to evaluate the impact of VAF and MAPD parameters, separately and together, firstly on the positive percent agreement (PPA) between dPCR and NGS (NGS-Oncomine) and secondly on the PPA between two independent NGS platforms (NGS-Oncomine and NGS-GeneReader).

Each mutation was treated as a separate measurement for statistical analysis; therefore, 137 measurements were used in this study.

The correlation between VAFs measured by dPCR and NGS was assessed with simple linear regression analysis, using the concordance correlation coefficient (p) and Spearman's coefficient (r). For comparisons between numerical variables, Mann–Whitney U test was used. Comparisons between categorical variables were made using Fisher's exact test or chi-squared test, whichever was most appropriate.

To describe how often NGS and dPCR methods agreed on *EGFR* calls, as well as concordance between the two different NGS platforms, we calculated the PPA.

The threshold of $p < 0.05$ was considered as statistically significant. Statistical software used was Stata v16.0 (StataCorp 2019. Stata Statistical Software Release 16. College station, TX: StataCorp LLC) and R version 3.6.3. (R core team 2020. The R Foundation for Statistical Computing Platform, Vienna, Austria) URL https://www.R-project.org/ (last accessed on 26 July 2021).

3. Results

3.1. EGFR Mutation Detection by dPCR and NGS-Oncomine

EGFR mutation status was evaluated in 85 plasma samples from 82 *EGFR*-positive NSCLC patients in parallel by dPCR and NGS-Oncomine. All samples used in this study

3. Results

3.1. EGFR Mutation Detection by dPCR and NGS-Oncomine

EGFR mutation status was evaluated in 85 plasma samples from 82 EGFR-positive NSCLC patients in parallel by dPCR and NGS-Oncomine. All samples used in this study had detectable *EGFR* driver mutations by dPCR. The mutation detected by dPCR was always concordant with the *EGFR* mutation detected on the pre-treatment tissue sample as reported by pathologists. Among the total number of detected *EGFR* mutations (N = 137), 62% were activating mutations, among which the most common mutations were exon 19 deletions (55.3%) or L858R (36.5%). The rest of the *EGFR* driver mutations were L861Q (3.5%), G719A (2.3%), S768I (1.2%), and exon 20 insertions (1.2%). Regarding T790M resistance mutation, 61.2% of samples were identified as T790M positive by dPCR. Data for T790M status in tissue samples were not available. Of note, 42 (30.6%) mutations detected by dPCR were not found using NGS-Oncomine. When analysing mutations separately, a lower PPA was measured in L858R mutation (67.74%; 95%CI 50.31–85.17) compared with exon 19 deletion (76.60%; 95%CI 64.03–89.16). Less common *EGFR* mutations such as L861Q, S768I, and G719A were detected by both methods. It should be noted that the exon 20 insertion (c.2310_2311insGGT; p.D770_N771insG) was not found by NGS-Oncomine.

Finally, regarding T790M resistance mutation, 52 (61.2%) samples were identified as T790M positive by dPCR, whereas only 28 (33%) samples were T790M positive using NGS-Oncomine (53.85% of agreement; 95% CI 39.83–67.86).

3.2. VAF and MAPD Involvement in the Agreement between dPCR and NGS-Oncomine Calls

Overall, there were 91 concordant calls by both technologies and 46 discordant calls with a PPA of 66.42% (95% CI 58.42–74.43).

First, we evaluated the overall correlation between VAF values assessed by dPCR and NGS-Oncomine when the mutation was detected by both methods. According to our data, VAFs measured by NGS-Oncomine were significantly correlated to VAFs assessed by dPCR ($r = 0.89$; $p < 0.001$) (Figure S2). Next, VAFs values and MAPD scores were compared between discordant and concordant calls. Overall, dPCR VAFs values were significantly lower in discordant calls compared with concordant calls ($p < 0.001$) (Figure 1A). Specifically, 1.1% and 10.9% of concordant calls have VAF ≤ 0.1% and ≤ 0.5%, respectively, compared with 8.9% and 46.7% in discordant calls. Likewise, MAPD score was significantly higher in discordant samples compared with concordant samples ($p < 0.001$) (Figure 1B).

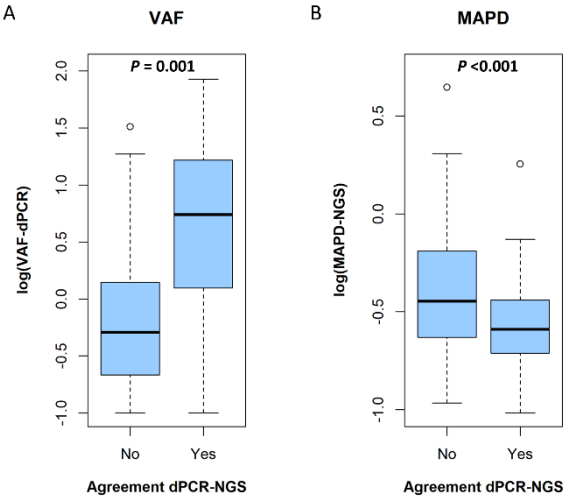

Figure 1. Boxplot. (**A**) VAF values in concordant and discordant calls (dPCR-NGS-Oncomine) in logarithmic scale. (**B**) MAPD values in concordant and discordant calls (dPCR-NGS-Oncomine) in logarithmic scale.

Next, we sought to evaluate the combined effect of VAF and MAPD parameters. Dot plots in Figure 2 show the concordance between dPCR and NGS-Oncomine on variant calls according to VAF and MAPD parameters. Discordant calls are coloured in red and concordant calls are coloured in blue. Figure 2A is divided into four quadrants using as cut-offs the logarithmic median values of VAF and MAPD according to our data set.

logarithmic scale. (**B**) MAPD values in concordant and discordant calls (dPCR-NGS-Oncomine) in logarithmic scale.

Next, we sought to evaluate the combined effect of VAF and MAPD parameters. Dot plots in Figure 2 show the concordance between dPCR and NGS-Oncomine on variant calls according to VAF and MAPD parameters. Discordant calls are coloured in red and concordant calls are coloured in blue. Figure 2A is divided into four quadrants using as cut-offs the logarithmic median values of VAF and MAPD according to our data set. As shown, the highest PPA (96.9% 95% CI: 89.8–99.9%) was observed in the lower right quadrant. Conversely, the PPA descended as much as 27.6% (95% CI: 12.7–47.2%) for calls clustered in the upper left quadrant, meaning that, the higher the VAF and the **lower the MAPD, the higher the PPA. Similar results were obtained when quadrants were divided using thresholds according to technical specifications for each parameter (Figure 2B). As illustrated, PPA between NGS and dPCR calls was 0% (95% CI: 0–20.7%) when using a cut-off of −0.301 for VAF and > −0.301 for MAPD, whereas in the opposite conditions, the PPA increased to 84.9% (95% CI: 74.5–90.9%).**

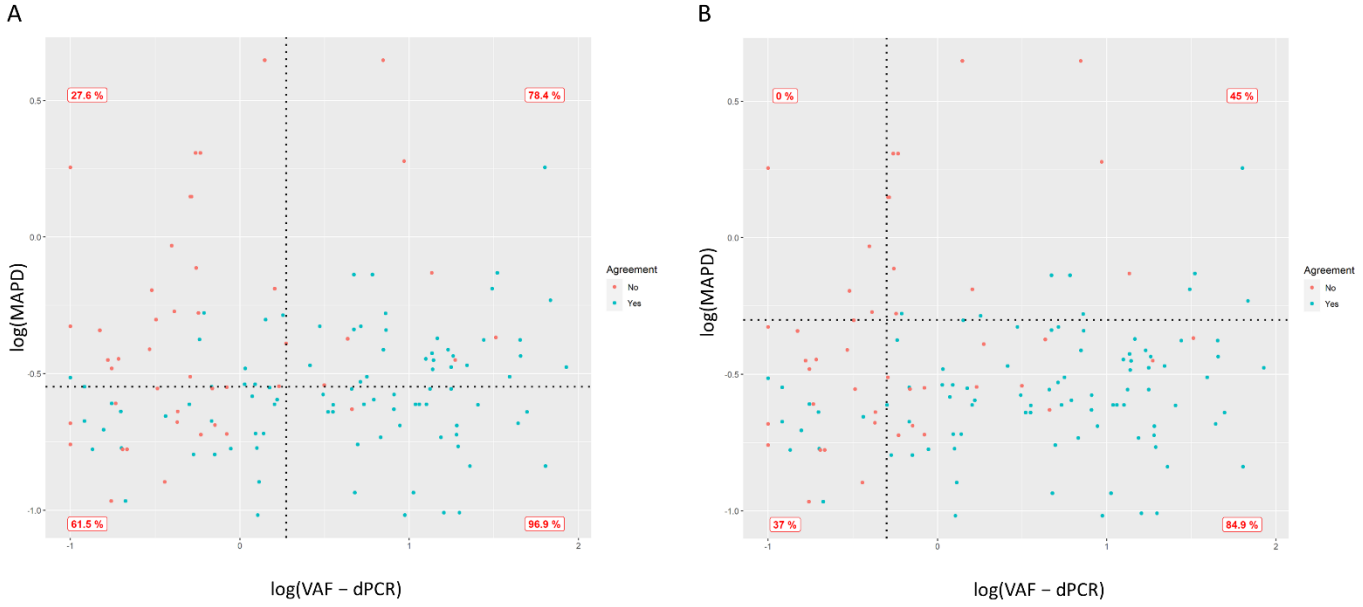

Figure 2. Dot plot showing the agreement in variant calls between dPCR—NGS-Oncomine, according to VAF and MAPD. VAF and MAPD values, both in logarithmic scale, are represented in the *x* and *y*-axis, respectively. Concordant calls are coloured in blue, while discordant calls are coloured in red. PPA for calls clustered in each quadrant is shown. (**A**) Dot plot divided into four quadrants using as cut-off the logarithmic median values of VAF and MAPD. In this way, the median VAF in our data set was 1.87, which is 0.272 on logarithmic scale, and the median MAPD was 0.28, which corresponds to −0.553 on logarithmic scale. (**B**) Dot plot divided into four quadrants according to technical specifications. MAPD threshold was selected following Ion Reporter recommendations [17]. According to the manufacturer, a value of MAPD above 0.5 is considered too high. Samples with high MAPD values have low coverage uniformity, which can result in missed or erroneous variant calls. The VAF threshold was chosen based on results from previous studies [18]. Therefore, both axes were divided using −0.301 value for VAF and MAPD (log(0.5)).

3.3. R-Score Is a Useful Parameter to Select Reliable Variant Calls

Based on previous observations, we proposed a new parameter, named R-score, which is defined as follows:

$$\text{R-score} = \log(\text{MAPD}/\text{VAF}) \quad (3)$$

In order to evaluate the utility of R-score for assessing the quality of an *EGFR* variant call, we evaluated the PPA between NGS-Oncomine and dPCR and NGS-Oncomine and NGS-GeneReader according to R-score.

First, we assessed the correlation between VAF values from NGS-Oncomine and NGS-GeneReader when the mutation was detected by both methods. According to our data, VAFs values from NGS-Oncomine significantly correlated with VAFs from NGS-GeneReader (r = 0.80; $p < 0.001$).

R-score was then calculated for each variant detected by NGS-Oncomine using the VAF and MAPD provided by the corresponding analysis software. MAPD and R-score values were significantly higher in discordant calls between dPCR and NGS-Oncomine compared with concordant calls ($p < 0.001$) (Figure 3A and Table S1). Conversely, VAF values were

NGS-GeneReader when the mutation was detected by both methods. According to our data, VAFs values from NGS-Oncomine significantly correlated with VAFs from NGS-GeneReader (r = 0.80; $p < 0.001$).

R-score was then calculated for each variant detected by NGS-Oncomine using the VAF and MAPD provided by the corresponding analysis software. MAPD and R-score values were significantly higher in discordant calls between dPCR and NGS-Oncomine compared with concordant calls ($p < 0.001$) (Figure 3A and Table S1). Conversely, VAF values were significantly lower in discordant calls between dPCR and NGS-Oncomine (Table S1). Subsequently, the PPA for *EGFR* variant calling between both NGS platforms was evaluated using different arbitrary R-score cut-offs (−1.25, −1, −0.75, −0.5, −0.25, 0, and 0.25). As shown in Figure 3C, there was a clear linear correlation between the PPA and the R-score (r = −0.97; $p < 0.001$). Of note, the PPA of samples with an R-score ≤ −1.25 was 95.83%, whereas PPA falls to 81.63% in samples with an R-score ≤ 0.25 (Figure 3B). A complete list of all mutations detected according to the NGS platform is available in Table S2.

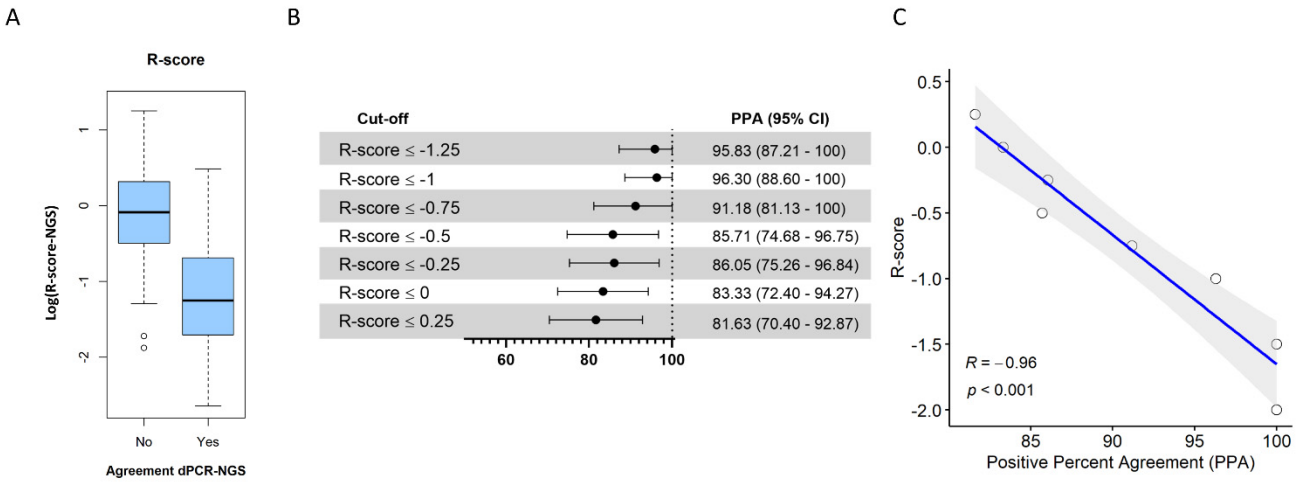

Figure 3. (**A**) R-score values in logarithmic scale in concordant and discordant samples (dPCR—NGS-Oncomine). R-score was calculated for each variant detected with Oncomine panel, using VAF and MAPD values from Ion Reporter (v5.10) analysis software. (**B**) Positive percent agreement (PPA) with corresponding 95% confidence interval (95% CI) between Oncomine and NGS-GeneReader according to R-score cut-off. The following arbitrary cut-offs for R-score were established: −1.25, −1, −0.75, −0.5, −0.25, 0, and 0.25, and PPA between both NGS platforms was estimated. (**C**) Correlation between PPA values and R-score cut-off values. As shown, there was a linear correlation between PPA and the R-score cut-off values; the lower the R-score, the greater the PPA. Abbreviations: R = Spearman correlation coefficient.

4. Discussion

Biomarker testing in NSCLC has been demonstrated to improve survival outcomes [19–21]. Of note, the number of biomarkers that need to be tested is constantly increasing in NSCLC as new targeted therapies are becoming available [7]. Unlike PCR-based platforms, which only allow a few mutations to be analyzed, NGS enables for interrogating multiple genomic alterations simultaneously in a single test. Indeed, National Comprehensive Cancer Network guidelines recommend that, when feasible, biomarker testing should be performed via a broad, panel-based approach by NGS [2]. However, NGS profiling of liquid biopsies, although feasible [22,23], remains challenging. On one hand, the sensitivity of the assays remains a major limitation [24], and approaches aimed to increase sensitivity might risk false positive calls. Moreover, it has been reported that tumor mutational burden (TMB) analysis, which has been proposed as a predictive biomarker for the identification of patients most likely to respond to immune checkpoint inhibitors, through liquid biopsies, is feasible [25]. TMB is optimally assessed by whole exome sequencing (WES) [26], but targeted panels provide a time-effective and cost-effective alternative [27]. Nevertheless, TMB analysis requires sequencing over 0.5 Mb [28,29]. In this scenario, it is of particular interest to reduce as much as possible the risk of false-positive and false-negative calls. Thus, new parameters evaluating the quality of NGS calls are needed. A recent comprehensive study, in which several methodologies for the analysis of circulating tumor DNA were compared, revealed that the agreement between platforms significantly improved when discarding samples with VAF ≤ 0.5% [16]. Likewise, a study comparing BEAMing and droplet dPCR for ctDNA analysis using plasma samples from advanced breast cancer patients enrolled in the PALOMA-3 trial showed that discordant calls occurred

at VAFs < 1% [30]. In the view of our findings, we hypothesized that the combination of VAF with MAPD could further improve the assessment of the reliability of a variant call. According to our data, MAPD was significantly higher in discordant samples compared with concordant calls ($p < 0.001$), while VAF values were significantly lower in discordant calls compared with concordant samples ($p < 0.001$). Remarkably, as shown in Figure 2, the highest PPA (96.9%; 95%CI: 83.8–99.9%) was observed in the lower-right quadrant. Conversely, the PPA descended as much as 27.6% (95%CI: 12.7–47.2%) for calls clustered in the upper-left quadrant.

Our results are limited to *EGFR* locus as the cohort included exclusively *EGFR*-positive NSCLC patients. Nonetheless, mutations in other key genes were found. Specifically, in our data set, there were two samples testing positive for *KRAS* mutations by both NGS platforms (data not shown). Larger cohorts assessing the utility R-score for assessing the reliability of variant calls in other loci different may be of particular interest.

Taken together, we propose the R-score defined as the log(MAPD/VAF). According to our results, *EGFR* variants with positive R-score are particularly sensitive to genotyping errors. As presented in Figure 3, a significant correlation was found between PPA and the R-score cut-off values, indicating that R-sore can be useful to discriminate between true and false calls in the *EGFR* locus.

5. Conclusions

VAF and MAPD have an impact on *EGFR* variant calling. Combining this information in a score (R-score) can further improve the assessment of the reliability of a variant call. Using a dataset of 85 *EGFR*-positive NSCLC patients, we find that *EGFR* variants with positive R-score are particularly sensitive to erroneous variant calls in the *EGFR* gene.

Supplementary Materials: The following are available online at https://www.mdpi.com/article/10.3390/biology10100954/s1, Figure S1: Two samples electropherogram showing a 180 bp peak corresponding to low fragment cfDNA and peaks corresponding to mono-, di-, and tri-nucleosomes. (B) Gel-like image of cfDNA samples an-alysed with Bioanalyzer 2100; Figure S2: Correlation between variant allele fraction assessed by dPCR and Oncomine-NGS. Linear regression line is shown in black and the 95% confidence interval is shaded in grey. Pearson's correlation coefficient and *p*-value are shown in the graph; Table S1: Effect size and *p*-values for VAF, MAPD, and R-score parameters when assessing significant differences between concordant and discordant calls; Table S2: Table with all *EGFR* mutations detected by dPCR, NGS-Oncomine, and NGS-GeneReader with VAF values for each assay and cfDNA concentration.

Author Contributions: All authors confirmed they have contributed to the intellectual content of this paper and have approved the submitted version and agree to be personally accountable for the author's own contributions and for ensuring that questions related to the accuracy or integrity of any part of the work, even ones in which the author was not personally involved, are appropriately investigated, resolved, and documented in the literature. All authors have read and agreed to the published version of the manuscript.

Funding: This paper is part of a project that has received funding from the European Union's Horizon 2020 research and innovation program under grant agreement No. 875160 and PI16/18018. Roberto Serna-Blasco is supported by Plan de Empleo Juvenil Comunidad de Madrid (PEJD-2018-PRE/BMD-8640). Estela Sánchez-Herrero is supported by the Consejería de Ciencia, Universidades e Innovación of the Comunidad de Madrid (Doctorados Industriales of the Comunidad de Madrid IND2019/BMD-17258).

Institutional Review Board Statement: The study was conducted according to the guidelines of the Declaration of Helsinki, and the study protocol was approved by the Hospital Puerta de Hierro Ethics Committee (internal code PI-154/17).

Informed Consent Statement: Informed consent was obtained from all subjects involved in the study.

Data Availability Statement: All data generated or analyzed during this study are included in this published article (and its additional files).

Acknowledgments: We wish to thank all the patients and staff who participated in the study.

Conflicts of Interest: Atocha Romero reports personal fees from Boehringer and Takeda during the conduct of the study. Mariano Provencio reports grants, personal fees, and non-financial support from BMS, ROCHE, and ASTRAZENECA, as well as personal fees from MSD and TAKEDA, outside the submitted work.

References

1. Provencio, M.; Torrente, M.; Calvo, V.; Gutiérrez, L.; Pérez-Callejo, D.; Pérez-Barrios, C.; Barquín, M.; Royuela, A.; Rodriguez-Alfonso, B.; Sotelo, M.; et al. Dynamic circulating tumor DNA quantificaton for the individualization of non-small-cell lung cancer patients treatment. *Oncotarget* **2017**, *8*, 60291–60298. [CrossRef]
2. Ettinger, D.S.; Wood, D.E.; Aisner, D.L.; Akerley, W.; Bauman, J.; Chirieac, L.R.; D'Amico, T.A.; Decamp, M.M.; Dilling, T.J.; Dobelbower, M.; et al. Non-small cell lung cancer, version 5.2017: Clinical practice guidelines in oncology. *JNCCN J. Natl. Compr. Cancer Netw.* **2017**, *15*, 504–535. [CrossRef]
3. Pérez-Callejo, D.; Romero, A.; Provencio, M.; Torrente, M. Liquid biopsy based biomarkers in non-small cell lung cancer for diagnosis and treatment monitoring. *Transl. Lung Cancer Res.* **2016**, *5*, 455–465. [CrossRef]
4. Romero, A.; Serna-Blasco, R.; Calvo, V.; Provencio, M. Use of Liquid Biopsy in the Care of Patients with Non-Small Cell Lung Cancer. *Curr. Treat. Options Oncol.* **2021**, *22*, 86. [CrossRef]
5. Provencio, M.; Serna-Blasco, R.; Franco, F.; Calvo, V.; Royuela, A.; Auglytė, M.; Sánchez-Hernández, A.; de Julián Campayo, M.; García-Girón, C.; Dómine, M.; et al. Analysis of circulating tumour DNA to identify patients with epidermal growth factor receptor–positive non-small cell lung cancer who might benefit from sequential tyrosine kinase inhibitor treatment. *Eur. J. Cancer* **2021**, *149*, 61–72. [CrossRef] [PubMed]
6. McLean, A.; Barnes, D.; Troy, L. Diagnosing Lung Cancer: The Complexities of Obtaining a Tissue Diagnosis in the Era of Minimally Invasive and Personalised Medicine. *J. Clin. Med.* **2018**, *7*, 163. [CrossRef]
7. Schrank, Z.; Chhabra, G.; Lin, L.; Iderzorig, T.; Osude, C.; Khan, N.; Kuckovic, A.; Singh, S.; Miller, R.J.; Puri, N. Current molecular-targeted therapies in NSCLC and their mechanism of resistance. *Cancers* **2018**, *10*, 224. [CrossRef] [PubMed]
8. Hallin, J.; Engstrom, L.D.; Hargi, L.; Calinisan, A.; Aranda, R.; Briere, D.M.; Sudhakar, N.; Bowcut, V.; Baer, B.R.; Ballard, J.A.; et al. The KRASG12C inhibitor MRTX849 provides insight toward therapeutic susceptibility of KRAS-mutant cancers in mouse models and patients. *Cancer Discov.* **2020**, *10*, 54–71. [CrossRef] [PubMed]
9. Hong, D.S.; Fakih, M.G.; Strickler, J.H.; Desai, J.; Durm, G.A.; Shapiro, G.I.; Falchook, G.S.; Price, T.J.; Sacher, A.; Denlinger, C.S.; et al. KRAS G12C Inhibition with Sotorasib in Advanced Solid Tumors. *N. Engl. J. Med.* **2020**, *383*, 1207–1217. [CrossRef] [PubMed]
10. Stewart, E.L.; Tan, S.Z.; Liu, G.; Tsao, M.S. Known and putative mechanisms of resistance to *EGFR* targeted therapies in NSCLC patients with *EGFR* mutations-a review. *Transl. Lung Cancer Res.* **2015**, *4*, 67–81. [PubMed]
11. Dal Maso, A.; Lorenzi, M.; Roca, E.; Pilotto, S.; Macerelli, M.; Polo, V.; Cecere, F.L.; Del Conte, A.; Nardo, G.; Buoro, V.; et al. Clinical Features and Progression Pattern of Acquired T790M-positive Compared With T790M-negative *EGFR* Mutant Non–small-cell Lung Cancer: Catching Tumor and Clinical Heterogeneity Over Time Through Liquid Biopsy. *Clin. Lung Cancer* **2020**, *21*, 1–14.e3. [CrossRef]
12. Romero, A.; Serna-Blasco, R.; Alfaro, C.; Sánchez-Herrero, E.; Barquín, M.; Turpin, M.C.; Chico, S.; Sanz-Moreno, S.; Rodrigez-Festa, A.; Laza-Briviesca, R.; et al. ctDNA analysis reveals different molecular patterns upon disease progression in patients treated with osimertinib. *Transl. Lung Cancer Res.* **2020**, *9*, 532–540. [CrossRef]
13. Provencio, M.; Torrente, M.; Calvo, V.; Pérez-Callejo, D.; Gutiérrez, L.; Franco, F.; Pérez-Barrios, C.; Barquín, M.; Royuela, A.; García-García, F.; et al. Prognostic value of quantitative ctDNA levels in non small cell lung cancer patients. *Oncotarget* **2018**, *9*, 488–494. [CrossRef] [PubMed]
14. Salk, J.J.; Schmitt, M.W.; Loeb, L.A. Enhancing the accuracy of next-generation sequencing for detecting rare and subclonal mutations. *Nat. Rev. Genet.* **2018**, *19*, 269–285. [CrossRef]
15. Kivioja, T.; Vähärautio, A.; Karlsson, K.; Bonke, M.; Enge, M.; Linnarsson, S.; Taipale, J. Counting absolute numbers of molecules using unique molecular identifiers. *Nat. Methods* **2012**, *9*, 72–74. [CrossRef] [PubMed]
16. Romero, A.; Jantus-Lewintre, E.; García-Peláez, B.; Royuela, A.; Insa, A.; Cruz, P.; Collazo, A.; Pérez Altozano, J.; Vidal, O.J.; Diz, P.; et al. Comprehensive cross-platform comparison of methods for non-invasive *EGFR* mutation testing: Results of the RING observational trial. *Mol. Oncol.* **2021**, *15*, 43–56. [CrossRef] [PubMed]
17. Ion Reporter™ Software 5.12 USER GUIDE. Available online: https://assets.thermofisher.com/TFS-Assets/LSG/manuals/MAN0018032_IonReporterSoftware_5_12_UG.pdf (accessed on 5 July 2021).
18. Deveson, I.W.; Gong, B.; Lai, K.; LoCoco, J.S.; Richmond, T.A.; Schageman, J.; Zhang, Z.; Novoradovskaya, N.; Willey, J.C.; Jones, W.; et al. Evaluating the analytical validity of circulating tumor DNA sequencing assays for precision oncology. *Nat. Biotechnol.* **2021**, 1–14. [CrossRef]
19. Le Tourneau, C.; Delord, J.P.; Gonçalves, A.; Gavoille, C.; Dubot, C.; Isambert, N.; Campone, M.; Trédan, O.; Massiani, M.A.; Mauborgne, C.; et al. Molecularly targeted therapy based on tumour molecular profiling versus conventional therapy for advanced cancer (SHIVA): A multicentre, open-label, proof-of-concept, randomised, controlled phase 2 trial. *Lancet Oncol.* **2015**, *16*, 1324–1334. [CrossRef]

20. Fisher, K.E.; Zhang, L.; Wang, J.; Smith, G.H.; Newman, S.; Schneider, T.M.; Pillai, R.N.; Kudchadkar, R.R.; Owonikoko, T.K.; Ramalingam, S.S.; et al. Clinical Validation and Implementation of a Targeted Next-Generation Sequencing Assay to Detect Somatic Variants in Non-Small Cell Lung, Melanoma, and Gastrointestinal Malignancies. *J. Mol. Diagn.* **2016**, *18*, 299–315. [CrossRef]
21. Cottrell, C.E.; Al-Kateb, H.; Bredemeyer, A.J.; Duncavage, E.J.; Spencer, D.H.; Abel, H.J.; Lockwood, C.M.; Hagemann, I.S.; O'Guin, S.M.; Burcea, L.C.; et al. Validation of a next-generation sequencing assay for clinical molecular oncology. *J. Mol. Diagn.* **2014**, *16*, 89–105. [CrossRef]
22. Provencio, M.; Pérez-Barrios, C.; Barquin, M.; Calvo, V.; Franco, F.; Sánchez, E.; Sánchez, R.; Marsden, D.; Cristóbal Sánchez, J.; Martin Acosta, P.; et al. Next-generation sequencing for tumor mutation quantification using liquid biopsies. *Clin. Chem. Lab. Med.* **2019**, *58*, 306–313. [CrossRef]
23. Sánchez-Herrero, E.; Serna-Blasco, R.; Ivanchuk, V.; García-Campelo, R.; Dómine Gómez, M.; Sánchez, J.M.; Massutí, B.; Reguart, N.; Camps, C.; Sanz-Moreno, S.; et al. NGS-based liquid biopsy profiling identifies mechanisms of resistance to ALK inhibitors: A step toward personalized NSCLC treatment. *Mol. Oncol.* **2021**, *15*, 2363–2376. [CrossRef]
24. Merker, J.D.; Oxnard, G.R.; Compton, C.; Diehn, M.; Hurley, P.; Lazar, A.J.; Lindeman, N.; Lockwood, C.M.; Rai, A.J.; Schilsky, R.L.; et al. Circulating tumor DNA analysis in patients with cancer: American society of clinical oncology and college of American pathologists joint review. *J. Clin. Oncol.* **2018**, *142*, 1242–1253.
25. Gandara, D.R.; Paul, S.M.; Kowanetz, M.; Schleifman, E.; Zou, W.; Li, Y.; Rittmeyer, A.; Fehrenbacher, L.; Otto, G.; Malboeuf, C.; et al. Blood-based tumor mutational burden as a predictor of clinical benefit in non-small-cell lung cancer patients treated with atezolizumab. *Nat. Med.* **2018**, *24*, 1441–1448. [CrossRef]
26. Rizvi, N.A.; Hellmann, M.D.; Snyder, A.; Kvistborg, P.; Makarov, V.; Havel, J.J.; Lee, W.; Yuan, J.; Wong, P.; Ho, T.S.; et al. Mutational landscape determines sensitivity to PD-1 blockade in non-small cell lung cancer. *Science* **2015**, *348*, 124–128. [CrossRef]
27. Kowanetz, M.; Zou, W.; Shames, D.S.; Cummings, C.; Rizvi, N.; Spira, A.I.; Frampton, G.M.; Leveque, V.; Flynn, S.; Mocci, S.; et al. Tumor mutation load assessed by FoundationOne (FM1) is associated with improved efficacy of atezolizumab (atezo) in patients with advanced NSCLC. *Ann. Oncol.* **2016**, *27*, vi23. [CrossRef]
28. Chalmers, Z.R.; Connelly, C.F.; Fabrizio, D.; Gay, L.; Ali, S.M.; Ennis, R.; Schrock, A.; Campbell, B.; Shlien, A.; Chmielecki, J.; et al. Analysis of 100,000 human cancer genomes reveals the landscape of tumor mutational burden. *Genome Med.* **2017**, *9*, 34. [CrossRef] [PubMed]
29. Merino, D.M.; McShane, L.M.; Fabrizio, D.; Funari, V.; Chen, S.J.; White, J.R.; Wenz, P.; Baden, J.; Barrett, J.C.; Chaudhary, R.; et al. Establishing guidelines to harmonize tumor mutational burden (TMB): In silico assessment of variation in TMB quantification across diagnostic platforms: Phase I of the Friends of Cancer Research TMB Harmonization Project. *J. Immunother. Cancer* **2020**, *8*, e000147. [CrossRef] [PubMed]
30. O'Leary, B.; Hrebien, S.; Beaney, M.; Fribbens, C.; Garcia-Murillas, I.; Jiang, J.; Li, Y.; Bartlett, C.H.; André, F.; Loibl, S.; et al. Comparison of beaming and droplet digital PCR for circulating tumor DNA analysis. *Clin. Chem.* **2019**, *65*, 1405–1413. [CrossRef]

ESMO GOOD SCIENCE BETTER MEDICINE BEST PRACTICE

ESMO OPEN CANCER HORIZONS

ORIGINAL RESEARCH

KRAS p.G12C mutation occurs in 1% of *EGFR*-mutated advanced non-small-cell lung cancer patients progressing on a first-line treatment with a tyrosine kinase inhibitor

R. Serna-Blasco[1], E. Sánchez-Herrero[1,2], S. Sanz-Moreno[1], A. Rodriguez-Festa[1], E. García-Veros[1], M. Casarrubios[1], B. Sierra-Rodero[1], R. Laza-Briviesca[1], A. Cruz-Bermúdez[1], X. Mielgo-Rubio[3], A. Sánchez-Hernández[4], E. A. Uribelarrea[5], V. Calvo[6], A. Romero[1,6*] & M. Provencio[1,6*]

[1]Molecular Oncology Laboratory, Biomedical Sciences Research Institute Puerta de Hierro-Majadahonda University Hospital, Majadahonda; [2]Atrys Health, Barcelona; [3]Medical Oncology Department, Hospital Universitario Fundación Alcorcón, Alcorcón, Madrid; [4]Medical Oncology Department, Hospital Provincial Centre de Castelló, Castellón de la Plana, Castellón; [5]Medical Oncology Department, Hospital Universitario de Cruces, Barakaldo, Vizcaya; [6]Medical Oncology Department, Hospital Universitario Puerta de Hierro-Majadahonda, Spain

Available online xxx

Background: *KRAS* is mutated in ∼30% of non-small-cell lung cancer (NSCLC) but it has also been identified as one of the mechanisms underlying resistance to tyrosine kinase inhibitors (TKIs) in *EGFR*-positive NSCLC patients. Novel *KRAS* inhibitors targeting *KRAS* p.G12C mutation have been developed recently with promising results. The proportion of *EGFR*-positive NSCLC tumours harbouring the *KRAS* p.G12C mutation upon disease progression is completely unexplored.

Materials and methods: Plasma samples from 512 *EGFR*-positive advanced NSCLC patients progressing on a first first-line treatment with a TKI were collected. The presence of *KRAS* p.G12C mutation was assessed by digital PCR.

Results: Overall, *KRAS* p.G12C mutation was detected in 1.17% of the samples ($n = 6$). In two of these cases, we could confirm that the KRAS p.G12C mutation was not present in the pre-treatment plasma samples, supporting its role as an acquired resistance mutation. According to our data, $KRAS^{G12C}$ patients showed similar clinicopathological characteristics to those of the rest of the study cohort and no statistically significant associations between any clinical features and the presence of the mutation were found. However, two out of six $KRAS^{G12C}$ tumours harboured less common *EGFR* driver mutations (p.G719X/p.L861Q). All $KRAS^{G12C}$ patients tested negative for the presence of p.T790M resistance mutation.

Conclusions: The *KRAS* p.G12C mutation is detected in 1% of *EGFR*-positive NSCLC patients who progress on a first line with a TKI. All $KRAS^{G12C}$ patients were negative for the presence of the p.T790M mutation and they did not show any distinctive clinical feature.

Key words: *KRAS*, G12C, NSCLC, *EGFR*

INTRODUCTION

KRAS is the most frequently mutated oncogene in human cancers being mutated in ∼30% of non-small-cell lung cancer (NSCLC).[1] It encodes a guanosine triphosphatase (GTPase) that in its active form [guanosine triphosphate (GTP)-bound] promotes cell proliferation. Mutated *KRAS* cannot return to the inactive guanosine diphosphate (GDP)-bound form leading to uncontrolled cell growth and proliferation.[2] NSCLC patients harbouring *KRAS* mutations constitute a heterogeneous group which have been associated to tobacco consumption and limited survival outcomes as well as resistance to *EGFR* tyrosine kinase inhibitors (TKIs).[1,3,4]

For more than three decades, the development of targeted therapies against *KRAS* mutant tumours has been largely unsuccessful.[1,5] Nevertheless, studies focusing on the potentially druggable *KRAS* p.G12C mutation have reported encouraging results.[6,7] This mutation, which causes

*Correspondence to: Dr Atocha Romero, Medical Oncology Department, Hospital Universitario Puerta de Hierro Hospital, Calle Joaquín Rodrigo, 1, 28222 Majadahonda, Madrid, Spain. Tel: +0034911917769
E-mail: atocha10@hotmail.com (A. Romero).
@LiquidBiopsyLab
*Dr Mariano Provencio, Medical Oncology Department, Hospital Universitario Puerta de Hierro Hospital, Calle Joaquín Rodrigo, 1, 28222 Majadahonda, Madrid, Spain. Tel: +0034655070914
E-mail: mprovenciop@gmail.com (M. Provencio).
@MARIANOPROVENCI

the replacement of glycine by cysteine at 12 position, promotes active state of the *KRAS* protein triggering proliferation and it is found in 13% of lung adenocarcinomas being the most frequent variant in NSCLC.[8] Specific *KRAS* p.G12C inhibitors are small molecules that bind irreversibly to the cysteine at residue 12, keeping *KRAS* at its inactive state.[9]

Nowadays, several direct $KRAS^{G12C}$ inhibitors have been developed and they are at different stages of clinical study. The first molecule developed AMG50 (sotorasib)[7] has reported promising results from the phase I trial conducted in patients with heavily pre-treated advanced NSCLC harbouring the *KRAS* p.G12C mutation.[10] In addition, a single-arm, phase II trial has recently reported a 37% response rate and 80% disease control rate in p.G12C-mutated advanced NSCLC previously treated with standard therapies.[11] Similarly, the covalent MRTX849 has shown antitumour activity in cell line- and patient-derived xenograft models from different cancer types harbouring *KRAS* p.G12C mutation.[12,13] Likewise, there are two novel inhibitors JNJ-74699157 and LY3499446 which are tested under phase I trials.

KRAS mutations have also been identified as an underlying mechanism of resistance to TKIs in *EGFR*-positive NSCLC.[14] However, the role of *KRAS* inhibitors after treatment failure with a TKI in *EGFR*-positive NSCLC is completely unexplored.

The aim of this study is to assess the prevalence of *KRAS* p.G12C mutation after progression to a first-line TKI in *EGFR*-positive NSCLC patients with advance disease. To this aim, the presence of *KRAS* p.G12C mutation was tested in 512 plasma samples collected upon disease progression analysed by digital PCR (dPCR).

MATERIALS AND METHODS

Patients and samples

This is an observational study in which plasma samples from 512 NSCLC patients were analysed by dPCR. The study was approved by the ethical committee of Hospital Puerta de Hierro, Madrid, Spain (internal code: PIE14/0064 and PI 178-18) and was conducted in accordance with the precepts of the Code of Ethics of The World Medical Association (Declaration of Helsinki). Briefly, eligibility criteria included patients aged $\geq$18 years, with stage IV *EGFR*-positive NSCLC, who were progressing on a first-line treatment with a TKI. Samples from patients in whom progression was clinically suspected but not confirmed were also accepted. All patients provided the appropriate signed informed consent.

Between 2015 and 2019, 512 samples were collected upon disease progression to a TKI, in an 8.5-ml PPT™ tubes (Becton Dickinson, Franklin Lakes, NJ). Plasma was isolated after two consecutive centrifugations. Specifically, samples were centrifuged at 1600*g* for 10 min at room temperature followed by a second centrifugation round at 6000*g* for 10 min. Circulating cell-free DNA (cfDNA) was isolated using a minimum starting volume of 3.5 ml of plasma and using the cfDNA QIAmp Circulating Nucleic Acid Kit (Qiagen®, Valencia, CA) following manufacturer's protocol.

dPCR analysis

KRAS p.G12C mutation status was analysed by dPCR using predesigned TaqMan® dPCR assays in a QuantStudio® 3D Digital PCR (Applied Biosystems®, South San Francisco, CA). dPCR reaction was carried out in a final volume of 18 µl; this reaction included 8.55 µl of template cfDNA, 9 µl of 20X QuantStudio® Master Mix (ThermoFisher Scientific®, Palo Alto, CA) and 0.45 µl of 40X TaqMan assay (ThermoFisher Scientific®). Subsequently, 14.5 µl of final reaction volume was loaded to QuantStudio® 3D Digital PCR 20K Chip (ThermoFisher Scientific®). Thermal cycler conditions were: initial denaturalisation at 96°C for 10 min, 40 cycles at 56°C for 2 min, 98°C for 30 s and finally 60°C for 2 min and were maintained at 22°C for at least 30 min. Chips were read using QuantStudio® 3D Digital PCR instrument (ThermoFisher Scientific®). Results were analysed with QuantStudio® 3D AnalysisSuite™ Cloud (ThermoFisher Scientific®). Default call assignments for each data cluster were manually adjusted when needed. Positive and negative controls were included in every run.

Mutant allele frequency (MAF) was defined as number of mutant molecules at a specific nucleotide location relative to the sum of total DNA molecules [mutant + wild type (wt)].

For sensitivity assays, DNA from a fresh tumour sample carrying the *KRAS* p.G12C mutation (as reported in the pathologist's report) was mixed at different allele concentrations (i.e. 1%, 0.5%, 0.1% and 0.05%) with wt DNA extracted from peripheral blood cells from healthy donors. The limit of detection (LOD) and limit of quantification (LOQ) were calculated based on the standard deviation (SD) of the response and the slope according to International Conference on Harmonisation Q2 (R1) guideline. The SD of the response was calculated based on standard error of the y-intercept.

Statistics

Discrete variables are presented as frequencies and proportions, and continuous variables as means and SDs. Associations between *KRAS* p.G12C mutation status and clinicopathological variables were assessed using Fisher's exact test or chi-square test according to which was most appropriate. The threshold of $P < 0.05$ was considered as statistically significant. Statistical software used was Stata v16.0 (StataCorp 2019, Stata Statistical Software Release 16, StataCorp LLC, College Station, TX). For survival analysis, median follow-up was estimated using reverse Kaplan—Meier method. Median overall survival (OS) and progression-free survival (PFS) were evaluated using Kaplan—Meier survival function. For OS analysis, time from the start of treatment with the first-line TKI to exitus or loss of follow-up was obtained, whereas for PFS, time was defined as the time from the start of treatment with the first-line TKI to disease progression, assessed by RECIST (Response Evaluation Criteria in Solid Tumours) criteria v1.1.

RESULTS

Frequency of KRAS p.G12C mutation upon treatment failure with a TKI

Clinical and epidemiologic characteristics of the 512 patients included in the study are presented in Table 1. The study population comprised mainly of females (64.45%) and never smokers (58.4%). The main histology was adenocarcinoma (93.36%). Regarding *EGFR* driver mutations, 90.74% were deletions in exon 19 or point mutations in exon 21 (56.77% and 33.97%, respectively). Mutations in exons 18 and 20 were also detected (3.56% and 5.23%, respectively). In two cases (0.48%), more than one driver mutation was detected. The p.T790M resistance mutation was present in 159 samples (31.83%).

The mean age at stage IV diagnosis was 66.17 years (192 patients with available data). First-line TKI was known for 193 patients with the following frequencies: 43.52% (n = 84) of the patients were treated with afatinib, 33.16% (n = 64) with gefitinib and 23.32% (n = 45) with erlotinib. Regarding metastases location at stage IV diagnosis, data were available for 190 patients, 50% (n = 95) of them showed local metastases, 31.05% (n = 59) had bone metastases, 18.42% (n = 35) presented metastases at central nervous system (CNS) and 13.16% (n = 25) showed liver metastases. Information about progression sites after first-line TKI treatment was available for 84 patients; among these patients, 63.10% (n = 53) presented progression disease at thoracic location and 26.19% (n = 22), 20.24% (n = 17) and 16.67% (n = 14) showed progression evidence at bone, CNS and liver, respectively. Finally, regarding second-line treatment, data were available for 99 patients, 51.52% (n = 51) of them received osimertinib, 21.21% (n = 21) were treated with first-/second-generation TKI, 18.18% (n = 18) received chemotherapy and 5.05% (n = 5), 3.03% (n = 3) and 1.01% (n = 1) received palliative care, immunotherapy and antiangiogenic agents, respectively.

The presence of the *KRAS* p.G12C mutation was evaluated in all samples. Only six samples (1.17%) were positive for this mutation (named as cases A-F) (Table 2) with an average MAF of 5.47% (SD: 8.08; min: 0.18%; max: 18.05%). In two (case E and F) of the six $KRAS^{G12C}$ patients we were able to analyse the pre-treatment plasma samples which resulted negative in both cases supporting that *KRAS* p.G12C mutation arose as a consequence of treatment failure. As presented in Table 1, patients in whom the *KRAS* p.G12C mutation was detected had similar characteristics to those of the global study population and no statistically significant associations were found between both populations. In this way, the majority of $KRAS^{G12C}$ patients were women (83.33%) and non-smokers (66.67%) with adenocarcinoma (100%), the mean age of diagnosis being 59.93 years. $KRAS^{G12C}$ patients were treated with afatinib (50%), gefitinib (33.33%) and erlotinib (16.67%). Half of the patients were of stage IVB and two cases harbour the uncommon *EGFR* mutations p.L861Q and p.G719X. All $KRAS^{G12C}$ samples were p.T790M negative. As second-line treatment, three patients were treated with chemotherapy and other patient received immunotherapy. Finally, survival data were available for five of six patients, and the median follow-up for those patients was not reached (NR) (29.8-NR). The median PFS and OS were 18.5 months (95% CI: 5.2-NR) and 43.7 months (95% CI: 14-NR), respectively (Table 2).

Table 1. Clinicopathological characteristics of the study cohort according to KRAS p.G12C mutation

Clinicopathological characteristics	*KRAS* p.G12C		*P* value
	Non-mutated (n = 506)	Mutated (n = 6)	
Age, mean (SD), years[a]	66.37 (10.99)	59.93 (7.66)	0.328
Sex, *n* (%) with data			
Female	325 (64.23)	5 (83.33)	0.430
Male	181 (35.77)	1 (16.67)	
Smoking, *n* (%) with data			
Never smoker	295 (58.30)	4 (66.67)	0.392
Former smoker	174 (34.39)	1 (16.67)	
Active smoker	37 (7.31)	1 (16.67)	
Histology, *n* (%) with data			
Adenocarcinoma	472 (93.28)	6 (100)	1.000
Adenosquamous	17 (3.36)	0 (0)	
Large cell	7 (1.38)	0 (0)	
Undifferentiated	9 (1.78)	0 (0)	
Other	1 (0.20)	0 (0)	
First-line TKI, *n* (%) with data			
Afatinib	81 (16.01)	3 (50)	1.000
Erlotinib	44 (8.70)	1 (16.67)	
Gefitinib	62 (12.25)	2 (33.33)	
NA	319 (63.04)	0 (0)	
Metastases location at stage IV, *n* (%) with data			
Local	94 (18.58)	1 (16.67)	0.621
Bone	59 (11.66)	0 (0)	0.312
CNS	34 (6.72)	1 (16.67)	0.560
Liver	24 (4.74)	1 (16.67)	0.434
NA	320 (63.24)	3 (50)	
EGFR mutation, *n* (%) with data			
Common	385 (76.09)	4 (66.67)	0.062
Uncommon	28 (5.53)	2 (33.33)	
NA	93 (18.38)	0 (0)	
EGFR p.T790M mutation, *n* (%) with data			
Non-mutated	341 (67.39)	6 (100.00)	0.184
Mutated	162 (32.02)	0 (0)	
NA	3 (0.59)	0 (0)	
Second-line treatment, *n* (%) with data			
First-/second-generation TKI	21 (4.15)	0 (0)	0.007
Antiangiogenic	1 (0.2)	0 (0)	
Immunotherapy	2 (0.4)	1 (16.67)	
Osimertinib	51 (10.08)	0 (0)	
Palliative care	5 (0.99)	0 (0)	
Chemotherapy	15 (2.96)	3 (50)	
NA	411 (81.23)	2 (33.33)	
Progression site, *n* (%) with data			
Local	52 (10.28)	1 (16.67)	0.552
Bone	22 (4.35)	0 (0)	0.563
CNS	16 (3.16)	1 (16.67)	0.497
Liver	12 (2.37)	2 (33.33)	0.071
NA	425 (83.99)	3 (50)	

CNS, central nervous system; *EGFR*, epidermal growth factor receptor; NA, not available; SD, standard deviation; TKI, tyrosine kinase inhibitor.
[a] Three hundred and twenty patients without information (all belong to the non-mutated group).

Assay performance

Measured *KRAS* p.G12C MAFs correlated with their theoretical expected frequencies (Pearson's correlation

Table 2. Clinical features of the six *KRAS*^{G12C} patients

	KRAS^{G12C} cases					
	A	B	C	D	E	F
Smoking status	Never smoker	Never smoker	Never smoker	Former smoker	Never smoker	Active smoker
Cigarettes/day						10
Sex	Female	Female	Female	Male	Female	Female
Previous cancer	No	NA	Testicle	NA	No	No
Age at diagnosis (years)	63	67	48	58	56	68
Histology	Adenoca.	Adenoca.	Adenoca.	Adenoca.	Adenoca.	Adenoca.
Metastasis location at stage IV diagnosis	Multiple brain metastases	NA	Liver	NA	NA	Extrathoracic lymph nodes | lung metastasis | adrenal glands |
Diagnosis stage	IVB	IVA	IVB	IVA	IVA	IVB
EGFR mutation	ExDel19	ExDel19	G719X	ExDel19	ExDel19	L861Q
First-line TKI treatment	Gefitinib	Erlotinib	Afatinib	Gefitinib	Afatinib	Afatinib
First-line TKI start date	16 March 2015	05 October 2012	27 June 2017	NA	04 February 2019	18 January 2018
First-line progression	Yes	Yes	Yes	Yes	Yes	Yes
First-line progression date	23 July 2018	23 January 2018	29 November 2017	09 November 2017	13 August 2020	04 January 2019
Progression-free survival (months)	40.8	64.5	5.2	NE	18.5	11.7
Toxicity	No	NA	Diarrhoea | skin	NA	NA	Diarrhoea | skin
Radiotherapy	NA	NA	No	NA	NA	No
Second-line TKI start date	15 August 2018	15 March 2018	19 December 2017		24 August 2020	—
Second-line TKI treatment	Nivolumab	CT	CT (CDDP + MTA)	—	CT	—
Second-line progression	Yes	Yes	Yes	—	Yes	—
Second-line progression date	17 October 2018	25 March 2019	27 March 2018	—	30 June 2021	—
Progression site	Brain	NA	Liver	NA	NA	Liver | thoracic node | lung metastasis
Exitus	Yes	Yes	Yes	NA	Yes	Yes
Exitus date/last date follow-up	17 October 2018	25 March 2019	20 August 2018	—	16 July 2021	29 April 2019
Overall survival (months)	43.7	78.7	14	NE	29.8	15.5

Adenoca, adenocarcinoma; CDDP, cisplatin; MTA, pemetrexed; NA, not available; NE, not estimated; CT, chemotherapy.

coefficient 0.997). LOD and LOQ for *KRAS* p.G12C assays were 0.414% and 1.255% (Figure 1), respectively. LODs were estimated for samples with an average of 300 copies/ml of wt DNA. Additionally, 10 wt cfDNA from healthy donors were used to evaluate the false-positive signals. *KRAS* p.G12C mutation was not detected in any of the wt samples.

DISCUSSION

The development of targeted therapies against the *KRAS* p.G12C mutation is shifting the paradigm in the treatment of advanced NSCLC. However, this mutation is not assessed routinely in many clinical laboratories. Nevertheless, the identification of patients, who might benefit from a *KRAS* inhibitor, is crucial to plan treatment strategies. *KRAS* functions downstream of *EGFR* and it is a known mechanism underlying *EGFR*-TKI tumour resistance.[14] It is well established that constitutive activation of *KRAS*, due to oncogenic mutations, activates *EGFR* pathway regardless of the *EGFR* status. Therefore, *KRAS*-mutated tumours are not expected to respond to *EGFR* blockade.[15] *MEK* (mitogen-activated protein kinase kinase) is a downstream effector of the Ras GTPase encoded by *KRAS*[16] and its activation plays a key role in intrinsic and acquired resistance to drugs targeting *EGFR*.[17] In this way, co-targeting *MEK* and *EGFR* has been shown to overcome third-generation *EGFR*-TKI resistance.[18] However, whether dual targeting of *KRAS* and *EGFR* may overcome drug resistance mutation or delay treatment failure in *EGFR*-positive NSCLC patients remains unknown. In this way, pre-clinical models suggest that blocking *EGFR* may reverse resistance to *KRAS* p.G12C.[19] In this scenario, we believe that it is of clinical interest to determine how often the *KRAS* p.G12C mutation arose after treatment failure with a TKI in *EGFR*-positive NSCLC patients and whether targeting both mutations could improve survival in this subset of patients.

To our knowledge, this is the first study assessing the frequency of *KRAS* p.G12C mutation in *EGFR*-positive NSCLC patients upon disease progression. Noteworthy, recent studies focused on *KRAS* p.G12C mutation incidence exclude the *EGFR*-positive NSCLC population.[20] Therefore, whether these patients could benefit from a *KRAS* inhibitor as a second-line treatment or concomitant to first-line *EGFR*-TKI is completely unexplored.

Overall, *KRAS* p.G12C is estimated to be mutated in 12% of all NSCLC.[21,22] In our patient cohort, only 1.17% ($n = 6$) of *EGFR*-positive NSCLC tumours carried the *KRAS* p.G12C mutation upon disease progression. Of note, 512 samples were analysed. Unfortunately, we were unable to identify any clinical feature associated with the presence of the *KRAS* p.G12C mutation. Yet, the *KRAS* p.G12C mutation appears to be more frequent in younger patients (median age 60 versus 66 years) whose tumours harbour less common *EGFR* mutations such as the p.G719X or the p.L861Q

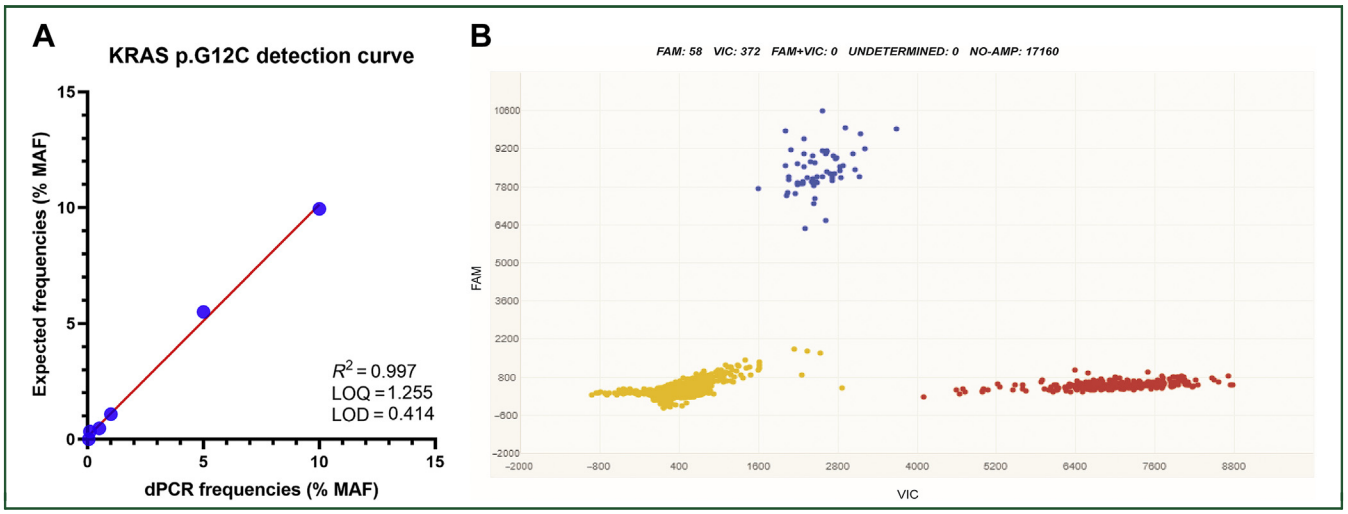

Figure 1. KRAS p.G12C detection.
(A) Calibration curve. Observed frequencies showed consistent correlation with expected frequencies (R^2 = 0.997). Limit of detection (LOD) was 0.414 and limit of quantification (LOQ) was 1.255. (B) Dot-plot from the digital PCR (dPCR) assay. Positive detection of p.G12C variant with 13% mutant allele frequency (MAF): mutated alleles were recognised by FAM probe and correspond to blue data points, while wild-type alleles are detected by VIC probe and are displayed as red dots. Yellow dots represent empty wells (no amplification).

mutations. These results suggest that dual targeting of *EGFR* and *KRAS* might benefit a small proportion of patients (1% of *EGFR*-positive NSCLC patients). This information might be useful for sample size estimations in clinical trials addressing the efficacy of dual or consecutive *EGFR* and *KRAS* blockage. Remarkably, all $KRAS^{G12C}$ tumours tested negative for the presence for the p.T790M mutation. In any case, we cannot derive any solid conclusion given the small number of tumours with *KRAS* p.G12C mutation, but special attention will have to be paid to this population in future studies.

In our study, we did not have the pre-treatment formalin-fixed paraffin-embedded biopsy available for molecular analysis and we could only assess *KRAS* p.G12C status in the plasma sample of two of the six positive cases, which may constitute a limitation of our study. However, in both cases, the mutation was not detected, suggesting that this mutation arose as a resistance mechanism. In this regard, *KRAS* and *EGFR* mutations have been reported to occur very rarely simultaneously and their presence is believed to be mutually exclusive.[23]

In summary, our results indicate that *KRAS* p.G12C occurs in 1% of NSCLC patients progressing to a first-line TKI. Larger cohorts will be needed to identify clinical characteristics of the patients (if any) whose tumour progress through *KRAS* activation. Our results are of particular interest for the design of new clinical trials.

ACKNOWLEDGEMENTS

We wish to thank all the patients and staff who participated in the study.

FUNDING

This work was supported by CLARIFY project (https://www.clarify2020.eu/). ES-H was supported by the Consejería de Ciencia, Universidades e Innovación of the Comunidad de Madrid (Doctorados Industriales of the Comunidad de Madrid) [grant number IND2019/BMD-17258]. EG-V was supported by AECC (Asociación española Contra el Cáncer) grant 'Programa de Prácticas de Laboratorio de curso académico AECC 2020' (no grant number).

DISCLOSURE

VC reports personal fees from Roche, BMS, MSD and Pfizer and other from Lilly, AstraZeneca, Boehringer, Novartis and Takeda during the conduct of the study. AS-H reports personal fees and non-financial support from Roche and personal fees from AstraZeneca and Boehringer, outside the submitted work. AR reports personal fees from Boehringer and Takeda outside the submitted work. MP reports grants, personal fees and non-financial support from BMS, Roche and AstraZeneca and personal fees from MSD and Takeda, outside the submitted work. The remaining authors have declared no conflicts of interest.

REFERENCES

1. Ryan MB, Corcoran RB. Therapeutic strategies to target RAS-mutant cancers. *Nat Rev Clin Oncol*. 2018;15(11):709-720.
2. Santos E, Martin-Zanca D, Reddy E, Pierotti M, Porta GD, Barbacid M. Malignant activation of a K-ras oncogene in lung carcinoma but not in normal tissue of the same patient. *Science*. 1984;223(4637):661-664.
3. Burns TF, Borghaei H, Ramalingam SS, et al. Targeting KRAS-mutant non-small-cell lung cancer: one mutation at a time, with a focus on KRAS G12C mutations. *J Clin Oncol*. 2020;38(35):4208-4218.
4. Chen H, Zhao J. KRAS oncogene may be another target conquered in non-small cell lung cancer (NSCLC). *Thorac Cancer*. 2020;11(12):3425-3435.
5. Jänne PA, Van den Heuvel MM, Barlesi F, et al. Selumetinib plus docetaxel compared with docetaxel alone and progression-free survival in patients with KRAS-mutant advanced non-small cell lung cancer: the SELECT-1 randomized clinical trial. *J Am Med Assoc*. 2017;317(18):1844-1853.

6. Ostrem JM, Peters U, Sos ML, Wells JA, Shokat KM. K-Ras(G12C) inhibitors allosterically control GTP affinity and effector interactions. *Nature*. 2013;503(7477):548-551.
7. Canon J, Rex K, Saiki AY, et al. The clinical KRAS(G12C) inhibitor AMG 510 drives anti-tumour immunity. *Nature*. 2019;575(7781):217-223.
8. Biernacka A, Tsongalis PD, Peterson JD, et al. The potential utility of remining results of somatic mutation testing: KRAS status in lung adenocarcinoma. *Cancer Genet*. 2016;209(5):195-198.
9. Passiglia F, Malapelle U, Del Re M, et al. KRAS inhibition in non—small cell lung cancer: past failures, new findings and upcoming challenges. *Eur J Cancer*. 2020;137:57-68.
10. Hong DS, Fakih MG, Strickler JH, et al. KRAS^{G12C} inhibition with sotorasib in advanced solid tumors. *N Engl J Med*. 2020;383(13):1207-1217.
11. Skoulidis F, Li BT, Dy GK, et al. Sotorasib for lung cancers with KRAS p.G12C mutation. *N Engl J Med*. 2021;384(25):2371-2381.
12. Hallin J, Engstrom LD, Hargi L, et al. The KRASG12C inhibitor MRTX849 provides insight toward therapeutic susceptibility of KRAS-mutant cancers in mouse models and patients. *Cancer Discov*. 2020;10(1):54-71.
13. Jänne PA, Rybkin II, Spira AI, et al. KRYSTAL-1: Activity and safety of adagrasib (MRTX849) in advanced/metastatic non—small-cell lung cancer (NSCLC) harboring KRAS G12C mutation. *Eur J Cancer*. 2020;138:S1-S2.
14. Rotow J, Bivona TG. Understanding and targeting resistance mechanisms in NSCLC. *Nat Rev Cancer*. 2017;17(11):637-658.
15. Amado RG, Wolf M, Peeters M, et al. Wild-type KRAS is required for panitumumab efficacy in patients with metastatic colorectal cancer. *J Clin Oncol*. 2008;26(10):1626-1634.
16. Roberts PJ, Der CJ. Targeting the Raf-MEK-ERK mitogen-activated protein kinase cascade for the treatment of cancer. *Oncogene*. 2007;26(22):3291-3310.
17. Martinelli E, Morgillo F, Troiani T, et al. Cancer resistance to therapies against the EGFR-RAS-RAF pathway: the role of MEK. *Cancer Treat Rev*. 2017;53:61-69.
18. Tricker EM, Xu C, Uddin S, et al. Combined EGFR/MEK inhibition prevents the emergence of resistance in EGFR-mutant lung cancer. *Cancer Discov*. 2015;5(9):960-971.
19. Amodio V, Yaeger R, Arcella P, et al. EGFR blockade reverts resistance to KRASG12C inhibition in colorectal cancer. *Cancer Discov*. 2020;10(8):1129-1139.
20. Sebastian M, Eberhardt WEE, Hoffknecht P, et al. KRAS G12C-mutated advanced non-small cell lung cancer: a real-world cohort from the German prospective, observational, nation-wide CRISP Registry (AIO-TRK-0315). *Lung Cancer*. 2021;154:51-61.
21. Mullard A. Cracking KRAS. *Nat Rev Drug Discov*. 2019;18(12):887-891.
22. Jordan EJ, Kim HR, Arcila ME, et al. Prospective comprehensive molecular characterization of lung adenocarcinomas for efficient patient matching to approved and emerging therapies. *Cancer Discov*. 2017;7(6):596-609.
23. Tam IYS, Chung LP, Suen WS, et al. Distinct epidermal growth factor receptor and KRAS mutation patterns in non—small cell lung cancer patients with different tobacco exposure and clinicopathologic features. *Clin Cancer Res*. 2006;12(5):1647-1653.

Campos-Silva *et al.*
Journal of Nanobiotechnology (2022) 20:72
https://doi.org/10.1186/s12951-022-01256-5

Journal of Nanobiotechnology

RESEARCH

Open Access

A simple immunoassay for extracellular vesicle liquid biopsy in microliters of non-processed plasma

Carmen Campos-Silva[1], Yaiza Cáceres-Martell[1], Estela Sánchez-Herrero[2,3], Amaia Sandúa[4], Alexandra Beneitez-Martínez[5], Álvaro González[4], Mariano Provencio[2,6], Atocha Romero[2,6], Ricardo Jara-Acevedo[5], María Yáñez-Mó[7,8] and Mar Valés-Gómez[1*]

Abstract

Background: Extracellular vesicles (EVs), released by most cell types, provide an excellent source of biomarkers in biological fluids. However, in order to perform validation studies and screenings of patient samples, it is still necessary to develop general techniques permitting rapid handling of small amounts of biological samples from large numbers of donors.

Results: Here we describe a method that, using just a few microliters of patient's plasma, identifies tumour markers exposed on EVs. Studying physico-chemical properties of EVs in solution, we demonstrate that they behave as stable colloidal suspensions and therefore, in immunocapture assays, many of them are unable to interact with a stationary functionalised surface. Using flocculation methods, like those used to destabilize colloids, we demonstrate that cationic polymers increase EV ζ-potential, diameter, and sedimentation coefficient and thus, allow a more efficient capture on antibody-coated surfaces by both ELISA and bead-assisted flow cytometry. These findings led to optimization of a protocol in microtiter plates allowing effective immunocapture of EVs, directly in plasma without previous ultracentrifugation or other EV enrichment. The method, easily adaptable to any laboratory, has been validated using plasma from lung cancer patients in which the epithelial cell marker EpCAM has been detected on EVs.

Conclusions: This optimized high throughput, easy to automate, technology allows screening of large numbers of patients to phenotype tumour markers in circulating EVs, breaking barriers for the validation of proposed EV biomarkers and the discovery of new ones.

Keywords: Extracellular vesicles, Cancer, Colloids, Flocculation, ELISA, Flow cytometry, Liquid biopsy

*Correspondence: mvales@cnb.csic.es
[1] Department of Immunology and Oncology, Spanish National Centre for Biotechnology, CNB-CSIC, Madrid, Spain
Full list of author information is available at the end of the article

Graphical Abstract

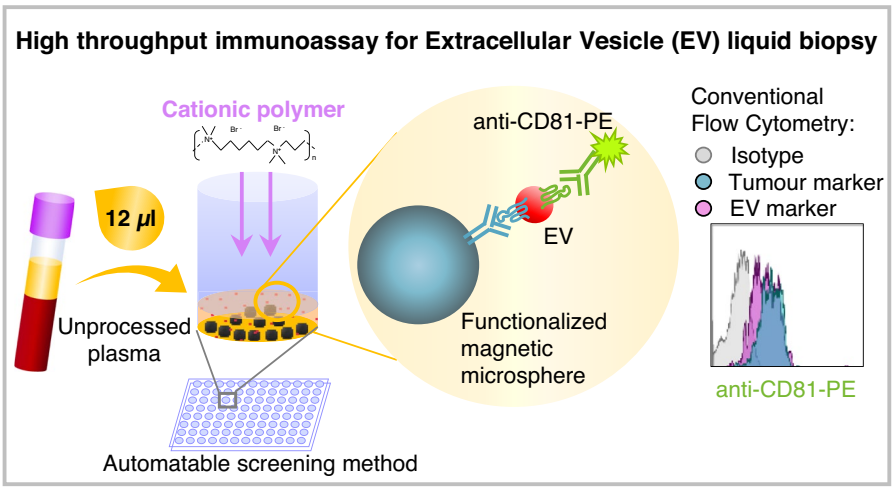

Background

During their normal life cycle, cells can release different types of vesicles originated from a variety of processes involving membrane invaginations and pinching-off events [1]. Thus, in biological fluids, different types of extracellular vesicles (EVs) can be found, providing information of the different physio-pathological processes occurring in any individual and allowing trafficking of diverse subcellular components which can act as mediators in the exterior milieu [2–4]. Exosomes are one type of such extracellular nanovesicles, generated from the endocytic pathway. Since vesicle cargo reflects cell composition, EVs are regarded as a potential useful tool displaying biomarkers and so, they have attracted great attention from scientists, clinicians and biotechnological companies recently [5–9].

Multiple candidate EV biomarkers have been suggested for different pathologies, however, for a routine translation into the clinics, high throughput comparative studies are still necessary to define the suitability of each particular biomarker in a given disease context. Such association studies, requiring the analysis of samples from large patient cohorts, are hampered by currently available methods which require either relatively large sample volumes or long protocols of nanovesicle pre-enrichment together with the use of sophisticated equipment or specialised personnel [10–13]. The development of nanosensors makes possible to specifically detect EVs using small sample volumes from large numbers of patients [14–16], but these new technologies require purpose-designed devices assembled in specialised laboratories and, data derived from this type of study are still scarce. Thus, carrying out large screening projects studying EVs in a research or clinical setting would require the adaptation of widely used techniques to allow the identification of vesicles in small volumes and with minimal sample manipulation. An extra level of complication arises from the fact that any biological fluid contains EVs from many cellular origins and samples can be very heterogeneous [17]. Therefore, marker selection is paramount for the characterization of the composition, number and size of the different vesicle subpopulations that can be released by any cell [2, 18–21].

To simplify the detection of EV proteins using a technique readily available in most clinical settings, we recently defined the critical parameters for improved flow cytometry detection of EVs after immunocapture [22]. To further improve these assays, we explored here the hypothesis that EVs are stable in suspension with the physico-chemical properties of colloids, in which EVs would correspond to the disperse phase and the buffer to the solvent of a colloidal suspension [23–25]. In a colloidal suspension the particles do not sediment as a consequence of gravity, instead they move erratically in such a manner that the electrostatic repulsion is significantly larger than the thermal energy, and molecular attraction forces, such as van der Waals, do not prevail [25]. This could limit the encounter with functionalised surfaces, such as antibodies on micro-beads, that, in contrast to EVs, would rapidly sediment to the bottom of the tube. If this hypothesis is true, destabilising the EVs suspension might increase the detection capacity in immunocapture experiments.

The stability of colloid suspensions has been studied in detail, in particular in several industrial settings such as

wastewater treatment. Depletion mechanisms and other destabilising factors including the addition of external particles, such as polymers, cause precipitation of the colloidal suspension, an effect known as flocculation [26, 27].

Here we analysed the effects on EV suspensions of two cationic polymers: poly-L-lysine (PL) and hexadimethrine bromide (PB) (polybrene, commercial brand name) commonly used to increase the efficiency of drug and virus delivery to cells via aggregation, sedimentation and adsorption [28]. We demonstrate that the addition of positively charged polymers to EV suspensions leads to the precipitation of vesicles and enhanced antibody capture of EVs in both ELISA and bead-based assays.

Thus, by taking advantage of the colloidal properties of EVs, we have developed a method combining cationic polymers with the maximization of EV-surface contact to directly phenotype tumour antigens contained in nanovesicles from patient biological samples. Using immunocapture in bead-assisted flow cytometry, tumour markers were easily detected in only a few microliters of body fluids, without previous ultracentrifugation or enrichment of vesicles. These new experimental conditions, that radically improve the efficiency of EV detection in immunocapture assays, open new possibilities for the study of samples from large cohorts of patients and controls with minimal effort in any laboratory setting.

Results

Standard antibody-binding conditions are not 100% efficient for the capture of extracellular vesicles

We have recently described a high sensitivity method for immunocapture and detection of EVs by flow cytometry, based on the use of antibody-coated beads followed by detection with a labelled antibody [22, 29]. During the optimisation of that method, we calculated the theoretical number of EVs that would bind the antibody-coated microspheres and analysed the saturation curve in experiments with increasing amounts of EVs. Although 6000 beads could theoretically bind 3.85×10^7 EVs, our experimental data showed that saturation of detection occurred when around 3.6×10^9 EVs (NTA measurement) were offered, suggesting that the beads were not capturing all the EVs that were present in the incubation mix. NTA measurement may overestimate the number of EVs, since the instrument does not discriminate protein aggregates from EVs, but a 2-log error in quantitation seemed improbable. Alternatively, since EVs are usually a heterogeneous mix, it could be possible that not all the EVs in the mixture contained the epitope for the capture antibody. To directly test these possibilities, nested rounds of incubations were carried out. EVs derived from a melanoma cell line were characterised (Fig. 1A–C) following MISEV2018 guidelines [30] and incubated with anti-CD63-coated beads for flow cytometry analysis. The supernatant from the first incubation was recovered and used with fresh anti-CD63-coated beads for successive rounds of flow cytometry analysis, until signal was minimal. Melanoma EVs were still detected on supernatants after several rounds of capture using anti-CD63-coated beads (Fig. 1D), suggesting that not all the EVs carrying the epitope were captured in a single step. We could observe the same behaviour with EV samples from different cell lines (Additional file 1: Fig. S1).

EVs in solution form stable colloidal suspensions, which are destabilised using charged polymers

Agitation did not improve the efficiency of EV binding to beads, while a long incubation time was crucial for good detection [22]. Thus, we decided to explore whether a more efficient capture of EVs could be achieved by affecting the physico-chemical properties of EVs. Because of their nanometric size, EV preparations could be considered colloidal suspensions, where EVs are stabilised in solution by steric (they are covered by proteins that would act as a solvated layer or halo) and electrostatic (amino acid and lipid charges) factors. Indeed, different methods initially developed for colloids, such as NTA, are used to characterise EV preparations [31, 32]. Thus, experiments to assess the colloidal behaviour of EVs were carried out including their stability versus flocculation properties.

In order to evaluate the effect of depletion forces, several biophysical parameters were analysed after incubation of melanoma-derived EV suspensions with two cationic polymers, commonly employed in biology for precipitation of nanometric structures [28]: hexadimethrine bromide (polybrene) and poly-L-lysine. First, the diameter and ζ-potential of metastatic melanoma derived EVs obtained by ultracentrifugation were measured by Dynamic Light Scattering (DLS) (NanoZS) (Fig. 2A). Melanoma-derived EVs usually have a negative ζ-potential and this parameter can be used as an approximation to evaluate colloidal stability, since electrostatic repulsion prevents aggregation [33]. When resuspended in regular isosmotic buffer, melanoma-derived EVs had, on average, a diameter of 196.5 nm by NTA. DLS readings of ζ-potential were − 15.27 mV in average, while diameter measurements render a higher value of 302.97 nm with this technique. Interestingly, when EVs were incubated with 4–8 μg/ml of either polybrene or poly-L-lysine for 5 min, the ζ-potential of EVs increased to a range between − 9.55 and + 2.65 mV. Similarly, the average diameter of the EV suspension increased dramatically in the presence of the charged polymers when measured by DLS, accompanied by a higher

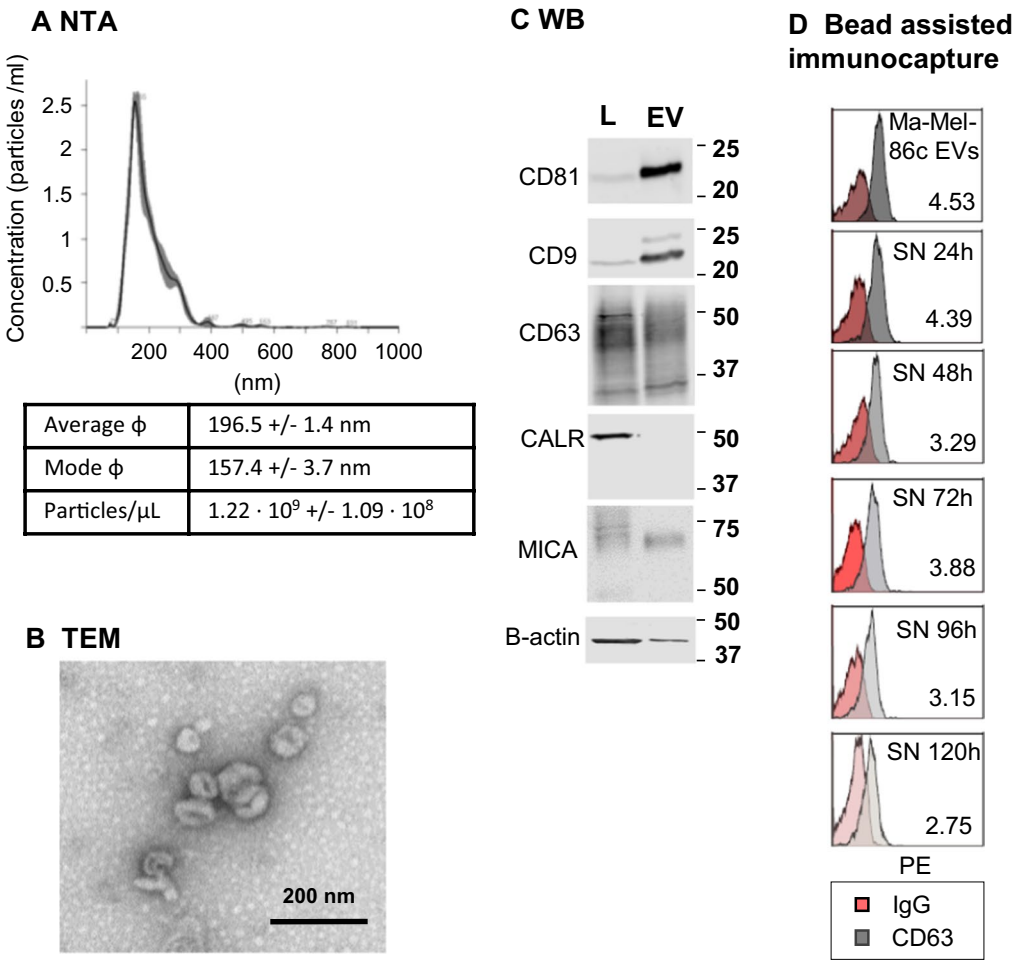

Fig. 1 Repeated incubations are needed to immuno-capture all available EVs. Melanoma-derived EVs (from Ma-Mel-86c cell line) were enriched by ultracentrifugation. **A** Nanoparticle tracking analysis (NTA) of melanoma-derived EVs. Average size and concentration of EVs were obtained in a Nanosight equipment capturing three videos of 60 s per measurement, with camera level 12, threshold 10 and temperature of 25 °C. Software NTA 3.1 (Malvern) was used for the analysis. ϕ: diameter. **B** Transmission Electron Microscopy (TEM). 1 µl EVs were diluted 1:10 in HBS and floated on a carbon-coated 400-mesh 240 Formvar grid, then incubated with 2% uranyl acetate and analysed using a Jeol JEM 1011 electron microscope operating at 245 100 kV with a CCD camera Gatan Erlangshen ES1000W. Pictures were taken at the Electron Microscopy Facility of the CNB. Bar: 200 nm. A representative image is shown. **C** EV characterization by Western Blot. Whole cell lysates (L) and EVs were loaded in 12% SDS-PAGE gels. Membranes were immunoblotted for detection of: tetraspanins CD9, CD63, CD81 as general EV markers; β-actin as loading control; MICA as cancer-related marker; and calreticulin (CALR) as an endoplasmic reticulum resident protein not present in the EV fraction. Two gels were loaded: one gel, under non-reducing conditions and the other under reducing conditions, for actin detection. One representative experiment out of three is shown. **D** EV immuno-capture followed by flow cytometry. 3000 anti-CD63-coated beads [or Isotype (IgG) coated as a negative control] were incubated with 3.5×10^6 Ma-Mel-86c derived EVs/µl in 100 µl (3.5×10^8 EVs/tube). Vesicles were detected by flow cytometry after incubation with anti-CD81-PE. Supernatants from the first incubation (SN 24 h), containing unbound vesicles, were incubated again with fresh anti-CD63 beads and EVs captured during this second incubation were analysed by flow cytometry. This procedure was repeated the following 4 days (SN 48 h, SN 72 h, etc., as indicated). The histograms with the Relative Fluorescence Intensity ($RFI = \frac{MFI\ sample}{MFI\ IgG}$) values from a representative experiment out of three is shown. MFI: mean fluorescence intensity

poly-dispersity index (Additional file 1: Fig. S2). Longer incubation times resulted in bigger ζ-potential or diameter changes only in a few cases (polybrene at 4 µg/ml and poly-L-lysine at 4 µg/ml respectively). The observed trend was also confirmed by NTA (Zetaview technology, Additional file 1: Fig. S3).

Since the diameter and charge data obtained by light scattering methods suggested that polymers could cause aggregation and flocculation of EVs, analytical ultracentrifugation was used to measure the sedimentation rate of nanoparticles in the presence of those positively charged polymers (Fig. 2B). Indeed, the weight

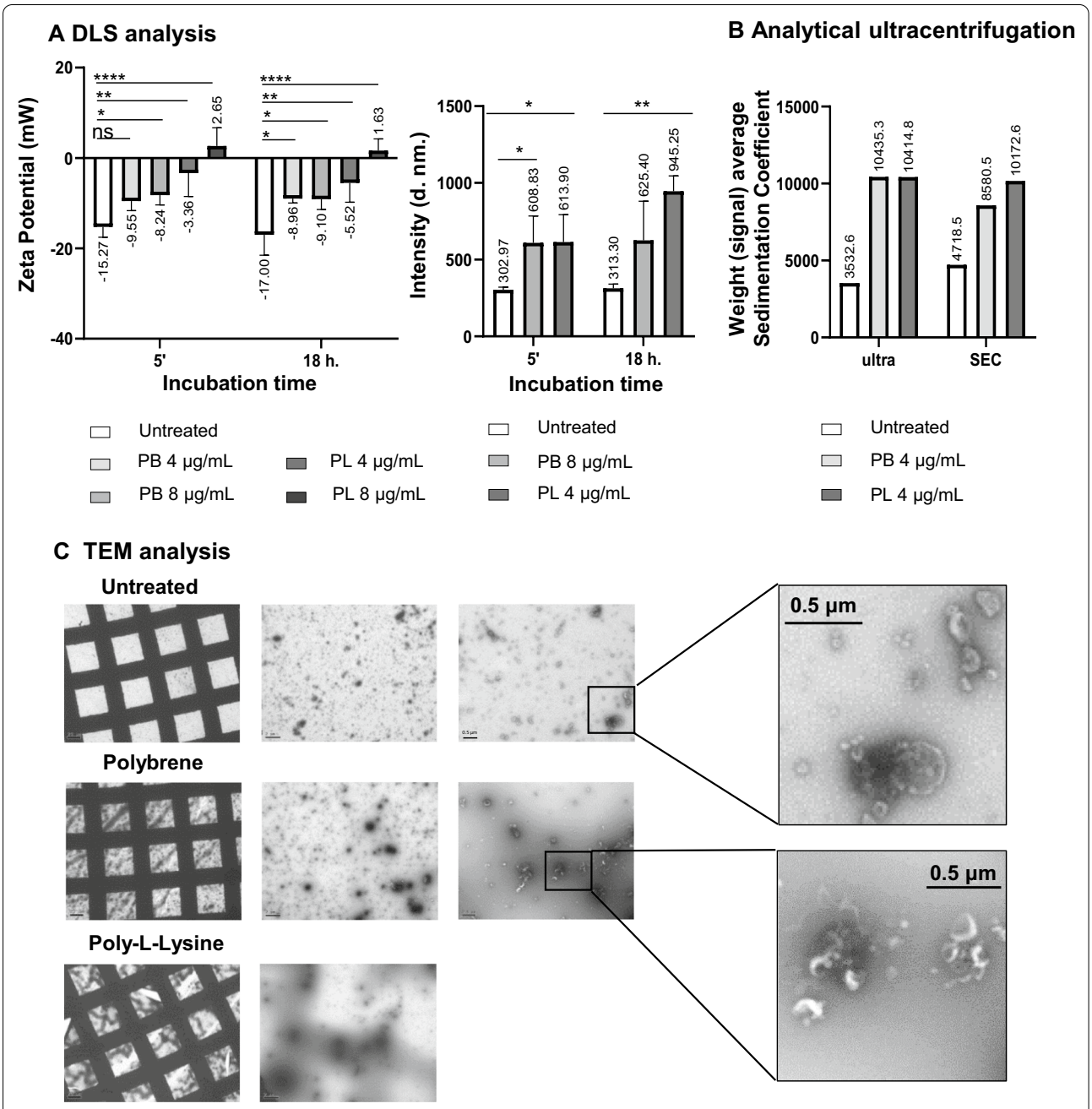

Fig. 2 Cationic polymers affect the biophysical properties of EV suspensions and result in precipitation of the nanoparticles. Metastatic melanoma derived EVs obtained by ultracentrifugation were incubated with or without 4 µg/ml or 8 µg/ml Polybrene (PB) or 4 µg/ml or 8 µg/ml Poly-L-lysine (PL). **A** Zeta Potential and Hydrodynamic diameter by Dynamic Ligh Scattering (DLS). EVs were incubated either 5 min or 18 h with the polymers and analysed using a DLS instrument. Data on Zeta Potential and Intensity Mean (average diameter in nm.) are depicted. Mean and Standard Deviation from three independent experiments is shown. Statistical analysis was performed by a one-way ANOVA Fisher's LSD test ($p < 0.05$). *$p < 0.05$, **$p < 0.01$, ***$p < 0.001$, ****$p < 0.0001$). **B** Analytical ultracentrifugation. The sedimentation coefficient of EVs was analysed either directly after ultracentrifugation (ultra) or after further purification by size exclusion chromatography (SEC). The graph represents data on the weight (signal) average sedimentation coefficient obtained after a 18 h-incubation with polymers of EVs obtained under these two methods. **C** Transmission Electron Microscopy. The left column shows the general aspect of the grid, followed by sequential magnifications [Bar: 2 µm (2nd column), 0.5 µm (3rd and 4th columns)]. Polymers caused precipitation of EV samples, affecting the integrity of the resin upon electron beam incidence. Thus, pictures from Poly-L-Lysine treated samples could not be obtained at high magnification. Electron dense areas correspond to EV aggregates

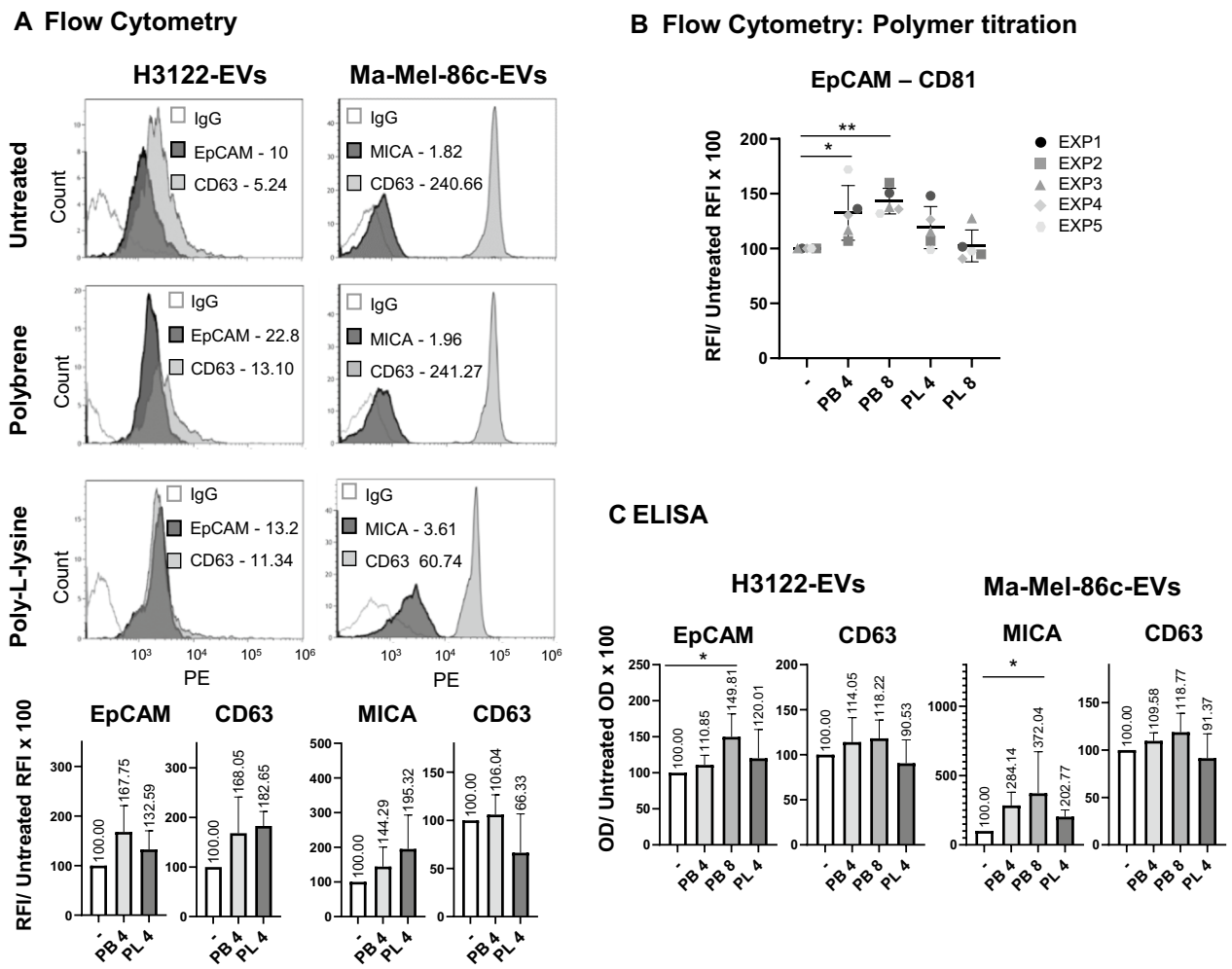

Fig. 3 Cationic polymer addition increased EV detection by flow cytometry and ELISA. Lung cancer-derived EVs (from H3122 cell line) and melanoma-derived EVs (from Ma-Mel-86c cell line) were enriched by ultracentrifugation. 1×10^6 H3122 EVs/µl or 1.8×10^7 Ma-Mel-86c EVs/µl in 100 µl of PBS-Casein 1% were treated with 4 or 8 µg/ml polybrene (PB), 4 or 8 µg/ml poly-L-lysine (PL) or kept untreated for 18 h, as indicated in each panel. **A** Flow Cytometry. EVs were incubated with 3000 of either anti-EpCAM, anti-MICA, anti-CD63 or IgG isotype control beads. Captured vesicles were detected by flow cytometry after incubation with anti-CD81-PE. Histograms from one representative experiment out of 3 are shown in the top panels. Relative Fluorescence Intensity ($RFI = \frac{MFIsample}{MFIIgG}$) values are shown in each plot. Bar plots in the bottom panels represent the change in the RFI relative to the untreated condition. Mean and Standard Deviation from three independent experiments are represented. MFI: Median Fluorescence Intensity. **B** Titration of cationic polymers. Tissue culture supernatant-derived EVs from the lung cancer cell line H3122 were incubated with either 3000 anti-EpCAM or IgG isotype control coated beads in 100 µl final volume of PBS-Casein 1%. EpCAM-captured vesicles were detected by flow cytometry after incubation with anti-CD81-PE. Relative increase of the RFI for EpCAM-CD81 detection, obtained in five experiment replicates (EXP), is shown. Statistical analysis was performed by a Two-way ANOVA Fisher's LSD test. (*$p < 0.05$). **C** ELISA. EVs enriched from tissue culture supernatant of the indicated cell lines were incubated in anti-EpCAM, anti-MICA or anti-CD63 antibody-coated plates. IgG Isotype-coated wells were used as negative control. Detection was performed with biotinylated anti-CD9 antibody followed by SA-HRP. Optical Density (OD) was measured at 450 nm. After subtraction of the negative control, binding relative to the untreated sample is represented. Statistics from three independent experiments are shown: one-way ANOVA Fisher's LSD (*$p < 0.05$; 95% confidence interval). A single representative experiment is shown in Additional file 1: Figure S6

average sedimentation coefficient of the EV suspension obtained by ultracentrifugation increased dramatically in the presence of the charged polymers. To eliminate any possible contribution of proteins co-precipitating with EVs in ultracentrifugation, samples were further purified by SEC, yielding a similar result (Fig. 2B). Interestingly, after an 18-h incubation with cationic polymers, samples presented high polydispersity with multiple peaks displaying a wide range of sedimentation coefficients (Additional file 1: Fig. S4). This implies

that larger particles of different sizes are present in the sample incubated with polymers compared to control samples. In line with these observations, electron microscopy imaging of EVs after an 18-h incubation with cationic polymers revealed large high electron dense structures (1–2 μm), consistent with high mass particles (Fig. 2C). In more detailed images, clusters of EVs could be observed. Inspection at low magnification of the grids already demonstrated the high density masses. In fact, when the electron beam struck high density spots observed in poly-L-lysine-incubated samples, the resin ruptured and high magnification images could not be obtained.

Altogether, these results indicated that adding cationic polymers to EV preparations, generated aggregates of particles of different sizes, leading to higher sedimentation rates, confirming that EV suspensions behave as colloids.

Cationic polymers increase the detection of EV proteins in immunoassays

Since cationic polymers destabilised EV suspensions, increasing the average diameter of the particles and the sedimentation coefficient, we hypothesised that this depletion force phenomenon, described for colloidal systems, could improve EV detection by immuno-capture methods. Thus, we tested how the inclusion of cationic polymers affected the precipitation of nanoparticles on antibody-coated surfaces either in bead-assisted flow cytometry or ELISA experiments. For these experiments, EVs obtained by ultracentrifugation from either the melanoma cell line Ma-Mel-86c or the lung cancer cell line H3122 were used. The characterization of these vesicles was performed first by classical methods including NTA, Western Blot and TEM to establish the tumour markers present on EVs derived from the different tumour cell lines (Fig. 1 and Additional file 1: Fig. S5). Ma-Mel-86c is positive for the tumour-associated immune ligand MICA as reported previously [34], while H3122 expresses the epithelial cell marker EpCAM (Additional file 1: Fig. S5). Enhanced detection of both tetraspanins and tissue-specific markers was observed using 4 μg/ml of either polybrene or poly-L-lysine, as shown in the RFI values (Fig. 3A), except for saturated signals (CD63-CD81 in Ma-Mel-86c EVs). Initial polymer titration experiments revealed that, in general, the best signal was obtained when polybrene was added at 8 μg/ml reaching a significant difference in the signal with respect to the untreated assay (Fig. 3B). Similar results were observed in the settings of a different immunoassay, such as ELISA, with no interference of the polymers in this experimental system either. Titration of different cationic polymers could be considered for optimization in ELISA. (Fig. 3C and Additional file 1: Fig. S6B). These data thus confirmed that the presence of cationic polymers does not interfere with immunodetection assays and suggest that their use could significantly enhance detection of several EV-contained markers after immunocapture.

Optimised immunocapture of EVs allows detection of tetraspanins and tumour-associated proteins directly in plasma from cancer patients

The immunocapture experiments shown above strongly suggest that disruption of EV stability in suspension improves immunodetection by increasing EV availability to bind to antibody-coated surfaces. An alternative way to facilitate the encounter of microbeads and nanometric EVs during the capture step, would be to maximize the contact area by incubating the beads and EVs in a relatively broad surface with minimal volume. To test whether the volume and geometry of the assay could affect the intensity of fluorescence detected, in addition to 5 ml tubes, micro-well plates were used (Fig. 4A) (Additional file 1: Fig. S7). In order to test whether small volumes of sample could still be detected in microtitre plates, the volume was reduced, keeping EV concentration constant (to facilitate the setup of this assay for biological samples tests). Using flat-bottom plates significantly increased detection when compared to 5 ml tubes. In fact, using low volumes in flat plates led to higher detection than using high volumes in 5 ml tubes. Thus, we concluded that reducing sample volume but maintaining EV concentration in flat-bottom plates increased detection signal. The great improvement in signal obtained in such small volumes, suggested that under these conditions this method might have enough sensitivity to directly detect EVs from biological samples. To test this hypothesis, antibodies against tetraspanins were used both for capture and detection in flow cytometry analysis of EVs directly in healthy donor plasma. CD63-CD81 EVs were efficiently captured and detected in plasma without any prior EV enrichment procedure, using as little as 12 μl of sample. Since, tumour-derived antigens are usually less abundant than tetraspanins on EVs, we also checked whether tumour-derived antigens in EVs could be directly detected in plasma using this methodology. As expected, healthy donor plasma was negative for EpCAM (Fig. 4B, left). However, when H3122 lung cancer-derived EVs (positive for EpCAM) were added to a healthy donor plasma sample before the immunocapture experiment (at a final concentration of 6.25×10^7 EVs/μl), the same sample showed a high positive signal for anti-EpCAM beads, as well as an increased signal for tetraspanins (Fig. 4B, right). In order to estimate the amount of EVs that could be recognised using

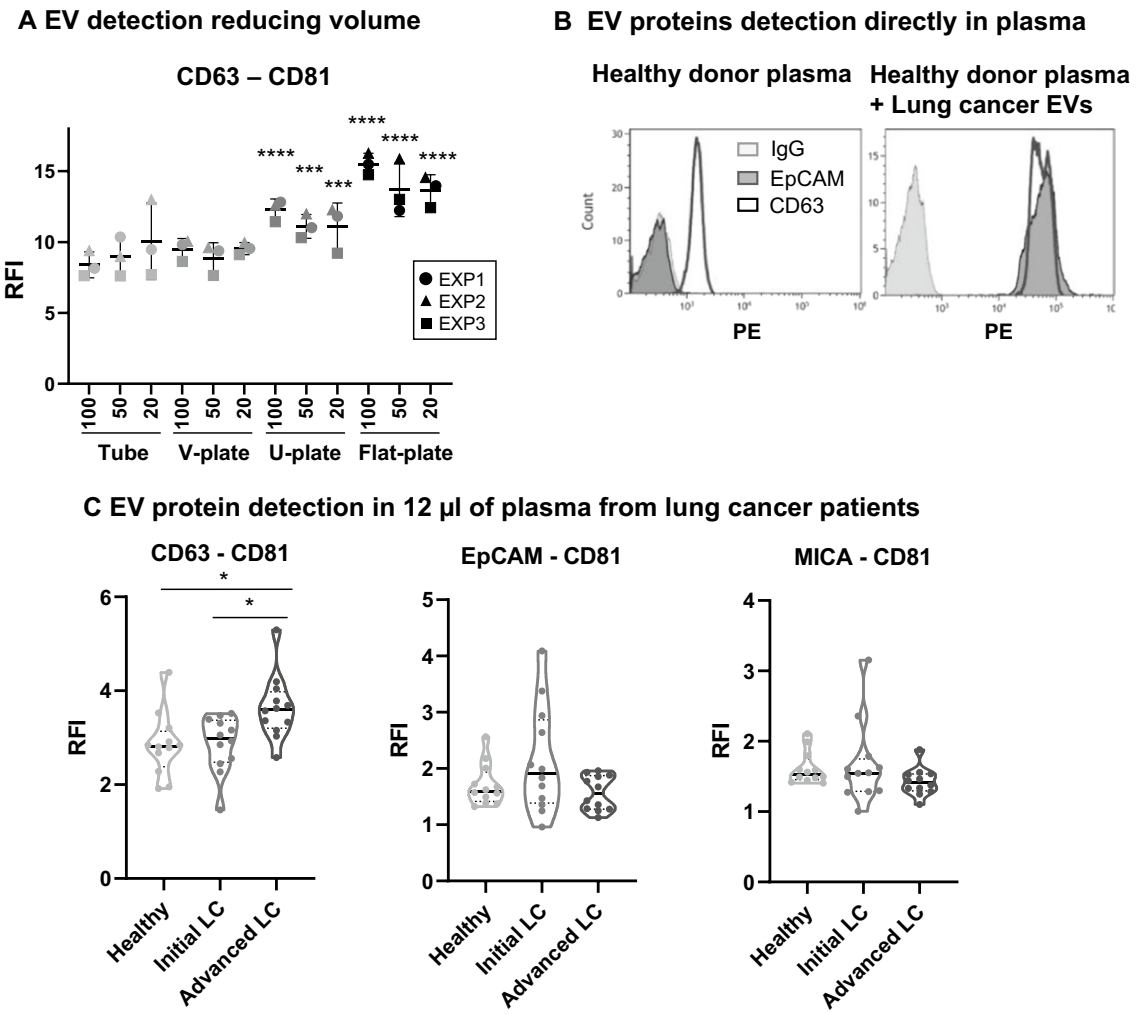

Fig. 4 EV detection in reduced volume of plasma. **A** Comparison of EV detection in decreasing volume. 3000 anti-CD63 beads were used per test in different incubation volumes (100 µl, 50 µl and 20 µl), using either 5 ml tubes or microtiter plates (96-well plates V-bottom, U-bottom or flat bottom, as indicated). Lung cancer-derived EVs (from H3122 cell line) were obtained by ultracentrifugation, incubated with beads for 16 h and, after staining with anti-CD81-PE, washed and analysed by flow cytometry. EV concentration was the same in all the conditions (4×10^6 H3122 EVs/µl). Relative Fluorescence Intensity (RFI) obtained in each condition is represented. Three independent experiments are shown. Statistical analysis was performed by a Two-way ANOVA Fisher's LSD test comparing each condition to the 100 µl tube condition as independent comparisons. (*$p < 0.01$, **$p < 0.01$, ***$p < 0.001$, ****$p < 0.0001$). **B** Detection of EV proteins directly in plasma. 12 µl of healthy donor plasma were incubated with 3000 anti-CD63, anti-EpCAM or IgG isotype control beads in a final volume of 25 µl. Captured EVs were detected with anti-CD81-PE. Left. Detection of EVs directly in 12 µl of healthy donor plasma. Right. 3.14×10^8 H3122-derived EVs (from the H3122 cell line) were added to 12 µl of the same healthy donor plasma (2.6×10^7 H3122 EVs/µl plasma). **C** EpCAM and MICA, can be detected directly in minimal volumes of plasma from a cohort of lung cancer (LC) patients by flow cytometry. 12 µl of PBS-1% casein containing 3000 beads conjugated either with anti-CD63, anti-EpCAM or anti-MICA were incubated for 16 h with 12 µl of plasma (EDTA-tubes) from a cohort of lung cancer patients (12 initial stage and 12 advanced stage) and 12 healthy donors. The final volume of the assay was 24 µl. EVs captured in each assay were detected with anti-CD81-PE, or IgG-PE as a negative control to calculate the Relative Fluorescence Intensity (RFI). The mean RFI from three independent repetitions was calculated for each patient and represented as a violin plot for each group of patients. Statistical analysis was performed by one-way ANOVA (Tukey test for correction of multiple comparisons) or Krustal-Wallis non-parametric test (Dunns test for correction of multiple comparisons) with the same results. *$p < 0.05$, **$p < 0.01$, ***$p < 0.001$, ****$p < 0.0001$). Patient samples were obtained at Clínica Universidad de Navarra

this method, a titration experiment was performed. The sensitivity of the assay was high enough to detect tumour associated antigens, such as EpCAM from H3122 lung cancer-derived EVs, at a concentration of 3.125×10^6 EVs/µl in plasma (Additional file 1: Fig. S8A).

The presence of tumour-associated EV markers expressed in the cell lines used in previous experiments was then analysed using plasma from a small cohort of lung cancer patients compared to healthy donors. We used two tumour markers validated in the cell line-derived EVs: EpCAM, which has been described in EVs from epithelial cells and has been widely used as an epithelial cancer marker in blood (e.g., in Circulating Tumour Cells). The second marker used, MICA, has been associated with cancer progression in many types of solid and haematological tumours [35]. Plasma obtained from 12 lung cancer patients in initial stages, 12 patients with advanced lung cancer and 12 healthy donors was analysed (demographic and clinical data are available in Additional file 1: Table S1). Western Blot sensitivity did not allow detection of EpCAM in EV enriched preparations from these donors and only faint bands of MICA were visible for certain patients in overexposed membranes (Additional file 1: Fig. S9). However, flow cytometry experiments using small amounts of non-processed plasma allowed detection of EpCAM and MICA in combination with tetraspanins (Fig. 4C). The EVs present in 12 µl of plasma were captured either on anti-MICA, anti-EpCAM or anti-CD63-conjugated beads. Detection was performed with anti-CD81-PE or isotype-PE, as the negative control to calculate the RFI. CD63-CD81 positive EVs were efficiently detected in all samples, with generally higher levels in cancer patients compared with healthy donors, although the difference was only statistically significant for advanced stage lung cancer patients. The intensity of EpCAM-CD81 EVs was higher in four initial stage lung cancer patients compared to healthy donors while MICA-CD81 positive EVs were observed to be higher in two initial stage lung cancer patients compared to healthy donors. Although the results obtained in flow cytometry agree with the biological decrease of EpCAM in advanced tumours, the objective of these experiments was to test whether this technique could be used to analyse EV proteins in non-processed plasma. Indeed, the results suggests a good detection by flow cytometry, however, the lack of sensitivity by WB did not allow comparison.

EV immunocapture combining small volume and cationic polymers in biological fluids has high sensitivity

We then analysed whether combining flat surfaces and minimal incubation volumes with cationic polymer addition further increased the signal detected in immunocapture assays using plasma from cancer patients. We first selected the best anti-coagulant for these assays (Additional file 1: Fig. S10A). EDTA resulted in general in better signal, especially when polybrene was added. Comparison of the absence or presence of 8 µg/ml polybrene in these assays with minimal volumes of cancer patients' plasma, confirmed a better signal when the cationic polymer was used (Additional file 1: Fig. S10B). However, since in small volumes the interaction of the EVs with the beads is already enhanced, the increment obtained with polybrene was not as significant as that observed in previous experiments performed in 100 µl (Additional file 1: Fig. S8B), being only significant when the Confidence Interval (CI) was reduced from 95 to 90%.

Because our pilot experiment using plasma from lung cancer patients did not allow detection of tumour markers by WB, to compare the sensitivity of immunocapture we used plasma from patients with other epithelial tumours in which high expression of EpCAM has been reported in EVs [36, 37]. Thus, to validate the methodology, this protein was studied together with tetraspanins, in plasma from 3 ovarian (Ov1-3) and 5 breast (Br1-5) cancer patients. 12 µl of plasma from each patient were captured on anti-EpCAM or anti-CD63-conjugated beads. Detection was performed with anti-CD81-PE, anti-CD9-PE or isotype-PE, as the negative control to calculate the RFI (Fig. 5A). CD63-CD81 positive EVs were successfully detected in every sample, with higher signal in Ov1, Br1 and Br5. One ovarian cancer patient (Ov1) plasma was clearly positive for $EpCAM^{+}$-$CD81^{+}$ EVs, followed by a moderate signal in samples from Br1 and Br2 patients and lower signals were observed for the rest of the patients. Interestingly, at least in these sample types, the use of CD9 as a detection antibody was associated with higher RFIs than when EVs were detected using a CD81-specific mAb. Next, 200 µl of the same plasma samples were ultracentrifuged and the EV-enriched preparation was analysed in parallel by: (1) Western Blot (1/3 of EV prep volume); and (2) immunocapture followed by flow cytometry (1/10 of EV prep volume). The intensity of the CD81 bands detected by WB corresponded to the fluorescence intensities obtained by flow cytometry (in Fig. 5B, compare WB bands with purple RFI heatmap). However, while flow cytometry detected different amounts of EpCAM in different patients (Fig. 5B, turquoise blue RFI heatmap), only a long exposure of the membrane allowed a clear visualization of the EpCAM band in Ov1. Thus, flow cytometry detection of proteins in EVs is far more sensitive than WB. However, it was not possible to test the capacity of quantitation in comparison.

Ascitic fluid from ovarian cancer patients has previously been reported to contain large amounts of EVs containing EpCAM [38, 39], and when 12 µl of ascites were tested by flow cytometry, EpCAM was successfully detected in all the ascitic fluid samples with high expression in several of them (Fig. 5C). The tumour antigen MICA was also tested, and the EVs of one patient (P2)

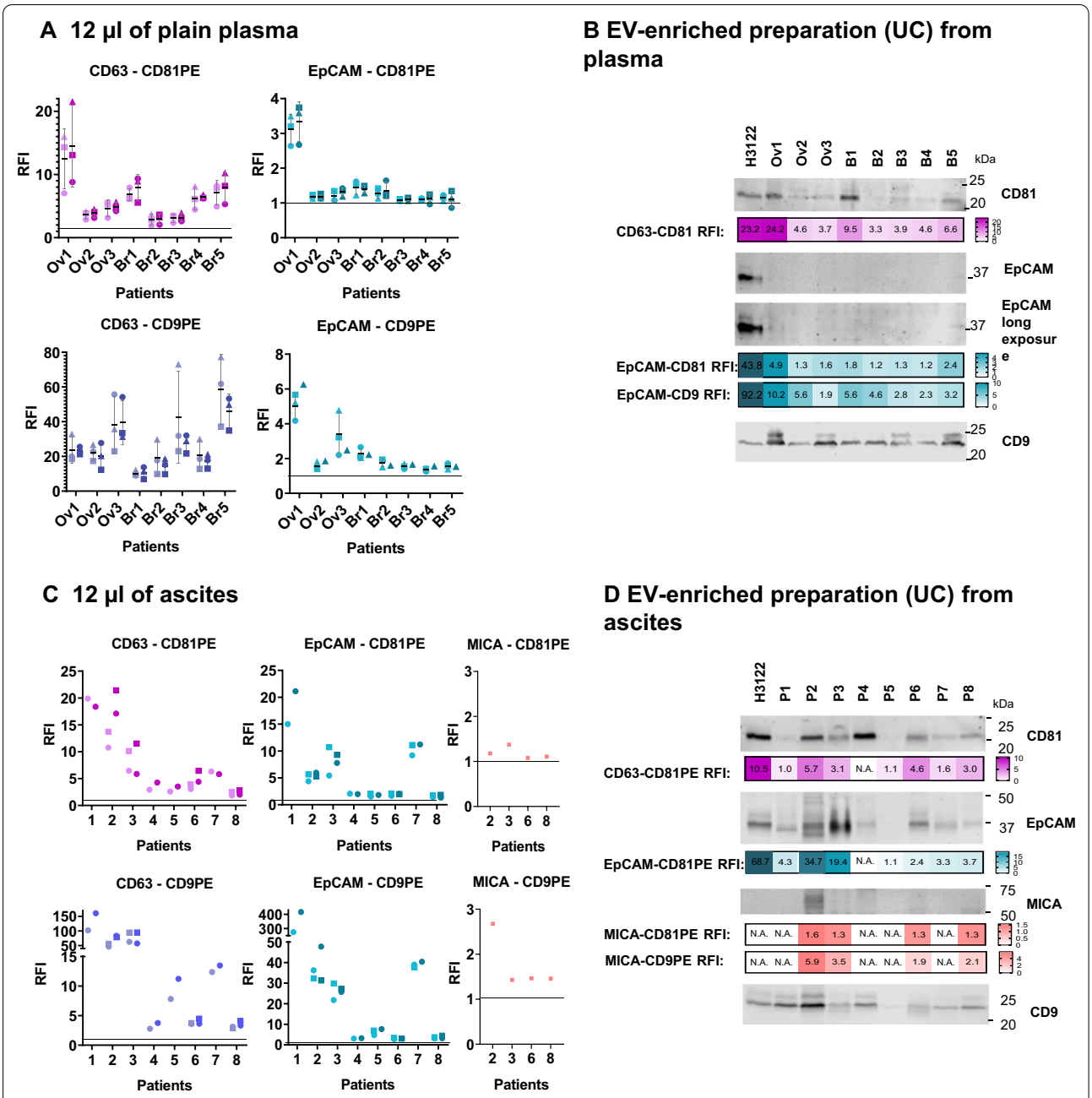

Fig. 5 Tetraspanins and EV tumour-related proteins, EpCAM and MICA, can be detected directly in minimal volumes of plasma and ascitic fluid from cancer patients by flow cytometry, with better sensitivity than Western Blot. Plasma (**A**, **B**). **A** 12 µl of PBS 1% casein containing 3000 beads conjugated with anti-CD63, anti-EpCAM or anti-MICA were incubated for 16 h with 12 µl of plasma (EDTA-tubes) from cancer patients (ovarian cancer Ov1-Ov3 and breast cancer Br1-Br5). Samples with addition of 8 µg/ml of polybrene were analysed in parallel (dark symbols). The final volume of the assay was 24 µl. EVs captured in each assay were detected with anti-CD81-PE, anti-CD9-PE or IgG-PE as a negative control to calculate the Relative Fluorescence Intensity (RFI). Mean and Standard Deviation of the RFI from 3 independent experiments (circles, squares and triangles) are represented. **B** After ultracentrifugation of 200 µl of each plasma, the EV enriched preparation was resuspended in 15 µl. 5 µl of this EV preparation were loaded in a 12% SDS-PAGE gel and transferred to nitrocellulose. The membrane was immunoblotted for detection of EpCAM and MICA and the tetraspanins CD9 and CD81, as general EV markers. In parallel, 1.5 µl of the same EV preparation were incubated for 16 h with 24 µl of PBS 1% casein containing 3000 beads conjugated with anti-CD63, anti-EpCAM or anti-MICA. EVs captured in each assay were detected by incubation with anti-CD81-PE or anti-CD9-PE. RFI values are represented as heatmaps (the number obtained is superimposed). EVs from the H3122 cell line were used as a control for EpCAM positive EVs (5.86×10^8 particles/well for WB and 1.76×10^8 particles/test for Flow Cytometry). Ascites (**C**, **D**). Ovarian cancer patients' ascites [1–8] were subjected to the same protocols as in **A**, **B**. Patient samples were obtained at Clínica Universidad de Navarra

contained high amounts of this protein. Comparison with WB of EV enriched preparations confirmed the semi-quantitative power of the immunocapture technique (in Fig. 5D, compare the intensities of the bands with the RFI heatmaps). In ascites, it was possible to visualize EpCAM clearly by WB and the intensity of the observed band for each patient could be related with the fluorescence intensity observed in the flow cytometry heatmap (Fig. 5D, turquoise blue heatmap). Similarly, the detection of MICA in P2 by immunocapture correlated with the visualisation of a clear MICA band after WB analysis.

It is interesting to note that unprocessed ascites had somewhat different relative amounts of each protein marker when compared with the ultracentrifuged sample (e.g., Patient 1 and 7 had high amounts of EpCAM in unprocessed plasma, but relatively lower in EVs after ultracentrifugation), highlighting the selection of different vesicle subpopulations during sequential centrifugation procedures.

In summary, direct immunocapture on 12 µl of patient plasma followed by flow cytometry yielded very sensitive results, compared to WB, and detection can be enhanced by the addition of cationic polymers. This procedure has the advantage of simple sample processing and eliminates the problems derived from sample manipulation, such as selection of EV subpopulations occurring after ultracentrifugation. The described EV characterization method may be applied to any biological fluid, such as plasma, ascitic fluid, serum, and saliva as well as conditioned tissue culture supernatant (Additional file 1: Figs. S10 and S11).

In conclusion, these experiments demonstrate that the optimised methodology for EV immunocapture can be used for a semi-quantitative analysis of EV tetraspanins as well as other proteins such as tumour-derived antigens, directly in 12 µl of plasma from cancer patients with minimal sample manipulation, opening the possibility for large screenings of multiple markers in patient cohorts.

Discussion

Immunocapture of EVs seems to yield, in general, lower detection levels than expected [18, 40–42]. Here, we demonstrate that EVs behave as stable colloids with limited particle sedimentation, so that treatments predicted to modulate the biophysics of the colloidal suspension increase EV contact with functionalised surfaces and markedly improve EV protein detection after immunocapture. Based on this observation, a straightforward method for EV immunocapture was optimised for bead-assisted flow cytometry. Modifying the geometry of the reaction conditions, decreasing the incubation volume in a broad surface, also significantly increased assay sensitivity, so that conclusive results could be obtained in plain plasma without the need to enrich EV samples. Detection could be further improved by the addition of cationic polymers. Thus, only 12 µl of plasma were enough for a clear detection of tetraspanins and other less abundant tumour markers by flow cytometry, with a sensitivity that is much higher than that of WB.

Although multiple previous reports have identified candidate disease markers in circulating EVs, their use in liquid biopsy still needs more definitive data. One of the biggest problems impeding marker validation is the difficulty of carrying out validation studies on large patient cohorts due to the limitation imposed by current EV enrichment methodology. By eliminating long manipulation protocols and increasing assay sensitivity, the method presented here could be used in high-throughput screenings in order to validate and discover new EV associated biomarkers. Further, these assays could be automatized in micro-titer plates, allowing standardization of the protocol.

The molecular basis of this enhanced immunocapture and detection can be explained by considering the physico-chemical characteristics of EVs as stable colloids. We hypothesized that EVs remain in suspension because gravity and buoyancy forces are not sufficient to counteract Brownian motion and electrostatic repulsion so that, in a bead-assisted assay, nanovesicles would remain in suspension while 6 µm beads precipitate relatively quickly, limiting the interaction of these particles. To test this hypothesis, polymer-induced colloidal flocculation was used. When cationic polymers were added to EV solutions, clusters of particles of different sizes were generated leading to higher sedimentation rates. These precipitation events correlated with an increase in protein detection. The cationic polymer-induced flocculation events occurring in this system could be due to particle aggregation after either neutralization of charges caused by adsorbed polyelectrolytes and/or formation of bridges between particles by simultaneous adsorption of polyelectrolyte chains onto more than two particles [43–45]. Adding flocculants, allowed EVs to precipitate in a controlled manner leading to enhanced interaction with antibody-coated surfaces. Since charged polymers were used, it could be anticipated that the interaction would be reversible and aggregates could be dissociated by successive washes, performed after the immunocapture step as it has been demonstrated previously [46–48]. This would be a clear advantage compared to other polymers commonly used for EV precipitation, such as polyethylene glycol (PEG), a non-ionic uncharged hydrophilic polymer, whose water excluding properties create a high osmotic pressure causing irreversible protein precipitation in complex solutions [49, 50]. In fact, DLS

measurement of the mean diameter of an EV solution with 8% PEG 6000 was not possible, due to the presence of extensive polydispersity index. In contrast, due to the presence of charged groups, polyelectrolytes provide stronger and more tunable interactions and they are also sensitive to the solution pH and amount of electrolytes [51]. In conclusion, these observations open a new avenue for further research on the interaction of polyelectrolytes with EV suspensions and biological fluids. Our data is also relevant for other applications involving EVs, such as isolation and recovery, in vitro EV-cell interaction, etc. [52, 53]. It is important to consider that, if downstream EV characterization methods are not based in immunocapture, the use of cationic polymers for EV enrichment needs to be evaluated since non-EV components may flocculate together with EVs. Interestingly, our results are in agreement with data from virus-containing solutions, where high molecular weight poly-L-lysine (up to 300 KDa) caused relatively higher aggregation than the lower molecular mass polymer polybrene (4–6 kDa) [28].

Immuno-detection was not enhanced by cationic polymers only when the untreated condition signal was already saturated, for example in some CD63-CD81 or CD63-CD9 combinations. In these cases, because tetraspanins are very abundant in EVs, the basal experiment already allows a high signal, probably saturating the capture beads. Thus, flocculation did not result in further EV capture when the polymer was added. All the epitopes tested in which the signal was low in the untreated condition, benefited from the addition of cationic polymers, except in the case of 8 µg/ml Poly-L-lysine (Fig. 3B). In colloid flocculation chemistry, it is well established that molecular weight of the polymer, its charge and distribution, as well as concentration are key factors in the effectiveness of the flocculation process [54]. Thus, it is important to define the optimal conditions in the context of EV protein detection for different experimental systems. Furthermore, EV aggregation induced by cationic polymers could sequester certain EV epitopes and therefore impede their capture on functionalized surfaces. This could also provoke the loss of these vesicles in the wash steps. In addition, it is still not known if different subsets of EVs could be more prone to aggregation and flocculation. In this situation, this assay might preferentially enhance detection of certain epitopes and impair detection of others. Our results showed an overall increase in the detection of the proteins assayed (except if the detection signal was already saturated without polymer). However, each protein epitope to be assayed in a given type of biofluid should be tested and optimized using appropriate controls, such as isotypes or EVs positive and negative for the epitope of interest.

The findings with polymers motivated the adaptation of bead-assisted flow cytometry to enhance EV interaction with antibody-coated surfaces, and the use of minimal incubation volumes with optimised geometry, yielded markedly improved immunocapture results. The method was firstly tried with tumour- derived EV-enriched preparations from tissue culture supernatant and limits of detection were obtained in spiking experiments using plasma from healthy donors. Since our goal was to compare flow cytometry with other commonly used techniques, we focused on two putative cancer biomarkers that have been well characterised in our in vitro models. So, tetraspanins were analysed in plasma together with EpCAM, an epithelial marker commonly used to identify epithelial cancer circulating tumour cells. The immune activating molecule MICA belongs to a family of proteins, which are overexpressed on stressed cells such as tumour transformed or viral infected cells, and bind to the activating immune receptor NKG2D present on T lymphocytes and Natural Killer cells [55, 56]. NKG2D-ligands have been shown to be overexpressed in most cancer cell lines and higher amounts of these soluble ligands in serum have been associated to worse cancer prognosis [57–62]. MICA was studied because this molecule can be released from the cell surface in EVs [63, 64].

In pilot experiments, since tumour staging and drug response can affect protein content in EVs, both initial and advanced lung cancer patient plasma were analysed. All samples were positive for CD63-CD81-EVs. Interestingly, advanced lung cancer patients had statistically significant higher levels of CD63-CD81-positive EVs compared with healthy donors and with initial stage patients. With respect to the detection by flow cytometry of tumour markers, EpCAM-CD81-containing EVs were efficiently detected in four initial stage lung cancer patients at higher levels than in healthy donor samples. MICA-CD81-containing EVs were also efficiently detected in two of these patients. According to published data, in some cases lung cancer patients EVs had low levels of EpCAM [36]. These data demonstrate the feasibility of our approach, but, of course, a large cohort needs to be studied for determination of cut-off values and for confirmation of the suitability of this particular tumour marker in diagnostics. Nevertheless, the finding of EpCAM-CD81-EVs in four initial stage patients, and not in advanced stage patients or healthy donors, agrees with previous observations that advanced tumour cells lose EpCAM expression as they undergo EMT (Epithelial to Mesenchymal Transition) [65, 66].

As we could not compare flow cytometry data with WB analysis in plasma from lung cancer patients, since no bands could be obtained for our molecules of interest, EpCAM and MICA, samples with higher expected

content of these proteins on EVs, ovarian and breast cancer-derived plasma and ascitic fluid, were also analysed. Analysis of EpCAM in these samples clearly demonstrated the sensitivity and semi-quantitative capacity of the immunocapture assays. Detection by flow cytometry was considerably more sensitive than WB, since data could be obtained using three-fold less EV preparation than the amount loaded in WB. Further, we demonstrated that the intensity of fluorescence obtained in immunocapture followed by flow cytometry follows the same pattern as the intensity of the bands visualised by WB for each specific molecule. These results demonstrate the semi-quantitative power and sensitivity of this approach. However, the suitability of these or other proteins as clinical biomarkers needs to be determined in larger cohorts with correspondent healthy controls for establishment of cut-off values and AUC curves. The improved techniques for EV immunocapture described here will surely aid in analyses of larger cohorts of patients. The results also show that addition of cationic polymers can improve the signal obtained in small volumes of sample, confirming that the method could be used for large screenings of patients. Interestingly, abundant markers can lead to signal saturation and, in this case, polymer addition does not increase detection.

The data presented here, also demonstrated detection of EpCAM-CD81-containing EVs in small volumes of other biological fluids such as ascites from ovarian cancer patients, in general, in higher concentration than in plasma samples, in line with previous observations in breast cancer [39].

Another interesting observation is that the results of analyses of EVs prepared by ultracentrifugation from patient samples differ somewhat from the data obtained when EVs from unmanipulated plasma are assayed. This finding strongly suggests the loss or enrichment of different vesicle subpopulations during sample preparation, emphasising the necessity to use methods that allow EV characterization directly in biological samples and so avoid possible biases in the results obtained. Further, the selection of markers can affect results due to the relative abundance of tetraspanins in plasma or tumour cells as well as in different EV subpopulations [18, 21]. For example, platelet derived EVs are devoid of CD81 but could contain CD9 [67]. Here, EV heterogeneity could be observed when capturing with either CD63 or EpCAM and comparing the signal obtained for CD9 or CD81. The method described here should be useful to detect any EV protein of interest, since beads can be conjugated to any capture antibody to enrich and detect any EV subpopulation.

Conclusions

The data presented here demonstrate that EVs behave as colloidal suspensions, so, in immunoassays, the interphase contact with functionalised surfaces should be maximised. Cationic polymers can be combined with immunocapture methods directly in the biological sample to increase detection, without previous sample manipulation for EV enrichment. The improved methodology, adaptable to any laboratory setting and easily automatable, has proven its potential to be used in high-throughput screenings of large cohorts of patients using multi-well plates. This will facilitate the validation and discovery of new body fluid EV-associated biomarkers, whose use can rapidly and easily be implemented in clinical settings.

Methods

Cells lines and reagents

Metastatic Melanoma cell lines: Ma-Mel-55, Ma-Mel-86c, (derived from melanoma patient metastases), provided by Prof. Annette Paschen (University Hospital of Essen, Germany), have been described elsewhere [34, 68, 69]. Lung cancer cell line H3122 from ATCC was authenticated by satellite analysis at the genomics service of the Institute of Biomedical Research (IIB-CSIC). Cells were regularly assayed for mycoplasma contamination.

Metastatic Melanoma and lung cancer cell lines were cultured in RPMI 1640 (Sigma-Aldrich Co., St Louis, MO, USA) with 10% fetal bovine serum (FBS), 1 mM L-Glutamine, 1 mM Sodium Pyruvate, 0.1 mM non-essential amino acids, 10 mM HEPES and Penicillin and Streptomycin at 100 µg/ml, at 37 °C, in 5% CO_2/95% air, and passaged when cells reached 80–90% confluence.

Unless otherwise stated, all chemicals were purchased from Merck & Co (Kenilworth, New Jersey, USA), including hexadimethrine bromide ≥ 94% also known as polybrene, and poly-L-lysine solution—0.1%(w/v) in H_2O.

Antibodies used for Western Blot include mouse monoclonal anti β-actin (clone AC-15, Sigma, St. Louis, MO, United States) at 0.13 µg/ml; anti tetraspanins: anti CD81 (clone M-38 kind gift from Vaclav Horejsi, Croatia), anti CD9 (clone VJ1/20), anti CD63 (clone Tea3/18); biotinylated anti-EpCAM (clone VU-1D9) (all from Immunostep S.L, Salamanca, Spain); all used at 1 µg/ml; and biotinylated goat polyclonal anti-MICA antibody (BAF1300, R&D Systems, Minneapolis, Minnesota, United States) at 2 µg/ml. For capture in immunoassays, antibodies used were monoclonal mouse anti-MICA (MAB13002, R&D biosystems), anti-EpCAM (clone VU-1D9), anti-CD63 (clone Tea3/18) (Immunostep S.L. Salamanca, Spain) or IgG1 (MOPC 21, Sigma, St. Louis, MO, USA), as isotype control. For detection in

immunoassays monoclonal mouse anti-CD81 (clone M38), anti-CD9 (Clone VJ1/20) (Immunostep, S.L., Salamanca Spain) and IgG1 (MOPC-21, Biolegend, San Diego, California, USA), all directly conjugated to PE were used at 0.02 µg/µl.

EV-enriched preparations

Cells were grown until 70% confluence and then changed into medium prepared with 1% EV-free FBS (prepared by ultracentrifugation at 100,000×*g* for 20 h), for EV accumulation during 3–4 days. Cell supernatants were centrifuged for 10 min at 200×*g* and small EVs enriched by sequential centrifugation as previously described [29, 70]. After ultracentrifugation at 100,000×*g* for 2 h at 4 °C, EVs were resuspended in 0.22 µm filtered HEPES-buffered saline (HBS: 10 mM HEPES pH 7.2, 150 mM NaCl) (2.67 µl/ml of starting cell culture supernatant) and stored at − 20 °C, for short term use, or at − 80 °C. For longer storage, EVs were lyophilised using a VirTis Freezemobile 12SL Freeze Dryer Lyophilizer (VirTis, Habour Group, St. Louis, MO, USA). Note that this protocol is used for exosomes enrichment, however, their specific origin cannot be assured so we refer to the enriched particles as EVs. For plasma and ascitic liquid EV enrichment, 200 µl of sample were diluted in 4 ml of HBS and ultracentrifuged at 110,000×*g* for 2 h at 4 °C, the EV pellet was resuspended in 15 µl of HBS and stored at − 20 °C for short term use.

EV quantitation

The concentration and size of enriched EVs in each preparation were determined by nanoparticle tracking analysis (NTA) in a Nanosight NS500 (Malvern Instruments Ltd, Malvern, UK) equipped with a 405 nm laser, a sCMOS camera and NTA 3.1 Software. Enriched EV preparations were diluted (1:1000) for measurement at a concentration range of 1×10^9 particles/ml, as recommended by manufacturer. The settings used were: Camera level:12, Threshold: 10, Capture: 60 s., Number of Captures: 3, Temperature 25 °C. The experiments were carried out at the laboratory of Dr. H Peinado, Spanish National Centre for Oncological Research (CNIO). Some measurements were double checked in a Zetaview (Particle Metrix).

Electron microscopy

For Transmission Electron Microscopy (TEM), 1 µl of the EV preparation obtained after sequential centrifugation was diluted 1:10 in filtered (0.22 µm) HBS. Ma-Mel-55 melanoma-derived EVs (0.6×10^9 particles/µl), were used for the experiment with polymers. Polymers were added at a final concentration of 4 µg/ml of polybrene or Poly-L-lysine and incubated for 18 h. Samples were floated on carbon-coated 400-mesh 240 Formvar grids, incubated with 2% uranyl acetate, and analysed using a Jeol JEM 1011 electron microscope (JEOL, Akishima, Tokyo, Japan) operating at 245 100 kV with a CCD camera Gatan Erlangshen ES1000W. The experiment was carried out at the Electron Microscopy Facility, Spanish National Centre for Biotechnology (CNB).

Western and dot blots

EV enriched preparations (either 6.8×10^9 particles or 5 µl of patient plasma EV preparation; 5.86×10^8 H3122 EVs were used as EpCAM positive control) or respective cell lysates (30 µg) were loaded in 12% SDS-PAGE gels, either under reducing or non-reducing conditions, as indicated in the experiments, and transferred to membranes with Trans-Blot® Turbo™ Transfer Packs (Biorad, Hercules, California, USA). Membranes were blocked using 5% non-fat dry milk in PBS containing 0.1% Tween-20 (PBS-T). Primary antibody was incubated for 1 h in PBS-T and, after washing, membranes were incubated with the appropriated secondary antibody. Secondary antibodies used were Alexa-700 GAM or Alexa-790-SA (ThermoFisher), when proteins were visualised using the Odyssey Infrared system (LI-COR Biosciences, Lincoln, NE, USA). When proteins were visualised using the ECL system (Amersham Biosciences, Amersham, UK), horseradish peroxidase-conjugated goat anti-mouse antibody (Sigma, St. Louis, MO, USA) was used at 0.8 µg/ml or horseradish peroxidase- streptavidin (Biolegend, San Diego, California, USA) at 0.1 µg/ml. For dot blots, 1 µl of EVs were immobilised onto nitrocellulose membranes, blocked and developed as for WB membranes.

Antibody coated magnetic beads preparation

Antibody-coated magnetic beads were obtained from the Exostep™ kit (Immunostep, S.L., Salamanca, Spain) or prepared by amine coupling capture antibodies onto magnetic fluorescent beads (APC and PerCP) either from Luminex (MagPlex Microsphere) or Bangs (QuantumPlex M SP Carboxil) as previously described [22].

EV detection by flow cytometry

EV samples were incubated with 3000 antibody-coated beads in either 100 µl, 50 µl or 12 µl of PBS containing 1% casein (EV enriched preparations diluted 1:100–1:1000) for 18 h, in either a 5 ml tube or a well in a 96 flat-bottom microtiter plate, as specified in each experiment, without agitation at room temperature (RT). Unless otherwise stated, when using biological samples, 12 µl of precleared samples were added to 12 µl of beads in PBS-casein (PBS containing 1% casein, Bio-rad Laboratories, Hercules,

California, USA). Background signals were determined by comparison with antibody isotype-coupled beads or PE-conjugated isotype antibody, as specified in each experiment. Cationic polymers were added and mixed before the 18-h incubation, unless otherwise stated, at a final concentration of 4 µg/ml of polybrene or poly-L-lysine. Control samples were incubated in the same volume of PBS-casein without polymer. After the capture step, beads were washed with PBS-casein and recovered using a Magnetic Rack (Ref Z5343, MagneSphere(R) (Promega, Madison, Wisconsin, USA), for tubes, or 40-285 Handheld Magnetic Separation Block (Millipore, Burlington, MA, USA), for 96 well plates. The recovered beads were stained with PE-conjugated anti-tetraspanin detection antibodies (at 0.02 µg/µl) during 1 h at 4 °C. After antibody binding, beads were washed with filtered PBS, and recovered using the Magnetic Rack. Beads were acquired by flow cytometry using Gallios, Cytomics FC 500 (Beckman Coulter) or CytoFLEX (Beckman Coulter) and data were analysed using Kaluza (Beckman Coulter) or FlowJo (Tree Star, Inc) software. Single beads were gated in Forward Scatter in the region corresponding to 6 µm [established using calibration beads (FlowCheck ProTM fluorospheres, Beckman Coulter, Brea, CA, USA)], excluding bead doublets and selecting APC-positive events [29]. PE MFI was analysed within the 6 µm-APC-positive events.

Dynamic light scattering (DLS)

For ζ-potential measurement, EVs enriched from Ma-Mel-86c melanoma cells (1.75×10^9 particles/µl), were diluted to a final concentration of 3.5×10^{10} EVs/ml in HBS (in the concentration range recommended for measurement by the instrument software) and treated, for 5 min or 18 h, with 8 µg/ml of cationic polymer polybrene or 4 µg/ml Poly-L-lysine (a non-treated control sample was prepared in parallel as a control), for 5 min or 18 h. The samples were then loaded in Zetasizer Nano DTS 1070 cuvettes for ζ-potential measurement at NanoZS (Red badge) ZEN3600 (Malvern Pranalytical, Malvern, UK) at 25 °C.

For size distribution measurement, EVs enriched from Ma-Mel-86c melanoma cells (1.9×10^9 particles/µl), were diluted to a final concentration of 1.9×10^9 EVs/ml in HBS (in the range recommended for measurement by the instrument software). EVs were treated, for 5 min or 18 h, with 8 µg/ml of cationic polymer polybrene or 4 µg/ml Poly-L-lysine (a non-treated control sample was prepared in parallel as a control) and loaded in a ZEN0040 disposable cell for diameter measurement using the same Zetasizer NanoZS (Red badge) ZEN3600 equipped with a 633 nm laser. Readings were performed at 25 °C.

DLS experiments were carried out at the Instituto de Ciencia de Materiales de Madrid—ICMM—CSIC. Malvern Pranalytical DTS Software Version 5.10 was used for data processing and analysis.

Analytical ultracentrifugation and sedimentation coefficient analysis

For analytical ultracentrifugation experiments, Ma-Mel-86c-derived EVs (2.6×10^9 particles/µl) were used, either directly after ultracentrifugation (diluted 1:10 in HBS) or subjected to further purification by size exclusion chromatography (SEC) to rule out any effect of co-precipitating proteins. For SEC, 26 µl of the EVs resuspended in HBS (pH 7.2, 0.22 µm filtered) after sequential centrifugation were layered on a 1 ml bed of sepharose CL-2B (Sigma CL2B300) in the same buffer. The eluate was collected in 0.2 ml fractions. Protein concentration was determined in each fraction, by measuring absorbance at 280 nm and the EV-containing fraction was determined by dot blot using anti-CD81 antibody. SEC was repeated 3 times and the EV-enriched fractions were pooled and used for sedimentation rate analysis experiments.

Both types of samples were treated either with 4 µg/ml of polybrene or 4 µg/ml of Poly-L-lysine (a non-treated sample was prepared in parallel as a control). After an 18-h incubation, all samples were run in an XLI analytical ultracentrifuge (Beckman Coulter, Brea, CA, USA) (wavelength: 280, 655×*g* (3000 rpm), 80 min, 20 °C). The results were analysed with SEDFIT 16.1c analysis Software with a confidence interval variation of the analysis of 0.68. The experiment was carried out at the Molecular Interactions Facility at Centro de Investigaciones Biológicas Margarita Salas (CIB-CSIC).

ELISA

Plates were coated with capturing antibodies at 6 µg/ml in BBS (Borate Buffered saline) overnight at 4 °C. After blocking the plates with 1% casein-PBS for 2 h at 37 °C, samples were added: EV enriched preparation diluted 1:100–1:1000 in PBS-casein and incubated 18 h at RT. When adding cationic polymers, they were mixed with the sample, at a final concentration indicated in each experiment, before the 18-h incubation. PBS-casein was added to controls to maintain the same final volume. Biotinylated secondary anti-tetraspanin antibodies were added at 0.4 µg/ml and followed by 0.25 µg/ml streptavidin-HRP (Amersham). The reaction was developed using

TMB (3,3′,5,5′-Tetramethylbenzidine) substrate (1-Step™ Ultra TMB-ELISA Substrate Solution; Thermo Scientific, Waltham, MA, USA). Absorbance was measured at 450 nm with Multiskan™ FC Filterbased Microplate Photometer (Thermo Scientific, Waltham, MA, USA).

Healthy donor plasma and patient selection

Experiments were carried out following the ethical principles established in the 1964 Declaration of Helsinki. Patients (or their representatives) were informed about the study and gave a written informed consent. This study used samples from 2 hospitals in Spain, Clínica Universidad de Navarra and Hospital Universitario Puerta de Hierro. Samples from Hospital Universitario Puerta de Hierro were obtained through the development of the research projects "PI17/01977" and "PIE14/00064". Both projects were approved by the Hospital Puerta de Hierro Ethics Committee (internal code 79-18 and PI144, respectively). Samples from Clínica Universidad de Navarra were obtained in the context of project 111/2010 "Estudio traslacional prospectivo de determinación de factores predictivos de eficacia y toxicidad en pacientes con cancer" included in the Spanish National Biobank Register with the code C.0003132 (Registro Nacional de Biobancos). A small cohort including 24 lung cancer patients and 12 healthy donors was used in this study. Demographic and clinical data from lung cancer patients are available in Additional file 1: Table S1. Plasma and ascites from breast and ovarian cancer patients were used to test the methodology with different biological fluids. The Ethics Committee of Clínica Universidad de Navarra evaluated this study and did not appreciate any ethical issues (internal project approval number 2021.145).

Blood was collected from each subject in a 5 ml EDTA tube containing a gel barrier (PPT™, BECTON DICKINSON) to separate the plasma from blood cells after centrifugation. Plasma samples were frozen at − 80 °C until test. Ascites were centrifuged 10 min at 1500×*g* after collection and frozen at − 80 °C until test. After the first thawing, aliquots were prepared and frozen to avoid further freezing–thawing cycles.

Statistics

Graphpad Prism 8 software was used for statistical analysis and representation of the data. Statistical tests used are indicated in each figure legend.

Abbreviations

BBS: Borate buffered saline; DLS: Dynamic light scattering; EMT: Epithelial to mesenchymal transition; ELISA: Enzyme-linked immunosorbent assay; EV: Extracellular vesicles; FBS: Fetal bovine serum; HBS: HEPES-buffered saline; HRP: Horse radish peroxidase; MICA: MHC class I chain-related protein A; NKG2D: Natural killer group 2D; NTA: Nano tracking analysis; PL: Poly-L-lysine; PB: Hexadimethrine bromide (polybrene, commercial brand name); PEG: Polyethylene glycol; SEC: Size exclusion chromatography; TEM: Transmission electron microscopy.

Supplementary Information

The online version contains supplementary material available at https://doi.org/10.1186/s12951-022-01256-5.

Additional file 1: Table S1. Lung cancer patients. Demographic and pathological data. **Figure S1.** Bead-assisted immunocapture does not result in binding of all the vesicles available in the mixture. 6000 antiCD63-coated beads were incubated with 2 µg of PC3-derived EVs and captured vesicles were detected by flow cytometry after incubation with anti-CD9-PE. IgG was used as a negative control. Supernatants of the first incubation (SN 24h), containing unbound exosomes, were incubated again with anti-CD63 beads and EVs captured during this second incubation were analysed by flow cytometry. This procedure was repeated the following 2 days (SN 48 h, SN 72 h). A. Histograms from a representative experiment out of 4. B. Relative Fluorescence Intensity (RFI) values. **Figure S2.** Polydispersity Index in the diameter measured by DLS increase in the presence of charged polymers. Metastatic melanoma (Ma-Mel-86c) derived EVs, obtained by ultracentrifugation, were diluted in HBS and incubated during 18 h with or without 8 µg/ml Polybrene (PB) or 4 µg/ml Poly-L-lysine (PL). The hydrodynamic diameter was measured by Dynamic Ligh Scattering (DLS). Intensity Mean (average diameter in nm) data from one representative experiment is shown together with the associated Polydispersity Index (PdI). **Figure S3.** Concentration and Z-potential measurement using NTA (Zetaview Technology). Ma-Mel-86c Metastatic melanoma-derived EVs obtained by ultracentrifugation were diluted 1:64000 in PBS and incubated during 5 minutes with either 8 µg/ml Polybrene (PB) or 1 µg/ml Poly-L-lysine (PL). Concentration and Z- potential were measured by NTA using a Zetaview Technology instrument. Measurement Parameters: Cell S/N: ZNTA-405. Sensed Electric Field: 3.1 V/cm (pulsed). Measurement Mode: Profile 11 Positions. Sensed Temperature: 31 ºC. The addition of cationic polymers led to an increase in the value of Z-potential. **Figure S4.** Sedimentation coefficient profile of EVs in the presence of charged polymers. Metastatic melanoma (Ma-Mel-86c)-derived EVs obtained by ultracentrifugation or further isolated by SEC, as indicated, were diluted in HBS and incubated during 18 h with or without 8 µg/ml Polybrene (PB) or 4 µg/ml Poly-L-lysine (PL). Sedimentation coefficient profiles and weight (signal) average sedimentation coefficient (inset) were obtained by analytical ultracentrifugation. Polydispersity increased when charged polymers were added to the EV solution. **Figure S5.** Characterization of cell lines-derived EVs. A. Size and concentration analysis by Nanoparticle tracking analysis (NTA). Average size and concentration listed in the table were obtained in a Nanosight equipment capturing 3 videos of 60 s per measurement, with camera level 12, threshold 10 and temperature of 25 °C. Software NTA 3.1 (Malvern) was used for the analysis. ϕ: diameter. B. Transmission Electron Microscopy (TEM) visualization. 1 µL EVs were diluted 1:10 in HBS and floated on a carbon-coated 400-mesh 240 Formvar grid, then incubated with 2% uranyl acetate and analysed using a Jeol JEM 1011 electron microscope operating at 245 100 kV with a CCD camera Gatan Erlangshen ES1000W. Pictures were taken at the Electron Microscopy Facility of the CNB. Bar: 100 nm. A representative image is shown. C. Protein marker characterization by Western Blot. EVs and whole cell lysates (L) were loaded in 12% SDS-PAGE gels. Membranes were immunoblotted for detection of: tetraspanins CD9, CD63, CD81 as general EV markers; βactin as loading control; EpCAM and MICA as cancer-related markers; and calreticulin (CALR) as an endoplasmic reticulum resident protein not present in the EV fraction. Two gels were loaded: one gel, under non-reducing conditions and the other under reducing conditions, for actin detection. One representative experiment out of 3 is shown. **Figure S6.** Cationic polymer addition increased cell lines-derived EV detection by Flow Cytometry and ELISA. **A.** Titration of cationic polymers. Tissue culture supernatant-derived EVs from the melanoma cell line H3122 were

incubated with 3000 anti-MICA coated beads in 100 µl final volume of PBS-Casein 1%. MICA-captured vesicles were detected by flow cytometry after incubation with anti-CD9-PE anti-CD81PE or isotype control. Relative increase of the RFI, obtained in three experiment replicates, is shown. Statistical analysis was performed by a Two-way ANOVA Fisher's LSD test. (* $p < 0.05$). **B. ELISA.** 100 µl containing 1 x 10^6 H3122 EVs/µl or 1.8 x 10^7 Ma-Mel-86c EVs/µl in PBS-Casein 1% were treated with 4 or 8 µg/ml polybrene (PB), 4 µg/ml poly-L-lysine (PL) or kept untreated and incubated for 18 h in antiEpCAM, anti-MICA or anti-CD63 antibody-coated plates. IgG coated wells were used as isotype control. EV detection was performed after incubation with biotinylated anti-CD9 antibody followed by SA-HRP. Optical Density (OD) was measured at 450 nm. Optical Density (OD) of the samples was represented after substraction of isotype OD. A representative experiment out of 3 is shown. **Figure S7.** Volume reduction increased cell lines-derived EV detection. A. Schematic representation of the binding surface. Diameter dimensions of the cytometry tube and the well of a 96-well plate are depited to scale. Beads are represented in black and EVs in red. **Figure S8.** A. Limit of detection of tetraspanins and EpCAM in plasma EVs, after addition of lung cancerderived EVs. 12 µl of plasma samples containing decreasing concentrations of lung cancer-derived EVs were incubated with 12 µl of PBS-casein containing 3000 anti-CD63, anti-EpCAM beads or IgG isotype coated beads. Captured EVs were detected with anti-CD81-PE. Bar plots represent RFI (Relative Fluorescence Intensity) values obtained. The limit of detection for EpCAM was below 3.125 x 10^6 EVs/µl. B. Titration of polymers for EpCAM detection in plasma after addition of lung cellsderived EVs. 3000 anti-EpCAM or IgG isotype-coated beads were incubated for 18 h with 2.6 x 10^6 H3122-derived EVs/µl in 12 µL of healthy donor's plasma in a final volume of 30 µL/test. Five different concentrations (0.5, 1, 2, 4 and 8 µg/ml) of Polybrene (PB) were compared to a polymeruntreated sample. Captured vesicles were detected by flow cytometry after incubation with antiCD81-PE. IgG was used as a negative control. Increase of EpCAM-CD81 RFI relative to the untreated condition in four experiment replicates (EXP) is shown. Statistical analysis was performed by a Twoway ANOVA Fisher's LSD test. (Confidence Interval CI = 90%) (* $p < 0.1$). Healthy donor samples were obtained at the University Hospital Puerta de Hierro. **Figure S9.** Western Blot detection of different proteins in the EV preparation by ultracentrifugation from lung cancer patient's plasma. 200 µl of plasma from 2 initial stage lung cancer patients (with EpCAM and MICA positive EVs detected by bead assisted flow cytometry), and from 2 healthy donors and 2 advanced stage patients plasma, were ultracentrifuged and the EV enriched preparation was resuspended in 15 µl. 5 µl of this EV preparation were loaded in a 12% SDS-PAGE gel and transferred to nitrocellulose. Lung cancer derived H3122 EVs (positive for EpCAM) were used as a positive control for EpCAM detection. The membrane was immunoblotted for detection of EpCAM and MICA and the tetraspanins CD9 and CD81, as general EV markers. EpCAM could not be detected even at high intensity exposure while MICA only showed a faint band in one of the initial stage patients after long exposure times. **Figure S10.** Direct EpCAM and MICA detection in cancer patient plasma can be improved by the combination of small volume and cationic treatment. A. Direct EpCAM and MICA detection in cancer patient plasma. 12 µl of PBS 1% casein containing 3000 beads conjugated with anti-CD63, anti-EpCAM or anti-MICA, as indicated, were incubated for 16 h with 12 µl of either serum (obtained in EDTA-tubes or heparin tubes) or plasma from each patient (cancer P1-P4 and non-cancer NC patients). The final volume of the assay was 26.5 µl, and two conditions were tested: either untreated EVs (in PBS 1% casein) (upper row) or treated with Polybrene at 8 µg/mL (lower row). EVs captured in each assay were detected with antiCD81-PE. The signal obtained from incubation of plasma with IgG isotype control-coated beads was used to calculate the Relative Fluorescence Intensity (RFI). Mean and Standard Deviation from three independent experiments are represented. Statistical analysis was performed by a multiple t-test correcting for multiple comparisons by the Holm Sidack method ($p < 0.05$). * $p < 0.05$, ** $p < 0.01$, *** $p < 0.001$, **** $p < 0.0001$). Patient samples were obtained at Clínica Universidad de Navarra. **B.** 12 µl of PBS-casein containing 3000 beads conjugated with anti-CD63, anti-EpCAM or anti-MICA, as indicated, were incubated for 16 h with 12 µl of EDTA-plasma from each patient (cancer P1-P4 and non-cancer NC patients) either treated with Polybrene at 8 µg/mL or untreated with polymer. The final volume of the assay was 26.5 µl. Captured EVs were detected with anti-CD81-PE. The signal obtained from incubation of plasma with IgG isotype control-coated beads was used to calculate the Relative Fluorescence Intensity (RFI). Mean and Standard Deviation from three independent experiments are represented. Statistical analysis was performed by a multiple t-test correcting for multiple comparisons by the Holm Sidack method ($p < 0.05$). * $p < 0.05$, ** $p < 0.01$, *** $p < 0.001$, **** $p < 0.0001$). Patient samples were obtained at Clínica Universidad de Navarra. **Figure S11.** Tetraspanins and EpCAM can be detected directly in minimal volumes of different biological fluids by flow cytometry. Polybrene can enhance low signals. PBS 1% casein containing 3000 beads conjugated either with anti-CD63, anti-MICA or anti-EpCAM (as indicated) were incubated for 16 h with the indicated volumes of conditioned medium (A), or saliva from a healthy donor (B), either untreated (PBS 1% casein) or treated with polybrene at 8 µg/mL. The final volume of the assay was 100 µl in A, and 26.5 µl in B. EVs captured in each assay were detected with anti-CD81-PE or anti-CD9-PE as indicated. Isotype-PE was used as a negative control to calculate the RFI: Relative Fluorescence Intensity. Samples were centrifuged once 10 min at 200 x g before analysis, except saliva which was centrifuged twice.

Acknowledgements
C. Campos-Silva and E. Sánchez-Herrero are registered PhD students at the Universidad Autónoma de Madrid. We acknowledge support of the publication fee by the CSIC Open Access Publication Support Initiative through its Unit of Information Resources for Research (URICI). The authors thank P Bergese (Institute for Research and Biomedical Innovation of Palermo—IRIB) for helpful discussions; A. Paschen (University Hospital Essen, Germany) for melanoma cell lines; V. Horejsi (Inst. of Molecular Genetics Academy of Sciences of the Czech Republic, Prague) for anti-CD81 antibody; H Peinado (National Centre for Oncological Research, CNIO, Spain) for the use of Nanosight NS500; MP Morales (Material Science Institute IICM-CSIC, Spain) for the use of Zetasizer NanoZS; C.A. Botello and J.R. Luque Ortega (Molecular Interactions Facility at Centro de Investigaciones Biológicas Margarita Salas (CIB-CSIC)) for the analytic centrifuge service. R. Manzanero-Cancela (Spanish National Centre for Biotechnology CNB-CSIC) for technical help with EV preparations. E Alegre (Clínica Universidad de Navarra) for help with patients' samples selection. H.T. Reyburn (Spanish National Centre for Biotechnology CNB-CSIC) for helpful discussions and critical review of the manuscript. The Flow Cytometry Service and the Electron Microscopy Service at the Spanish National Centre for Biotechnology (CNB-CSIC).

Authors' contributions
CCS, YCM, ESH, AS generated and analysed data. MVG, MYM, conceived, designed and supervised the study; MP, AG, AR, AS, ESH selected patient samples; MVG, MYM, AR, RJA provided material support; CCS and MVG wrote the manuscript with revisions from all authors. All authors read and approved the final manuscript.

Funding
This work was supported by the Spanish Ministry of Science and Innovation (MCIU/AEI/FEDER, EU) under Grants RTI2018-093569-B-I00 and RED2018-102411-T (Translational Network for clinical application of EV, Tentacles); Madrid Regional Government under Grant "IMMUNOTHERCAN" (S2017/BMD-3733-2) and IND2019/BMD-17258.

Availability of data and materials
All data generated in this study are included in this publication.

Declarations

Ethics approval and consent to participate
Experiments were carried out following the ethical principles established in the 1964 Declaration of Helsinki. Patients (or their representatives) were informed about the study and gave a written informed consent. This study used samples from 2 hospitals in Spain, Clínica Universidad de Navarra and Hospital Universitario Puerta de Hierro. Samples from Hospital Universitario

Puerta de Hierro were obtained through the development of the research projects "PI17/01977" and "PIE14/00064". Both projects were approved by the Hospital Puerta de Hierro Ethics Committee (internal code 79-18 and PI144, respectively). Samples from Clínica Universidad de Navarra were obtained through the development of the research project 111/2010 "Estudio traslacional prospectivo de determinación de factores predictivos de eficacia y toxicidad en pacientes con cáncer" approved by Clínica Universidad de Navarra Ethics Committee and included in the Spanish National Biobank Register with the code C.0003132 (Registro Nacional de Biobancos). A small cohort including 24 lung cancer patients and 12 healthy donors was used in this study. Demographic and clinical data from lung cancer patients are available in Additional file 1: Table S1. Plasma and ascites from breast and ovarian cancer patients were used to test the methodology with different biological fluids. Clínica Universidad de Navarra Ethics Committee evaluated this study and did not appreciate any ethical issues (Internal Project Approval Number 2021.145).

Consent for publication

Not applicable.

Competing interests

CCS, YCM, MYM, MVG, RJA are inventors on the European patent EP20382602. RJA is CEO of Immunostep, S.L. ABM is employed by Immunostep S.L. The rest of the authors declare no potential conflict of interest.

Author details

[1]Department of Immunology and Oncology, Spanish National Centre for Biotechnology, CNB-CSIC, Madrid, Spain. [2]Laboratorio de Biopsia Líquida, Instituto de Investigación Sanitaria Hospital Universitario Puerta de Hierro, Majadahonda, Madrid, Spain. [3]Atrys Health, Barcelona, Spain. [4]Service of Biochemistry, Clínica Universidad de Navarra, Pamplona, Spain. [5]Immunostep, S.L., Salamanca, Spain. [6]Medical Oncology Department, Hospital Universitario Puerta de Hierro, Majadahonda, Madrid, Spain. [7]Department of Molecular Biology, UAM - Centro de Biología Molecular Severo Ochoa, Madrid, Spain. [8]Instituto de Investigación del Hospital Universitario La Princesa, Madrid, Spain.

Received: 18 October 2021 Accepted: 9 January 2022
Published online: 08 February 2022

References

1. Yanez-Mo M, Siljander PR, Andreu Z, Zavec AB, Borras FE, Buzas EI, et al. Biological properties of extracellular vesicles and their physiological functions. J Extracell Vesicles. 2015;4:27066.
2. Bobrie A, Colombo M, Krumeich S, Raposo G, Thery C. Diverse subpopulations of vesicles secreted by different intracellular mechanisms are present in exosome preparations obtained by differential ultracentrifugation. J Extracell Vesicles. 2012. https://doi.org/10.3402/jev.v1i0.18397.
3. Verweij FJ, Balaj L, Boulanger CM, Carter DRF, Compeer EB, D'Angelo G, et al. The power of imaging to understand extracellular vesicle biology in vivo. Nat Methods. 2021. https://doi.org/10.1038/s41592-021-01206-3.
4. Yuana Y, Sturk A, Nieuwland R. Extracellular vesicles in physiological and pathological conditions. Blood Rev. 2013;27(1):31–9.
5. Shah R, Patel T, Freedman JE. Circulating extracellular vesicles in human disease. N Engl J Med. 2018;379(22):2180–1.
6. Simeone P, Bologna G, Lanuti P, Pierdomenico L, Guagnano MT, Pieragostino D, et al. Extracellular vesicles as signaling mediators and disease biomarkers across biological barriers. Int J Mol Sci. 2020. https://doi.org/10.3390/ijms21072514.
7. Tatischeff I. Current search through liquid biopsy of effective biomarkers for early cancer diagnosis into the rich cargoes of extracellular vesicles. Int J Mol Sci. 2021. https://doi.org/10.3390/ijms22115674.
8. Pietrowska M, Zebrowska A, Gawin M, Marczak L, Sharma P, Mondal S, et al. Proteomic profile of melanoma cell-derived small extracellular vesicles in patients' plasma: a potential correlate of melanoma progression. J Extracell Vesicles. 2021;10(4): e12063.
9. Hoshino A, Kim HS, Bojmar L, Gyan KE, Cioffi M, Hernandez J, et al. Extracellular vesicle and particle biomarkers define multiple human cancers. Cell. 2020;182(4):1044-61 e18.
10. Gardiner C, Di Vizio D, Sahoo S, Thery C, Witwer KW, Wauben M, et al. Techniques used for the isolation and characterization of extracellular vesicles: results of a worldwide survey. J Extracell Vesicles. 2016;5:32945.
11. Liangsupree T, Multia E, Riekkola ML. Modern isolation and separation techniques for extracellular vesicles. J Chromatogr A. 2021;1636: 461773.
12. Theodoraki MN, Hong CS, Donnenberg VS, Donnenberg AD, Whiteside TL. Evaluation of exosome proteins by on-bead flow cytometry. Cytometry A. 2021;99(4):372–81.
13. Liang Y, Lehrich BM, Zheng S, Lu M. Emerging methods in biomarker identification for extracellular vesicle-based liquid biopsy. J Extracell Vesicles. 2021;10(7): e12090.
14. Ibsen SD, Wright J, Lewis JM, Kim S, Ko S-Y, Ong J, et al. Rapid isolation and detection of exosomes and associated biomarkers from plasma. ACS Nano. 2017;11(7):6641–51.
15. Jeong S, Park J, Pathania D, Castro CM, Weissleder R, Lee H. Integrated magneto-electrochemical sensor for exosome analysis. ACS Nano. 2016;10(2):1802–9.
16. Im H, Lee K, Weissleder R, Lee H, Castro CM. Novel nanosensing technologies for exosome detection and profiling. Lab Chip. 2017;17(17):2892–8.
17. Witwer KW, Buzas EI, Bemis LT, Bora A, Lasser C, Lotvall J, et al. Standardization of sample collection, isolation and analysis methods in extracellular vesicle research. J Extracell Vesicles. 2013. https://doi.org/10.3402/jev.v2i0.20360.
18. Kowal J, Arras G, Colombo M, Jouve M, Morath JP, Primdal-Bengtson B, et al. Proteomic comparison defines novel markers to characterize heterogeneous populations of extracellular vesicle subtypes. Proc Natl Acad Sci USA. 2016;113(8):E968–77.
19. Mathieu M, Nevo N, Jouve M, Valenzuela JI, Maurin M, Verweij FJ, et al. Specificities of exosome versus small ectosome secretion revealed by live intracellular tracking of CD63 and CD9. Nat Commun. 2021;12(1):4389.
20. Willms E, Cabanas C, Mager I, Wood MJA, Vader P. Extracellular vesicle heterogeneity: subpopulations, isolation techniques, and diverse functions in cancer progression. Front Immunol. 2018;9:738.
21. Jeppesen DK, Fenix AM, Franklin JL, Higginbotham JN, Zhang Q, Zimmerman LJ, et al. Reassessment of exosome composition. Cell. 2019;177(2):428-45 e18.
22. Campos-Silva C, Suárez H, Jara-Acevedo R, Linares-Espinós E, Martinez-Piñeiro L, Yáñez-Mó M, et al. High sensitivity detection of extracellular vesicles immune-captured from urine by conventional flow cytometry. Sci Rep. 2019;9(1):2042.
23. Morrison ID, Ross S. Colloidal dispersions: suspensions, emulsions, and foams. New York: Wiley; 2002.
24. Stepto RFT. Dispersity in polymer science (IUPAC recommendation 2009). Polym Int. 2010;59(1):23–4.
25. Shboul AA, Pierre F, Claverie JP. A primer on polymer colloids: structure, synthesis and colloidal stability. In: Mario L, Robert G, editors. Functional materials: for energy, sustainable development and biomedical sciences. De Gruyter: Berlin; 2014. p. 9–36.
26. Tabujew I, Peneva K. CHAPTER 1 functionalization of cationic polymers for drug delivery applications. In: Samal S, Dubruel P, editors. Cationic polymers in regenerative medicine. The Royal Society of Chemistry: Cambridge; 2015. p. 1–29.
27. Murthy VS, Cha JN, Stucky GD, Wong MS. Charge-driven flocculation of poly(L-lysine)-gold nanoparticle assemblies leading to hollow microspheres. J Am Chem Soc. 2004;126(16):5292–9.
28. Davis HE, Rosinski M, Morgan JR, Yarmush ML. Charged polymers modulate retrovirus transduction via membrane charge neutralization and virus aggregation. Biophys J. 2004;86(2):1234–42.
29. Campos-Silva C, Caceres-Martell Y, Lopez-Cobo S, Rodriguez MJ, Jara R, Yanez-Mo M, et al. An immunocapture-based assay for detecting multiple antigens in melanoma-derived extracellular vesicles. Methods Mol Biol. 2021;2265:323–44.
30. Thery C, Witwer KW, Aikawa E, Alcaraz MJ, Anderson JD, Andriantsitohaina R, et al. Minimal information for studies of extracellular vesicles 2018 (MISEV2018): a position statement of the International Society for Extracellular Vesicles and update of the MISEV2014 guidelines. J Extracel Vesicles. 2018;7(1):1535750.
31. Lopez-Cobo S, Campos-Silva C, Moyano A, Oliveira-Rodriguez M, Paschen A, Yanez-Mo M, et al. Immunoassays for scarce tumour-antigens in exosomes: detection of the human NKG2D-Ligand, MICA, in

tetraspanin-containing nanovesicles from melanoma. J Nanobiotechnol. 2018;16(1):47.
32. Montis C, Zendrini A, Valle F, Busatto S, Paolini L, Radeghieri A, et al. Size distribution of extracellular vesicles by optical correlation techniques. Colloids Surf B Biointerfaces. 2017;158:331–8.
33. Oliveira-Rodriguez M, Lopez-Cobo S, Reyburn HT, Costa-Garcia A, Lopez-Martin S, Yanez-Mo M, et al. Development of a rapid lateral flow immunoassay test for detection of exosomes previously enriched from cell culture medium and body fluids. J Extracel Vesicles. 2016;5:31803.
34. Lopez-Cobo S, Pieper N, Campos-Silva C, Garcia-Cuesta EM, Reyburn HT, Paschen A, et al. Impaired NK cell recognition of vemurafenib-treated melanoma cells is overcome by simultaneous application of histone deacetylase inhibitors. Oncoimmunology. 2018;7(2): e1392426.
35. Sharma P, Diergaarde B, Ferrone S, Kirkwood JM, Whiteside TL. Melanoma cell-derived exosomes in plasma of melanoma patients suppress functions of immune effector cells. Sci Rep. 2020;10(1):92.
36. Wei P, Wu F, Kang B, Sun X, Heskia F, Pachot A, et al. Plasma extracellular vesicles detected by single molecule array technology as a liquid biopsy for colorectal cancer. J Extracell Vesicles. 2020;9(1):1809765.
37. Zhao Z, Yang Y, Zeng Y, He M. A microfluidic ExoSearch chip for multiplexed exosome detection towards blood-based ovarian cancer diagnosis. Lab Chip. 2016;16(3):489–96.
38. Runz S, Keller S, Rupp C, Stoeck A, Issa Y, Koensgen D, et al. Malignant ascites-derived exosomes of ovarian carcinoma patients contain CD24 and EpCAM. Gynecol Oncol. 2007;107(3):563–71.
39. Rupp AK, Rupp C, Keller S, Brase JC, Ehehalt R, Fogel M, et al. Loss of EpCAM expression in breast cancer derived serum exosomes: role of proteolytic cleavage. Gynecol Oncol. 2011;122(2):437–46.
40. Clayton A, Court J, Navabi H, Adams M, Mason MD, Hobot JA, et al. Analysis of antigen presenting cell derived exosomes, based on immuno-magnetic isolation and flow cytometry. J Immunol Methods. 2001;247(1–2):163–74.
41. Morales-Kastresana A, Jones JC. Flow cytometric analysis of extracellular vesicles. Methods Mol Biol. 2017;1545:215–25.
42. Wiklander OPB, Bostancioglu RB, Welsh JA, Zickler AM, Murke F, Corso G, et al. Systematic methodological evaluation of a multiplex bead-based flow cytometry assay for detection of extracellular vesicle surface signatures. Front Immunol. 2018;9:1326.
43. Lim VH, Yamaghita Y, Doan YTH, Adachi Y. Inhibition of cationic polymer-induced colloid flocculation by polyacrylic acid. Water. 2018;10:1215.
44. Adachi Y, Kobayashi A, Kobayashi M. Structure of colloidal flocs in relation to the dynamic properties of unstable suspension. Int J Polym Sci. 2012;2012: 574878.
45. Zhou Y, Franks GV. Flocculation mechanism induced by cationic polymers investigated by light scattering. Langmuir. 2006;22(16):6775–86.
46. Johnson L, Gray DM, Niezabitowska E, McDonald TO. Multi-stimuli-responsive aggregation of nanoparticles driven by the manipulation of colloidal stability. Nanoscale. 2021;13(17):7879–96.
47. Ghernaout D, Ghernaout B. Sweep flocculation as a second form of charge neutralisation—a review. Desalin Water Treat. 2012;44(1–3):15–28.
48. Antunes FE, Marques EF, Miguel MG, Lindman B. Polymer-vesicle association. Adv Colloid Interface Sci. 2009;147–148:18–35.
49. Effio CL, Hubbuch J. Next generation vaccines and vectors: Designing downstream processes for recombinant protein-based virus-like particles. Biotechnol J. 2015;10(5):715–27.
50. Koho T, Mantyla T, Laurinmaki P, Huhti L, Butcher SJ, Vesikari T, et al. Purification of norovirus-like particles (VLPs) by ion exchange chromatography. J Virol Methods. 2012;181(1):6–11.
51. Khan N, Brettmann B. Intermolecular interactions in polyelectrolyte and surfactant complexes in solution. Polymers. 2018. https://doi.org/10.3390/polym11010051.
52. Stranford DM, Hung ME, Gargus ES, Shah RN, Leonard JN. A systematic evaluation of factors affecting extracellular vesicle uptake by breast cancer cells. Tissue Eng Part A. 2017;23(21–22):1274–82.
53. Kim J, Lee H, Park K, Shin S. Rapid and efficient isolation of exosomes by clustering and scattering. J Clin Med. 2020. https://doi.org/10.3390/jcm9030650.
54. Maćczak P, Kaczmarek H, Ziegler-Borowska M. Recent achievements in polymer bio-based flocculants for water treatment. Materials. 2020;13(18):3951.
55. Fernandez-Messina L, Reyburn HT, Vales-Gomez M. Human NKG2D-ligands: cell biology strategies to ensure immune recognition. Front Immunol. 2012;3:299.
56. Campos-Silva C. NKG2D-ligands: putting everything under the same umbrella can be misleading. HLA. 2018;91(6):489–500.
57. Holdenrieder S, Stieber P, Peterfi A, Nagel D, Steinle A, Salih HR. Soluble MICA in malignant diseases. Int J Cancer. 2006;118(3):684–7.
58. Holdenrieder S, Stieber P, Peterfi A, Nagel D, Steinle A, Salih HR. Soluble MICB in malignant diseases: analysis of diagnostic significance and correlation with soluble MICA. Cancer Immunol Immunother. 2006;55(12):1584–9.
59. Zhao Y, Chen N, Yu Y, Zhou L, Niu C, Liu Y, et al. Prognostic value of MICA/B in cancers: a systematic review and meta-analysis. Oncotarget. 2017;8(56):96384–95.
60. Li K, Mandai M, Hamanishi J, Matsumura N, Suzuki A, Yagi H, et al. Clinical significance of the NKG2D ligands, MICA/B and ULBP2 in ovarian cancer: high expression of ULBP2 is an indicator of poor prognosis. Cancer Immunol Immunother. 2009;58(5):641–52.
61. Jinushi M, Takehara T, Tatsumi T, Hiramatsu N, Sakamori R, Yamaguchi S, et al. Impairment of natural killer cell and dendritic cell functions by the soluble form of MHC class I-related chain A in advanced human hepatocellular carcinomas. J Hepatol. 2005;43(6):1013–20.
62. Liu G, Lu S, Wang X, Page ST, Higano CS, Plymate SR, et al. Perturbation of NK cell peripheral homeostasis accelerates prostate carcinoma metastasis. J Clin Invest. 2013;123(10):4410–22.
63. Ashiru O, Lopez-Cobo S, Fernandez-Messina L, Pontes-Quero S, Pandolfi R, Reyburn HT, et al. A GPI anchor explains the unique biological features of the common NKG2D-ligand allele MICA*008. Biochem J. 2013. https://doi.org/10.1042/BJ20130194.
64. Lopez-Cobo S. Glycosyl-phosphatidyl-inositol (GPI)-anchors and metalloproteases: their roles in the regulation of exosome composition and NKG2D-mediated immune recognition. Front Cell Dev Biol. 2016;4:97.
65. Keller L, Werner S, Pantel K. Biology and clinical relevance of EpCAM. Cell Stress. 2019;3(6):165–80.
66. Byers LA, Diao L, Wang J, Saintigny P, Girard L, Peyton M, et al. An epithelial-mesenchymal transition gene signature predicts resistance to EGFR and PI3K inhibitors and identifies Axl as a therapeutic target for overcoming EGFR inhibitor resistance. Clin Cancer Res. 2013;19(1):279–90.
67. Koliha N, Wiencek Y, Heider U, Jungst C, Kladt N, Krauthauser S, et al. A novel multiplex bead-based platform highlights the diversity of extracellular vesicles. J Extracell Vesicles. 2016;5:29975.
68. Ugurel S, Thirumaran RK, Bloethner S, Gast A, Sucker A, Mueller-Berghaus J, et al. B-RAF and N-RAS mutations are preserved during short time in vitro propagation and differentially impact prognosis. PLoS ONE. 2007;2(2): e236.
69. Zhao F, Sucker A, Horn S, Heeke C, Bielefeld N, Schrors B, et al. Melanoma lesions independently acquire T-cell resistance during metastatic latency. Cancer Res. 2016;76(15):4347–58.
70. Ashiru O, Boutet P, Fernandez-Messina L, Aguera-Gonzalez S, Skepper JN, Vales-Gomez M, et al. Natural killer cell cytotoxicity is suppressed by exposure to the human NKG2D ligand MICA*008 that is shed by tumor cells in exosomes. Cancer Res. 2010;70(2):481–9.

Publisher's Note

original reports

Overall Survival and Biomarker Analysis of Neoadjuvant Nivolumab Plus Chemotherapy in Operable Stage IIIA Non–Small-Cell Lung Cancer (NADIM phase II trial)

Mariano Provencio, MD, PhD[1]; Roberto Serna-Blasco, MSc[1]; Ernest Nadal, MD[2]; Amelia Insa, MD[3]; M. Rosario García-Campelo, MD[4]; Joaquín Casal Rubio, MD[5]; Manuel Dómine, MD[6]; Margarita Majem, MD[7]; Delvys Rodríguez-Abreu, MD[8]; Alex Martínez-Martí, MD[9]; Javier De Castro Carpeño, MD[10]; Manuel Cobo, MD[11]; Guillermo López Vivanco, MD[12]; Edel Del Barco, MD[13]; Reyes Bernabé Caro, MD[14]; Nuria Viñolas, MD[15]; Isidoro Barneto Aranda, MD[16]; Santiago Viteri, MD[17]; Eva Pereira, MSc[18]; Ana Royuela, PhD[1]; Virginia Calvo, MD[1]; Javier Martín-López, MD[1]; Francisco García-García, PhD[19]; Marta Casarrubios, MSc[1]; Fernando Franco, MD[1]; Estela Sánchez-Herrero, MSc[1,20]; Bartomeu Massuti, MD[21]; Alberto Cruz-Bermúdez, PhD[1]; and Atocha Romero, PhD[1]

abstract

PURPOSE Neoadjuvant chemotherapy plus nivolumab has been shown to be effective in resectable non–small-cell lung cancer (NSCLC) in the NADIM trial (ClinicalTrials.gov identifier: NCT03081689). The 3-year overall survival (OS) and circulating tumor DNA (ctDNA) analysis have not been reported.

METHODS This was an open-label, multicenter, single-arm, phase II trial in which patients with stage IIIA NSCLC, who were deemed to be surgically resectable, were treated with neoadjuvant paclitaxel (200 mg/m^2 once a day) and carboplatin (area under curve 6) plus nivolumab (360 mg) once on day 1 of each 21-day cycle, for three cycles, followed by adjuvant nivolumab monotherapy for 1 year (240 mg once every 2 weeks for 4 months, followed by 480 mg once every 4 weeks for 8 months). The 3-year OS and ctDNA analysis were secondary objectives of the trial.

RESULTS OS at 36 months was 81.9% (95% CI, 66.8 to 90.6) in the intention-to-treat population, rising to 91.0% (95% CI, 74.2 to 97.0) in the per-protocol population. Neither tumor mutation burden nor programmed cell death ligand-1 staining was predictive of survival. Conversely, low pretreatment levels of ctDNA were significantly associated with improved progression-free survival and OS (hazard ratio [HR]: 0.20; 95% CI, 0.06 to 0.63, and HR: 0.07; 95% CI, 0.01 to 0.39, respectively). Clinical responses according to RECIST v1.1 criteria did not predict survival outcomes. However, undetectable ctDNA levels after neoadjuvant treatment were significantly associated with progression-free survival and OS (HR: 0.26; 95% CI, 0.07 to 0.93, and HR: 0.04; 95% CI, 0.00 to 0.55, respectively). The C-index to predict OS for ctDNA levels after neoadjuvant treatment (0.82) was superior to that of RECIST criteria (0.72).

CONCLUSION The efficacy of neoadjuvant chemotherapy plus nivolumab in resectable NSCLC is supported by 3-year OS. ctDNA levels were significantly associated with OS and outperformed radiologic assessments in the prediction of survival.

J Clin Oncol 00. © 2022 by American Society of Clinical Oncology

ASSOCIATED CONTENT

Data Sharing Statement
Data Supplement
Protocol

Author affiliations and support information (if applicable) appear at the end of this article.

Accepted on April 4, 2022 and published at ascopubs.org/journal/jco on May 16, 2022: DOI https://doi.org/10.1200/JCO.21.02660

INTRODUCTION

Lung cancer is a devastating disease, being the leading cause of cancer deaths worldwide.[1] Nevertheless, immunotherapy-based treatments have dramatically improved outcomes and become established as a major modality for the treatment of metastatic non–small-cell lung cancer (NSCLC).[2-5] Yet, its role in earlier stages needs to be established. In this regard, we previously published the results from the primary analysis of the NADIM trial, in which patients with resectable stage IIIA NSCLC were treated with neoadjuvant nivolumab plus chemotherapy, which showed a progression-free survival (PFS) at 24 months of 77.1% in the intention-to-treat (ITT) population.[6] In addition, a pathologic complete response (pCR) rate of 63.4% was reported. These are unprecedented results that outperform outcomes with the standard-of-care preoperative chemotherapy.[7] Consequently, currently, there is intense research ongoing focused on the efficacy of chemoimmunotherapy in the neoadjuvant setting. Without long-term survival data available, methodologies for the early measurement of treatment

CONTEXT

Key Objective

Our objectives were to evaluate the long-term clinical benefit of neoadjuvant nivolumab plus chemotherapy in operable stage IIIA non–small-cell lung cancer (NSCLC) and to assess the utility of circulating tumor DNA (ctDNA) as an early surrogate end point for treatment efficacy.

Knowledge Generated

Overall survival at 36 months was 81.9% in the intention-to-treat population, rising to 91.0% in the per-protocol population. Additionally, we report for the first time a significant association between ctDNA levels after neoadjuvant chemo-immunotherapy and survival outcomes in operable NSCLC. Indeed, ctDNA outperformed clinical responses, assessed on computed tomography scans and according to RECIST criteria v.1.1, in the prediction of survival.

Relevance

The efficacy of neoadjuvant chemotherapy plus nivolumab in resectable NSCLC is supported by unprecedentedly high survival rates. Overall survival was almost three times that reported in the historical series. Our data support the usefulness of ctDNA as an early surrogate end point in the context of neoadjuvant treatment.

efficacy are of particular interest. Scoring approaches for pathologic response assessments for neoadjuvant immunotherapy in NSCLC have been reported.[8] Specifically, Cottrell et al[9] proposed quantitative immune-related pathologic response criteria on the basis of the histologic features of the regression bed in the tumors. Similarly, Stein et al[10] have proposed a pan-tumor immune-related pathologic response score system. Yet, its capacity to predict long-term survival has not been established.

Here, we report the results of the planned secondary end point of 3-year overall survival (OS) of the NADIM trial. Finally, we evaluate the prognostic value of the circulating tumor DNA (ctDNA) and compare its capacity to predict long-term survival with classical survival surrogates.

METHODS

Study Design and Participants

This is an open-label, multicenter, single-arm phase II trial. The trial was conducted in accordance with the precepts established in the Declaration of Helsinki, Good Clinical Practice guidelines, and all applicable regulatory requirements. The study Protocol (online only) was approved by the ethics committee of Hospital Puerta de Hierro and the Spanish Agency of Medicines and Medical Devices. Full details of the NADIM trial (ClinicalTrials.gov identifier: NCT03081689) have been published elsewhere.[6] Briefly, eligible patients included patients age $\geq$ 18 years, with operable stage IIIA NSCLC (American Joint Committee on Cancer seventh edition criteria) and an Eastern Cooperative Oncology Group performance status of 0 or 1. Patients were treated with neoadjuvant intravenous paclitaxel (200 mg/m^2 once a day) and carboplatin (area under the curve 6; 6 mg/mL per min) plus nivolumab (360 mg) once on day 1 of each 21-day cycle, for three cycles before surgical resection, followed by adjuvant intravenous nivolumab monotherapy for 1 year (240 mg once every 2 weeks for 4 months, followed by 480 mg once every 4 weeks for 8 months). The primary end point was PFS at 24 months and it has been previously published.[6] Secondary end points included 3-year OS and the analysis of tissue and plasma biomarkers.

Peripheral blood and tissue from all patients were prospectively collected. Plasma samples were collected before and after neoadjuvant treatment. Post-treatment plasma samples were collected before surgery in all cases. Informed consent for the collection of research samples was obtained.

Procedures

Patients were assessed every 21 days for clinical response. Computed tomography (CT) scans were performed locally before and after neoadjuvant treatment, after surgery, every 3 months during the first-year follow-up, every 4 months during the second year of follow-up, and every 6 months thereafter. The tumor response to neoadjuvant treatment was evaluated by comparing before and after neoadjuvant treatment CT scans, and according to RECIST version 1.1.

The pathologic response was locally assessed in the pulmonary resection specimen (lobectomies, bilobectomies, or pneumonectomies) according to the pathologist of each of the 18 participating hospitals. A second evaluation was performed by two independent pathologists with 100% agreement. The number of sections reviewed for pathologic response assessment ranged from 8 to 28 (median 10, mean 12). In all cases, the pathologist was blinded to the patient's identity and outcome. pCR was defined as the absence of any viable tumor cell in the resected lung specimen and all regional lymph nodes. Major pathologic response was defined as the presence of 10% or fewer tumor cells in the primary tumor, and incomplete pathologic response was considered when there were 10% or more viable tumor cells present in the primary tumor.

Next-generation sequencing analysis of formalin-fixed paraffin-embedded and plasma samples is described in the Data Supplement (online only). Briefly, DNA from formalin-fixed paraffin-embedded samples was sequenced using the Oncomine Tumor Mutation Load Assay. Likewise, cfDNA, from plasma samples, was analyzed using the Oncomine Pan-Cancer Cell-Free Assay kit.

Mutant allele fraction (MAF) was defined as the number of mutant molecules at a specific nucleotide location relative to the sum of total DNA molecules (mutant plus wild-type). A cutoff of MAF $\geq$ 0.1% was established as the limit of detection.

Statistical Analysis

Median follow-up time was estimated by the reverse Kaplan-Meier (KM) method.[11] Estimation of the median follow-up and the ratio of the expected variance of S(t) to the current variance of S(t) at 36 and 42 months were used to quantify data maturity.[12]

OS was defined as the time from the start of neoadjuvant treatment to death from any cause. PFS was defined as the time between the start of neoadjuvant treatment and disease progression, as assessed by RECIST criteria v1.1, or death from any cause, whichever occurred first. Patients who were alive or without the event at the end of follow-up were censored at the time of the last contact. PFS and OS were assessed in the ITT population, which included all patients who received neoadjuvant treatment, and in the per-protocol (PP) population, which included all patients who underwent tumor resection and received at least one cycle of adjuvant therapy (Data Supplement). Cox proportional-hazards models were used to determine the association of each of the study variables with survival outcomes. The models were adjusted by surgery. Two patients died of COVID-19 disease, which represents a competing event for cause-specific mortality. Thus, competing risk analysis was also performed. Specifically, cumulative incidence functions and subhazard ratios on the basis of the Fine and Gray approach are presented to estimate the risks of progression and cancer-related death.

To avoid potential bias in the association of PFS and OS with response to treatment assessed by pathologic response, radiologic response, and ctDNA detection after neoadjuvant treatment, the landmark analysis approach[13] was used with the landmark chosen as the date of the end of neoadjuvant treatment.

The discrimination ability for each model was evaluated using Harrell's concordance index (C-index).[14,15] The C-index can take values from 0 to 1, with higher values indicating better discrimination. A value of 0.5 corresponds to no better discrimination than by chance. Likelihood ratio statistics of tumor response to treatment assessed by CT scans and ctDNA were also evaluated after accounting for surgery status. Models were first conditioned on one predictor, and then the significance of the other was tested. P values of $< .05$ were considered to be statistically significant.

Role of Funding Source

The study was sponsored by the Spanish Lung Cancer Group.[16] The study funders had no role in study design, data collection, data analysis, data interpretation, or writing of the manuscript.

RESULTS

Clinical Outcomes

The demographic characteristics of the patients at baseline have been reported previously.[6] All patients (N = 46) were stage IIIA. Regarding nodal status, nine (19.6%) patients were N0, three (6.5%) patients were N1, and 34 (73.9%) were N2. The median follow-up time was 38.0 months (95% CI, 36.7 to 40.7), with 94% maturity at 36 months and 90% maturity at 42 months. There were no events (death or disease progression) during neoadjuvant treatment. Among the ITT population (N = 46), 41 patients underwent tumor resection and 37 patients, constituting the PP population, received subsequent adjuvant therapy (90.2% of the planned population; Data Supplement). Of these, 29 (78.4%) patients completed the adjuvant treatment (14-17 cycles), eight (21.6%) patients received between three and 13 cycles of adjuvant therapy. There was no interruption of nivolumab administration in any of the 17 cycles. KM curve according to completion of adjuvant therapy is presented in the Data Supplement. Details of the patients who did not undergo surgery (n = 5) or did not receive adjuvant treatment (n = 4) are available in the Data Supplement.

At the time of data cutoff (March 2021), disease progression had been diagnosed in 12 patients and nine deaths had been recorded. Three of these deaths were of patients who did not undergo surgery and had disease progression, four were of patients who underwent surgery and had disease progression, and two were of patients diagnosed as being disease-free after surgery but who died of COVID-19 disease. The Data Supplement shows the cumulative incidence function curves for each cause of death. The median PFS and the median OS were not reached in the ITT or PP population (Fig 1). The median time to progression for patients who had progressive disease was 19.4 months (P25-P75: 10.6-25.1 months; Data Supplement).

PFS at 36 and 42 months in the ITT population was 69.6% (95% CI, 54.1 to 80.7) in both cases. Similarly, PFS at 36 and 42 months in the PP population was 81.1% (95% CI, 64.4 to 90.5) in both cases. OS at 36 and 42 months in the ITT population was 81.9% (95% CI, 66.8 to 90.6) and 78.9% (95% CI, 63.1 to 88.6), respectively. Likewise, OS at 36 and 42 months in the PP population was 91.0% (95%

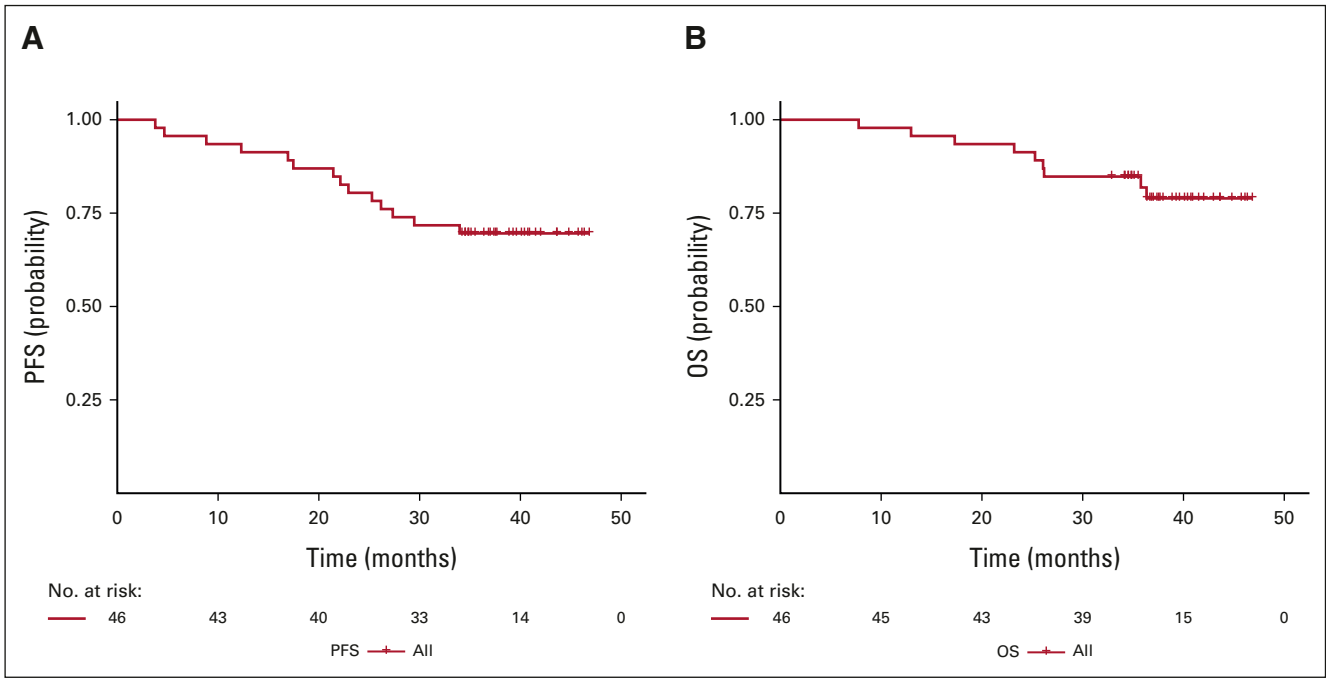

FIG 1. Kaplan-Meier curves for (A) PFS and (B) OS in the ITT population (N = 46). ITT, intention-to-treat; OS, overall survival; PFS, progression-free survival.

CI, 74.2 to 97.0) and 87.3% (95% CI, 69.3 to 95.1), respectively.

In univariate Cox regression analyses, no statistically significant associations were noted between the baseline characteristics of the patients and PFS or OS, except for Eastern Cooperative Oncology Group performance status (0 *v* 1) and the tumor lesion size (maximum diameter), which were both associated with inferior OS (hazard ratio [HR]: 4.91; 95% CI, 1.01 to 23.80; and HR: 1.03; 95% CI, 1.01 to 1.06, respectively; Data Supplement). Finally, patients who underwent surgery had significantly improved OS (HR: 0.14; 95% CI, 0.04 to 0.59; Data Supplement).

Treatment-related adverse events (AEs) during neoadjuvant treatment have been reported previously.[6] Of note, any of them were associated with surgery delays or deaths. There was no intraoperative or in-hospital mortality either at 30 or 90 days after surgery. AEs of grade 1 or 2 during adjuvant treatment were noted in 27 (73.0%) patients. The most common grade 1 or 2 AE was fatigue that was noted in 10 patients (27.0%; Data Supplement). AEs of grade 3 or 4 during adjuvant treatment were notified in five (13.5%) patients, being the most common toxicity increased lipase which was reported in four (10.8%) patients (Data Supplement). No long-term toxicities were noted.

Baseline Biomarkers

Of the 46 patients included in the trial, 35 (76.1%) had a biopsy sample available for next-generation sequencing analysis and 29 (63.0%) had valid data for tumor mutation burden (TMB) assessment. Similarly, programmed cell death ligand-1 (PD-L1) data were available for 28 (60.9%) samples. In total, 43 pretreatment plasma samples were collected.

TABLE 1. HR and Corresponding 95% CI According to Each Biomarker (TMB, PD-L1, and ctDNA levels at baseline)

Biomarker	No.	Deaths	Progressions	HR (PFS)[a]	95% CI[a]	*P*[a]	HR (OS)[a]	95% CI[a]	*P*[a]
Basal ctDNA < 1%	43	9	12	0.20	0.06 to 0.63	.006	0.07	0.01 to 0.39	.002
TMB ≥ 10 mut/Mb	29	6	6	1.67	0.41 to 6.83	.474	2.13	0.37 to 12.40	.399
PD-L1 ≥ 1%	28	5	8	0.64	0.17 to 2.40	.508	0.35	0.06 to 2.12	.252

NOTE. A cutoff of MAF ≥ 1% was established. Among patients with low ctDNA (MAF < 1%), 77.4% (95% CI, 58.4 to 88.5) were progression-free, and 93.6% (95% CI, 76.6 to 98.4) were alive at 36 months, whereas only 41.7% (95% CI, 15.3 to 66.5) and 46.7% (95% CI, 16.8 to 72.2) patients with baseline ctDNA ≥ 1% were progression-free and alive, respectively.

Abbreviations: ctDNA, circulating tumor DNA; HR, hazard ratio; MAF, mutant allele fraction; OS, overall survival; PD-L1, programmed cell death ligand-1; PFS, progression-free survival; TMB, tumor mutation burden.

[a]Multivariate analyses adjusted by surgery.

The expression of PD-L1 in tumor cells was not associated with improved PFS or OS (Data Supplement). Similarly, TMB assessment was not associated with survival outcomes (Data Supplement; Table 1).

Baseline ctDNA was detected in 30 of 43 (69.8%) of the pretreatment plasma samples (Data Supplement). ctDNA levels at baseline were significantly associated with tumor size (maximum diameter; Data Supplement).

To explore the prognostic value of the amount of ctDNA at baseline, for each positive plasma sample, we calculated the sum of MAFs for all detected mutations. Different MAF thresholds were evaluated (Data Supplement), and 1% MAF was selected (Table 1). In the multivariate analysis, patients with low ctDNA levels (< 1% MAF), at baseline, had significantly improved PFS and OS than patients with high ctDNA levels (adjusted HR: 0.20; 95% CI, 0.06 to 0.63; $P = .006$; and adjusted HR: 0.07; 95% CI, 0.01 to 0.39; $P = .002$ for PFS and OS, respectively; Fig 2; Data Supplement).

Tumor Response to Treatment Assessment: Comparative Analysis of Different Surrogates for the Prediction of Long-Term Survival

Tumor response to treatment was evaluated by CT scans in all patients (N = 46), the pathologic response was assessed in all patients who underwent surgery (n = 41), and a plasma sample collected after neoadjuvant treatment but before surgery was available in 40 cases (Data Supplement).

According to RECIST v1.1 criteria, two (4.3%) patients had a complete response, 33 (71.7%) had a partial response, and 11 (23.9%) showed stable disease. Regarding pathologic response, 34 (82.9%) patients had a major pathologic response, including 26 (63.4%) patients who showed pCR, and seven (17.1%) had an incomplete response.

Radiologic response according to CT scans did not show any association with PFS or OS ($P = .698$ for PFS and 0.848 for OS). Likewise, pCR was not significantly associated with survival ($P = .111$ for PFS and 0.102 for OS; Table 2). However, when treating COVID-19 deaths as competing risk events, pCR (but not radiologic response) identified patients with improved PFS (adjusted subHR, 0.23; 95% CI, 0.06 to 0.86; $P = .030$ for PFS and adjusted subHR: not estimable for OS because of lack of events). Of note, two of the 26 patients diagnosed as having pCR were deceased. Both patients died of COVID-19 disease and did not show disease progression according to CT scans during the study. ctDNA dynamics at the individual level and according to pathologic response are available in the Data Supplement.

Improved PFS and OS were observed for patients with undetectable ctDNA (limit of detection established at 0.1% MAF) after neoadjuvant treatment (adjusted HR: 0.26; 95% CI, 0.07 to 0.93; $P = .038$; and HR: 0.04; 95% CI, 0.00 to 0.55; $P = .015$ for PFS and OS, respectively; Table 2; Fig 3; Data Supplement). As mentioned, 13 of 43 patients had undetectable ctDNA at baseline. Adjusted HRs remained significant when excluding patients who were ctDNA-negative at baseline (Data Supplement).

To evaluate the ability of each survival surrogate to discriminate between deceased and nondeceased patients

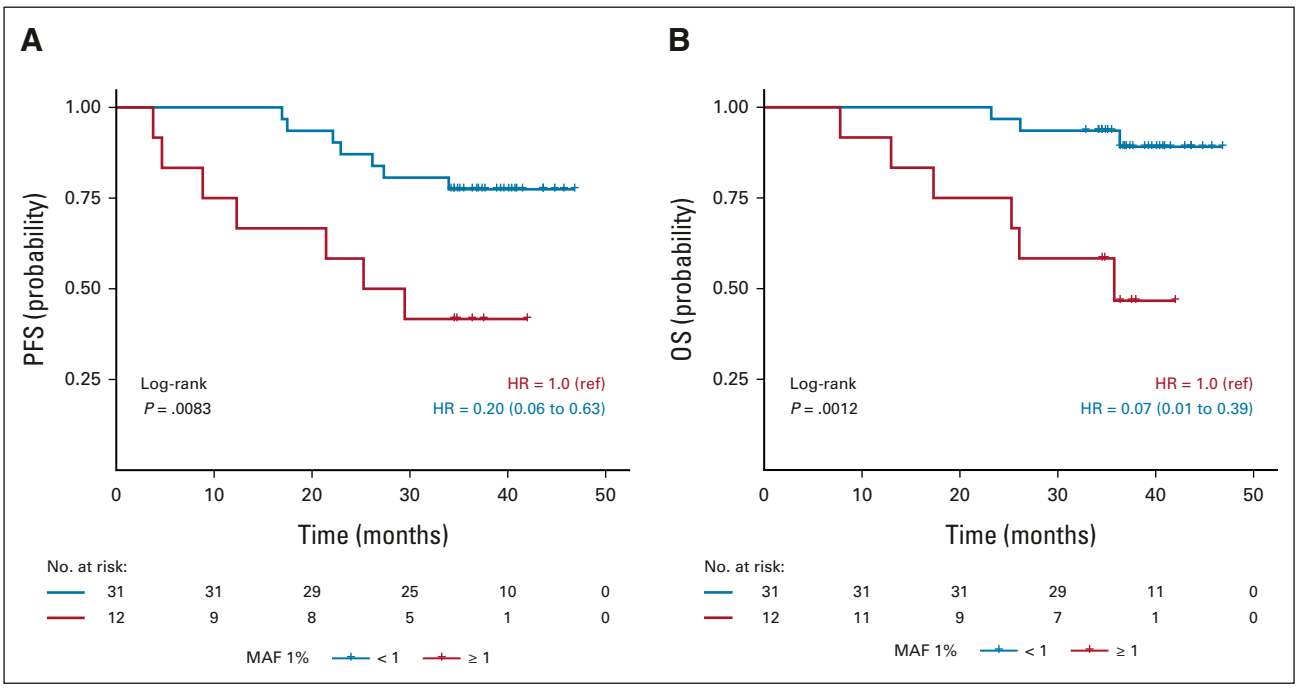

FIG 2. Kaplan-Meier curves for (A) PFS and (B) OS by ctDNA levels at baseline, using a cutoff of < 1% MAF. ctDNA, circulating tumor DNA; HR, hazard ratio; MAF, mutant allele fraction; OS, overall survival; PFS, progression-free survival; ref, reference category.

TABLE 2. Prognostic Value of Tumor Response to Treatment Assessments on the Basis of CT Scans, Pathologic Evaluation, and ctDNA (landmark analysis)

Survival surrogate	No.	HR (PFS)[a]	95% CI[a]	P[a]	C-index (PFS)	95% CI	HR (OS)[a]	95% CI[a]	P[a]	C-index (OS)	95% CI
Clinical response (CR plus PR *v* SD)	46	0.79	0.24 to 2.59	.698	0.62	0.47 to 0.77	0.87	0.20 to 3.75	.848	0.72	0.51 to 0.90
Pathologic response (pCR *v* major plus incomplete)	41	0.38	0.12 to 1.25	.111	0.63	0.47 to 0.78	0.24	0.04 to 1.33	.102	0.65	0.43 to 0.86
Undetectable ctDNA after treatment	40	0.26	0.07 to 0.93	.038	0.63	0.45 to 0.81	0.04	0.00 to 0.55	.015	0.82	0.61 to 1.00

NOTE. HR and corresponding 95% CI and C-indices and their corresponding 95% CI, to predict OS and PFS, by pathologic response, clinical response assessed according to RECIST v1.1 criteria, and ctDNA after neoadjuvant treatment. PFS and OS at 36 months in patients who showed pCR was 80.8% (95% CI, 59.8 to 91.5) and 92.3% (95% CI, 72.6 to 98.0), respectively. Among patients who showed incomplete pathologic response or major pathologic response after neoadjuvant treatment, only 60.0% (95% CI, 31.8 to 79.6) of the patients were progression-free and 61.9% (95% CI, 25.0 to 84.7) of the patients were alive. PFS and OS at 36 months for patients showing radiologic response was 71.3% (95% CI, 53.2 to 83.4) and 79.2% (95% CI, 58.4 to 90.4), respectively, compared with 63.6% (95% CI, 29.7 to 84.5) and 72.7% (95% CI, 37.1 to 90.3) in patients diagnosed as having stable disease. The probability of being alive and with no evidence of disease at 36 months in patients who showed undetectable ctDNA levels after neoadjuvant treatment (n = 27) was 96.3% (95% CI, 76.5 to 99.5) and 81.5% (95% CI, 61.1 to 91.8), respectively, compared with 57.7% (95% CI, 24.9 to 80.4) and 53.8% (95% CI, 24.8 to 76) in patients who had detectable ctDNA (n = 13) after neoadjuvant treatment.

Abbreviations: C-index; concordance index; CT, computed tomography; ctDNA, circulating tumor DNA; CR, complete response; HR, hazard ratio; OS, overall survival; pCR, pathologic complete response; PFS, progression-free survival; PR, partial response; SD, stable disease.

[a]Multivariate analyses adjusted by surgery.

and between progressed and nonprogressed patients, we calculated Harrell's C-index. The adjusted C-index to predict OS of ctDNA (0.82) was higher than the C-index for the RECIST criteria (0.72; Table 2).

Finally, we investigated whether the prognostic information provided by radiologic responses can improve by adding ctDNA information. In our hands, ctDNA added a significant degree of prognostic information to the radiologic response in terms of OS (P = .003; Data Supplement).

DISCUSSION

The main objective of any neoadjuvant study should be to contribute to the cure of the patients and increase their OS.[18] Our study shows an OS of 81.9% at 3 years in the ITT population and 91.0% in the PP population. These are unprecedentedly high survival rates in patients with stage IIIA NSCLC and have not been reported in prior studies evaluating neoadjuvant approaches.[7,19] Importantly, data maturity was 94% at 36 months. Consistent with this, a clear plateau in the KM curves for OS and PFS was observed (Fig 1). Moreover, the median time to progression was 19.4 months in patients who showed progression disease, exceeding that of the overall follow-up from the previous series.[19] We previously reported a pCR rate of 63.4% and a major pathologic response rate of 82.9%.[6] Similarly, preliminary data from the CheckMate 816 randomized phase III trial showed that neoadjuvant nivolumab plus chemotherapy increased the pCR rate compared with chemotherapy alone (24.0% *v* 2.2%; odds ratio: 13.94; 99% CI, 3.49 to 55.75).[20] Nevertheless, pathologic responses have not always resulted in prolonged OS. In this way, despite neoadjuvant treatments with chemoradiotherapy demonstrating significant benefit in terms of pathologic response rates compared with chemotherapy alone, they did not have any impact on the PFS or OS.[21]

The marked difference between the current standard of care and the NADIM-based treatments is shifting our perspective on stage IIIA NSCLC from being a lethal disease to one where it may be considered potentially curable. Accordingly, there are a significant number of ongoing clinical trials addressing the role of chemoimmunotherapy in the neoadjuvant setting. It should be acknowledged that the development of novel neoadjuvant strategies for resectable NSCLC has been hampered by a lack of surrogate end points that can be measured much faster than the end points they are meant to predict.[22] Currently, we continue to lack surrogate end points for immunotherapy-based treatment efficacy that accurately predict long-term survival. Although major pathologic response has been proposed as a surrogate end point in neoadjuvant trials for resectable NSCLC,[23] the hitherto accepted definition of major pathologic response as ≤ 10% of residual viable tumor in NSCLC regardless of histologic subtype is under debate. Several alternative approaches have been proposed so far,[8-10,24] yet its capacity to predict long-term survival has not been reported. In our study, all patients diagnosed as having pCR were alive at data cutoff, except for two patients who died of COVID-19 disease. A recent study from the International Neoadjuvant Melanoma Consortium supports the role of pCR as an early surrogate end point for recurrence-free survival and OS.[25] In this regard, it appears that pCR is a distinct biological entity being associated with specific microenvironmental features.[26,27]

In our study, neither TMB nor PD-L1 staining predicted long-term survival. Similar results have been obtained in the metastatic setting where none of these biomarkers have proved to be predictive for chemoimmunotherapy.[28]

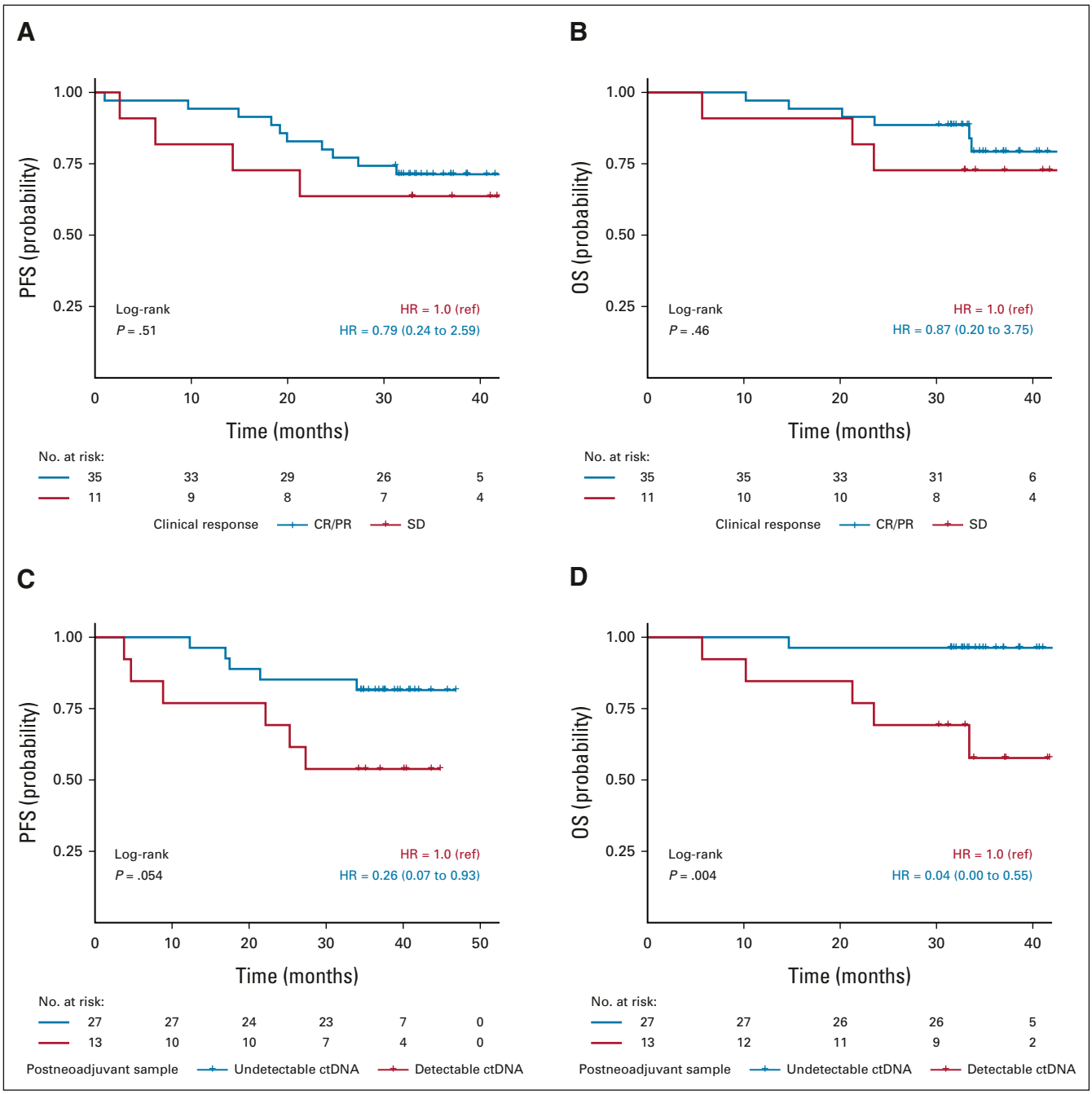

FIG 3. Kaplan-Meier curves for (A) PFS and (B) OS according to ctDNA detection after neoadjuvant treatment and Kaplan-Meier curves for (C) PFS and (D) OS by clinical response assessed on CT scans (landmark approach). Among patients who had undetectable ctDNA after neoadjuvant treatment,[17] five were diagnosed as having progression disease. All of these patients (n = 5) underwent surgery. Regarding pathology assessments, two of them were diagnosed as having pCR, one as having major pathologic response and two were diagnosed as incomplete pathologic response. One of the patients showing undetectable ctDNA after treatment but incomplete pathologic response died, representing the unique death event among patients with undetectable ctDNA after treatment. Among patients with ctDNA detection after treatment (n = 13), two patients did not undergo surgery, three patients showed an incomplete pathologic response, one patient showed a major pathologic response, and seven patients had pCR. Of these, two patients showed progressive disease despite having pCR. CR, complete response; CT, computed tomography; ctDNA, circulating tumor DNA; HR, hazard ratio; OS, overall survival; pCR, pathologic complete response; PFS, progression-free survival; PR, partial response; ref, reference category; SD, stable disease.

Specifically, the KEYNOTE-189 trial demonstrated that the addition of pembrolizumab to chemotherapy, as a first-line treatment, significantly improved both PFS and OS in NSCLC patients with metastatic disease, regardless of status.[17] Similarly, Rothschild et al[29] reported that no significant association was found between PD-L1 expression

and major pathologic response or nodal downstaging in patients with NSCLC treated with neoadjuvant chemotherapy followed by durvalumab. However, it should be acknowledged that in our study, the sample size for PD-L1 and TMB analyses was rather low, which makes any association difficult to demonstrate as being statistically significant.

In our study, patients with low ctDNA levels (MAF < 1%) at baseline had significantly improved PFS and OS than patients with high pretreatment ctDNA levels. Currently, there is not a standardized methodology to quantify ctDNA. We hypothesize that the sum of MAFs from all detected mutations would better recapitulate the status of disease as different tumor lesions may harbor different somatic mutations. Although this approach would be dependent on the total number of genes included in the panel as well as TMB, it is plausible to think that it may be less limited by tumor heterogeneity than measuring only the mutation at the highest MAF. Anyhow, similar results were obtained when using maximum MAF (Data Supplement). This approach has been used by other researchers.[30] Consistent with our findings, numerous reports have shown that the baseline ctDNA level is a prognostic factor in a wide range of patients with lung cancer.[31-33] Indeed, it has been proposed to incorporate ctDNA levels in a modified TNM staging system.[34]

Tumor response to treatment according to RECIST criteria was not associated with survival questioning the usefulness of radiologic response as a survival surrogate or even PFS as a trial end point when evaluating the efficacy of immunotherapy-based treatments. On the contrary, undetectable ctDNA at the end of neoadjuvant treatment clearly identified patients with improved OS. Although our analysis is exploratory, the notable effect size (HR: 0.04) prompts us to postulate ctDNA as being a pivotal surrogate for long-term OS in the immunotherapy field, with a similar prognostication capacity as pCR. Prior studies have noted an association between ctDNA dynamics and response to immunotherapy in NSCLC,[35] but the NADIM set is larger and the associations are more robust. Likewise, ctDNA clearance was associated with pCR in the CheckMate 816 trial.[20] In addition, it is well established that conventional imaging cannot always reliably predict long-term OS in patients undergoing immunotherapy and it has been shown that immunotherapy-based treatments can significantly improve OS rather than PFS.[2,36,37]

Longer follow-up has not revealed any signs of any unexplained or unexpected toxicities or deaths. There have been two deaths in the context of the COVID-19 pandemic, both involving patients without active tumor disease. This is an expected outcome, considering the high morbidity and mortality of this infection in patients with lung cancer.[38]

In our study, adjuvant nivolumab was administered for up to 12 months. It remains to be determined how much this treatment contributes to the OS. In this regard, adjuvant atezolizumab following lung resection and adjuvant chemotherapy has been shown to extend disease-free survival in patients with NSCLC,[39] although this has not been replicated in other tumors.[40]

In conclusion, here we report mature OS data, with more than 3 years of follow-up, in patients with resectable stage IIIA NSCLC treated with neoadjuvant chemo-immunotherapy. Survival time was almost three times that reported in the historical series, in which the 3-year OS did not exceed 30%.[19] Pretreatment ctDNA levels were significantly associated with survival but not classical biomarkers such as TMB or PD-L1 staining. Finally, undetectable ctDNA levels after neoadjuvant treatment outperformed radiologic responses assessed according to RECIST criteria v 1.1 in the prediction of OS.

AFFILIATIONS

[1]Hospital Universitario Puerta de Hierro-Majadahonda, Madrid, Spain
[2]Institut Català d'Oncologia, L'Hospitalet De Llobregat, Barcelona, Spain
[3]Fundación INCLIVA, Hospital Clínico Universitario de Valencia, Valencia, Spain
[4]Hospital Universitario A Coruña, A Coruña, Spain
[5]Hospital Universitario de Vigo, Pontevedra, Spain
[6]Hospital Universitario Fundación Jiménez Díaz (IIS-FJD), Madrid, Spain
[7]Hospital de la Santa Creu i Sant Pau, Barcelona, Spain
[8]Hospital Insular de Gran Canaria, Las Palmas, Spain
[9]Vall d'Hebron Institute of Oncology (VHIO), Hospital Universitari Vall d'Hebron, Barcelona, Spain
[10]Hospital Universitario La Paz, Madrid, Spain
[11]Hospital Universitario Regional de Malaga, Spain
[12]Hospital Universitario Cruces, Barakaldo, Spain.
[13]Hospital Universitario de Salamanca, Salamanca, Spain
[14]Hospital Universitario Virgen del Rocio, Seville, Spain
[15]Hospital Clínic, Barcelona, Spain
[16]Hospital Universitario Reina Sofia, Córdoba, Spain
[17]Instituto Oncológico Dr. Rosell. Hospital Universitario Quiron Dexeus, Grupo QuironSalud, Barcelona, Spain
[18]Spanish Lung Cancer Group, Barcelona, Spain
[19]Centro de Investigación Principe Felipe, Valencia, Spain
[20]Atrys Health, Barcelona, Spain
[21]Hospital General de Alicante, Alicante, Spain

CORRESPONDING AUTHOR

Mariano Provencio, MD, PhD, Medical Oncology Department, Hospital Puerta de Hierro, Calle Joaquín Rodrigo, 1, 28222 Majadahonda, Madrid, Spain; Twitter: @MARIANOPROVENCI; e-mail: mprovenciop@gmail.com.

PRIOR PRESENTATION

Presented in part at the World Conference on Lung Cancer Virtual Meeting, September 8-14, 2021.

SUPPORT

Supported by Bristol Myers Squibb. This study was supported by the European Union Horizon 2020 Research and Innovation program under

grant agreement no. 875160. In addition, the project received funds from Instituto de Salud Carlos III (ISCIII) PI19/01652 (Cofunded by European Regional Development Fund/European Social Fund 'A way to make Europe'/'Investing in your future'). R.S-B. is supported by PEJD-2018-PRE/BMD-8640 contract from European Social Fund (ESF). M.Ca. is supported by PEJD-2019-PRE/BMD-17006 contract from European Social Fund (ESF). E.S-H was funded by the Consejería de Ciencia, Universidades e Innovación of the Comunidad de Madrid (Doctorados Industriales of the Comunidad de Madrid IND2019/BMD-17258). A.C-B. is supported by Sara Borrell fellowship grant no. CD19/00170, Instituto de Salud Carlos III (ISCIII).

CLINICAL TRIAL INFORMATION

NCT03081689 (NADIM)

AUTHORS' DISCLOSURES OF POTENTIAL CONFLICTS OF INTEREST

Disclosures provided by the authors are available with this article at DOI https://doi.org/10.1200/JCO.21.02660.

DATA SHARING STATEMENT

A data sharing statement provided by the authors is available with this article at DOI https://doi.org/10.1200/JCO.21.02660.

AUTHOR CONTRIBUTIONS

Conception and design: Mariano Provencio, Manuel Dómine, Bartomeu Massuti, Alberto Cruz-Bermúdez, Atocha Romero
Financial support: Mariano Provencio
Administrative support: Eva Pereira, Bartomeu Massuti
Provision of study materials or patients: Mariano Provencio, Ernest Nadal, Margarita Majem, Javier De Castro Carpeño, Manuel Cobo, Edel Del Barco, Santiago Viteri, Virginia Calvo, Fernando Franco, Bartomeu Massuti, Atocha Romero
Collection and assembly of data: Mariano Provencio, Roberto Serna-Blasco, Amelia Insa, Manuel Dómine, Margarita Majem, Alex Martínez-Martí, Javier De Castro Carpeño, Manuel Cobo, Reyes Bernabé Caro, Nuria Viñolas, Isidoro Barneto Aranda, Santiago Viteri, Eva Pereira, Virginia Calvo, Javier Martín-López, Marta Casarrubios, Bartomeu Massuti, Alberto Cruz-Bermúdez, Atocha Romero
Data analysis and interpretation: Mariano Provencio, Roberto Serna-Blasco, Ernest Nadal, Delvys Rodríguez-Abreu, Alex Martínez-Martí, Javier De Castro Carpeño, Edel Del Barco, Isidoro Barneto Aranda, Ana Royuela, Francisco García-García, Fernando Franco, Estela Sánchez-Herrero, Alberto Cruz-Bermúdez, Atocha Romero
Manuscript writing: All authors
Final approval of manuscript: All authors
Accountable for all aspects of the work: All authors

ACKNOWLEDGMENT

The authors would like to thank Phil Mason for language editing.

REFERENCES

1. Siegel RL, Miller KD, Fuchs HE, et al: Cancer statistics, 2021. CA Cancer J Clin 71:7-33, 2021
2. Borghaei H, Paz-Ares L, Horn L, et al: Nivolumab versus docetaxel in advanced nonsquamous non–small-cell lung cancer. N Engl J Med 373:1627-1639, 2015
3. Herbst RS, Baas P, Kim DW, et al: Pembrolizumab versus docetaxel for previously treated, PD-L1-positive, advanced non-small-cell lung cancer (KEYNOTE-010): A randomised controlled trial. Lancet 387:1540-1550, 2016
4. Reck M, Rodríguez-Abreu D, Robinson AG, et al: Pembrolizumab versus chemotherapy for PD-L1–positive non–small-cell lung cancer. N Engl J Med 375: 1823-1833, 2016
5. Hellmann MD, Ciuleanu T-E, Pluzanski A, et al: Nivolumab plus ipilimumab in lung cancer with a high tumor mutational burden. N Engl J Med 378:2093-2104, 2018
6. Provencio M, Nadal E, Insa A, et al: Neoadjuvant chemotherapy and nivolumab in resectable non-small-cell lung cancer (NADIM): An open-label, multicentre, single-arm, phase 2 trial. Lancet Oncol 21:1413-1422, 2020
7. NSCLC Meta-analysis Collaborative Group: Preoperative chemotherapy for non-small-cell lung cancer: A systematic review and meta-analysis of individual participant data. Lancet 383:1561-1571, 2014
8. Ling Y, Li N, Li L, et al: Different pathologic responses to neoadjuvant anti-PD-1 in primary squamous lung cancer and regional lymph nodes. NPJ Precis Oncol 4:1-7, 2020
9. Cottrell TR, Thompson ED, Forde PM, et al: Pathologic features of response to neoadjuvant anti-PD-1 in resected non-small-cell lung carcinoma: A proposal for quantitative immune-related pathologic response criteria (irPRC). Ann Oncol 29:1853-1860, 2018
10. Stein JE, Lipson EJ, Cottrell TR, et al: Pan-tumour pathologic scoring of response to PD-(L)1 blockade. Clin Cancer Res 26:545-551, 2020
11. Clark TG, Bradburn MJ, Love SB, et al: Survival Analysis Part I: Basic concepts and first analyses. Br J Cancer 89:232-238, 2003
12. Gebski V, Garès V, Gibbs E, et al: Data maturity and follow-up in time-to-event analyses. Int J Epidemiol 47:850-859, 2018
13. Anderson JR, Cain KC, Gelber RD: Analysis of survival by tumor response and other comparisons of time-to-event by outcome variables. J Clin Oncol 26: 3913-3915, 2008
14. Harrell FE, Califf RM, Pryor DB, et al: Evaluating the yield of medical tests. JAMA 247:2543-2546, 1982
15. White IR, Rapsomaniki E, Wannamethee SG, et al: Covariate-adjusted measures of discrimination for survival data. Biometrical J 57:592-613, 2015
16. Spanish Lung Cancer Group: www.gecp.org
17. Gadgeel S, Rodríguez-Abreu D, Speranza G, et al: Updated analysis from KEYNOTE-189: Pembrolizumab or placebo plus pemetrexed and platinum for previously untreated metastatic nonsquamous non–small-cell lung cancer. J Clin Oncol 38:1505-1517, 2020
18. Blumenthal GM, Bunn PA, Chaft JE, et al: Current status and future perspectives on neoadjuvant therapy in lung cancer. J Thorac Oncol 13:1818-1831, 2018
19. Ramnath N, Dilling TJ, Harris LJ, et al: Treatment of stage III non-small cell lung cancer: Diagnosis and management of lung cancer, 3rd ed: American College of Chest Physicians evidence-based clinical practice guidelines. Chest 143:e314S-e340S, 2013 (5 suppl)
20. Forde PM, Spicer J, Lu S, et al: Nivolumab (NIVO) + platinum-doublet chemotherapy (chemo) vs chemo as neoadjuvant treatment (tx) for resectable (IB-IIIA) non-small cell lung cancer (NSCLC) in the phase 3 CheckMate 816 trial. Cancer Res 81, 2021 (suppl 13; abstr CT003)
21. Xu YP, Li B, Xu XL, et al: Is there a survival benefit in patients with stage IIIA (N2) non-small cell lung cancer receiving neoadjuvant chemotherapy and/or radiotherapy prior to surgical resection: A systematic review and meta-analysis. Medicine 94:e879, 2015
22. Mauguen A, Pignon JP, Burdett S, et al: Surrogate endpoints for overall survival in chemotherapy and radiotherapy trials in operable and locally advanced lung cancer: A re-analysis of meta-analyses of individual patients' data. Lancet Oncol 14:619-626, 2013

23. Hellmann MD, Chaft JE, William WN, et al: Pathological response after neoadjuvant chemotherapy in resectable non-small-cell lung cancers: Proposal for the use of major pathological response as a surrogate endpoint. Lancet Oncol 15:e42-50, 2014
24. Qu Y, Emoto K, Eguchi T, et al: Pathologic assessment after neoadjuvant chemotherapy for NSCLC: Importance and implications of distinguishing adenocarcinoma from squamous cell carcinoma. J Thorac Oncol 14:482-493, 2019
25. Menzies AM, Amaria RN, Rozeman EA, et al: Pathological response and survival with neoadjuvant therapy in melanoma: A pooled analysis from the International Neoadjuvant Melanoma Consortium (INMC). Nat Med 27:301-309, 2021
26. Casarrubios M, Cruz-Bermúdez A, Nadal E, et al: Pre-treatment tissue TCR repertoire evenness is associated with complete pathological response in patients with NSCLC receiving neoadjuvant chemoimmunotherapy. Clin Cancer Res 27:5878-5890, 2021
27. Laza-Briviesca R, Cruz-Bermúdez A, Nadal E, et al: Blood biomarkers associated to complete pathological response on NSCLC patients treated with neoadjuvant chemoimmunotherapy included in NADIM clinical trial. Clin Transl Med 11:e491, 2021
28. Paz-Ares L, Ciuleanu TE, Cobo M, et al: First-line nivolumab plus ipilimumab combined with two cycles of chemotherapy in patients with non-small-cell lung cancer (CheckMate 9LA): An international, randomised, open-label, phase 3 trial. Lancet Oncol 22:198-211, 2021
29. Rothschild SI, Zippelius A, Eboulet EI, et al: SAKK 16/14: Durvalumab in addition to neoadjuvant chemotherapy in patients with stage IIIA(N2) non-small-cell lung cancer-A multicenter single-arm phase II trial. J Clin Oncol 39:2872-2880, 2021
30. Pairawan S, Hess KR, Janku F, et al: Cell-free circulating tumor DNA variant allele frequency associates with survival in metastatic cancer. Clin Cancer Res 26: 1924-1931, 2020
31. Provencio M, Majem M, Guirado M, et al: Phase II clinical trial with metronomic oral vinorelbine and tri-weekly cisplatin as induction therapy, subsequently concomitant with radiotherapy (RT) in patients with locally advanced, unresectable, non-small cell lung cancer (NSCLC). Analysis of survival and value of ctDNA for patient selection. Lung Cancer 153:25-34, 2021
32. Provencio M, Serna-Blasco R, Franco F, et al: Analysis of circulating tumour DNA to identify patients with epidermal growth factor receptor–positive non-small cell lung cancer who might benefit from sequential tyrosine kinase inhibitor treatment. Eur J Cancer 149:61-72, 2021
33. Giroux Leprieur E, Herbretau G, Dumenil C, et al: Circulating tumour DNA evaluated by Next-Generation Sequencing is predictive of tumour response and prolonged clinical benefit with nivolumab in advanced non-small cell lung cancer. Oncoimmunology 7:e1424675, 2018
34. Yang M, Forbes ME, Bitting RL, et al: Incorporating blood-based liquid biopsy information into cancer staging: Time for a TNMB system? Ann Oncol 29: 311-323, 2018
35. Anagnostou V, Forde PM, White JR, et al: Dynamics of tumor and immune responses during immune checkpoint blockade in non-small cell lung cancer. Cancer Res 79:1214-1225, 2019
36. Brahmer J, Reckamp KL, Baas P, et al: Nivolumab versus docetaxel in advanced squamous-cell non–small-cell lung cancer. N Engl J Med 373:123-135, 2015
37. Motzer RJ, Escudier B, McDermott DF, et al: Nivolumab versus everolimus in advanced renal-cell carcinoma. N Engl J Med 373:1803-1813, 2015
38. Provencio M, Mazarico Gallego JM, Calles A, et al: Lung cancer patients with COVID-19 in Spain: GRAVID study. Lung Cancer 157:109-115, 2021
39. Wakelee HA, Altorki NK, Zhou C, et al: IMpower010: Primary results of a phase III global study of atezolizumab versus best supportive care after adjuvant chemotherapy in resected stage IB-IIIA non-small cell lung cancer (NSCLC). J Clin Oncol 39, 2021 (suppl 15; abstr 8500)
40. Bellmunt J, Hussain M, Gschwend JE, et al: Adjuvant atezolizumab versus observation in muscle-invasive urothelial carcinoma (IMvigor010): A multicentre, open-label, randomised, phase 3 trial. Lancet Oncol 22:525-537, 2021

AUTHORS' DISCLOSURES OF POTENTIAL CONFLICTS OF INTEREST

Overall Survival and Biomarker Analysis of Neoadjuvant Nivolumab Plus Chemotherapy in Operable Stage IIIA Non–Small-Cell Lung Cancer (NADIM phase II trial)

The following represents disclosure information provided by authors of this manuscript. All relationships are considered compensated unless otherwise noted. Relationships are self-held unless noted. I = Immediate Family Member, Inst = My Institution. Relationships may not relate to the subject matter of this manuscript. For more information about ASCO's conflict of interest policy, please refer to www.asco.org/rwc or ascopubs.org/jco/authors/author-center.

Open Payments is a public database containing information reported by companies about payments made to US-licensed physicians (Open Payments).

Mariano Provencio
Consulting or Advisory Role: Bristol Myers Squibb, Roche, MSD, AstraZeneca, Takeda
Speakers' Bureau: BMS, Roche, AstraZeneca, MSD
Research Funding: Pierre Fabre (Inst), Roche (Inst), Boehringer Ingelheim (Inst), Bristol Myers Squibb (Inst)
Travel, Accommodations, Expenses: Roche, BMS, AstraZeneca

Ernest Nadal
Consulting or Advisory Role: MSD, Bristol Myers Squibb, Roche, Boehringer Ingelheim, Pfizer, Takeda, AstraZeneca, Lilly, Amgen, Bayer, Sanofi
Research Funding: Roche (Inst), Pfizer (Inst), Roche (Inst), Bristol Myers Squibb (Inst), Merck Serono (Inst)
Travel, Accommodations, Expenses: MSD, Bristol Myers Squibb, Pfizer, Roche, Lilly

Amelia Insa
Consulting or Advisory Role: Pfizer, Amgen, AstraZeneca Spain
Expert Testimony: Bristol Myers Squibb/Celgene, Roche Molecular Diagnostics, AstraZeneca Spain, MSD Oncology
Travel, Accommodations, Expenses: Roche/Genentech, Pfizer

M. Rosario García-Campelo
Consulting or Advisory Role: Roche/Genentech, MSD Oncology, AstraZeneca, Bristol Myers Squibb, Pfizer, Novartis, Takeda, Boehringer Ingelheim, Janssen Oncology
Speakers' Bureau: Roche, AstraZeneca, Bristol Myers Squibb, Pfizer, Novartis, Takeda, Boehringer Ingelheim, MSD Oncology, Sanofi/Aventis, Janssen Oncology, Amgen
Travel, Accommodations, Expenses: Roche/Genentech, MSD Oncology, Pfizer

Manuel Dómine
Consulting or Advisory Role: AstraZeneca, Bristol Myers Squibb, Boehringer Ingelheim, MSD Oncology, Pfizer, Roche, Takeda

Margarita Majem
Consulting or Advisory Role: AstraZeneca, Roche, Bristol Myers Squibb, Merck Sharp & Dohme, Pfizer, Boehringer Ingelheim, Novartis, Tesaro, Helsinn Therapeutics, Takeda, Sanofi, Janssen Oncology, Pierre Fabre
Research Funding: BMS (Inst)
Travel, Accommodations, Expenses: AstraZeneca, Roche, Lilly

Delvys Rodríguez-Abreu
Consulting or Advisory Role: Roche, Bristol Myers Squibb, MSD, AstraZeneca Spain, Novartis
Speakers' Bureau: Roche, Bristol Myers Squibb, MSD
Travel, Accommodations, Expenses: Roche, Bristol Myers Squibb, MSD

Alex Martínez-Martí
Consulting or Advisory Role: Bristol Myers Squibb, Roche, Merck Sharp & Dohme, Pfizer, Boehringer Ingelheim, MSD Oncology, AstraZeneca/MedImmune
Speakers' Bureau: Roche, Bristol Myers Squibb, Merck Sharp & Dohme, Pfizer, Boehringer Ingelheim, AstraZeneca/MedImmune
Travel, Accommodations, Expenses: Roche, Bristol Myers Squibb, Pfizer, Merck Sharp & Dohme, Boehringer Ingelheim, AstraZeneca/MedImmune

Javier De Castro Carpeño
Consulting or Advisory Role: AstraZeneca, Boehringer Ingelheim, Bristol Myers Squibb, Merck Sharp & Dohme, Roche, Pfizer, Takeda, GlaxoSmithKline, Janssen Oncology, Sanofi, Bayer, Lilly
Travel, Accommodations, Expenses: AstraZeneca Spain, Merck Sharp & Dohme, Roche

Edel Del Barco
Travel, Accommodations, Expenses: Bristol Myers Squibb

Nuria Viñolas
Speakers' Bureau: Pfizer, Roche, Bristol Myers Squibb/Medarex

Santiago Viteri
Consulting or Advisory Role: Roche, Bristol Myers Squibb, Janssen, Takeda, Reddy Pharma Iberia, Merck KGaA, Puma Biotechnology
Speakers' Bureau: Bristol Myers Squibb, Roche, MSD, AstraZeneca Spain
Travel, Accommodations, Expenses: Roche, MSD, Merck KGaA

Virginia Calvo
Consulting or Advisory Role: Roche/Genentech, Bristol Myers Squibb/Celgene, Merck Sharp & Dohme, Takeda, AstraZeneca Spain, Boehringer Ingelheim, Lilly, Pfizer

Javier Martín-López
Speakers' Bureau: Roche
Travel, Accommodations, Expenses: EUSA Pharma

Bartomeu Massuti
Consulting or Advisory Role: Roche, Boehringer Ingelheim, Bristol Myers Squibb, AstraZeneca, Takeda, Merck Serono, Janssen
Speakers' Bureau: Roche, AstraZeneca, Boehringer Ingelheim, Bristol Myers Squibb
Travel, Accommodations, Expenses: Roche

Atocha Romero
Consulting or Advisory Role: Takeda, AstraZeneca Spain
Research Funding: Bristol Myers Squibb Foundation (Inst), Boehringer Ingelheim (Inst), Takeda (Inst)
Expert Testimony: Vivo Diagnostics

No other potential conflicts of interest were reported.

cancers

MDPI

Article

Molecular Divergence upon *EGFR*-TKI Resistance Could Be Dependent on the Exon Location of the Original *EGFR*-Sensitizing Mutation

Roberto Serna-Blasco [1], Estela Sánchez-Herrero [1,2], Lucía Robado de Lope [1], Sandra Sanz-Moreno [1], Alejandro Rodríguez-Festa [1], Dunixe Ares-Trotta [1], Alberto Cruz-Bermúdez [1], Fabio Franco [3], Alfredo Sánchez-Hernández [4], María de Julián Campayo [4], Carlos García-Girón [5], Manuel Dómine [6], Ana Blasco [7], José M. Sánchez [8], Juana Oramas [9], Joaquim Bosch-Barrera [10], María Á. Sala [11], María Sereno [12], Atocha Romero [1,3,*] and Mariano Provencio [3]

1 Liquid Biopsy Laboratory, Instituto de Investigación Sanitaria Hospital Puerta de Hierro—Segovia de Arana, 28222 Madrid, Spain
2 I+D Department, Atrys Health, 08025 Barcelona, Spain
3 Medical Oncology, Hospital Puerta de Hierro, 28222 Majadahonda, Spain
4 Medical Oncology, Hospital Provincial Centre de Castelló, 120002 Castellón de La Plana, Spain
5 Medical Oncology, Hospital Universitario de Burgos, 09006 Burgos, Spain
6 Medical Oncology, Fundación Jiménez Díaz, 28040 Madrid, Spain
7 Medical Oncology, Hospital General Universitario Valencia, 46014 Valencia, Spain
8 Medical Oncology, Hospital de La Princesa, 28006 Madrid, Spain
9 Medical Oncology, Hospital Universitario de Canarias, 38320 La Laguna, Spain
10 Medical Oncology, Hospital ICO Girona, 8908 Girona, Spain
11 Medical Oncology, Hospital Basurto, 48013 Bilbao, Spain
12 Medical Oncology, Hospital Universitario Infanta Sofía, 28703 San Sebastián de Los Reyes, Spain
* Correspondence: atocha10@hotmail.com; Tel.: +34-1917769

Simple Summary: In this study, we report that the exon location of the original *EGFR*-sensitizing mutation could drive resistance mechanisms underlying tumor progression in advanced *EGFR*-positive NSCLC patients under targeted therapies. In our study, plasma detection of the p.T790M *EGFR* resistance mutation, upon disease progression, was more frequent in tumors with an *EGFR* exon 19 deletion ($p = 0.0028$). Furthermore, oncogenic mutations of *KRAS*, arising upon disease progression in 5.6% of the cases, were always detected in patients with tumors harboring *EGFR* exon 18 or 21-sensitizing mutations ($p < 0.001$).

Abstract: Tumor molecular profiling upon disease progression enables investigations of the tumor evolution. Next-generation sequencing (NGS) of liquid biopsies constitutes a noninvasive readily available source of tumor molecular information. In this study, 124 plasma samples from advanced *EGFR*-positive NSCLC patients, treated with a first-line *EGFR* tyrosine kinase inhibitor (*EGFR*-TKI) were collected upon disease progression. The circulating cell-free DNA (cfDNA) was sequenced using the Oncomine Pan-Cancer Cell-Free Assay™. Excluding *EGFR* mutations, the most frequently mutated gene was *TP53* (57.3%), followed by *APC* (11.3%), *FGFR3* (7.3%), and *KRAS* (5.6%). Different molecular alterations were observed upon disease progression depending on the location of the original *EGFR*-sensitizing mutation. Specifically, the detection of the p.T790M mutation was significantly associated with the presence of exon 19 mutations in *EGFR* (Fisher *p*-value: 0.028). All *KRAS* activating mutations ($n = 8$) were detected in tumors with *EGFR* mutations in exons 18 and 21 (Fisher *p*-value < 0.001). Similarly, mutations in *NRAS* and *HRAS* were more frequently detected in samples from tumors harboring mutations in exons 18 or 21 (Fisher *p*-value: 0.050 and Fisher *p*-value: 0.099, respectively). In conclusion, our data suggest that the mechanisms underlying *EGFR*-TKI resistance could be dependent on the exon location of the original *EGFR*-sensitizing mutation.

Keywords: *EGFR*; NGS; *KRAS*; NSCLC; liquid biopsy

check for updates

Citation: Serna-Blasco, R.; Sánchez-Herrero, E.; Robado de Lope, L.; Sanz-Moreno, S.; Rodríguez-Festa, A.; Ares-Trotta, D.; Cruz-Bermúdez, A.; Franco, F.; Sánchez-Hernández, A.; Campayo, M.d.J.; et al. Molecular Divergence upon *EGFR*-TKI Resistance Could Be Dependent on the Exon Location of the Original *EGFR*-Sensitizing Mutation. *Cancers* **2022**, *14*, 4446. https://doi.org/10.3390/cancers14184446

Academic Editor: Roberta Alfieri

Received: 19 August 2022
Accepted: 8 September 2022
Published: 13 September 2022

Publisher's Note: MDPI stays neutral with regard to jurisdictional claims in published maps and institutional affiliations.

1. Introduction

Lung cancer is currently a serious public health problem. In the United States, the incidence of lung cancer is responsible for approximately one in seven cases of cancer in both sexes, but one in four deaths, being by far the leading cause of cancer death [1]. According to pathology reports, lung cancer can be classified into two main groups: non-small-cell lung cancer (NSCLC) and small-cell lung cancer, accounting for 85% and 15% of the cases, respectively. Among NSCLCs, *EGFR*-positive tumors define a subtype that may benefit from targeted therapies. Overall, *EGFR* mutations are mainly detected in young patients, females, and Asians. The age-standardized incidence rate of *EGFR*-positive NSCLC has been reported to be five per 100,000 person-years [2,3].

Despite *EGFR* inhibitors having dramatically improved the survival outcomes and quality of life of *EGFR*-positive NSCLC patients, drug-resistance mechanisms invariably emerge after treatment, leading to tumor progression within 2 years [4]. Currently, there is intense ongoing research focused on new treatment strategies for *EGFR*-mutated NSCLC patients. As a result, several third-generation *EGFR* tyrosine kinase inhibitors (*EGFR*-TKIs) are in the late stage of clinical development [5–7], and fourth-generation *EGFR* inhibitors are being evaluated in preclinical stages and phase I trials [8]. Similarly, the efficacy of the combinations of an *EGFR*-TKI with chemotherapy or antiangiogenic drugs has been evaluated in several trials [9,10]. Other drug combinations such as the third-generation *EGFR*-TKI lazertinib plus amivantamab, a human antibody targeting *EGFR* and *MET*, are under investigation. Furthermore, encouraging results have been reported with more than one-third of *EGFR*-mutant NSCLC patients that progressed on osimertinib showing durable responses [11].

A wide range of survival outcomes is observed in *EGFR*-positive NSCLC. Hence, some *EGFR*-mutant NSCLC patients exhibit a particularly good prognosis with a time to progression exceeding 30 months, while others are diagnosed as having tumor progression within 6 months of *EGFR*-TKI treatment initiation [12]. Heterogeneity caused by different clonal populations may underlie different clinical responses. Indeed, a high clonal diversity has been observed in early-stage *EGFR*-positive NSCLC patients [13–15]. In this regard, it was reported that, in advanced *EGFR*-positive NSCLC, tumors harboring concurrent *TP53* or *RB1* mutations showed a higher risk of histologic transformation and inferior sensitivity to *EGFR*-TKI [16,17]. Tumor biopsies in lung cancer upon disease progression are often not feasible or they may not reflect intratumoral heterogeneity and other relevant mutations that may arise in secondary lesions [18–20]. In such a scenario, liquid biopsy emerges as an attractive approach for tumor molecular profiling upon disease progression.

In this study, we performed a thorough explorative analysis of *EGFR*-positive NSCLC through NGS profiling of the plasma sample collected upon disease progression of 124 patients in order to characterize the molecular mechanisms via which tumors may progress and to identify the molecular mechanisms underlying different prognoses.

2. Materials and Methods

2.1. Patients and Samples

A total of 124 patients were recruited by 35 hospitals from February 2016 to September 2021. Written consent was obtained for all enrolled patients. This study was approved by the Ethical Committee of Hospital Puerta de Hierro, Madrid, Spain (internal code: PI 02/16), and conducted in accordance with the precepts of the Code of Ethics of the World Medical Association (Declaration of Helsinki). All patients included in this study were diagnosed with stage IV *EGFR*-positive NSCLC (as per the criteria of the American Joint Committee on Cancer, seventh edition). *EGFR* testing in the FFPE tissue sample was carried out in the pathology department of each participating hospital. Patients were at least 18 years old with a life expectancy of over 12 weeks. All patients were treated with a first-line *EGFR*-TKI. The choice of TKI therapy was left to the discretion of the physician. A plasma sample was collected in an 8.5 mL PPT™ tube (Becton Dickinson, Franklin Lakes, NJ, USA) upon disease progression (n = 124). Treatment response was assessed as per

Response Evaluation Criteria in Solid Tumors (RECIST) version 1.1 criteria. The average time between the diagnosis disease progression and blood drawn was 5.4 days.

2.2. Laboratory Procedures

Blood samples were centrifuged at 1600× *g* for 10 min then immediately at 6000× *g* for 10 min; both centrifugations were performed at room temperature. Hemolyzed samples were excluded. Circulating cell-free DNA (cfDNA) was extracted from the resulting plasma using cfDNA QIAmp Circulating Nucleic Acid kit (Qiagen, Hiden, Germany) following the manufacturer's protocol. cfDNA was quantified using Qubit 2.0 Fluorometer with a Qubit 1× dsDNA HS Assay Kit (Thermo Fisher, Palo Alto, CA, USA). Libraries were prepared using the Oncomine™ Pan-Cancer Cell-Free Assay kit (Thermo Fisher, Palo Alto, CA, USA), according to the manufacturer's instructions (the list of genes covered by this panel is available in Supplementary Data S1). The minimum input of cfDNA from each sample required for library preparation was 10 ng, and the maximum volume was 10.4 µL. If less volume of cfDNA was used, RNase-free water was added up to a total volume of 10.4 µL. For library purification, AMPureXP magnetic beads (Beckman Coulter, Inc., Brea, CA, USA) were used. Finally, libraries were diluted to 50 pM using the quantification values obtained from an Ion Library TaqMan® Quantitation Kit (Thermo Fisher, Palo Alto, CA, USA) in a StepOnePlus™ qPCR machine (Thermo Fisher, Palo Alto, CA, USA). Libraries were prepared in batches of eight and were stored at −20 °C up to a maximum of 2 weeks until pool preparation.

A total of 16 samples were sequenced in every NGS run using two Ion 550™ Chips, each of them loaded with eight pooled samples. Templating and Ion 550™ Chip loading were carried out with an Ion Chef™ System (Thermo Fisher, Palo Alto, CA, USA), and then chips were sequenced on an Ion GeneStudio™ S5 Sequencer (Thermo Fisher, Palo Alto, CA, USA). Torrent Suite Software v5.12.2 was used to perform raw sequencing data analysis. The CoverageAnalysis v5.12.2 plugin was used for sequencing coverage analysis. Raw reads were aligned to the human reference genome hg19. Variant calling was carried out on the Ion Reporter platform v.5.18 using Oncomine TagSeq Pan-Cancer Liquid Biopsy—w2.5—Single Sample (workflow versions from w2.1 to w2.5 were used). Variant filtering was performed using an internal pipeline. The pipeline uses the raw data in the non-filtered-oncomine.tsv, which contains variants that have passed the OncomineVariants (v.5.12) filter and variants that have not. Specific conditions were established for single-nucleotide variants (SNVs), insertions or deletions (indels), multiple-nucleotide polymorphisms (MNP), fusions, and copy number variant (CNV) calls. Detailed information about the pipeline is available in Supplementary Figure S1. All candidate mutations were manually reviewed using the Integrative Genomics Viewer (IGV) v.2.3.40, (Broad Institute, Cambridge, MA, USA). The clinical significance of somatic variants was determined according to the Standards and Guidelines for the Interpretation and Reporting of Sequence Variants in Cancer [21]. The pathogenicity of *TP53* and *APC* variants was assessed according to *TP53*-specific ACMG/AMP guidelines [22].

Genomic variants identified by NGS were further confirmed by digital PCR (dPCR) (the mutant allele frequency concordance between NGS and dPCR is shown in Supplementary Figure S2). A complete list of validated variants is available in Supplementary Data S2. In addition, variants identified as potential resistance mechanisms were retrospectively tracked using dPCR (or NGS in the case of CNVs) in all cases in which a baseline sample (before treatment initiation) was available (Supplementary Data S3). dPCR was carried out using predesigned or customized TaqMan® dPCR assays in a QuantStudio® 3D Digital PCR (Applied Biosystems®, South San Francisco, CA, USA). An 18 µL final reaction mix was obtained with 8.55 µL of template cfDNA, 9 µL of 20× QuantStudio® Master Mix, and 0.45 µL 40× TaqMan assay. Then, 14.5 µL of the final reaction volume was loaded to a QuantStudio® 3D digital PCR 20K chip. Positive and negative controls were included in every run. Thermal cycler conditions were defined as a first denaturalization step at 96 °C for 10 min, followed by 40 cycles at 56 °C for 2 min and 98 °C for 30 s, an elongation step at

72 °C for 10 min, before finally maintaining the samples at 22 °C for at least 30 min. Then, chip fluorescence was read twice using two independent QuantStudio® 3D Digital PCR instruments. The analysis was performed with QuantStudio® 3D AnalysisSuite™ Cloud; the default call assignment for each read was manually adjusted when needed. The limits of detection and quantitation of the dPCR TaqMan® assays were estimated according to the recommendations of The International Council for Harmonization of Technical Requirements for Pharmaceuticals for Human Use; ICH Q2 (R1) guidelines (validation of analytical procedures: text and methodology), as published elsewhere [23].

2.3. Statistical Analysis

Categorical variables are summarized as frequencies, and potential associations were evaluated using the chi-square test or Fisher's test as appropriate, whereas continuous variables are shown as the mean and standard deviation (non-normally distributed variables are displayed as the median, along with 25th and 75th percentiles), and potential associations were tested using Student's *t*-test or the Mann–Whitney U test.

Overall survival (OS) was defined as the time from diagnosis of stage IV NSCLC to death from any cause or the censored date of the last follow-up for patients who were alive when the data were extracted. Progression-free survival (PFS) was defined as the time between the start of *EGFR*-TKI treatment and disease progression, as assessed by RECIST criteria, and death from any cause or the censored date of the last follow-up, whichever occurred first. Survival was evaluated using the Kaplan–Meier method with Cox proportional hazards model assumption. The log-rank test was used to assess statistical differences between Kaplan–Meier survival curves. Hazard ratios (HRs) were estimated from the Cox model using a univariate approach. The statistical analysis was performed using R software (v.4.1.2) and Stata version 16.0 (StataCorp 2019, Stata Statistical Software Release 16; StataCorp LLC, College Station, TX, USA).

3. Results

3.1. Study Cohort

Between February 2016 and September 2021, 124 blood samples from advanced *EGFR*-positive NSCLC patients were collected upon disease progression to a first-line *EGFR*-TKI. The clinical characteristics of the study population are presented in Table 1. Patients were mostly women (77; 62.1%) and never-smokers (71; 57.3%). The mean age at diagnosis was 65.8 years (range 38–89). A total of 116 (93.6%) cases were adenocarcinomas, and the majority were stage IVB (64; 51.6%). Most patients had an Eastern Cooperative Oncology Group Performance Status (ECOG-PS) of 0 or 1 (72; 58.1%). All patients were treated with a first-line *EGFR*-TKI; 62 received afatinib (50%), 26 received erlotinib (21%), 33 received gefitinib (26.6%), and three were treated with osimertinib (2.4%).

According to the pathologist´s report, 68 (54.8%) tumors tested positive for deletions in exon 19, 43 (34.7%) tumors harbored the point mutation p.L858R in exon 21, and six (4.8%) tumors harbored insertions in exon 20. Point mutations at codon 719 (p.G719X), in exon 18, were found in three (2.4%) cases, and the p.L861Q mutation, in exon 21, was also detected in three (2.4%) cases. Lastly, one tumor harbored two concomitant *EGFR*-sensitizing mutations, namely, the p.S768I mutation, in exon 20, and the deletion p.E746_A750del, in exon 19.

Survival data were available for 91 patients. The median follow-up for this population was 46.7 (37.3 to 49.8) months, and the median OS was 23.6 (17.7 to 33) months. Kaplan–Meier curve for PFS, according to the original sensitizing mutations, is depicted in Supplementary Figure S3.

Table 1. Descriptive analysis of the study cohort.

Clinicopathologic Characteristics	*N* = 124
Age, mean (SD), years	65.8 (11.1)
Sex, No. (%) with data	
Female	77 (62.1)
Male	47 (37.9)
Smoking, No. (%) with data	
Never-smokers	71 (57.3)
Active smokers	9 (7.2)
Former smokers	44 (35.5)
ECOG-PS [a], No. (%) with data	
0	35 (28.2)
1	37 (29.8)
2	5 (4.0)
Stage, No. (%) with data	
IVA	60 (48.4)
IVB	64 (51.6)
Histology, No. (%) with data	
Adenocarcinoma	116 (93.6)
Adenosquamous	2 (1.6)
Large cell	4 (3.2)
Squamous	2 (1.6)
Metastases at IV stage diagnosis [b], No. (%) with data	
Local	88 (71)
Bone	61 (49.2)
CNS	18 (14.5)
Liver	17 (13.7)
Progression site [c], No. (%) with data	
Bone	21 (16.9)
CNS	13 (10.5)
Liver	13 (10.5)
EGFR mutation, No. (%) with data	
Del19	68 (54.8)
G719X	3 (2.4)
Ins20	6 (4.8)
L858R	43 (34.7)
L861Q	3 (2.4)
>1 mut.	1 (0.8)
Treatment, No. (%) with data	
Afatinib	62 (50)
Erlotinib	26 (21)
Gefitinib	33 (26.6)
Osimertinib	3 (2.4)
Second line treatment [d], No. (%) with data	
Osimertinib	63 (50.8)
Others	25 (20.2)
None	8 (6.4)
Exitus [e]	
Yes	59 (47.6)
No	32 (25.6)

[a] 47 patients without information; [b] 5 patients without information; [c] 52 patients without information; [d] 28 patients without information; [e] 33 patients without information. Abbreviations: CNS: central nervous system; ECOG-PS: Eastern Cooperative Oncology Group Performance Status.

detected in three (2.4%) cases. Lastly, one tumor harbored two concomitant *EGFR*-sensitizing mutations, namely, the p.S768I mutation, in exon 20, and the deletion p.E746_A750del, in exon 19.

Survival data were available for 91 patients. The median follow-up for this population was 46.7 (37.3 to 49.8) months, and the median OS was 23.6 (17.7 to 33) months. Kaplan–Meier curve for PFS, according to the original sensitizing mutations, is depicted in Supplementary Figure S3.

3.2. Molecular Landscape upon Disease Progression

In total, 365 somatic variants were detected across 32 genes (Figure 1). The most frequent types of variants detected were SNPs (73.9%), followed by indels (24.8%) and CNVs (1.3%). A database containing all detected mutations is available in Supplementary Data S4.

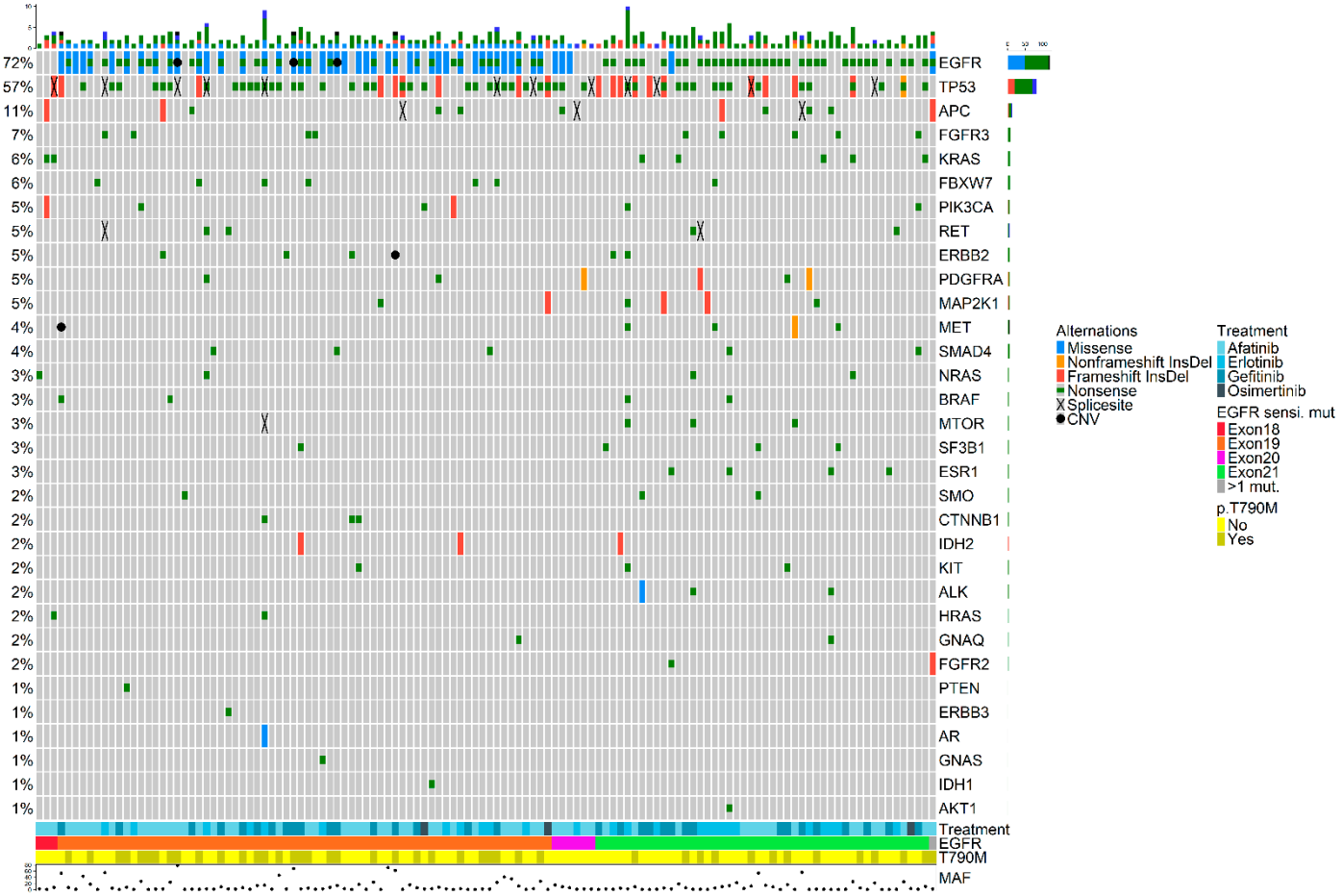

Figure 1. OncoPrint plot showing the distribution of genomic alterations detected in the plasma samples collected upon disease progression. Overview of genomic alterations (legend) in particular genes (rows) for each sample (columns). Missense mutations, non-frameshift deletions or insertions, frameshift deletions or insertions, nonsense mutations, splice site mutations, and CNVs are shown as green rectangles, blue rectangles, red rectangles, black crosses, orange rectangles, and a black dots, respectively. At the bottom of the plot, the following features are presented: first the *EGFR*-TKI type of original *EGFR*-sensitizing mutation, and detection of the p.T790M resistance mutation at disease progression. The maximum value of MAF from all detected variants is also shown. Co-occurring mutations were not associated with smoking history and did not have an impact on overall survival (OS). CNV: copy number variant; InsDel: insertion or deletion; MAF: mutated allele frequency.

The mean number of detected mutations per sample was 2.9 (range 1–16) with a median mutant allele frequency (MAF) of 5.2% (range 0.1–77.7%) (Supplementary Table S1). Excluding *EGFR* mutations, the most frequently mutated gene was *TP53*, which was mutated in 57.3% of the cases, followed by *APC* (11.3%), *FGFR3* (7.3%), and *KRAS* (5.6%) (Supplementary Table S2). Patients in whom a pathogenic mutation (class 5 or class 4) in *TP53* or *APC* was detected upon disease progression did not show inferior OS compared to patients who did not.

As depicted in Figure 1, a widespread presence of co-occurring genetic alterations was observed. Specifically, 67.7% of the samples had concomitant mutations alongside

the original *EGFR*-sensitizing mutation which was detected in the plasma sample of 89 patients (71.8%).

Plasma detection of the original *EGFR*-sensitizing mutation was more challenging in samples from patients with tumor progression exclusively at the brain level, compared with patients diagnosed as having disease progression in other locations (*EGFR* detection rate of 61.5% vs. 76.3%, respectively). On the contrary, the original *EGFR* mutation was detected in all samples from patients with disease progression at the hepatic level (13/13) ($p = 0.015$). The *EGFR* p.T790M resistance mutation was detected in 43 patients.

Oncogenic mutations in other genes were also observed. Specifically, the gain-of-function mutation p.P124L in *MAP2K1* was observed in two cases. Furthermore, the p.E545K mutation in *PIK3CA* was detected in one patient. This mutation was absent at baseline, as well as at 3 months from treatment initiation, further supporting its role as a resistance mutation (Table 2). Similarly, the p.V600E mutation in *BRAF* was detected at disease progression in one case and tested negative in samples collected previously (Table 2; Supplementary Data S3).

Table 2. dPCR Validation and retrospective tracking of oncogenic mutations detected upon disease progression.

Sample	Gene	Coding Transcript Change	Protein Change	Functional Classification	PFS [b]	OS [b]	B	≈3	≈6	P
400003	*KRAS*	c.35G>T	p.G12V	Missense	5.8	NA	-	-	-	🟢
1000040	*KRAS*	c.182A>G	p.Q61R	Missense	9.7	NA	-	-	-	🟡
8500002	*KRAS*	c.34G>A	p.G12S	Missense	12.3	NA	-	-	-	🟢
03-002 [a]	*MET*	CNV	CNV	CNV	2.8	3	🟢			🟢
11-006	*KRAS*	c.34G>T	p.G12C	Missense	11.7	15.5	🔴	🔴	🔴	🟢
11-008	*PIK3CA*	c.1633G>A	p.E545K	Missense	7.7	15	🔴	🔴	-	🟢
13-014	*BRAF*	c.1799T>A	p.V600E	Missense	15.8	34.2	🔴	🔴	🔴	🟢
13-015 [a]	*EGFR*	CNV	CNV	CNV	9.5	18.5	🔴			🟢
15-012 [a]	*EGFR*	CNV	CNV	CNV	3.9	5.9	🟢			🟢
19-001 [a]	*EGFR*	CNV	CNV	CNV	21.3	25.5	🔴			🟢
21-005 [a]	*ERBB2*	CNV	CNV	CNV	7.5	25.9	🔴			🟢
26-004	*KRAS*	c.436G>A	p.A146T	Missense	2.8	14.3	🟢	-	-	🟢
33-001	*KRAS*	c.44G>T	p.G15V	Missense	11.9	30.4	🔴	🔴	🔴	🟡
36-005	*KRAS*	c.183A>C	p.Q61H	Missense	7.6	9.7	🔴	🔴	🔴	🟡
36-005	*KRAS*	c.35G>A	p.G12D	Missense	7.6	9.7	🔴	🔴	🔴	🟢

[a] Samples from this patient were evaluated by NGS. [b] Calculated in months. Red dots represent that the variant was absent in the sample, green dots indicate detection of the mutation in the sample, and yellow dots are depicted when the variant could not be validated by dPCR due to the lack of sample. In this case, only the NGS data are available. Three *KRAS* variants (p.G15V, p.Q61H, and p.Q61R) were not confirmed by dPCR because of a lack of sample, whereas the remaining *KRAS* mutations were validated by dPCR. Unfortunately, there were no previous samples for the patients whose tumors harbored p.G12V, p.Q61R, and G12S mutations. Abbreviations: B: baseline sample (before the start of treatment); ≈3: sample extracted during treatment (after 3 months of treatment approximately); ≈6: sample extracted during treatment (after 6 months of treatment approximately); P: sample extracted at the moment of disease progression; PFS: progression-free survival; OS; overall survival.

Eight oncogenic variants in *KRAS*, namely, p.G12C, p.G12V, p.G12S, p.G12D, p.G15V, p.Q61R, p.Q61H, and p.A146T were detected in seven samples (5.6%) (Table 3). Of them, the p.G12C, p.G15V, p.Q61H, and p.G12D mutations were imputed as acquired resistance mechanisms as they were not detected in the previous samples from the corresponding cases. Conversely, the *KRAS* mutation p.A146T was found at baseline and corresponded to a patient showing the worst PFS (2.8 months) among all *KRAS*-positive cases (Table 2).

Table 3. Clinicopathological features of *KRAS* mutated cases.

	400003	1000040	8500002	11-006	26-004	33-001	36-005
***KRAS* mutation by NGS (coding/protein)**	c.35G>T/p.G12V	c.182A>G/p.Q61R	c.34G>A/p.G12S	c.34G>T/p.G12C	c.436G>A/p.A146T	c.44G>T/p.G15V	c.183A>C/p.Q61H c.35G>A/p.G12D
MAF *KRAS* mutation (%)	4.15	0.18	0.62	18.11	0.19	0.57	3.67/0.64
***EGFR* mutation by NGS (coding/protein)**	Not detected	c.2573T>G/p.L858R	c.2573T>G/p.L858R	c.2582T>A/p.L861Q	Not detected	Not detected	c.2573T>G/p.L858R
MAF *EGFR* mutation (%)	-	0.30	9.77	2.15	-	-	25.63
p.T790M by NGS	Not detected	Not detected	Detected	Not detected	Not detected	Not detected	Not detected
***EGFR* mutation in tumor at stage IV diagnosis**	p.G719X	p.L858R	p.L858R	p.L861Q	p.G719X	p.L858R	p.L858R
Sex	Male	Female	Male	Female	Female	Female	Female
Age (years)	74	76	74	68	58	79	52
Smoking	Former smoker	Former smoker	Former smoker	Smoker	Never-smoker	Never-smoker	Never-smoker
Histology	Adenocar.	Adenocar.	Adenocar.	Adenocar.	Adenocar.	Adenocar.	Adenocar.
ECOG-PS	NA	NA	NA	0	1	1	1
Metastasis location at stage IV diagnosis	Thoracic and bone	Bone	Thoracic	Thoracic	Bone and CNS	Thoracic	CNS
Stage	IVB	IVB	IVA	IVA	IVB	IVA	IVB
First-line TKI	Afatinib	Gefitinib	Afatinib	Afatinib	Afatinib	Erlotinib	Afatinib
PFS (months)	5.8	9.7	12.3	11.7	2.8	11.9	7.6
Progression site	NA	NA	NA	CNS	Liver	NA	NA
Second-line treatment	None	Gefitinib	Osimertinib	None	None	Chemoth.	Osimertinib
Exitus	NA	NA	NA	Yes	Yes	No	Yes
OS (months)	NA	NA	NA	15.5	14.3	30.4	9.7

Adenocar.: adenocarcinoma; Chemoth.: chemotherapy; CNS: central nervous system; ECOG-PS: Eastern Cooperative Oncology Group Performance Status; MAF: mutant allele frequency; NA: not available; NGS: next-generation sequencing; OS: overall survival; PFS: progression-free survival.

Lastly, CNVs in *EGFR* (n = 3), *MET* (n = 1), and *ERBB2* (n = 1) were detected in five cases. These CNVs were absent in the pretreatment samples in three cases but were detected at baseline in two cases with *MET* and *EGFR* amplification. Patients in whom CNVs were detected at baseline showed the shortest PFS (2.8 and 3.9 months), suggesting primary resistance through amplification of *MET* or *EGFR*, respectively (Figure 2 and Table S2).

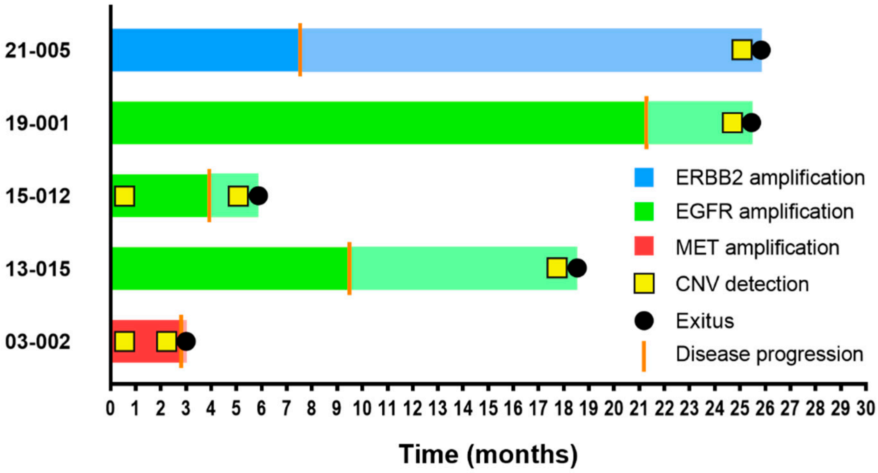

Figure 2. Swimmer plot of PFS and OS in CNV-positive patients. The PFS bar plot appears in dark color, whereas OS is represented continuing the same bar but in attenuated color. Disease progression and exitus events are shown on bar plots as a vertical orange line and a black dot, respectively. CNV detection by NGS is represented with a yellow square.

Figure 2. Swimmer plot of PFS and OS in CNV-positive patients. The PFS bar plot appears in dark color, whereas OS is represented continuing the same bar but in attenuated color. Disease progression and exitus events are shown on bar plots as a vertical orange line and a black dot, respectively. CNV detection by NGS is represented with a yellow square.

3.3. Exon Location of the Original Sensitizing Mutation Determines Distinct Molecular Profiles upon Disease Progression

3.3. Exon Location of the Original Sensitizing Mutation Determines Distinct Molecular Profiles upon Disease Progression

Detection of the p.T790M mutation was more frequent in tumors harboring an *EGFR* mutation in exon 19 compared with tumors harboring an *EGFR* mutation in exon 21 (p = 0.028). Among p.T790M-negative cases, two cases showed clinically actionable mutations upon disease progression, which included a *MET* amplification and the p.G12C mutation in *KRAS*. The druggable p.V600E mutation in *BRAF* was detected in one case, which harbored an exon 19 deletion and tested positive for the p.T790M mutation.

We further tested whether other specific genetic co-alterations tended to be *EGFR* exon-dependent. Comparison of the frequency of genetic co-alterations present in samples from tumors harboring an exon 19 mutation with those with a mutation in exon 21 revealed significant enrichment for *KRAS* mutations in tumors harboring *EGFR*-sensitizing mutations in exons 18 and 21 (p < 0.001) (Figure 3). Noteworthy, three of the *KRAS* mutated cases (n = 7) harbored an uncommon *EGFR* mutation: the p.G719X mutation in two cases and the p.L861Q mutation in one case. The associations between uncommon *EGFR*-sensitizing mutations and *KRAS* mutations was also significant (p = 0.002).

Detection of the p.T790M mutation was more frequent in tumors harboring an *EGFR* mutation in exon 19 compared with tumors harboring an *EGFR* mutation in exon 21 (p = 0.028). Among p.T790M-negative cases, two cases showed clinically actionable mutations upon disease progression, which included a *MET* amplification and the p.G12C mutation in *KRAS*. The druggable p.V600E mutation in *BRAF* was detected in one case, which harbored an exon 19 deletion and tested positive for the p.T790M mutation.

We further tested whether other specific genetic co-alterations tended to be *EGFR* exon-dependent. Comparison of the frequency of genetic co-alterations present in samples from tumors harboring an exon 19 mutation with those with a mutation in exon 21 revealed significant enrichment for *KRAS* mutations in tumors harboring *EGFR*-sensitizing mutations in exons 18 and 21 (p < 0.001) (Figure 3). Noteworthy, three of the *KRAS* mutated cases (n = 7) harbored an uncommon *EGFR* mutation: the p.G719X mutation in two cases and the p.L861Q mutation in one case. The associations between uncommon *EGFR*-sensitizing mutations and *KRAS* mutations was also significant (p = 0.002).

A similar pattern was observed for *NRAS* (n = 4) (Supplementary Table S3) and *HRAS* (n = 2) (Supplementary Table S4); mutations in these genes were more frequently detected in samples from tumors harboring mutations in exons 18 or 21 (p = 0.050 and p = 0.099, respectively) (Figure 3).

3.4. Prognostic Value of Circulating Tumor DNA

The prognostic value of circulating tumor DNA (ctDNA) levels was evaluated using different methodological approaches. To this aim, we calculated the mean, maximum, and sum of MAF from the set of all detected variants for each sample, and we established different MAF thresholds (ranging from 1% to 10%). In addition, the prognostic value of the MAF of the original *EGFR*-sensitizing mutation was tested. As presented in Table 4 and Figure 4A, the amount of ctDNA was of prognostic significance regardless of the approach used. Overall, patients with high ctDNA at disease progression had significantly worse

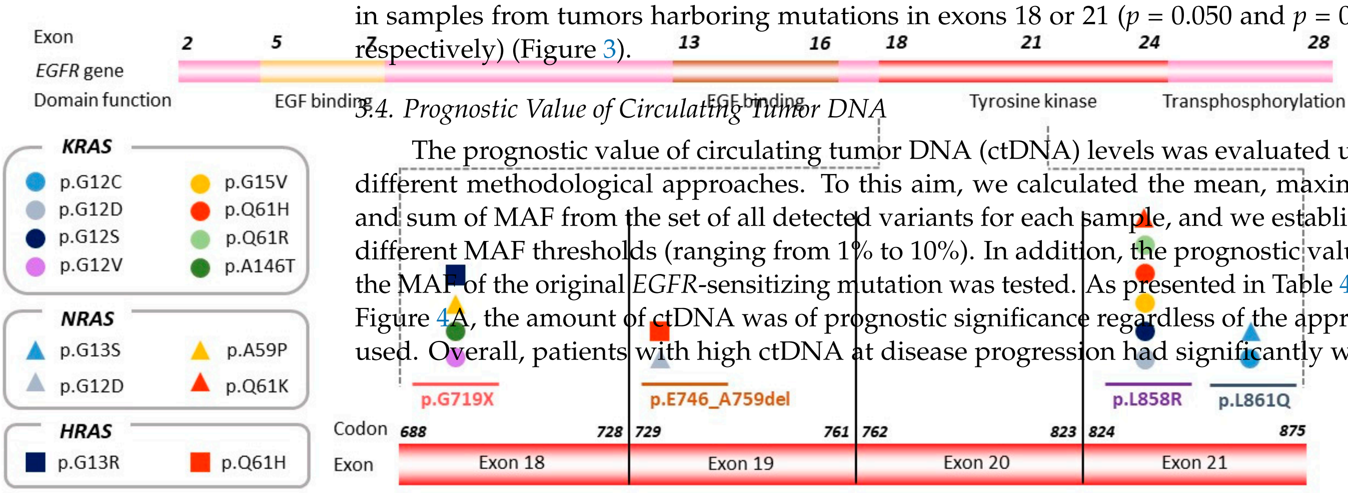

Figure 3. *KRAS*, *NRAS*, and *HRAS* mutations detected by NGS according to exon location of the

0.028). Among p.T790M-negative cases, two cases showed clinically actionable mutations upon disease progression, which included a *MET* amplification and the p.G12C mutation in *KRAS*. The druggable p.V600E mutation in *BRAF* was detected in one case, which harbored an exon 19 deletion and tested positive for the p.T790M mutation.

We further tested whether other specific genetic co-alterations tended to be *EGFR* exon-dependent. Comparison of the frequency of genetic co-alterations present in samples from tumors harboring an exon 19 mutation with those with a mutation in exon 21 revealed significant enrichment for *KRAS* mutations in tumors harboring *EGFR*-sensitizing mutations in exons 18 and 21 ($p = 0.001$) (Figure 3). Noteworthy, three of the *KRAS*-mutated cases ($n = 7$) harbored an uncommon *EGFR* mutation: the p.G719X mutation in two cases and the p.L861Q mutation in one case. The associations between uncommon *EGFR*-sensitizing mutations and *KRAS* mutations was also significant ($p = 0.042$).

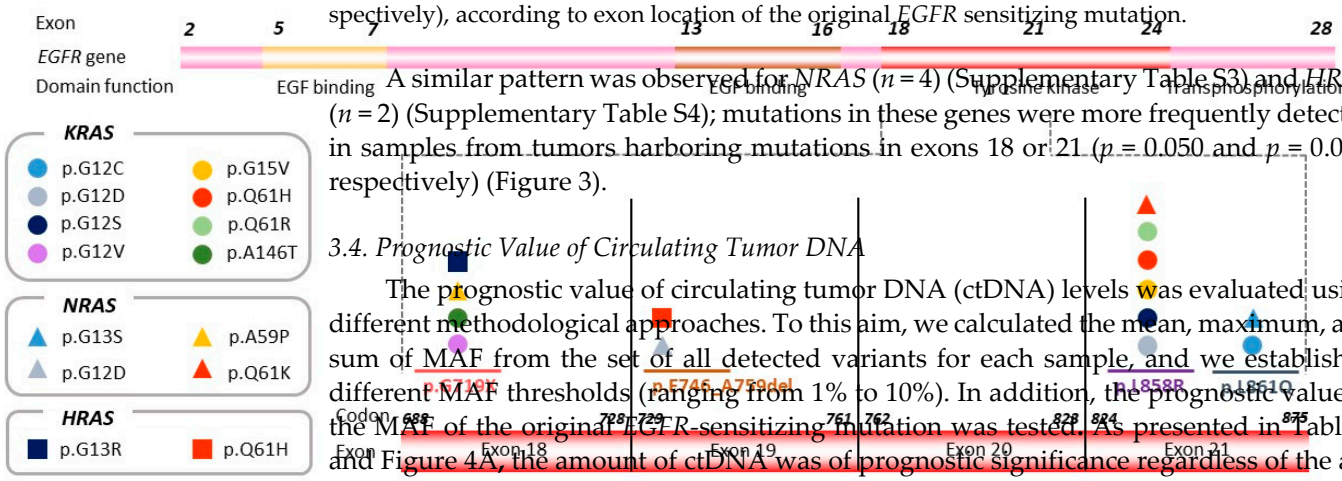

Figure 3. *KRAS*, *NRAS*, and *HRAS* mutations detected by NGS according to exon location of the original *EGFR*-sensitizing mutation. The *EGFR* gene is represented, and the region including exons 18–21 is magnified in order to show the distribution of *KRAS*, *NRAS*, and *HRAS* variants detected in the plasma sample upon disease progression (represented by circles, rectangles, and squares, respectively), according to exon location of the original *EGFR* sensitizing mutation.

A similar pattern was observed for *NRAS* ($n = 4$) (Supplementary Table S3) and *HRAS* ($n = 2$) (Supplementary Table S4); mutations in these genes were more frequently detected in samples from tumors harboring mutations in exons 18 or 21 ($p = 0.050$ and $p = 0.099$, respectively) (Figure 3).

3.4. Prognostic Value of Circulating Tumor DNA

The prognostic value of circulating tumor DNA (ctDNA) levels was evaluated using different methodological approaches. To this aim, we calculated the mean, maximum, and sum of MAF from the set of all detected variants for each sample, and we established different MAF thresholds (ranging from 1% to 10%). In addition, the prognostic value of the MAF of the original *EGFR*-sensitizing mutation was tested. As presented in Table 4 and Figure 4A, the amount of ctDNA was of prognostic significance regardless of the approach used. Overall, patients with high ctDNA at disease progression had significantly worse OS than those patients in which the opposite situation occurred (Table 4 and Figure 4B–E). Kaplan–Meier curves for the <5% MAF cutoff are shown in Figure 4B–E. Using a cut-off of sum MAF < 5%, the median OS was 16 months (95% CI: 14 to 21.2) in patients with high ctDNA levels (MAF ≥ 5%) compared with 43.7 months (95% CI: 23.6 to NR) for patients with ctDNA levels below that cutoff.

Figure 4. OS according to ctDNA levels upon disease progression. (**A**) Hazard ratios (HRs) for OS are depicted for each MAF cutoff value and according to the quantification approach (mean: blue circles; max: blue squares; max driver: purple triangles; sum: pink upside-down triangles). The horizontal dashed line delimits the confidence intervals. Large red rectangles highlight the MAF cutoff represented in the Kaplan–Meier curves. (**B**–**E**) Kaplan–Meier curves for OS according to MAF cutoff (5%) measured using different methodological approaches. Median OS for each group; log-rank *p*-values and HRs are shown at the left bottom side and right upper side, respectively. Mean MAF was calculated as the mean of the MAF from the set of all variants detected for each sample. Max MAF was defined as the maximum MAF among the set of variants detected for each sample. Driver

circles; max: blue squares; max driver: purple triangles; sum: pink upside-down triangles). The horizontal dashed line delimits the confidence intervals. Large red rectangles highlight the MAF cutoff represented in the Kaplan–Meier curves. (**B**–**E**) Kaplan–Meier curves for OS according to MAF cutoff (5%) measured using different methodological approaches. Median OS for each group; log-rank *p*-values and HRs are shown at the left bottom side and right upper side, respectively. Mean MAF was calculated as the mean of the MAF from the set of all variants detected for each sample. Max MAF was defined as the maximum MAF among the set of variants detected for each sample. Driver MAF was defined as the MAF of the *EGFR*-sensitizing mutation. This analysis was carried out using 89 samples which had detectable *EGFR* variants. Sum MAF was calculated as the sum of MAF from the set of variants detected for each sample. CI: confidence interval; CNV: copy number variant; HR: hazard ratio; MAF: mutant allele frequency; NA: not available; Ref.: reference category.

Table 4. HR and corresponding 95% CI according to MAF cutoff assessed using four different approaches.

MAF Cutoff	Mean MAF [a]		Max MAF [b]		Driver MAF [c]		Sum MAF [d]	
	HR (95%CI)	*p*-Value	HR (95%CI)	*p*-Value	HR (95%CI)	*p*-Value	HR (95%CI)	*p*-Value
1%	0.40 (0.23–0.71)	0.002	0.44 (0.25–0.81)	0.008	0.39 (0.23–0.68)	0.001	0.71 (0.38–1.34)	0.295
2%	0.40 (0.23–0.67)	0.001	0.39 (0.23–0.66)	0.001	0.44 (0.26–0.74)	0.002	0.47 (0.26–0.82)	0.009
3%	0.48 (0.29–0.81)	0.006	0.38 (0.23–0.65)	<0.001	0.45 (0.27–0.75)	0.003	0.39 (0.22–0.67)	0.001
4%	0.53 (0.31–0.91)	0.022	0.37 (0.22–0.63)	<0.001	0.43 (0.26–0.73)	0.002	0.40 (0.23–0.68)	0.001
5%	0.40 (0.23–0.69)	0.001	0.46 (0.28–0.78)	0.004	0.50 (0.30–0.84)	0.009	0.38 (0.22–0.65)	<0.001
6%	0.45 (0.25–0.79)	0.006	0.48 (0.29–0.82)	0.007	0.50 (0.30–0.85)	0.010	0.43 (0.26–0.73)	0.002
7%	0.41 (0.22–0.74)	0.003	0.43 (0.25–0.72)	0.002	0.44 (0.26–0.75)	0.003	0.45 (0.27–0.76)	0.003
8%	0.44 (0.24–0.81)	0.008	0.46 (0.27–0.78)	0.004	0.47 (0.28–0.81)	0.007	0.49 (0.29–0.82)	0.006
9%	0.44 (0.24–0.81)	0.008	0.40 (0.23–0.70)	0.001	0.42 (0.24–0.72)	0.002	0.43 (0.26–0.73)	0.002
10%	0.41 (0.22–0.77)	0.005	0.42 (0.25–0.73)	0.002	0.44 (0.25–0.76)	0.003	0.49 (0.29–0.82)	0.007

[a] Mean MAF was calculated as the mean of the MAF set of variants detected for each sample. [b] Max MAF was defined as the maximum MAF among the set of variants detected for each sample. [c] Driver MAF was defined as the maximum MAF among *EGFR*-sensitizing variants detected for each sample. This analysis was carried out using 89 samples which had detectable *EGFR* variants. [d] Sum MAF was calculated as the summation of the MAF set of variants detected for each sample. HRs and *p*-values were calculated using univariate Cox model analysis. All data were estimated for overall survival. CI: confidence interval; HR: hazard ratio; MAF: mutant allele frequency.

4. Discussion

Several different mechanisms of acquired resistance to *EGFR* inhibitors have been described so far [24–26]. The wide variety of resistance mutations highlights the importance of tumor heterogeneity in shaping tumor resistance to targeted therapies. To our knowledge, here, we report for the first time that *EGFR*-TKI resistance through acquired *KRAS* mutation could be dependent on the exon location or type of mutation of the original *EGFR*-sensitizing mutation, suggesting that tumor resistance could be driven by the position in the genome of the original *EGFR* mutation. This hypothesis is plausible considering

that it is well established that *EGFR*-mutant NSCLC patients have different sensitivity to targeted therapies according to the exon in which the original sensitizing mutation is detected [27]. This circumstance was also observed in our cohort (Supplementary Figure S3). In other words, *EGFR*-positive NSCLC tumors can be classified into different subtypes with different survival outcomes defined by the location of the *EGFR*-sensitizing mutation. In this way, unlike *EGFR* exon 19 deletions and point mutations in exon 21, most NSCLC tumors harboring *EGFR* exon 20 insertion mutations do not benefit from *EGFR*-TKIs with response rates reported to be below 5% and short intervals of disease control [28]. Indeed, important efforts have been made in order to develop effective therapies for this particular subset of patients in recent years [29].

Overall, TKI resistance can be classified into *EGFR*-dependent and *EGFR*-independent mechanisms. The p.T790M mutation is the most commonly observed resistance mechanism in NSCLC patients treated with first- and second-generation *EGFR*-TKIs [30–32]. In our study, the p.T790M mutation was significantly more frequently detected in tumors harboring a mutation in exon 19. This finding is consistent with previous reports [12,33]. Furthermore, in our cohort, amplifications in *EGFR*, *MET*, and *ERBB2* were detected in five cases. *MET* gene amplification has been identified as a resistance mechanism for afatinib, gefitinb, erlotinib, and osimertinib [34–37]. Indeed, dual inhibition of *EGFR* and *MET* represents a promising treatment strategy [11]. Similarly, *ERBB2* amplifications have been observed in tumors with acquired resistance to erlotinib, gefitinib, and osimertinib [38,39]. Oncogenic mutations in *MAP2K1* and *PIK3CA* genes were also found in three cases. It is well established that activation of downstream *EGFR* signaling pathways such as *MAPK*/*ERK* or *PIK3CA*/*AKT* signaling pathways play an important role in *EGFR*-TKI resistance [40,41]. Similarly, acquired mutations in *BRAF* have been shown to underline *EGFR*-TKI resistance [42,43]. In our cohort, the p.V600E mutation in *BRAF* was detected alongside the p.T790M resistance mutation in one patient whose tumor harbored a deletion in exon 19. Similarly, a case report by Chao-Chi Ho et al. reported the acquisition of the mutation *BRAF* p.V600E in a patient with p.T790M at the time of progression while being treated with osimertinib [42]. In our study, ctDNA profiling was carried out with a relatively small NGS panel. The Oncomine™ Pan-Cancer Cell-Free Assay kit (Thermo Fisher, Palo Alto, CA, USA) covers hotspots in 52 genes. Therefore, these results should be interpreted with caution and they must be validated with larger cohorts.

The fact that *KRAS* mutations were more frequently detected in tumors harboring mutations in exon 18 and 21 or uncommon mutations may have important implications for the development of clinical trials evaluating the efficacy of dual or consecutive *EGFR* and *KRAS* blockage. It has previously been documented that the druggable mutation *KRAS* p.G12C is found in approximately 1% of *EGFR*-positive NSCLC patients progressing on a first-line treatment with an *EGFR*-TKI, and it tended to arise in tumors harboring *EGFR* uncommon mutations [44], supporting our findings.

Lastly, the amount of ctDNA at disease progression significantly correlated with OS. There is large evidence indicating that ctDNA levels significantly correlate with tumor bulk and, therefore, can be used to monitor disease [12,45,46]. Moreover, ctDNA levels are of prognostic significance [12]. Indeed it has been proposed to include ctDNA in the tumor staging system [47]. Nevertheless, it is not well established how ctDNA should be measured, especially when tumors do not harbor druggable mutations. As an exploratory approach, here, we evaluated the prognostic value using different methods (median of MAF from all mutations detected, maximum MAF of all detected mutation, MAF of the original *EGFR*-sensitizing mutation, and summation MAF of all detected mutations), and similar results were obtained.

5. Conclusions

Different molecular heterogeneous alterations were observed upon disease progression, highlighting the importance of heterogeneity driving tumor resistance. Our data suggest that the mechanisms underlying resistance could be dependent on the exon loca-

tion of the original *EGFR*-sensitizing mutation. Further studies are warranted to confirm this observation.

Supplementary Materials: The following are available online at https://www.mdpi.com/article/10.3390/cancers14184446/s1, Figure S1: Flowchart of the bioinformatic pipeline optimized for processing and assessing variants using the Oncomine™ Pan-Cancer Cell-Free Assay; Figure S2: Linear correlation between MAF assessed by NGS and dPCR for driver EGFR and p.T790M mutations; Figure S3: Kaplan–Meier curve for PFS according to exon location of EGFR-sensitizing mutation at diagnosis of advanced NSCLC; Table S1: Types of mutations detected using NGS. MAF and MAPD parameters; Table S2: Number of patients with tumors harboring mutations in each gene covered by the NGS panel; Table S3: Relevant information regarding *NRAS*-mutated patients; Table S4: Relevant information regarding *HRAS*-mutated patients; Data S1: Datasheet with a list of genes included in the Oncomine™ Pan-Cancer Cell-Free Assay kit (Thermo Fisher, Palo Alto, CA, USA) (Format: .xlsx); Data S2: Datasheet with all TaqMan® dPCR assays (predesigned or customized) (Thermo Fisher, Palo Alto, CA, USA) available in our laboratory (format: .xlsx); Data S3: Datasheet with variants considered as potential mechanism of resistance with information about validation by dPCR/NGS and its detection in previous samples (format: .xlsx); Data S4: Final list of the genetic variants (N = 365) found through NGS for this study (format: .xlsx).

Author Contributions: Conceptualization, A.R. and M.P.; data curation, R.S.-B., E.S.-H., L.R.d.L., S.S.-M., A.R.-F., D.A.-T., A.S.-H., M.d.J.C., C.G.-G., M.D., A.B., J.M.S., J.O., J.B.-B., M.Á.S. and M.S.; formal analysis, R.S.-B. and A.R.; funding acquisition, F.F. and M.P.; investigation, S.S.-M., A.R.-F. and D.A.-T.; methodology, R.S.-B., E.S.-H., S.S.-M. and A.R.-F.; project administration, A.R. and M.P.; resources, M.P.; software, R.S.-B.; supervision, A.R. and M.P.; writing—original draft, R.S.-B., L.R.d.L. and A.R.; writing—review and editing, R.S.-B., E.S.-H., L.R.d.L., A.C.-B., A.R. and M.P. All authors have read and agreed to the published version of the manuscript.

Funding: This study was supported by Boehringer Ingelheim. Boehringer Ingelheim had no role in the design, analysis, or interpretation of the results in this study. Boehringer Ingelheim was given the opportunity to review the manuscript for medical and scientific accuracy as it relates to Boehringer Ingelheim substances, as well as intellectual property considerations. This article is part of a project that received funding from Instituto de Salud Carlos III through the project "PI21/01500" (co-funded by European Regional Development Fund/European Social Fund: "A way to make Europe"/"Investing in your future"). The work presented in this paper also received funding from the European Union's Horizon 2020 research and innovation program under grant agreement No 875160. E.S.-H. was funded by the Consejería de Ciencia, Universidades e Innovación of the Comunidad de Madrid (Doctorados Industriales of the Comunidad de Madrid IND2019/BMD-17258). D.A.-T. was funded by the Consejería de Educación, Juventud y Deporte of the Comunidad de Madrid and by the Fondo Social Europeo (Programa Operativo de Empleo Juvenil, and Iniciativa de Empleo Juvenil), PEJ2019-TL/SAL-14607.

Institutional Review Board Statement: This study was approved by the Ethical Committee of Hospital Puerta de Hierro, Madrid, Spain (internal code: PI 02/16), and conducted in accordance with the precepts of the Code of Ethics of the World Medical Association (Declaration of Helsinki).

Informed Consent Statement: A total of 124 patients were recruited by 35 Hospitals from February 2016 to September 2021. Informed consent was obtained from all subjects involved in the study.

Data Availability Statement: In this study, an internal bioinformatics pipeline, designed using R, was used. A schematic flowchart of the pipeline is shown in Supplementary Figure S1. The data presented in this study are available on request from the corresponding author.

Acknowledgments: The authors would like to thank their patients and their families for making the study possible.

Conflicts of Interest: A.S.-H. reports personal fees and nonfinancial support from Roche, AstraZeneca, and Boehringer, outside the submitted work. M.d.J.C. reports personal fees from Roche, Pierre Fabre, and MSD and other fees from AstraZeneca, Boehringer Ingelheim, AstraZeneca, and Lilly, outside the submitted work. M.D. reports personal fees from AstraZeneca, BMS, Boehringer Ingelheim, MSD, Pfizer, and Roche, outside the submitted work. J.B.-B. reports grants and personal fees from Roche-Genentech, Pfizer, and Pierre Fabre and personal fees from MSD, BMS, AstraZeneca,

and Novartis. A.R. reports personal fees from Boehringer and AstraZeneca. M.P. reports personal fees from Roche, BMS, MSD, Pfizer, Lilly, Novartis, and Takeda, as well as grants and personal fees from AstraZeneca and Boehringer during the conduct of the study. The remaining authors declare no conflicts of interest.

Abbreviations

cfDNA, circulating cell-free DNA; CI, confidence interval; CNS, central nervous system; CNV, copy number variant; ctDNA, circulating tumor DNA; dPCR, digital PCR; ECOG eastern cooperative oncology group; *EGFR*-TKI, *EGFR* tyrosine kinase inhibitor; HR, hazard ratio; IGV, integrative genome visualizer; Indel, insertion or deletion; MAF, mutated allele frequency; MNP, multiple-nucleotide polymorphism; NGS, next-generation sequencing; NR, not reached; NSCLC, non-small-cell lung cancer; OS, overall survival; PFS, progression-free survival; RECIST, Response Evaluation Criteria in Solid Tumors; SNV, single-nucleotide variant.

References

1. Siegel, R.L.; Miller, K.D.; Jemal, A. Cancer Statistics, 2020. *CA Cancer J. Clin.* **2020**, *70*, 7–30. [CrossRef] [PubMed]
2. Thress, K.S.; Brant, R.; Carr, T.H.; Dearden, S.; Jenkins, S.; Brown, H.; Hammett, T.; Cantarini, M.; Barrett, J.C. EGFR Mutation Detection in CtDNA from NSCLC Patient Plasma: A Cross-Platform Comparison of Leading Technologies to Support the Clinical Development of AZD9291. *Lung Cancer* **2015**, *90*, 509–515. [CrossRef] [PubMed]
3. Aye, P.S.; McKeage, M.J.; Tin, S.T.; Khwaounjoo, P.; Elwood, J.M. Population-Based Incidence Rates and Increased Risk of EGFR Mutated Non-Small Cell Lung Cancer in Māori and Pacifica in New Zealand. *PLoS ONE* **2021**, *16*, e0251357. [CrossRef] [PubMed]
4. Soria, J.C.; Ohe, Y.; Vansteenkiste, J.; Reungwetwattana, T.; Chewaskulyong, B.; Lee, K.H.; Dechaphunkul, A.; Imamura, F.; Nogami, N.; Kurata, T.; et al. Osimertinib in Untreated EGFR-Mutated Advanced Non-Small-Cell Lung Cancer. *N. Engl. J. Med.* **2018**, *378*, 113–125. [CrossRef] [PubMed]
5. Yang, J.C.H.; Camidge, D.R.; Yang, C.T.; Zhou, J.; Guo, R.; Chiu, C.H.; Chang, G.C.; Shiah, H.S.; Chen, Y.; Wang, C.C.; et al. Safety, Efficacy, and Pharmacokinetics of Almonertinib (HS-10296) in Pretreated Patients with EGFR-Mutated Advanced NSCLC: A Multicenter, Open-Label, Phase 1 Trial. *J. Thorac. Oncol.* **2020**, *15*, 1907–1918. [CrossRef]
6. Ahn, M.J.; Han, J.Y.; Lee, K.H.; Kim, S.W.; Kim, D.W.; Lee, Y.G.; Cho, E.K.; Kim, J.H.; Lee, G.W.; Lee, J.S.; et al. Lazertinib in Patients with EGFR Mutation-Positive Advanced Non-Small-Cell Lung Cancer: Results from the Dose Escalation and Dose Expansion Parts of a First-in-Human, Open-Label, Multicentre, Phase 1-2 Study. *Lancet Oncol.* **2019**, *20*, 1681–1690. [CrossRef]
7. Zhou, Q.; Wu, L.; Feng, L.; An, T.; Cheng, Y.; Zhou, J.; Li, J.; Feng, J.F.; Zhang, L.; Han, B.; et al. Safety and Efficacy of Abivertinib (AC0010), a Third-Generation EGFR Tyrosine Kinase Inhibitor, in Chinese Patients with EGFR-T790M Positive Non-Small Cell Lung Cancer (NCSLC). *J. Clin. Oncol.* **2019**, *37*, 9091. [CrossRef]
8. Du, X.; Yang, B.; An, Q.; Assaraf, Y.G.; Cao, X.; Xia, J. Acquired Resistance to Third-Generation EGFR-TKIs and Emerging next-Generation EGFR Inhibitors. *Innovation* **2021**, *2*, 100103. [CrossRef]
9. Noronha, V.; Patil, V.M.; Joshi, A.; Menon, N.; Chougule, A.; Mahajan, A.; Janu, A.; Purandare, N.; Kumar, R.; More, S.; et al. Gefitinib Versus Gefitinib Plus Pemetrexed and Carboplatin Chemotherapy in EGFR-Mutated Lung Cancer. *J. Clin. Oncol.* **2020**, *38*, 124–136. [CrossRef]
10. Nakagawa, K.; Garon, E.B.; Seto, T.; Nishio, M.; Ponce Aix, S.; Paz-Ares, L.; Chiu, C.H.; Park, K.; Novello, S.; Nadal, E.; et al. Ramucirumab plus Erlotinib in Patients with Untreated, EGFR-Mutated, Advanced Non-Small-Cell Lung Cancer (RELAY): A Randomised, Double-Blind, Placebo-Controlled, Phase 3 Trial. *Lancet Oncol.* **2019**, *20*, 1655–1669. [CrossRef]
11. Bauml, J.; Cho, B.C.; Park, K.; Lee, K.H.; CHO, E.K.; Kim, D.-W.; Kim, S.-W.; Haura, E.B.; Sabari, J.K.; Sanborn, R.E.; et al. Amivantamab in Combination with Lazertinib for the Treatment of Osimertinib-Relapsed, Chemotherapy-Naïve EGFR Mutant (EGFRm) Non-Small Cell Lung Cancer (NSCLC) and Potential Biomarkers for Response. *J. Clin. Oncol.* **2021**, *39*, 9006. [CrossRef]
12. Provencio, M.; Serna-Blasco, R.; Franco, F.; Calvo, V.; Royuela, A.; Auglytė, M.; Sánchez-Hernández, A.; de Julián Campayo, M.; García-Girón, C.; Dómine, M.; et al. Analysis of Circulating Tumour DNA to Identify Patients with Epidermal Growth Factor Receptor–Positive Non-Small Cell Lung Cancer Who Might Benefit from Sequential Tyrosine Kinase Inhibitor Treatment. *Eur. J. Cancer* **2021**, *149*, 61–72. [CrossRef] [PubMed]
13. Nahar, R.; Zhai, W.; Zhang, T.; Takano, A.; Khng, A.J.; Lee, Y.Y.; Liu, X.; Lim, C.H.; Koh, T.P.T.; Aung, Z.W.; et al. Elucidating the Genomic Architecture of Asian EGFR-Mutant Lung Adenocarcinoma through Multi-Region Exome Sequencing. *Nat. Commun.* **2018**, *9*, 216. [CrossRef]
14. Hong, S.; Gao, F.; Fu, S.; Wang, Y.; Fang, W.; Huang, Y.; Zhang, L. Concomitant Genetic Alterations with Response to Treatment and Epidermal Growth Factor Receptor Tyrosine Kinase Inhibitors in Patients with EGFR-Mutant Advanced Non-Small Cell Lung Cancer. *JAMA Oncol.* **2018**, *4*, 739–742. [CrossRef] [PubMed]

15. Blakely, C.M.; Watkins, T.B.K.; Wu, W.; Gini, B.; Chabon, J.J.; McCoach, C.E.; McGranahan, N.; Wilson, G.A.; Birkbak, N.J.; Olivas, V.R.; et al. Evolution and Clinical Impact of Co-Occurring Genetic Alterations in Advanced-Stage EGFR-Mutant Lung Cancers. *Nat. Genet.* **2017**, *49*, 1693–1704. [CrossRef]
16. Canale, M.; Petracci, E.; Delmonte, A.; Chiadini, E.; Dazzi, C.; Papi, M.; Capelli, L.; Casanova, C.; De Luigi, N.; Mariotti, M.; et al. Impact of TP53 Mutations on Outcome in EGFR-Mutated Patients Treated with First-Line Tyrosine Kinase Inhibitors. *Clin. Cancer Res.* **2017**, *23*, 2195–2202. [CrossRef]
17. Offin, M.; Chan, J.M.; Tenet, M.; Rizvi, H.A.; Shen, R.; Riely, G.J.; Rekhtman, N.; Daneshbod, Y.; Quintanal-Villalonga, A.; Penson, A.; et al. Concurrent RB1 and TP53 Alterations Define a Subset of EGFR-Mutant Lung Cancers at Risk for Histologic Transformation and Inferior Clinical Outcomes. *J. Thorac. Oncol.* **2019**, *14*, 1784–1793. [CrossRef]
18. Collisson, E.A.; Campbell, J.D.; Brooks, A.N.; Berger, A.H.; Lee, W.; Chmielecki, J.; Beer, D.G.; Cope, L.; Creighton, C.J.; Danilova, L.; et al. Comprehensive Molecular Profiling of Lung Adenocarcinoma. *Nature* **2014**, *511*, 543–550.
19. Chen, Z.; Fillmore, C.M.; Hammerman, P.S.; Kim, C.F.; Wong, K.K. Non-Small-Cell Lung Cancers: A Heterogeneous Set of Diseases. *Nat. Rev. Cancer* **2014**, *14*, 535–546. [CrossRef]
20. Diaz, L.A.; Bardelli, A. Liquid Biopsies: Genotyping Circulating Tumor DNA. *J. Clin. Oncol.* **2014**, *32*, 579–586. [CrossRef]
21. Li, M.M.; Datto, M.; Duncavage, E.J.; Kulkarni, S.; Lindeman, N.I.; Roy, S.; Tsimberidou, A.M.; Vnencak-Jones, C.L.; Wolff, D.J.; Younes, A.; et al. Standards and Guidelines for the Interpretation and Reporting of Sequence Variants in Cancer. *J. Mol. Diagn.* **2017**, *19*, 4–23. [CrossRef] [PubMed]
22. ClinGen TP53 Expert Panel Specifications to the ACMG/AMP Variant Interpretation Guidelines Version 1 TP53 Rule Specifications for the ACMG/AMP Variant Curation Guidelines Gene Disease (MONDO ID) Clinically Significant Transcript TP53 Li-Fraumeni Syndrome (0007903) Pathogenic Criteria Criteria Original Criteria Description Specification(S). Available online: https://www.clinicalgenome.org/affiliation/50013 (accessed on 15 August 2022).
23. Provencio, M.; Torrente, M.; Calvo, V.; Pérez-Callejo, D.; Gutiérrez, L.; Franco, F.; Pérez-Barrios, C.; Barquín, M.; Royuela, A.; García-García, F.; et al. Prognostic Value of Quantitative CtDNA Levels in Non Small Cell Lung Cancer Patients. *Oncotarget* **2018**, *9*, 488–494. [CrossRef] [PubMed]
24. Zhang, Z.; Lee, J.C.; Lin, L.; Olivas, V.; Au, V.; Laframboise, T.; Abdel-Rahman, M.; Wang, X.; Levine, A.D.; Rho, J.K.; et al. Activation of the AXL Kinase Causes Resistance to EGFR-Targeted Therapy in Lung Cancer. *Nat. Genet.* **2012**, *44*, 852–860. [CrossRef] [PubMed]
25. Bivona, T.G.; Hieronymus, H.; Parker, J.; Chang, K.; Taron, M.; Rosell, R.; Moonsamy, P.; Dahlman, K.; Miller, V.A.; Costa, C.; et al. FAS and NF-KB Signalling Modulate Dependence of Lung Cancers on Mutant EGFR. *Nature* **2011**, *471*, 523–526. [CrossRef] [PubMed]
26. Ono, M.; Kuwano, M. Molecular Mechanisms of Epidermal Growth Factor Receptor (EGFR) Activation and Response to Gefitinib and Other EGFR-Targeting Drugs. *Clin. Cancer Res.* **2006**, *12*, 7242–7251. [CrossRef]
27. Jackman, D.M.; Yeap, B.Y.; Sequist, L.V.; Lindeman, N.; Holmes, A.J.; Joshi, V.A.; Bell, D.W.; Huberman, M.S.; Halmos, B.; Rabin, M.S.; et al. Exon 19 Deletion Mutations of Epidermal Growth Factor Receptor Are Associated with Prolonged Survival in Non-Small Cell Lung Cancer Patients Treated with Gefitinib or Erlotinib. *Clin. Cancer Res.* **2006**, *12*, 3908–3914. [CrossRef]
28. Yasuda, H.; Kobayashi, S.; Costa, D.B. EGFR Exon 20 Insertion Mutations in Non-Small-Cell Lung Cancer: Preclinical Data and Clinical Implications. *Lancet Oncol.* **2012**, *13*, e23–e31. [CrossRef]
29. Piper-Vallillo, A.J.; Sequist, L.V.; Piotrowska, Z. Emerging Treatment Paradigms for EGFR-Mutant Lung Cancers Progressing on Osimertinib: A Review. *J. Clin. Oncol.* **2020**, *38*, 2926–2936. [CrossRef]
30. Kobayashi, S.; Boggon, T.J.; Dayaram, T.; Jänne, P.A.; Kocher, O.; Meyerson, M.; Johnson, B.E.; Eck, M.J.; Tenen, D.G.; Halmos, B. EGFR Mutation and Resistance of Non-Small-Cell Lung Cancer to Gefitinib. *N. Engl. J. Med.* **2005**, *352*, 786–792. [CrossRef]
31. Arcila, M.E.; Oxnard, G.R.; Nafa, K.; Riely, G.J.; Solomon, S.B.; Zakowski, M.F.; Kris, M.G.; Pao, W.; Miller, V.A.; Ladanyi, M. Rebiopsy of Lung Cancer Patients with Acquired Resistance to EGFR Inhibitors and Enhanced Detection of the T790M Mutation Using a Locked Nucleic Acid-Based Assay. *Clin. Cancer Res.* **2011**, *17*, 1169–1180. [CrossRef]
32. Chen, H.J.; Mok, T.S.; Chen, Z.H.; Guo, A.L.; Zhang, X.C.; Su, J.; Wu, Y.L. Clinicopathologic and Molecular Features of Epidermal Growth Factor Receptor T790M Mutation and C-MET Amplification in Tyrosine Kinase Inhibitor-Resistant Chinese Non-Small Cell Lung Cancer. *Pathol. Oncol. Res.* **2009**, *15*, 651–658. [CrossRef] [PubMed]
33. Matsuo, N.; Azuma, K.; Sakai, K.; Hattori, S.; Kawahara, A.; Ishii, H.; Tokito, T.; Kinoshita, T.; Yamada, K.; Nishio, K.; et al. Association of EGFR Exon 19 Deletion and EGFR-TKI Treatment Duration with Frequency of T790M Mutation in EGFR-Mutant Lung Cancer Patients. *Sci. Rep.* **2016**, *6*, 36458. [CrossRef] [PubMed]
34. Politi, K.; Fan, P.D.; Shen, R.; Zakowski, M.; Varmus, H. Erlotinib Resistance in Mouse Models of Epidermal Growth Factor Receptor-Induced Lung Adenocarcinoma. *Dis. Model. Mech.* **2010**, *3*, 111–119. [CrossRef] [PubMed]
35. Nanjo, S.; Arai, S.; Wang, W.; Takeuchi, S.; Yamada, T.; Hata, A.; Katakami, N.; Okada, Y.; Yano, S. MET Copy Number Gain Is Associated with Gefitinib Resistance in Leptomeningeal Carcinomatosis of EGFR-Mutant Lung Cancer. *Mol. Cancer Ther.* **2017**, *16*, 506–515. [CrossRef] [PubMed]
36. Martinez-Marti, A.; Felip, E.; Matito, J.; Mereu, E.; Navarro, A.; Cedrés, S.; Pardo, N.; de Castro, A.M.; Remon, J.; Miquel, J.M.; et al. Dual MET and ERBB Inhibition Overcomes Intratumor Plasticity in Osimertinib-Resistant-Advanced Non-Small-Cell Lung Cancer (NSCLC). *Ann. Oncol. Off. J. Eur. Soc. Med. Oncol.* **2017**, *28*, 2451–2457. [CrossRef]

37. Deng, L.; Kiedrowski, L.A.; Ravera, E.; Cheng, H.; Halmos, B. Response to Dual Crizotinib and Osimertinib Treatment in a Lung Cancer Patient with MET Amplification Detected by Liquid Biopsy Who Acquired Secondary Resistance to EGFR Tyrosine Kinase Inhibition. *J. Thorac. Oncol.* **2018**, *13*, e169–e172. [CrossRef]
38. Mazières, J.; Peters, S.; Lepage, B.; Cortot, A.B.; Barlesi, F.; Beau-Faller, M.; Besse, B.; Blons, H.; Mansuet-Lupo, A.; Urban, T.; et al. Lung Cancer That Harbors an HER2 Mutation: Epidemiologic Characteristics and Therapeutic Perspectives. *J. Clin. Oncol.* **2013**, *31*, 1997–2003. [CrossRef]
39. Planchard, D.; Loriot, Y.; André, F.; Gobert, A.; Auger, N.; Lacroix, L.; Soria, J.C. EGFR-Independent Mechanisms of Acquired Resistance to AZD9291 in EGFR T790M-Positive NSCLC Patients. *Ann. Oncol.* **2015**, *26*, 2073–2078. [CrossRef]
40. Sun, Y.; Meyers, B.A.; Czako, B.; Leonard, P.; Mseeh, F.; Harris, A.L.; Wu, Q.; Johnson, S.; Parker, C.A.; Cross, J.B.; et al. Allosteric SHP2 Inhibitor, IACS-13909, Overcomes EGFR-Dependent and EGFR-Independent Resistance Mechanisms toward Osimertinib. *Cancer Res.* **2020**, *80*, 4840–4853. [CrossRef]
41. Oxnard, G.R.; Hu, Y.; Mileham, K.F.; Husain, H.; Costa, D.B.; Tracy, P.; Feeney, N.; Sholl, L.M.; Dahlberg, S.E.; Redig, A.J.; et al. Assessment of Resistance Mechanisms and Clinical Implications in Patients With EGFR T790M-Positive Lung Cancer and Acquired Resistance to Osimertinib. *JAMA Oncol.* **2018**, *4*, 1527–1534. [CrossRef]
42. Ho, C.C.; Liao, W.Y.; Lin, C.A.; Shih, J.Y.; Yu, C.J.; Chih-Hsin Yang, J. Acquired BRAF V600E Mutation as Resistant Mechanism after Treatment with Osimertinib. *J. Thorac. Oncol.* **2017**, *12*, 567–572. [CrossRef] [PubMed]
43. Linardou, H.; Dahabreh, I.J.; Kanaloupiti, D.; Siannis, F.; Bafaloukos, D.; Kosmidis, P.; Papadimitriou, C.A.; Murray, S. Assessment of Somatic K-RAS Mutations as a Mechanism Associated with Resistance to EGFR-Targeted Agents: A Systematic Review and Meta-Analysis of Studies in Advanced Non-Small-Cell Lung Cancer and Metastatic Colorectal Cancer. *Lancet Oncol.* **2008**, *9*, 962–972. [CrossRef]
44. Serna-Blasco, R.; Sánchez-Herrero, E.; Sanz-Moreno, S.; Rodriguez-Festa, A.; García-Veros, E.; Casarrubios, M.; Sierra-Rodero, B.; Laza-Briviesca, R.; Cruz-Bermúdez, A.; Mielgo-Rubio, X.; et al. KRAS p.G12C Mutation Occurs in 1% of EGFR-Mutated Advanced Non-Small-Cell Lung Cancer Patients Progressing on a First-Line Treatment with a Tyrosine Kinase Inhibitor. *ESMO Open* **2021**, *6*, 100279. [CrossRef] [PubMed]
45. Provencio, M.; Torrente, M.; Calvo, V.; Gutiérrez, L.; Pérez-Callejo, D.; Pérez-Barrios, C.; Barquín, M.; Royuela, A.; Rodriguez-Alfonso, B.; Sotelo, M.; et al. Dynamic Circulating Tumor DNA Quantificaton for the Individualization of Non-Small-Cell Lung Cancer Patients Treatment. *Oncotarget* **2017**, *8*, 60291–60298. [CrossRef] [PubMed]
46. Iwama, E.; Sakai, K.; Azuma, K.; Harada, T.; Harada, D.; Nosaki, K.; Hotta, K.; Ohyanagi, F.; Kurata, T.; Fukuhara, T.; et al. Monitoring of Somatic Mutations in Circulating Cell-Free DNA by Digital PCR and next-Generation Sequencing during Afatinib Treatment in Patients with Lung Adenocarcinoma Positive for EGFR Activating Mutations. *Ann. Oncol.* **2017**, *28*, 136–141. [CrossRef]
47. Yang, M.; Forbes, M.E.; Bitting, R.L.; O'Neill, S.S.; Chou, P.C.; Topaloglu, U.; Miller, L.D.; Hawkins, G.A.; Grant, S.C.; DeYoung, B.R.; et al. Incorporating Blood-Based Liquid Biopsy Information into Cancer Staging: Time for a TNMB System? *Ann. Oncol.* **2018**, *29*, 311–323. [CrossRef]